Faculty of Engineering and Science

Geochemical Characteristics of Water, Sediments and Suspended Solids in Sibuti River Estuary and Its Potential Effect on the Miri-Sibuti Coral Reefs

RAKESH ROSHAN GANTAYAT

0000-0001-5296-1784

This thesis presented for the Degree of
Doctor of Philosophy
of
Curtin University

June 2021

Declaration

To the best of my knowledge and belief this thesis contains no material previously published by any other person except where due acknowledgment has been made. This thesis contains no material which has been accepted for the award of any other degree or diploma in any university.

Rakesh Roshan Gantayat

16th Dec 2021

Dedication

To my parents

Mr. Kedar and Mrs. Kanak

My brother and sister

Mr. Omm and Mrs. Monalisa

Thank you for the irreplaceable love, care and support

Acknowledgements

I would like to express my sincere gratitude to my main supervisor **Assoc/Prof. M.V. Prasanna** and my Co-supervisor **Prof. Nagarajan Ramasamy** for their invaluable support, guidance, suggestions and comments throughout my research work. I am truly grateful to Associate supervisor **Prof. S. Chidambaram** for his valuable inputs and paramount support, suggestions and encouragements throughout this journey and before. I would like to convey sincere thanks to my Chairperson **Assoc/Prof Perumal Kumar** for his unwavering support. I would like to thank Curtin University, for providing Curtin Malaysia Postgraduate Research Scholarship, The Dean, Graduate School, Faculty of Engineering and Science, Curtin University for their financial assistance throughout my research.

A very special thanks to Dr. Eswaramoorthi for support, encouragement and teaching of greatest importance during my experimental and interpretation work. A heartfelt thanks to my former colleague Dr. Prabakaran Krishnamurthy for his suggestions and help during my proposal and preliminary study. I would also like to convey my exceptional gratitude towards Mr. Stephen Ongetta, Mr. Farooq Ismail, Mr. Paramesh Pydiah, Mr. Navakanesh and Mr. Sulaimaan Hassan for helping me out in my field work. A very special thanks to Mr. Navakanesh for providing me the Geological details of Sarawak and Mr. Pritam Chaudhury for guiding me through ArcGIS during the time of need. A heartfelt thanks to Mr. Thomas Mienczakowski for modifying the fish tank pump used in the experiment. Without all of your inputs it was difficult to overcome the hurdles.

This research work would have been impossible to carry without the help from the lab staffs and friends. My sincere gratitude to Mrs. Rassti and Mrs. Marilyn, for being a constant helping hand in handling the instruments and providing chemicals throughout analytical work. A special thanks to Ms. Yuanna and Ms. Diana for the invaluable help. A very heartfelt thanks to Mr. Odvut, Mr. Wajdan, Mr. Farooq, Mr. Thomas, Mr. Majoob and Mr. Sulaimaan for their continuous help provided during analytical work. A sincere thanks to Ms. Esther for the encouragement and linguistic corrections.

This journey would have been impossible without the support and encouragement of my friends and well-wishers. I am immensely thankful to Mr. Odvut, Mr. Farooq, Mr. Thomas, Mr. Farhan, Ms. Khyati, Ms. Udita, Ms. Shehnee, Ms. Zara, Mr. Mahjoob,

Mr. Steve, Mr. Majeed, Ms. Shima, Mr, Paramesh, Mr. Wajdan, Mr. Shahin, Mr. Hassan, Mr. Murtuza, Mr. Lee, Mr. Maruf, Ms. Levina. Ms. Sherlina, Mr. Majeed and Mr. Oshil for being a support system throughout this time. I am really blessed to have you people around me through these years. A very genuine thanks for being there for me during my ups and downs. I am truly blessed to be under the care of my precious family. It would have never been possible to carry on without their unconditional love and care for all my life. Finally, my profound thanks my HDR friends and administrative staff's at the Curtin University for their encouragement and support which made my stay and studies more enjoyable.

Frequently used list of abbreviations

AAS	Atomic Absorption Spectroscopy
ANZECC	Australian And New Zealand Environment and Conservation Council
APHA	American Public Health Association
AU	Absorbance Unit
BCR	Community Bureau of Reference
BDL	Below Detection Limit
CF	Contamination Factor
CR	Corrosivity Ratio
DGT	Diffusive Gradient Thin Film
DO	Dissolved Oxygen
EC	Electrical Conductivity
EDL	Electrode Cathode Lamps
EF	Enrichment Factor
EPA	Environmental Protection Agency
ERL	Effect Range Low
ERM	Effect Range Medium
GBR	Great Barrier Reef
HCL	Hollow Cathode Lamps
IBE	Indices of Base Exchange
I_{geo}	Geoaccumulation Index
ITCZ	Intertropical Convergence Zone
MANRED	Ministry of Modernisation of Agriculture, Native Land and Regional Development
mg kg^{-1}	Milligram Per Kilogram
mg L^{-1}	Milligram Per Liter
MSCR	Miri-Sibuti Coral Reef
MSCRNP	Miri-Sibuti Coral Reef National Park
Na%	Sodium Percentage
NEM	North-East Monsoon
NGS	National Geographic Society

NIWA	National Institute of Water and Atmospheric Research
NOAA	National Oceanic and Atmospheric Administration
NTU	Nephelometric Turbidity Unit
OM	Organic Matter
PAAS	Post-Archean Australian Shale
PCA	Principal Component Analysis
pCO_2	Partial Pressure of Carbon Dioxide
PDO	Pacific Decadal Oscillation
PERI	Potential Ecological Risk Index
PI	Permeability Index
PLI	Pollution Load Index
RAC	Risk Assessment Code
RSC	Residual Sodium Carbonate
SCS	South China Sea
SI	Saturation Index
SPI	Sediment Pollution Index
SPSS	Statistical Package for Social Science
SS	Suspended Solids
SWM	South-West Monsoon
TDS	Total Dissolved Solids
TSS	Total Suspended Solids
TTM	Total Trace Metal
UNEP	United Nations Environment Programme
USEPA	United State Environmental Protection Authority
USGS	United States Geological Survey
USSL	United States Salinity Laboratory
UV	Ultraviolet
WHO	World Health Organization

Abstract

Estuaries are the most challenging environments on earth to study the origin, pathways and fates of various dissolved and solid materials. Freshwater discharge and tidal forcing change on daily and turbulent mixing usually give rise to various geochemical processes with abrupt changes in major parameters such as temperature, salinity, turbidity and pH. The Sibuti river basin spreads over 1020 km^2 and gets geological inputs from 3 major and 6 minor formations aging from Oligocene to Pliocene. The major geological formations are dominated by siliciclastic sediments made up of sandstones, mudstones, shale, marl lenses, limestone beds along with thin lenses of coal and pyrite concretions. The basin is heavily influenced by deforestation over the years and the major anthropological inputs include agricultural activities in the basinal area and inputs from small towns like Bekenu along with several other villages located along the shore of the river. The hydrological regime of the river is controlled mainly by rainfall associated with Pacific Decadal Oscillation (PDO). To understand the geochemical nature of the Sibuti river, 36 samples of water and sediments and 5 samples of suspended solids were collected from 30 to 35 km stretch of estuary starting from the river mouth. The collected water samples were analysed for various physico-chemical parameters (pH, dissolved oxygen (DO), electrical conductivity (EC), total dissolved solids (TDS), turbidity, velocity, salinity, temperature, carbon dioxide (CO_2) and total suspended solids (TSS)), major ions (calcium (Ca^{2+}), magnesium (Mg^{2+}), sodium (Na^+), potassium (K^+), bicarbonate (HCO_3^-), carbonate (CO_3^-) and Chloride (Cl^-)), nutrients (sulfate (SO_4^{2-}), phosphate (PO_4^{3-}), nitrate (NO_3^-), ammonia (NH_3) and ammonium (NH_4^+)) and trace metals (cobalt (Co), copper (Cu), manganese (Mn), lead (Pb), zinc (Zn), selenium (Se), iron (Fe), aluminium (Al), cadmium (Cd), chromium (Cr) and barium (Ba)), whereas sediment and suspended solids were analysed for trace metals. To reveal detailed metal behaviour in sediments, a sequential extraction technique was adopted.

The study of hydrochemistry revealed that seawater's influence during South-West monsoon (SWM) and mixed dynamic of freshwater and seawater mixing during North-East monsoon (NEM) mainly controls the water chemistry in the estuary. The Schoeller's water classification revealed base ion exchange and reverse ion exchange during SWM and NEM respectively. The Piper plot revealed Na-Cl water type domination in the estuary during SWM, whereas reverse ion exchange in NEM altered

the ionic composition of water with increase in Ca^{2+} and Mg^{2+}. As a result, Ca-Cl and Na-Mg-Cl are the dominating water type in the upper part, whereas Na-Cl prevails in the lower part of estuary during NEM. Factor analysis revealed that ions and nutrients like Cl^-, Mg^{2+}, Ca^{2+}, Na^+, K^+, SO_4^{2-} are regulated by seawater intrusion during both seasons. Nutrients like NO_3^- and NH_3 are part of agricultural inputs with the fluctuation of DO that controls the nitrification and ammonification processes in the estuary. Log pCO_2 values revealed higher respiration of organic matter controlling the pH. Higher residence time of river water is controlled by high tidal regime and low monsoonal rainfall and vice versa. Saturation index (SI) shows that carbonate, sulfate and halide group of minerals are in undersaturated condition and heavily dependent on freshwater infusion into the estuary. On the other hand, oxide and oxyhydroxides like goethite and magnetite were found in oversaturated condition during low flow regime of river (SWM). Sequential extraction of sediments revealed the association of Cd, Mn, Ba, Zn and Se with exchangeable and carbonate fraction, whereas Fe was found higher in oxidizable fraction and is an indicative of high degree of humification. Metals in the water, sediments and suspended solids (Co, Cu, Mn, Pb, Zn, Se, Fe, Al, Cr and Ba) were mostly found to be geogenic in origin except for Cd, which is contributed by leaching from agricultural fields. Fe and Mn hydroxides and clay minerals controlled the trace metal absorption/desorption and are mainly dependent on salinity variation, concentration of DO, turbidity and pH in the estuary. Association of Mn with exchangeable fraction such as Mn-hydroxide controlled the majority of the variance in metals like Cu, Zn, Ba and Co in sediments. Fe and clay minerals with high degree of humification played a vital role in absorption of metals like Ba, Co, Cd, Zn, Cd and Cr in low salinity and high pH conditions. Stratification of water during NEM contributed to 2-fold increase in Mn hydroxide formation in oxygenated layer of water and absorption of metals like Cu and Zn in turbidity maximum zones. Study of partition coefficient revealed metal absorption's nature in estuary under prevailing ideal conditions of pH (4-7), salinity conditions and high degree of humification on suspended solids.

The acidic condition of water and high turbidity at all the stations overwhelming the concentration of ions such as Na^+, Mg^{2+}, K^+, Cl^-, nutrients such as PO_4^{3-} and metals such as Fe, Mn, Cr, Se indicate unsuitability of water for drinking purposes. Residual sodium carbonate (RSC), EC and U.S. salinity laboratory (USSL) classifications

suggested permissible to excellent category, which indicate suitability for irrigational purposes. Low EC and salinity at majority of the stations away from the mouth region and absence of CO_3^- in estuarine water are mainly found to be responsible for such suitability. On contrary, Na% and Permeability index (PI), Sodium absorption ratio (SAR) and Kelly's ratio suggested unsuitability of water during SWM, whereas majority of NEM water were found suitable for irrigation. In such conditions, mechanical aeration, water diversion and dilution might work as proficient mitigation measures to reduce the effects in the contaminant zones. Corrosivity ratio (CR) found estuarine water to be corrosive in nature due to high concentration of Cl^- and SO_4^{2-}. Geoaccumulation index (I_{geo}), Enrichment factor (EF), Contamination factor (CF) indicated estuarine sediments are contaminated with Se, Co, Cu, Ba and Cd whereas suspended solids are contaminated with Co, Cu, Cd and Ba. Risk indices like Sediment pollution index (SPI), Pollution load index (PLI) and Potential ecological rick index (PERI) categorized sediments as highly polluted with toxic for biological community, whereas same indices placed suspended solids in highly polluted category as well and can cause moderate harmful effects on the biological community. Effect range low (ERL) and Effect range median (ERM) value comparison suggested Cu in sediments poses maximum possible biological effects to living organisms and adverse effects can be expected from Zn and Cr. Risk assessment code (RAC) placed Cd, Pb, Mn Se, Ba and Zn to be posing high risk during SWM, whereas Cd, Mn, Ba, Cu and Co during NEM pose medium to high risk towards benthic community of the estuary. In Sibuti river estuary, water carries high concentration of nutrients like NO_3^-, NH_3, metals such as Co, Mn, Zn, Cu, Fe and Cr in sediments whereas suspended solids are the major carrier of Mn, Zn and Cd compared to Baram river discharges. These contaminants are found discharging into the coastal water with the help of monsoonal rain especially during NEM and carried mainly by the help of sea currents flowing in Northern and N-Eastern direction into Miri-Sibuti coral reef (MSCR) region. The positive association of such contaminants with turbidity confirmed that influence of Sibuti river discharges are highly dependent on seasonal rainfall and terrestrial run-off associated with it. During SWM, influence is minor due to low flow regime of river and tidal dominance in the estuary. However, high rainfall and high flow regime during NEM is helping to push the contaminants into South China Sea (SCS) effectively, which has a major influence on MSCR region. Such situation can be dealt with the help of flocculation, precipitation, oxidation and algaecides, which helps to

remove the suspended solids. Sediments dredging might be useful in removing contaminated sediments from the river bottom. These remedial measures will be helpful in removing the contaminants from estuary and their influence in the coastal region.

Contents

List of Tables

List of Figures

Chapter-1

Background

1.1 Introduction

Geochemistry is a science of systematic study about various mechanisms behind major geological systems on earth and is linked to almost all aspects of geology (Correns, 1969). It is mainly concerned with the structure, composition and various physical and chemical aspects such as the distribution of elements and minerals in rocks along with their movement into the soil and water bodies (Albarède, 2009). Since the earth is composed of various chemical elements, it will not be wrong to examine most geologic materials and processes from a chemical point of view. Furthermore, these chemical reactions involve major processes like weathering (due to rock water interaction depending upon several factors) which give rise to dissolution and mobility of elements. This weathering product solution in many water bodies such as the lake, river, and sea leads to progressive chemical and mineralogical changes, thus affecting the biodiversity. So, an assimilated approach of geochemistry in a particular water body or location can reveal the influence and behavior of these contaminants with regard to innumerable environmental factors. Keeping that in mind, the "river system", a major functioning carrier of the hydrological cycle on the earth, has some key factors that make it different from other sources of water bodies. The most important one is the course or unidirectional flow towards its estuary/sea (Geyer and MacCready, 2014; UNEP, 2017). But the spatial distribution of river systems, their quantitative characteristics, and temporal changes in any region of the world depend on a range of physiographic factors (including climatic factors) and the effects of human activities (Dooge, 2009). The key changes in the river's ecosystem are always contributed by the headwaters, in its catchment area or floodplains and concluding in the estuary before entering the ocean or sea (Alexander et al., 2007).

1.2 Origin of river or headwater

The river origin, also known as the headwaters, is the beginning of a river, which is often located in the mountains and usually steep and erosional in nature (Alexander et al., 2007). The source of a river may be fed by an underground spring or by runoff from rainwater, snowmelt, or glacial melt (USGS, 2021). These sources contribute a

major amount of water to the river and enriches various minerals and nutrients due to the interaction with rocks of different origins. Some other conditions in the headwater region like temperate environments result in well-oxygenated water that is apparently rich in organic matter. This kind of origin helps to increase the organic matter in the river basin by helping the photosynthesis process (Chapman, 1996; Pedersen et al., 2013). In most cases, the source water is used to be free of contaminated substances, but under various circumstances, point sources such as volatile organic compounds (solvents and oil products in groundwater), micro-organisms, an excess amount of nutrients and ions comes into the river usually are responsible for the contamination (Zogorski et al., 2006). Furthermore, if the source of river water comes from various tributaries instead of a single source, there is a higher chance that the river will be enriched with many non-point source pollutants. Furthermore, this flow of diverse contaminants becomes the core part of the river in the catchment. Other factor such as temperature also plays a significant role in the source area. The increase in temperature and higher nutrient load in the headwaters can cause the micro-organisms to grow extreme amount, leading to aquatic hypoxia-like conditions in the catchment and estuarine region (Naidoo et al., 2013). As dissolved oxygen in water is also essential for all aquatic life, such hypoxic conditions can be considered as a major threat to their life (Chapman, 1996; Vaquer-Sunyer et al., 2008).

1.3 Catchment

The river, which is in a continuous state of unidirectional flow, brings along the chemical changes that had already happened in the source area to the catchment (Alexander et al., 2007). Furthermore, the catchment area where runoff from the land area is prominent further exposes the river water to some high degree of spatial and temporal changes. It is the most affected region of the river because both point and non-point sources of pollution are present here and play a vital role in changing the water chemistry (Santhi et al., 2001). With the increase of human settlement along the riverbanks, the contaminants increase, aggravated by erosion from the land. Some of the non-point sources include excess fertilizers, herbicides and insecticides from agricultural lands and residential areas, oil, grease and toxic chemicals from urban runoff and energy production, sediment from improperly managed construction sites, crop and forest lands, and eroding streambanks, salt from irrigation practices and acid drainage from abandoned mines, bacteria and nutrients from livestock, pet wastes and

faulty septic systems, atmospheric deposition and hydro modification etc. (Ongley, 1996; Costanzo et al., 2003; Savci et al., 2012; Edokpayi et al., 2017; Jarsjö et al., 2017). Moreover, catchment area is home to plants, animals, micro-organisms, non-living physical and chemical components (McCabe, 2010). The catchment is exposed to rainwater, atmospheric and human-made influences due to higher area coverage (Lintern et al., 2018). It also gets airborne contaminants through rainfall, which further acts as the main transporter of sediments and other inorganic contaminants into the river basin (Taylor et al., 2009). On the other hand, various weather events like heavy rainfall and flood provide a better transport medium for the sediment to spread in the river basin along with the increased velocity of the water. Regular sediment deposition can build bars for aquatic habitats, but increased sedimentation can destroy more habitats than it creates (NIWA, 2020). Increased sedimentation from the catchment area is one of the primary causes of habitat degradation. Depending on the local geology and terrain, sediment build-up can damage aquatic ecosystems not only in downstream sites but in upstream headwaters as the deposits grow (Lintern et al., 2018). Total maximum daily load helps in establishing a limit for measurable pollutants and parameters in river water. This daily load is established depending upon several factors such as sediment load, including total suspended solids, nutrient impairment, pathogens and siltation (Hart, 2006). The major process that works in the catchment is precipitation of such load, which can also bring a high amount of faecal materials into the water source, resulting in a pathogen breakthrough.

1.4 Estuary

Estuaries are the part of the river, where the freshwater gets mixed with the sea/ocean water. Being a transitional zone between river and sea, estuaries also play a major role in the case of health and growth of various marine plants and animals and is called as “nurseries of sea” because it provides a protected environment and abundant food supplies for the fish and shellfish to reproduce (Ohrel & Register, 2006). The presence of mangrove forest near estuaries also makes it even more productive in nature (Carugati et al., 2018). Most of the marine organisms feed in estuaries as a healthy estuary produces 4 to 10 times more organic matter than a cornfield of similar size (Ohrel & Register, 2006). It removes excess nutrients by bordering salt marshes and results in clear water for marine organisms. These are highly diverse biologically and

huge in productivity due to their shallowness, protected waters and availability of nutrients derived from different sources of rivers (Saifullah et al., 2014).

Many plant and animal communities survive in this particular environment due to the brackish nature of water, which is the result of the mixture of fresh and saline water. This combination provides a unique environment for the plants and animals to grow near it. Some common estuarine habitats are oyster reefs, kelp forests, rocky and soft shorelines, submerged aquatic vegetation, coastal marshes, mangroves, deep-water swamps, and riverine forests (Thayer, 2003) (Fig. 1.1). Furthermore, fishes available all over the world spend at least some parts of their life in the estuaries. In the case of humans, besides being a food source, estuaries are also helpful in creating jobs, recreation and even homes. As a result, 22 out of 32 of the largest cities are situated near the estuaries, which is proof of the importance of this environment (NOAA, 2020).

There are thousands of estuarine systems all over the world, which range in different shapes and sizes. The shape of the estuaries is determined depending upon various factors such as sea level influence, geology, topography, tidal currents, sediment supply, wave action, and human activities (Narayana, 2015). In general, estuaries are divided into 3 broad groups depending on their influencing characters (Dalrymple et al., 1992; Scanes et al., 2017) such as

a. Open embayment
b. Tide dominated estuaries
c. Wave dominated estuaries

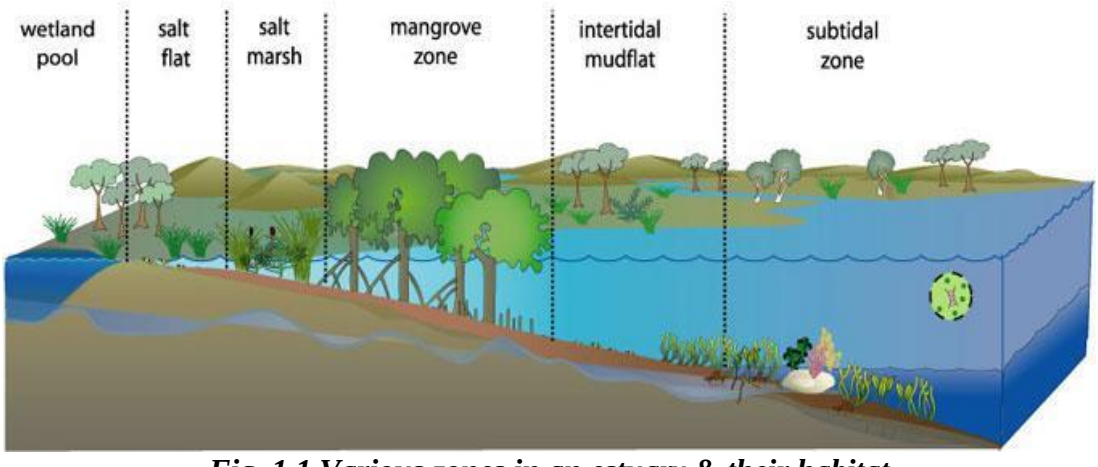

Fig. 1.1 Various zones in an estuary & their habitat (Source: https://microbewiki.kenyon.edu/index.php/Estuaries)

1.4.1 Open embayment

These types of estuaries, where tide and wave influence are limited by the presence of friction provided by the seabed and localized landforms, act as a protective barrier, which limit the penetration of seawater into embayment (e.g. Fly river estuary, Papua New Guinea) (Dalrymple et al., 1992; Narayana, 2015; Davidson, 2018). These types of estuaries are semi-enclosed bodies characterized by limited marine water influence with limited freshwater inflow and helps in creating more sheltered environments (Whitfield & Elliott, 2011).

1.4.2 Tide dominated estuaries

These are landward tapering funnel-shaped valleys surrounded by intertidal sedimentary environments like mangroves, intertidal flats, saltmarshes, etc (e.g. Baram river, Borneo) (Dalrymple et al., 1992; Whitfield & Elliott, 2011; Dalrymple et al., 2012). This type of estuarine system is distinguished by high tidal energy at the mouth similar to ocean, large and deep entrances (Narayana, 2015; Davidson, 2018). Tide-dominated estuaries have a tendency to fill the riverine part of the estuary with marine and terrestrial sediments, leading to the transitional nature of the geomorphic and sedimentary environment in seaward direction (Dalrymple et al., 2012).

1.4.3 Wave dominated estuaries

The estuaries that have smaller entrances than tide-dominated estuaries with a barrier formed by beach sand or flood tides fall into this category. In this type of estuaries, the tidal influence range is significantly lesser (~ 5-10%) (Dalrymple et al., 1992; Scanes et al., 2017). These are predominantly affected by river discharges more than ocean or sea influence (e.g. Brunswick river, Australia) (Narayana, 2015; Davidson, 2018). Furthermore, wind-induced water movement is the dominant mechanism for the sediment transport system. The unpredictable rain in tropical regions influences the ecosystem in a huge manner, making the salinity gradient highly variable (Whitfield & Elliott, 2011; Iglesias et al., 2019).

1.5 Estuarine processes

An estuary is a fascinating place from the largest landscape features to the smallest microscopic organisms. The services of this ecological system and the natural capital is critical to the functioning of the Earth's life-support system, directly and indirectly

(Narayan, 2015; Davidson, 2018; Iglesias et al., 2019). This dynamic system consisting of various cycles and processes pilot a range of spatial and temporal changes. Mechanisms like hydrodynamic mixing processes, geomorphological influence, water quality parameters and rock water interaction are the controlling factors of such activities under the changing circumstances in it (Fatema et al., 2012; Kumar et al., 2015).

1.5.1 Hydrodynamic mixing processes

The main agents carrying processes might include tides, wave actions, water density variation in all the estuaries. However, agents like wind action, Coriolis effect and gravitational effects have greater influence in the case of bigger estuaries and are due to external forces. In general, the tides and Coriolis effect depend on the gravitational pull of cosmic objects, such as the sun and moon along with the rotation of the Earth (NGS, 2011). It tends to dictate the changes in the estuary with effects like high and low tides along with the denser push of ocean water, which helps these materials to settle down or pushes them into the ocean floor (Fig.1.2). In addition, the spatially-variable and oscillatory nature of estuarine tidal currents give rise to several transport mechanisms depending on the conditions (Dronkers, 2005). This kind of periodic oscillation induced by the tide controls the volume of water fluxes into and out of estuaries and can cause effects like tidal pumping, which is a significant mechanism responsible for the up-estuary transport of saltwater and sediments (Salas-Monreal et al., 2008; Mathew et al., 2020). Such effects are responsible for creating turbidity maxima zones with elevated suspended solids and enhanced sediment trapping in tidal freshwater zones of the estuary (Mathew et al., 2020). However, such effects are limited to the high tidal period whereas baroclinic circulation is dominant during the low tide period while being a medium for terrestrial material transport. Here, intense mixing happens due to near-bottom currents directed up-estuary and near-surface currents directed down-estuary. This induces an up-estuary flux of sediment that extends up to the limit of salinity intrusion and resulting in the formation of turbid zones co-located with the salt front (Burchard et al., 2018). Similarly, hydrodynamic mixing like the fluvial effect is well known for its association with episodical or seasonal rainfall and pushes the salt-front seaward, enhancing bed shear stress, and potentially causing erosion and export of sediments from the estuary (Ralston et al., 2013; Mathew et al., 2020). Estuaries require a natural balance of freshwater and

saltwater. Droughts reduce freshwater input into tidal rivers and bays, which raise salinity in estuaries, and enable saltwater to mix farther upstream. The increase of salinity in brackish water environments can threaten to degrade ecosystem health. The intrusion of saltwater within groundwater or further upstream also possesses risks for coastal drinking water infrastructure.

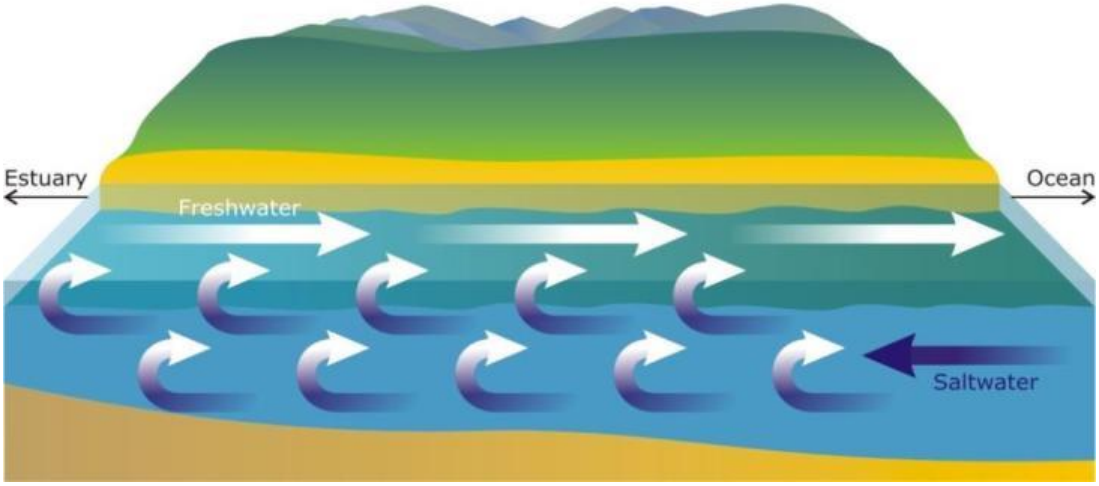

Fig. 1.2 Saline water and freshwater flow in estuary
(Source: https://www.britannica.com/science/estuary)

1.5.2 Geomorphological influence

These processes mainly have ascendancy with the help of disparity of catchment run-off and ingress of marine sediments into the estuarine environment along with changes in estuarine river channels (Dalrymple et al., 2012). These can also be derived by the effect exerted by catchment erosion, biological effects and aeolian transport. Contrarily, polarity in tidal currents leads to an increase of marine sediments in the estuary (Mathew et al., 2020; Li et al., 2020). These processes determine the fate and transport of contaminants in an estuary and sediment-related processes such as rate of erosion in the river basin, suspended sediment and sediment transport, sedimentation in the estuary. Li et al. (2020) explained that the amount of fine sediment particles deposited on the estuary tidal flat is directly related to the amount of sediments transported by the river and is inversely proportional to the ability of rivers to transport fine matter. Chemical processes such as precipitation, adsorption by suspended sediments and degradation, determine the distribution of a contaminants over the (suspended) sediments, the water column and even the atmosphere (volatilization) (Villars et al., 2001; Lin et al., 2018). However, coastal development, introduction of invasive species, harmful agricultural practices, and dumping of riverine pollutants

have led to a decline in the health of estuaries (Kennish et al., 2002). Habitats associated with estuaries, such as salt marshes and mangrove forests, act as filters. As water flows through a salt marsh, marsh grasses and peat (a spongy matrix of live roots, decomposing organic material, and soil), pollutants such as herbicides, pesticides, and heavy metals from the water, as well as excess sediments and nutrients are filtered out (Thayer et al., 2003). Due to the increase in pollutants through human activities in the catchment area and highland, it becomes a dump yard with a huge amount of riverine pollutants, leading to sophisticated chemical reactions.

1.5.3 Rock-water interaction

Rock–water interaction is the major process in aqueous systems because solid phases (inorganic and organic matter) are the primary sources and sinks of dissolved constituents in water (Elango et al., 2007). During the transition from land to river, various chemical processes take places in water due to contact with different rock types in its pathway, causing chemical reactions, which vary spatially and temporally, depending on the chemical nature of the initial water, geological formations and residence time (Brantley et al., 2017). In an environment like an estuary, hydraulic settings are controlled by tidal influence and freshwater regimes. In such a variable system, the residence time of rock as sediments usually varies according to flow regimes of the river and gives rise to various chemical reactions such as dissolution/precipitation, ion exchange processes, oxidation-reduction and absorption/desorption of metals (Elango et al., 2007; Villars et al., 2001). Sediments are more prone to the absorption of trace metals and containing organic matter, which are probably due to the chemical reaction and density of electrons on the surface in the aquatic environment (Rieuwerts et al., 1998). This absorption process significantly influences the physical and chemical form of metal and reduces the potential risk of these metals towards the environment (Saeedi et al., 2003; Tchounwou et al., 2012). But, a certain change in physico-chemical characters like pH, DO, temperature and rate of flow can release the trace metals from sediments. A study conducted by Li et al. (2013) showed that under the condition of acidic and alkaline water, high temperature, low DO and high-rate flow in the river can give rise to higher trace metal released from sediments. Moreover, the heavy metals release rates are in much greater extent in low pH (4–7) conditions. Whereas higher temperature (30–35°C) can release more metals than low temperature. Sediments in estuarine conditions can also absorb

metals from overflowing water through ionic bonding, which may be released at higher oxygen conditions due to oxidation of organic compounds (Li et al., 2013). This release can give rise to a higher concentration of trace metal in riverine water, especially in the case of estuary, where pH level fluctuates along with the rate of flow of the river. On the other hand, organic matters are decayed particles of dead animals and plants, which may be in dissolved form or it may be settled in sediments. These are very rich in carbon, oxygen and nitrogen (Zimmer, 2008) and are very helpful for the growth of estuarine animals and plants.

1.6 Estuaries and Coral reefs

Estuary, with all its dynamic strings, has many attributes that promote destruction in the coastal environment along with its own. Estuary traps sediments, suspended solids, and the associating trace metals in it due to the encounter of salt fronts during the flow of freshwater into the sea. However, during the flooding of river or storm, the contaminated sediments and suspended solids are wiped into the sea (Beiras, 2018). Sometimes, tides help in bringing suspended solids into the water column due to resuspension, which enters the sea with the flow. These contaminated sediments, suspended solids, and nutrients in water play a major role in the destruction of a marine ecosystem like coral reefs. Kroon et al. (2012) reported that degradation in the Great Barrier Reef (GBR) is directly linked with the land-based run-off of suspended solids, nutrients and sediments. Wiedenmann et al. (2013) observed that elevated sediment concentration can induce various negative impacts when exposed to coral reefs. These negative impacts include reduced reproduction, calcification rates, skeletal density, or linear extension along with the reduction of heat stress tolerance of corals. D'Angelo et al. 2014 reported that elevated nitrogen and phosphorus might not affect negatively the physiological performance of zooxanthellae, but an unnaturally high concentration of nitrogen and deficiency of phosphorous can lead to a detrimental effect on zooxanthellae, eventually leading to an algal bloom. This may lead to a reduction of light and dissolved oxygen, creating a starvation zone for the corals resulting in coral bleaching (Wiedenmann et al., 2013). Furthermore, Dunn et al. (2012) reported that the increased phosphorus levels in the coral ecosystem can reduce the skeletal density of corals which makes them susceptible to mechanical damage. On the other hand, sediments and suspended solids by river inputs can harm the coral reefs directly by smothering (sedimentation) and reduced light availability for photosynthesis due to

turbidity in the water column (Bartley et al., 2013; Browne et al., 2019). An experiment by Weber et al. (2012) showed that grain size and associated organic matter are the main factors behind coral stress. Sedimentation in the experiment kills corals through microbial processes triggered by the organic matter in the sediments, namely respiration and presumably fermentation and desulfurization of products from tissue degradation. An increase in the same microbial respiration results in reduced O_2 and pH, initiating tissue degradation in corals. In contrast, trace metals are also able to stress the early life stage of corals by accompanying river water, sediment, and suspended solids (Kroon et al., 2012; Krawczyk et al., 2020). They can affect larval motility, larval settlement success and reduce fertilization success (Reichelt-Brushett et al., 2005). Various studies revealed that trace metals like copper, lead, zinc, cadmium, and nickel can result in acute or chronic toxicity causing lethal effects or long-term impacts to key biological processes of corals such as respiration, fertilization, and metamorphosis (Reichelt-Brushett et al., 2005) and larvae settlement (Berry et al., 2013). These can also result in physiological stress (van Dam et al., 2011; Kroon et al., 2012), loss of zooxanthellae, reduced growth, enhanced mortality (Rebecca et al., 2013), and reduced biodiversity (Berry et al., 2013). Furthermore, as per ANZECC (2000) water quality guidelines, the trigger value for copper in marine water to conserve 99% of species is 0.3µg/L, whereas the same percentage of species can be conserved with 2.2µg L^{-1}, 7.0µg L^{-1}, 7.0µg L^{-1}, 0.7µg L^{-1} of lead, zinc, nickel, and cadmium respectively.

1.7 Regional overview

1.7.1 Geographical and meteorological details

Malaysia, a federal constitution situated in South-East Asia located between 2º and 7º N of the equator has a total landmass of 330,621 km^2, and is separated by the South China Sea into two landmasses called Peninsular Malaysia (West Malaysia) and Malaysian Borneo (East Malaysia) (Lockard, 2020). It has a population close to 28 million. East Malaysia has two states named Sabah and Sarawak, which share international borders with Indonesia and Brunei respectively (Lockard, 2020). Malaysia's major revenue comes from petroleum and natural resources, palm oil production and tourism, in which these two states are also involved in revenue contribution. In the case of Sarawak, the oil rigs are present in the South China Sea

(Ahmad, 2020). Forests and caves are well known for their economic influence in various manners. Sarawak hosts 37.5% of the total area of Malaysia and is home for 4 major cities: Kuching, Bintulu, Miri and Sibu, and possesses 41 small and big rivers, 15 major tourist destinations (DSMOP, 2020) and 17 diving destinations due to the presence of corals reefs near NW and SW coasts (Pulau Talang Talang near Sematan river and Katori Maru near Santubong) (RCM, 2018). The average annual rainfall over Malaysia varies from region to region. The average rainfall is recorded 2420 mm for Peninsular Malaysia, 2630 mm for Sabah and 3830 mm for Sarawak (Ahmad et al. 2017) and mainly controlled by Pacific Decadal Oscillation (PDO) (Krawczyk et al., 2020). The positive PDO mainly brings dry sinking air and reduced rainfall termed as southwest monsoon (SWM) and negative PDO brings more cold air and more rainfall termed as northeast monsoon (NEM). The precipitation prevailing over the southern South China Sea (SCS) region results in highest rainfall over Borneo, whereas the vice versa effect is visible during SWM. This happens as an effect of high pressure over Asia and low pressure over Australia that pushes the Intertropical Convergence Zone (ITCZ) towards the south (Steinke et al., 2010; Stephens et al., 2008). This region experiences the SW monsoon from late May to September and the NE monsoon from October to March, making Sarawak the region the wettest region in Malaysia (Saifullah et al., 2014; Lockard, 2020; Krawczyk et al., 2020).

1.7.1 Regional geology

The geology of Sarawak can be divided into 4 zones, namely the West Borneo Basement, Kuching Zone, Sibu Zone and Miri Zone (Haile, 1974; Hutchison, 1989; Hall and Breitfeld, 2017). The basin covers both onshore and offshore that is divided into several provinces aging from Paleogene to recent age (Madon et al., 1999). The West Borneo Basement is made up of Middle-Upper Carboniferous to Permian mica schists, hornfels and metaquartzites, which are the oldest rocks in the zone and are intruded by Middle Jurassic to Late Cretaceous plutonic suites (Madon et al., 1999; Hutchison, 1989). The Kuching zone in the southwestern part of Sarawak consists of Upper Cretaceous shelf deposits mainly made up of marine limestones and is overlain mainly by siliciclastic sequences and minor carbonates (Hutchison, 1989; Breitfeld et al., 2018). The Sibu zone is separated by Lupar line from Kuching zone (Haile, 1974; Hall and Breitfeld, 2017) (Fig. 1.4) and underlain by Rajang Group of formations. This zone has rocks of similar age as Kuching zone but mainly composed of intensely

folded, thrust and low-grade metamorphosed turbidites of Late Cretaceous to Eocene age (Madon et al., 1999; Hall and Breitfeld, 2017; Ahmed et al., 2020). Moving up north, shallow marine sediments of the Neogene age dominate the Miri zone (Madon et al., 1999). This zone imparts fringe towards Sibu zone separated by Bukit Mersing fault line (Fig. 1.3), which is strike-slip in nature and was active through Eocene to the central Miocene (Hutchison, 2007; Najar et al., 2020).

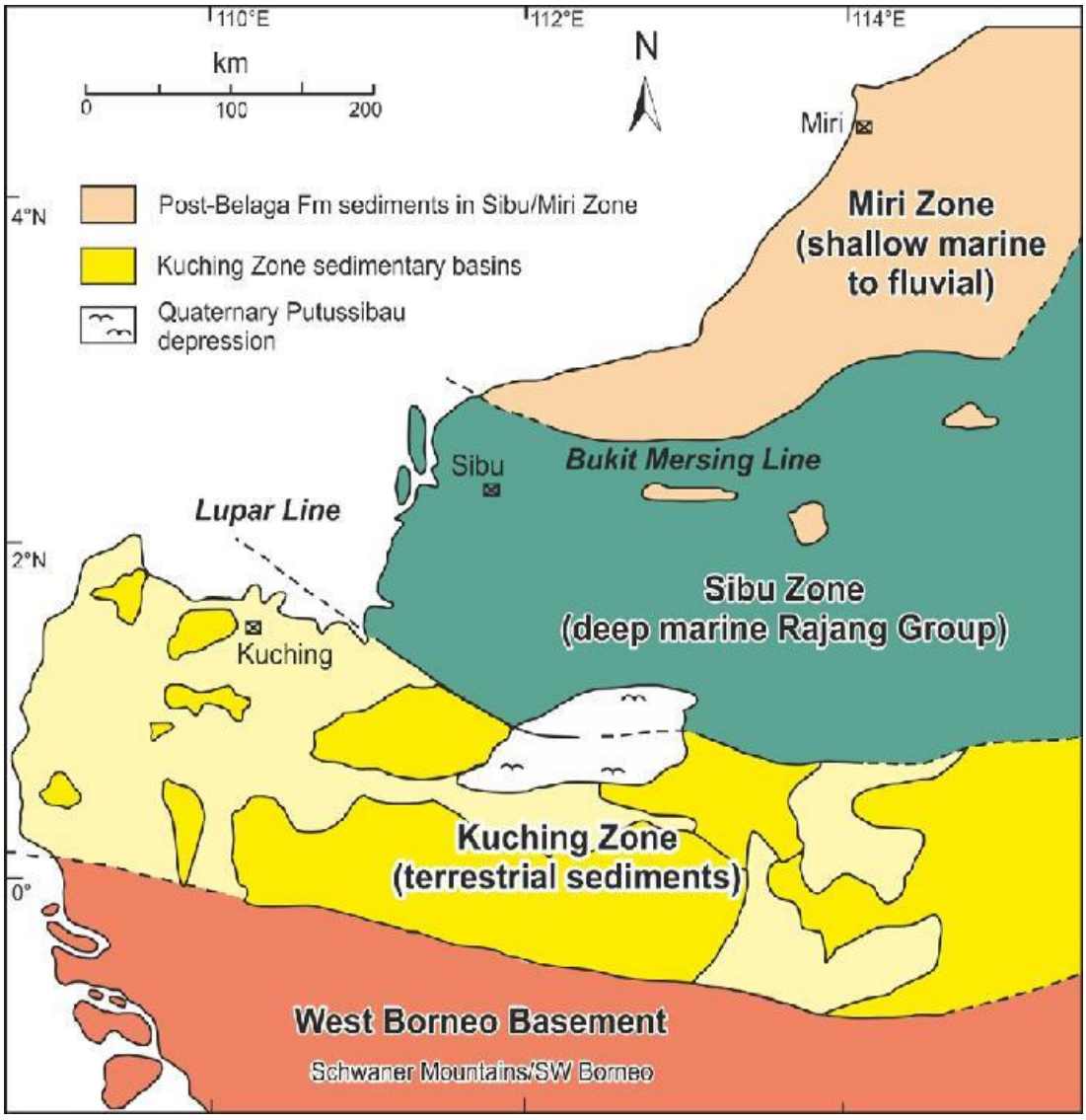

Fig. 1.3 Geological zones of NW Borneo (Source: Haile, 1974, Hall & Breitfeld, 2017)

In this zone, Rajang group of rocks were overlain by terrestrial and shallow marine sediments and are largely undeformed caused by collisional event named Sarawak Orogeny (Hutchison et al., 1996; Hutchison, 2005). After this Orogeny, the recycling, transportation and deposition of sediments from this collision zone of Rajang group are the main sources of sediments deposited in Lambir and Sibuti formation

(Nagarajan et al., 2015; Nagarajan et al., 2017a) of this zone. The deposition took place until Middle Miocene. The turbidites of Rajang formation aging from early Cretaceous to Late Eocene are also found in Miri zone but these are inlier within eastern Miri zone in Kelalan and Mulu formations (Hutchison et al., 1996; Hall & Breitfeld, 2017). Some of the main rock types in this zone are basalt, tuff and radiolarian chert (Madon et al., 1999). A decrease in stratigraphic and structural complexity has been noted towards the east in all 4 zones (Madon et al., 1999).

1.7.2 Regional overview of Miri-Sibuti coral reefs

The coral reefs of the Southeast Asian region are considered endangered globally as 95% of the reef's decline is happening because of the local sources (Burke et al., 2011; Browne et al., 2019). The hard coral cover in this region has decreased at a rate of 2% per year from 1980 to 2000s (Browne et al., 2019). The reduction in reef cover was mainly attributed to the rapid land developments along the coasts, insufficient environmental policies leading to deforestation, poor water quality, higher sediment load from the rivers and various anthropogenic activities. In the Sarawak region, deforestation is a major issue with only 3% forest intact in the region (Bryan et al., 2013; Browne et al., 2019) and the 26% loss of forest cover since 1970 (Krawczyk et al., 2020) becomes a hotspot which threatens corals in form of nutrient load and sedimentation, with the influence of major rivers flowing in this region (Miri, Sibuti and Baram) (Pilcher, 2000; Long, 2014; Browne et al., 2019; Krawczyk et al., 2020). For example, the Baram river delta is noted to be in destructive phase due to the rising sea levels, along with increased frequency and intensity of rainfall in the region that is discharging 2.4×10^{10} kg/year of sediment load in the coastal zone, which is likely to increase this load in the future (Nagarajan et al., 2015; Browne et al., 2019). In addition, studies carried out by Krawczyk et al. (2020) on the corals near the Miri coast pointed out that significant change in coral hydrology is directly linked to the local precipitation and river discharges in the region. The nutrient study done by Saifullah et al. (2014) shows the seasonal fluctuation of nitrogen and phosphorous which can act as a threat to the corals. The same study also highlighted the presence of nitrate and ammonium in the Sibuti river water and might be associated with increased sediment load in the river (Browne et al., 2019). Pilcher (2000) showed that the suspended sediment concentration in the Miri river is more than 4500 mg L^{-1} because of increased run-off load in the highlands over 3 decades ago while live tissues of

many hard corals are covered by filamentous algae indicating the increasing nutrient enrichment. The algal cover on the reefs near the Miri coast is 50% higher as compared to reefs near northern Borneo and low diversity in corals is noted because of poor water quality near the shore (Browne et al., 2019). This shows the influence of the rivers on the coral reef with the help of sediment load and suspended solids and the filamentous algae demonstrate the occurrence of metabolic energy waste in the Miri-Sibuti coral ecosystem. The coral survey conducted by Fenner (2001) also shows that corals present near the river mouths of the north-western Sarawak coast are already near the tolerance limits of turbidity and sedimentation. As a supporting example, we can consider the eutrophic coast of Jakarta, Indonesia, where no live coral is visible, whereas the offshore reefs are in better condition (Koop et al., 2001). Such conditions were also noted in recent studies done by Browne et al. (2019), where bioerosion during wet season and pigmentation during the dry season is a major threat to reefs along with high suspended solid load. He also found an increase in diversity and health parameters in corals that are away from the river mouths. Studies conducted by Moollye (2017) in Miri-Sibuti coral reef national park (MSCRNP) found increase in nutrients such as NO_3^-, PO_4^{3-}, SO_4^{2-} and NH_3 and trace metals like Cd, Cd and Ni in surface seawater during post southwest monsoonal period. He concluded that such increase is a direct effect of river run-off and coastal development and is responsible for coral bleaching and overwhelming algae cover. Hence, it is evident from the above studies that Miri-Sibuti coral reef region is getting influenced by the river discharges over a long period of time and the reefs seem to be in temporary stable condition from such threats (Browne et al., 2019), which is likely to increase in future.

1.8 Study Area

1.8.1 Geographical and meteorological details

The present study area belongs to Miri zone in northern Sarawak, more specifically, the Sibuti river estuary is located between latitude 3°59'32.0" N and longitude 113°43'36.2" E (mouth of the river) and latitude 4°0’44.21” N and longitude 113°53’50.96” E (maximum reach of tidal water) (Fig. 1.6). The river basin covers an area of 1020 km^2. The river receives tides at a maximum height of 2-3m during high tides (Source: www.tide-forecast.com) and receives run-off deliberately in its bank from the land. Based on the above classification, Sibuti river estuary falls under tide

dominated estuary especially in micro-tidal type (Tidal height: 2-3 meters) (Boothroyd, 1978), where limited tidal influence can be expected irrespective of the season. However, during high tide seawater can influence major portion of the estuary especially during dry season. The presence of dense mangrove and Nipa palm (Mangrove palm) is observed along the bank of the estuary. The rainfall in the study area follows the similar pattern as regional and mainly regulated by PDO as mentioned before bringing two monsoon seasons in a year such as SWM and NWM. This monsoonal effect is mainly responsible for hydrological balance in this region and controlling the river run-offs (Krawczyk et al., 2020; Browne et al., 2019). The average annual rainfall is around 3022 mm in Miri region (Anandkumar, 2016), with rainfall spanning over 220 days a year (Geography of Sarawak, 2015). The monthly rainfall data for these 2 monsoons during the study (2017 and 2018) is presented in Table 1.1.

Table 1.1 Rainfall details of monsoons over Miri during 2017 and 2018 (Acquired from : www.worldweatheronline.com)

SW Monsoon (2017)			**NE Monsoon (2017-2018)**		
Months	**Days rained**	**Rainfall data (in mm)**	**Months**	**Days rained**	**Rainfall data (in mm)**
June	23	105	December (2017)	29	598
July	24	53	January (2018)	31	354
August	24	277	February (2018)	25	255

The average daily temperature varies from 23 °C (73 °F) in the morning to 32 °C (90 °F) in the afternoon. The Sibuti river mainly passes through dense forests, various agricultural fields and urbanized areas like Bekenu along with many villages (Fig. 1.4). Among these, major land use activity in the river basin is agricultural activities and mainly concentrates around Bekenu and several other villages. Due to such, Bekenu is growing in agro-activity drive in this region and agriculture becoming a major source of income for the locals. The main agricultural products of these areas might include Palm tree plantation, Pandan coconut plantation, lemon grass, ginger, turmeric, shallots, chilies and other herbs (MANRED, Sarawak, 2020). The river gets

continuous discharges from the terrestrial sources through various drainage channels and tributaries. Major tributaries contributing to the estuarine influence region are Sungai Tiris (Station 19) and Sungai Kejapil (Station 24) (Fig. 1.4). Other than that direct drainage channels from agricultural fields connecting to the estuary were also observed during preliminary study and sampling period and are marked in Fig. 1.4. The notable major drainage channels are marked near station 3, 4, 6, 12, 13, 16, 21 and 28 (Fig. 1.4).

1.8.2 Geology of Sibuti river basin

1.8.2.1 Lithological details

The river basin is mostly influenced by 3 major and 6 minor formations, namely the Sibuti Formation, Lambir Formation and alluvium near the coast, whereas the minor formations may include Miri, Belait, Tukau, Nyalau, Setap shale, and Tangap formations (Fig 1.6). The Sibuti Formation is reported to be dominated by sandstone and mudstone (Nagarajan et al., 2017a) Shale deposition is also reported with prominent marl lenses, thin limestone bed and high content of fossils in it (Peng et al., 1997; Nagarajan et al., 2015). The siliciclastic sediments of this formation are rich in light minerals such as quartz, pyrite clay minerals, along with heavy minerals such as zircon, rutile, or ilmenite (Nagarajan et al., 2015). The mineralogical constituents of rocks in Sibuti formations are quartz, mica, clay minerals such as illite, kaolinite, and chlorite, zeolites with little feldspar (Nagarajan et al., 2019). The Lambir formation is mainly comprised of sandstones, sandy intercalations with shale and siltstones, mudstone and limestone (Table 1.2). The sediments found in this formation are organically rich, and sandstones are laminated with fine to medium-grained lignites (Nagarajan et al., 2017a). The siliciclastic rocks were classified by Nagarajan et al. (2017a) and were found to be shale, wacke, arkoses, lithrarenites, Fe-sands, and quartz arenites. Mineralogically, sandstones are comprised of quartz, illite/muscovite, along with a minor amount of plagioclase, whereas the limestone consists of calcite, ankerite, quartz, chlorite, illite/muscovite, and a trace amount of aragonite (Nagarajan et al. 2017a). In addition, mudstones of this formation are dominated by quartz, illite/muscovite, amorphous phase, chlorite, plagioclase, and calcite (Nagarajan et al., 2017a; Nagarajan et al., 2019). The lithological layers of the Tukau formation are dominated by an alternate layer of siltstone and mudstone with occasional massive

sandstones with thin lenses of coal (Nagarajan et al., 2017b). Mineralogically, quartz, clay minerals like detrital illite, mica and kaolinites, heavy minerals like zircon, rutile/anatase and relatively less tourmaline, chromite, ilmenite, monazite and garnet were reported in the Tukau formation (Nagarajan et al., 2017b). The Setap Shale Formation is a thick, extensive and monotonous succession of shale with subordinate thin sandstone beds and a few thin lenses of limestone. Apart from these major lithological details, the concretion of pyrites was reported to be present in Sibuti, Setap shale (Azrul NIsyam et al., 2013; Nagarajan et al., 2019) and Tukau formations (Nagarajan et al., 2017b) in the river basin. In the case of the Miri Formation, the southern part of this formation falls under Sibuti basinal area. This part of rich Neogene sedimentary rocks and alluvium in the lower river section includes thick peat soils. The Neogene sediments are comprised of irregular sandstone-shale alternations, with the sandstone beds passing gradually into clayey sandstone and sandy or silty shale (Nagarajan et al., 2019). The lithology of other minor formations is listed in Table 1.2.

1.8.2.2 Sediment chronology and depositional history of the basin

The stratigraphic age of the formations in the river basin ranges from Oligocene to Pliocene. The major formation of Sibuti was formed during Miocene and is considered a member of Setap Shale Formation, which was formed between mid to early Miocene (Nagarajan et al., 2015). Other major formations in Miri and Lambir formation lies over the Sibuti and Setap Shale Formation and are separated by mid-Miocene unconformity. The silliciclastic sediments in these formations are derived from physical and chemical weathering of Rajang group (Nagarajan et al., 2015; Nagarajan et al., 2017a) due to the collisional event termed as Sarawak Orogeny (Hutchison, 1996). The depositional environment of Sibuti and Setap Formation is an open marine environment, whereas Belait, Lambir, Tukau, and Miri formations are deposited under shallow marine to intertidal and coastal environments (Kessler et al., 2009; Nagarajan et al., 2017a). The sedimentary rocks of the former are deposited mainly during the intervals of transgression and regression and tectonic events (Nagarajan et al., 2017b). The Tukau Formation is the youngest of all the formations observed in the river basin and overlies the Lambir Formation (Fig. 1.5).

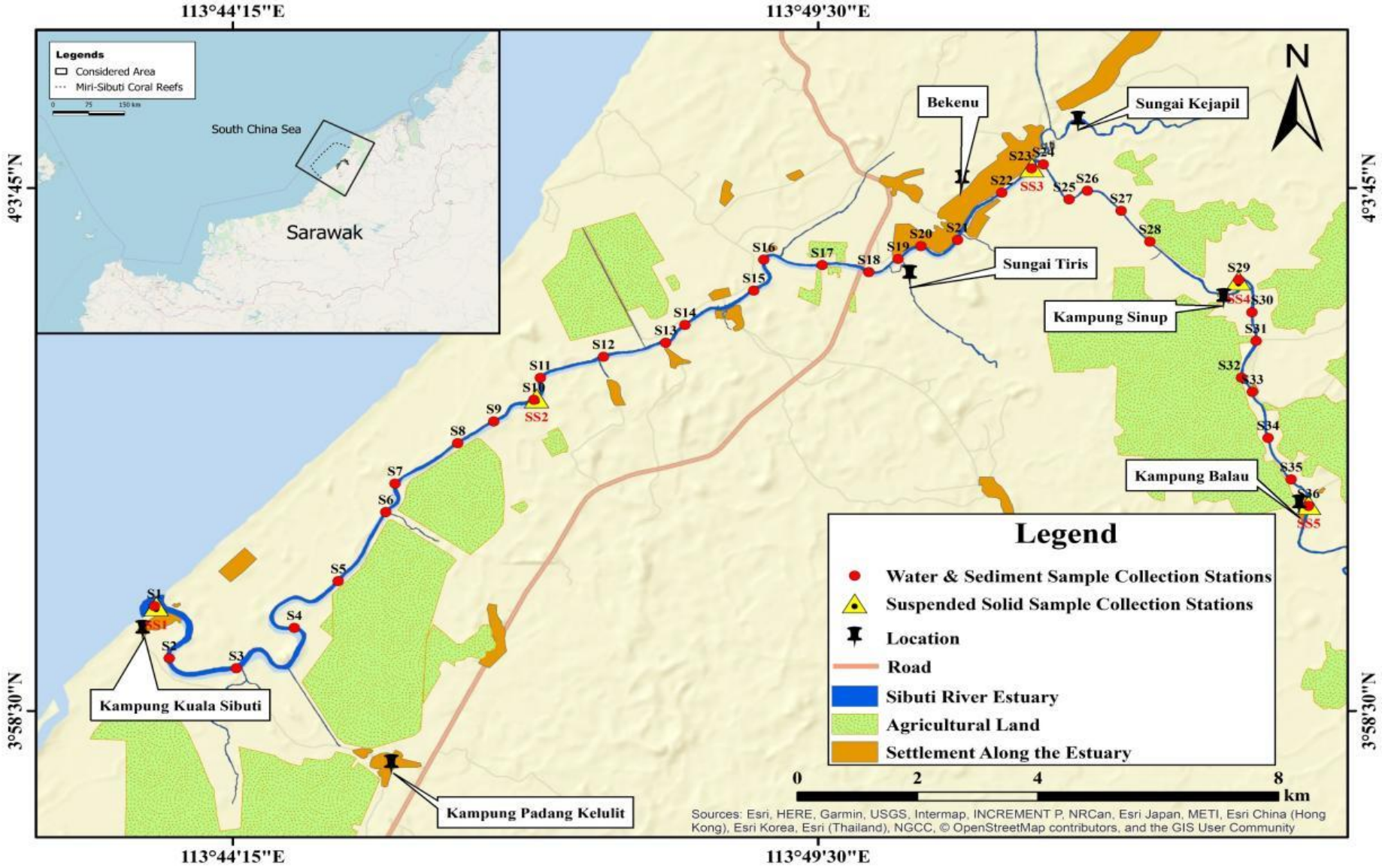

Fig. 1.4 Map of Sibuti river estuary showing sampling stations and land use pattern near it.

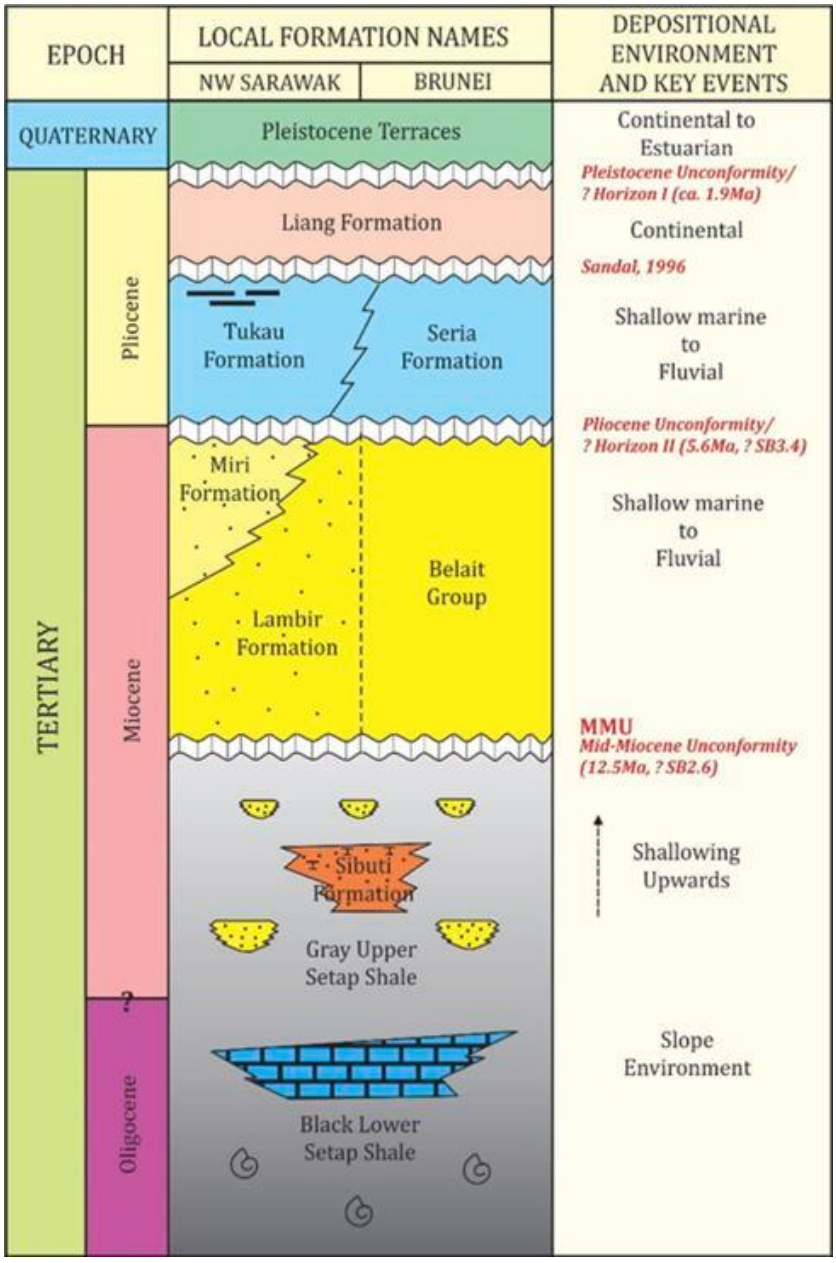

Fig 1.5 Litho-stratigraphy of formations observed in Sibuti river basin (Source: Kessler and Jong, 2015; Nagarajan et al., 2017a)

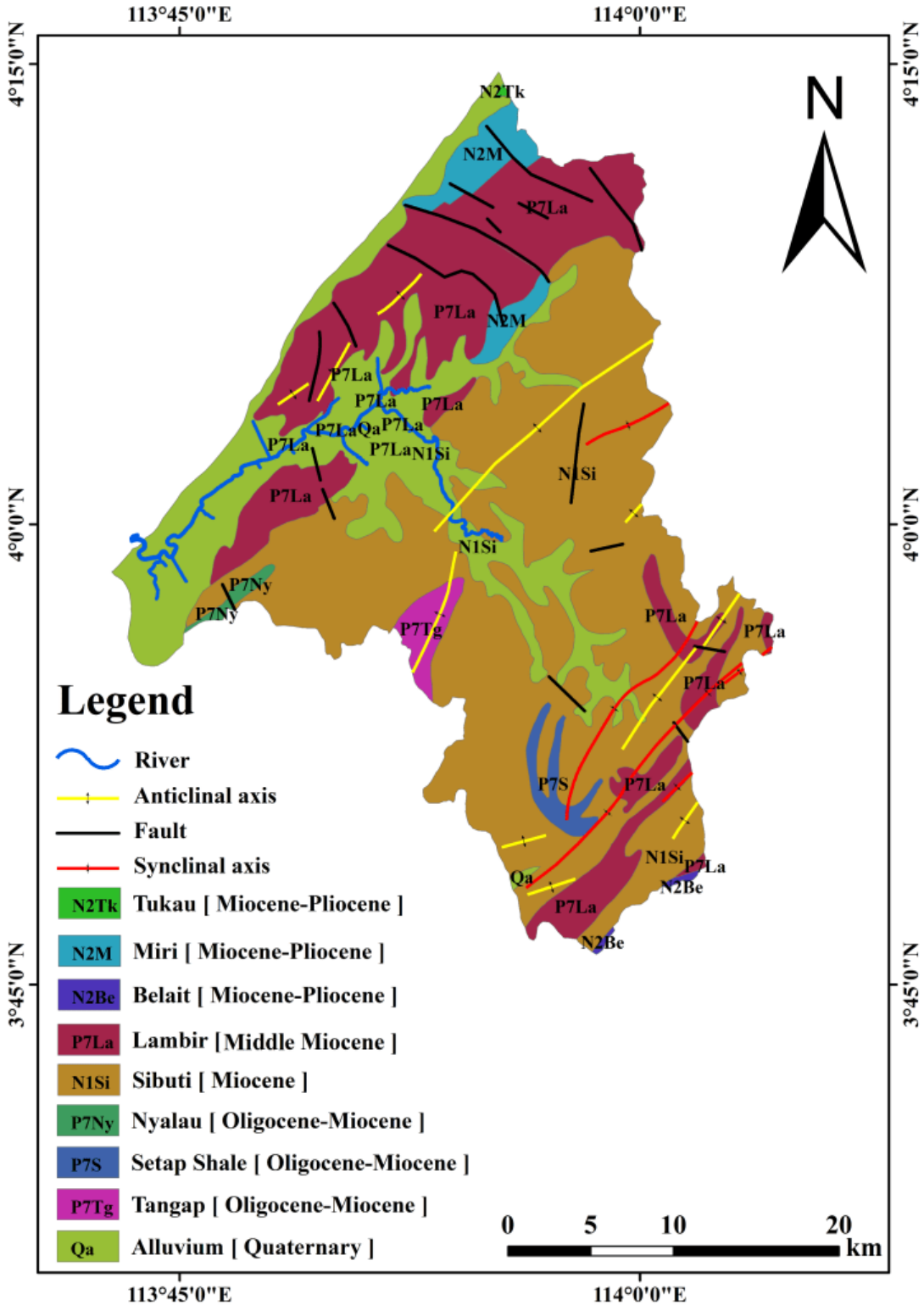

Fig. 1.6 Geological map of the Sibuti river basin

Table 1.2 Geological units of Sibuti basin and their lithological details

Code	Lithology	Area (in km^2) and significance of the formations in the river basin	Age
N2Tk	**Tukau Formation:** Sandstone, siltstone, shale, sand, clay with some conglomerate and lignite: poorly consolidated in general	0.389 km^2 (Minor)	Miocene-Pliocene
N2M	**Miri Formation:** Sandstone, siltstone, shale, sand, clay with some conglomerate and lignite: poorly consolidated in general	32.635 km^2 (Intermediate)	Miocene-Pliocene
N2Be	**Belait Formation:** Sandstone, siltstone, shale, sand, clay with some conglomerate and lignite: poorly consolidated in general	1.370 km^2 (Minor)	Miocene-Pliocene
P7La	**Lambir Formation:** Sandstone, shale, mudstone, limestone, lignite with some marlstone, siltstone and calcareous sandstone	238.201 km^2 (Major)	Middle Miocene
N1S1	**Sibuti Formation:** Sandstone, shale, mudstone, siltstone with some limestone and conglomerate lenses	500.433 km^2 (Major)	Miocene
P7Ny	**Nyalau Formation:** Sandstone, shale, mudstone, limestone, lignite with some marlstone, siltstone and calcareous sandstone	3.780 km^2 (Minor)	Oligocene-Miocene
P7S	**Setap Shale Formation:** Sandstone, shale, mudstone, limestone, lignite with some marlstone, siltstone and calcareous sandstone	13.741 km^2 (Intermediate)	Oligocene-Miocene
P7Tg	**Tangap Formation:** Sandstone, shale, mudstone, limestone, lignite with some marlstone, siltstone and calcareous sandstone	13.251 km^2 (Intermediate)	Oligocene-Miocene
Qa	Marine and fluviatile alluvium (Regoliths)	203.033 km^2 (Major)	Quaternary-Holocene

1.9 Problem statement

The Sibuti river estuary in Sarawak receives a large amount of sediment and suspended solids along with the nutrient loads depending upon various seasons (Saifullah et al., 2014). The uncertain rain event apart from the seasonal rain in this region is also adding garbage and fertilizers from agricultural lands and chemicals from industrial waste to the Sibuti river. The changes in land use pattern such as deforestation and increased agricultural activities in the river basin are also contributing to land inputs in the river over the years. In addition, complex geology of Northern Borneo is a

challenging aspect and important towards contribution of trace metals of geogenic origin in various rivers in the region. Considering these aspects and comparing these to the studies done on various rivers estuaries around the world, it is admittedly difficult to obtain the necessary details regarding the contamination agents and factors in the Sibuti river estuary depending on previous studies. The catchment of the river is around 1020 km^2 (Tenaga, 2003) and receives an average seasonal rainfall similar to the regional rain fall (3126 to 3246 mm, average: 3022 mm) spanning over 220 days a year (Anandkumar, 2016). The estuary has more than 30 kms of pristine mangrove and Nipa palm (Mangrove palm) forest in the vicinity with a number of agricultural fields, small towns such as Bekenu, and a number of villages that are present around the river. The river gets majority of the run-off water from the northern and south-eastern parts of the basin (Fig. 1.4). Geologically, the basin is made up of sedimentary rocks aging from Oligocene-Miocene and the depositional nature of the basin is identified as shallow marine (Simon et al., 2014). With a high amount of rain, deforestation, settlements along the shore and weathering prone rocks in the catchments, the river is likely to get continuous input of run-off water and sediments accompanied with various ions, nutrients and metal. Therefore, these ions, nutrients, metals in water and sediment have a tendency to get deposited at the intertidal zone of the river. The intertidal sediments in the study area are mainly consisting of mud and sand and pose a tendency of resuspension of such metals from the sediments under varying environmental conditions. These leached ions, metals and nutrients in the river water and resuspended metals from the sediments pose a huge threat to the estuarine ecosystem and can be responsible for harmful chemical processes in the estuary. Hydrological factors like pH, DO, salinity and temperature are very important for the species' composition, and are responsible for the abundance and diversity of estuary, in which they can get affected under such extreme circumstances. Sarawak region has a tropical climate with high rainfall intensity, which can act as a major cause in case of soil erosion. Surface runoff from high terrains and agricultural lands can increase sedimentation and suspended solid load in the rivers' ecosystem.

There have been a few studies carried out in the estuary and the river, but they are only focused on physico-chemical standards and the number of nutrient loads, indicating the emerging pollution levels. However, a huge gap still remains because the studies have not concentrated on major ions, trace metals and various nutrients in this region.

Detailed sediment and suspended solid analysis have not been considered for evaluation in the previous studies, even though these play a major role in the contamination of the riverine ecosystem. The lack of attempts undoubtedly exists in identifying the major pollutants, their origin and controlling factors of this riverine environment.

Apart from gaining importance due to the riverine pollution, Sibuti river's influence in the Miri-Sibuti coral reefs is still unknown despite the fact that its estuary is much closer to them. The role of terrestrial inputs was identified to be affecting the coral reefs in various previous studies as discussed before. The role of the Sibuti river in this matter is lacking in various manners. As such, consideration of riverine aspects near the coral region has been fruitful in the case of the Great Barrier Reef, Australia, Corals Triangle, Indonesia and Corals near Porto Rico to reveal the major reasons behind their degradation. In such a scenario, a detailed study is required in the Sibuti river estuary to determine the geochemical characteristics of the river by analyzing the water, sediments and suspended solids. Hence, this focused study will provide details regarding major geochemical processes, the spatial and temporal variation of water and sediment quality (bedload and suspended) along with source identification of pollutants. Therefore, it will be helpful to analyze the contribution of Sibuti river which carries contaminants on Miri-Sibuti coral reefs.

1.10 Significance of the study

This study was carried out by analyzing the water, sediment and suspended solids in the estuary to determine the concentration of ions, nutrients in the water and various trace metal concentration present in water sediment and suspended solids. This study is distinctive because it will provide a detailed view of the Sibuti river and its estuary in case of water, sediment, and suspended solid contamination levels. This will also consider the effect of nutrient and trace metals flowing in water and association with the sediments and suspended solids. With the help of sequential extraction of metals in sediments, the characteristics of metal behavior in the estuary can be revealed. The study will also help to identify major geochemical processes in the estuary by identifying the linkage between various parameters in both water and sediment, while revealing the factors responsible for it. As river water contamination is a major concern in various parts of the world, the study will identify the suitability of water

for public water supply, recreation purposes, wildlife suitability, agriculture, treated water transportation, etc. Although outstanding outlines exist for various river estuaries in Malaysia, the perceptible data is still lacking in the case of the Sibuti river estuary, where previous studies have only focused on physico-chemical standards and the amount of nutrient loads, indicating the emerging pollution levels. The study of such extent will help to get a clear picture of pollution status of the Sibuti river estuary and will help the researchers, local government and Department of Environment (DOE), Malaysia to formulate a management plan in the future.

After being confirmed about the contamination levels and pollutants, the results can be compared to the results obtained from coral reefs (Moollye, 2017) and Miri coastal studies (Anandkumar, 2016) in a predictive manner. This will be helpful to measure the influence of Sibuti river based contaminants in coastal environment. This will allow researchers and relevant authorities to obtain certain effective parameters, which can help to conserve the mortality of the corals present. In this scenario, where coral mortality is concerned, the study will also concentrate on various unique factors like turbidity, the concentration of suspended solids, sediment load and its compositional behavior, which are proven to be the main reasons behind the reduction of coral reefs around the world. Hence, the study can discover results that can be used for various purposes for the betterment of the Sibuti estuarine ecosystem and strategies to deal with coral reef conservation.

1.11 Research questions

1. What is the present status of the Sibuti river estuary in terms of water and sediment quality?
2. What are the major pollutants in the river, their origin and their source?
3. What are the major geochemical processes controlling these pollutants in the estuarine water-sediment interface?
4. Is there any influence of these pollutants on Miri-Sibuti coral reefs?

1.12 Aim and objectives

The aim of this research is to investigate and quantify geochemical contaminants in water, sediment and suspended solids in Sibuti river estuary and identify major geochemical processes controlling it. A comprehensive analysis of ecological risk assessment of such pollutants and projection of the acquired results on MSCR region is conducted to assess their potential influence. The analysis includes the following.

1. Analysis of physico-chemical parameters, major ions, nutrients, trace metals in water and trace metal concentration in sediments (Bed load and suspended) of the Sibuti river estuary.
2. Determine the controlling geochemical processes in freshwater-saltwater and sediment-water interface.
3. Evaluation of the spatial and temporal variations of major pollutants in the estuary, their risk assessment and source.
4. Determine the potential influence of river carried pollutants on the Miri-Sibuti coral reefs present near the estuary.

1.13 Structure of the thesis

The first three objectives were addressed by focusing on the three main transport mediums (water, sediments and suspended solids) of the contaminants in the estuary and the fourth objective was achieved with the help of comparison and projection of acquired outputs with respect to the Miri coastal waters and Miri-Sibuti coral reefs region. **Chapter-2** highlights the literature regarding major chemical processes with respect to major components in estuarine systems such as nutrients, major ions, trace metals and controlling physico-chemical parameters. The importance of sediment extraction methods and digestion protocols followed for the experimental work were discussed. To support the importance of tropical estuaries such as Sibuti river estuary in coral reef region, critical case studies at international levels were considered and are also discussed in this chapter. **Chapter-3** describes all the methods adopted for this study, which include sample collection, field and lab measurements, sample preparation, digestion and analysis. This chapter also discusses the instruments, their calibration and precision adopted to conduct the experiments. In addition, it provides an overview of various indices adopted for risk and quality assessment of sediments and suspended solids.

Chapter-4 discusses regarding spatial and seasonal distribution of physico-chemical parameters, major ions, nutrients and trace metals in estuarine water. This chapter further discusses hydrochemistry of water with the help of Indices of base exchange (IBE), Piper plot, Gibbs plot, Saturation Index (SI) and statistical analysis including Pearson's correlation and Principal component analysis (PCA). For drinking water quality assessment, WHO (2017) and Malaysian standards (2004) were used at threshold values, whereas irrigational suitability of water was assessed using Electrical conductivity (EC), Corrosivity ratio (CR), USSL classification, Sodium hazard, Residual sodium carbonate (RSC), Permeability Index (PI) and hardness of water. **Chapter-5** explores the seasonal and spatial distribution of considered metal concentration in bed load sediments. The discussion of these results includes statistical analysis of both total metal concentration and metal concentration in various fractions of sediments. The source of considered metals are reported with the help of statistical techniques such as Pearson's correlation and PCA using total metal concentration in sediments. In the same way, sediment chemistry, metal distribution and their influence on other transporting medium like suspended solids and water metals are emphasized in the chapter with the help of statistical factor model created using metal concentration in various fractions. This chapter also reports sediment quality with the help of Geoaccumulation index (I_{geo}), Enrichment factor (EF), Contamination factor (CF), Pollution load index (PLI), Potential ecological risk index (PERI), Sediment pollution index (SPI), Effect low range (ERL), Effect medium range (ERM) and Risk assessment code (RAC) values. In a similar manner, **Chapter-6** discusses about the seasonal and spatial distribution of considered metals in the estuarine suspended solids. This chapter reports regarding the suspended solid behavior under estuarine condition and source of metals in it using similar statistical approach like bed load sediments. In addition, speciation of metal (K_d) between suspended solid matter and liquid phase are also discussed. Suspended solid quality is reported in this chapter using Geoaccumulation index (I_{geo}), Enrichment factor (EF), Contamination factor (CF), Pollution load index (PLI), Potential ecological risk index (PERI) and Sediment pollution index (SPI). **Chapter-7** discusses about the seawater circulation in the region in regard to the river influenced and compares the results acquired in the study area to pre-acquired results from Miri coastal waters and Miri-Sibuti coral reef national park (MSCRNP). The statistical outputs from the previous studies are also compared with current study area and discussed in this chapter. The determined influence of Sibuti

river in the coastal waters including the MSCR region is discussed in this chapter using these comparisons. **Chapter-8** discusses the summary and insights obtained from the thesis and recommendations for future studies are addressed in this chapter.

Chapter-2

Literature Review

2.1 Introduction

Estuaries have been used by humans for a multitude of purposes over centuries. While the effect of some usages has been innocuous to this ecosystem, others had a derogatory impact on this sensitive ecosystem and have affected the habitat areas and aquatic communities surviving in it. Estuaries' main work is to act as major repositories for disposal of the riverine system, atmospheric deposition and non-point sources such as run-off from land (Kennish et al., 1994). These disposals contain municipal waste, sewage sludge and agricultural inputs, which are known to have high nutrients and metal concentration, whereas geogenic dredged materials disposals may contain a high amount of dissolved ions, trace metals and nutrients (Benson et al., 1988). These contaminants go through complex chemical processes in a sophisticated and changing ecosystem due to both riverine and tidal forces working at both ends (Matthiessen et al., 2002). The increase in such a process is a growing threat not only to the estuarine aquatic habitat but also to the coastal environment, which is continuing to prevail and grow over time (Hennessey et al., 1994). Numerous analytical studies have been carried out on natural water and sediments in estuaries to assess their complexity and environmental risks. To support the aim and objective of the current research, a critical literature review was carried out to acquire information on various relevant aspects such as major contaminants and their controlling processes for water, sediment and suspended solids. The evolution of extracting trace metals and their interaction between sediments and water columns, the various methodologies adopted and related mechanisms and methodologies used for the extraction of metals from the sediments are also discussed.

2.2 Major ions in estuaries

Understanding hydrochemistry in estuaries is critical in the context of increasing anthropogenic and geogenic pressure. The knowledge of the water circulation and its mixing is increasingly relevant to identify the fate of particle-bound and dissolved contaminants, the ecology of benthic communities and the morphological evolution of the surrounding (Garel et al., 2009). The circulation of water in estuaries is governed

by the density differences and the interaction between fresh and salt waters. Typically, a distinction is made between the baroclinic density-driven and barotropic pressure-driven components of the flow. With significant tidal forcing, these pressure gradients may interact and produce internal tidal asymmetries leading to the mixing of water in the influential region (French et al., 2008). The major components of water that are affected in such process are the changes in physico-chemical parameters and ionic concentration, nutrients and trace metals available in the estuarine ecosystem. Major ion concentrations in the riverine estuaries are derived as a result of either weathering of catchments or the increasing influence of tidal water. Most major ions in estuarine system exhibit dilution effects with the flow of river, where higher concentrations at baseflow (tidal water) are diluted depending on the river flow conditions (Jarvie et al., 1997; Sultan et al., 2012; Huang et al., 2014; Wu et al., 2014; Frazar et al., 2019). In principle, salinity can refer to any inorganic ions, while in practice, it is mostly the result of the following major ions: Na^+ , Ca^{2+}, Mg^{2+}, K^+, Cl^-, CO_3^{2-} and HCO_3^- (Williams et al., 1987; Shammi et al., 2017). The sea's influence in the case of estuaries can be monitored by their salinity, where this influence and concentration of ions are greater (Huang et al., 2014), so is the salinity. Similarly, the effects of freshwater discharged from hydrographic basins can be observed in the ocean in terms of reduced salinity through dilution (Loitzenbauer et al., 2012). The ions have significant control over other physico-chemical parameters like pH, etc. For instance, the presence of CO_3^- and H^+ are very much useful in evaluating the pH of water. A higher amount of CO_3^- shows the alkaline nature of water whereas a higher amount H^+ ions is a sign of acidic water (Lower et al., 1999). These two ions typically occur in the form of a carbonate system of chemical equilibrium (Hamid et al., 2020). Similarly, seawater maintains a pH level of 8.0-8.5, which mainly shows the dominance of CO_3 and HCO_3 (Anthoni et al., 2006; Mewes et al., 2014). Contrarily, CO_3^{2-} and HCO_3^-, Ca^{2+} and Mg^{2+} (Nikanorov et al., 2009; Nikanorov et al., 2012) ions can be released from erosion of carbonate rocks (limestone, dolomite, magnesite) in river systems with precipitation of CO_2. Apart from these, chemical disintegration like organic decomposition and dissolution of carbonic acid (H_2CO_3) also give rise to HCO_3^- while reducing the pH in open aquatic systems (Ramesh et al., 2012). In the case of K^+, the main terrestrial source in open systems like rivers and estuaries would be weathering of potash silicate minerals and agrochemicals like potash fertilizers in agricultural fields (Van Straaten, 2002). Weathering of Na–K-bearing minerals/rocks

such as halite, feldspar and montmorillonite enhanced by ion (cation) exchange process can give rise to K^+ and Na^+ concentration in the riverine system (Hamid et al., 2020).

Table 2.1 Case studies explaining behavior and source of major ions in estuaries

Author	Study area	Findings
Patra et al., 2012	Changjiang river, China	Na^+, Ca^{2+}, Mg^{2+} are part of the fluvial contribution in the estuary, whereas Cl^- and K^+ are controlled by seawater influx. Two components mixing between river and seawater was observed where fluvial contribution was removed by suspended particles interaction and active phase change in the quantity of both organic and inorganic components.
Shammi et al., 2017	Estuaries of Bangladesh	K^+, Na^+, Ca^{2+}, Cl^- are the principal components of salinity along with EC and TDS irrespective of the seasons.
Jiang et al., 2020	Tuo river and Bian river, China	The ion composition of the two rivers was mainly affected by rock weathering. Water quality evaluation showed that both river was greatly affected by agricultural non-point source pollution, and its water quality was poor.
Serder et al., 2020	River estuaries, Bangladesh	Na^+ and Cl^- are the abundant ions in the river estuaries. Seawater intrusion regulated the water types and ion abundancy and water quality deterioration with varying seasons. Na-Cl type was observed during pre and post monsoonal period whereas mixed water type Na-Cl-HCO_3 dominated during monsoon.
Sheeja et al., 2020	Neyyar river, India	Rock weathering controlled ionic chemistry of the river water where Cl-HCO_3-Na water type is dominant during monsoon. The presence of mineral varieties of quartz, feldspars, pyroxene, biotite, etc., in the Pre-Cambrian crystalline namely Khondalite and Charnockites, could be the source of major ions
Wen et al., 2020	Yangtze estuarine coastal zone of Qidong, China	HCO_3^--Cl-Na type and Na-Cl being the dominant water types in the coastal strip. Major influencer of such types were mainly controlled by to the ongoing influence of seawater intrusion, ion exchange processes, freshwater infiltration, and mineral (carbonate and silicate) dissolution.
Al-Asadi et al., 2020	Shatt Al-Arab river, Iraq	Highest concentration of Ca^{2+}, Mg^{2+}, Na^+, $Cl^-$and K^+ major ions and TDS were observed due to saltwater intrusion from Arabian Gulf during dry season. During other seasons, higher inflow from the Tigris river regulated these parameters.

2.3 Nutrient in estuaries

Nutrients like nitrate, nitrite, ammonia and phosphate naturally enter estuarine waters when freshwater runoff passes over geologic formations rich in phosphate or nitrate (Tahir, 2008), or when decomposing organic matter and wildlife waste get flushed into rivers and streams. Meanwhile, manmade sources of nutrients entering estuaries include sewage treatment plants, leaky septic tanks, industrial wastewater, acid rain, and fertilizer runoff from agricultural, residential and urban areas (Chen et al., 2015; Frazar et al., 2019). These nutrients are helpful in supporting the growth of algae and aquatic plants by giving the required amount of nitrogen and phosphorus, which helps in providing food and habitat for fish, shellfish and smaller organisms (Howarth et al., 2000; USEPA, 2017). However, only small amounts of each are required in a natural ecosystem. Excess levels of nitrates and nitrites in water can create conditions that make it difficult for aquatic organisms to survive and in the case of drinking water utility (Conley et al., 2009; WHO, 2011; Stumpf et al., 2016). This extended level of nitrite and nitrate also causes disease in fishes called “Brown blood disease” (Kumar et al., 2012; Stumpf et al., 2016). On the other hand, ammonia is toxic to aquatic life and a common cause of fish kills following large agricultural runoff events, industrial and agricultural spills (Loken et al., 2016). In contrast, phosphate above 0.025 mg L^{-1} is unsuitable for consumption (WHO, 2011) and can cause digestive problems for humans (Kumar et al., 2012). Furthermore, nitrogen and phosphorus levels increase in the estuarine ecosystem in form of nitrate, nitrite, ammonia and phosphate (Jaworski et al., 1981; Ngatia et al., 2019). Excess in amount and length of time that nutrients stay in estuaries dictates their availability to communities and affects the potential for biological utilization and impact (Scott et al., 1990). This can cause eutrophication, leading to a huge increase in algal and plant growth that leads to oxygen deficiency in the estuarine ecosystem. This effect is also called as “algal bloom” where it alters stream habitat and is critical for fish and other aquatic life. According to Eric et al. (2008), 0.08 to 0.10 mg L^{-1} phosphate can trigger a periodic algal bloom in the estuarine ecosystem. This algal bloom can also shade submersed aquatic vegetation, reducing or eliminating photosynthesis and productivity with the help of turbidity. Conversely, the residence time of these nutrients in estuary initiates chemical cycles like nitrogen (Fig. 2.1) (Loken et al., 2016) and phosphorus cycle (Fig. 2.2), which increases the threat of biological response to it (Scott et al., 1990).

Sulfates naturally occur in water that passes through rock or soil containing gypsum and other common minerals, or of atmospheric deposition (Porowski et al., 2019). Point sources include runoff from fertilized agricultural lands and various industrial discharges (Bo et al., 2012). In an aquatic environment, bacterial sulfate reduction, free sulfides and iron sulfides are the main components of organic and inorganic sulfur. But in estuaries, iron sulfides is mainly controlled by the availability of reactive iron and in anaerobic condition, this leads to an increase of metals, sulfate ion, and organic matter, which facilitates sulfate reduction and consequently, metal sulfide formation in bottom sediments (Matson et al., 1985; Mirlean et al., 2020). In addition, under increasing oxic conditions, it is possible to produce the SO_4^{2-} under biochemical (not chemical) oxidation of pyrite (Matson et al., 1985; Bianchi et al., 2007; Colin et al., 2017). Though sulfates are well-oxygenated and less harmful, they can give rise to hydrogen sulfide in the sulfur cycle, which is quite soluble in water and toxic to both humans and fishes (Boyd et al., 2014; Long et al., 2016; Verma et al., 2020). Moreover, these hydrogen sulfides are formed in low oxygen areas (algal bloom) (Long et al., 2016).

$$SO_4^{2-} + 5H_2(g) \rightarrow H_2S + 4H_2O \quad \text{……..(eq. 2.1)}$$

In humans, concentrations of 250 - 500 mg/L (WHO, 2011) sulfate can cause a temporary laxative effect. At very high concentrations, sulfates are harmful. However, a major threat with sulfate is its ability to form strong acids in water, which can change the pH in the estuarine ecosystem rapidly.

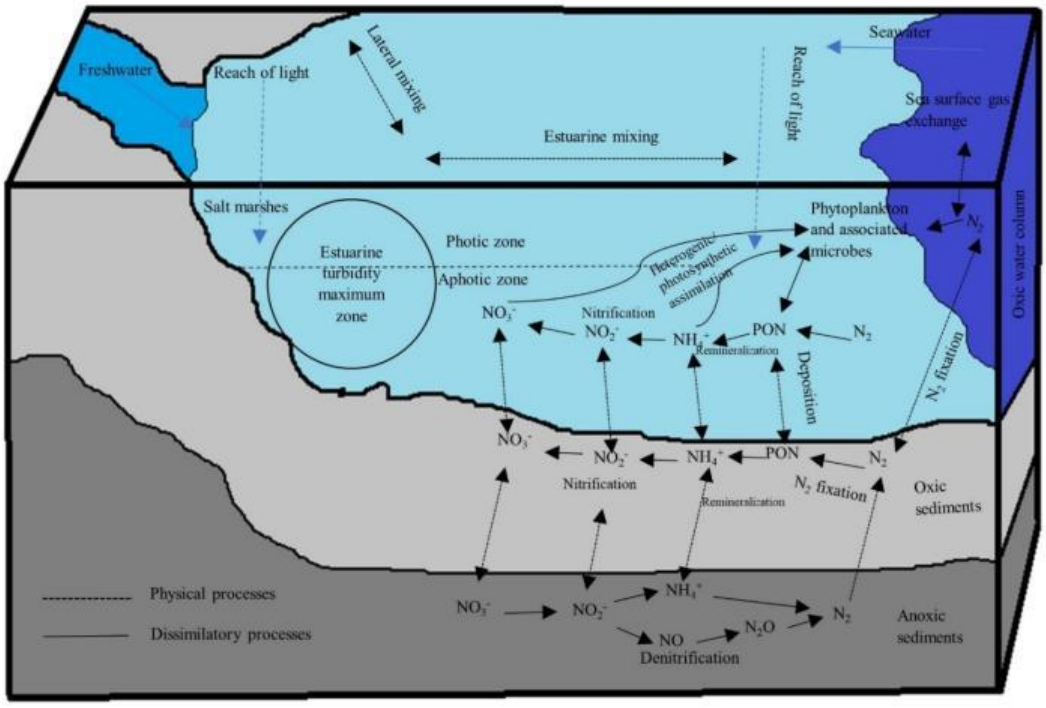

Fig. 2.1 Nitrogen cycle in an estuary (Adapted from Damashek et al., 2018)

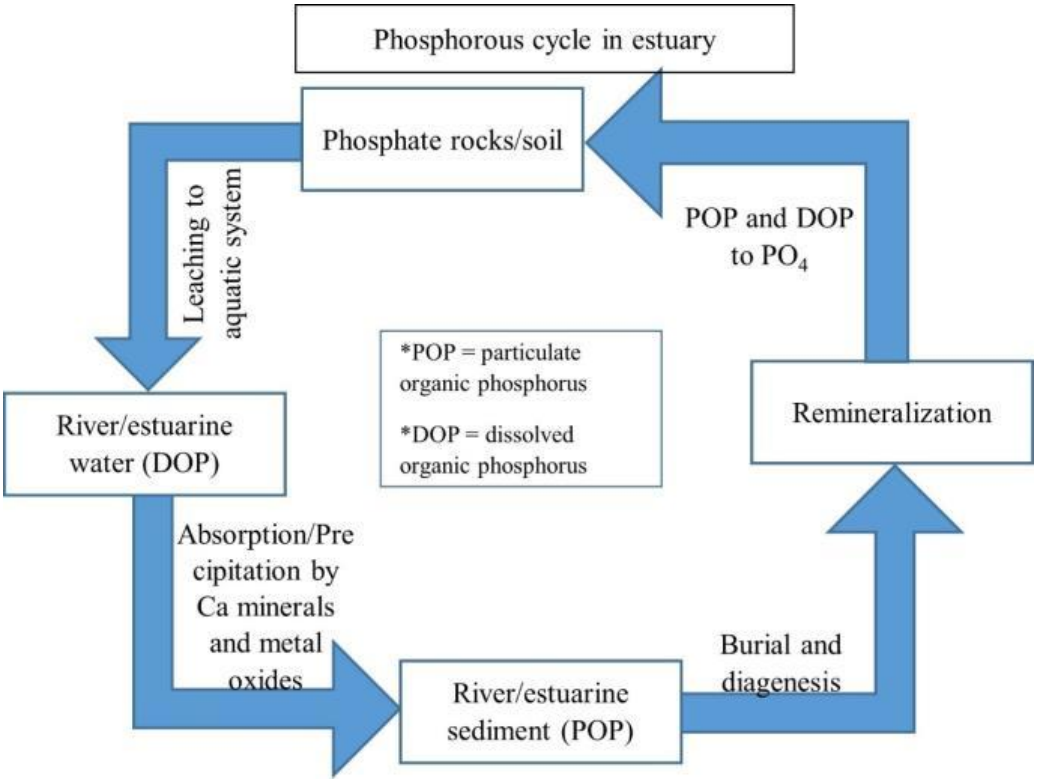

Fig. 2.2 Phosphorous cycle in an estuary (Turner et al., 2019)

Table 2.2 Case studies explaining behavior and source of nutrients in estuaries

Author	Study area	Findings
Global scenario		
Somura et al., 2012	Hii river basin, Japan	Primary source of Phosphorous and Nitrogen is agricultural and fertilizer applications in it.
Meybeck et al., 2012	Rivers of temperate and semi-arid regions (USA and western Europe)	High flow events in river contribute disproportionately to water and nutrient export from agricultural land.
Longphuirt et a. 2016	Irish river estuaries	Major input of P and N related nutrients from agricultural practices
Vaughan et al., 2017	Coastal waters	Higher nitrogen flux from agricultural than urban watersheds.
Scavia et al., 2017	Northern Gulf of Mexico, Mississippi river	Hypoxia zone forms nearly every summer in the northern Gulf of Mexico because of nutrient inputs from the Mississippi River Basin and water column stratification.
Zhu et al., 2018	Hangzhou bay, China	Nitrification and denitrification in the water column were detected and strongly controlled by suspended sediments.
Frazar et al., 2019	Maidford river, USA	Dissolved nutrient flux is mainly from agricultural lands and increases during an increase in flux.
Mori et al., 2019	Coffs Creek estuary, Australia	Nitrate in the fluvial endmember to ammonium and dissolved organic nitrogen toward the marine end member. Nitrogen cycling in estuaries is driven by a complex interaction of DO, organic matter supply, microbial activity and mixing of different water masses.
Adams et al., 2020	South African estuaries	Stormwater run-off and agricultural return flow responsible for dissolved nutrients increase. Estuaries are eutrophic with phytoplankton blooms and bottom-water hypoxia.
Geisler et al., 2020	Qishon river, Israel	High heterotrophic N_2 fixation related to N cycles was approximately three-fold higher at an upstream location compared to the lower estuary.
National and regional scenario		
Saifullah et al., 2014	**Sibuti river estuary, Sarawak, Malaysia**	NO_3^-, PO_4^{3-} and NH_4^+ concentrations ranged from 0.40 to 3.53 mg L^-, 0.01 to 1.92 mg L^- and 0.06 to 1.24 mg L^-.Distribution of nutrients is mainly influenced by seasonal variation, rate of freshwater discharge, land run-off and tidal condition. Source of nitrate in the estuary are anthropogenic input, land runoff and oxidation of ammonia in a form of nitrogen to nitrite and consequently, to nitrate.
Gandaseca et al., 2011	**Sibuti river, Sarawak, Malaysia**	pH ranged from 6.02-8.07, DO varied from 2.76-4.7 mg L^{-1}, conductivity from 0.805-96.1 µS cm^{-1}, TSS ranged from 0.00119-0.4361 mg L^{-1}, turbidity ranged from 10.2-15.3 NTU and ammoniacal nitrogen ranged from 0.1-0.31 mg L^{-1}. All water quality parameters in this study are found to be in class I and II (good water quality)

		except for the BOD and DO which indicate fairer and moderate river water quality status.
Soo et al., 2017	Southwestern coast of Sarawak, Borneo, Malaysia	High NO_3-N, NO_2-N, NH_4^+ sources from surface river runoff through agriculture and domestic wastewater discharge and closely related to deforestation and oil palm plantation. DO content in coastal water also accelerates the decomposition and nitrification process where organic content was converted to the end product of NO_3 -N.
Suratman et al., 2018	Terengganu river estuary, Malaysia	N nutrients behave non-conservatively with addition of tidal water, except for nitrate which shows removal behavior. Stronger water turbulence related resuspension of nutrients in bottom sediment lead to the increase in N compounds concentrations in the surface water. The presence of a breakwater at the lower part of the estuary contributed high nutrient content in the estuary due to restricted outflow of nutrients to the coastal area.
Nasir et al., 2019	Besut river estuary, Malaysia	Nutrients were found flocculating with increasing influence of seawater. Coastal waters were the major source of total particulate phosphorous in the estuary and found at high salinity zones. The major source of nutrients was found to be input of organic matter and nutrients from anthropogenic activities such as agricultural run-off. Denitrification played major role in removal of nitrate under low DO conditions converting nitrate to nitrite and ammonia.
Sia et al., 2019	Rajang river, estuary, Sarawak, Malaysia	Dissolved organic and inorganic phosphorous exhibit non-conservative behavior towards mixing. Inorganic phosphorous subjected to removal whereas organic phosphorous subjected to addition with salinity gradient. Addition of NO_3-N during monsoon was noticed.
Jiang et al., 2019	Rajang river estuary, Sarawak, Malaysia	Dissolved nitrogen and related nutrients (NO_3^- and NO_2^-) resulting from the decomposition of terrestrial organic matter. Strong precipitations, induced by La Niña events, might inhibit soil ammonification in the watershed and hence decreased NH_4^+ concentrations in the river water. This indicates causal chain between climate events and N cycling in tropical soils and rivers. Denitrification was major process on particle surfaces in the estuary.

*Case studies related to the current study area are marked in bold

2.4 Trace metal in estuaries

Estuaries are considered to be the most significant reservoir of trace metals originating from terrestrial and anthropogenic sources (Melville et al., 2006). This circumstance is even more complex due to estuaries multi-source character receiving water and

sediment loadings from multiple tributaries and contaminants from different sources and seasonal circulation flow dynamics (Kennish et al., 2002; Wang et al., 2012). The biochemical changes and sedimentological processes determine the fate of the metals in such an environment (Zhang et al., 2015; Catianis et al., 2018; Mori et al., 2019; Gaulier et al., 2021). Furthermore, elemental partition between liquid phase and solid phase (sediments) can give rise to drastic chemical and physical changes during estuarine mixing (Chapman et al., 2021; Ip et al., 2007; Pavoni et al., 2021). These conditions are mainly supported by input of freshwater water (low density) and seawater (high density), which usually generate hydrodynamic circulation by bringing in strong physicochemical gradients such as salinity, density, flow velocity, and suspended matter composition (Xia et al., 2019). Such factors exhibit the highest influences on the fate of metals in sediment and dissolved metals in the estuary (Elliott et al., 2002; de Souza et al., 2016; Gaulier et al., 2021).

Trace element contamination is a major ecological crisis in marine environments because they are potentially destructive, non-degradable, and bio-accumulative in tissues of organisms through the food web (Alsamadany et al., 2020). Therefore, trace metals play a major role in the quality criteria and standards of the estuarine environment. According to Gabriela et al. (2015), the speciation of trace metals is much effective to get the effect of these on biota rather than the total concentration in water. The toxicity of trace metals is largely dependent on the physical and chemical parameters of the river. Studies carried out by Neubeker et al. (1983) and William et al. (1987) found that varying pH and higher concentrations of organic ligands can give rise to the most toxic free metal such as Cu^{2+} and $CuOH^{+}$. Similarly, under changing salinity and pH conditions, Cd^{2+} ions can form soluble forms like $CdCl^{-}$, $CdCl_2(aq)$ and $CdCl_3^{-}$, which can be taken up by aquatic animals. This absorption can cause problems in enzymatic regulation of carbohydrate metabolism, lysosomal damage and mortality (Md. Badiuzzaman et al., 2014). Moreover, Cd, in addition to Cu, As, Hg and Pb, influences the reproduction of fishes in an estuarine environment (Scott et al., 2004). For mammals, it can destroy red blood cells and give harmful effects to kidneys when it is present in a higher amount (Andre et al., 2005). Lead is not essential for humans or organisms, nutritionally or physiologically. Organometallic forms of lead can easily penetrate and bioaccumulate in food chains, which damage the aquatic organisms (Monisha et al., 2014). The main dissolved form of lead are $PbCO_3$ and

PbOH. It mainly affects various physical and chemical properties of surface water and sediments such as pH, total hardness and organic matter present in them (Md. Badiuzzaman et al., 2014). It mainly affects mammals by replacing Ca^{2+} in their bones and may cause damage to their DNA and reproductive system (Monisha et al., 2014). Similarly, long-term exposure is poisonous to the fishes in the estuarine ecosystem. On the other hand, Zn in estuarine condition is absorbed by suspended solids and anaerobic sediments in high turbidity conditions. In low saline conditions, it can be mobilized from sediments due to microbial degradation of organic matter by displacing Ca^{2+} and Mg^{2+} (Md. Badiuzzaman et al., 2014). As a result, it can impact the reproduction process of various organisms in the estuary. Especially in fishes, it can get accumulated in the digestive tract and affects the liver and kidney (Clearwater et al., 2002). According to Oliveira et al. (2012), Cr uptake in water varies in terms of change in temperature, salinity and pH. This uptake can impact the photosynthesis in algae and stop the growth of some fishes (Chandra et al., 1997). In the estuarine condition, it can also settle on the sediments, which can cause remobilization in the form of chromate and organic Cr (Md. Badiuzzaman et al., 2014; Nayak et al., 2016). Similarly, Co in estuarine conditions is affected by various factors like pH, salinity, and dissolved oxygen. It is an essential element for algae, nitrogen bacteria and animals, and it can substitute various trace metals like Cu, Pb, Zn, Cd due to its similar geochemical properties (Sunda et al., 2012; Md. Badiuzzaman et al., 2014; Facey et al., 2019). Fe plays a very important role in photosynthesis, respiration and nitrogen fixation in plants (Gyana et al., 2015). Meanwhile, organic complexation in estuarine waters keeps iron in a dissolved phase at higher salinities, whereas the non-organic complexes become aggregates and are absorbed onto particles and stay in the estuary for a longer time (Md. Badiuzzaman et al., 2014). It can affect the metabolism and enzyme in mammals and fishes (Abbaspour et al., 2014; Chanda et al., 2017). In contrast, Cu at higher concentration can limit the growth in organisms in the estuary (Schuler et al., 2008; Ali et al., 2019). Bioaccumulation of Cu is highly dependent on variation in salinity, which mainly increases with decreasing salinity and accumulates on sediments and suspended solids (Ali et al., 2019). The free forms like Cu^{+} and Cu^{2+} are among the most toxic metals for various organisms surviving in aquatic conditions (Md. Badiuzzaman et al., 2014).

Table 2.3 Case studies explaining behavior and source of trace metals in estuaries

Author	Study area	Findings
Global scenario		
Priya et al., 2014	Muthupet estuary, India	The river discharge controlled the concentration of Fe in water during the post-monsoon and resuspension of bed sediments during the pre-monsoon, whereas Cu, Cd, and Zn are supplemented by the resuspension of the bed sediments.
Wang et al., 2017	Jiulong river Estuary, China	Trace metals (Cu, Zn, Ni, Co, Pb, Cd, Mn, and Fe) behaviors controlled by early diagenetic reactions. The organic matter oxidation led to Cu and Cd concentration and the reductive dissolution of Mn/Fe (hydr)oxides in suboxic layer led to which Zn and Co concentration increase.
Monte et al., 2019	Iguaçu river estuary, Brazil	A higher release of Cu and Zn with massive increase on the bioavailable fraction after resuspension of sediments due to oxidation of sulfides.
Mori et al., 2019	Coffs Creek estuary, Australia	High concentrations of Ba, Mn and Fe in mangrove porewaters suggest porewater discharge as an important source of dissolved metals in estuarine water. Dissolution of Ba from riverine particles in the fluvial-mangrove transition in low-medium salinity.
Xie et al., 2020	Pearl river estuary, China	Estuarine mixing controlled the distribution of dissolved metals (Mn, Cu, Zn and Cd) in the estuary; meanwhile, removal and addition processes also induced anomalies in the distribution.
Asha et al., 2020	Sundarban mangrove estuary, Bangladesh	Fe, Mn and Cu were found to be non-crustal in origin and mainly controlled in sediments through sediment and macroalgae interaction.
Huang et al., 2020	Xiangjiang river estuary, China	Cr, Co are geogenic in nature and Pb, Zn, As, Cu, and Cd are anthropogenic inputs. Organic matter and grain size are the main factors affecting the distribution of trace metals in the sediment
Gaulier et al., 2021	Scheldt estuary, Netherlands	Gradients like turbulent mixing mechanisms, an increasing salinity, temperature and DO in the mid-zone of the estuary responsible for metal (Cd and Cu solubilization and remobilization processes through biochemical processes.
Pavoni et al., 2021	Karstic Timavo river estuary, Italy	Fe and Mn redox behavior appears to play a crucial role in the recycling of dissolved trace elements in the water column. Cr, Ni, and Co are mainly from lithogenic origin and mainly carried by sediment and suspended solids in the river.
National and regional scenario		
Mokhtar et al., 2015	Langat river estuary, Malaysia	Ni and Zn have been identified as a major metals contamination in Langat river estuary which mainly comes from anthropogenic activity in Port Klang and Langat river water ways. The unique of geographical of Langat rivers estuary also has influenced depositions of metals ions in sediment.

Sim et al., 2018	Baram river, Sarawak, Malaysia	Al, Fe and Mn are major constituents of the sediments. High metal concentration mainly attributed through surface run-off and possible anthropogenic disturbances. Enrichment of Al, Fe, Mn and Zn in sediments are more likely associated with the intensive land clearing activities in the region.
Ibrahim et al., 2020	Sembilang river, Malaysia	Effluent from the landfill material, and wastewater from industry, agricultural runoff and residential area are the major source of trace metals (Al, Fe, Mn, Cr, Zn, Cu, Cd and Pb). Al and Mn found higher than the permissible values.
Salam et al., 2020	Perak river, Malaysia	Fe and Cd were found to be highest in concentration. Cd, Fe and Pb are pose high risk towards the aquatic animals and human consumption.
Prabakaran et al., 2020	Baram river estuary, Sarawak, Malaysia	Partition coefficient of metals showed Mn-oxyhydroxides has predominant role in the transportation of trace elements in the river. Factor model illustrated the dissolution of Al and authigenic clay formations. Fe and Al are within permissible limits both in dissolved and particulate form.
Chang et al., 2020	Estuaries in Malaysia	In acidic, low-oxygen, organic-rich blackwater (peatland-draining) rivers, dissolved Se found to be higher in concentration. Positive correlation of organic Se with humification index and humic-like chromophoric dissolved organic matter components in freshwater river suggest that peat soils are probably the main source.
Salam et al., 2021	Kelantan coastline area estuaries, Malaysia	Concentrations of metals in the estuarine surface sediment differ from one estuary to another following the order of: Fe (39.08%) > Zn (37.02 μg/g) > Pb (20.78 μg/g) > Cu (6.68 μg/g) > Cd (3.69 μg/g). The source of these metals were more or less anthropogenic in nature and is revealed through cluster analysis.

2.5 Major Influential mechanisms

2.5.1 Ion-exchange

River sediments consist of clay minerals, metal hydroxides and organic matter. These materials present with dissolved solutes encounter water of increased ionic strength (seawater) while entering the estuarine environment (Hao et al., 2020; Weiduo et al., 2020). Differences between the chemistry of rivers (pH ranging from 2 to 8, ionic strength <0.01M) and oceans (average pH 8.1, ionic strength from 0.56M to 0.7M) result in variations in both the aqueous speciation of trace elements and clay surface properties (Weiduo et al., 2020). Widely available minerals like quartz and feldspar are less capable of such an exchange process whereas clay minerals and metal oxides

thrive in such environment due to their higher surface area for absorbance and increased reactivity due to increased ionic strength (Regnier et al., 1993; Manning et al., 1997; Hu et al., 2015; Ugwu et al., 2019). In addition, the isomorphous substitution of one cation with another within crystal structures leads to a charge imbalance in silicate clay minerals particles, which accounts for the permanent negative charge on it, hence, enhances the ability of clays to attract cations to the surface. The presence of amphoteric OH groups at the surface of clays also contributes to surface charge (pH-dependent reversible charge) (Alshameri et al., 2019). Apart from that, permutolites (clay minerals like kaolinite, illite, chlorite, halloysite, glauconite, zeolites and organic matter) have certain qualities of absorption and tend to exchange their cations with cations present in water (Thilagavathi et al., 2012). In such conditions, ion exchange between the solid phase and liquid phase commonly takes place, where ions are absorbed onto the surface of the particles. In addition, the resuspended particles from bed load sediments due to intertidal mixing become involved in these solute-particle interactions (Hunter et al., 1982; Fitzsimons et al., 2012; Cochran, 2014). This process is responsible for the alteration of water composition as well as solid composition involved with it. Furthermore, this process leads to absorption and dissolution with the varying chemical conditions in the aqueous systems.

As explained before, major ions like Ca^{2+} and Mg^{2+} in rivers are part of the fluvial contribution, while Na^{+} and Cl^{-} are the major contributions from seawater influence (Patra et al., 2012). These contributions sometimes lead to continuous phenomena of ion exchange and reverse ion exchange in a mixed dynamic environment like estuaries. Generally, chloro-alkaline indices (Schoeller, 1965) are used to measure the rock-water interaction and ion exchange between them (eq. 2.1 and 2.2) and the major reaction involved in this process can be represented as eq. 2.3.

$$CAI1 = [Cl^- - (Na^+ + K^+)]/Cl^- \quad \text{.....(eq. 2.1)}$$

$$CAI2 = [Cl^-(Na^+ + K^+)]/[Cl^-(SO_4^- + HCO_3^- + CO_3^- + NO_3^-)] \quad \text{.....(eq. 2.2)}$$

$$Na^+ + K^+ \Leftrightarrow Ca^{2+} + Mg^{2+} \quad \text{.....(eq. 2.3)}$$

When Na^+ and K^+ in solution are exchanged with Ca^{2+} and Mg^{2+} in the weathered solid phase, the index value would be positive for eq.1 and 2 and is termed as ion exchange. The vice versa situation is termed as reverse ion exchange.

During high flow regimes or increased terrestrial input as during monsoons, solid phases that are rich in Ca^{2+} and Mg^{2+} due to a higher amount of weathering in the catchment area gets replaced by Na^+ and K^+, leading to ion exchange phenomenon. This process increases Ca^{2+} and Mg^{2+} in solution while decreasing Na^+ and K^+ in water (Zaidi et al., 2015; Patra et al., 2012). Contrarily, during limited terrestrial recharge of river that mixes with seawater during the horizontal mixing process, the overwhelming amount of Na^+ and K^+ ions from the seawater and solids dominate the process, leading to absorption of Ca^+ and Mg^{2+} on surfaces like clay mineral and metal oxyhydroxides (Sridharan et al., 2017). When Na-Cl type of water passes through a solution rich in calcium and magnesium in solution (fresh river run-off), the latter will be replaced with sodium. If calcium and magnesium-containing water prefer to be attached to the absorption site such as clay minerals, the sodium goes back into the aqueous medium, giving rise to a mixed mechanism of ion and reverses the ion exchange process, while promoting Na^+ and Cl^- dominating water during mixing. This refers to the higher tendency of Ca^+ and Mg^{2+} for absorption over Na^+ and K^+ in chemically reactive conditions (Barzegar et al., 2018). This is also an indication of continuous seawater infusion in an estuarine environment (Sridharan et al., 2017). Unlike groundwater, estuaries' nature of continuous changes in their hydro-dynamics leads to the mixed phenomenon of ion and reverse ion exchange process in general.

2.5.2 Water density stratification and Oxidation-reduction

Water in estuaries exchanges in both horizontal and vertical directions, leading to self-restoration and purification (Pfeiffer et al., 2015; Zhu et al., 2015; Sun et al., 2020). Horizontal mixing controls factors such as sediment deposition and ion exchange (Kärnä et al., 2016), whereas vertical circulation pattern can be attributable to various dynamic conditions of tidal currents, freshwater discharge and density gradient of water (Geyer & MacCready, 2014). Vertical stratification is a common phenomenon in microtidal estuaries. Meanwhile, it is an impending factor of a vertical exchange of water and dissolved materials (Qian et al., 2018) and is a physical condition for hypoxia development (Tian et al., 2020). The tidal current observed in this type of

estuaries is not strong enough to eliminate stratification of the water column. In such conditions, tidal currents promote turbulence and facilitate reaeration, and sometimes leading to hypoxia during the insufficient vertical renewal of DO reaeration in the water column (Muller et al., 2016; Zhang et al., 2017; Sun et al., 2020). This bottom water hypoxia condition mainly occurs due to the presence of suspended organic particulate and their respiration despite the high rate of mixing of tidal waters in the turbidity maximum zones (Tomasko et al., 2006; Sun et al., 2020). Such hypoxic condition combined with increased organic matter can significantly enhance anaerobic nitrate reduction to ammonia in estuaries, further contributing towards nitrogen cycles (McCarthy et al., 2008; Walker et al., 2020) while also being responsible for the release of iron-bound phosphate into the water table from the bottom sediments (Sinkko et al., 2013). In addition, these stratified zones are the main reason for the upstream movement of marine sediments during the low flow of the river, but it also creates an enhanced sediment trapping zone in the tidal freshwater zone of the estuary (Mathew et al., 2020). This process is most active near the sediment-water interface with a steep gradient of pore water DO and pH (Silburn et al., 2017). Thus, microbially driven oxidation of OM, dissolution of Fe and Mn oxyhydroxides and other metals carrying phases along with upward diffusion of the dissolved materials are the common phenomena observed in such zones which give rise to metal concentration in the water table (Turner et al., 2000; Tankere et al., 2007; Santos et al., 2009; Rigaud et al., 2013; Dang et al., 2015; Mori et al., 2019; Jokinen et al., 2020). Contrarily, these trace metals face absorption and flocculation on suspended solids in case of overlying well-oxygenated conditions in estuarine water (Turner et al., 2000; Venkatramanan et al., 2015; Mori et al., 2019).

Table 2.4 Case studies explaining Oxidation-reduction and density stratification in estuaries

Author	Study area	Findings
Global scenario		
Rigauda et al., 2013	Berre lagoon, France	Under oxic conditions and in the absence of benthic organisms, the main redox reactions were well identified vertically in the surface sediments and followed the theoretical sequence of oxidant consumption: O_2 > NO_3/MnO_2 > $Fe(OH)_3$ > SO_4^{2-}. Under anoxic conditions, only MnO_2, $Fe(OH)_3$ and SO_4^{2-} reduction were identified, occurring at the sediment-water interface.
Li et al., 2018	Pearl river estuary, China	During summer, the fresh and saline-water intersection where is characterized by severe

		stratification and high heterotrophic bacteria abundance. Low DO phenomenon presented in the sub-layer water column during the summer but not winter period
Sun et al., 2020	Pearl river estuary, China	Seasonal variations of river discharge heavily causing water density stratification and DO depletion in bottom waters.
Walker et al., 2020	Estuaries in Texas, USA	Stratification at the mid to lower estuary contributed to the low bottom water pH and DO condition. Increase in external organic matter loadings due to flooding and strengthen vertical stratification. Nitrogen cycle observed at intermediate salinities.
Tian et al., 2020	Chester river estuary, USA	Seasonal and tidal influenced stratification to die to bottom saltwater intrusion are significant factors controlling determining hypoxia occurrence while bringing DO < 2 mg L^{-1}. PO_4^{3-} load is impacted highly due to this hypoxia condition than nutrients controlling dissolved nitrogen.
National and regional scenario		
Ishak et al., 2000	Selangor river estuary, Malaysia	Estuary goes from partially mixed type to well mixed type depending upon the tidal force. Strong density stratification observed during higher river discharge due to monsoonal rain. Turbidity maxima zones were observed with suspended solid concentration reaching values up to 2000 mg L^{-1}.Tidal pumping was identified to be a dominant factor identified as compared to estuarine circulation.
Lee et al., 2016	Terengganu river estuary, Malaysia	Water stratification, high contamination of nutrient, low current speed and the geometrical formation are recognized as important role in formatting the hypoxia at the Terengganu river mouth. Estuary is free from hypoxia condition during wet season, but rapid development of hypoxia noticed during dry season with DO level going to 0.78 mg L^{-1}.
Jiang et al., 2019	Rajang river estuary, Sarawak, Malaysia	Addition of dissolved nitrogen, and NO_3^- was evident from pore-water both cohesive and sandy sediments and surface water due to large contact area. this exchange can be driven by tidal pumping, wave actions and density difference. Undersaturated DO observed in the mixing zone suggesting active aerobic respiration on the basis of organic matter decomposition.

2.5.3 Mineral dissolution and precipitation

Dissolution and precipitation of minerals determine the concentration of various cations and anions in the solid and liquid phase of open aquatic systems (Reiss et al., 2021). Dissolution attributes to higher concentration in the liquid phase, whereas precipitation of minerals leads to higher concentration in the solid phases. For instance, aluminosilicates give rise to kaolinites upon physical weathering and K^+ in

the aqueous system during the chemical breakdown, whereas carbonate minerals result in a higher concentration of Ca^{2+} and CO_3^- in aqueous solution during the same process (Chidambaram et al., 2011; Venturelli et al., 2003). Similarly, sulfate minerals give rise to Ca^{2+} and SO_4^{2-} upon dissolution in aqueous solutions. This kind of process is highly dependent on the pH of the solution and mainly controlled by the CO_2 equilibrium with atmosphere (in an open aqueous environment) and their residence time in considered aqueous solution (Prasanna et al., 2010; Chidambaram et al., 2011; Srinivasamoorthy et al., 2014; Naderi et al., 2016). Chemical weathering particularly consumes CO_2 in minerals in order to maintain equilibrium with the atmosphere. However, such a process makes the minerals unstable when exposed to surface conditions. In an open aqueous system like estuaries, CO_2 is regulated by atmospheric interaction and as a result, it produces weak acid like H_2CO_3 (eq. 2.4), which creates an acidic environment at the rock-water interface and is responsible for dissolution (Sheikhy et al., 2014).

$$H_2O + CO_2 \rightarrow H_2CO_3 \text{.....(eq. 2.4)}$$

In addition, estuarine systems are known to be organically rich in nature, phenomenon such as stratification and oxidation-reduction causes hypoxia conditions resulting in respiration of organic matter at the bottom of the water, bringing more CO_2 into the system. This leads to increased dissolution of these minerals. This process of dissolution increases with more residence time of river water in the estuary for carbonate minerals (Glynn et al., 2005; Al-Ghanimy et al., 2019). On the other hand, continuous and higher recharge enhances the dissolution of sulfate minerals in estuarine systems (Murray et al., 1964; Hamzaoui et al., 2013; Juen et al., 2015; Naderi et al., 2016; Al-Ghanimy et al., 2019) and precipitation is higher in stagnant water environment such as seawater conditions (Reiss et al., 2021).

2.5.4 Flocculation of metals

Estuarine environment works as a geochemical reactor during the process of estuarine mixing of freshwater and salt water effectively, attributing to the flocculation process (Fig. 2.3), which plays an important role in self-purification by accumulating the dissolved trace metals (Sholkovitz et al., 1978; Biati et al., 2010; Biati et al., 2010; Chenar et al., 2013; Samani et al., 2015; Hassani et al., 2017; Sun et al., 2020; Vane et al., 2020). Various researchers have identified salinity (Hassani et al., 2017), pH

(Karbassi et al., 2014), colloidal stability, surface properties (Chenar et al., 2013), turbulence and concentration of suspended matters (Mhashhash et al., 2018), ionic strength, and algal concentration (Biati et al., 2010) as the main governing factors of such process during mixing. In this process, dissolved metals (from the upstream region) move to a particulate phase where a lower salinity regime is dominant and eventually depositing themselves in the lower part of the estuary (Fig. 2.3) (Regnier et al., 1993; Biati et al., 2010; Hassani et al., 2017). This helps to maintain a significant chemical balance between river and sea (Karbassi et al., 2008; Karbassi et al., 2013; Mosley et al., 2020). At low salinity, colloids do not tend to settle out of the water column due to the low gravitational settling rate. Thus, the destabilizing influence of tidal water cations in the estuary enhances the aggregation of these colloidal materials (Fig. 2.3) (Sholkovitz et al., 1976; Chaudhuri et. al., 2019; Mosley et al., 2020).

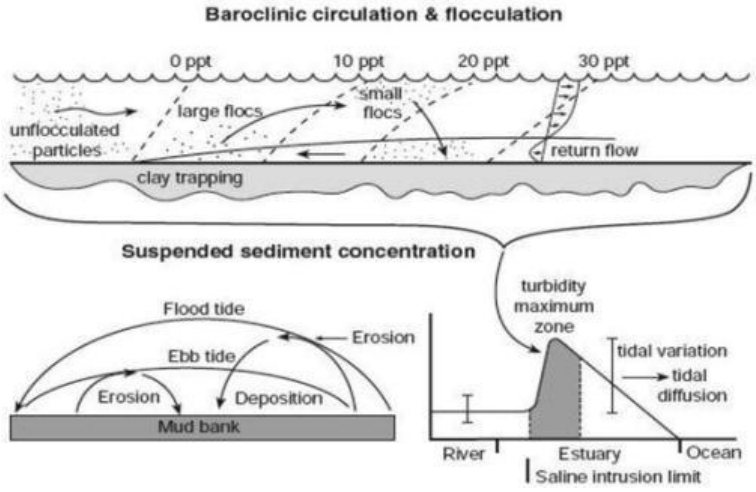

Fig. 2.3 Flocculation of particles in turbidity maximum zone created due to tidal pumping (Chaudhuri et al., 2019)

However, an increase in salinity sometimes leads to hypoxia condition attributing towards low pH conditions (due to stratification and less exchange of DO between the top and bottom waters), causing to a sharp decrease in flocculation rates (Duinker et al., 1983; Saeedi et al., 2003; Biati et al., 2010; Karbassi et al., 2013). In the case of turbulence, which is an important component of turbidity, cohesive sediments play a major role in controlling the flocculation rate in estuarine environments (Fennessy et al., 1994). Under certain salinity threshold (2.5 ppt-experimental value: Allersma et al., 1967; Lintern et al., 2003), these sediments come together to form micro (diameter < 100 μm; settling velocity < 1 mm s−1: Lafite, 2001) and macro flocs (diameter > 100 μm). With salinity crossing such threshold value, floccules formed by these

cohesive sediments are slowed down. In addition, increased tidal influence near the river mouth generates the turbidity maxima zones and increases in suspended solids concentration in the water table. In such conditions, these flocs are more likely to bump into each other leading to breakdown and absorption by these suspended solids, which eventually leads to settlement (Mhashhash et al., 2018) (Fig. 2.3). Trace metals like Fe, Mn, Cu, Zn and Al's affinity towards humic acid is dependent on high salinity. Such affinity and their colloidal nature in estuaries often leads to flocculation of these metals in association with dissolved and colloidal organic matter (Sholkovitz et al., 1978; Illuminati et al., 2020). Contrarily, desorption of metals from river suspended matter and/or the addition of dissolved trace metals from pore solutions of estuarine sediments are the major mechanisms, which counterbalance the removal of metals by flocculation (Sholkovitz et al., 1978). The recommended pattern of flocculation metals in estuarine mixing can be seen as solids > free ions » hydroxides > oxides (Biati et al., 2010).

Table 2.5 Case studies explaining flocculation of metals in estuaries

Author	Study area	Findings
Global scenario		
Biati et al., 2010	Minab river estuary, Iran	Solids and oxides have the highest and lowest flocculation levels. The general pattern of flocculation of studied metals is manganese (180 µg/L) > zinc (88 µg/L)> nickel (73µg/L)> copper (30µg/L)> lead (19 µg/L). Dissolved organic carbon plays a major role in the flocculation of metals during estuarine mixing except for Pb as it is present as oxide.
Karbassi et al., 2014	Aras river estuary, Azerbaijan	The flocculation trend of Pb (100 %) [Ni (62.5 %) [Zn (30.43 %), Mn (25 %), Cu (18.18 %) at different salinity regimes (0.5–2.5 %) at pH 7 during estuary mixing.
Karbassi et al., 2017	Sardabroud river, Iran	The flocculation rate of Ni (25%) > Zn (18.59%) > Cu (16.67%) > Mn(5.83%) > Pb(4.86%) indicates that lead and manganese have relatively conservative behavior, but nickel, zinc and copper have non-conservative behavior during Sardabroud river's estuarine mixing. The highest removal efficiencies were obtained between salinities of 1 to 2.5%
Liu et al., 2019	Yangtze river, China	Increasing dissolved organic matter values at constant salinities, lead to an increment of maximum flocculation rate of Cu during estuarine mixing.
Tarpley et al., 2020	York river estuary, USA	Flocculation increased particle size, which reduced suspended solids by half in the turbidity maximum zone through increased settling velocity. Stratification of water had negligible influence on flocculation.

National and regional scenario		
Anandkumar, 2016	Miri coast, Sarawak, Malaysia	Fe, Mn, Cu and Zn are mainly associated with silt fractions and indicated flocculation of these metals in during estuarine mixing in river estuaries such as Baram, Miri and Sibuti rivers.
Prabakaran et al., 2019	Baram river estuary, Sarawak, Malaysia	Factor analysis revealed that Cu, Zn and Pb were more enriched in the estuarine sediments as compared to upstream sediments, whilst flocculation is the major process behind it
Zhang et al., 2020	Rajang river estuary, Sarawak, Malaysia	Intense removal of dissolved Fe in low-salinity waters (salinity < 15 PSU) was observed. The reason behind it was salt-induced flocculation and absorption of Fe in suspended solids. Higher concentration of Fe observed during monsoon due to leaching of peat-lands by the backwaters.

2.5.5 Absorption and desorption of metals

Absorption generally represents the attraction between negatively charged metal ions and positively charged solid or particulate surfaces, while the vice versa condition is termed as desorption (Thompson et al., 2012). In estuaries, the dwell time of water in an estuary determines the period of dissolved and particulate reactants held under less fluctuating salinity, pH, turbidity and DO condition (riverine system), whereas flushing time mainly determines the absorption and desorption under varying conditions towards the downward region. During this flushing period, a convergent zone prone to elevated suspended solid matter promotes solid–solution reactions in the freshwater-seawater interface. This zone is also termed as turbidity maxima zone where maximum (Mathew et al., 2020) absorption takes place. Generally, sorption reactions involving dissolved metals are not unidirectional as the propagation of variable riverine conditions is not the only source of such dissolved metals (Morris et al., 1979). The subsidiary inputs such as infusions of sediment porewaters and bankside discharges also work as additional source of metals (Turner et al., 2000).The biogeochemical reactions happening in this porewaters are responsible for the contribution of higher metal concentration, leading to non-conservative behavior of metal in the estuary (Millward et al., 2003). The trace metal absorption (dissolved, particulate, and colloidal) in estuaries commonly have major association with metal oxyhydroxides (Fe, Mn and Al), organic matter and clay particles (Nystrand et al., 2012; Warren et al., 1994; Jokinen et al., 2020). Fe and Mn oxyhydroxide precipitation and its scavenging nature are responsible for a higher amount of absorption (Rigaud et al., 2013), whereas dissolved organic matter in bottom pore water controls the

vertical flow of metals by forming complexes (Jokinen et al., 2020). On the other hand, clay minerals are known for their surface reactivity and availability as suspended solids in an estuarine environment (Sposito et al., 1999; Lackovic et al., 2003; Zhao et al., 2018). In addition, the absorption is not only dependent on the reactive surface but also works in combination with Fe, Mn amorphous oxides, and organic materials, some of which may cover clay surfaces (Li et al., 2009; Chen et al., 2016). This process alters the surface reactivity of clay minerals and promotes varieties of new sites for the absorption of metals in the mineral-water interface (Hirst et al., 2017; Zhou et al., 2020).

This absorption and aggregation process stimulates the flux of terrestrial and biogenic materials in estuaries and works as a sinking medium as well as recycling and redistribution of such riverine materials into the coastal environment (Elderfield et al., 1975; Gibbs et al., 1986). The recycling (desorption) into the water table may be driven by microbial oxidation of organic matter and is associated with reductive dissolution of Fe and Mn oxyhydroxides (Tankere-Muller et al., 2007; Prajith et al., 2016; Jokinen et al., 2020). In the case of organic-rich sediments, mineralization of organic matter can lead to a steep gradient of pH and DO near sediment-water interface at the bottom, enhancing the desorption due to dissolution of such reactive metal carrying phases (Canfield et al., 1993; Silburn et al., 2017). These influencing physico-chemical parameters also influence the dissolution during remobilization (Jokinen et al., 2020) and stratification of the water table (Turner et al., 2000). In clay minerals, an increase in pH of aqueous solution promotes deprotonation of functional group surfaces, while high ionic strength due to seawater influence attenuates the negative electrostatic field, leading to diminished cation adsorption at the clay surface (Hao et al., 2018; Hao et al., 2019). The main variation in ionic strength of clay minerals can be seen in the transition from river and seawater with changing pH, which is below 0.01 mol L^{-1} in the river and can increase up to 0.56-0.7 mol L^{-1} with the introduction of seawater, with varying pH range of 2 - 8 (Gu et al., 20008; Hao et al., 2020).

Table 2.6 Case studies explaining absorption/desorption of trace metals in estuaries

Author	Study area	Findings
Global scenario		
Robert et al., 2004	Gironde estuary, France	Intense metal mobilization due to redox-induced dissolution and resuspension, releasing trace metals into the water column in the lower part of the estuary. Absorption onto reactive particles such as freshly precipitated Mn oxyhydroxides is stabilizing the dissolved metal phase.
Ingri et al., 2014	Bothnian bay, Sweden	Trace metals have been transferred from permanently buried sulfides to Fe–Mn-oxyhydroxides. The absorption by these oxyhydroxide layers restrict the flux of trace metals from the sediment to the oxic bottom water. Hence, Fe–Mn cycling in the suboxic sediment enriches a number of trace metals in the surface sediment.
Wang et al., 2017	Kelantan river estuary, Malaysia	The major type of sediments was clay silt and the organic carbon in surficial sediments. The critical role of retention of trace metals mainly controlled by the combined effect of clay minerals and total organic carbon.
Hirst et al., 2017	Lena river, Russia	Fe oxides are found attached to the surface of primary produced organic matter and clay particles and working together with high reactive surfaces for higher metal absorption.
Priya et al., 2020	Muthupet estuary, India	The location of turbidity maxima and peak metal concentration was identified to be the same as the estuary due to resuspension and dissolution. The removal of Fe as Fe oxyhydroxides from liquid phase under increasing salinity condition while absorbing metals like Cu and Zn.
Wang et al., 2020	Yangtze river estuary, China	Cu, Zn, Pb, and Ni are controlled by strong absorption on a large surface area of clay minerals originating from clastic sediments.
Zhou et al., 2020	Coastal environment	Organic bacteria accumulate on clay mineral (kaolinite, montmorillonite and illite) surfaces, promoting the development of larger micro aggregates while absorbing Cd to the relative sites on the clay mineral surfaces.
National and regional scenario		
Lim et al., 2012	Langat river estuary, Malaysia	pH changes mainly controlled absorption and desorption of trace metals on sediment surfaces. Alkaline condition in sediments increased As, Cr, and Ni concentration in water. With decrease in water pH Co desorbed from organic ligands and other particulate matters. Change in salinity increased metal concentration water column by increasing the competition between cations and metals for binding sites on clay-organic particle surfaces.
Mohamed et al., 2019	Kelantan river, Malaysia	TSS in the water column along Sungai Kelantan increased from 14.0% at upstream to 38.3% at downstream with ranging from 68.8 - 571.8 mg L^{-1}.

		Mobilization and resuspension enhances absorption of Ga on suspended solids and Cr sediments. Diffusion from the water column towards surface sediment due to the presence of dissolved particulate Cr may increase the total concentration of Cr in surficial sediment.
Salam et al., 2021	Estuaries along Kelantan Coastline Area, Malaysia	pH and total organic matter greatly controlled metal (Pb, Zn and Cu) retention on sediment surfaces. Organic matter deposited on the aquatic sediment surface is originated from plant derivatives, animal detritus, and fecal matter and acted as absorption site for majority of the metals. The was noticed at pH above 3.

2.6 Significance of metal partitioning in sediments

Sediments in aqueous systems work as sink and store houses of dissolved/particulate metals (Usero et al., 1998). Solid components of sediments govern the dissolved levels of trace metals with the processes like absorption/desorption, precipitation/dissolution and flocculation reactions, which are coupled to complexation, acidification and redox reactions (Kersten et al., 2002). However, trace metals in sediments can be associated with various solid phases such as in absorbed phase on solid surfaces of clay minerals or metal oxyhydroxides, co-precipitated with carbonates phases of carbonate minerals, organic matter either in living or detrital form and matrix-bound such as aluminosilicates (Tessier et al., 1987; Simpson et al., 2000). Some of these phases like metal oxyhydroxides and organic matter have their scavenging actions associated with them, which are far out of proportion to their concentrations (Li et al., 2000; Knox et al., 2006; Laing et al., 2009). On the other hand, some phases like the matrix-bound metals do not pose the tendency to be mobile in an aqueous medium easily. In such a scenario, the weak binding phases are subjected to change in physico-chemical condition of over laying the water table. In changing aqueous system like estuaries, factors such as dredging of anoxic sediment or acidification of overlaying water, change in redox potential, ion strength and salinity can increase the mobility of these metals easily (Tessier et al., 1987; Chapman et al., 1998; Burton et al., 2006; Gómez et al., 2007). Even though the total concentration of metals in sediments is a good tool to measure the contamination levels, it does not provide sufficient details regarding the mobility of these metals in overlying aqueous medium and the toxicity possessed by their higher concentration on aquatic organisms (Gómez et al., 2007; Farkas et al., 2007; Rinklebe et al., 2014; Baran et al., 2015). Based on this, quantification of metals in geochemical phases of sediments is an effective tool to evaluate their mobility,

bioavailability and toxicity (Morillo et al., 2004; Burton et al., 2006; Baran et al., 2015).

Sequential extraction of sediments is an important method to study and quantify the metals in various phases while revealing their binding strength in the solid matrix (Tessier et al., 1987; Tessier et al., 1979; Ruttenberg et al., 1992). The extraction proposed by Tessier et al. (1979) partitions metals into 5 fractions: exchangeable, carbonates or acid-soluble, reducible or Fe-Mn oxide association, oxidizable or organic matter controlled, and residual. The metals associated with exchangeable and carbonate fractions are considered to be easily bioavailable as compared to metals in reducible and oxidizable fractions (Zhang et al., 2014). The latter fractions have the potential to stabilize metals in elevated oxidative–reductive potential and changing the hydrological regime in estuaries (Burton et al., 2006; Iwegbue et al., 2007). This extraction is also very helpful in analyzing detailed information about the origin, mode of occurrence of metals, which might be geogenic or anthropogenic (Borgese et al., 2013; Saleem et al., 2015; Ali et al., 2019).

2.7 Sequential extraction review

Accumulation of trace metals in an aquatic environment like estuaries takes place in a similar way despite its origin, i.e., geogenic or anthropogenic, making it difficult to identify its effect and mobility under varying conditions (Saleem et al., 2015). To gain a better understanding of geochemical and biological processes and solid speciations involved in it, sequential extraction techniques are widely employed in sediment studies (Zhang et al., 2014). Beyond the importance of sampling and pretreatment of sediments, it has been observed that the specificity and the reproducibility of the method greatly depend upon the chemical properties of the element and the chemical composition of the samples (Prohić et al., 1987; Martin et al., 1987). This method provides a gradient for physico-chemical association strength between trace metals and the solid phase particles rather than their actual speciation (Martin et al., 1987). Geochemists consistently utilize this method to estimate either the amount of trace elements involved in authigenesis (removal from dissolved to particulate phase) or conversely, their remobilization during the early diagenesis or resuspension of deposited sediments (Martin et al., 1987). The exchangeable amorphous oxides of Fe, Mn and A1, organic matter, carbonates, phosphates and sulfides can be considered as

important sinks for trace elements and/or are susceptible to modification under certain environmental conditions. Keeping such processes in consideration, extraction techniques have focused on five fractions for sediments speciation, namely, exchangeable/water-soluble, carbonate/acid-soluble, Fe and Mn hydroxides and reducible, organic/oxidizable and residual fraction. In current times, various extraction procedures emerged in the geochemical field to quantify the trace metals depend on their solid phase characteristics behavior (Zhang et al., 2014; Saleen et al., 20015). Different popular methods of extraction are depicted in Table 2.7. Wong et al. (1980) observed that the discrepancy in metal concentration might increase depending on differences in extraction time, extraction rate and storage conditions even when the same procedures for extraction and analysis are used in various laboratories participating in calibration studies. The utilization of dried sediment samples is useful in improving the precision of measurement in a great manner.

Table 2.7 Characteristics of popular sequential extraction procedures

Name of extraction method	Extraction step needed	Extracted metal species	Reference
Modified BCR	3-step	Exchangeable and weak acid-soluble fraction, Reducible fraction, Oxidizable fraction and Residual fraction.	Pueyo et al., 2008
Tessier	5-step	Exchangeable fraction, Carbonate fraction, Fe and Mn oxides fraction, oxidizable fraction and Residual fraction.	Tessier et al., 1979
Diffusive gradient	One-off	Labile species	Davison and Zhang, 1994
Diffusive gradient thin film (DGT)		Bioavailable	
Kersten and Forstner sequential extraction	6-step	Exchangeable ions, Carbonates, Mn oxides amorphic and Fe oxides, acid volatile sulfides (AVS), organic matter and Metals bound in lithogenic minerals	Kersten and Förstner 1986

Exchangeable fraction deals with metal that shares a weak electrostatic bond with the surface of the solid and can be easily retained in solution through ion exchange process (Narwal et al., 1999). Exchangeable metals are the measure of those metals, which are easily available in the aquatic environment and have the highest potential to be the cause of toxicity (Masindi et al., 2018; Devi et al., 2018). The concentration of metals

in this fraction is generally below 2% of the total concentration sediments and are easily obtained through action of common reagents such as $MgCl_2$, and sodium acetate (pH 5.4) by acetic acid (Okoro et al., 2012). Carbonates are a major absorbent of trace metals when there is a reduction of Fe/Mn hydroxides and organic matter and are the most sensitive to pH changes (Okkoro et al., 2014; Zhang et al., 2014; Caporale et al., 2016). It is also considered as a loosely bound phase and subjected to metal release under pH 5. The metal release of this fraction is achieved by the usage of reagents like 1M sodium acetate adjusted to pH 5.0 with acetic acid (Mseddi et al., 2010; Okoro et al., 2012). The process of absorption by Fe/Mn hydroxides in the aqueous phase operates mainly through a combination of precipitation, adsorption, surface complex formation and ion exchange, making it one of the most scavenging solid phase among others (Singh et al., 1985; Tessier et al., 1987; Balistrieri et al., 2008). Hydroxylamine, oxalic acid and dithionite are the most commonly used reagents used for this phase to retain the metals in it. However, the efficiency of the reagent is determined by its reduction potential and its ability to attack the different crystalline forms of Fe and Mn oxyhydroxides (Anschutz et al., 2005). For instance, 1M hydroxylamine can be more useful in obtaining amorphous Mn hydroxide phase whereas 5M hydroxylamine gives an effective attack on Fe oxide phases during retention (Okoro et al., 2012). The bioaccumulation and complexation of metals is the major contributor of metals in the organic fraction of sediments (Zhang et al., 2014; Ali et al., 2019). In aqueous solutions, organic substances tend to have high degree of selectivity for individual ions compared to monovalent ions into the organic matter where Cu > Pb > Zn > Co (Giacalone et al., 2005; Okoro et al., 2019). This phase is well known for keeping the absorbed metals for a longer period of time unless the decomposition process is initiated under oxidizing conditions and degradation of organic matter (Giacalone et al., 2005). The most commonly used reagent for the extraction of metals in organic phases is hydrogen peroxide with ammonium acetate (Rodgers et al., 2015). The residual phase serves as a tool for long-term threat assessment of trace metals or toxic metals entering the aquatic environment. The metals in this phase are associated with the crystal lattice structure of minerals present in the sediments (Sundaray et al., 2011; Sarkar et al., 2014). To obtain such metals, complete digestion is required and strong acids like HF, $HClO_4$, HCl and HNO_3 work as very good reagents in such process (Okoro et al., 2012; Koki et al., 2015; Das et al., 2017).

The protocols provided by Tessier et al. (1979) are widely used to satisfy such purpose, and speciation is mainly achieved by the usage of appropriate reagents to the sediment samples. This protocol mainly employs the technique of speciation of sediments into exchangeable, carbonate, Fe-Mn hydroxide, organic matter, and residual-related geochemical fractions (Tessier et al., 1979). Reagents like magnesium chloride, sodium acetate-acetic acid, hydroxyl ammonium chloride, hydrogen peroxide and hydrofluoric perchloric acid are usually employed to retain the metals bound to various fractions with an additional procedure like agitation and heating for complete dissolution and retention (Davidson et al., 1994). The study with the Tessier scheme shows the best reproducibility, when obtained with the acid-soluble, reducible and residual fractions (Filgueiras et al., 2002). The long experimental procedure associated with this extraction provides more information about the distribution of a particular element over the chemical fractions. However, the use of $MgCl_2$ for exchangeable fraction sometimes causes a considerable matrix effect especially when the graphite furnace is used in analytical processing and increase of time and the amount of H_2O_2 added in the oxidizable fraction are needed when applying the Tessier scheme to organic-rich sediments (Dollar et al., 2001; Filgueiras et al., 2002).

Table 2.8 Critical case studies that employed extraction methods to assess the trace metals in estuarine sediments

Authors	Study area location	Extraction method	Findings
Global scenario			
Brayner et al., 2001	Capibaribe river estuary, Brazil	3-steps BCR sequential extraction method	The concentrations of exchangeable Mn suggest that the metal exists in a reduced form and oxidation of Mn much slower than Fe. concentration values of transition metals like Zn, Cr, Mn and Fe in the natural waters indicate low bioavailability and counterbalance is noted for anthropic release by scavenging mechanisms.
Wepener et al., 2005	Richards bay harbour, South Africa	Tessier sequential extraction	Mn and Zn had more than 50% of this concentrated in the easily reducible fractions. More than 70% of Cr was concentrated in the inert fractions nevertheless concentrations recorded at some sites were still above action levels when considering only the bioavailable fractions.
Rosado et al., 2016	Huelva estuary, Spain	BCR and Tessier	The metal extracted at the highest percentage and most bioavailable metal

		sequential extraction	available is Cd, followed by Zn, Mn, Cu, Pb, Ni, Cr and Fe
Barrio et al., 2018	Mediterranean estuarine system	Tessier sequential extraction	Co and Mn fractionation and bioavailability were controlled by the environmental conditions generated by the advance of seawater into the estuarine system during high tide. Co in Fe and Mn hydroxides is due to soils suffering catalyst spills or direct sludge disposal. The prevailing effect of pH in the fractionation of Co and Mn in this estuarine environment. Co and Mn pose medium to high risk in case of bioavailability according to the fractionation.
He et al., 2019	Yangtze river estuary, China	Modified Tessier sequential extraction	The sequential extraction results suggest that most of these trace metals (Zn, Cu, Ni, Pb, Cr) except Cd, are bound in the geochemically inert residual fractions, and primarily determined by the Changjiang input from natural weathering sources.
Ben et al., 2019	Meliane river and Rades-Hamam life coast, Tunisia	Modified Tessier sequential extraction	Metal like Cd is dominant in the exchangeable fraction of sediments and has high potential bioavailability. Cr and Cu were mostly bound to the residual fraction indicating their low toxicity and bioavailability.
Sakan et al., 2020	Kupa river, Croatia	BCR sequential extraction technique	Most of the elements were considered to be immobile due to the high availability in the residual fraction. Pb was present mainly in the reducible fraction, while more easily mobile and bioavailable forms were predominant for Cd and Ba.
Pavoni et al., 2021	Karstic Timavo river estuary, Italy	Modified Tessier sequential extraction	Sulfate-reductive state of the bottom saltwater causing potential anoxia at the sediment-water interface, driving trace element accumulation in the residual fraction of the sediments.
National and regional scenario			
Nemati et al., 2011	Buloh river, Malaysia	BCR sequential extraction	Dominant proportion of Co found in organic fraction. Zn and Pb mainly controlled by Fe-Mn oxyhydroxides. Major proportion of Cd obtained from exchangeable fraction and possess highest rick among all the elements.
Idriss et al., 2012	Juru river, Malaysia	BCR sequential extraction technique	Concentration of Cu, Cd and Pb are higher in residual fraction followed by organic fraction. Change in concentration of organic matter and pH of sediment responsible for increase in concentration of Cu and Pb whereas percentage of Cd is higher in exchangeable fraction than Cu and Pb.

Ghazali et al., 2016	Brunei bay, Borneo	Tessier sequential extraction	Monsoon and anthropogenic source are the major controllers of distribution of metals. Al, Fe and Pb in Brunei Bay sediment were dominantly bound to the mineral fraction which is also an indicator of natural source. Cu was more dominant in the ion exchangeable fraction which is the most bioavailable fraction. Fe and Pb are in low-risk category as per RAC and Cu is in high-risk category.
Prabakaran et al., 2019	Baram river estuary, Borneo, Malaysia	Tessier sequential extraction	Fe-Mn oxides and the organic-bound fractions greatly controls the mobility of all the trace metals. Higher concentration of Mn in the exchangeable fraction was observed. Cu was found in high concentration mainly in the organic bound fraction irrespective of seasonal and redox condition changes. Reason behind such was noted to be dredging activities, which stimulates the release of Cu into the overlying waters of the Lower Baram River.
Hing et al., 2020	Terengganu river estuary, Malaysia	3-steps BCR sequential extraction method	The highest concentration of Co, Cu, and Zn reside in the residual fraction. However, a bioavailable fraction like an exchangeable fraction has 2nd highest amount of the 3 metals.

2.8 Tropical riverine influence on Coral reefs

Rainfall and seasonal variability in river flow are the major components that push the contaminants from the estuarine system to the coastal system which affect the coastal environments such as coral reefs. In the case of tropical rivers, variability is modulated by El Niño –Southern Oscillation (ENSO) events and the Pacific Decadal Oscillation (PDO) (Lough et al., 2007). With high variability in rainfall between seasons, the magnitude and extent of freshwater river flood plumes increase and push more terrestrial materials towards the coastal region (Lough et al., 2015). Such flood plumes were observed to have a significant impact on the Great Barrier Reef (GBR) (Lough et al., ,2007; Lough et al., 2015). Similar impacts have also been noticed in the case of the Miri-Sibuti coral reef region as well by Krawczyk et al. (2020), where terrestrial materials were pushed forward with the influence of PDO. Apart from this, these river run-offs or plumes are generally influenced by Coriolis effect, which is a deflection of water caused by a rotation of the earth. This deflection is to the left in the southern hemisphere and to the right in the northern hemisphere. Therefore, river plumes

generally move northward as a geostrophic, density current and mix with oceanic water eventually (Devlin et al., 2001). During high flow conditions, inshore ecosystems like rivers experience the highest concentrations of dissolved nutrients throughout the year. Suspended sediment concentrations and particulate nutrients are high at these times though higher loads may be generated by resuspension of inshore sediments (Woolfe et al., 1998).

Such terrestrial inputs usually affect the water quality and clarity of the coastal environment. The discrepancy of water clarity or turbidity mainly impacts the resources for photosynthetic organisms living in the coral system (Anthony et al., 2003; Fabricius et al., 2014). It has been clearly established that this turbidity is a major effect of sediment resuspension from shallow shelves mainly contributed by river system by terrestrial run-off (Storlazzi et al., 2009; Brodie et al., 2012; Fabricius et al., 2013). The shore currents are capable of transporting the particulate loads such as silt, clay, plankton and organic-rich sediment flocs for tens to hundreds of kilometers northwards away from the river mouths, and typically remain initially within ~5 km off the coast (Bainbridge et al., 2012). After these particles are dissipated, they undergo repeated resuspension and deposition process (Wolanski et al., 2008; Storlazzi et al., 2009; Kroon et al., 2012). Due to such effects, turbidity is measured 43% higher during higher river run-off and takes weeks to years to neutralize in the GBR region (Fabricius et al., 2013). These plankton blooming in coral reefs develop in response to the detritus run-off from rivers nutrients, iron and other trace elements released from sediment resuspension through the seabed (Walker et al., 1981; McKinnon et al., 1993; Smith et al., 2009; Kroon et al., 2012; Orpin et al., 2012; Fabricius et al., 2014). This effect usually neutralizes in 3 mechanisms such as gradual transport of suspended particles to deeper self of sea or ocean where resuspension will require higher wave or energy, the gradual decline of plankton biomass after depletion of nutrients and trace metals, and sediment compaction and break down of organic flocs (Lambrechts et al., 2010; Fabricius et al., 2014). Other than that, clay particles, and TSS have a higher tendency to travel further into the sea and affect the coastal turbidity compared to large grain sediments where these particles are major carriers of nutrients and trace metals in river estuaries due to higher cation exchange capacity, less particle size, and higher charge density (Douglas et al., 2006; Lewis et al., 2013). The fresh discharge of these materials is organically more enriched and has a higher

tendency to go through resuspension than the traditional seafloor sediments (Van et al., 2014; Seers et al., 2015).

Table 2.9 Literature summary of riverine influence on coral reefs in the tropical region

Authors	Study area location	Findings
Global scenario		
Fabricius et al., 2014	Central GBR region	Predominantly terrigenous sediments accumulated particular downstream of Burdekin river and the fine river-derived sediments remain available on the seabed for resuspension for years after floods. Turbidity rose 43% higher after the monsoonal run-off of rivers.
Fabricius et al., 2016	GBR region, Australia	Expanding agricultural development of the GBR catchments, river sediment and nutrient supplies to the GBR have markedly increased since European settlement. Water clarity in this high-risk GBR region is strongly determined by these river nutrient and sediment loads.
Hwang et al., 2018	Danshui estuarine influenced region, Taiwan	Higher concentrations of Zn, Cd, Cr and Pb at the lower and inner reef areas are explained by the likely higher ambient metal contents in these areas that were polluted by river run-offs from Danshui estuary.
Heery et al., 2018	Coral assemblages in East and South-east Asia	Corals and coral reefs near coastal cities are subject to a suite of intense stressors. Sediment pollution constrains urban reefs to shallow depths and limits complexity. Species diversity near Jakarta, Indonesia are closely tied with water quality, as inshore sites influenced by terrestrial inputs such as higher turbidity, mean temperature, pH, dissolved oxygen, and chlorophyll-a concentrations. In Hong Kong, freshwater inputs from the Pearl (Zhujiang) river is the major contributor of marine contamination, nutrient enrichment, and elevated sedimentation rates. In Japan, coral diversity tends to be particularly low (<20%) near river outputs. The input of nutrients and pollutants such as endocrine disrupters and bisphenol A (BPA) to coastal waters by rivers in southern Okinawa is responsible for it.
Cybulski et al., 2020	Greater bay area, China	Output from resource extraction, agricultural outputs destructive, trace metals, and riverine driven turbidity from through influx of eutrophic water from the Pearl River are the major stressors of the Coral system.
National and regional scenario		
Moollye, 2017	**Miri-Sibuti coral reefs (MSCR), Sarawak and Coral reefs in Sipadan, Sabah**	Turbidity in Miri-Sibuti coral reef region found associated with nutrients like NO_3^-, NH_3 and trace metals such as Co and Cu. This nutrients and trace metal flow are mainly contributed by local rivers during monsoonal flow. Heavy sedimentation was also found in this region as a major stressor. In Sipadan, corals were healthier as compared to MSCR due to limited terrestrial freshwater flow into

		it. Trace metals like Cd, Co, Pb and Co are below detection levels.
Browne et al., 2019	**Miri-Sibuti coral reefs, Sarawak, Malaysia**	Strong inshore to the offshore gradient in hard coral cover, diversity and community composition as a direct result of spatial differences in sediment at distances <10 km. Seasonal differences are responsible for higher bioerosion rates, which increased five-fold after the wet season.
Krawczyk et al., 2020	**Miri-Sibuti coral reefs, Sarawak, Malaysia**	Seawater around Miri is influenced by the balance between precipitation and evaporation (the P-E balance), and freshwater runoff. So, local precipitation near the coast and local river discharges have significant control over hydrological balance in reef waters.

*Studies related to the current study area are marked in bold

2.9 Summery

The Northern region of Sarawak region in Malaysia has gone through rapid industrialization over the last few decades and will continue to grow in such manner into the distant future. This has attributed vastly to practices of increased land use over this period of time. Concurrently, subsistence and agro-industrial agriculture accounted for more than 23% deforestation in this region since 1973. This has been accompanied by 65,000 km^2 palm oil plantation during 2010. Such activities have paved way for significant increase in geological processes such as physical and chemical weathering aided by high seasonal rainfall in the region. Being in this region, Sibuti river basin has gone through such transformation over the same period and draining around 1020 km^2 of basinal area while bringing in weathered sediment and suspended solids into the riverbed. This basin is highly agriculture-prone where extensive use of fertilizers is a common practice for increased agricultural outputs. So, the river stream might be carrying natural, agricultural, domestic or industrial affluents with it which are rich in nutrients and contain high trace metals. Such discharge usually interferes gradually with the health of riverine and estuarine ecosystem and is a threat to the aquatic biota surviving in it. Once these terrestrial constituents are delivered to South China Sea through driving agents like water and sediments, they can profoundly impact the coastal ecosystems such as the coral reefs.

As the literature elucidates, estuaries has been a focal point around to the world because of its variable and complex nature due to tidal and riverine influence from both ends. It works as a reservoir for riverine-based pollutants and entry point of these contaminants into the coastal ecosystem. Although significant outlines are available

on various river and estuarine systems around Malaysia, only limited studies on nutrients and physico-chemical changes have been conducted on the Sibuti river estuary in the past (Table 2.2). A huge research gap exists in case of assessment of the contaminants in Sibuti river estuary in regard to both water and sediments. Hence, an attempt has been made here to assess the ionic composition, quantification of nutrients and trace metals in water, along with quantification of the trace metals in sediments and suspended solids. This will answer the suitability of water for human consumption and agricultural usage whereas risk assessment of trace metals in sediment and suspended solids will be done to assess the impact on aquatic biota. The nature and behavior under estuarine environment and bioavailability of trace metals sequential extraction technique has been employed. The study will help to identify the sources of contaminants and their controlling factors in the river and estuary. This will also help to draw some outlines regarding the influence of this river on the coastal ecosystems such as Miri-Sibuti coral reefs.

Chapter-3

Methodology

3.1 Introduction

The monsoonal or seasonal rainfall and associated weathering contributes major chemical and physical changes in river system and estuary. Assessing such inputs, their associated parameters and changes in the estuarine system is the main focus of this study and is limited to the river estuary. On the other hand, tidal water in estuaries are the major short term influencers of spatial and chemical changes due to the intrusion of saline water from the sea and are helpful in demarcate the boundary of estuaries. Thus, high tidal conditions were taken into consideration during preliminary study. During sampling process, observed tidal conditions were noted to assess their influence on riverine constituents during both seasons.

3.2 Preliminary study and sampling strategy

An estuary is an area where freshwater from the river meets the seawater, where high tide and low tide play major roles in the advancement and retreat of saline water into the river system. In such system, coastal wetlands such as mangrove and Nipa palm (Mangrove palm) swamps are usually found because of their tendency to survive in both salt and fresh water especially in tidal regions (EPA, 2016; Armitage, 2014). In order to differentiate the boundary of such system from the river and identify the seawater influence, salinity of water and extent of mangroves generally work a determinator. In current study area, preliminary study was conducted 14th of June, 2017 during the high tide (Fig. 3.1) and salinity was analyzed and used as a key parameter to determine the influence of seawater in the river (Fig. 3.2). The extent of mangroves present near the bank of the river was helpful in determining the maximum reach of the saline water in the river. By combining both the factors, borders of the estuary have been drawn and was identified to be extending up to 30-35 kms towards the upstream direction starting from the mouth (Fig. 3.2). The increase and decrease of water during high and low tide time can be clearly visible at the riverbank through the influenced region and the photographic evidence are presented in fig. 3.7. Along with that, major tributaries, agricultural input channels and meandering points were also identified and marked during the preliminary studies.

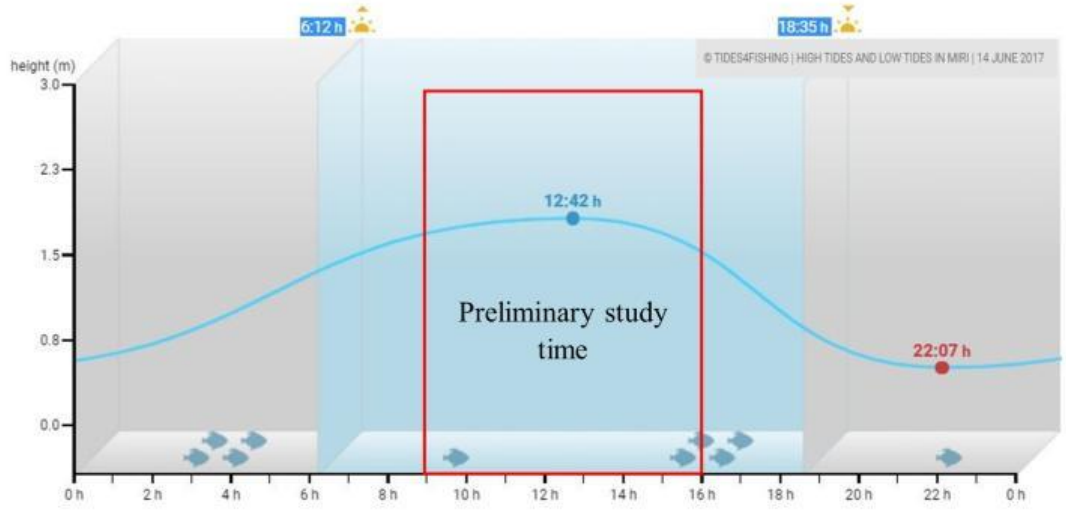

Fig. 3.1 High tide time considered for preliminary study to identify the salinity boundary (Source: https://tides4fishing.com/as/malaysia/miri)

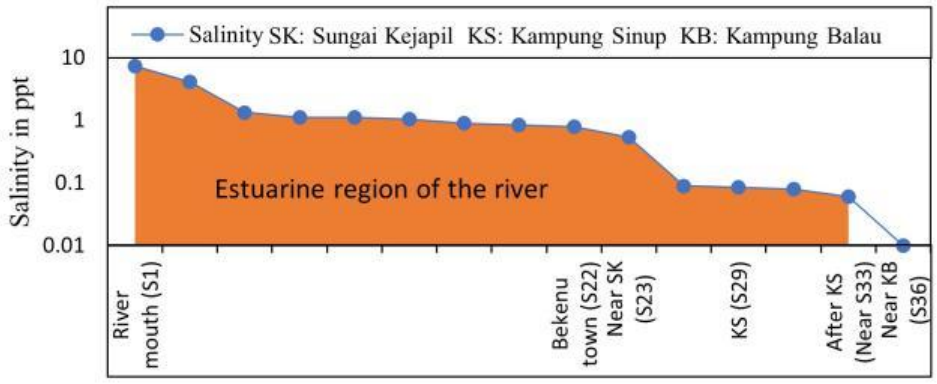

Fig. 3.2 Determined estuarine boundary during preliminary studies (Salinity stations are in accordance with Fig. 1.4)

3.2.1 Practical difficulties during sampling

The width of the river is considerably more near river mouth and becomes narrower towards Bekenu. The width further narrows down after Bekenu and station near Sungai Kejapil (Stations 23; Fig. 1.4). In such conditions, the presence of dense mangroves and mangrove palm (Nipa palm) near the bank of river makes it difficult to collect the sediment samples. Similar conditions persists in case of river meandering and small agricultural channels near the bank. Materials such as plant roots and garbage were mainly obtained through grab samples rather than usable bottom sediments. So, the samples were collected at the middle of the river at all the stations. The availability of larger boats (recommended for study) in the study area is limited to Kampung Kuala Sibuti and Bekenu town. But these larger boats are not suitable in case of small agricultural channels present near the bank. In addition, the presence of small walking bridges near Kampung Sinup and Kampung Balau makes

is difficult of larger boats to pass through especially during high tide. So smaller boats with capacity of carrying maximum 3 persons or 2 persons and very limited instruments and samples were hired from these villages and utilized to do the preliminary study and sampling during such conditions. The presence of crocodiles in the river is very common and it is not recommended to enter the river water even near the bank. For instance, two crocodiles were observed at the riverbank between Kampung Sinup and Kampung Balau during the sampling process, which made agricultural channels and riverbank nearby inaccessible for collection of water and sediments.

3.3 Sample Collection

Sampling was carried out for two monsoon seasons during 2017 and 2018 using a fiber boat. The 1st sampling was carried out on 25th and 26th of August during SW monsoon (May to September), when the rain was milder, whereas the 2nd sampling was done on 14th and 15th of February 2018 during NE monsoon (November and March). The details of rainfall data during sampling seasons is given in Table 1.1. During SWM, 1st day sampling (25th August 2017) was done during high tide time in the lower part of the estuary and 2nd day (26th August 2017) sampling was done during low tide in the upstream region of the estuary (Fig. 3.4). However, during NEM, the 1st day (14th February 2018) sampling was done during the transition from low to high tide near the mouth region, whereas sampling was carried out under similar conditions in upstream region of the estuary (Fig. 3.5).

The water (surface; n=36 for each season), and sediment samples (riverbed; n=36 for each season) were collected at the regular internal (at least 1 km) by considering the following aspects, such as influence of tributaries, evidence of anthropogenic activities, meanders/major turnings, etc. These stations are segregated in groups and shown in fig. 3.3 according to their influencing factors.

In addition, ~20L of water samples were collected to quantify the suspended solids at different location at the interval of at least 10km between the samples (i.e., 5 samples in each season). The interval has been considered to identify the changes occurring in the suspended solids amount and its constituents with respect to the river, its tributaries and influence of tides in relation to the resuspension of the sediments along the estuary and various geochemical processes.

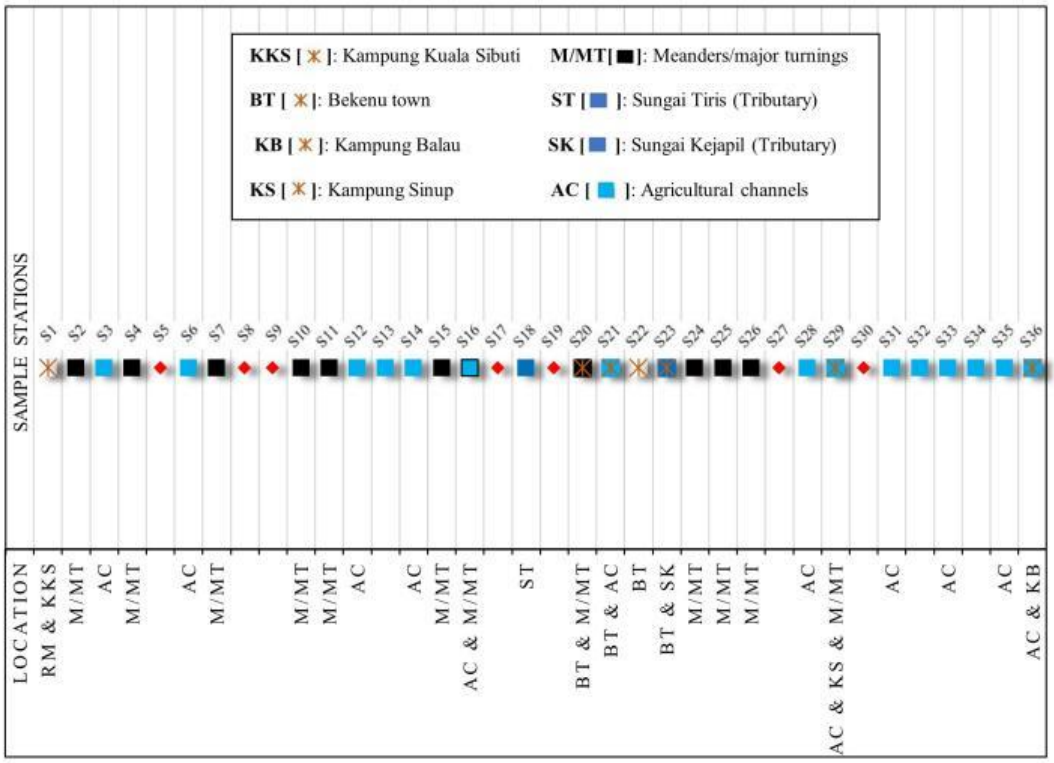

Fig. 3.3 Sample locations situated near various influencing factors in accordance with Fig. 1.4

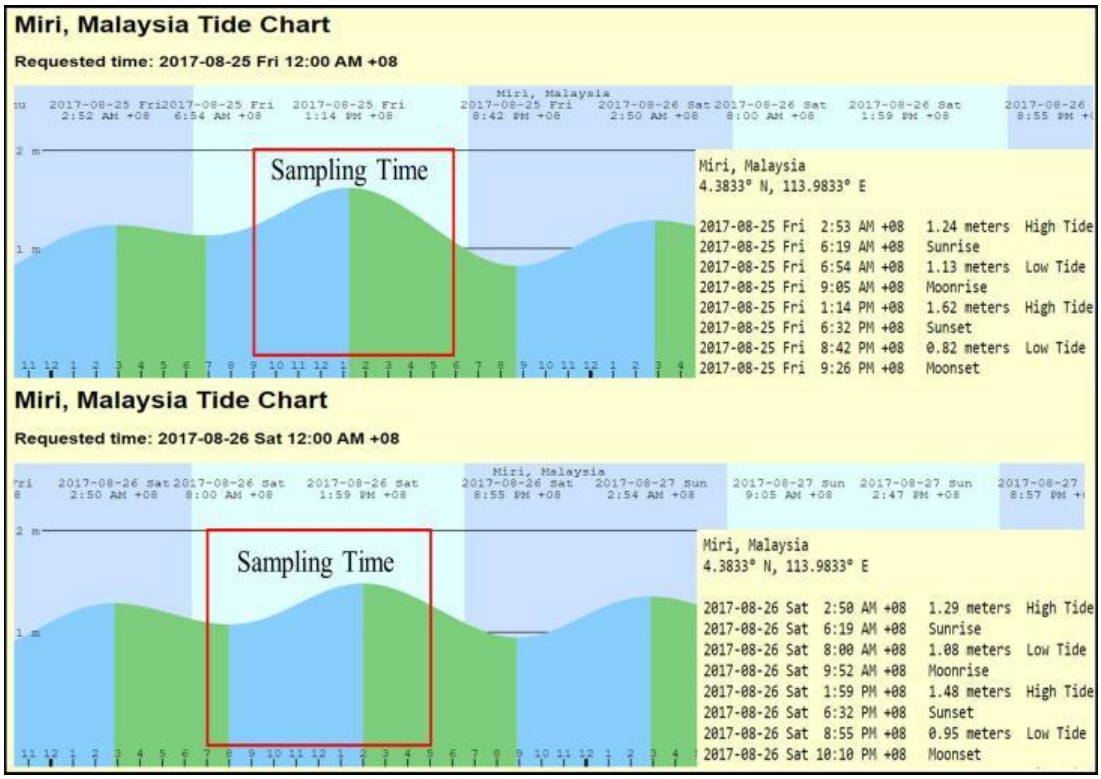

Fig. 3.4 Tidal conditions and sampling time details during SWM (Source: https://tides4fishing.com/as/malaysia/miri)

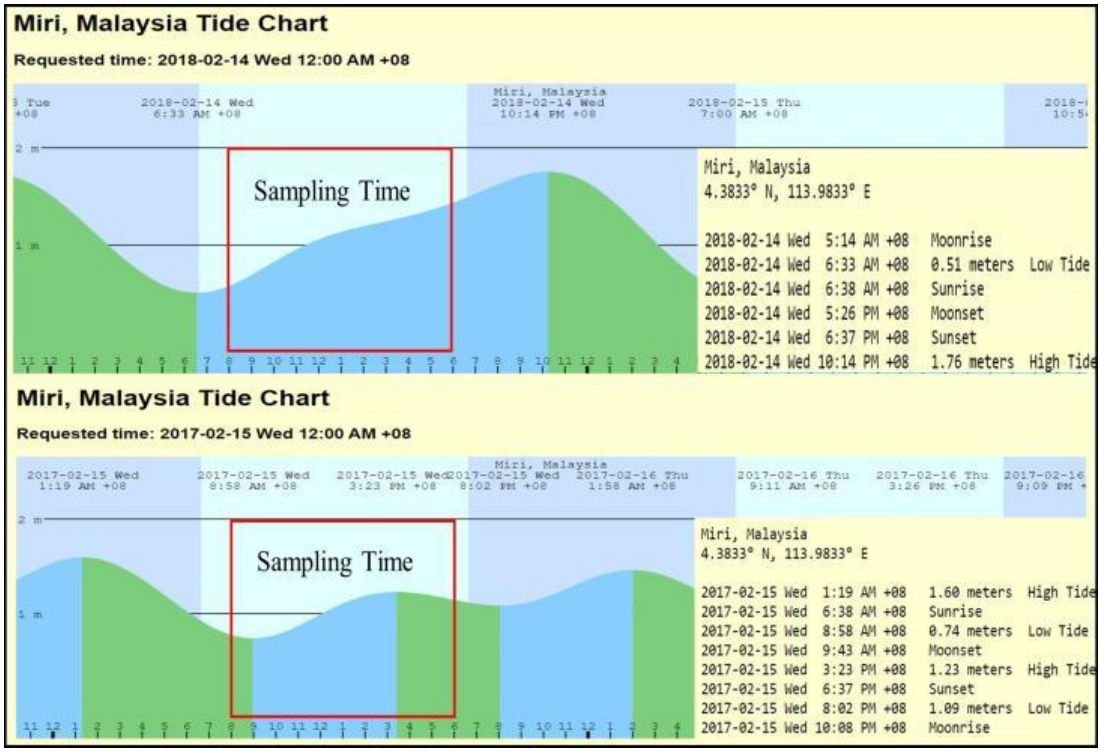

Fig. 3.5 Tidal conditions and sampling time details during NEM (Source: https://tides4fishing.com/as/malaysia/miri)

3.3.1 Water sample collection

Three liters of water samples were collected in 3 clean polyethylene sample containers with depth reaching a maximum of 1-2m at every point. All three liters of water was filtered with 0.45µ Whatman filter paper and suspended solid amount (TSS) collected per liter of water through filtration was recorded for each station. The first bottle of water was used for nutrient (SO_4^{2-}, PO_4^{3-}, NH_3, NH_4^+, NO_3^-, NO_3-N) analysis. The second bottle of water was used for the measurement of various major ion concentrations in water such as Cl^-, CO_3^-, HCO_3^-, Ca^{2+}, Mg^{2+}, whereas the third bottle of water was acidified to pH < 2 for determination of trace metal- Na^+ and K^+ concentration in water using nitric acid (30%). These samples were stored in a refrigerator at 4°C until further processes such as digestion and trace metal analysis using Flame Atomic Absorption Spectroscopy were conducted (Perkin Elmar A Analyst 400).

3.3.1.1 Field measurements (On-site)

Physico-chemical parameters such as pH, temperature, Electrical Conductivity (EC), Total Dissolved Solids (TDS), salinity, turbidity and Dissolved Oxygen (DO) were measured in situ in the field. Amongst the parameters, pH, temperature, EC, TDS and

DO were measured using respective probes in Lovibond meter. Turbidity of the water was measured with turbidity meter and Hach salinity probe and meter was used to measure the salinity. Apart from this, flow meter was used to measure the velocity of water at all the sampling locations. The depth of velocity measurement was kept 3-4 meters (maximum reach of Flow meter).

3.3.2 Sediment sample collection

Meanwhile, bed load sediments were collected using grab sampler and stored in a plastic container and sealed to avoid any contamination. The sample numbers were recorded on the container with starting number from the river mouth of Sibuti river and moved upstream. The central portion of the grab samples was considered to avoid the contamination from the wall of the sampler. The sampler was washed on the river water before and after the sampling at each location and followed throughout the sampling. The sediment samples were collected at the middle of river at each station. In addition to that, specific depositional areas such as meandering points, presence of tributaries and settlements were preferred for the collection of the samples along the estuary (Fig. 3.3).

3.3.2.1 Sediment sample preparation

These samples were brought to the laboratories and dried in oven at 60°C. The dried samples were homogenized using a stone mortar and pestle. Meanwhile, the roots, leaves, gravels and other anthropogenic/natural vegetable matters were removed manually. The samples were sieved for particle size analysis where 250, 125, 75 and 63 µm trays were used. The samples below 63 µm were stored for further digestion to analyze trace metal.

3.3.3 Suspended solid sample collection

To get the suspended solids in a good amount, 20 liters of water samples were collected from 5 locations with an interval of 10 km starting from the river mouth. The samples were stored for some weeks to settle the suspended solids down. Once they were settled, the upper half of the water layer was pumped out from the container using a small submersible pump without disturbing the lower half of the tank and filtration through 0.45-micron filter paper was done using a vacuum pump. The water in the lower half of the container was subjected through centrifuge to extract the settled

suspended solids. The samples were dried at 60°C to remove the water content, weighed and stored for trace metal analysis using the Flame Atomic Absorption Spectroscopy (Perkin Elmar A Analyst 400) after the digestion.

3.4 Sample digestion and analysis

3.4.1 Water sample digestion and analysis

The stored water samples after acidification were digested using acid digestion method 3005A (USEPA, 1992), where HNO_3 and HCl were used as main reagents for digestion. This digestion was done for the analysis of Na, K and metals such as Co, Cu, Mn, Pb, Zn, Se, Fe, Al, Cd, Cr and Ba in water. The protocols adopted for analysis of physico-chemical parameters, nutrients, major ions and trace metals are as follows.

Table 3.1 Methodology overview of water samples

Category	Parameter	Method	Instrument
Physico-chemical Parameters	pH Temperature Electrical Conductivity Total Dissolved Solids	-	pH meter (Lovibond Sensodirect 150 Meter)
	Salinity	-	Salinity Probe (Hach, HQ 4000 Portable meter)
	Velocity	-	Valeport current flow meter
	Turbidity	-	Turbidity meter (LAMOTTE 2020)
	Dissolved Oxygen	-	DO probe (Hach, HQ 4000 Portable meter)
	CO_2	Titration (APHA, 1998)	-
Cations and Anions	Calcium (Ca^{2+}) Magnesium (Mg^{2+}) Chlorine (Cl^-) Bicarbonate (HCO_3^-) Carbonate (CO_3)	Titrimetric method (APHA, 1998)	-
	Sodium (Na^+) Potassium (K^+)	-	Flame Atomic Absorption Spectroscopy (Perkin Elmar A Analyst 400)
Nutrients	Nitrate (NO_3^-) Nitrate-Nitrogen ($NO3^-$-N)	Cadmium Reduction Method LR	UV Spectrophotometer (DR 2800)

Nutrients	Ammonia (NH_3) Ammonium (NH_4^+)	Salicylate Method	
	Sulfate (SO_4^{2-})	SulfaVer 4	
	Phosphate (PO_4^{3-})	PhosVer 3 (Ascorbic Acid) Method	
Trace Metals	Digestion of water samples	Acid digestion method (USEPA, 1992)	-
Trace Metals	Aluminum (Al) Barium (B) Chromium (Cr) Manganese (Mn) Iron (Fe) Cobalt (Co) Copper (Cu) Zinc (Zn) Cadmium (Cd) Selenium (Se) Lead (Pb)	-	Flame Atomic Absorption Spectroscopy (Perkin Elmar A Analyst 400)

3.4.2 Sediment digestion and analysis

Sieving analysis was performed for each of the samples considering the sieving pans of various particle sizes, such as 63, 75, 125, 150 and 250 microns. The sediments collected in the pan with < 63 microns were used to perform sequential analysis (Tessier et al., 1979) to extract the distribution of metals in sediments of various fractions. However, the 5th fraction digestion was done by Perkin Elmer Titan MPS Microwave digestion system following guidelines provided by Perkin Elmer. The process used 2ml of 49% Hydrofluoric acid (HF) and 6.6ml of 35% Hydrochloric Acid (HCL) to digest 200 mg of each sample. The solution of HF, HCL and samples were contained in high-pressure 100ml digestion vessels and subjected to following the temperature (Table 3.2) and pressure setting in the instrument. After the digestion, 2ml of Boric acid (H_3BO_3) was added into the digested solution and heated using hotplate until visible white fumes appeared to remove the excess HF. Later, the solution was diluted with ultrapure distilled water and made into 100ml for further analysis.

Table 3.2 Instrument settings adopted for sediment digestion using Titan MPS Microwave Digester

Step	Target Temperature (°C)	Pressure Limit (bar)	Ramp Time (min)	Hold Time (min)	Power (%)
1	170	60	5	5	80
2	210	60	3	20	100
3	50	60	1	30	0

All the digested sediment samples of 5 fractions were subjected to analysis of trace metals using Perkin Elmar A Analyst 400 (Table 3.3).

Table 3.3 Methodology overview of sediment samples

Category	Parameters	Method	Instrument
Particle size analysis		-	Sieving Machine
Sediment digestion	Fraction 1-4	Sequential Extraction (Tessier et al., 1979)	Orbital Shaker Hettich Centrifuge 320 R Memmrtz Water Bath Memmrtz Oven
Sediment digestion	Fraction 5	Microwave digestion	Perkin Elmar Titan MPS Microwave Digester
Analysis of trace metals	Al, Cr, Mn, Fe, Co, Cu, Zn, Cd, Ba, Se, Pb		Flame Atomic Absorption Spectroscopy (Perkin Elmar A Analyst 400)

3.4.3 Suspended solid digestion and analysis

In order to analyze the bulk chemistry in the suspended solids, the digestion process adopted for 5th fraction was applied and the same instrument such as Perkin Elmer Titan MPS Microwave digestion system and Flame Atomic Absorption Spectroscopy (Perkin Elmar A Analyst 400) were used for digestion and trace metal analysis (Table 3.4).

Table 3.4 Methodology overview of suspended solid samples

Parameters		Method
Trace metals	Al, Cr, Mn, Fe, Co, Cu, Zn, Cd, Ba, Se, Pb	Perkin Elmar Titan MPS Microwave Digester and Flame Atomic Absorption Spectroscopy (Perkin Elmar A Analyst 400)

3.5 Accuracy and precision of analysis

3.5.1 Apparatus and reagents

All glassware and plastic containers that were used during analysis were rinsed properly using 20% HNO_3 and distilled water. The reagents used in the experiments were bought from Merck (Darmstadt, Germany) and Fisher Scientific and were of analytical grade. The Safety Data Sheet for all the chemicals was filled thoroughly according to the guidelines provided by the Merck or Fisher Scientific. This was done for all the chemicals prior to the lab works that were conducted. The wastes produced by the chemicals in labs were disposed of according to Curtin University, Local State and Federal Regulations.

3.5.2 Standard solution for metal analysis

The standard solutions (1000ppm) used for the calibration of Perkin Elmer A Analyst 400 were purchased from Perkin Elmer. These solutions were used to prepare the standard sub-stock solutions of 100 ppm and 10 ppm using 2% HNO_3 and pure water according to recommended instructions. The sub-stock solutions were further diluted to prepare standards according to the need of limit required for each element to be calibrated and analyzed using the instrument. Normally, 4 to 5 standard solutions were prepared for each element for calibration using 100ppm and 10ppm solutions.

3.5.3 Calibration of Atomic Analyst 400

For the accuracy of Atomic Absorption Spectrometer, calibration curves were obtained first using the standards prepared from the stock and sub-stock. These standard curves were obtained before the analysis of water and sediment samples. One preliminary analysis was also done prior to the analysis to check the limits of concentration of metals in the samples and the range was adjusted according to the need depending on the obtained results. The correlation co-efficient (R^2) for each metal was determined from the calibration curve and made sure that it was above 0.995 to ensure reliable results. To ensure the stability in accuracy of results, Quality Check (QC) was done with every 20-sample interval for all the standards. The specific instrument conditions used for metal analysis can be obtained from Table 3.5.

Table 3.5 Instrument conditions of AAS for various elements as per Perkins Elmar recommendations.

Element	Wavelength (nm)	Char. Conc (mg/l) [a]	Sensitivity Check (mg/l) [b]	Linear Range (mg/l) [c]	Slit Width (nm)	Oxidant	Oxidant Flow (L/min)	Acetylene/N_2O Flow (L/min)	Light Sources (Lamp) [d]
Co	243.58	0.4	20	-	1.8/1.35	Air	10	2.5	HCL
Cd	228.80	0.01	0.5	1	2.7/1.35	Air	10	2.5	EDL & HCL
Cu	216.51	0.15	6.5	6.5	1.8/1.35	Air	10	2.5	HCL
Fe	346.59	3.6	180	-	1.8/0.6	Air	10	2.5	HCL
Pb	283.31	0.18	8	10	2.7/1.05	Air	10	2.5	EDLs & HCL
Mn	279.83	0.016	1	0.6	1.8/0.6	Air	10	2.5	HCL
Zn	213.86	0.006	0.3	0.75	2.7/1.8	Air	10	2.5	HCL
Se	196.03	0.3	15	100	2.7/2.3	Air	10	2.5	HCL
Al	309.27	1.1	50	100	2.7/0.8	N_2O	6	7.5	HCL
Cr	357.87	0.078	4	5	2.7/0.8	N_2O	10	3.3	HCL
Ba	553.55	0.46	20	20	1.8/0.6	N_2O	6.2	8.2	HCL
Na^+	330.24	0.9	45	-	2.1/0.8	Air	10	2.5	HCL
K^+	404.41	4	180	300	2.7/0.6	Air	10	2.5	HCL

[a] Characteristic Concentration is the minimum absorbance value of the instrument.

[b] Sensitivity check is the concentration giving approximately 0.2 absorbance unit (AU)

[c] Linear range is the maximum absorbance value of the instrument

[d] Light source is the Electrode Cathode Lamps (EDL) and Hollow Cathode Lamp (HCL)

3.6 Ecological risk assessment of sediments and suspended solids

Ecological risk assessment of sediments and suspended solids was done by classifying trace metal concentration into various pollution indices, such as Geo-accumulation index (I_{geo}) (Muller et al., 1969), Enrichment Factor (EF) (Bloundi et al., 2009), Contamination Factor (CF), Pollution Load Index (PLI), and Potential Ecological Risk Index (PERI). These indices are proven to be able to identify risks posed by various elements in the aquatic sediments and SS (Elias et al., 2018; Vu et al., 2018).

3.6.1 Geoaccumulation index (I_{geo})

Geo-accumulation index (I_{geo}) was developed by Muller (1969) and is usually applied to assess the status metal concentrations by comparing the current concentration and pre-industrial background concentration of the metal (Elias et al., 2018). The quantification of the degree of metal pollution in sediments is done according to the formula proposed by Muller et al. (1979) and can be represented as follows:

$$I_{geo} = log_2 \left[\frac{C_n}{1.5 * B_n}\right] \text{.....(eq. 3.1)}$$

Where 'C_n' is identified as the concentration analyzed metal 'n', and B_n represents the background concentration of the continental crustal average of the metal (PAAS Value) (Taylor & McLennan, 1985, 1995; McLennan, 2001) for sediments, while world metal average concentration of riverine suspended solids (Viers et al., 2009) is used. The 1.5 factor was introduced to minimize the effect of possible variations in the continental crustal average values, which may occur due to the influence of lithological variations and anthropogenic effects (Zahra et al., 2014; Elias et al., 2018).

Table 3.6 Sediment and suspended solid quality guidelines for I_{geo} index

I_{geo} Values	Quality guidelines
< 0	Uncontaminated
0-1	Uncontaminated to moderate contamination
1-2	Moderately contaminated
2-3	Moderate to strong contamination
3-4	Strongly contaminated
4-5	Strong to extreme contamination
> 5	Extremely contaminated

3.6.2 Enrichment factor (EF)

The metal concentration in sediments is primarily the part of their natural constituents depending upon the parental materials (Barbieri et al., 2016). In recent years, it has been noticed that these metal concentrations are increasing with the influence of various anthropogenic activities such as the distribution of fertilizers, pesticides, industries, waste disposal and air pollution. This effect is increasing the selected metal's concentration above the safe threshold standards, leading to the release of

these metals into the environment under various environmental conditions and poses a significant potential environmental threat to the health of people and animals living around such environments (Taylor et al., 2010; Barbieri et al., 2016). To measure such parameters above the threshold values and determine the enormity of anthropogenic influence on the aquatic sediment's enrichment factor, EF is used as a tool. In the current study area, Al is used as a normalization element because of its lithospheric origin and its compensation towards granulometric and mineralogical effects (Ho et al., 2012). The PAAS values (Taylor & McLennan, 1985, 1995; McLennan, 2001) and world metal average concentrations on suspended solids (Viers et al., 2009) were considered as background values in the calculation to determine this factor. Enrichment factor is calculated based on the formula (Szefer et al., 1998) as follows:

$$EF = \left[\frac{\left(\frac{C_n}{RE}\right)_{Soil}}{\left(\frac{B_n}{RE}\right)_{Background}}\right] \text{.....(eq. 3.2)}$$

Where n represents the considered element and RE represents the adopted referenced element (Al).

The values deduced for EF is as per Sutherland (2000), and a detailed sediment quality classification depending on enrichment levels is described in Table 3.7. Depending on the EF values of each element, the origin of these metals can be explained easily where EF values between 0.5 to 1.5 are assumed as the result of natural weathering, whereas values above 1.5 indicate the mixing of significant portions of metal from non-crustal sources like point and non-point pollutants (Barbieri et al., 2016).

Table 3.7 Sediment and suspended solid quality guidelines for EF

EF Values	Sediment quality
EF < 2	Deficiency to minimal enrichment
2< EF <5	Moderate enrichment
5< EF <20	Significant enrichment
20< EF <40	Very high enrichment
EF > 40	Extremely high enrichment

3.6.3 Contamination factor (CF)

The contamination factor (CF) can be described as the contamination of a toxic substance in a given environment and is an effective method to determine the effect of pollution (Özkan et al., 2012; Hakanson et al., 1980). It is determined by considering the ratio of considered elemental concentration to the pre-industrial reference value of the element.

$$CF = \frac{C_n}{B_n} \text{.....(eq. 3.3)}$$

Where C represents the measured concentration of element n, and B represents the PAAS value of the respective element given by Taylor and McLennan (1985, 1995) and McLennan (2001) for sediments. In case of suspended solids, world metal average concentrations on suspended solids given by Viers et al. (2009) were used as B_n values.

Table 3.8 Contamination standards as per Hakanson et al. (1980)

CF Values	Contamination levels
CF<1	Low contamination
1<CF<3	Moderate contamination
3<CF<6	Considerable contamination
CF>6	Very high contamination

3.6.4 Pollution load index (PLI)

The pollution load index (PLI) is used to evaluate the pollution levels in sediments associated with various aquatic environments. It was proposed by Tomlinson (1980) and depends mainly on the contamination factors (CF) of various elements expressed as below.

$$PLI = \sqrt[n]{(CF_1 \times CF_2 \times CF_3 \times \ldots\ldots \times CF_n)} \text{.....(eq. 3.4)}$$

Where 'n' represents the number of elements. The classification of the sediments depending on PLI can be done by considering PLI>1 as polluted sediment, whereas PLI<1 is considered as non-polluted (Rabee et al., 2011; Harikumar et al., 2009).

3.6.5 Potential ecological risk index (PERI)

The potential ecological risk index (PERI) is a useful diagnostic tool for aquatic system assessment. It is based on sediment constituent chemistry and combined with environmental chemistry and ecotoxicology (Hakanson et al., 1980). It calculates the level of metal associated with pollution in aquatic ecosystems depending upon the toxic effects of the respective metals and ecological risks posed by them. PERI can be calculated by the formula proposed by Hakanson (1980) as follows:

$$PERI = \sum E_r^i = \sum T_r^i \times C_r^i = \sum T_r^i \times \frac{C_0^i}{C_n^i} \text{.....(eq. 3.5)}$$

Where C_r^i is the pollution coefficient of a particular metal that has been used to observe the pollution intensity of the various metals. C_0^i represents the measured concentration of metal in the current study area and C_n^i is the respective background value of the respective metal as per McLennan et al. (1995). E_r^i represents the potential ecological risk coefficient whereas T_r^i in the formula is expressed as a toxic response factor of various metals.

As per Hakanson (1980), the toxic response factor based on their toxicity can be presented as Cu=Pb=5, Cr=2, Zn=1. The evaluation of metal associated pollution is done depending on certain classifications related to calculated PERI values as follows.

Table 3.9 PERI guidelines for sediments and suspended solids

PERI Values	Ecological Risk Indicator
PERI<150	Low ecological risk
150<PERI<300	Moderate ecological risk
300<PERI<600	Considerable ecological risk
PERI>600	Very high ecological risk

3.6.6 Sediment pollution index (SPI)

The sediment pollution index (SPI) is a multi-metal-based approach to assess the sediment quality with respect to its heavy metal concentration and consideration of the toxicity of the respective metal. It was established by Singh et al. (2002) and defined as the linear sum of metal enrichment factors along with the account of metal toxicity weight. SPI can be expressed as follows:

$$SPI = \frac{\sum(EF_m \times W_m)}{\sum W_m} \text{.....(eq. 3.6)}$$

$$EF_m = \frac{C_n}{C_r} \text{.....(eq.3.7)}$$

Where EF_m is the ratio between the analyzed value of the considered C_n and its respective background value C_r (Sediments: PAAS values given by Taylor and McLennan (1985, 1995), McLennan (2001) and suspended solids: average metal concentration of riverine suspended solids given by Viers et al. (2009)) and W_m represents the toxicity weight of the considered metal.

The toxicity weight of various metals was assigned by Singh et al. (2002), which is Cr=Zn=1, Ni=Cu=2, Pb=5 and Cd=300. SPI was classified into 5 classes to categorize and identify the levels of pollution at various stations.

Table 3.10 SPI Guidelines for sediments and suspended solids

SPI values	Related Pollution levels
0<SPI<2	Natural Sediments
2<SPI<5	Low polluted sediments
5<SPI<10	Moderately polluted sediments
10<SPI<20	Highly polluted sediments
SPI>20	Dangerous sediments

3.6.7 Effect range low (ERL) and Effect range median (ERM)

The effect range low (ERL) and effect range median (ERM) are the sediment quality guidelines (SQGs) and the purpose is to assess the relative likelihood or potential for adverse biological effects occurring due to exposure of biota to toxicants present in the sediments. These guidelines are developed by Long et al. (1995) as informal tools to evaluate whether a concentration of a contaminant in sediment might have toxicological effects. The ERL and ERM values of selected metals (Cu, Pb, Zn, Cd and Cr) are compared with such metals' concentrations measured in the current study area. The compared results are shown in Table 5.18 and 5.19 for both seasons.

The ERL and ERM measures are expressed as specific chemical concentrations of a toxic substance in sediment. The ERL indicates the concentration below in which toxic effects are scarcely observed or predicted, whereas between ERL-ERM, it represents possible biological effects and is in a range within which effects would occasionally

occur. The concentrations above ERM represents toxic effects that are always observed

3.6.8.7 Risk assessment code (RAC)

The ecologic risk assessment (RAC) of sediments based on the total metal content is questionable because the bioavailability of metal largely depends on its speciation. The metal phases in sediments mainly influence the toxicity for organism in the aquatic system depending on their availability, especially for exchangeable and carbonate fraction (Yuan et al., 2014). These fractions have higher mobility under minimal environmental changes in the aquatic environment as these elements are weakly bonded to the sediments or are the results of anthropogenic activities (Yuan et al., 2014; Sakan et al., 2020). The risk assessment code (RAC) was first introduced by Perin et al. (1985) for evaluating the mobility and bioavailability of PTEs in sediments based on the exchangeable fraction (F1) and carbonate fraction (F2) content. So, it is possible to assess the availability of these metals by applying the percentage presence of these metals in these 2 fractions, where <1% presence represents no risk (N), 1-10% represents low risk (L), 11-30% represents medium risk (M) and 31-50% represents high risk (H), while more than 50% represents very high risk (V) (Perin et al., 1985).

3.7 Methodology overview

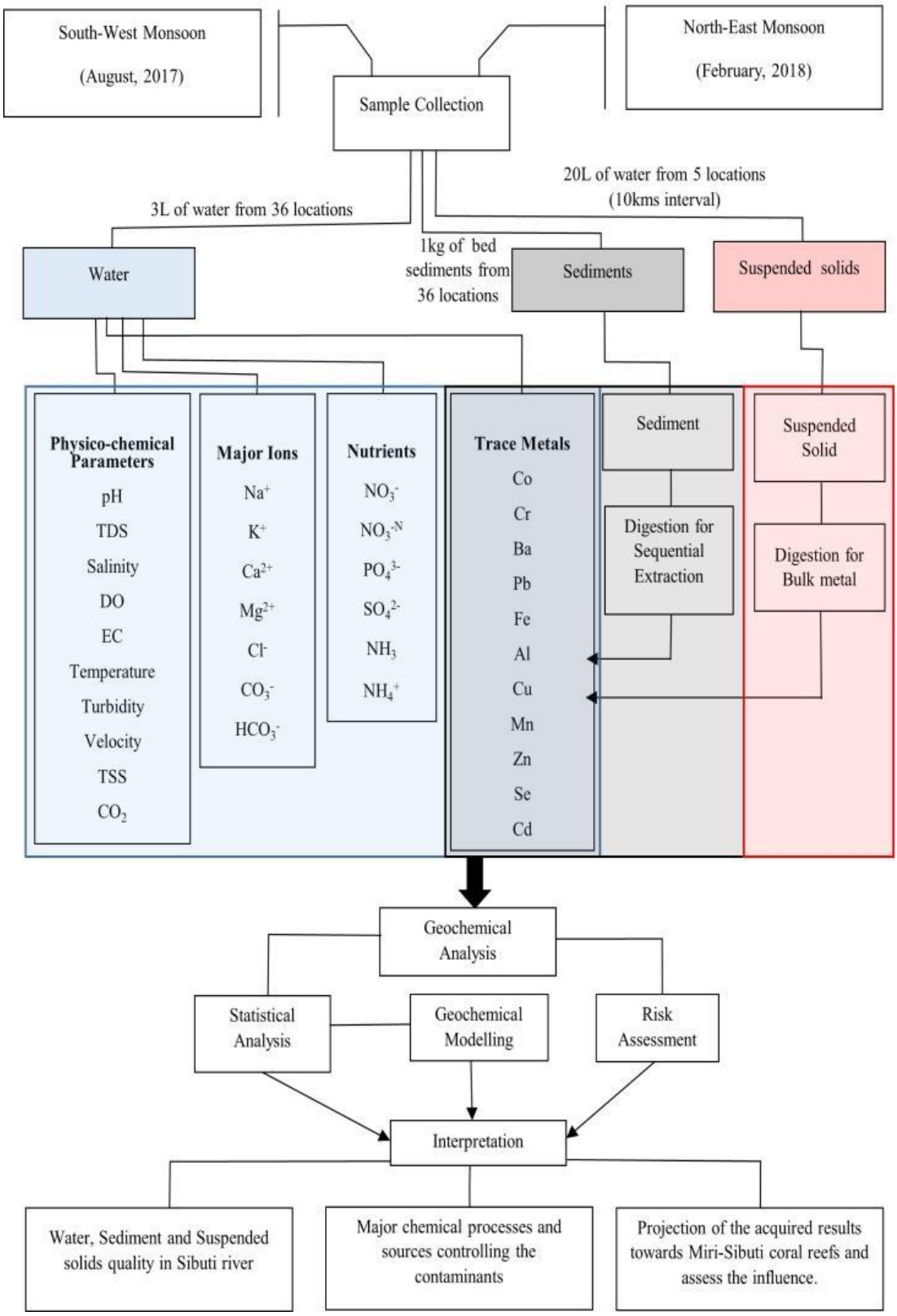

Fig. 3.6 Flow chart of the methodology carried out for sample collection, chemical analysis and interpretations

(A) ***(B)*** ***(C)***

Fig. 3.7 Mangrove and Nipa palm (Mangrove palm) presence near Sibuti river mouth (A) and far away from the mouth (B, C)

(A) ***(B)*** ***(C)***

Fig. 3.8 Mixing zones in Sibuti river estuary (A, B and C)

(A) *(B)* *(C)*

Fig. 3.9 River water upwelling due to tidal water influence at (A)near the river mouth (B)near Bekenu (C) near Kampung Sinup

(A) *(B)* *(C)*

Fig. 3.10 Major settlements near Sibuti river estuary (A) Kampung Kuala Sibuti, (B) Bekenu Town, (C) Kampung Balau

(A) ***(B)*** ***(C)***

Fig. 3.11 Major tributary Sungai Kejapil (A) and major water canals connecting river to agricultural fields (B, C)

(A) ***(B)*** ***(C)***

Fig. 3.12 Water (A), Sediment (B) and Suspended Solid (C) sample collection

(A) ***(B)*** ***(C)***

Fig. 3.13 Instruments used for laboratory analysis (A) Perkin Elmar AA400 (B) Perkin Elmar MPS Titan digester (C) Hettich Centrifuge

Chapter-4

Water Geochemistry

4.1 Physico-chemical parameters

4.1.1 South-West Monsoon (SWM)

The descriptive statistics of major physico-chemical parameters during SWM are shown in Table 4.1. The pH in the study area ranged from 4.60 to 6.88 with a mean value of 6.16. The fluctuation of DO varied from 3.66 to 6.44 mg L^{-1} with an average of 4.44 mg L^{-1}. The study sites exhibited EC and TDS values in a similar manner, where EC ranged from 107.60 to 3170 µS cm^{-1} and TDS is ranged from 153.8 to 4528.6 mg L^{-1} with a respective average of 409.60 µS cm^{-1} and 585.15 mg L^{-1}. The turbidity in the study area varied from 7.87 to 53.90 NTU with an average of 27.9 NTU. Furthermore, the velocity of water in the river varied between 0.7 and 11.84 m/s depending on the flow condition and its environment. Salinity in the estuary ranged from 0.02 to 1.65 ppt with an average of 0.61 ppt. Meanwhile, the temperature in the study area ranged between 21.4 and 30°C with an average value of 28.40°C. The concentration of CO_2 in estuarine water varied from 4.4 to 15.40 mg L^{-1} with an average of 6.91 mg L^{-1}. The total suspended solids (TSS) ranged from 20.2 to 178.6 mg L^{-1} with mean values of 55.62 mg L^{-1} (Table 4.1).

4.1.2 North-East Monsoon (NEM)

The descriptive statistics for surface water during NEM are given in Table 4.1. The pH ranged from 5.45 to 7.60 with a mean value of 6.61. The levels of DO range from 13.20 to 35.1 mg L^{-1} with an average of 2.49 mg L^{-1}. The study site exhibited mean values of EC and TDS at 1707.25 µS cm^{-1} and 1195.08 mg L^{-1}. The levels of EC and TDS ranged from 139.59 to 11971.44 µS cm^{-1} and 97.71 to 8380.01 mg L^{-1} respectively. Turbidity varied from 15.1 to 50.1 NTU with mean values of 31.69 NTU. The velocity ranged from 0.29 to 2 m/s with mean values of 0.88 m/s. The value of salinity varied from 0.04 to 11.70 ppt with an average of 1.05 ppt. The temperature varied from 29.80 to 32 °C with an average of 30.04 °C. Water carrying CO_2 during NEM varied from 11 to 39.60 mg/L with a mean value of 20.96 mg L^{-1}. The total suspended solids (TSS) varied from 44 to 383.3 mg L^{-1} with an average value of 156.82 mg L^{-1} (Table 4.1).

Table. 4.1 Descriptive Statistics of Physico-chemical parameters of surface water (n=36) during SWM and NEM

Parameters	Units	SWM				NEM			
		Min	Max	Mean	St. Dev.	Min	Max	Mean	St. Dev.
pH	-	4.6	6.88	6.16	0.33	5.45	7.6	6.61	0.4
DO	mg L^{-1}	3.66	6.44	4.44	0.44	13.2	35.1	20.49	5.15
EC	µS cm^{-1}	107.6	3170	409.6	719.63	139.59	11971.44	1707.25	2805.01
TDS	mg L^{-1}	153.8	4528.6	585.15	1028.05	97.71	8380.01	1195.08	1963.51
Turbidity	NTU	7.87	53.9	27.9	9.61	15.1	50.1	31.69	8.37
Velocity	m/s	0.7	11.84	3.58	2.02	0.29	2	0.88	0.48
Salinity	ppt	0.02	1.65	0.61	0.59	0.04	11.7	1.05	2.12
Temp	°C	21.4	30	28.4	1.39	29.8	32	30.04	0.44
CO_2	mg L^{-1}	4.4	15.4	6.91	2.42	11	39.6	20.96	5.84
TSS	mg L^{-1}	20.2	178.6	55.62	39.3	44	384.3	156.81	92.33

4.1.3 Seasonal and spatial distribution

4.1.3.1 EC and TDS

From the data collected during SWM, it was inferred that river water quality is being highly affected by the sea water's influence near the mouth. Parameters such as EC and TDS showed a decline in trend while moving away from the river mouth during both seasons (Fig. 4.4). TDS and EC both are dependent on the concentration of dissolved ions in water, which is much higher in seawater compared to freshwater (Gasim et al., 2015). In addition, Miri coastal water is reported to have a higher concentration of ions along with EC and TDS (Anandkumar, 2016), which might be responsible for the sharp increase in EC and TDS near the mouth. On contrary, some stations like no. 4 during SWM showed an increase in both values. This may be due to the influence of the agricultural channel near Kampung Padang, which is mixed with the main course of the Sibuti river before the sampling station (Fig. 1.4). Both the parameters are perfectly correlated with each other during both seasons besides the fact that samples during NEM showed a higher concentration of TDS than SWM (eq. 4.1) (Fig. 4.1). This satisfies the relation between TDS and EC as the conductivity goes high with a higher concentration of dissolved solids in water (Rusydi et al., 2018).

$$TDS\left(\frac{mg}{L}\right) = k * EC\left(\frac{\mu S}{cm}\right) \quad \text{.....(eq. 4.1)}$$

Where k is represents the ratio between TDS/EC and can vary from 0.55 to 0.7 depending upon the type of water and contained EC concentration (Rusydi et al., 2018).

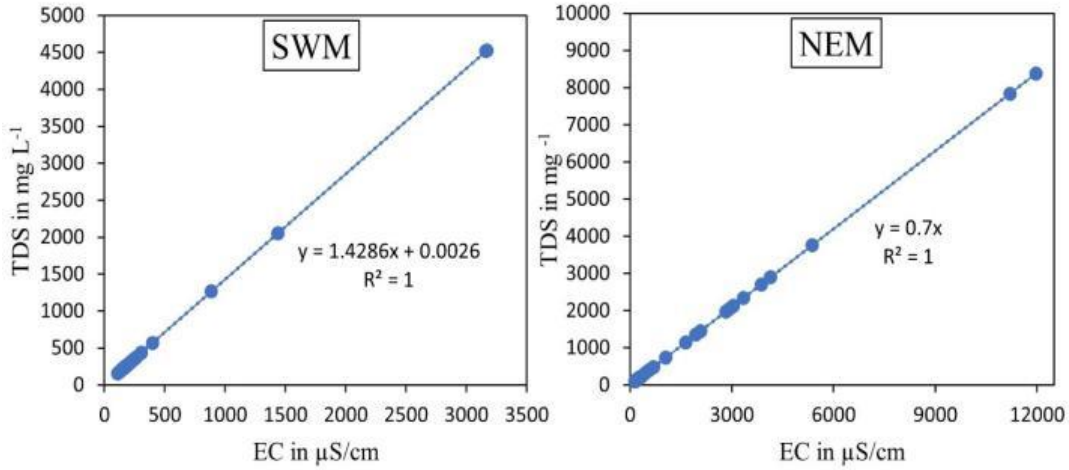

Fig. 4.1 Comparison of EC & TDS at different stations during SWM and NEM

4.1.3.2 pH and CO_2

The trend of pH decreases towards the lower part and remains higher in the freshwater dominating region of the estuary during both seasons. However, average values suggest that it is higher during NEM as compared to SWM. A sudden decrease of pH with increase of CO_2 and vice versa situation has been noted at various stations during both seasons as shown in Fig. 4.2 (red zones). This might be due to the respiration of organic matter caused by the stratification of water with increasing tidal influence in the lower part. Under such conditions, degradation of these organic matters gives rise to CO_2, which makes the water more acidic in nature with the formation of carbonic acid during photosynthesis which expels O_2 (Krachler et al., 2009; NOAA, 2021). The CO_2 concentration during NEM than SWM and shows a gradual increase in concentration towards upstream as well. As the river basin is dominated by carbonate rocks such as limestone, mudstone, dolomite and calcareous sandstones along aluminosilicate minerals in shales in Sibuti and Lambir formations (Nagarajan et al., 2015; Nagarajan et al., 2017a), weathering of such rocks with the help of higher run-off during NEM must be responsible for high dissolved CO_2 (Cole & Prairie, 2014).

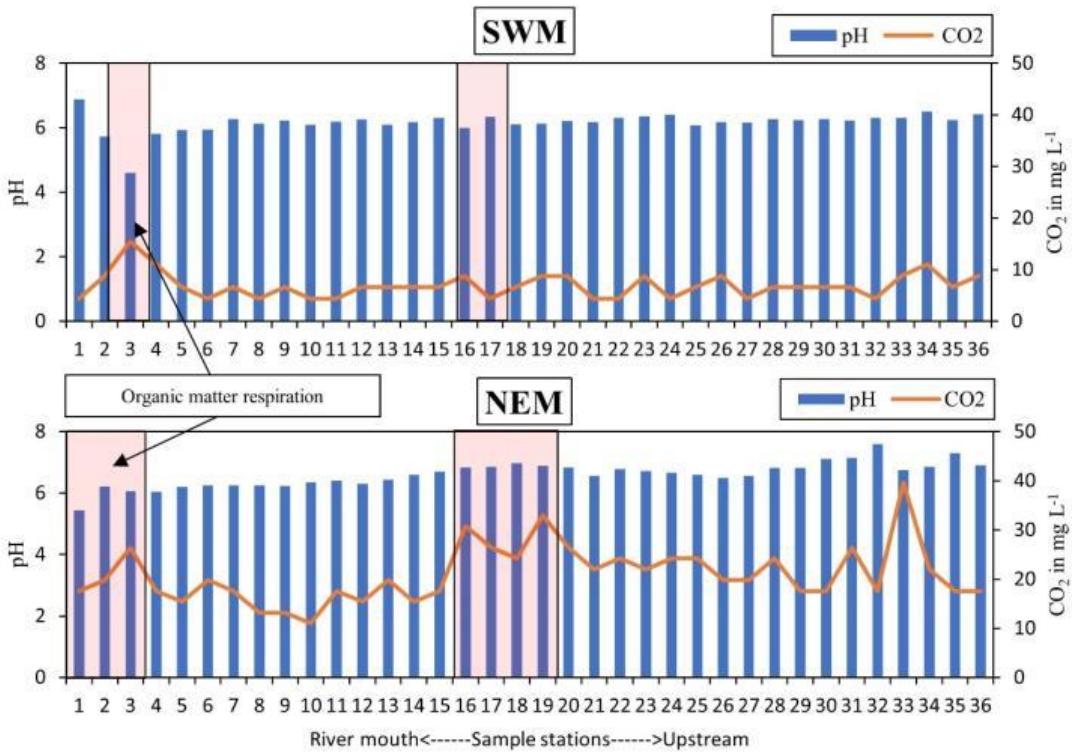

Fig. 4.2 Comparison of pH and CO_2 at different stations during SWM and NEM

4.1.3.3 Salinity

Salinity in the study area near the mouth has the highest values during both SWM and NEM, whereas the lowest value during SWM and NEM is recorded far from the mouth. The influence of high-tide and low-tide (Fig. 3.1) is clearly visible in the graph below (Fig. 4.3), particularly during SWM. In this season, the 1st day sampling was done during peak high tide, including stations like 16, 18, 21 and 23. The 2nd day sampling was carried out during low tide, including the stations like 15, 17, 19, 20 and 22. These observations indicate the domination of saline water in the intertidal zones of the estuary. The tidal straining in tidal estuaries destabilize the water column during high tides and increases stratification during low tides, generating variable vertical mixing over the tidal cycle, which controls the salinity (Simpson et al., 1990; Bolaños et al., 2013; Bakri et al., 2020). So, the lower salinity observed during SWM in high-tidal period might be due to vertical mixing of water as low flow of river and strong tidal currents eliminate vertical layering of water (e.g. Frota et al., 2013). On the other hand, during NEM sample collection which started during low tide from the mouth of the river (Fig. 3.2), station one recorded relatively the highest salinity. A sudden drop can be noticed at station two (Fig. 4.3) as compared to station one, which is indicative salt-front near the mouth against the flow of the river. The saline water's influence

decreasing gradually towards the upstream region. The low tide condition and high rainfall during NEM and sharp salt front at the mouth are the indication of partial mixing or density stratification in inter tidal zones as tidal straining is not enough against flow of river (Simpson et al., 1990; Frota et al., 2013; Bolaños et al., 2013; Bakri et al., 2020). The field evidence of this salt front during is given in Fig. 3.5A. These observations also indicate limited tidal influence in the lower part of the estuary prevails even during high rain-associated seasons such as NEM and low tidal condition.

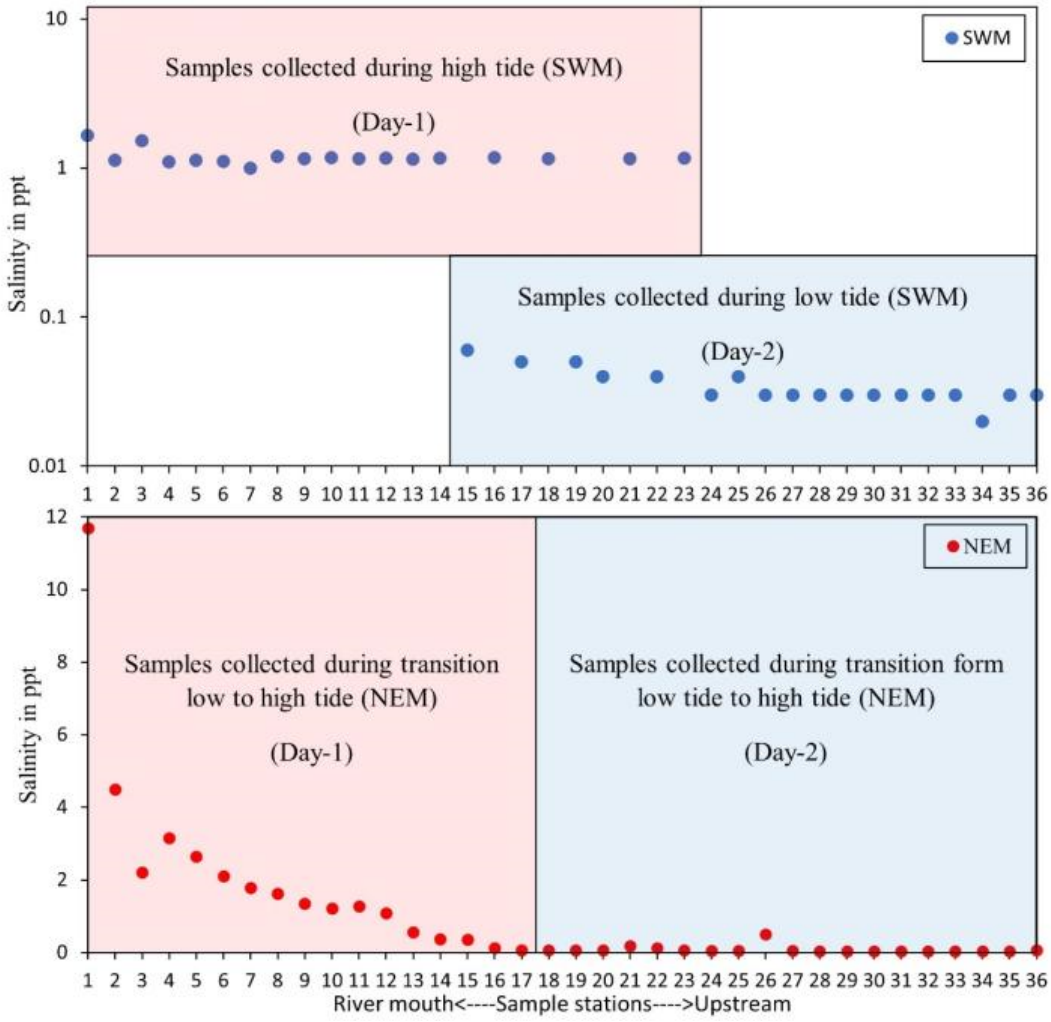

Fig. 4.3 Comparison of Salinity with tidal influence in the river during SWM and NEM

4.1.3.4 Turbidity

Turbidity during SWM and NEM has higher values near the mouth region of the estuary. However, the turbidity during SWM shows a decreasing trend towards the upstream direction, whereas the increasing trend observed in NEM and reported higher

in the upper part (Fig. 4.4). The higher turbidity near the mouth may be generated due to the oscillatory nature of estuarine tidal currents (Mathew et al., 2020). During SWM, barotropic effects and tidal pumping due to high tide is giving rise to an increase of sediment particles in the water column, hence high turbidity is noticed in the lower part zone. On contrary, the fluvial effect (Mathew et al., 2020) during NEM brings freshwater recharge in the upstream region, which brings suspended solids along with it, and suspension of clay from bottom sediments might be the main reason for the turbidity in the upper part of the estuary (Tripathy et al., 1990). The higher turbidity noted at station 1 during NEM is due to the same tidal pumping observed during SWM, but the intensity is much lower as compared to SWM due to the lower rate of saltwater flow due to low tide conditions observed during sampling.

4.1.3.5 Velocity

Velocity of river water was measured at the middle of the river at all the sampling locations with the flow meter reaching up to 3 to 4 meters. Velocity during SWM is noted to be higher than NEM at almost every station (Fig. 4.4) despite the fact that NEM is associated with a higher amount of run-off and discharge. There are two ways in which tides can modulate river discharge in tidal rivers like Sibuti. It is either governed by an oscillatory gradient of tidal water or steady gradients in subtidal water level (Sassi et al., 2013). As SWM is associated with the low discharge of river and samples were collected during high tide, governance of oscillatory gradient dominant in the estuary explains the higher fluctuation rate of velocity during this season. Sassi et al. (2013) also explained that such gradient is not directly related to river flow and water movement is mainly controlled by tidal friction during river-tide interaction, which might be responsible for high average velocity observed during SWM. On the other hand, higher river run-off and low tidal influence are responsible for a steady gradient of velocity during NEM with lesser tidal friction (Hidayat et al., 2011; Sassi et al., 2013). However, the highest velocity is recorded at station one during SWM (Fig. 4.4), which might be due to the high tidal influx towards the upstream direction of the river. It was also observed from the flow meter direction that the flow was towards the upstream direction at station one.

4.1.3.5 Dissolved oxygen

Dissolved Oxygen (DO) concentration in water during NEM is much higher than in SWM (Fig. 4.4), which might be due to the addition of freshwater run-off to the river water (Mackay et al., 1969; Tomaso et al., 2015) influenced by high rainfall associated with NEM (Saifullah et al., 2014). The changes in DO are a direct and indirect result of a change in pH, algal photosynthesis, aquatic respiration, water temperature and oxidative decomposition of organic matter (Zang et al., 2011). Moreover, the consumption and production of CO_2 in an aquatic environment is a direct result of an increase or decrease in DO (Zang et al., 2011). In the study area, effects of oxidation-reduction properties of freshwater play a vital role for higher levels of DO during NEM, which is mainly related to acidity (eq. 4.2 and 4.3) (Zang et al., 2011; Wang et al., 2001). With higher pH value such as freshwater, the redox reaction shifts towards left, which produces more DO (eq. 4.3) in the aquatic system (Wang et al., 2001, 2012).

$$2\mathrm{H}^+ + 2\mathrm{e}^- \Leftrightarrow \mathrm{H}_2(\mathrm{g});\ \mathrm{e}_0 = 0 \quad \text{..... (eq. 4.2)}$$

$$O_2(g) + 4H^+ + 4e^- \Leftrightarrow 2H_2O(aq);\ E_0 = +1.23V \quad \text{..... (eq. 4.3)}$$

4.1.3.6 Temperature

The temperature in the study area shows a similar decreasing trend towards the lower part of the estuary, where the upper part stays warmer during both seasons. The main factors controlling water temperature in estuaries are driven primarily by the interactive effects of river runoff, tidal exchange, and mouth state (Wooldridge et al., 2012). The water temperature of a tropical ocean or sea typically exceeds 20°C. In the case of the South China Sea, a study by Krawczyk et al. (2020) suggested that the seawater's surface temperature varies between 26 and 27°C during January to March (NEM), whereas the same varies from 28 to 29°C during July to September (SWM) and are expected to be colder at the bottom due to less influence of sunlight. In general, tropical ocean or sea surface water sinks at downwelling's where surface currents flow toward a continental coastline, or where two surface currents converge. Deep ocean water rises to the surface at upwellings where surface currents flow away from land, or where surface currents diverge (Wooldridge et al., 2012). Depending upon the above observations, deep water upwellings in the form of tidal water, and low river

runoff might be the driving factors of the low temperature observed near the river mouth during SWM (Fig. 4.4). The higher average surface water temperature observed during the NEM might be due to the surface generated temperature surging in streams after localized rainstorms, complimented by heating through interaction with warmer air (Briciu et al., 2020). Additionally, higher river runoff (Wooldridge et al., 2012) during NEM seems to be limiting the tidal influence during low tide and working as the major controlling factor of temperature during NEM.

4.1.3.7 Total suspended solids (TSS)

TSS during SWM maintains a linear relationship with seawater infusion in the estuary and shows a gradual decreasing trend towards the upstream direction and the highest concentration is also recorded near the river mouth (Fig 4.4). However, TSS during NEM shows a mixed influence of freshwater infusion in the upper part and seawater intrusion in the lower region of the estuary, besides also showing increased concentration at both ends (Fig 4.4). With regard to the concentration, NEM shows a 3-fold increase in TSS concentration as compared to SWM in the estuary, which might be due to the combined effect of both seawater borne particles near the mouth and freshwater run-off containing particles in the upper part. The highest concentration of TSS is observed at stations in the upper part of the estuary during this season (Fig. 4.4).

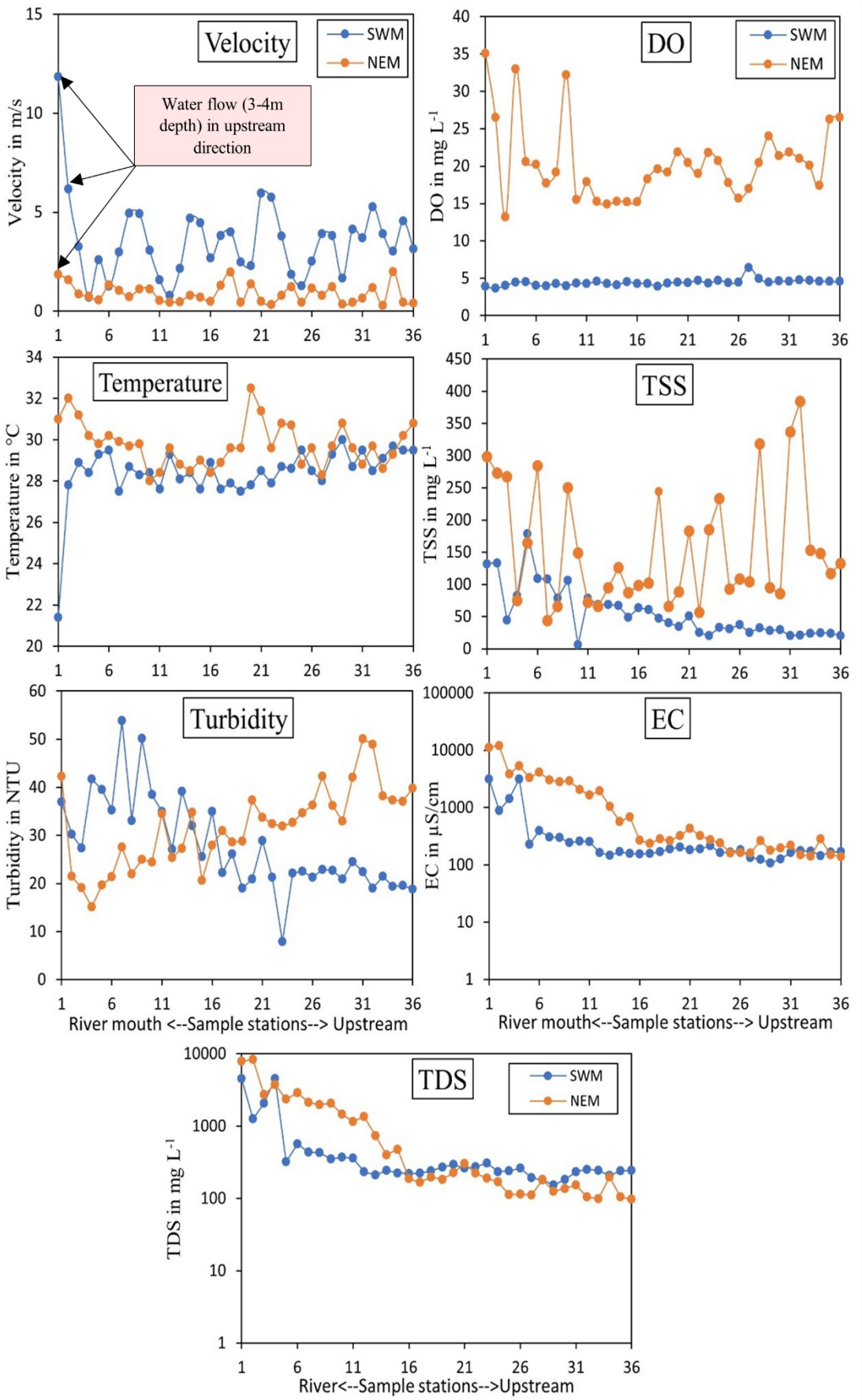

Fig. 4.4 Variation of Turbidity, Velocity, DO, Temperature and TSS during SWM and NEM

4.2 Major Ions

4.2.1 South-West monsoon (SWM)

The descriptive statistics of various cations and anions analysed in water during SWM are given in table 4.2. Ca^{2+} in the study area ranged from 2 to 14 mg L^{-1} with a mean value of 4.83 mg L^{-1}. The concentration of Mg^{2+} varied from BDL to 54 mg L^{-1} with a mean value of 4.70 mg L^{-1}. Cations such as Na^{+} and K^{+} varied from 20.40 to 1252.80 mg L^{-1} and 7.96 to 75.05 mg L^{-1} with mean values of 134.70 and 15.89 mg L^{-1} respectively. The study area exhibited anion concentration Cl^{-} ranging from 26.58 to 2153.58 mg L^{-1} with an average value of 182.17 mg L^{-1}, whereas HCO_3^{-} varied from 18.30 to 54.90 mg L^{-1} with an average value of 31.35 mg L^{-1} (Table 4.2). On the other hand, CO_3^{2-} is not detected in the study area during SWM.

During SWM, the concentration of various cations and anions were observed in the following order:

Overall mean abundance of ionic concentration: $Cl^{-} > Na^{+} > HCO_3^{-} > K^{+} > Ca^{2+} > Mg^{2+}$

Mean abundance of cations: $Na^{+} > K^{+} > Ca^{2+} > Mg^{2+}$

Mean abundance of anions: $Cl^{-} > HCO_3^{-}$

4.2.2 North-East monsoon (NEM)

The descriptive statistics observed in case of various cations and anions during NEM are given in Table 4.2. During NEM, Ca^{2+} varied from 2 to 286 mg L^{-1} with an average value of 60.58 mg L^{-1} . The variation of Mg^{2+} ranged from BDL to 1082 mg L^{-1} with an average value of 125.92 mg L^{-1} (Table 4.2). Na^{+} ranged between 2.76 to 3034 mg L^{-1} with a mean value of 292.97 mg L^{-1}, whereas K^{+} varied between 2.88 to 98.26 mg L^{-1} with an average value of 17.10 mg L^{-1}. In addition to that, the concentration of Cl^{-} varied from 17.72 to 5742.90 mg L^{-1} with a mean value of 621.85 mg L^{-1}. HCO_3^{-} ranged from 12.20 to 61 mg L^{-1} with an average value of 27.45 mg L^{-1}, whereas CO_3^{2-} remained undetected during NEM.

During NEM, the abundance of various cations and anions were observed in the following order:

Overall mean abundance of ionic concentration: $Cl^- > Na^+ > Mg^{2+} > Ca^{2+} > HCO_3^- > K^+$

Mean abundance of cations: $Na^+ > Mg^{2+} > Ca^{2+} > K^+$

Mean abundance of anions: $Cl^- > HCO_3^-$

Table 4.2 Descriptive Statistics of Cations and Anions (n=36) during SWM and NEM (in mg L^{-1})

Parameters	SWM				NEM			
	Min	Max	Mean	St. Dev.	Min	Max	Mean	St. Dev.
Ca^{2+}	2	14	4.83	3.1	2	286	60.58	67.59
Mg^{2+}	BDL	54	4.7	9.47	BDL	1082.4	125.92	233.3
Na^+	20.4	1252.8	134.7	261.2	2.76	3034	292.97	582.29
K^+	7.96	75.05	15.89	13.1	2.88	98.26	17.1	16.3
HCO_3^-	18.3	54.9	31.35	7.46	12.2	61	27.45	10
Cl^-	26.58	2153.58	182.17	441.71	17.72	5742.9	621.85	1131.22

4.2.3 Seasonal and spatial distribution

4.2.3.1 Bicarbonate (HCO_3^-)

The highest concentration of HCO_3^- is noted at station 10 during SWM and station 1 during NEM (Fig. 4.6). The trend of HCO_3^- stays very similar during both the seasons and concentration during SWM is noted to be higher at the majority of the station as compared to NEM. The concentration of HCO_3^- in the Miri coastal water was noted to have a mean value of 86.75 mg L^{-1} during NEM and 111.76 mg L^{-1} during SWM (Anandkumar, 2016). Considering this observation, the higher average concentration of HCO_3^- observed during SWM. HCO_3^- is mainly indicative of seawater influence (Gasim et al., 2015) irrespective of the seasons. However, the dilution of seawater due to high freshwater infusion might be playing a major role in lowering the average concentration of HCO_3^- in the middle part estuary (Fig. 4.5) despite the higher concentration observed near the mouth due to high salinity during NEM. In addition, in open environments like an estuary, diluted freshwater from river reacts with seawater carrying CO_2 while mixing, which gradually increases the acidity (decrease in pH) forms of carbonic acid, eventually giving rise to H^+ and HCO_3^- on further reaction (eq. 4.2) (Mook et al., 1975; Dickson et al., 2007; Mucci et al., 2011; Saifullah et al., 2014; Van Dam et al., 2019).

$$H_2O + CO_2 \Leftrightarrow H_2CO_3 \Leftrightarrow H^+ + HCO_3^- \quad \text{..... (eq. 4.2)}$$

Similar conditions have been observed in the study area at multiple stations (Fig. 4.5) (blue box), where the concentration of CO_2 decreased with an increase in HCO_3^- and acidity with the influence of salinity and vice versa. Under such conditions, depending upon the alkalinity of freshwater and seawater, CO_3^{2-} can be very low even with relatively high salinity (Mook et al., 1975), which is the condition in the case of the Sibuti river estuary.

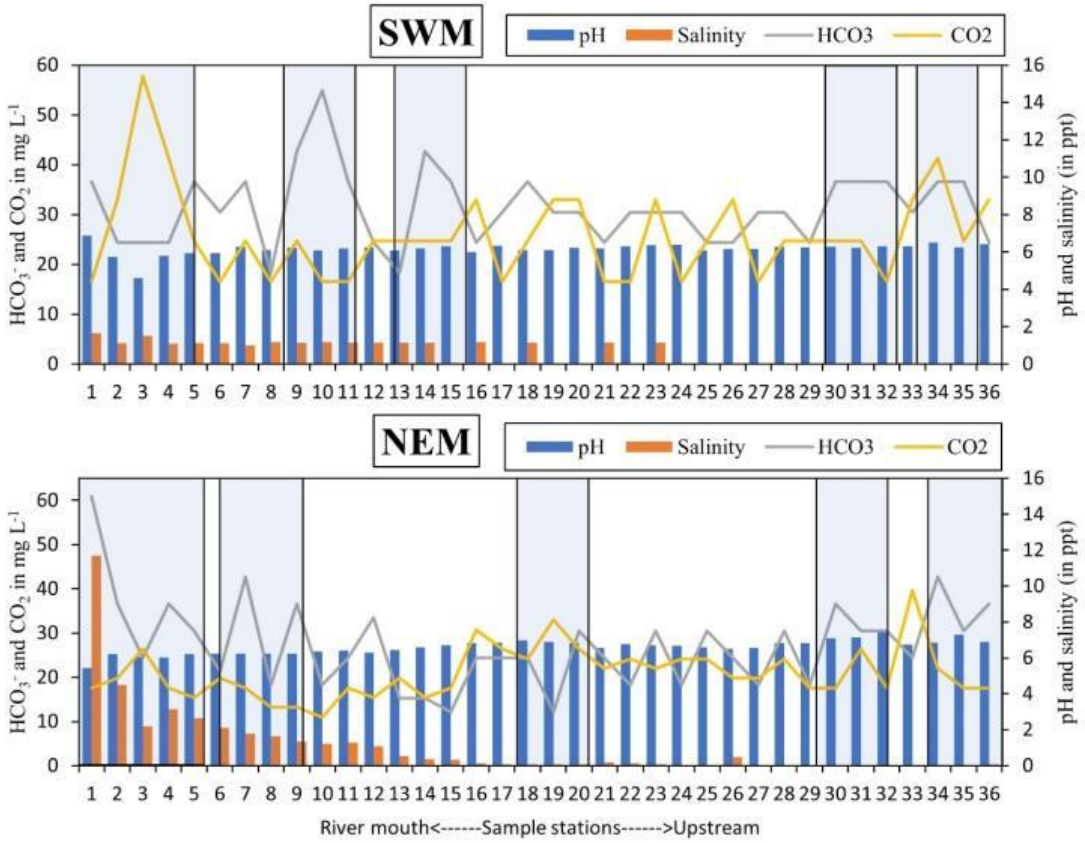

Fig. 4.5 HCO_3 forming zones in the Estuary with the help of salinity and CO_2

4.2.3.2 Chloride (Cl^-)

Chloride (Cl^-) concentration in the estuary is higher during NEM than concentration recorded in SWM, particularly in the estuary region. During both the seasons, the highest concentration is recorded in the lower region of the estuary (Fig. 4.6). The fluctuation of Cl^- shows a direct decline towards the upstream direction in the estuary, which is an indication of seawater influence. Additionally, the minor contribution of Cl^- from agricultural land can also be expected in the study area because of the use of various fertilizers (WHO, 1993). Specifically, potash related fertilizers, which use

potassium chloride and are applied to increase the fertility of the soil, act as sources of chloride in the river because of leaching (WHO, 1993; Hunt et al., 2012; Khatri et al., 2015).

4.2.3.3 Calcium (Ca^{2+}) and Magnesium (Mg^{2+})

Ca^{2+} and Mg^{2+} during SWM and NEM are increasing in concentration towards the lower part of the estuary (Fig. 6). The increase in concentration might be influenced by the high concentration of Ca^{2+} and Mg^{2+} present in seawater naturally (Mewes et al., 2014) and its mixing with the river water. Moreover, during NEM, Ca^{2+} and Mg^{2+} concentration is increased by 13 and 27% as compared to SWM in the estuary (Table 4.6). This indicates the enrichment of such cations in the upper part of the river (catchment area) with the help of rock water interaction resulting in weathering of such ions (Khatri et al., 2015) during NEM. The weathering of mica-bearing rocks such as shale and limestone in the river basin (Nagarajan et al., 2017a) might be the reason for such enrichment (Panigrahy et al., 2005). The deviation is also much higher during NEM (Table 4.6), which might be due to the intense intrusion of freshwater in the estuary as compared to SWM. A similar condition has been noted by Tripathy et al. (1990) in the Rushikulya River Estuary in Odisha, India. In summary, in the upper part of the estuary, the river carried water is noted to be the driving force of Ca^{2+} and Mg^{2+} due to weathering, whereas the mixing of saltwater from the South China Sea (SCS) with river water is the controlling factor of the increase in the concentration of these ions in the lower region.

4.2.3.4 Sodium (Na^{+})

There is a two-fold increase in Na^{+} concentration during NEM as compared to SWM (Table 4.6). A sharp increase in concentration was noticed in the lower part of the estuary as compared to the upper part (Fig. 4.6). The trend is similar during both seasons and a sudden increase in Na^{+} concentration near the lower region indicates the seawater influx in the estuarine zone. However, in the upstream region, the concentration gradually decreases due to the mixing with fresh water. The lower concentration of Na^{+} in the upstream region and overall lower concentration as compared to Cl^{-} in the estuary might have been attributed to the preferential absorption and incorporation of Na^{+} into silicates in the estuary (Patra et al., 2012).

4.2.3.4 Potassium (K^+)

The concentration of Potassium (K^+) during SWM is recorded to be abundant after Na^+ among the cations. However, it is recorded to be the least abundant during NEM despite its minor increase in concentration. K^+ is the least affected ion during NEM as compared to other ions and shows negative relation to infusion of freshwater associated with weathering in the upper part of the river basin. The trendline during SWM shows a decrease in the concentration of K^+ towards the upstream direction of the estuary (Fig. 4.6), which matches the saltwater distribution during the same period. Hence, seawater in the estuary might be the main carrier of K^+ during SWM. On the contrary, NEM shows a higher concentration of K^+ in the upper part of the estuary (Fig. 4.6), where freshwater infusion is dominant. This might be attributed to the weathering of potassium-bearing clay minerals such as potassium-micas (Saha et al., 2019; Rich et al., 1968), illites (Środoń, 1999) and leaching of potassium from the agricultural lands containing potash fertilizers (Kolahchi et al., 2007). However, the concentration K^+ further declines in the intermediate zones before increasing to the highest in the lower part of the estuary. The lower concentration in the intermediate zones might attribute to the absorption of K^+ through ion exchange by Na^+ and Mg^{2+} on the clay minerals (Adesina et al., 2017), whereas the highest concentration recorded in the lower part is the result of K^+ rich saline water influenced from SCS.

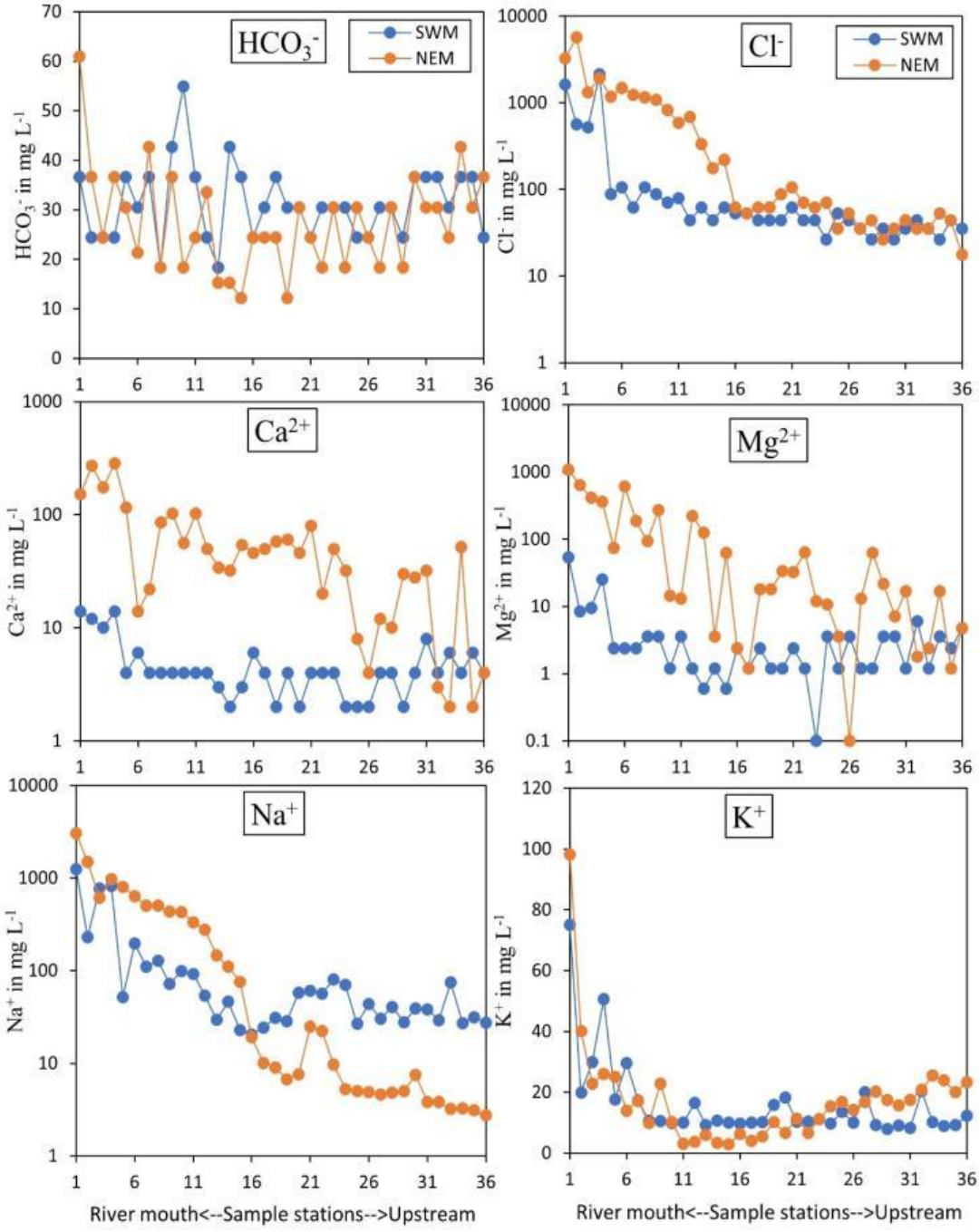

Fig. 4.6 Variation of cations and anions in water during SWM and NEM

4.3 Nutrients

4.3.1 South-West monsoon (SWM)

During SWM, sulfate (SO_4^{2-}) varied from 6 to 89 mg L^{-1} with an average value of 34.97 mg L^{-1} (Table 4.3). The concentration of PO_4^{3-} in water ranged from BDL to 3.45 mg L^{-1} with mean value of 0.87 mg L^{-1}. Likewise, the concentration of NO_3-N and NO_3^- in water ranged from BDL and 0.1 mg L^{-1} to 0.08 and 0.34 mg L^{-1} with

respective mean values of 0.03 and 0.12 mg L^{-1}. The exhibiting value of NH_3 and NH_4^- in the study area ranged from 0.01 and 0.04 mg L^{-1} to 0.9 and 0.32 mg L^{-1} with a respective average value of 0.18 and 0.15 mg L^{-1}. The mean abundance of nutrient concentration during SWM is in the following order:

$SO_4^{2-} > PO_4^{3-} > NH_3 > NH_4^+ > NO_3^- > NO_3$-N

4.3.2 North-East Monsoon (NEM)

The SO_4^{2-} varied from 2 to 133 mg L^{-1} with an average value of 46.86 mg L^{-1}, whereas PO_4^{3-} ranged from 0.03 to 0.35 mg L^{-1} with a mean value of 0.11 mg/L (Table 4.3). The concentration exhibited by NO_3-N and NO_3^- varied from BDL to 0.86 and 4.09 mg/L with mean values of 0.19 and 0.85 mg/L respectively. The analysed NH_3 and NH_4^+ varied from 0.17 and 0.18 to 0.97 and 1.03 mg/L with respective average values of 0.85 and 0.61 mg/L. The mean abundance of nutrient concentration during NEM is in the following order:

$SO_4^{2-} > NO_3^- > NH_4^+ > NH_3 > NO_3$-N $> PO_4^{3-}$

Table. 4.3 Descriptive Statistics of Nutrients (n=36) during NEM (in mg L^{-1})

Parameters	SWM				NEM			
	Min	Max	Mean	St.Dev.	Min	Max	Mean	St.Dev.
SO_4^{2-}	6	89	34.97	20.35	2	133	46.86	45.05
PO_4^{3-}	BDL	3.45	0.87	0.92	0.03	0.35	0.11	0.06
NO_3-N	BDL	0.08	0.03	0.02	BDL	0.86	0.19	0.32
NH_3	0.01	0.9	0.18	0.23	0.17	0.97	0.58	0.21
NH_4^+	0.04	0.32	0.15	0.07	0.18	1.03	0.61	0.22
NO_3^-	0.01	0.34	0.12	0.07	BDL	4.09	0.85	1.43

4.3.3 Seasonal and spatial distribution

4.3.3.1 Sulfate (SO_4^{2-})

The concentration of SO_4^{2-} in estuarine water increased during NEM as compared to SWM. The trend shows higher enrichment of SO_4^{2-} towards the lower part of the estuary during NEM (Fig. 4.8), which may be due to seawater influence, as the sea is rich in SO_4^{2-} as high as 2570 mg L^{-1} (Hoz et al., 2003). The low concentration and disparity in the concentration of SO_4^{2-} during the SWM might be due to the anoxic condition of bottom water because of salt water dominated in the water table, while

increase in organic matter results in SO_4^{2-} reduction in bottom water and saline sediments (Matson et al., 1985; Hartzell et al., 2012). In such reducing conditions during SWM, with less rainwater infusion in the estuary, Fe (II) precipitates to sulfides formed by SO_4^{2-}. However, with reoxygenation through freshwater infusion, these sulfides will oxidize to sulfates and remineralization of organic matter in such situation also gives rise to SO_4^{2-} concentration in water (Patra et al., 2012; Matson et al., 1985; Malcolm et al., 1986). The oxygenated freshwater influx during NEM might be giving rise to a significant increase in the concentration of SO_4^{2-} and responding towards the mixing of saline water with freshwater (Fig 4.7).

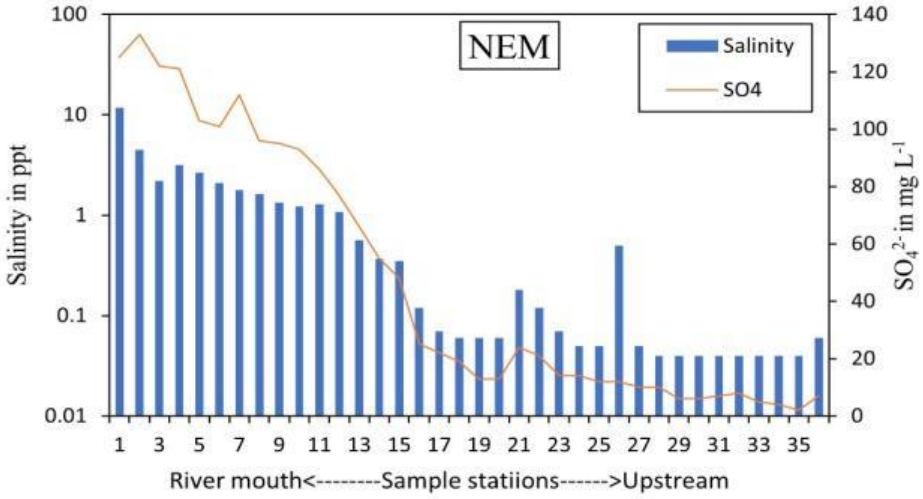

Fig. 4.7 Variation of SO_4^{2-} and salinity in the estuary during NEM

4.3.3.2 Phosphate (PO_4^{3-})

PO_4^{3-} in the study area shows an increasing trend towards the upstream direction during both seasons (Fig. 4.8). During NEM, a significant decrease in average concentration of PO_4^{3-} has also been observed (Table 4.3) and is the least dominant nutrient found in estuarine water. This may be due to the saline nature of the estuary during SWM. In such an environment, terrigenous Fe (III) bounds to P deposited in the estuary and releases PO_4^{3-}, making it freely available in surface water (Hartzell et al., 2012). This condition occurs more in saline sediments rather than freshwater sediments, which also explains the low concentration of PO_4^{3-} in the lower part of the estuary during both seasons. In both freshwater and saline water zones, PO_4^{3-} bounds with Fe (III) oxides and is released to solutions when Fe (III) reduces to Fe (II) under anoxic conditions (Hartzell et al., 2012). Moreover, in sulfate rich seawater sediments, Fe (II) precipitates to sulfides formed by SO_4^{2-}, thus preventing PO_4^{3-} to precipitate

with Fe (II) in anaerobic conditions (Roden et al., 1997; Gächter et al., 2003; Hartzell et al., 2012). However, the aerobic condition of the estuary and freshwater dominated sediments favour PO_4^{3-} to bond with particulate Fe (III), thus removing it from the water table as during NEM.

4.3.3.3 Ammonia (NH_3) and Ammonium (NH_4^+)

The concentration of NH_4^+ is higher than NH_3 in both the seasons and follow a similar trend as in aqueous solution, ammonia acts as a base and drags H^+ ions from water to form NH_4^+ and OH^-. With the effect of pH below 7 and higher temperature, both the parameters acquired their value by being in the equilibrium (eq. 4.3) (Körner et al., 2001).

$$NH_3(aq) + H_2O \Leftrightarrow NH_4^+(aq) + OH^-(aq) \quad \text{..... (eq. 4.3)}$$

The concentration of NH_3 in domestic wastewater generally ranges from 10 to 50mg L^{-1} and can increase up to 200 mg L^{-1} in the case of industrial wastewater (Körner et al., 2001; Konig et al., 1987). In comparison to that, the concentration of NH_3 is much lesser in the study area and rules out the higher influence of domestic and industrial wastewater. The concentration of NH_3 and NH_4^+ shows an increasing trend towards the lower part of the estuary during NEM (Fig. 4.8). This might be due to the nitrification process happening in the estuary infusion of higher O_2 containing freshwater during NEM, which gives rise to more ionised NH_4^+ and NO_3^- in latter process with increase in H^+ ion in water in absence of carbonates (eq. 4.4) (Müller et al., 2018; Thompson, 2007).

$$NH_3 + H_2O + 2O_2 \Leftrightarrow NH_4^+ + OH^- + 2O_2 \Leftrightarrow NO_3^- + 2H_2O + H^+ \quad \text{.....(eq. 4.4)}$$

A similar condition is observed in the study area where NH_3, having the third highest mean concentration during SWM, has been reduced to the fourth highest mean during NEM. Similarly, there is a significant increase in NO_3^- and NH_4^+ concentration and they are the second and third most dominant nutrients during NEM.

4.3.3.3 Nitrate (NO_3^-) and Nitrate-nitrogen (NO_3-N)

The concentration of NO_3^- and NO_3-N during NEM is recorded higher than SWM, and this might be due to the nitrification process happening in the estuary (eq. 4.4). The highest concentrations are observed far from the river mouth during SWM, whereas

the highest concentration during NEM is observed in the lower region of the estuary. In contrast, the concentration of the nutrients is responding with the distance of sample stations from the river mouth and has a decreasing trend towards the upstream direction during NEM (Fig. 4.8).

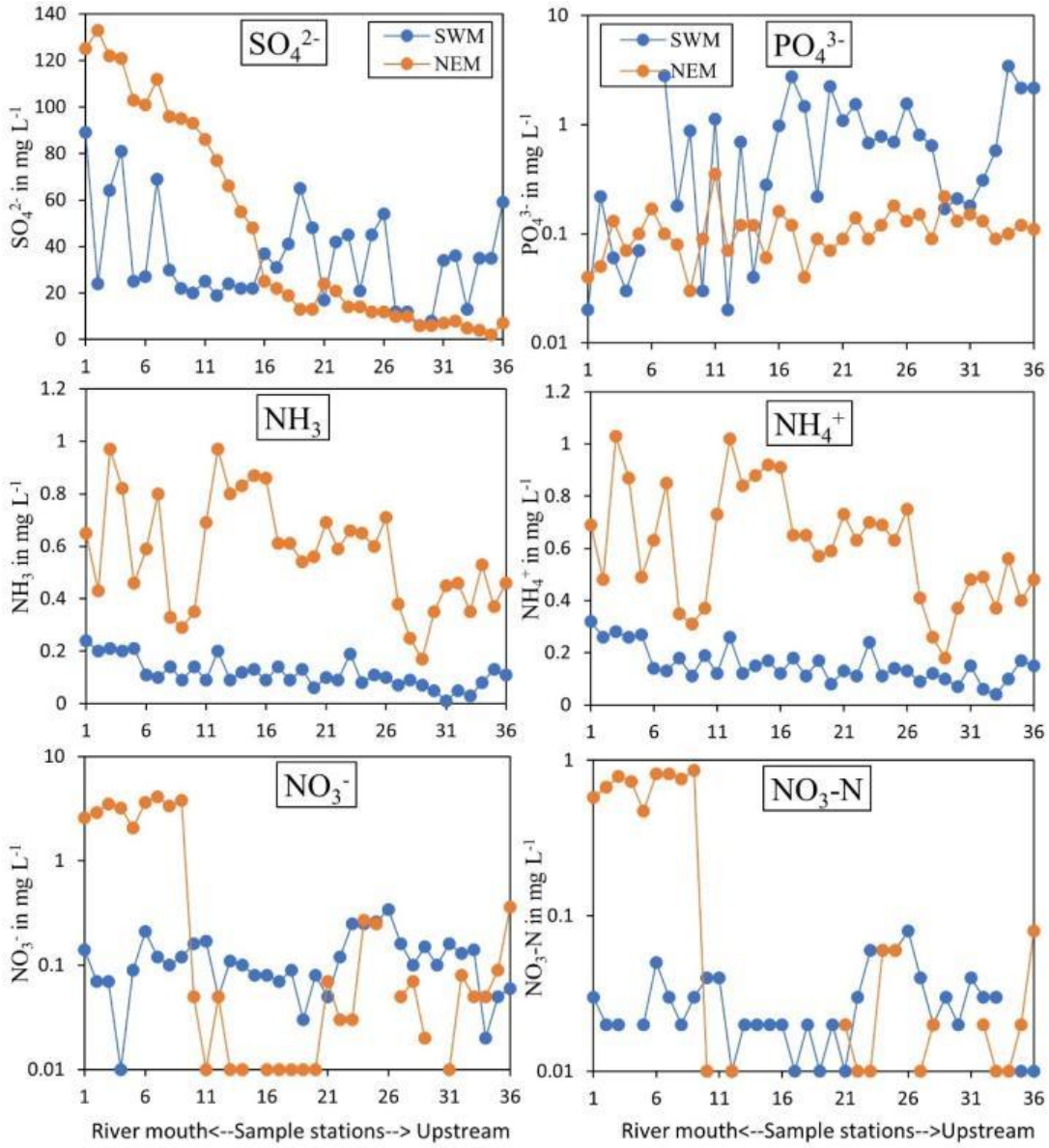

Fig. 4.8 Variation of nutrients in water during SWM and NEM

4.4 Trace Metals

The concentration of various trace metals was measured for the estuarine-influenced region of the Sibuti river during SWM and NEM periods. Descriptive statistics of the data acquired are presented in Table 4.4 for both seasons.

4.4.1 South-West Monsoon (SWM)

Copper (Cu) concentration is ranged between BDL to 0.386 mg L^{-1}, with a mean value of 0.036 mg L^{-1}. The concentration of Zinc (Zn) ranged from BDL to 0.534 mg L^{-1} during SWM with its highest concentration at station 31. The lowest value of zinc (Zn) is reported at a few stations along with an average of 0.109 mg L^{-1}. The Iron (Fe) concentration is higher near the river mouth at station 1. The concentration fluctuated from 3.950 to 1.375 mg L^{-1} in the estuary with a mean value of 2.294 mg L^{-1} and the lowest is recorded at station 31. The concentration of Cobalt (Co) varied from BDL to 0.046 mg L^{-1} along the estuary with an average of 0.003 mg L^{-1}. The highest value is recorded at station 1 and BDL in most of the stations. The range of Manganese (Mn) in the study area stood between 0.096 and 0.306 mg L^{-1} with an average of 0.164 mg L^{-1}. The concentration of Cadmium (Cd) was considerably low during SWM, ranging from 0.016 to 0.077 mg L^{-1} with an average of 0.026 mg L^{-1}. The concentration of Chromium (Cr) in the study area ranged between 0.007 to 0.541 mg L^{-1} with an average of 0.324 mg L^{-1}. The highest reading is recorded at station 22. The concentration exhibited by Se and Ba during this season ranged from 3.445 mg L^{-1} and BDL to 8.559 and 0.996 mg L^{-1} with respective average values of 6.236 and 0.074 mg L^{-1}. Apart from that, elements like Lead (Pb) and Aluminium (Al) are absent in all the water samples during SWM. The mean abundance of metal concentration during SWM is in the following order:

Se > Fe > Cr > Mn > Zn > Ba > Cu > Cd > Co

4.4.1 North-East Monsoon (NEM)

During NEM, copper (Cu) concentration ranged from 0.178 to 0.556 mg L^{-1} with an average of 0.293 mg L^{-1}. The fluctuation of zinc (Zn) was from 0.015 to 1.065 mg L^{-1} with the mean value of 0.151 mg L^{-1}, with the highest and lowest values recorded at stations 31 and 14 respectively. Similarly, the concentration of iron (Fe) fluctuated from 0.240 to 67.480 mg L^{-1}. The average concentration stood at 6.507 mg L^{-1} with the highest value recorded at station 31, and the lowest value recorded closer to the mouth at station 7. The concentration is cobalt (Co) varied from 0.179 to 0.351 mg L^{-1} with an average value of 0.261 mg L^{-1}. The highest value is recorded at station 29. Manganese (Mn) concentration in the estuary ranged from BDL to 0.238 mg L^{-1} with a mean value of 0.042 mg L^{-1}. The highest value for manganese is recorded at station

31 and the lowest value is recorded at multiple stations (i.e. 35 and 36). The highest recorded value of Cd is captured near the river mouth at station 1, where the value stood at 0.025 mg L^{-1}. However, the lowest value (BDL) is recorded at station 21. The concentration of lead (Pb) is recorded at only 2 stations near the river mouth (stations 1 and 2), with recorded values of 0.097 and 0.018 mg L^{-1}. The variance in concentration of chromium (Cr) ranged from BDL to 0.424 mg L^{-1} with an average value of 0.118 mg L^{-1} and had the highest concentration recorded at station 34 along with the lowest at multiple stations. The metals, Se and Ba during this season ranged from 2.784 mg L^{-1} and BDL to 6.47 and 0.536 mg L^{-1} with a respective average of 5.522 and 0.031 mg L^{-1}. In contrast, the concentration of Al at all stations was below detection limit. The mean abundance of metal concentration during NEM is in the following order:

Fe > Se > Cu > Co > Zn > Cr > Zn > Ba > Cd = Pb

Table. 4.4 Descriptive Statistics of Trace Metals (n=36) during SWM and NEM (in mg L^{-1})

Parameters	SWM				NEM			
	Min	Max	Mean	St. Dev.	Min	Max	Mean	St.Dev.
Cu	BDL	0.386	0.036	0.089	0.178	0.556	0.293	0.068
Zn	BDL	0.534	0.109	0.102	0.015	1.065	0.151	0.189
Fe	1.375	3.950	2.294	0.556	0.240	67.480	6.507	11.348
Co	BDL	0.046	0.003	0.009	0.179	0.351	0.261	0.063
Mn	0.096	0.306	0.164	0.052	BDL	0.238	0.042	0.047
Cd	0.016	0.077	0.026	0.011	BDL	0.025	0.003	0.005
Pb	BDL	BDL	BDL	BDL	BDL	0.097	0.003	0.016
Cr	0.007	0.541	0.324	0.136	BDL	0.424	0.118	0.135
Al	BDL	BDL	BDL	BDL	BDL	BDL	BDL	BDL
Se	3.445	8.559	6.236	1.153	2.784	6.47	5.522	0.640
Ba	BDL	0.996	0.074	0.199	BDL	0.536	0.031	0.102

4.4.3 Seasonal and spatial distribution

The concentrations of all metals during NEM are higher than SWM with exception of Cr, Mn, Ba and Se (Fig. 4.9). A significant increase in concentration is noted in the case of elements like Fe, Cu and Co. The concentrations of Se and Fe have significant dominance in the estuarine waters during both seasons.

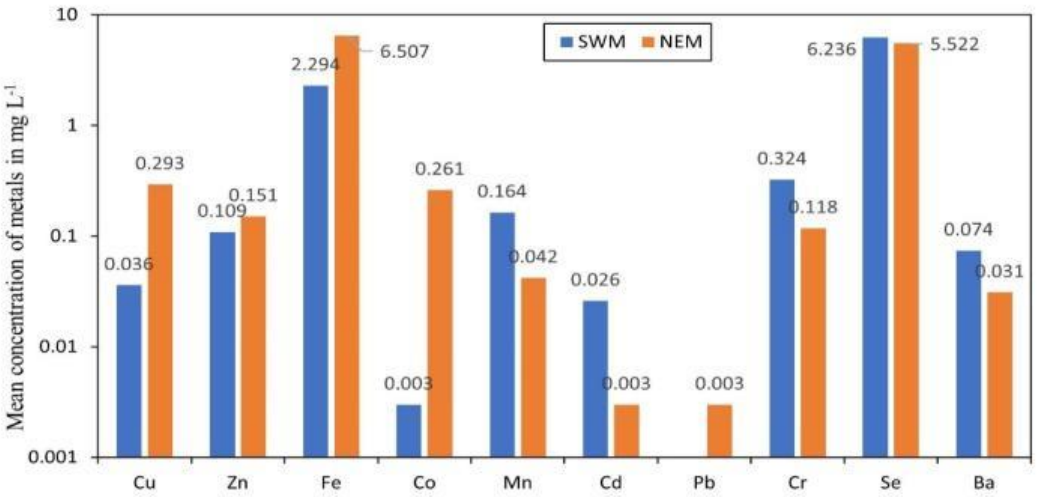

Fig. 4.9 Comparison of mean concentration of metals during SWM and NEM

4.4.3.1 Iron (Fe) and Manganese (Mn)

During SWM, Fe and Mn both respond conservatively towards salinity gradient in the estuary and have a declining trend in the upstream direction of the river (Fig. 4.10). In contrast, similar trend has not been observed for both parameters during NEM. On the other hand, a spike in the concentration of Fe in water has been noticed during NEM as compared to SWM, whereas the vice-versa condition prevails for Mn in the estuary (Table 4.4). A spike in concentration in the upstream region and a decrease in the lower region has been noticed for both parameters (Fig. 4.10). Biturbation, physical disturbance at the bottom, and higher velocity scour might be introducing Mn-rich pore water to the water column, which initiates the spike in Mn concentration during low flow conditions like SWM (Callaway et al., 1988). The considered estuarine area is tidally driven and rich in the mangrove, which indicates a stronger effect towards the biogeochemical cycling in the estuary with the help of saline water and run-off from the mangroves during dry seasons (Mori et al., 2019), such as SWM. Therefore, the lower concentration and trend of Fe observed during SWM might be the effect of seawater driven flocculation in the estuary with the help of turbidity and can be released through Fe(hydr)oxide formation under suboxic to anoxic conditions in intertidal systems (Mayer et al., 1982; Jilbert et al., 2016).

On the other hand, when there is intense mixing of estuarine oxygenated surface waters and marine water such as in NEM, a strong decrease of these organic compounds happens to suggest their removal by photodegradation and co-precipitation with particles such as Mn(hydr)oxides up to 100% (Oldham et al., 2017;

Mori et al., 2019). Furthermore, Oldham et al. (2017) explained that these Mn complexes are kinetically stabilized against Fe reduction even if the concentration of Fe is much higher in water. The presence of these oxidized forms of Mn during NEM might be the reason behind the decrease in concentration as compared to SWM, whereas the decrease in Fe concentration in the lower region of the estuary might be due to the precipitation and formation of iron monosulfides (FeS) under sulfidic conditions or Fe(hydr)oxides in oxygen-rich environments (Mori et al., 2019; Beck et al., 2008).

4.4.3.2 Copper (Cu) and Zinc (Zn)

Cu and Zn in the study area are observed to be behaving non-conservatively towards the distance from SCS during both seasons. The mean concentration calculated for both parameters shows a significant increase in Cu concentration during NEM whereas mild increase in concentration was observed for Zn (Table 4.4 and Fig. 4.9) as compared to SWM. The increase in concentration might be due to the weathering for Cu and Zn containing feldspar rich sandstones such as wackes in Sibuti formation (Nagarajan et al., 2015) and lithrarenites, Arkoses and wackes present in Lambir formation in the study area (Nagarajan et al., 2015; Nagarajan et al., 2017a)). Both formations indicated to be going through extreme weathering conditions (Nagarajan et al., 2015) and are major contributors in Sibuti river basin (Fig 1.6).

4.4.3.3 Cobalt (Co)

The concentration of Co in water was observed to be BDL at the majority of the stations during SWM, whereas a significant increase in concentration was noticed during NEM (Fig. 4.9) while showing a gradual increase in concentration away from the mouth (Fig. 4.10). This indicates the high Co-carrying nature of the Sibuti river during the wet season (NEM) and chemical weathering of Co happening in the upper region of the river basin. The presence of Co in the siliciclastic rocks were reported in the Sibuti and Lambir formation (Nagarajan et al., 2015; Nagarajan et al., 2017a).

4.4.3.4 Cadmium (Cd)

Cd concentration is noticed to be higher during SWM and much lower during NEM (Fig. 4.9), where most of the stations reported to be BDL. The recorded concentrations did not show any conservative behavior with the distance of sample stations from the

sea. The drainage basin of the Sibuti river estuary is extensively prone to weathering and predominantly consists of agricultural land, particularly downstream. However, the absence of a potential source of Cd such as phosphate rocks in the study area (Table. 1.2) indicates the infusion of such metal through extensive agricultural activities in the drainage basin (Fig. 1.4). According to Zaharah et al. (2014), P fertilizers are mainly derived from imported Phosphate rocks of maximum yield and are used in Sarawak's peat soil for oil palm's growth over the years. These fertilizers are the major source of Cd (De Boo et al., 1990) in the river and estuarine water, and dissolved value of Cd exhibits higher values during less rain associated months (Monbet et al., 2004) such as SWM in the considered area.

4.4.3.5 Chromium (Cr)

Cr during SWM is reported to be higher in concentration than NEM (Fig. 4.9). The measured concentrations during SWM showed a decreasing trend towards the lower region of the estuary (Fig. 4.10). The sample stations showed a decrease in concentration in the mixing zone of the estuary during NEM (Fig. 4.10). The presence of Cr in the river and estuary can be attributed to the presence of siliciclastic sediments of the Lambir and Sibuti formations, which has chromite and Cr that is associated with the organic rich layers (Nagarajan et al., 2015; Nagarajan et al., 2017a). In freshwaters, predominant inorganic forms of Cr are found in hydro complexes ($Cr(OH)^{2+}$, $Cr(OH)_3$), and with the influence of Cl^- (seawater), it forms hexaaquo complex ($[Cr(H_2O)_6]Cl_3$). These inorganic Cr also have an affinity to form complexes with natural or anthropogenic organic substances and to get adsorbed on suspended particulate matter (Pađan et al., 2019). The intense removal of Cr in the freshwater and saltwater interface during SWM and NEM might be because of hexaaquo complex and Cr-organic associations, which are stable in freshwater but destabilize with an increase in ionic strength and precipitate as floccules in high turbid zones (Pađan et al., 2019; Campbell et al., 1984). Apart from that, the precipitation of dissolved Fe and Mn may also provide a mechanism for the removal of dissolved Cr through co-precipitation or adsorption of Cr on newly formed Fe and Mn precipitates (Bewers & Yeats, 1978; Campbell et al., 1984).

4.4.3.6 Barium (Ba)

Ba concentration in the water is recorded only at 6 stations in the lower part of the estuary (Mid salinity zone) during both seasons despite the presence of a higher Ba concentration in the lithology exposed in the basin area. The Ba in water is mainly from the constituents of particulate matter in the estuary (Coffey et al., 1997; Moore & Shaw, 2008; Samanta & Dalai, 2016; Mori et al., 2019). According to a study by Coffey et al. (1997), large discharge rivers such as Zaire, Ganges-Brahmaputra, and Amazon desorb Ba in a low salinity range, whereas in the river with smaller discharge such as Sibuti, which has a relatively compressed salinity gradient with distance, the dissolved Ba peak tends to be observed at a higher salinity. The increase in salinity along the estuarine transect drives Ba desorption from the riverine particles (Mori et al., 2019; Coffey et al., 1997). Furthermore, under low-salinity conditions such as the upper part of the estuary, removal of dissolved Ba is possible in association with coprecipitation with Fe and Mn oxyhydroxides because of higher oxygen saturation in the water column (Mori et al., 2019). Likewise, higher saturation of oxygen in the water column during NEM might also be the reason behind the decrease in the concentration of Ba in water as compared to SWM in the estuary (Fig. 4.9).

4.4.3.7 Aluminum (Al) and Lead (Pb)

The concentrations of Al and Pb recorded BDL during both seasons despite the presence of Al and Pb bearing siliciclastic sedimentary rocks in the river basin (Nagarajan et al., 2015; Nagarajan et al., 2017a). This indicates a combination of three mechanisms responsible for complete Al removal such as flocculation, authigenic aluminosilicate formation and adsorption (Takayanagi et al., 2000; Simonsen et al., 2019). During the high river discharge such as NEM, the major form of dissolved Al in the river water was presumably colloidal, flocculated and adsorbed onto suspended particles. These mechanisms are responsible for the absence of Al in the estuarine water. On contrary, dissolved Al presumably exists as inorganic forms, authigenic aluminosilicate formations and in adsorbed forms on suspended particles. These mechanisms are more important in the estuarine processes due to the introduction of higher salinity during SWM. On the contrary, dissolved Pb, whose associated sources are industrial outputs like electroplating activity, manufacturing batteries and stainless-steel production, and machinery part in Malaysia (Mokhtar et al., 2015), is observed to be BDL to very low in concentration in the study area due to lack of such

sources in the river basin. According to Li et al. (2013), in acidic (pH<4) and alkaline (pH>8) conditions, a higher temperature range in aquatic conditions leads to release of Pb from underlying sediments and particulate matters present in the estuary. However, lower concentration observed in the lower part of the estuary during NEM might be due to the high flow rate of water and aerobic condition observed in the estuary (Li et al., 2013). In addition to that, flocculation related to an increase in salinity might be responsible for the absence of Pb in estuarine water as 84% of flocculation of Pb is noted by Samani et al. (2015) in Tadjan River, Iran.

4.4.3.8 Selenium (Se)

Selenium (Se) in the study area is dominant during both seasons while showing higher concentration in the upper part of the estuary and eventually decreasing towards the lower part. However, it does not show any significant relation with the sample stations during both seasons. During NEM, the concentration of Se is recorded to be decreasing as compared to SWM (Fig. 4.9; Table 4.4). The aerobic condition that occurred during NEM due to infusion of freshwater might be the reason for the decline in Se concentration as compared to SWM. Under such reoxygenated conditions, sorption or dissolved form of Se such as SeO_3^{2-} and SeO_4^{2-} on sediments and suspended solid happens in aqueous conditions (Kieliszek et al., 2019; Söderlund et al., 2016; Hung et al., 1995). This retention is closely linked with the presence of organic matter in water (Söderlund et al., 2016). The source of Se is believed to be from riverine inputs (Hung et al., 1995). Clay minerals, pyrites, and accessory sulfides constitute major fractions of coal (Paikaray et al., 2016) while organic-rich deposits (Fordyce, 2007) can be enriched in Se. There is an abundance of clay minerals in both Sibuti and Lambir formations and pyrite concretion present in the sandstones and limestones in Sibuti formation reported by Nagarajan et al. (2015) are rich in chalcophile elements. These concretions may host Se in it and might be the source of Se concentration in the river and estuary. Apart from that, excessive fertilization in the agricultural area, which is rich in peat soil along with possible anthropogenic activities such as combustion of coal and lignite, crude oil (Kieliszek et al. 2019) might contribute high concentration of Se in the study area. The presence of lignite in the various formations such as Belait, Miri, Tukau, Lambir, Nyalau, Setap and Tangap formation (Fig. 1.6; Table 1.2) might give rise to Se in coastal systems. A similar condition was reported in Hubei Province, China where Se content in coal oscillates was at 6 to 8.4 g kg^{-1} (Kieliszek et al., 2019).

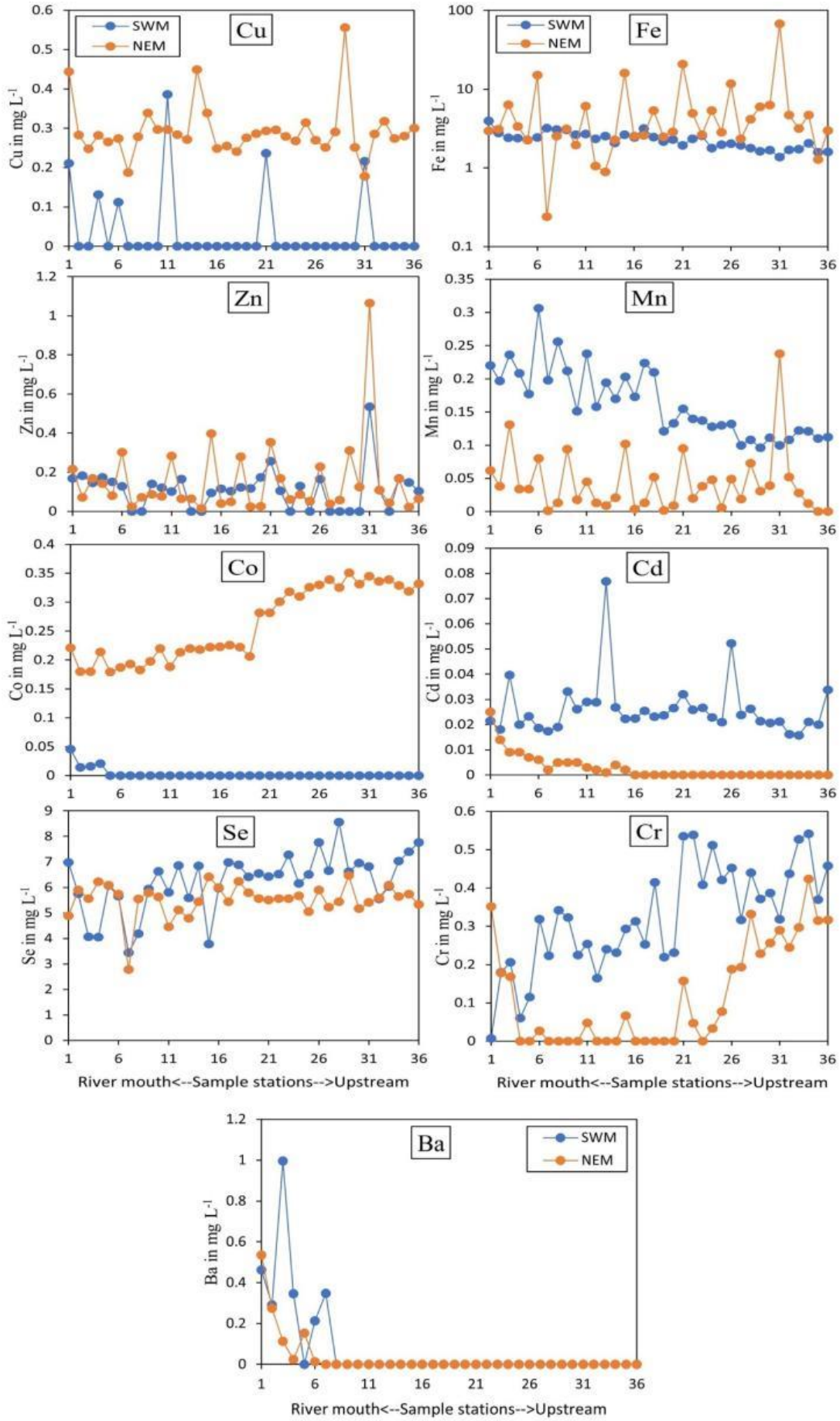

Fig. 4.10 Variation of metals in water during SWM and NEM

4.5 Drinking water quality measurement

Water during both seasons is observed to be acidic and not considerable under drinking water standards as 35 stations during SWM and 13 stations during NEM have recorded pH below the limits of both WHO (2017) and MWQSI (2021). Meanwhile, the recorded Ca^{2+} is within the limit of WHO (2017) during SWM. However, the levels of Ca during NEM seasons are much higher. Samples from 9 stations have recorded higher Ca^{2+} during NEM. Some of the samples showed Mg^{2+} concentration to be above the limits of WHO in both seasons, but the Malaysian limits stand higher at 150 mg L^{-1}. Moreover, 4 and 12 consecutive stations near the lower region of the estuary recorded higher concentrations of Na^{+} than the recommended values from WHO's (2017) standard. This is mainly because of the seawater influence during both seasons. High concentration of K^{+} exceeding the recommended WHO (2017) values are observed at 16 stations during SWM and 21 stations during NEM. The HCO_3^{-} in both seasons is recorded lower compared to the limit of drinking purpose as per the WHO (2017) guidelines. Cl^{-} concentration in water during both seasons showed higher concentration at 4 and 13 stations than the recommended value by WHO (2017). EC in water signifies the ability to conduct current through it, therefore, it is directly related to the enrichment of salts in it. The stations representing EC > 1500 µS/cm (WHO, 2017) and EC > 1000 µS/cm (Malaysian Water Quality Standard and Index, 2021) are considered unsafe for human consumption. During SWM and NEM, 2 and 12 stations in the lower part of the estuary have reported higher concentrations of more than 1500 µS/cm. Similarly, for TDS, 5 and 13 stations exceeded the levels set by WHO (2017) and (MWQSI, 2021) during SWM and NEM respectively. According to the Malaysian standards for drinking water, the turbidity of water should be within 5 NTU, whereas WHO has not specified any limits for the turbidity of water. In the study area, all the samples showed higher turbidity and are unsuitable for drinking purposes. SO_4^{2-} concentration in the study area is recorded to have very low values as compared to the standards followed by WHO (2017) and the MWQSI (2021), which stands at 250 mg $L^{-}1$. NH3 and NH_4^{+} have concentrations within the limits given by WHO (2017). NO_3^{-} also showed lower concentration at all the stations as compared to the highest value (45 mg L^{-1}) set by WHO (2017) and considered safe for drinking water usage. The concentration of Cu and Zn at all the stations was recorded lower than the recommended values given by WHO(2017) during both seasons. On the

contrary, the concentration of Fe is recorded more than the standard value of 0.3 mg L^{-1} (WHO, 2017) at all the stations during SWM and NEM. The concentrations of Mn at all the stations during SWM are above the recommended limits (Mn=0.05) given by WHO (2017) whereas 10 stations recorded higher concentration during NEM. The Cd concentration is recorded low at all the stations during SWM and NEM as compared to the recommended value of 0.03 mg L^{-1} (WHO, 2017) except for 6 stations during SWM. The Cr concentration during both seasons fell under the unsafe category as compared to the recommended value of 0.03mg L^{-1} (WHO, 2017). About 35 stations during SWM and 17 stations during NEM have been reported to have higher Cr concentrations. The concentration of Se reported at all the stations during SWM and NEM exceeded the recommended values (0.04 mg L^{-1}) given by WHO (2017) and MWQSI (2021) (0.01 mg L^{-1}). The concentration of Ba at all the stations reported lesser values as compared to 1.3 mg L^{-1} (WHO, 2017) and 0.7 mg L^{-1} (MWQSI, 2021) during both seasons, except station 3 during SWM, which has higher value than the recommended value of Malaysian standard.

Table. 4.5 Comparison of all the parameters with WHO (2017) and MWQSI (2021) drinking water standards. (All parameters are in mg L^{-1} except pH, EC (µS/cm) & Turbidity (NTU))

Parameters	SWM		NEM		WHO (2017)	MWQSI (2021)	No. of samples exceeding the limits	
	Range	Avg	Range	Avg			SWM	NEM
pH	5.74-6.88	6.16	5.45-7.6	6.5-9.0	6.5-8.5	6.5-9.0	35	13
Ca^{2+}	2-14	4.83	2-286	--	75	--	0	9
Mg^{2+}	0.6-54	4.7	0-1082.4	150	50	150	1	14
Na^{+}	20.4-1252.8	134.7	2.76-3034	200	200	200	4	13
K^{+}	7.96-75.05	15.89	2.88-98.26	--	12	--	14	21
HCO_3^{-}	24.4-54.9	31.35	12.2-61	--	500	--	0	0
Cl^{-}	35.45-2153.58	182.17	17.73-5742.9	250	250	250	4	13
EC	107.6-3161.2	409.6	97.7-11971.44	1000	1500	--	2	12
TDS	153.8-4516	585.15	139.59-8380	500	500	1000	5	13
Turbidity	7.87-53.9	27.9	15.1-50.1	5	--	5	36	36
SO_4^{2-}	6-89	34.45	2-133	250	--	250	0	0

Parameters	SWM		NEM		WHO (2017)	MWQSI (2021)	No. of samples exceeding the limits	
	Range	Avg	Range	Avg			SWM	NEM
PO_4^{3-}	0-3.45	0.87	0.03-0.35	--	0.025	--	36	36
NH_3	0.03-0.9	0.18	0.17-0.97	1.5	--	1.5	0	0
NH_4^+	0.09-0.32	0.15	0.18-1.03	--	1.5	--	0	0
NO_3^-	0.07-0.34	0.12	0-4.09	10	45	10	0	0
Cu	0-0.39	0.04	0.18-0.56	1	2	1	0	0
Zn	0-0.53	0.11	0.02-1.07	3	3	3	0	0
Fe	1.38-3.95	2.29	0.24-64.48	0.3	0.3	0.3	36	34
Co	0-0.05	0.003	0.18-0.35	--	--	--	--	--
Mn	0.1-0.31	0.16	0-0.24	0.1	0.05	0.1	36	6
Cd	0.02-0.08	0.03	0-0.03	0.01	0.03	0.03	3	0
Pb	0	0	0-0.09	0.01	0.01	0.05	0	2
Cr	0.01-0.54	0.32	0-0.42	0.05	0.05	0.05	35	17
Al	0	0	0	0.2	0.9	0.2	0	0
Se	3.45-8.56	6.24	2.78-6.47	0.01	0.04	0.01	36	36
Ba	0-0.996	0.074	0.536	1	1.3	0.7	0	0

4.6 Suitability of water for Irrigation

4.6.1 Electrical conductivity (EC)

Electrical Conductivity (EC) is an effective parameter to measure the salinity hazard for crops as it reflects the salt content in water. Higher EC in water can affect the productivity of crops by increasing the incapability of plants to compete with the ions present in the soil solution (Mohamed et al., 2017). The major components for the increase in EC are salt, more specifically Na^+ and Cl^-. So, higher EC is an indication of the presence of higher salt content in the soil or salinity hazard, which is not suitable for irrigation. Depending on such properties, Wilcox (1955) has proposed the classification of EC in which water samples can be categorized according to the level of EC and their suitability for agricultural purposes.

Table 4.6 Comparison of samples depending on their EC conductivity during SWM and NEM

EC (µS/cm)	Suitability	SWM (Total samples-36)	NEM (Total samples-36)
<250	Excellent	27	12
250-750	Good	5	11
750-2250	Permissible	2	4
2250-5000	Doubtful	2	6
>5000	Unsuitable	0	3

According to the classification (Table 4.6), out of 36 samples, SWM has 27 samples in the excellent category, whereas 5 and 2 samples are within good and permissible limits respectively. However, during the NEM, the number of samples in the excellent category is lesser than SWM, but a majority of the samples are above permissible limits with 12, 11, and 4 samples falling in excellent, good and permissible category respectively. On the contrary, 2 and 6 samples from SWM and NEM respectively are in the doubtful category along with 3 samples that are considered unsuitable for agricultural purposes during NEM. The TDS, Na^+ and Cl^- concentrations increase during NEM as compared to SWM in which this might be due to the combined effect of seawater intrusion and contribution of Cl^- from agricultural fields, specifically from potash-related fertilizers which uses potassium chloride and are applied to increase the fertility of the soil (Hunt et al., 2012; Khatri et al., 2015). This mixed effect is contributing more towards the decrease in excellent suitability reporting stations during NEM despite the infusion of fresh water.

4.6.2 Corrosivity ratio (CR)

Corrosivity Ratio (CR) is defined as the corrosive tendency of water due to the proportional occurrence of alkaline earths and saline salts along with sulfates in groundwater (Varade et al., 2018). Corrosion causes significant loss in the hydraulic capacity of pipes and pipe fittings. So high corrosive water is not meant to be transported through them (Balasubramanian, 1986; Aravindan, 2004; Shankar et al., 2011; Rawat et al., 2018). Corrosion is mainly an electrolytic process, which creates a series of damages and gradually destroys and corrodes away a metal surface, particularly Pb and Cu (Bardal & Derby, 2004). The range of corrosion continuous relative to chemical equilibrium reactions as well as upon specific physical influence

such as temperature, pressure and velocity of flow (Moncmanová et al., 2007). In addition to that, lack of carbonate minerals' intensity concentration of Cl^- and SO_4^{2-} can increase the corrosion rate as well (Rawat et al., 2018; Abhay et al., 2018). Additional studies conducted by NAWQA (2021) placed pH out of neutral range, elevated concentrations of dissolved and suspended solids, and lower alkalinity as the major factors controlling corrosivity in surface water conditions.

Ryzner (1944) proposed a ratio to assess the corrosive nature of the groundwater on metals. Lawrence (1995) and Sridhar (2001) used this methodology to identify the corrosive nature of water in Ramanathapuram District and the Kodavanar basin (South India) respectively. If the CR is < 1, then the water is non-corrosive, and if the CR > 1, then the water is corrosive (Rengarajan & Balasubramaniam, 1990). The corrosiveness of water can be expressed as follows:

$$\text{Corrosivity Ratio} = \frac{\left[\frac{Cl^-}{35.5}\right]+2\left[\frac{SO_4^-}{96}\right]}{2\left[\frac{[HCO_3^-+CO_3^-]}{100}\right]} \quad \text{……..(eq. 4.4)}$$

(All ion concentrations are expressed in meq L^{-1})

In the study area, all the samples in SWM and NEM have values higher than 1 and are corrosive in nature. It cannot be transported through metal pipes and transporting through PVC pipes will be a better option in such conditions.

4.6.3 USSL classification

United States Salinity Laboratory (USSL, 1954) has proposed a classification for the rating of irrigation water with reference to salinity and sodium hazard (Richards, 1954). The total dissolved solids' content is measured in terms of specific electrical conductance (EC in µS/cm) and gives the salinity hazard of irrigation water. The sodium hazard in irrigation water is expressed by determining the Sodium Adsorption Ratio (SAR) and is a measure of alkali/sodium hazard to crops. It is estimated by the formula in which concentrations are expressed in milliequivalents per liter (meq L^{-1}).

$$\text{SAR} = \frac{Na^+}{\left\{\frac{Ca^{2+}+Mg^{2+}}{2}\right\}^{\frac{1}{2}}} \quad \text{……..(eq. 4.5)}$$

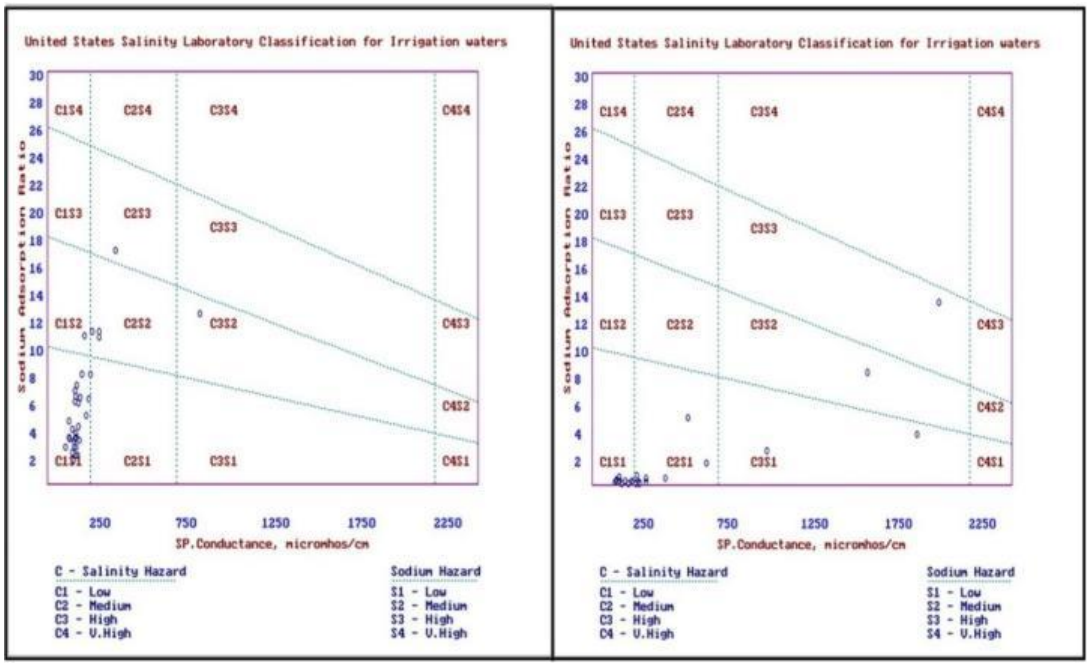

Fig. 4.11 USSL Classification of water for irrigational use for SWM (left) and NEM (right)

In conclusion, 90% of the samples in the study area are under the excellent category (C1S1) for irrigation purposes irrespective of the seasons. The samples fall under low sodium and low salinity hazard. Apart from this, C2S2 in SWM consists of three samples falling under the category of medium salinity and sodium hazard. Categories like C1S2, C2S3 and C3S2 consist of one sample each, which is represented by low salinity-medium sodium hazard, medium salinity-high salinity hazard and high salinity-medium sodium hazard respectively. In NEM, the C2S1 category has eight samples, which indicates that it falls under medium salinity-hazard and medium sodium-hazard. Moving onto C3S1, the category upholds three samples, which fall under high-salinity and low-sodium hazard. C3S2 includes only one sample and it falls under high salinity hazard and medium sodium hazard. C3S3 also has only one sample and it has high salinity and high sodium hazard.

4.6.4 Sodium percentage (Na%) or Sodium hazard

Irrigation water containing large amounts of sodium is of special concern due to sodium's effects on soil and poses a sodium hazard. This is also caused because of the relative proportion of sodium to other principal cations (Wilcox, 1948; Eaton, 1950). Excess sodium in water produces the undesirable effects of changing soil properties and reducing soil permeability as well. Na^+ reacts with CO_3^{2-} and forms alkaline soils, while Na^+ reacts with Cl^- and forms saline soils. Na^+ affected soil (alkaline/saline)

retards crop growth (Todd, 1980; Rawat et al., 2018). Excessive sodium in water renders it unsuitable for soils, as it contains exchangeable Ca^{2+} and Mg^{2+} ions. If the percentage of Na^{+} to Ca^{2+}+Mg^{2+}+Na^{+} is considerably above 50 ppm in irrigation waters, soils containing exchangeable Ca^{2+} and Mg^{2+} make up Na^{+} in base-exchange reaction will cause deformation (Rawat et al., 2018) and harm to the permeability of soil (Saleh et al., 1999; Kumar et al., 2007).

For irrigational purpose, sodium is usually presented as percent sodium and can be obtained using the following formula.

$$Na^{+}\% = \frac{Na^{+}}{Ca^{2+}+Mg^{2+}+K^{+}} \times 100 \quad \text{..... (eq. 4.6)}$$

(where the quantities of Ca^{2+}, Mg^{2+} Na^{+} and K^{+} are expressed in milliequivalents per litre (meq L^{-1}).

Table. 4.7 Comparison of water samples during SWM and NEM depending on Na%

Na%	Remark on Water Quality	SWM (Total samples-36)	NEM (Total samples-36)
0-20	Excellent	0	11
20-40	Good	0	9
40-60	Permissible	0	7
60-80	Doubtful	8	8
>80	Unsuitable	28	1

In the study area, samples from 28 stations during SWM fell under the unsuitable level along with 8 samples, which fell under the doubtful category and are very prone to salinity hazard, thus not very suitable for irrigation purposes. However, during NEM, the opposite trend has been noticed, where only 1 sample came under the unsuitable category and 11 samples are placed in the excellent category for the irrigation purposes. Apart from this 9, 7 and 8 samples fell under the good, permissible, and doubtful category respectively (Table 4.7) during NEM. An improved condition of sodium hazard during NEM is due to freshwater water infusion influenced by monsoonal rainfall in the estuary. The increase in concentration of Ca^{2+} and Mg^{2+} in water (Fig. 4.6) is also observed during this season, which might have diluted the Na^{+} concentration (Rawat et al., 2018) in estuarine water.

4.6.5 Residual sodium carbonate (RSC)

When CO_3^{2-} levels exceed the total amount of Ca^{2+} and Mg^{2+}, water quality drops. If the excess CO_3^{2-} (residual) concentration becomes too high, CO_3^{2-} combines with Ca^{2+} and Mg^{2+} to form a solid material (scale) which precipitates. The relative abundance of Na^+ with respect to alkaline earth metals (Mg^{2+} and Ca^{2+}), and the quantity of HCO_3^- and CO_3^{2-} in excess of alkaline earths also influences the suitability of water for irrigation (Kumar et al., 2007; Kumarasamy et al., 2014; Rawat et al., 2018). This condition is represented as the residual sodium carbonate (RSC) index of irrigation water and indicates the alkalinity hazard for soil (Richards, 1954). The RSC index is used to find the suitability of the water for irrigation in clay soils, which have a high cation exchange capacity. Excess quantity of sodium bicarbonate ($NaHCO_3$) and carbonate ($NaCO_3$) (expressed as RSC) causes dissolution of organic matter in the soil (Kumar et al., 2007), which in turn leaves a black stain on the soil surface on drying, and is detrimental to the physical properties of soils. RSC values are expressed as follows:

$$\mathrm{RSC(meql^{-1})} = (\mathrm{HCO_3^-} + \mathrm{CO_3^{2-}}) - (\mathrm{Ca^{2+}} + \mathrm{Mg^{2+}}) \quad \text{.....(eq. 4.7)}$$

Where the concentration of HCO_3^-, CO_3^{2-}, Ca^{2+} and Mg^{2+} are expressed in meq L^{-1}.

The Residual Sodium Carbonate (RSC) during the survey is found to be less than 1.25 meq L^{-1} in all the samples irrespective of seasons (Table 4.8). According to Eaton (1950), waters with RSC greater than 2.5 meq L^{-1} may be regarded as deleterious while those with less than 1.25 meq L^{-1} are considered safe, thus suggesting that HCO_3^- content is higher than the dissolved Ca^{2+} and Mg^{2+} ions in water.

Table 4.8 Comparison of water samples depending on their RSC values during SWM and NEM

RSC Values	Remarks on Quality	SWM (Total samples-36)	NEM (Total samples-36)
<1.25	Good	36	36
1.25-2.5	Medium	0	0
>2.5	Bad	0	0

4.6.6 Sodium absorption ratio (SAR)

SAR is one of the most commonly used indices to assess irrigational suitability of water keeping in the observation that excess sodium can reduce soil permeability and soil structure (Saleh et al., 1999; Kumar et al., 2007). It measures sodicity in terms of the relative concentration of sodium ions to the sum of calcium and magnesium ions in a water sample (Subbarao et al., 2018). SAR can be calculated using the following formula:

$$SAR = \frac{Na^{+}}{\sqrt{(Ca^{2+}+Mg^{2+})/_{2}}} \text{.....(eq. 4.8)}$$

Where the ionic concentrations are expressed in meq L^{-1}.

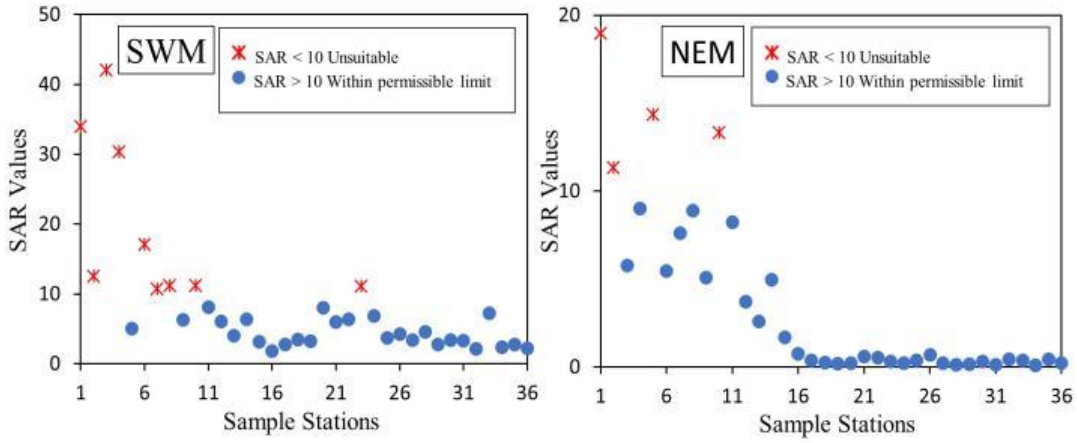

Fig. 4.12 SAR values of water sample during SWM and NEM

SAR values during SWM and NEM varied between 1.77 to 33.96 meq L^{-1} and 0.1 to 18.97 meq L^{-1} respectively (Fig. 4.12). The majority of the sample stations were observed to have SAR values below permissible limits and suitable for irrigation. Nine sample stations during SWM and 5 sample stations during NEM fall under the unsuitable category and possess a high chance of sodicity upon use in case of irrigation purposes.

4.6.7 Kelly's ratio

Kelly (1940; 1963) has found the hazardous effect of sodium on water quality for irrigation usage in terms of Kelly's ratio (KR). Kelly's ratio was calculated from the formula given in equation 4.9 and all concentrations were expressed in meq/l.

$$Kelly's\ ratio = \frac{Na^+}{(Ca^{2+}+Mg^{2+})} \text{.....(eq. 4.9)}$$

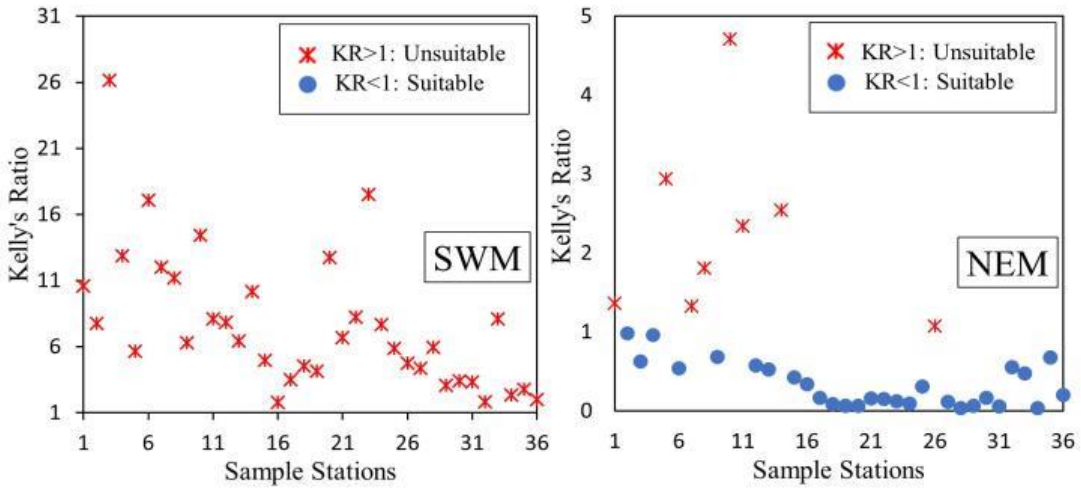

Fig. 4.13 Kelly's ratio of water sample during SWM and NEM

According to Kelly's ratio, samples <1 are suitable for irrigation, while those with a ratio >1 are unsuitable. In the study area, all the samples during SWM along with 8 samples during NEM are unsuitable for irrigation purposes (Fig. 4.13), whereas the rest and majority of the stations during NEM are suitable with <1 values (Fig. 4.13). Seawater intrusion due to high tidal influence during SWM caused excessive Na^+ at all the stations. On the other hand, freshwater input during NEM due to monsoonal rainfall has reduced the possibility of hazardous Na^+ influence at majority of the stations.

4.6.8 Permeability index (PI)

The Permeability Index (PI) values also depict the suitability of water for irrigation purposes since long-term use of irrigation water can affect the soil permeability. This is mainly influenced by the Na^+, Ca^{2+}, Mg^{2+} and HCO_3^- contents of the soil. The PI can be expressed as:

$$\text{PI} = \frac{\text{Na}^+ + \sqrt{\text{HCO}_3^-}}{\text{Ca}^{2+} + \text{Mg}^{2+} + \text{Na}^+} \times 100 \text{ (Doneen, 1964) .....(eq. 4.10)}$$

The concentrations are reported in meq L^{-1}. Doneen (1964) developed a criterion for assessing the suitability of water for irrigation based on PI, where waters can be classified as classes I, II, and III. Class I and II water are categorized as good for

irrigation with 75% or more of maximum permeability. Class III water is unsuitable with 25% of maximum permeability.

During SWM, all the samples fall in class III and can be categorized as unsuitable for irrigation. One sample falls under class II and can be categorized as good for irrigational purposes with more than 75% of permeability. As explained before in section 4.6.4, the increased possibility of sodium hazard in SWM might be responsible for the unsuitable permeability index in majority of the samples. Such hazard can cause Ca^{2+} and Mg^{+} deficiency resulting in low permeability of soil (Rawat et al. 2018).

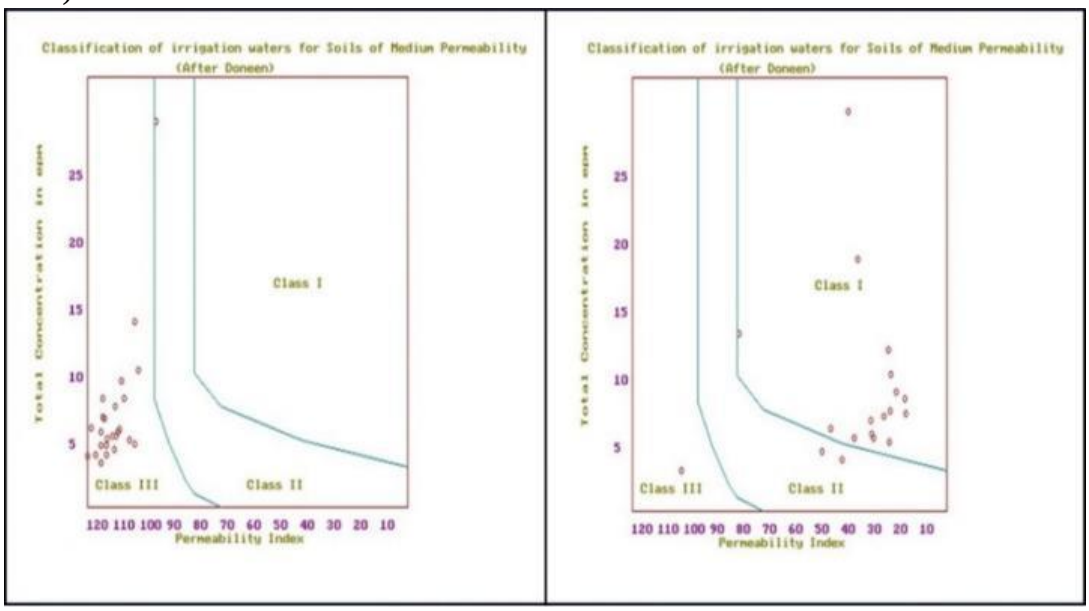

Fig. 4.14 Permeability Index of water during SWM (left) and NEM (right)

On the contrary, most of the samples during NEM are classified under class I and II and possess a permeability of 75% or more and are considered suitable for irrigation purposes. However, one sample (Station 1) in this season is categorized under class III, which is unsuitable. This might be due to the effect of an increase in Ca^{2+} and Mg^{2+} type water along with an increase in SO_4^{2-}.

4.6.9 Hardness of water

The main natural sources of hardness in water are dissolved polyvalent metallic ions from sedimentary rocks, seepage, and runoff from soils (Akram et al., 2018; WHO, 2011). Keeping this in mind, Ca^{2+} and Mg^{2+} can be categorized as two principal ions that play an essential role in increasing the hardness of water (WHO, 2009; Sengupta et al., 2013). These ions originate from sedimentary rocks, most commonly from

limestone and chalk. Some other cations like Al, Ba, Fe, Mn and Zn can also contribute to this process (WHO, 2009). Although the hardness of water is caused by mainly cations, it can also involve carbonate (temporary) and non-carbonate (permanent) hardness (Handa, 1964). According to WHO (2009), removal of hardness can be done by removing responsible ions through boiling. But such method becomes difficult in case of permanent hardness. This is caused by the high amount of dissolved Ca^{2+} and Mg^{2+} ions in water. However, the removal is much easier in case of carbonate hardness or temporary hardness and can be removed with the help of boiling. The hardness in water is derived from the solution of CO_2 and released by bacterial action into the soil through percolating rainwater. Total Hardness (TH) is expressed as

$$TH = (Ca^{2+} + Mg^{2+}) \times 50 \quad \text{.....(eq. 4.11)}$$

Where TH, Ca^{2+} and Mg^{2+} are measured in meq L^{-1}.The Total Permanent Water Hardness is expressed as equivalent of $CaCO_3$ (WHO, 2009) and can be calculated with the following formula.

$$\text{Total Permanent Hardness } CaCO_3(mg/l) = 2.5(Ca^{2+}) + 4.1(Mg^{2+}) \quad \text{...(eq. 4.12)}$$

According to Sawyer and McCarty's (1967) classification of hardness, samples can be presented in various groups as shown in Table 4.9. This categorization shows 34 samples falling under the soft category in SWM along with 1 sample each in the slightly hard and moderately hard category respectively. On the contrary, the highest number of samples fall under the very hard category during NEM is standing at 15, followed by 8, 7 and 6 samples falling under moderately hard, slightly hard and soft category respectively. Similarly, Handa's hardness classification (1964) is also presented in Table 4.9, which has placed 8 (A3) and 28 (B3) samples in the permanent hardness and temporary hardness category during SWM. However, during NEM, permanent hardness category holds 24 samples in A2 and 7 samples in the A3 group (Table 4.9). The temporary hardness category has 5 samples under the B3 group. This significant increase in NEM samples in the permanent hardness category might be due to the increase in the concentration of Ca^{2+} and Mg^{2+} in water, which can be noticed in figure 4.8.

Table 4.9 Various Classification depending on the Hardness of water during SWM and NEM

Sawyer and McCarty Hardness				Handa (1964) Hardness Classification							
Water Condition	$CaCO_3$ equivalent (mg/l)	Samples falling in the Category		SWM				NEM			
		SWM	NEM	NCH (Permanent Hardness)		CH (Temporary Hardness)		NCH (Permanent Hardness)		CH (Temporary Hardness)	
Soft	<75	34	6	**A1**	0	**B1**	0	**A1**	0	**B1**	0
Slightly Hard	75-150	1	7	**A2**	0	**B2**	0	**A2**	24	**B2**	0
Moderately Hard	150-300	1	8	**A3**	8	**B3**	28	**A3**	7	**B3**	5
Very Hard	>300	0	15								

4.6.10 Schoeller's water type

The water types in the study area in both monsoons have been identified according to the classification of Schoeller (1967) and can be explained as follows:

Schoeller (1977) described the first and foremost water in the system as those in which $rCO_3^{2-} > rSO_4^{2-}$……..Type-I

as the total concentration in water changes the above relation changes to $rSO_4^{2-} > rCl^-$ ……Type-II,

at similar higher conditions water may also change to $rCl^- > rSO_4^{2-} > rCO_3^{2-}$ ……..Type-III,

and in the final stages $rCl^- > rSO_4^{2-} > rCO_3^{2-}$ and $Na^+ > Mg^{2+} > Ca^{2+}$……..Type-IV.

Depending on the above types, 20 and 14 samples during SWM fall under type-III and type-I respectively. In addition to that, 2 samples fall in type-II and none of the samples fall in type-IV. Similarly, 20 and 16 falls under type-III and type-I respectively during NEM where none of the samples came under type-II and type-IV (Table 4.11). This indicates the domination of Cl^- ions in the study area. But the equivalent distribution of both the ions can be attributed to the domination of CO_3^{2-} based fresh water in the upper part of the estuary, which is becoming Cl^- based water as it nears the river mouth. The excess of chloride in the study area may be due to the seawater's influence or the

input of anthropogenic activities contributed by the agricultural run-off (Srinivasamoorthy et al., 2014; Vengosh et al., 2002).

Table 4.10 Classification of water according to Schoeller's classification (1967) during SWM and NEM

Schoeller's Classification	SWM (Total sample-36)	NEM (Total sample-36)
Type-I	14	16
Type-II	2	0
Type-III	20	20
Type-IV	0	0

4.6.11 Chloride classification

Stuyfzand (1989) classified water types depending on Cl^- content, alkalinity, important (Na^+, Ca^{2+}, Mg^{2+}) cations and anions (HCO_3^-, SO_4^{2-}, Cl^-), where [$Na^+ + K^+ + Mg^+$] was corrected for the sea salt. Depending on the mentioned parameters, 8 water types are brought as follows:

Table 4.11 Comparison of water samples and type depending on the Cl^- content in water during SWM and NEM

Main Type	Cl^- in meq L^{-1}	SWM (Total samples-36)	NEM (Total samples-36)
Very Oligohaline	<0.141	0	0
Oligohaline	0.141-0.846	4	2
Fresh	0.846-4.231	28	19
Fresh Brackish	4.231-8.462	0	2
Brackish	8.462-28.206	2	4
Brackish salt	28.206-282.064	2	9
Salt	282.064-564.127	0	0
Hypersaline	>564.127	0	0

According to the classification (Table 4.12), freshwater is dominating the estuary as 28 and 19 samples fell in this category during SWM and NEM respectively. Additionally, 4 and 2 samples from SWM and NWM are oligohaline in nature, along with 2 samples in NEM that showed fresh-brackish nature. Along with the other samples, 2 and 4 samples were brackish in nature while brackish-salt nature are shown by 2 and 9 samples in SWM and NEM respectively. The high rainfall during NEM

and freshwater infusion into the estuary is responsible for the reduced fresh chloride in water.

4.7 Hydrochemistry

4.7.1 Indices of base exchange (IBE)

The ion exchange and geochemical process happening between the river water and its host environment during the travel process can be verified using an index of Base Exchange (Schoeller, 1965). According to Thilagavathi et al. (2012), there are substances called permutolites, which have certain qualities of absorption and tend to exchange their cations with cations present in water. These substances may include clay minerals like kaolinite, illite, chlorite, halloysite, glauconite, zeolites and organic matter. Kaolinite, illite, chlorite and halloysite are the clay minerals in which ions are held at edges and their ionic exchange capacity is low. But, in the case of montmorillonite and vermiculite, the scenario is opposite and the exchange capacity tends to be higher when the number of ions held on the surface is more. Chloro-alkaline indices, CAI1 and CAI2 (eq. 4.14 and 4.15), are used to measure the extent of base exchange during rock–water interaction. When Na^+ and K^+ ions in water are exchanged with Mg^{2+} or Ca^{2+} ions in weathered materials, the index value will be a positive value, indicating base exchange, whereas negative value indicating chloro-alkaline disequilibrium (Schoeller, 1965). This is also known as reverse ion-exchange reaction (eq. 4.13).

$$Na^+ + K^+ \Leftrightarrow Ca^{2+} + Mg^{2+} \quad \text{.....(eq. 4.13)}$$

The Chloro-alkaline indices used for the evaluation can be expressed as:

$$CAI1 = [Cl^- - (Na^+ + K^+)]/Cl^- \quad \text{.....(eq. 4.14)}$$

$$CAI2 = [Cl^-(Na^+ + K^+)]/[Cl^-(SO_4^- + HCO_3^- + CO_3^- + NO_3^-)] \quad \text{.....(eq. 4.15)}$$

Where all ions were measured in meq L^{-1} for calculation.

During this process, the host rocks are the primary sources of dissolved solids in the water (Srinivasamoorthy et al., 2014). In the study area, the dominance of Na^+ and K^+ in rock with Mg^{2+} or Ca^{2+} in water during SWM is observed, where 30 samples showed indication of exchange between Na^+ and K^+ in rock with Mg^{2+} or Ca^{2+} in water, whereas 6 samples in the same condition showed exchange between Na^+ and K^+ in

water with Mg^{2+} or Ca^{2+} in rock (Table 4.10). On the contrary, during NEM, this process is opposite and showed 33 samples under exchange between Na^{+} and K^{+} in water with Mg^{2+} or Ca^{2+} in rock. These samples also included 3 samples in the exchange between Na^{+} and K^{+} in rock with Mg^{2+} or Ca^{2+} in the water category (Table 4.10). Considering the sharp increase in the concentration of Ca^{2+} and Mg^{2+} during NEM, it is an indication of the mixing of various weathered ions in river water through runoff from its catchment, which mainly consists of sandstones and calcareous sandstone, shale, limestone and marl and are dominant in Sibuti and Lambir formations (Fig. 1.6 and Table 1.2) (Nagarajan et al., 2015; Nagarajan et al., 2017a). These rocks are prominent to weathering and consist of calcite ($CaCO_3$), dolomite ($CaMg(CO_3)^2$) and less prominent feldspars along with weathering resistant minerals like quartz (Nagarajan et al., 2015; Simon et al., 2014). On the other hand, chloride in water is a result of saline intrusion from the sea but the sharp increase in concentration from SWM to NEM can be attributed to the base exchange of Na^{+} for Ca^{2+} and Mg^{2+} as mentioned earlier. It may also be due to agricultural return flow of water, which is characterized by higher ratios of SO_4^{2-}/Cl^{-} (>0.05), attributing to the application of gypsum fertilizers (Vengosh et al., 2002; Srinivasamoorthy et al., 2014), which has also been identified in the reconstructed piper plot given by Lawrence and Balasubramanian (1994).

Table 4.12 Classification of base exchange Schoeller (1965) during SWM and NEM

Exchange conditions	SWM (Total samples-36)	NEM (Total samples-36)
Na^{+} and K^{+} in rock with Mg^{2+} or Ca^{2+} in water	30	3
Na^{+} and K^{+} in water with Mg^{2+} or Ca^{2+} in rock	6	33

4.7.2 Piper's plot

A trilinear plot is used to study the water chemistry and quality (Piper, 1944). In this diagram, cations and anions were normalized to 100% and plotted in their appropriate triangle (Shelton et al., 2018). The main function of the Piper diagram is to identify the hydro-facies, nevertheless, it also helps us to understand the several geochemical processes along the flow path of water. It provides a convenient method to classify and compare water types based on the ionic composition of different water samples (Shelton et al., 2018; Wanda et al., 2012). This diagram is very useful for bringing out

the chemical relationship among waters in more definite terms (Wanda et al., 2012). Piper (1944) presented a graphical technique, which is used to assess the nature of hydro geochemistry of the estuary waters. It is an effective tool in separating hydro-chemical analysis for critical studies with respect to the sources of dissolved constituents (major cations: Ca^{2+}, Mg^{2+}, Na^{+}, K^{+} and major anions: Cl^{-}, NO_3^{-}, SO_4^{-}, CO_3^{-}, HCO_3^{-}) in waters, modifications in the character of water as it passes through an area and related to geochemical problems (Shelton et al., 2018; Wanda et al., 2012). The central plotting field (diamond shape) of the trilinear diagram is divided into nine areas and water is classified in to nine types depending upon the area in which the analysis results fall and the alkali cations (Na^{+} and K^{+}) are called primary constituents and the alkaline earth cations (Ca^{2+} and Mg^{2+}) are called secondary constituents. The strong acid cations (SO_4^{2-}, Cl^{-}) are treated as saline constituents while CO_3^{2-} and HCO_3^{-} are treated as a weak acid. The approximate balancing of these cations and anions determines the chemical character of water. There are various water types found, such as Ca-HCO_3 type, Na-Cl type, Ca-Mg-Cl type, Ca-Na-HCO_3 type, Ca-Cl type and Na-HCO_3 type, etc.

During SWM, most of the sampling stations in the cation triangle fall in Na+K type, whereas in the anion triangle, the majority of samples fall under Cl type while a minority of the sample have no dominant anions. When this is extended to the diamond area, all the samples fall under the Na-Cl type of water and are directly influenced by seawater in the estuarine region (Fig. 4.15). This phenomenon can be explained by the variety of conditions like gentle coastal hydraulic gradients, tidal and estuarine activity, sea level rises, low infiltration, excessive withdrawal and local hydrogeological conditions (Sivakumar et al., 2008; Sivasubramanian et al., 2013; Senthilkumar et al., 2017). In this study, the Na-Cl type of water is mainly dominating because of the high tidal influence, considering the time of sample collection along with the low flow of the Sibuti river system due to less rainfall during the SWM period.

However, in the diagrams for NEM, samples show various water types in the cation triangle including Ca type, Na+K type, Mg type and no dominant type, whereas in the anion triangle all the samples fall under Cl type. When extended to the diamond area, these samples fall under various facies including Na-Cl type, Ca-Cl type and Ca-Mg-Cl type, unlike the SWM. This pattern suggests that the water chemistry in the study area changes due to the cation exchange reaction, as well as the simple mixing with

seawater as a result of seawater intrusion (Sivasubramanian et al., 2013). The dominant water type in NEM can be represented as Ca-Cl type > Na-Cl type > Ca-Mg-Cl type (Fig. 4.15). The noticeable variation in this season can be attributed to the mixing of fresh rainwater and run-off from the ground into the river as samples were collected during the monsoon. Generally, the anionic composition of freshwater in estuaries changes systematically from bicarbonate dominance to Cl^- dominance as water flows from a freshwater zone to the mouth (Appelo & Postma, 1996). Samples falling in the Ca–Cl type are prominent at the most upstream side of the estuary, which indicate the weathering of limestones and dolomites in the upstream areas or direct recharge from rainwater (e.g. Ravikumar et al., 2015).

During the phase of seawater intrusion, underneath the freshwater flow, there is an initial increase in salinity and a rapid and marked reverse exchange of Na/Ca, which is recognized by the characteristic Ca-Mg-Cl facies (e.g. Ravikumar et al., 2017). This type of water evolves towards facies that are closer to seawater (Na-Cl). This coastal region possibly represents ion-exchange reactions or a hydrochemical evolutionary path from Ca–Cl and Ca-Mg-Cl water type to Na–Cl water type. Here, Ca–Cl and Ca-Mg-Cl represent the bedrock interaction with the water and reverse ion exchange processes, whereas samples representing Na–Cl type indicate seawater mixing, which is mostly constrained in the coastal region and weathering characteristics are noted in the upstream region of the estuary.

The factors that influence the change of chemical composition of water can be investigated graphically by plotting the difference in milliequivalent concentrations between alkaline earth elements ($Ca^{2+} + Mg^{2+}$) and alkali metal elements ($Na^+ + K^+$) on the x-axis and the difference in milli-equivalent concentrations between weak acids (HCO_3^-) and strong acids ($Cl^- + SO_4^{3-}$) on the y-axis.
The water classification of hydrogeochemical facies of the Piper diagram was reconstructed by Lawrence and Balasubramanian (1994) in the new reconstructed diamond field (Fig. 4.16 and 4.17). It classifies water in the various zones based on various reactions occurring in the estuarine water system. According to the diagram, all samples from SWM fall into category number 12 (Fig. 4.16).

This means the water is highly contaminated with gypsum during SWM. Na-Cl water type from the sea during this season might be the main source of gypsum-influenced

water in the estuary as the concentration of gypsum is highly saturated in seawater up to 3.8 g/L (Kopittke et al., 2005). This condition can be attributed to the erosion of sedimentary deposits in association with halite, anhydrite, sulfur, calcite, and dolomite. Erosion of rocks like limestones, calcite rich sandstones, shales present at the various formations of the Sibuti River basin (Simon et al., 2014; Nagarajan et al., 2015; Nagarajan et al., 2017a) (Fig. 1.6 and Table 1.2) might be a source of the high amount of gypsum in the study area. Apart from that, 673 to 881 kg/m^3 gypsum are used in the palm oil plantation in Malaysia for various benefits such as to reduce of magnesium toxicity, increase the efficiency of crops, correct sub-oil acidity, reduce water run-off and erosion and remove salt from the soil (Tiemann et al., 2018). The leaching of gypsum from vast palm oil plantations and farming near the estuary and nearby areas might also be attributed to the gypsum influence in the estuary.

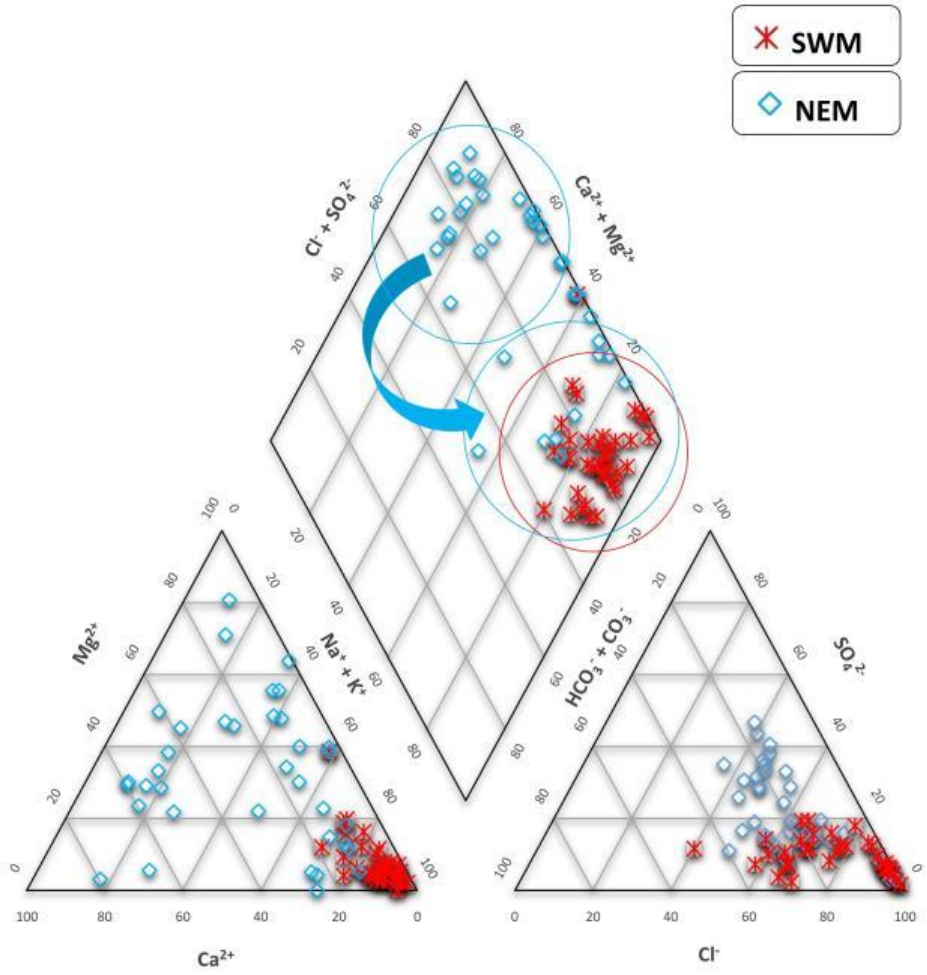

Fig. 4.15 Water Samples presented in Piper plot during SWM and NEM

Notably, the sampling process was carried out during the end of the SWM, which has less amount of rainfall, unlike the NEM. Similarly, alkalies (Na^++K^+) exceed alkaline earth elements (Ca^{2+}+Mg^{2+}) while strong acids (SO_4^{3-}+Cl^-) exceed weak acids (CO_3^{2-}+HCO_3^-) at 36 stations in this season (Table 4.13), which indicate the major influence of seawater in the estuary. Hence, gypsum from the seawater and agricultural run-off is playing a major role, unlike weathering in this season, and are dominating any other facies in the estuary.

During NEM, alkaline earth elements (Ca^{2+}+Mg^{2+}) exceed alkalis (Na^++K^+) where 25 samples and 11 samples fall under alkalis (Na^++K^+) exceed alkaline earth (Ca^{2+}+Mg^{2+}), whereas strong acids (SO_4^{3-}+Cl^-) exceed weak acids (CO_3^{2-}+HCO_3^-) were noted in 36 samples (Table 4.13). This type of water indicates the influence of weathering of bedrocks with the release of Ca^{2+} and Mg^{2+}, mostly by intensive weathering (Ravikumar et al., 2017; Sharma et al., 2012) from shale, calcareous sandstones, marl and limestones lenses in the river basin (Nagarajan et al., 2017a; Simon et al., 2014) (Fig. 1.6 and Table 1.2). The weathering of such rocks is contributing high Ca^{2+}+Mg^{2+} and SO_4^{3-}+Cl^- facies (Fig. 4.17) in the upper part of the estuary that is rich in such weathered rock content and fresh in nature. In contrast, gypsum-contaminated water samples were contributed by agricultural run-off and saltwater intrusion near the mouth region.

Table 4.13 Characteristics of corresponding subdivisions of diamond-shaped field during SWM and NEM

Characteristics of corresponding subdivisions of diamond-shaped field	SWM	NEM
Left Triangle (Fig. 4.15)		
Alkaline earth (Ca^{2+}+Mg^{2+}) Exceed alkalis (Na^++K^+)	0	25
Alkalis (Na^++K^+) exceed alkaline earths (Ca^++Mg^+)	36	11
Right Triangle (Fig. 4.15)		
Weak acids (CO_3^{2-}+HCO_3^-) exceed Strong acids (SO_4^{3-}+Cl^-)	0	0
Strong acids (SO_4^{3-}+Cl^-) exceed weak acids (CO_3^{2-}+HCO_3^-)	36	36
Diamond Area (Fig. 4.15)		
Magnesium bicarbonate type	0	0
Calcium-chloride Type	0	20
Sodium-chloride Type	36	11
Sodium-Bicarbonate Type	0	0
Mixed type (No cation-anion exceed 50%)	0	5

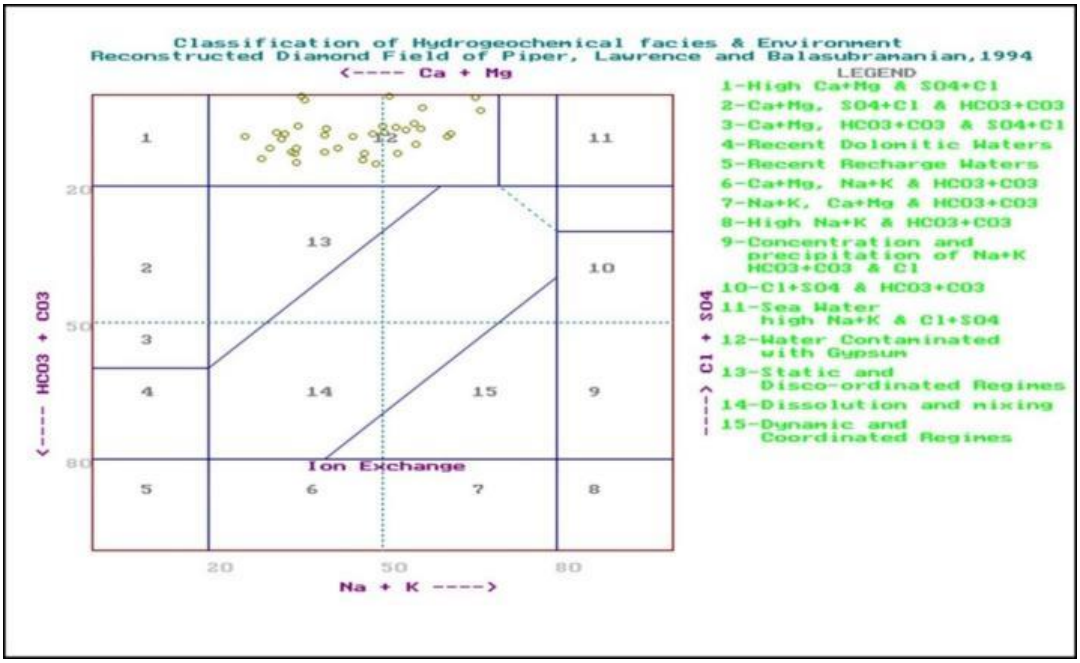

Fig 4.16 Classification of hydrochemical facies and environment according to Lawrence and Balasubramanian, (1994) during SWM

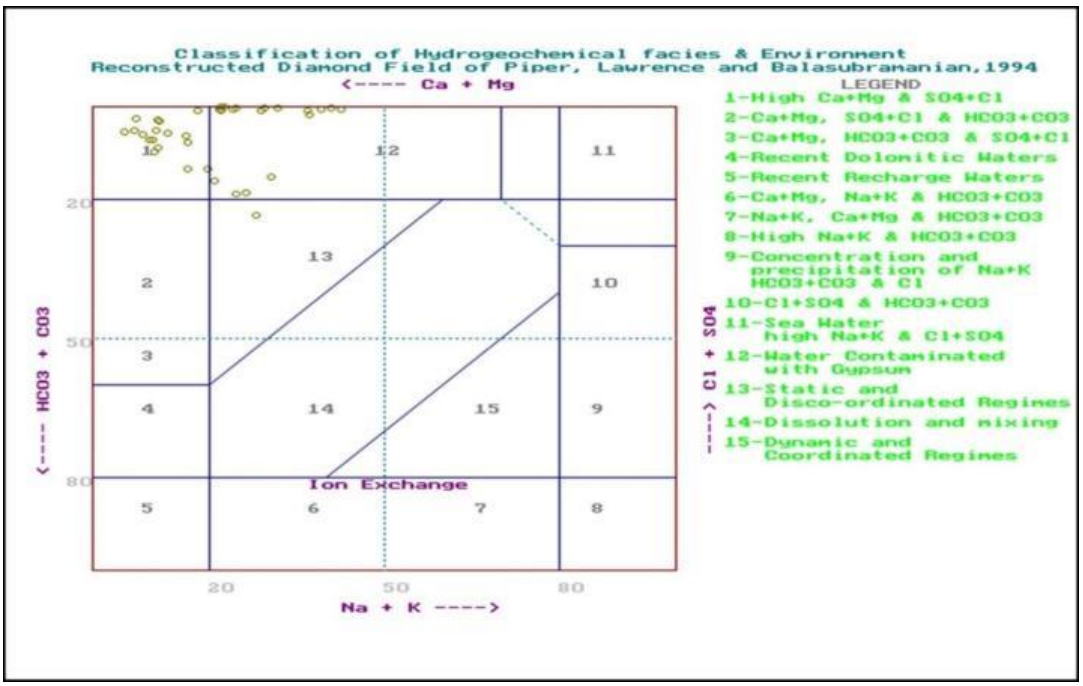

Fig 4.17 Classification of hydrochemical facies and environment according to Lawrence and Balasubramanian, (1994) during NEM

4.7.3 Gibbs plot

Gibbs diagram (Gibbs, 1970) is used to explain the major geochemical processes in water. Gibbs (1970) demonstrated that if TDS is plotted against $(Na^+ + K^+)/(Na^+ + K^+ + Ca^{2+})$, this would provide information on the mechanism controlling the chemistry of waters. It helps to explain the relationship between water composition and their respective aquifer characteristics, such as rock-water interaction, rainfall dominance and evaporation dominance along with the interacting environments. In the study area, all the samples fall outside the defined field during SWM indicate the integrated mechanism of high weathering, low evaporation and precipitation along with input from other sources (Annapoorna et al., 2015). These sources might include the effect of seawater intrusion because of the tides along with the agricultural run-off. In contrast, NEM has shown a major variation in the plot by placing the number of samples in weathering due to rock-water interaction and evaporation phase. The majority of the cations fall in rock weathering defined field, which may be due to the weathering happening in upstream and downstream region of the river as mentioned earlier. On the contrary, the rest of the cations and all the anions fall outside the defined zone (Fig. 4.18), indicating the integrated mechanism of weathering and evaporation with the help of agricultural run-off and seawater intrusion noticed during SWM. Some of the samples, which fall in the evaporation dominance phase might be due to the semi-arid climatic condition along with surface contamination sources such as fertilizers, irrigation return flow, and domestic discharges from the land. The palm oil plantations might be the major contributors, whereas settlements near river coasts might be minor contributors towards such an integrated mechanism.

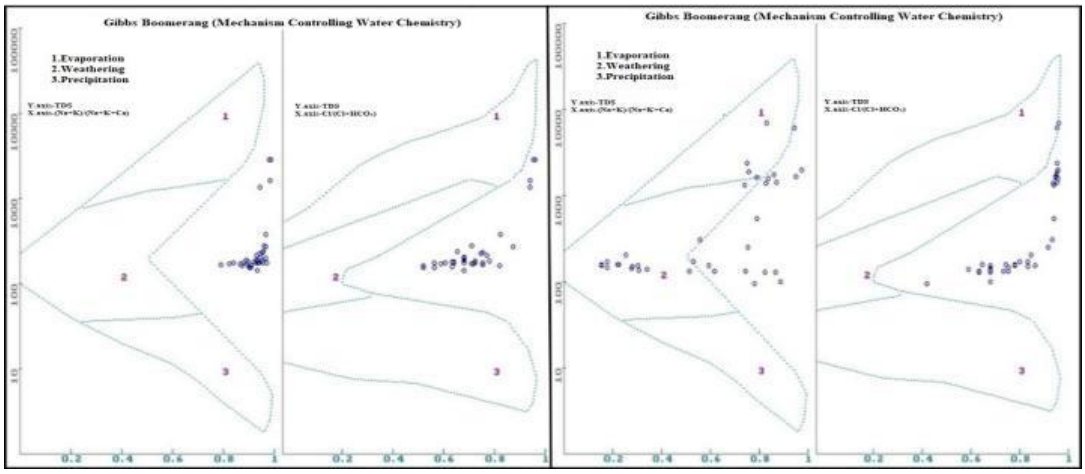

Fig. 4.18 Gibbs Classification of water samples according to mechanisms controlling the water chemistry during SWM (left) and NEM (right)

4.7.4 Correlation matrix

Karl Pearson's measure or Pearson's correlation coefficient between two variable series X and Y, where r is denoted as the ratio of covariance between X and Y to the product of standard deviation of both series. Symbolically:

$$r = \frac{\sum(dx \times dy)}{\sqrt{\sum(dx)^2 \times \sum(dy)^2}} \quad \text{.....(eq. 4.16)}$$

Where, R is the correlation coefficient

X and Y are variables

dx and dy are the deviations of x and y mean of x and y variables

This correlation helps to identify mathematical relationships between various physico-chemical parameters, ions, nutrients and metals in water (Khatoon et al., 2013). The relation between these parameters is correlation coefficients or degree of association and can establish positive and negative correlations between the parameters (Shroff et al., 2015; Jothivenkatachalam et al., 2015; Thivya et al., 2015). The matrix value above 0.5 and less than -0.5 has been considered for interpretation, where values above 0.5 contemplate high correlation and vice versa condition is presumed for -0.5. The Pearson correlation matrix analysis has been carried out for the acquired data from both seasons using IBM Statistical Package for Social Sciences (SPSS) version 25. The analysis is believed to be helpful in identifying major variations and chemical processes (Jothivenkatachalam et al., 2010; Thivya et al., 2015) taking place in the surface water of the estuary.

4.7.4.1 South-West monsoon (SWM)

During SWM, none of the parameters showed any positive or negative correlation with pH except for CO_2, which is negative, which means that CO_2 is inversely proportional with pH in the estuary (Table 4.14). This might be due to the degradation of organic matter in the estuary (Krachler et al., 2009). The respiration of organic matter, which involves CO_2 originated both from the sea and river water can generate various organic acids along with carbonic acid in water (Hu et al., 2013; Krachler et al., 2009). This can increase the level of H^+ in water as a secondary product, which is an indication of an increase in acidity levels of the estuarine water.

The dissolved oxygen (DO) in this season also showed a negative correlation with salinity, Fe and Mn. This negative correlation of DO can be attributed by the presence of bacteria, fungi and other decomposers in the estuary, which are responsible for the reduction of DO through consumption in presence of elevated saline intrusion from the sea (Rath et al., 2015). According to Ayolabi et al. (2013), the mass loading of metal in estuary drops comparatively with the higher intrusion of seawater and lower infusion of freshwater. In such conditions, the estuarine region becomes a large exporter of Fe and Mn because of internal recycling between the bedload sediment and water body under anaerobic conditions. This process is seemingly significant in this case as SWM is prone to less freshwater discharge into the estuary than the saline discharge from the sea. This can be further strengthened by the fact that transition and transformation of reduced soluble and oxidized solid-phase Mn and Fe usually take place with microbial mediation processes (Zhang et al., 2014), which is the main source of reduction of DO in estuarine water.

Total Dissolved Solids (TDS) and Electrical Conductivity (EC) during SWM are highly correlated with each other as the capacity of water to conduct electric charge directly depends on the concentration of dissolved ions (Rsuydi et al., 2018). Likewise, both the parameters show a high positive correlation with Cl^-, Mg^{2+}, Na^+, Ca^{2+}, SO_4^{2-} and NH_4^+. In contrast, they also have a negative correlation with parameters like temperature and Cr. The positive correlation of Cl^-, Mg^{2+}, Na^+, Ca^{2+}, SO_4^{2-} and NH_4^+ with TDS can be signified by considering the higher concentration and contribution whereas inorganic compounds like Cl^-, Mg^{2+}, Na^+, Ca^{2+}, SO_4^{2-} and NH_4^+ contribute to the ability of water to pass through electricity (Choo et al., 2019). Higher correlation of TDS with Na^+ and Cl^- indicates the input of saltwater from the sea, however, the higher correlation with Mg^{2+}, Ca^{2+} and nutrients like SO_4^{2-} and NH_4^+ indicates the input of agricultural and residential effluents (Choo et al., 2019) as these are the major sources in the study area.

The bottom velocity of river and seawater work as major influencers in increasing and decreasing the concentration of suspended solids in the water column (Pejrup et al., 1986). However, in the study area, both parameters do not show a correlation between each other. This might be due to the shear velocity of saline water at the bottom, because of the high tide and freshwater flow in horizontal gradient at the top. The TSS concentration shows a higher correlation with salinity. Similar saline factor

and tidal influence are also noticed to be influencing various shallow estuaries near the European Wadden Sea (Pejrup et al., 1986). Turbidity is produced in water with the help of suspended solids in the water table (Bilotta et al., 2008). As per the comparison of both parameters, the turbidity is highly influenced by the suspended solids' concentration. Turbidity is highly correlated to salinity and its correlations with velocity is quite low, indicating that an increase of suspended solids in water is due to the flow of water of saline origin at the bottom. The positive correlation with salinity can be defined by saltwater-freshwater interaction in the estuarine environment, where high-density saltwater intrusion influences the deposition of sediments directly. This marine transgression and regression initiated by the tides are responsible for the upbringing of sediments into the water column, making it more turbid (Pejrup et al., 1986; Uncles et al., 1993). Turbidity and TSS in the study area also share a significant correlation with Fe and Mn with r values of 0.572 and 0.604 respectively, whereas a high negative correlation has been noted with Cr and Se with respective r values of -0.544 and -0.536. In the case of Fe and Mn during SWM, the correlation indicates the association of Fe and Mn with organic matter. With an increase in salinity and turbidity due to characteristic tide and wave action, Fe and Mn from the sediment resuspension are adsorbed onto particulate organic matter (Yamamoto et al., 2016). This leads to the formation of cation-induced coagulation of negatively charged humic colloids containing bound Fe and Mn and is found during the mixing (Jilbert et al., 2016; Mayer et al., 1982; Boyle et al., 1977; Sholkovitz et al., 1976; Shapiro et al., 1964).

Salinity shows high correlation with NH_4, Fe, Mn and a negative correlation with DO in the estuary (Table 4.14). The correlation matrix is shown by salinity with NH_4 standing at 0.588, whereas the r values of 0.636 and 0.707 are observed for Fe and Mn respectively. On the contrary, -0.573 matrix has been noted between salinity and DO. Considering the fact that freshwater hold more amount of DO than the relatively warm saline water (Chabot et al., 2013; Prasad et al., 2014), the stratification of saline water and fresh water in intertidal zones have a tendency to saturate the level of DO carried by freshwater, whilst the amount of DO decreases in the estuarine environment during the high tidal time (Scully et al., 2016). The correlation with NH_4^+ can be signified by the reduction of the nitrification process linked to the nitrogen cycle running in the estuary. With the increase in salinity in the estuarine environment, the nitrification process decreases with a decrease in absorption of NH_4^+ by the sediments along with

the decrease in DO (Rysgaard et al., 1999; Prasad et al., 2014). This gives rise to the increase in NH_4^+ in the water column. In addition to that, Fe and Mn load from the riverine side is low in the estuary and seaward influence is higher during SWM. Such conditions can enhance the resuspension of Fe and Mn in the estuary, promoted by pore water species into the water column (Zhou et al., 2003). Furthermore, these metals might be forming stable Fe-organic matter complexes with an increase in salinity gradient (Herzog et al., 2019) and push towards the upstream region of the estuary through tidal forces (Zhou et al., 2003). A similar condition has been visible under intermediate salinity conditions in Conwy estuary, North Wales as per the study done by Zhou et al. (2003). This justifies the high positive correlation of salinity with Mn and Fe in the study area as salinity conditions stand at intermediate and tidal forces holding major upward force during SWM.

The temperature in the study area does not show a positive correlation to any of the parameters. In contrast, it has a high negative correlation towards EC, TDS, velocity, Cl^-, Mg^{2+}, Na^+, K^+, Fe and Co. In a similar manner, HCO_3^- also does not show any major positive or negative correlation with any of the parameters. However, it has a low r-value of 0.257 with pH during SWM.

Chloride (Cl^-) has a high positive correlation with Mg^{2+}, Na^+, K^+, Ca^{2+}, Co, TDS and EC during SWM (Table 4.14). Likewise, it shows a significant positive correlation with SO_4^{2-} and NH_4^+ along with a negative correlation with Cr. The conservative behaviour of both Na^+ and Cl^- in the estuary with Ca^{2+}, Mg^+, K^+ and SO_4^{3-} indicates the enrichment and association of all these ions depend on varying saline water influence (e.g. Patra et al., 2012; Serder et al., 2020). The gradual decline in the concentration of these ions during this season might be due to the precipitation of NaCl, $MgCl_2$, KCl, Na_2SO_4 and $CaCl_2$ in mixing zones of estuarine water (Looi et al., 2013) attributing towards the deficiency of these ions in the water towards the upper part of the estuary. Such formation of salt was also reported by Eckert and Sholkovitz (1976) as a result of subsequent processes in the post mixing period. They also observed a rapid increase in the amount of these precipitated materials with an increase in salinity, and at equimolar concentration, the effectiveness of precipitation by different sea salt cations increased while forming NaCl, $MgCl_2$ and $CaCl_2$. Furthermore, the concentration of Cl^- in the study area is higher than Na^+ concentration, which is also an indication of seawater influence coupled with the

leaching of secondary salt from various agricultural fields situated near the estuary. This correlation of SO_4^{2-} with Cl^-, Na^+, K^+, Mg^{2+} and Ca^{2+} also indicates the intrusion of various salts from the sea and anthropogenic sources present near the estuary (e.g. Prasanna et al., 2019) as SO_4^{2-} concentration of water can also be derived from the seawater due to presence of gypsum ($CaSO_4$. H_2O) (e.g. Singaraja et al., 2013). The correlation of K^+ and Cl^- is also an indication of the ion exchange process in the estuary (e.g. Thivya et al., 2015; Banaja et al., 2018; Singaraja et al., 2013). The anthropogenic sources may include various agricultural run-off and domestic sewage, which is widely observed in the study area.

The correlation of Ca^{2+} with Cl^- is an indicator of the addition of halite and gypsum, which has also been noticed in the reconstructed diagram proposed by Lawrence and Balasubramanian (1994) (Fig. 4.16). Major ions such as Na^+, K^+, Ca^{2+}, Mg^{2+}, SO_4^{3-}, NH_4^+ and Cl^- are highly correlated to each other along with a high correlation with TDS and EC. All these ions also have a very similar trend in the estuary during SWM, which is highest at the river mouth and gradually decreasing towards the upstream direction (Fig. 4.6 and 4.7). This indicates that the majority of these ions are seawater borne and dominating the estuary because of tidal influence.

The high correlation of ionized ammonia (NH_4^+) with Cl^-, Mg^{2+}, Na^+, K^+ and salinity may be due to the influence of salinity as mentioned above. The saline water is the main carrier of these cations and anions along with few anthropogenic sources such as fertilizers in the agricultural fields (Eddy et al., 2005). According to studies by Rysgaard et al. (1999), NH_4^+ absorption's capacity of estuarine sediment decreases with increasing salinity. This limits both in situ nitrification and denitrification, giving rise to free NH_4^+ ions in aqueous solution and increases in concentration along with other seawater influenced cations and anions.

Ba in the estuary shows a high correlation with all the major ions (Na^+, K^+, Ca^{2+}, Mg^{2+}, SO_4^{3-}, NH_4^+ and Cl^-) (Table 4.14) along with a high negative correlation with CO_2 and pH. Ba in estuaries are mainly the constituents of particulate matter in water (Mori et al., 2019; Samantha & Dalai, 2016) and tend to desorb from it under high salinity conditions in case of small river discharge (Coffey et al., 1997) such as Sibuti. The decrease in acidity with the influence of degradation of the organic matter involving

CO_2 (Hu et al., 2013; Krachler et al., 2009) near the river mouth area provides a condition for the release of Ba into estuarine water (Coffey et al., 1997).

Table 4.14 Correlation Matrix of Water contained physico-chemical parameters, major ions, nutrients and trace metals during SWM

	pH	DO	EC	TDS	Tur	Vel	Sal	TSS	Temp	HCO_3^-	Cl^-	Mg^{2+}	Na^+	K^+	Ca^{2+}	CO_2	SO_4^{2-}	PO_4^{3-}	NO_3N	NH_3	NH_4^+	NO_3^-	Cu	Zn	Fe	Mn	Cd	Cr	Se	Ba
pH	1.000																												
DO	0.186	1.000																											
EC	-0.150	-0.264	1.000																										
TDS	-0.150	-0.264	1.000	1.000																									
Tur	-0.165	-0.399	0.325	0.325	1.000																								
Vel	0.311	-0.150	0.336	0.336	0.027	1.000																							
Sal	-0.343	-0.573	0.441	0.441	0.643	0.181	1.000																						
TSS	-0.121	-0.472	0.387	0.387	0.699	0.190	0.627	1.000																					
Temp	-0.315	0.241	-0.592	-0.592	-0.265	-0.698	-0.329	-0.368	1.000																				
HCO_3^-	0.257	-0.044	-0.086	-0.086	0.201	0.224	0.020	-0.028	-0.179	1.000																			
Cl^-	-0.118	-0.226	0.982	0.982	0.328	0.263	0.394	0.379	-0.522	-0.112	1.000																		
Mg^{2+}	0.146	-0.246	0.907	0.907	0.259	0.567	0.367	0.388	-0.768	0.006	0.858	1.000																	
Na^+	-0.215	-0.296	0.957	0.957	0.300	0.417	0.494	0.373	-0.638	-0.064	0.888	0.912	1.000																
K^+	-0.040	-0.183	0.922	0.922	0.300	0.398	0.415	0.455	-0.685	-0.040	0.872	0.920	0.925	1.000															
Ca^{2+}	-0.269	-0.262	0.851	0.851	0.261	0.380	0.402	0.390	-0.418	-0.099	0.835	0.741	0.823	0.766	1.000														
CO_2	-0.577	-0.190	0.257	0.257	-0.131	-0.252	0.057	-0.087	0.240	-0.270	0.244	0.041	0.264	0.101	0.317	1.000													
SO_4^{2-}	-0.090	-0.337	0.652	0.652	0.127	0.167	0.209	0.167	-0.483	-0.117	0.605	0.598	0.637	0.645	0.483	-0.299	1.000												
PO_4^{3-}	0.295	0.054	-0.283	-0.283	-0.138	-0.059	-0.352	-0.207	0.068	0.025	-0.277	-0.218	-0.302	-0.290	-0.299	0.295	-0.337	1.000											
NO_3N	0.079	0.091	-0.175	-0.175	-0.131	-0.111	-0.094	-0.138	-0.001	0.058	-0.214	-0.099	-0.106	-0.088	-0.246	0.079	-0.090	0.295	1.000										
NH_3	-0.094	-0.181	0.043	0.043	0.041	0.133	0.239	0.051	-0.125	-0.062	0.043	0.034	0.032	0.002	0.043	-0.094	-0.181	0.054	0.091	1.000									
NH_4^+	-0.299	-0.388	0.626	0.626	0.209	0.208	0.588	0.514	-0.349	-0.086	0.587	0.529	0.643	0.581	0.621	-0.299	-0.388	0.098	0.145	0.104	1.000								
NO_3^-	0.145	0.098	-0.182	-0.182	-0.151	-0.114	-0.120	-0.150	0.009	0.024	-0.217	-0.085	-0.117	-0.098	-0.283	0.145	-0.156	-0.516	0.039	-0.071	-0.190	0.247							
Cu	0.104	-0.143	0.344	0.344	0.211	0.146	0.295	0.210	-0.321	0.070	0.331	0.375	0.341	0.325	0.354	0.104	-0.143	-0.580	-0.331	0.183	0.438	0.364	0.257	1.000					
Zn	-0.071	-0.156	0.183	0.183	-0.007	0.101	0.028	0.064	-0.030	0.117	0.180	0.163	0.163	0.144	0.372	-0.071	-0.156	-0.073	-0.190	0.438	0.364	0.257	1.000	0.183	1.000				
Fe	0.039	-0.516	0.438	0.438	0.572	0.386	0.636	0.613	-0.698	0.097	0.385	0.472	0.480	0.468	0.318	0.039	-0.516	0.326	0.247	0.364	0.257	1.000	0.183	1.000	1.000				
Mn	-0.331	-0.580	0.364	0.364	0.604	0.068	0.707	0.656	-0.313	0.068	0.324	0.264	0.411	0.367	0.314	-0.331	-0.580	0.326	0.247	0.257	1.000	0.183	1.000	1.000	1.000	1.000			
Cd	-0.190	-0.073	-0.081	-0.081	0.101	-0.153	0.172	-0.037	-0.008	-0.323	-0.099	-0.101	-0.036	-0.134	-0.190	-0.190	-0.073	0.326	0.247	0.183	1.000	0.183	1.000	1.000	1.000	1.000	1.000		
Cr	0.247	0.326	-0.593	-0.593	-0.544	-0.063	-0.561	-0.634	0.480	-0.099	-0.579	-0.501	-0.568	-0.615	-0.530	0.247	0.326	0.255	0.446	-0.286	0.669	-0.286	0.669	0.669	0.669	0.669	1.000	1.000	
Se	0.446	0.255	-0.286	-0.286	-0.536	0.107	-0.364	-0.361	0.081	0.127	-0.285	-0.085	-0.277	-0.222	-0.264	0.446	0.255	-0.286	0.446	0.286	0.669	0.286	0.669	0.669	0.669	0.669	1.000	1.000	1.000
Ba	-0.639	-0.351	0.669	0.669	0.296	0.183	0.471	0.314	-0.308	-0.140	0.569	0.524	0.785	0.635	0.677	-0.639	-0.351	0.669	-0.639	0.669	0.669	0.669	0.669	0.669	0.669	0.669	1.000	1.000	1.000

	pH	DO	EC	TDS	Tur	Vel	Sal	TSS	Temp	HCO_3^-	Cl^-	Mg^{2+}	Na^+	K^+	Ca^{2+}	CO_2	SO_4^{2-}	PO_4^{3-}	NO_3N	NH_3	NH_4^+	NO_3^-	Cu	Zn	Fe	Mn	Cd	Cr	Se	Ba
CO_2																1.000	0.394	0.082	-0.242	0.017	0.243	-0.275	-0.251	0.090	-0.146	-0.057	0.165	-0.104	-0.153	0.513
SO_4^{2-}																	1.000	0.177	-0.047	0.180	0.451	-0.077	0.129	0.194	0.372	0.206	0.023	-0.373	-0.213	0.542
PO_4^{3-}																		1.000	-0.162	0.087	-0.347	-0.137	-0.132	-0.002	0.018	-0.150	0.045	0.368	0.200	-0.183
NO_3N																			1.000	-0.111	-0.153	0.988	0.057	-0.075	-0.051	-0.071	0.109	0.244	0.140	-0.094
NH_3																				1.000	0.046	-0.144	-0.122	0.015	0.198	0.173	-0.056	0.067	0.015	0.013
NH_4^+																					1.000	-0.181	0.133	0.237	0.487	0.404	0.007	-0.695	-0.169	0.552
NO_3^-																						1.000	0.055	-0.130	-0.066	-0.083	0.142	0.276	0.193	-0.143
Cu																							1.000	0.459	0.141	0.283	-0.035	-0.188	-0.053	0.115
Zn																								1.000	-0.112	-0.017	-0.051	-0.120	0.073	0.104
Fe																									1.000	0.738	0.041	-0.570	-0.387	0.357
Mn																										1.000	0.075	-0.469	-0.561	0.453
Cd																											1.000	-0.029	0.096	0.032
Cr																												1.000	0.349	-0.457
Se																													1.000	-0.476
Ba																														1.000

**Blue cells: Positive correlation; Grey cells: Negative correlation*

4.7.4.2 North-East monsoon (NEM)

During NEM, pH shows a positive correlation with turbidity and Co with a matrix value of 0.555 and 0.634 respectively (Table 4.15). However, it has a significant negative correlation with TDS, EC, salinity, Na^{+}, Ca^{2+}, Mg^{2+}, Cl^{-}, SO_4^{2-}, NO_3^{-} (Table 4.15). The positive correlation of pH with Co and turbidity may be due to the complexation of Co to dissolved organic substances, which reduces its sediment sorption in water with increasing pH conditions (Byrd et al., 1990). Furthermore, the aerobic nature of the estuary during monsoon helps to reduce the uptake of Co from water to sediments as compared to the anaerobic condition, where it is much higher subjected to the change in pH from 5 to 7.5 in water (WHO, 2006). Considering the above assumptions, Co stays in the water column and contributes more towards the turbidity during NEM. Total dissolved solids (TDS) are mainly represented by the presence of inorganic salts and organic matter in the water where the main constituents are various ions and nutrients (Islam et al., 2017). This is the main reason behind the high correlation of TDS and EC with salinity, Na^{+}, Ca^{2+}, Mg^{2+}, Cl^{-}, SO_4^{2-}, NO_3^{-} as these are the dominating ions, nutrients and metals during NEM. On the other hand, the acidity of water helps in the dissolution of various ions, nutrients and metals and is an indication of strong acid presence (Islam et al., 2017). This is the case in the current study where the pH of the estuary is negatively correlated with TDS, EC, salinity, Na^{+}, Ca^{2+}, Mg^{2+}, Cl^{-}, $SO_4^{2-}$and NO_3^{-}.

Cl^{-} shows a positive correlation with Na^{+}, Ca^{2+}, Mg^{2+}, SO_4^{-}, NO_3^{-} (Table 4.15) indicating the formation of secondary salts like NaCl, $MgCl_2$, KCl, Na_2SO_4 and $CaCl_2$ from direct seawater influence and anthropogenic activities (e.g. Singaraja et al., 2013) and ions exchange process (e.g. Thivya et al., 2015) in the estuary. A similar condition has been noticed during SWM. Moreover, the concentration of Cl^{-} is much higher as compared to Na^{+} concentration during NEM, which might be due to the addition of chloride from agricultural or irrigation discharges (i.e. Brandt et al., 2017).

A positive correlation of HCO_3^{-} with Mg^{2+} and Na^{+} indicates the chemical weathering of ions in the upstream region (i.e. Prasanna et al., 2010). It has a positive correlation with salinity and TDS during NEM as well, which might be the result of HCO_3^{-} enriched seawater intrusion into the estuary.

The positive correlation of dissolved nitrate (NO_3^-) with salinity, Na^+, Ca^{2+}, Mg^{2+}, $SO_4^{2-}$and Cl^- (seawater parameters) and the negative correlation of NO_3^- with pH signifies nitrification process where NO_3^- is getting enriched in the estuary in presence of DO in water creating an acidic condition (Muller et al., 2018; WHO, 2017). In this process, NH_3, in the presence of DO, forms NO_3^- while giving rise to increasing H^+ which is responsible for the reduction of pH (eq. 16). Ammonia (NH_3) during NEM shows a correlation matrix of 1 with ionized ammonium (NH_4^+) in the study area, which means ammonium ions exist in equilibrium with ammonia (eq. 4.16).

$$NH_3 + H_2O + 2O_2 \Leftrightarrow NH_4^+ + OH^- + 2O_2 \Leftrightarrow NO_3^- + 2H_2O + H^+ \text{.....(eq. 4.17)}$$

$$NH_3^-(aq) + H_2O \Leftrightarrow NH_4^-(aq) + OH^-(aq) \text{ .....(eq. 4.18)}$$

This an indication of the use of ammonia-rich fertilizers in the agricultural fields, which have been added into the estuary with the help of agricultural run-off.

Heavy metals like Fe, Mn and Zn show a significant correlation with each other during NEM. These metals do not show any correlation with any other parameters in the estuary. Low correlation with salinity, TDS and pH excludes the possibility of saline carrier and dissolution due to organic matter of these elements in the estuary (Zhang et al., 2018). This attributes towards the source of these metal to be terrestrial in origin and the run-off might be the carrier of these metals during NEM as terrestrial input during this season is much higher while there has been a significant increase in the concentration of these metals as compared to SWM.

Turbidity in the estuary has a positive correlation with Co and Cr and this indicates the binding of these metals with the organic matter present in the water. As observed by Campbell et al. (1984) in the St. Lawrence estuary, stable chromium-organic matter association exists in fresh water-salt water mixing zones and produces organic-rich floccules in the waters of the turbidity zone. He also explained the dominancy of Cr (VI) as CrO_4^{2-} in oxic water, which is the case during NEM due to infusion of freshwater containing more DO (Fig. 4.4).

Table 4.15 Correlation Matrix of Water contained physico-chemical parameters, major ions, nutrients and trace metals during NEM

CO_2	**Ca^{2+}**	**K^+**	**Na^+**	**Mg^{2+}**	**Cl^-**	**HCO_3^-**	**TSS**	**Temp**	**Sal**	**Vel**	**Tur**	**TDS**	**EC**	**DO**	**pH**										
															1.000	**pH**									
														1.000	-0.213	**DO**									
													1.000	0.508	-0.735	**EC**									
												1.000	1.000	0.508	-0.735	**TDS**									
											1.000	-0.363	-0.363	0.087	0.555	**Tur**									
										1.000	0.012	0.393	0.393	0.186	-0.181	**Vel**									
									1.000	0.382	-0.158	0.893	0.893	0.537	-0.752	**Sal**									
								1.000	0.313	0.245	-0.105	0.407	0.407	0.478	-0.174	**TSS**									
							1.000	0.251	0.278	0.494	0.242	0.301	0.301	0.296	0.037	**Temp**									
						1.000	0.279	0.357	0.603	0.400	0.228	0.517	0.517	0.614	-0.282	**HCO_3^-**									
					1.000	0.436	0.276	0.413	0.771	0.368	-0.404	0.973	0.973	0.445	-0.652	**Cl^-**									
				1.000	0.822	0.530	0.382	0.420	0.904	0.413	-0.271	0.910	0.910	0.506	-0.727	**Mg^{2+}**									
			1.000	0.914	0.831	0.590	0.286	0.327	0.993	0.385	-0.222	0.934	0.934	0.549	-0.764	**Na^+**									
		1.000	0.843	0.760	0.604	0.729	0.438	0.356	0.862	0.373	0.183	0.723	0.723	0.670	-0.473	**K^+**									
	1.000	0.405	0.660	0.601	0.783	0.309	0.125	0.381	0.601	0.225	-0.549	0.775	0.775	0.439	-0.605	**Ca^{2+}**									
1.000	-0.170	-0.080	-0.281	-0.184	-0.257	-0.174	0.049	-0.021	-0.259	-0.090	0.204	-0.271	-0.271	-0.194	0.308	**CO_2**									
-0.452	0.717	0.349	0.744	0.719	0.777	0.259	0.083	0.162	0.695	0.197	-0.667	0.806	0.806	0.205	-0.842	**SO_4^{2-}**									
0.040	-0.261	-0.294	-0.284	-0.288	-0.295	-0.283	-0.200	-0.325	-0.266	-0.383	0.238	-0.305	-0.305	-0.312	0.183	**PO_4^{3-}**									
-0.302	0.593	0.411	0.623	0.692	0.683	0.361	0.211	0.350	0.575	0.242	-0.555	0.706	0.706	0.398	-0.683	**NO_3N**									
0.073	0.209	-0.166	0.097	0.168	0.037	-0.044	-0.217	-0.019	0.123	-0.016	-0.343	0.083	0.083	-0.366	-0.313	**NH_3**									
0.072	0.221	-0.160	0.107	0.178	0.054	-0.042	-0.210	-0.012	0.131	-0.008	-0.348	0.097	0.097	-0.361	-0.317	**NH_4^+**									
-0.301	0.572	0.402	0.613	0.680	0.670	0.367	0.194	0.341	0.566	0.240	-0.548	0.693	0.693	0.384	-0.679	**NO_3^-**									
-0.236	0.035	0.296	0.249	0.200	0.079	-0.027	-0.043	0.124	0.270	-0.067	0.045	0.147	0.147	0.290	-0.184	**Cu**									
0.050	0.004	0.022	-0.008	0.038	-0.059	-0.016	0.352	-0.058	0.009	0.001	0.247	-0.034	-0.034	0.046	0.117	**Zn**									
0.150	-0.084	-0.047	-0.119	-0.058	-0.116	-0.046	0.370	-0.073	-0.109	-0.069	0.321	-0.117	-0.117	-0.006	0.211	**Fe**									
0.256	-0.570	-0.005	-0.481	-0.468	-0.541	0.041	0.088	-0.016	-0.437	-0.160	0.766	-0.550	-0.550	0.046	0.634	**Mn**									
0.069	0.145	0.125	0.087	0.192	0.064	0.033	0.630	0.073	0.093	0.091	0.127	0.094	0.094	0.092	-0.023	**Cd**									
-0.300	0.712	0.797	0.980	0.910	0.842	0.506	0.316	0.318	0.966	0.375	-0.289	0.936	0.936	0.503	-0.779	**Cr**									
0.123	-0.146	0.520	0.092	0.097	-0.001	0.436	0.378	0.125	0.125	0.121	0.632	0.031	0.031	0.268	0.262	**Se**									
0.172	0.166	-0.068	-0.132	-0.101	-0.051	-0.342	0.176	0.096	-0.155	0.004	-0.201	-0.082	-0.082	0.139	0.208	**Ba**									

	pH	DO	EC	TDS	Tur	Vel	Sal	TSS	Temp	HCO_3^-	Cl^-	Mg^{2+}	Na^+	K^+	Ca^{2+}	CO_2	SO_4^{2-}	PO_4^{3-}	NO_3N	NH_3	NH_4^+	NO_3^-	Cu	Zn	Fe	Mn	Cd	Cr	Se	Ba
SO_4^{2-}																	1.000	-0.175	0.815	0.296	0.305	0.811	0.025	-0.082	-0.172	-0.833	0.085	0.784	-0.347	-0.224
PO_4^{3-}																		1.000	-0.267	-0.004	-0.007	-0.262	0.079	0.201	0.136	0.172	-0.002	-0.286	0.036	-0.209
NO_3N																			1.000	0.058	0.068	0.999	-0.067	-0.076	-0.107	-0.607	0.158	0.648	-0.177	-0.160
NH_3																				1.000	1.000	0.068	-0.183	-0.004	-0.033	-0.423	0.021	0.123	-0.415	-0.231
NH_4^+																					1.000	0.078	-0.186	-0.003	-0.032	-0.430	0.025	0.133	-0.416	-0.228
NO_3^-																						1.000	-0.078	-0.079	-0.109	-0.606	0.147	0.633	-0.183	-0.198
Cu																							1.000	-0.091	-0.244	0.078	-0.141	0.286	0.142	0.284
Zn																								1.000	0.943	0.162	0.838	-0.008	0.241	0.126
Fe																									1.000	0.234	0.839	-0.115	0.237	0.082
Mn																										1.000	0.040	-0.531	0.627	0.130
Cd																											1.000	0.142	0.225	0.152
Cr																												1.000	0.066	-0.045
Se																													1.0000	-0.148
Ba																														1.000

**Blue cells: Positive correlation; Grey cells: Negative correlation*

4.7.5 Factor analysis

In an attempt to understand the geochemical processes in estuarine water, factor analysis was carried out for SWM and NEM with help of IBM SPSS 25. This analysis also helps to group the parameters related to various chemical processes happening in the estuary. In order to avoid issues arising due to different units of each parameter the

data was standardized by the SPSS package itself to carry out the PCA extraction using correlation matrix. The extracted factors were from varimax rotation so that orthogonal factors can be obtained, which directly relates the factors to independent geochemical processes occurring in the study area. As physico-chemical parameters, major ions, nutrients and trace metals frequently interact with each other in the water column, they are considered for the analysis and presented in Table 4.16 and 4.17. The factor scores are obtained to analyse locations where these factors-associated processes are taking place. These scores are represented in Fig. 4.19 and 4.21 for SWM and NEM respectively, where higher positive and lower negative factors are indicative of the intensity of the chemical processes.

4.7.5.1 South-West monsoon (SWM)

Eight factors are dominant in this factor model explaining 82.27% of the variance, in which factor-1 being the highest explaining 30.179% of the total variance. Factor-1 during SWM is loaded with EC, TDS, velocity, Cl^-, Mg^{2+}, Ca^{2+}, Na^+, K^+, SO_4^{2-}, NH_4^+ and Ba (Table 4.16). This factor has a major association at station 1 with a factor score of 4.383 (Fig. 4.19). The association and trend of these parameters in water indicate the domination of seawater in the estuary during SWM (e.g. Patra et al., 2012). The seawater is the major source of these parameters and the main reason for domination as well. The precipitation of secondary salts like NaCl, $MgCl_2$, KCl, Na_2SO_4, $CaCl_2$ and NH_4Cl is evident in the intermediate and upper part of the estuary (Singaraja et al., 2013; Eckert & Sholkovitz, 1976; Looi et al., 2013). The formation of these secondary salts might be carried out during the ion exchange process mainly by Ca^{2+}, Mg^{2+} and K^+ (Thivya et al., 2015; Banaja et al., 2015; Singaraja et al., 2013) in the mixing zone and upper part of the estuary. The same influence of saline water intrusion also gives rise to the release of Ba from suspended solid matter in the estuary (Coffey et al., 1997).

Factor-2 is loaded with turbidity, salinity, TSS, Fe and Mn, where a negative load of DO is also associated with the process, contributing to 14.49% of the total variance. This indicates towards the tidal induced turbidity in the estuary initiating resuspension of suspended solids (Peirup et al., 1986; Uncles et al., 1983) and reveals the injection of Fe and Mn into the water column from the hydroxide phases available in the sediments and suspended solids (Turner et al., 2000; Callaway et al., 1988). Such a

process is commonly related to anaerobic conditions created at the bottom of water due to seawater dominance (Kristensen et al., 2003) and can be confirmed in the study area with negative loading of DO in this factor. This factor is dominant in the mid zones of the estuary (stations 6 to 13) and the process is taking place just after factor 1, which is mainly because of the direct influence of seawater (Fig 4.18). The association of TSS also indicates towards particulate organic matter association of sediments and suspended solids with the formation of cation-induced coagulation of negatively charged humic colloids containing Fe and Mn, while forming Fe and Mn oxides in a water solution with reduction of DO in water (Shapiro et al., 1964; Sholkovitz et al., 1976; Boyle et al., 1977; Mayer et al., 1982; Zhou et al., 2003; Jilbert et al., 2016; Wen et al., 2019). The absorption of Cr by bottom sediments is evident by having negative loading in this factor because of its affinity to form complexes with natural or anthropogenic organic substances (Campbell et al., 1984; Pađan et al., 2019), which is found to be associated with increasing pH in sediments in the same zone and is discussed further in the sediment chapter. In the case of Se, absorption by the organic Fe, Mn complexes (Bewers & Yeats, 1978; Campbell et al., 1984) and sediments and suspended particulate matter (Pađan et al., 2019) is happening near the mouth with the influence of increasing seawater induced turbidity. The evidence of such absorption of Se is further discussed in both suspended solids and sediment chapter.

Factor-3 during SWM shows a positive loading of pH and negative loading of CO_2 and Ba in estuarine water, while contributing 9.65% variance. This indicates towards the reaction of water with CO_2 with seawater to cause respiration of organic matter with the generation of various organic acids including formation of carbonic acid in water, making the water acidic (eq. 4.19) (Mook et al., 1975; Mucci et al., 2007; Krachler et al., 2009; Xingping et al., 2013; Saifullah et al., 2014; Van Dam et al., 2019).

$$H_2O + CO_2 \Leftrightarrow H_2CO_3(\text{carbonic acid}) \Leftrightarrow H^+ + HCO_3^- \quad \text{.....(eq. 4.19)}$$

Factor-4 represents 7.47% of the total chemical processes in the estuary and has major loading of NO_3^- and NO_3-N. The high factor scores for this component is observed at stations 6, 23, 24, 25 and 26 (Fig. 4.19). At station 6 a major agricultural channel is located whereas rest of the stations are situated near Sungai Kejapil and other smaller

Table 4.16 Rotated Component Matrix of water contained physico-chemical parameters, major ions, nutrients and trace metals during SWM

Parameters	Communalities	Components							
		1	2	3	4	5	6	7	8
pH	0.862	-0.049	-0.254	0.837	0.033	-0.004	0.272	-0.079	-0.110
DO	0.649	-0.145	-0.593	0.131	-0.011	-0.243	-0.093	-0.435	-0.050
EC	0.964	0.956	0.179	-0.064	-0.076	0.075	-0.053	-0.025	0.001
TDS	0.964	0.956	0.179	-0.064	-0.076	0.075	-0.053	-0.025	0.001
Turbidity	0.761	0.146	0.831	0.057	-0.109	0.029	-0.036	-0.166	-0.062
Velocity	0.693	0.438	-0.025	0.530	-0.068	0.006	-0.056	0.423	-0.182
Salinity	0.843	0.287	0.732	-0.047	-0.033	0.119	-0.325	0.278	0.155
Temperature	0.872	-0.660	-0.274	-0.553	-0.067	0.036	-0.101	-0.196	-0.002
TSS	0.708	-0.392	0.601	0.396	-0.077	-0.118	-0.026	0.077	-0.104
HCO_3	0.563	-0.110	0.130	0.319	0.041	0.174	-0.014	0.064	-0.629
Cl^-	0.898	0.914	0.152	-0.062	-0.133	0.076	-0.058	-0.087	0.002
Mg^{2+}	0.955	0.935	0.098	0.251	-0.004	0.076	-0.012	0.059	-0.010
Na^+	0.958	0.946	0.209	-0.077	0.013	0.061	-0.081	0.059	0.015
K^+	0.928	0.941	0.174	0.073	0.007	0.016	-0.064	-0.037	-0.040
Ca^{2+}	0.859	0.819	0.110	-0.191	-0.183	0.250	-0.167	0.059	-0.110
CO_2	0.809	0.251	-0.144	-0.775	-0.193	-0.018	0.178	0.136	0.194
SO_4^{2-}	0.815	0.698	0.113	-0.191	0.068	0.064	0.477	0.189	0.081
PO_4^{3-}	0.876	-0.231	-0.096	0.088	-0.154	0.012	0.879	0.088	0.052
NO_3-N	0.981	-0.095	-0.055	0.043	0.981	0.003	-0.062	-0.041	0.010
NH_3	0.581	-0.014	0.091	-0.033	-0.080	-0.076	0.069	0.743	-0.046
NH_4^+	0.687	0.590	0.274	-0.155	-0.113	0.145	-0.341	0.264	0.141
NO_3^-	0.984	-0.101	-0.080	0.100	0.972	-0.025	-0.050	-0.073	0.066
Cu	0.757	0.274	0.220	0.244	0.103	0.705	-0.033	-0.255	0.000
Zn	0.840	0.145	-0.090	-0.105	-0.086	0.881	0.024	0.085	-0.094
Fe	0.889	0.380	0.748	0.283	0.015	-0.147	0.112	0.261	0.034
Mn	0.800	0.207	0.855	-0.079	0.026	0.035	-0.043	0.114	0.051
Cd	0.819	-0.112	0.135	-0.019	0.100	0.035	0.027	-0.009	0.881
Cr	0.689	-0.519	-0.523	0.013	0.231	-0.048	0.282	0.086	-0.056
Se	0.754	-0.169	-0.643	0.399	0.076	0.193	-0.040	0.251	0.213
Ba	0.810	0.657	0.311	-0.518	0.032	-0.015	-0.013	0.109	-0.007
Percentage Variance Explained		30.179	14.499	9.658	7.476	5.391	5.195	5.066	4.812
Total Variance Explained		82.27%							
Eigen Value		Greater than 1							

**Blue cells: Positive factor loading; Grey cells: Negative factor loading*

agricultural streams (Fig. 3.3 and Fig. 1.4). Such observation indicate towards the leaching of these nutrients from the agricultural fields present in the study area and anaerobic denitrification processes in the estuary (e.g. Haaijer et al., 2006).

Factor-5 shows major loading of Cu and Zn and represents around 5.391% variance. The major loading such chalcophile metals are mainly associated with oxidation of pyrites (Anandkumar, 2016) (Fig. 4.20), which are widely available in Sibuti and Lambir formations (Nagarajan et al., 2015; Nagarajan et al., 2017a). This metal association is not associated with any physico-chemical parameters indicating the release of such metal in source rocks due to chemical weathering. During chemical weathering of pyrites, chalcophile metals like Cu and Zn are released in aqueous solution (Fig. 4.20) (Lu et al., 2005; Fernandez et al., 2009; Chopard et al., 2017) and act as a major source in river water (Galán et al., 2003; Nieto et al., 2007). The factor scores for this component is higher at stations 11, 21 and 31 (Table 4.18) and indicative of the major input zones for such metal mainly through direct run-off from land or through tributaries.

Factor-6 is loaded with PO_4^{3-} and weak loading of SO_4^{2-}, represents 5.195% of the variance. This association does not relate to any other parameters. The factor score of this component higher at station 7, 17, 20, 26, 34 and 36. These stations are near agricultural fields and are part of indicates PO_4^{3-} input from agricultural inputs around the river basin (Hartzell et al., 2012; Nystrand et al., 2016). The station 26 reported higher factor for both factor 4 and 6 along with decrease in DO concentration at this station (highest DO reported at the previous station 27) (Fig. 4.4). This observation and weak loading of SO_4^{2-} in this factor indicate the process of denitrification coupled to sulfide oxidation and organic matter respiration with consumption of DO at station 26. This process leads to increase in PO_4^{3-} mobilization (e.g. Lamers et al., 2002; Boomer & Bedford, 2008).

Factor-7 has major loading of NH_3 with weak negative loading of DO and represents a 5.06% of the total variance. Higher factor scores are observed at station 1, 2, 3, 16, 18, 22 and 23. The stations are situated closer proximity to various agricultural channels (Fig. 3.3) and tributaries such as Sungai Kejapil near Bekenu except station 22 which is closer near Bekenu town (Fig. 1.4 and Fig. 3.3). These observations indicate that NH_3 is a derived initially from agricultural and wastewater affluents from Bekenu town. Furthermore, the weak negative association of DO with this factor is an indication of the combined effect of ammonification and NO_3 reduction to NH_4^+, where DON (dissolved organic nitrogen) and NO_3 give rise to NH_4^+ (Scott et al., 1999)

(Fig. 4.20). This process is continuing to form NH_3 with the consumption of available DO in the water column (Müller et al., 2018).

Factor-8 represents 4.81% of the total variance and has major loading of Cd along with negative loading of HCO_3^- during SWM. Despite being a chalcophile group of element independent behavior of the metal in this component indicate the leaching of Cd from agricultural fields as phosphate-based fertilizers is widely used in agricultural fields and are the major source of Cd in Malaysian rivers (De Boo et al., 1990) (Fig. 4.19). This practice is common in Borneo where these fertilizers provide maximum growth to palm oil plantations in peat-based soil (Zaharah et al., 2014). The factor score for this component is higher at stations 13, 14, 26 and 36 (Fig 4.19). Considering the land use map (Fig. 1.4), the proximity of these stations (13,14 and 36) (Fig. 3.3) is very close to the agricultural fields situated near the estuary, which further validates the source of such metal in estuarine water. The association of station 36 with nutrients dominated component such as factor 4, 6 and Cd in factor 8 indicate the direct input of nutrients rich agricultural input near these stations whereas station 26 is situated near a major tun of the river leading to deposition of such inputs. The oxidation of sediments derived from these agriculture inputs under anaerobic conditions and decomposition of organic matter (Fig. 4.4) is giving rise to spike in concentration of these nutrients and related to chemical processes such as denitrification and coupled oxidation of sulfate (Lamers et al., 2002) and metals especially at station 26.

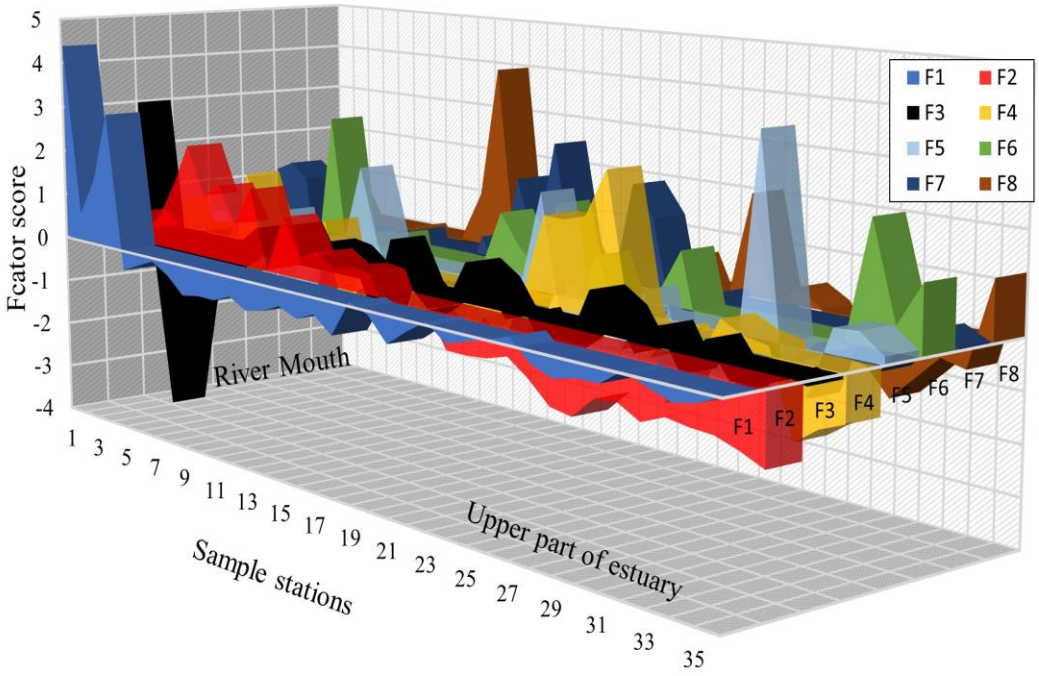

Fig. 4.19 Graphical representation of factor scores for various components during SWM

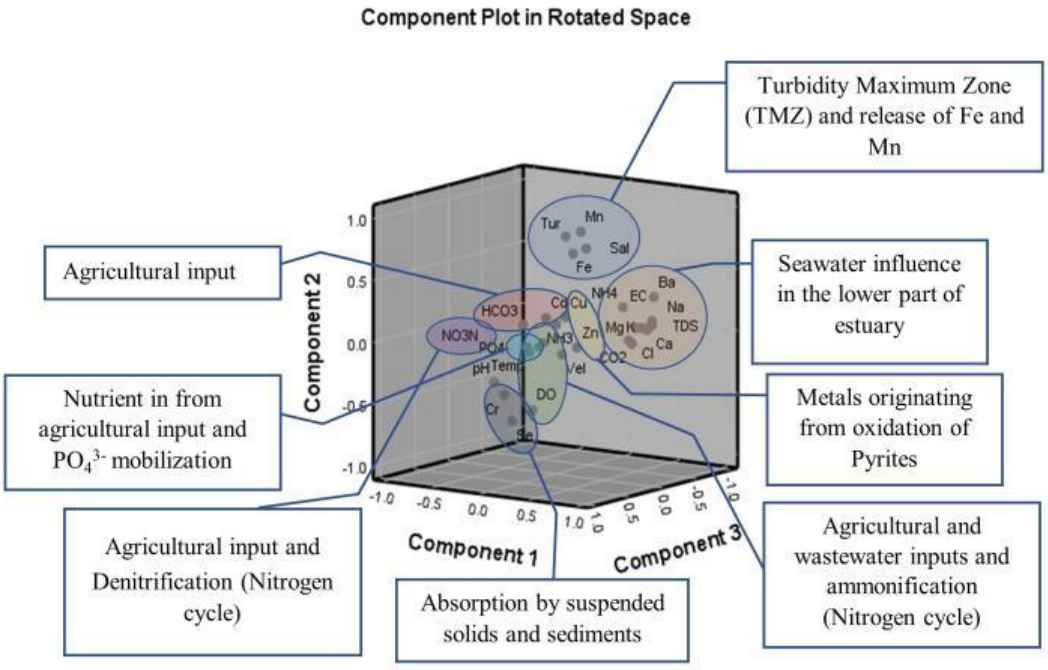

Fig. 4.20 Dominant principal components during SWM and its associated processes and sources

4.7.5.2 North-East Monsoon (NEM)

Factor-1 is during NEM has major loading of EC, TDS, DO, salinity, HCO_3^-, Cl^-, Mg^{2+}, Ca^{2+}, K^+, SO_4^{2-}, Cd, Ba and Cr along with negative loading of pH, while controlling 35.51% of the total variance (Table 4.17). The association of the mentioned parameters indicates saline water influenced processes like SWM despite the large infusion of freshwater during NEM from the riverine side. The high concentration of all the above parameters near the mouth and the factor score of 5.36 and 1.62 at stations 1 and 2 (Fig. 4.21) reveal the influence of seawater in the lower part of the estuary (Fig. 4.22). The loading of HCO_3^- with Cl^-, Mg^{2+} and Ca^{2+} is illustrative of their contribution from seawater as HCO_3^- presence in natural water varies from pH 4.5 to 8.3 (Millero, 1979) and the dissolution of these ions are ensured by the acidic condition near the mouth and indicated by negative pH loading. Metal desorption from sediments and suspended matter increases with increasing salinity (De Souza et al., 2016) due to the complexation of metals such as Cd with Cl^- and SO_4^{2-} forming soluble inorganic complexes (De Souza et al., 2016; Greger et al., 1995). Water-borne Cd is observed to rise 4-fold under salinity increase from 0-10 ppt (Greger et al., 1995; De Souza et al., 2016). So, positive loading of Cd and Ba attributes towards the immediate increase in salinity near the mouth and is giving rise to the concentration of Ba (Coffey et al., 1997) and Cd (Greger et al., 1995) from the suspended particles and sediments.

Factor-2 has major loading of EC, TDS, Mg^{2+}, Cl^-, Ca^{2+}, SO_4^{2-} and NO_3^- and has negative affinity towards pH, Co, Cr and turbidity, which contributes 20.27% of the total variance. This factor indicates the intense mixing of fresh water in the lower region of the estuary, where high factor scores observed from stations 2 to 9 have a higher affinity with this component. The association of EC, TDS, Mg^{2+}, Cl^-, Ca^{2+} indicates towards ion exchange process (Thivya et al., 2015) in the estuary (Fig. 4.21), where Na^+ is replaced by the water-borne Ca^{2+} and Mg^{2+} along with precipitation of various secondary salts (Singaraja et al., 2013). Regarding negative loading of Co and Cr and turbidity, these metals are removed from the water column and finding their way to the sediments with an increase in the influence of Cl^- (seawater). Under such conditions, Cr forms hexaaquo complex ($[Cr(H_2O)_6]Cl_3$). These hexaaquo complex and Cr-organic associations are stable in freshwater but destabilize with an increase in ionic strength and precipitate as floccules (Pađan et al., 2019; Campbell et al., 1984). Due to the intensive mixing of freshwater and seawater, DO carried by river water

plays a major role in the positive loading of both SO_4^{2-} and NO_3^-. Sulfides under reoxygenated conditions are oxidizing to sulfates and remineralization of organic matter gives rise to more SO_4^{2-} in the water column (Patra et al., 2012; Matson et al., 1985; Malcolm et al., 1986). In addition, the nitrification process (nitrogen cycle) increases with the availability of DO to produce more NO_3 in the water column from NH_3 and NH_4^+. Such a process gives rise to more H^+ ions and acidic conditions in water, which justifies the negative loading of pH in factor-2 (Muller et al., 2018; Scott et al., 1999). The negative loading of NH_3 and NH_4^+ in factor-4 validates this reaction (eq. 4.16) and high positive loading of DO is observed at the same stations while representing 9.14% of variance. As NH_3 and NH_4^+ are the by-products of degradation of organic matter under anaerobic conditions (Canfield et al., 1993; Baric et al., 2002), an increase in DO eliminates the enrichment of NH_3 and NH_4^+ in the estuary. The factor scores at station 9 (2.001) and 29 (2.162) suggest that nitrification (nitrogen cycle) is a dominating process during NEM mainly in the upper part and mixing zones (Fig 4.21) of the estuary (Fig 4.22).

Factor-3 has major loading of Fe, Mn, and Zn contributing 9.495% of the total variance. The factor score at station 32 (4.962) is observed to have an affinity to this association (Fig 4.21). Although pH has been a major influencer in Fe and Mn oxide dissolution in aquatic conditions, as well as absorption of metals onto it (Lion et al., 1982; Tipping & Heaton, 1983), this association seems to be independent of any ionic or pH influence in the estuarine water. This attributes towards the source of these metals association to be terrestrial in origin (Nguyen et al. 2005) and the run-off might be the carrier of these metals during NEM as terrestrial input. As the metal association is mainly composed of chalcophile elements, oxidation of pyrites might be the major source of these metals in estuarine waters (Galán et al., 2003; Lu et al., 2005; Nieto et al., 2007; Fernandez et al., 2009; Chopard et al., 2017). The higher factor scores in the upper part of the estuary (station 32) (Fig. 4.21) imply the source to be mainly from Sibuti formation, where pyrites concretions are common (Nagarajan et al., 2015; Nagarajan et al., 2017a) (Fig. 1.6). On the other hand, higher rub-off during NEM does not permit the saline water to impact the association in the upper part of the estuary.

Factor-5 is loaded positively with temperature, TSS and velocity along with high negative loading of PO_4^{3-}, which represents 7.09% of the total variance. PO_4^{3-} remobilization in estuary mainly happens under reducing conditions (Deborde et al.,

2007). The absorption of PO_4^{3-} by sediments happens under an increase in temperature with decreasing salinity conditions (Zhang et al., 2011) (Fig 4.21). During NEM, infusion of freshwater rich in DO decreases the reducing conditions, whereas resistance provided by such freshwater input towards saline water input can be validated by positive loading of velocity from the riverine side (Fig. 4.21). Positive loading of temperature and negative loading of PO_4^{3-} indicate the sorption of PO_4^{3-} under such conditions where it is finding its way to suspended solids and sediments. The factor scores suggest this process to be dominant in the upper part of the estuary. On contrary, stations 2 and 4 are observed to have higher factor scores (Fig. 4.21), which is mainly because of the higher turbidity and concentration of DO observe in these stations.

Factor-6 has positive loading of HCO_3^- and negative loading of Cu and Se while representing 5.44% variance. The negative loading of Cu might be due to the formation of insoluble $[Cu(HCO_3)_2]$ and association with organic compounds that exist in colloidal form favoured by an increase in HCO_3^- concentration in water (Drogowska et al., 1994; Namieśnik et al., 2010) while removing it from the water column (Fig. 4.22). Similarly, under well-oxygenated conditions, sorption of the dissolved form of Se such as SeO_3^{2-} and SeO_4^{2-} on sediments and suspended solid happens in aqueous conditions (Kieliszek et al., 2019; Hung et al., 1995), and such retention is closely linked with the presence of organic matter in water (Söderlund et al., 2016). This process is dominant in the lower part of the estuary (Fig. 4.21).

Table 4.17 Rotated Component Matrix of water contained physico-chemical parameters, major ions, nutrients and trace metals during NEM

Parameters	Extraction	Component					
		1	2	3	4	5	6
pH	0.803	-0.588	-0.631	0.090	0.212	0.078	-0.030
DO	0.681	0.533	0.101	0.043	0.528	0.322	-0.063
EC	0.946	0.784	0.531	0.017	0.018	0.215	0.011
TDS	0.946	0.784	0.531	0.017	0.018	0.215	0.011
Turbidity	0.910	0.105	-0.832	0.189	0.273	-0.120	0.293
Velocity	0.404	0.346	0.030	0.003	-0.014	0.506	0.156
Salinity	0.963	0.936	0.300	-0.001	-0.039	0.074	0.055
Temperature	0.463	0.293	0.117	-0.009	0.135	0.585	-0.087
TSS	0.769	0.291	-0.059	0.423	0.225	0.578	-0.046
HCO_3	0.806	0.626	-0.055	-0.012	0.193	0.344	0.499
Cl^-	0.832	0.658	0.574	0.010	0.054	0.257	-0.007
Mg^{2+}	0.893	0.822	0.407	0.084	-0.058	0.203	0.042
Na^+	0.975	0.911	0.376	-0.004	-0.008	0.101	0.038
K^+	0.943	0.913	-0.045	0.030	0.237	0.211	0.091
Ca^{2+}	0.732	0.458	0.606	0.086	-0.098	0.305	-0.217
CO_2	0.449	-0.171	-0.442	0.125	-0.288	0.327	-0.134
SO_4^{2-}	0.971	0.462	0.850	-0.014	-0.151	-0.037	0.103
PO_4^{3-}	0.603	-0.160	-0.134	0.134	0.000	-0.719	0.101
NO_3-N	0.882	0.330	0.808	0.055	0.138	0.231	0.218
NH_3	0.916	0.060	0.146	0.008	-0.935	-0.009	0.088
NH_4^+	0.917	0.066	0.154	0.012	-0.934	-0.002	0.087
NO_3^-	0.877	0.321	0.803	0.048	0.129	0.223	0.251
Cu	0.756	0.430	-0.111	-0.237	0.236	-0.364	-0.559
Zn	0.935	0.047	-0.097	0.951	0.004	-0.131	-0.049
Fe	0.950	-0.074	-0.141	0.959	0.013	-0.047	0.039
Co	0.845	-0.176	-0.805	0.113	0.382	0.015	0.030
Mn	0.891	0.084	0.061	0.934	0.002	0.065	-0.037
Cd	0.972	0.879	0.437	0.022	-0.028	0.090	-0.054
Cr	0.733	0.354	-0.564	0.240	0.430	0.104	0.130
Se	0.883	-0.125	-0.052	0.135	0.164	0.267	-0.866
Ba	0.923	0.944	0.115	0.009	-0.023	0.159	-0.035
Percentage Variance Explained		31.510	20.270	9.495	9.140	7.092	5.445
Total Variance Explained		82.951%					
Eigen Value		Greater than 1					

**Blue cells: Positive factor loading; Grey cells: Negative factor loading*

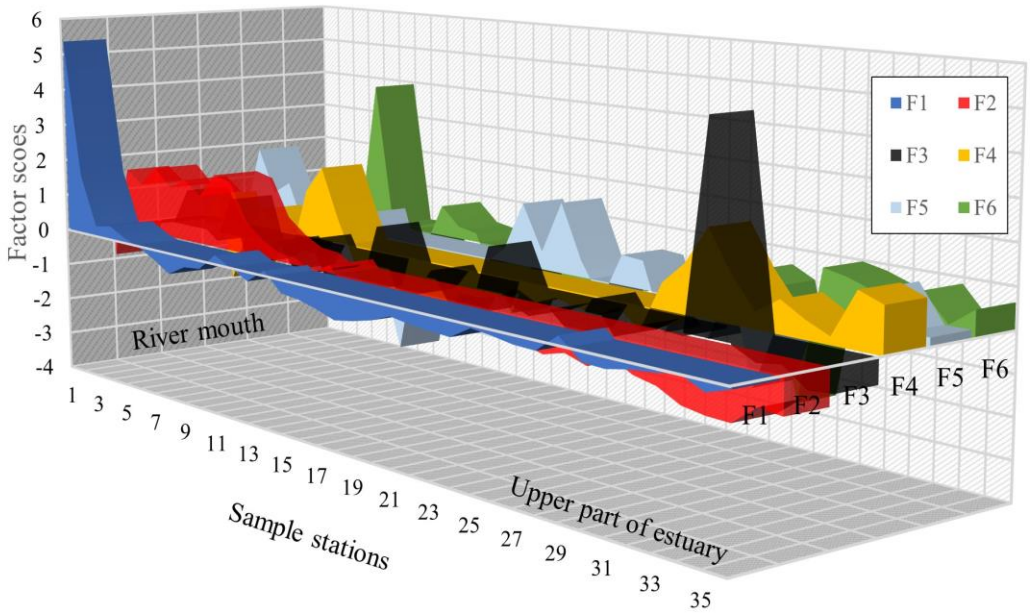

Fig. 4.21 Graphical representation of factor scores of various components during NEM

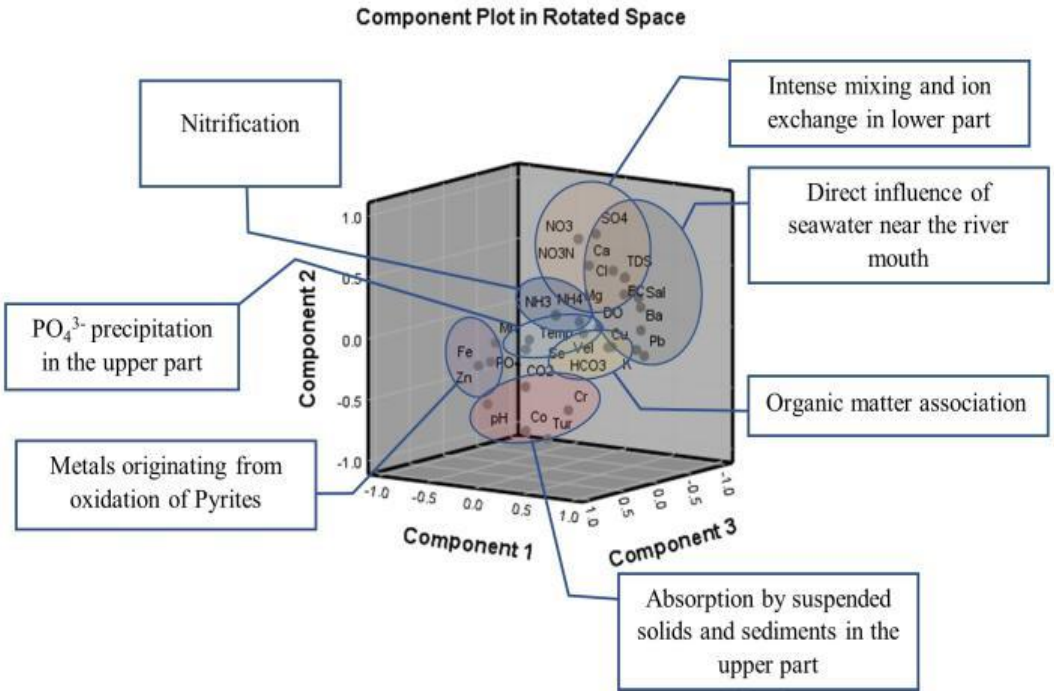

Fig. 4.22 Dominant principal components during NEM and its associated processes and sources

4.7.6 Saturation index (SI)

Saturation index (SI) is a tool that characterizes the thermodynamic stability of water with respect to specific minerals (Mackenzie & Garrels, 1971; Stumm & Morgan,

1981; Chidambaram et al., 2011). The Earth's crust is dominated by aluminosilicates and water flowing from the land to the river system comes in contact with these minerals frequently on its way. These aluminosilicates (e.g. muscovite) sometimes give rise to another mineral (e.g. kaolinite) of the same group in aqueous solutions depending on pH along with ions like K^+ (eq. 4.18). Similarly, carbonate minerals give rise to ions like Ca^{2+} and CO_3^{2-} with changing pH and temperature (Chidambaram et al., 2012) (eq. 4.19). Furthermore, the amorphous calcium carbonates are 100 times more soluble than calcites (Chidambaram et al., 2012).

$$2KAlSi_3O_8 + 2H^+ + 9H_2O \Leftrightarrow Al_2Si_2O_5(OH)_4 + 2K^+ + 4H_4SiO_4 \text{……..(eq. 4.20)}$$

$$Ca^{2+} + CO_3^{2-} \Leftrightarrow CaCO_3 \text{……..(eq. 4.21)}$$

In such scenarios, determining SI values of such minerals helps to understand the reactions taking place on its pathways and their contribution to the riverine water ecosystem (Chidambaram et al., 2011). Many researchers have used the SI of silicate, carbonate along with other mineral groups such as fluoride and oxide as an indicator to determine the weathering conditions in groundwater (Chidambaram et al., 2007; Vasanthavigar et al., 2009; Prasanna et al., 2010; Juen et al., 2015) from the source region. The SI can be calculated by the log-ratio value of ionic activity product in water (IAP) (Ferrer, 1988) with respect to the solubility product of the mineral (K_{sp}).

$$SI = \log(IAP/K_{sp}) \text{……(eq. 4.22)}$$

The index is calculated to know if.

SI = 0; Equilibrium state

SI < 0; Undersaturated state (mineral dissolution condition)

SI > 0; Oversaturated state (mineral precipitation condition)

Among all groups of minerals, SI of mineral groups like carbonate (calcite, magnesite, aragonite and dolomite), sulfate (gypsum, anhydrite), oxide (magnetite, goethite) and halide (halite) are taken into consideration. This consideration is done depending on their availability in the study area during SWM and NEM.

4.7.6.1 South-West monsoon (SWM)

In SWM, oxides like goethite and magnetite have SI values > 0 and are oversaturated in the water, whereas carbonate minerals like calcite, dolomite, aragonite and magnesite have SI values < 0 at all the stations and in the dissolution phase. Among

these carbonate minerals, the dissolution of dolomite is 2-fold higher than others. The dissolution phase of halite is highest in estuarine water indicate Na-Cl water type which also supports the seawater influence in the estuary during SWM (Juen et al., 2015). The sulfate group of minerals, gypsum and anhydrite are in the undersaturated stage in estuarine water. The super-saturation of minerals like magnetite might be due to excess oxide minerals dissolved under equilibrium conditions and the undersaturation phase of calcite, gypsum, dolomite and anhydrite might be due to the ongoing ion exchange process in the estuary (Juen et al., 2015). The saturation state of considered minerals according to their group in descending order is as follows:

Oxides and oxyhydroxides: $SI_{Magnetite} > SI_{Goethite}$ (Oversaturated state)

Carbonate minerals: $SI_{Calcite} > SI_{Aragonite} > SI_{Magnesite} > SI_{Dolomite}$ (Undersaturated state)

Sulfate minerals: $SI_{Gypsum} > SI_{Anhydrite}$ (Undersaturated state)

Halide minerals: SI_{Halite} (Undersaturated state)

4.7.6.2 North-East monsoon (NEM)

In NEM water samples, carbonate minerals like calcite, dolomite, aragonite and magnesite have SI values < 0 and are in the dissolution phase. Dissolution of these carbonate minerals is lower as compared to SWM. However, dissolution of dolomite stays highest among carbonate minerals. Likewise, halite is observed to be in the dissolution phase and has SI values lower than 0 at all stations. Higher dissolution of halite during NEM and saline water intrusion validate the presence of Na-Cl water type observed in the lower part of the estuary (Juen et al., 2015). However, dissolution of sulfate minerals, gypsum and anhydrite indicates an increase in ion-exchange process. Ions like Ca^{2+} and Mg^{2+} are replacing Na^{+} from various chloride complexes. The higher dissolution of halite mineral is known to produce conservative Cl^{-} ions that help with other available cations and metals in forming dissolved chloride complexes (Juen et al., 2015). The dissolution is lower for the group of minerals during NEM as compared to SWM samples. The saturation state of considered mineral groups in descending order is as follows:

Carbonate minerals: $SI_{Calcite} > SI_{Aragonite} > SI_{Magnesite} > SI_{Dolomite}$ (Undersaturated state)

Sulfate minerals: $SI_{Gypsum} > SI_{Anhydrite}$ (Undersaturated state)

Halide minerals: SI_{Halite} (Undersaturated state)

4.7.6.3 pH and Log pCO_2

Log pCO_2 is defined as the partial pressure of CO_2 of water bodies and stays in equilibrium with the atmosphere in open aquatic systems like an estuary. The state of saturation of minerals is closely related to the partial pressure of CO_2 (pCO_2) (Chidambaram et al., 2011). The equilibrium of calcium carbonate in contact with natural water, either surface or ground, is one of the most important geochemical reactions. Neutral water when exposed to CO_2 in the atmosphere will dissolve CO_2 equal to the partial pressure. The CO_2 will react with H_2O to form H_2CO_3, a weak acid, and the resulting solution will have a pH of about 5.7. Here, CO_2 in the soil is mainly generated from organic decomposition and plays an important role in the dissolution. Excess CO_2 can cause less supersaturated solution with respect to all the carbonate minerals (Chidambaram et al., 2011; Venturelli et al., 2003).

Log pCO_2 during SWM ranges from -2.307 to 0.132 and gains higher values in acidic conditions (Fig. 4.23). During NEM, the majority of dissolution and precipitation take place between log pCO_2 in the range of -2.742 to -0.59, and pH range of 5.45 to 7.6. In the lower part of the estuary, low pH and high log pCO_2 are observed at station 3 during SWM, where pH drop is observed due to respiration of organic matter and increasing log pCO_2, causing higher dissolution (Chidambaram et al., 2011) (Fig. 4.23). Similarly, a higher value of log pCO_2 is observed during NEM, with decrease in pH in the lower part of the estuary at station 1, and most probably associated with organic respiration due to water density stratification. In both seasons, the log pCO_2 is higher than the atmosphere (-3.5) (Njitchoua et al., 1997; Prasanna et al., 2010; Srinivasamoorthy et al., 2014), which means CO_2 is higher than the atmospheric equilibrium. In such a case, respiration of organic matter and dissolution of carbonate minerals play a major role in the increase of CO_2. Meanwhile, pH in the estuary is inversely related to log pCO_2 (Fig. 4.23). Factor such as atmospheric equilibrium is frequently used as an indicator of recharge and residence time of water in rivers (Prasanna et al., 2010; Chidambaram et al., 2011). The samples showing log pCO_2 values nearer to atmospheric equilibrium value (-3.5) are considered recharged due to fresh rainfall along with lesser residence time (Prasanna et al., 2010). During SWM, the lowest value of log pCO_2 is near the river mouth and at station 1, indicating a direct

flow of seawater into the estuary, whereas the highest value of log pCO_2 is also found in the lower region at station 3 maximum respiration of organic matter and dissolution of carbonate in this part. On the other hand, NEM log pCO_2 values indicate a clear influence of recharge and discharge in the estuary (Fig. 4.23). This season has a lower log pCO_2 value in the upper part of the estuary and is considered part of the fresh recharge because of higher rainfall during this time. The highest value is observed at station 1, indicating higher residence time of the recharged water in the lower part due to continuous tidal influence. Overall, the average value of log pCO_2 during NEM (-1.776) is lower than SWM (-1.494) and is an indication of less residence time of river water in the estuary as compared to SWM.

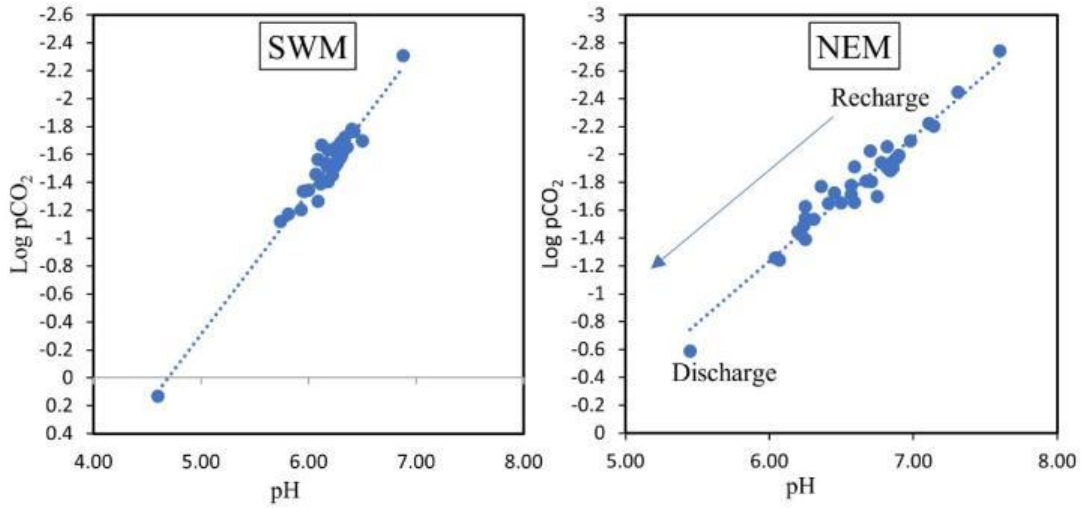

Fig. 4.23 Relation between log pCO_2 and pH

4.7.6.4 SI of Carbonate minerals

Saturation of carbonate minerals mainly depends on factors like log pCO_2, pH and HCO_3^- concentration (Prasanna et al., 2010; Chidambaram et al., 2011), whereas EC enhances other anions such as HCO_3^- present in water, which associates with other cations and helps saturation of carbonate minerals (Chidambaram et al., 2011). According to Chidambaram et al. (2011), bicarbonates derived from weathering and other sources stay in solution in aqueous solution and equilibrate with Ca^{2+} and Mg^{2+} or attain saturation with various carbonate minerals. In the current study, carbonate mineral dissolution does not show any significant relation with HCO_3^- concentration (Fig. 4.24) in water, indicating the source of such is mainly from seawater rather than weathering. Likewise, EC in estuarine water can be influenced mainly by seawater intrusion (Chidambaram et al., 2005), the interaction of rock and water

(Srinivasamoorthy et al., 2007) and presence of fine sediments (Fenn et al., 1987; Chidambaram et al., 2011). However, EC is noted higher near the river mouth and is mainly influenced by seawater intrusion in the study area during both seasons. There is no definite trend noted between EC and SI values of carbonate minerals (Fig. 4.24), indicating that EC is not the governing factor for the dissolution of these minerals. In the case of log pCO_2 and pH, an increase in dissolution of all carbonate minerals has been observed with increasing log pCO_2 and decreasing pH (Fig. 4.24). The saturation during NEM is higher than SWM and degassing of CO_2 is evident from the saturation of carbonate minerals (Chidambaram et al., 2011) and is confirmed by an observed higher average of CO_2 during this season (Fig. 4.2).

4.7.6.5 SI of Sulfate minerals

Gypsum and anhydrite have been observed to be undersaturated during both seasons, where dissolution is between -1 and -2 log pCO_2 whey they did not show any increasing or decreasing trend towards lower log pCO_2 values during SWM. According to Murray et al. (1964), higher CO_2 concentration in water reduces the dissolution of gypsum by 20-30 times and dissolution mainly depends on the flow and gradient of flow in the surrounding. Seawater is generally susceptible to the higher dissolution of sulfate minerals (Murray et al., 1964) and dissolution of such minerals is observed to be between -1 and -5 during both seasons. In such a scenario, the flow rate of the river and reactivity of clay minerals seemed to be playing a major role in dissolution patterns. The lack of sufficient recharge (Al-Ghanimy et al., 2019) during low flow period (SWM), tidal resistance to the fresh flow of the river and stratification at the bottom aforementioned might be the reasons for the non-reactivity of both minerals towards pH and log pCO_2 (Fig. 4.25). In addition, the Na-Cl water found dominating in the estuary, thus leaving less possibility of ion exchange or reverse ion exchange, which is major process for dissolution of gypsum and anhydrite in aquatic systems, is keeping the dissolution in near-constant stage during SWM. The lack of these controlling factors during SWM is limiting the dissolution and minerals stay closer to the saturation phase. On contrary, dissolution of both minerals is found to be more aligned and falling along the recharge line of the river during NEM (Fig. 4.25). Lower log pCO_2 values indicate less residence time of the water in the estuary and both minerals near to saturation at the discharge zone, attributing towards the higher influence of tidal water near the river mouth. Such conditions can be supported by

sulfate minerals' tendency to dissolve more with recharge and higher flow (Murray et al., 1964; Al-Ghanimy et al., 2019), higher saturation of calcite and dedolomization (Glynn et al., 2005; Al-Ghanimy et al., 2019) and action of clay minerals as they have more potential towards ion exchange process (Kalin et al., 1996). The estuary has a higher average of TSS during NEM, which confirms the abundance of clay minerals. Higher pH and lower log pCO_2 have been observed in the upper part and the reverse ion exchange process identified in the piper plot refers to higher dissolution in these minerals in the upper part and responds very well towards log pCO_2 and pH in the estuary. With respect to EC, the dissolution of these minerals also behave conservatively during NEM (Fig. 4.25). Higher EC has been noted at the river mouth due to seawater influence while bringing the dissolution of gypsum and anhydrite near saturation stage. However, the concentration of HCO_3^- does not respond to sulfate group of minerals, indicating its non-controlling nature in the river. Dissolution of gypsum and anhydrite are observed to be very close to each other in all the samples, unlike carbonate minerals, which may be due to the solubility of both minerals that are equivalent to each other. In addition, conversion of gypsum to anhydrite and back to gypsum is common due to the thermodynamic instability of these minerals within the physicochemical range of the common geologic environment (Murray et al., 1964). Anhydrite dissolved in water produces a solution of $CaSO_4$ that eventually attains equilibrium as gypsum in water (Klimchouk et al., 1996).

4.7.6.5 SI of Halide minerals

The dissolution is highest for halite than any other minerals considered in the current study, which may be due to its nature of high solubility (Klimchouk et al., 1996; Naderi et al., 2016). The saturation index of halite validates the dominance of Na-Cl water type during SWM and partial presence during NEM. SI of halite does not share any significant relation with log pCO_2, pH and HCO_3 during SWM and is mostly concentrated around -1 to -2 log pCO_2 values, indicating moderate residence of saline water in the estuary. It responds to EC during both seasons perfectly with dissolution decreases with higher EC values. During SWM, higher dissolution takes place between 100 to 200 µS/cm of EC, whereas dissolution is well spread during NEM due to reducing saline water influence through freshwater recharge (Fig. 4.26). On the other hand, SI values of halite relate significantly with log pCO_2 and pH, indicating a lower residence time of saline water (Prasanna et al., 2010; Naderi et al., 2016) while

an increase in dissolution in the seawater's flow direction (towards upstream direction) is due to the intensive mixing and ion exchange process caused by dissolution of gypsum and anhydrite (Hamzaoui et al., 2013; Juen et al., 2015; Naderi et al., 2016) and validates the Ca-Mg-Cl type of water observed during NEM.

4.7.6.5 SI of Oxides

Fe oxides are found to be precipitating during SWM, whereas such precipitation/dissolution is missing in NEM water samples. These oxides show an increasing trend with an increase in pH and a decrease in log pCO_2 values of water in the estuary (Fig. 4.27). The supersaturation state of magnetite is responsible for lowering the concentration of dissolved Fe in estuarine water. Both oxide and oxyhydroxides approach saturation with a decrease in pH condition, attributing towards the changes in redox conditions, pH and hydrolysis reactions (Mapoma et al., 2017). The main control of Fe content in water samples studied is dissolution and precipitation mechanisms of Fe-containing minerals. In the study area, siliciclastic rocks with pyrite concretions in the river basin are the major source of Fe (Nagarajan et al., 2015; Nagarajan et al., 2017a). The oxidization of pyrites mainly releases this metal into the river (Anandkumar, 2016). According to Tosca et al. (2019), effluent-seawater mixing with river water strongly reduces the flux of dissolved Fe into the sea due to the formation of oxides and oxyhydroxides. These observations suggest the precipitation of Fe is mainly associated with the residence time of river water for a longer period during SWM as compared to NEM. This might be due to increased tidal resistance observed in the river and low flow (seasonal fluctuation) which is allowing Fe to precipitate (Mapoma et al., 2017) in the estuary in the form of magnetite and goethite. The EC and HCO_3^- do not show any significant relation with both the minerals as they are not the major controlling factors for magnetite and goethite.

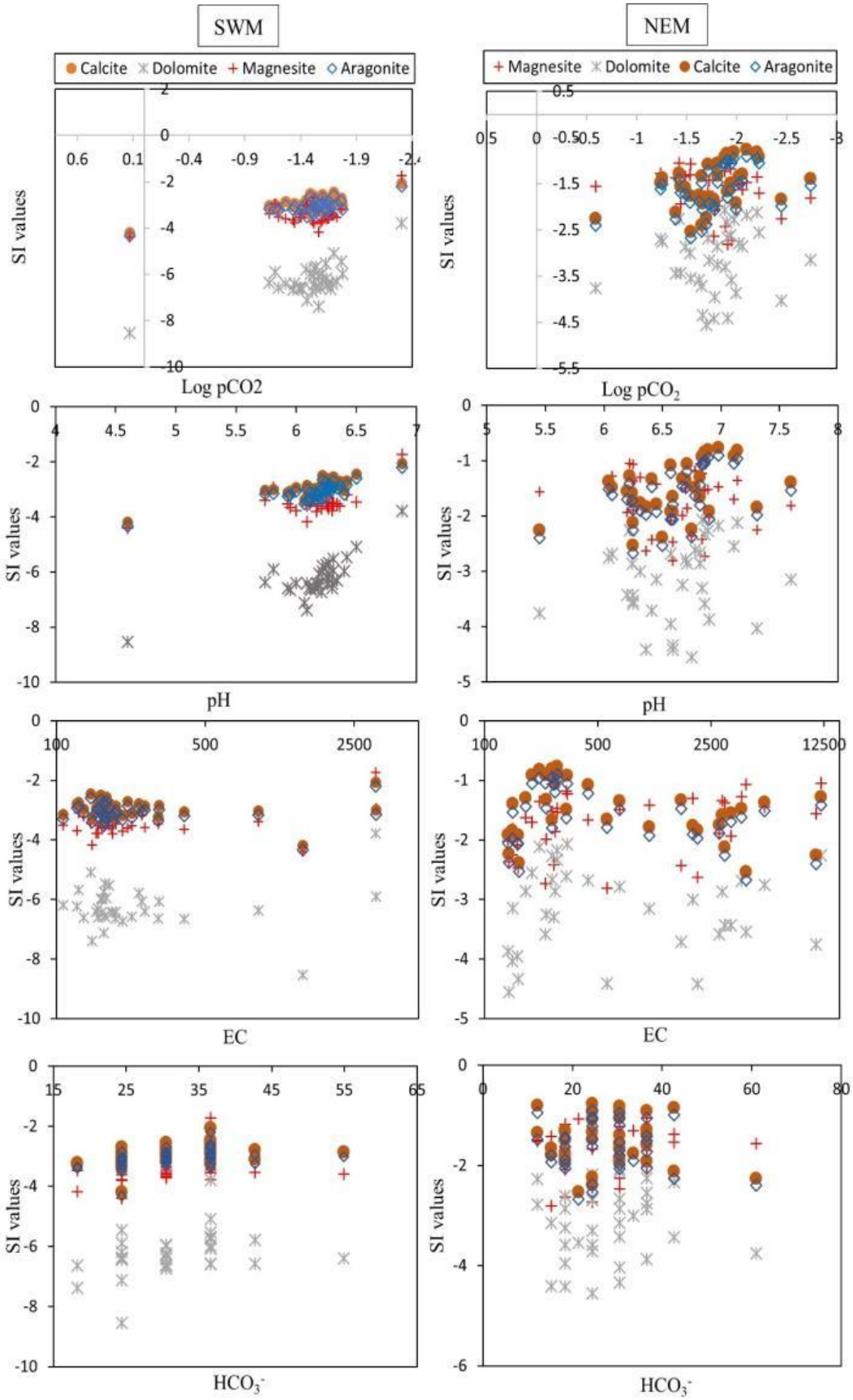

Fig. 4.24 Relationship of log pCO_2, pH, EC and HCO_3^- with SI of carbonate minerals

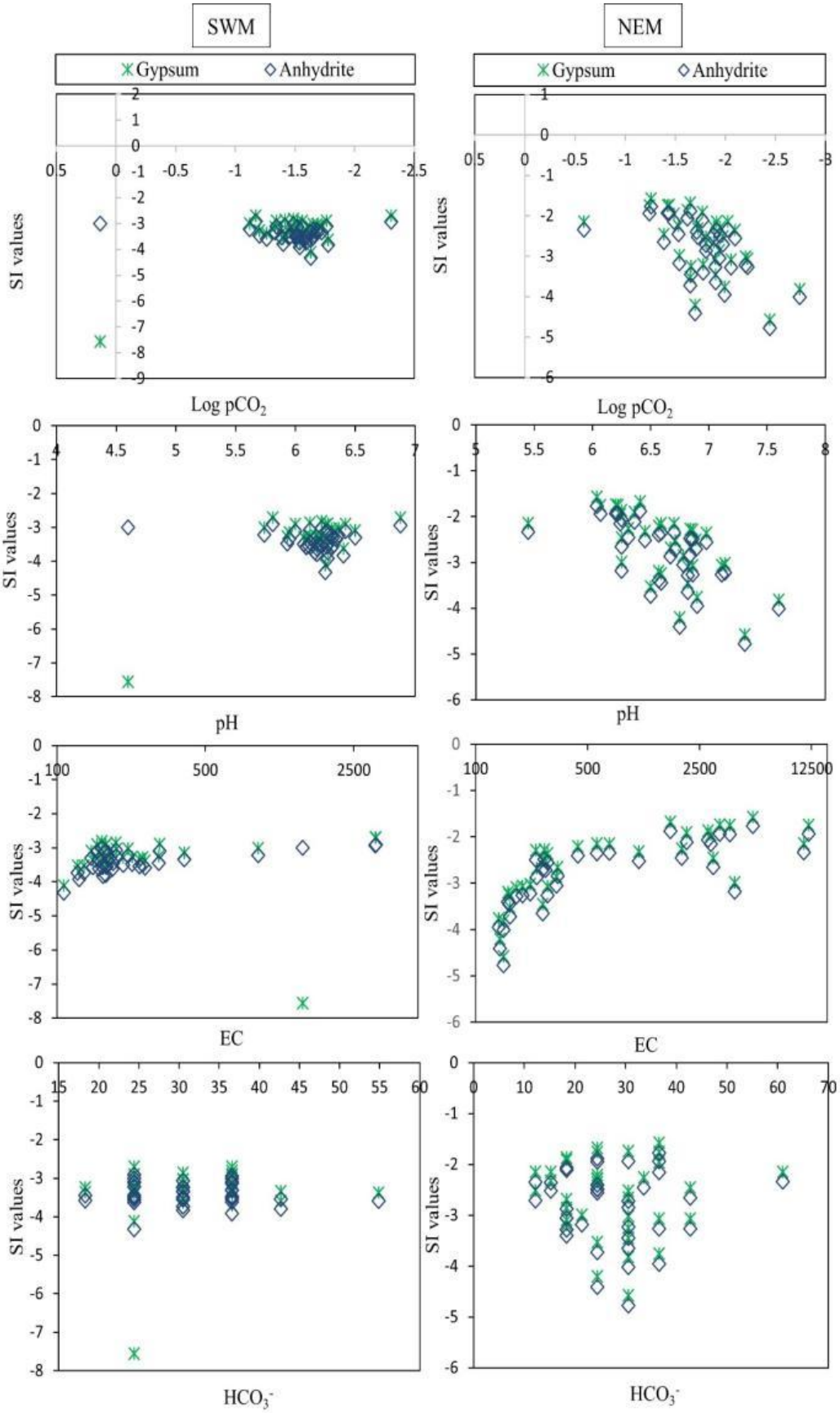

Fig. 4.25 Relationship of log pCO_2, pH, EC and HCO_3^- with SI of Sulfate minerals

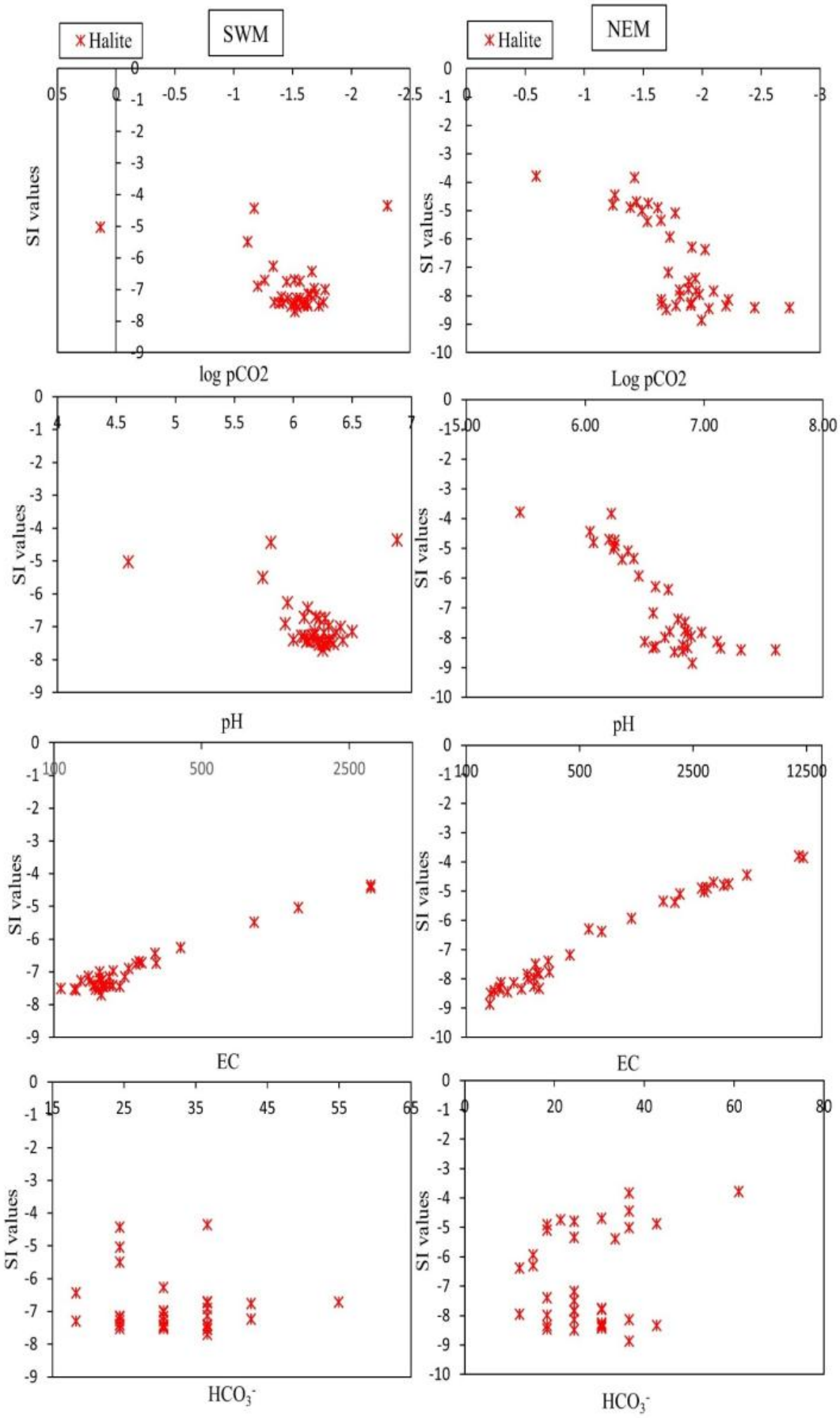

Fig. 4.26 Relationship of log pCO_2, pH, EC and HCO_3^- with SI of Halite

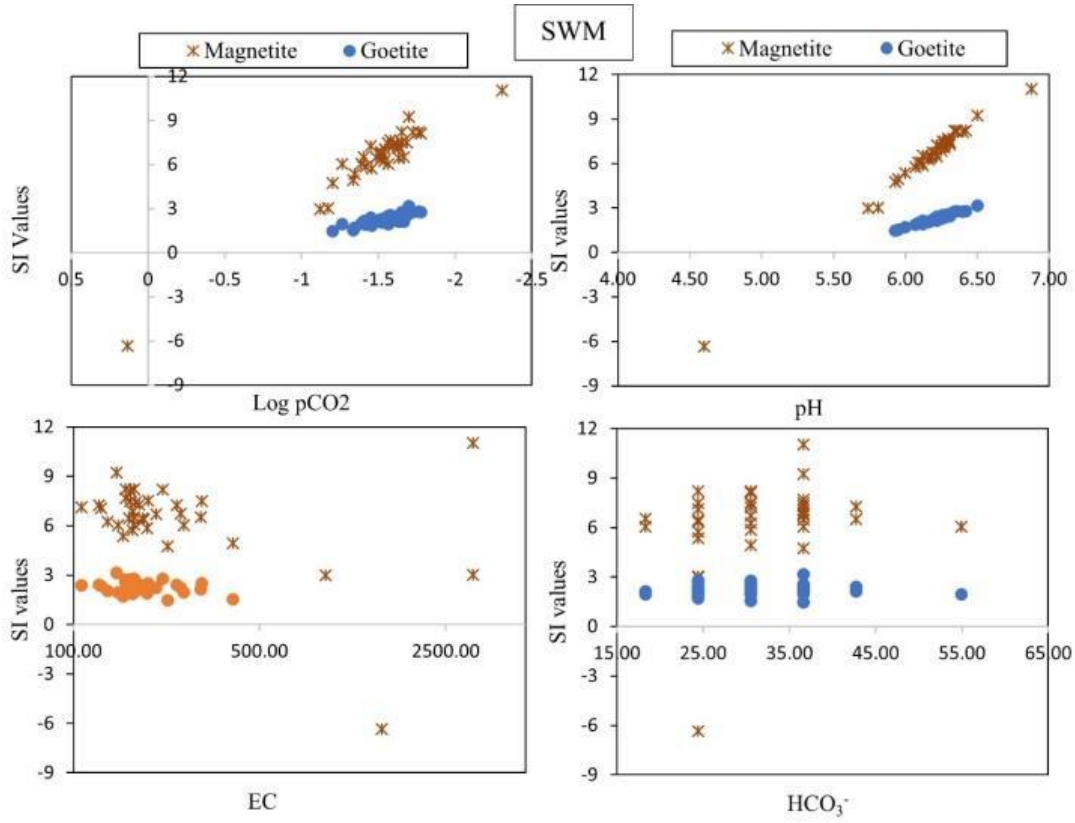

Fig. 4.27 Relationship of log pCO_2, pH, EC and HCO_3^- with SI of Oxide and Oxyhydroxide

4.8 Summary

- Parameters such as DO, salinity, EC, turbidity, TSS, Ca^{2+}, Mg^{2+}, Na^{+}, Cl^{-}, SO_4^{2-}, NO_3^{-}, PO_4^{3-}, Cu and Fe showed significant variation between the seasons, where Cl^{-}, SO_4^{2-}, and Fe remained the dominant ion, nutrient and metal respectively.
- Estuarine water was found unsuitable for drinking purposes and corrosive in nature. Samples were found to be suitable for irrigational purposes based on the USSL and RSC index irrespective of the seasons. However, SAR, Kelly's ratio, Permeability index and Na% suggested the possibility risk of sodium hazard in the majority of SWM samples.
- Hydrochemistry of the estuary suggested reverse ion exchange during NEM with Ca-Cl water type dominated the estuary, whereas Na-Cl water type dominated during SWM due to high tidal influence.
- Factor analysis along with factor scores revealed seawater-related parameters controlled major geochemical processes during SWM. Evidence of denitrification and ammonification process was confirmed by the factor models and the source of the nutrients (PO_4^{3-}, SO_4^{2-}, NO_3^{-}, NH_3) along with Cd were found to be from agricultural affluents mainly through the tributaries.

- During NEM, major geochemical processes were also controlled by seawater and intense mixing of fresh and sea water in the lower part of the estuary. Nitrification process was dominant in the mixing zone, unlike SWM due to availability of DO in the water column.
- SI revealed dissolution of carbonate, sulfate and halide group of minerals during both seasons except oxides and oxyhydroxides, which are found in oversaturated states during SWM.

Chapter-5
Sediment Geochemistry

5.1 Introduction

Environmental pollution in the aquatic system like coastal waters, estuaries, and rivers is a global concern due to the increase in land deforestation, human activities, agriculture and economic activities as these are closely linked to human survival. An increase in such activities can have deleterious effects on aquatic living resources, human health, besides posing a hindrance to marine activities and cause impairment in the quality of use of such systems for our benefit in the future (Dan et al., 2014; Shazili et al., 2006). Most of the human-induced pollution is mainly transported from land to sea through river with it being a medium and estuaries being a transition zone between them. Although the riverine ecosystem primarily functions and transports with the help of 3 main interfaces simultaneously such as water, suspended particles and sediment load, sediments hold ought to be the most important interface to be paid attention to as the global contribution of river-derived sediments comprises up to 95% of the material entering the world oceans (Lučić et al., 2019). In addition to that, 30 to 98% of toxic materials like metals from geogenic/anthropogenic sources transported by rivers get deposited on sediments under varying environmental conditions like in estuaries (Gibbs et al., 1973; Yang et al., 2017). These metals' presence in sediments is of utmost concern because of their environmental persistence, biogeochemical recycling, and potential ecological risks towards many aquatic organisms and humans (Zhang et al., 2018; Yao et al., 2019).

The study of sediment composition in estuaries helps to reflect the geochemical nature of the river basin and helps to elucidate the overall character of the material transported by rivers from adjacent land areas, derived from shoreline erosion, carried by marine currents from external sources, produced in situ by organisms and contribution by human activities (Prabakaran et al., 2020). It is also an important indicator of ongoing environmental pollution in the aquatic system like estuaries as deposition of surface sediments are fresh due to continuous inputs (Fernandes et al., 1997). The sediment input in the Sibuti River is mainly influenced by Sibuti and Lambir formations, exposed in the river basin, which is reported to have mineral concretions that are rich in Fe_2O_3, MnO and P_2O_5 and selected trace metals (Azrul Nisyam et al., 2013;

Nagarajan et al., 2015; Nagarajan et al., 2017a). Deforestation due to rapid urbanization, which stands above 26% since 1970 in Borneo (Krawczyk et al., 2020), is mostly contributing to the high sediment load from the river basin. Apart from that, land-use factors such as vast agricultural practices are observed in the study area. Considering such a scenario, the Sibuti river is expected to be getting a high amount of metals with sediment run-off over the years, which is eventually transported towards South China sea through its estuary. In order to decipher the behavior of these inputs in the intertidal zones of the estuary, assessment of major metals (Co, Cu, Mn, Pb, Zn, Se, Fe, Al, Cd, Cr, Ba) in surface sediments of the Sibuti River estuary was taken into consideration for the study during two major seasons which are the SW monsoon (SWM) and the NE monsoon (NEM). Besides, to understand the geochemical processes and distribution of the metals, 36 samples were collected from the estuarine zone and the elements were studied using sequential extraction methods and statistical analyses like correlation and factor analysis were used to interpret the data set. Besides, to assess the level of pollution, indices such as Geoaccumulation index (I_{geo}), Enrichment factor (EF), Contamination factor (CF), Pollution load index (PLI), Potential ecological risk index (PERI), Sediment pollution index (SPI), ERL and ERM along with Risk assessment code (RAC) were used and discussed in this chapter.

5.2 Results

5.2.1 South-west monsoon (SWM)

The descriptive statistics of total trace metal (TTM) concentrations are shown in Table 5.1 for SWM. The observed abundance of trace metals in estuarine sediments in descending order during SWM is as follows:

Al > Fe > Ba > Co > Cu > Se > Mn > Zn > Cr > Pb > Cd

Based on the results, the concentration of Co varies from 796.5 to 2337.2 mg kg^{-1} with mean values of 1318.11 mg kg^{-1}. The concentrations of Al and Fe are recoded higher and their ranges are 33205.70 to 90397.50 mg kg^{-1} and 16651.50 to 227258.10 mg kg^{-1} to mg kg^{-1} and with average values of 54123.51 and 52496.30 mg kg^{-1} respectively. The Ba also exhibits a wider range as 774.1 and 7511.3 mg kg^{-1} with an average of 2301.48 mg kg^{-1} during SWM. The concentration of Cu is widely varied between the

samples and it ranges from 76.80 to 3901.3 mg kg^{-1} with an average value of 1050.78 mg kg^{-1}. The concentration of Mn is ranged from 38.70 to 523.30 mg kg^{-1} with an average of 174.19 mg kg^{-1}. The concentration of Pb is varied from BDL to 11.40 mg kg^{-1} with an average value of 3.35 mg kg^{-1}, whereas Zn is varied between 86.40 and 213.5 with an average value of 174.19 mg kg^{-1}. Similarly, the Se concentration during SWM is recorded as 527.7 to 1081.1 mg kg^{-1} (avg. 789.87 mg kg^{-1}). The Cd shows a minimum variation as 0.99 to 1.74 mg kg^{-1} with an average value of 1.25, whereas Cr shows a significant variation as 29.7 to 113.8 mg kg^{-1} with an average of 92.63 mg kg^{-1}.

5.2.2 North-east monsoon (NEM)

The descriptive statistics of TTM concentrations observed during NEM are presented in Table 5.1. The observed abundance of trace metals in estuarine sediments in descending order during NEM is as follows:

Fe > Al > Co > Ba > Se > Cu > Mn > Zn > Cr > Cd > Pb

There is a significant change in the overall trend of the elemental concentrations, where Fe has recorded the highest concentration during NEM and ranges from 27,673.6 to 65400.8 mg kg^{-1} (avg. 39527.7 mg kg^{-1}) followed by Al recording the 2nd highest concentration at 1862.4 to 102302 mg kg^{-1} with an average of 27635.9 mg kg^{-1}.Co varies from 1331.40 to 2902.90 mg kg^{-1} (avg. 1969.36 mg kg^{-1}), and Ba ranges from 210.3 to 3186 mg kg^{-1} with an average of 1487.73 mg kg^{-1}. The concentrations of Cu and Mn are recorded as 134 to 952.90 mg kg^{-1} (355.67), and 39 to 399.3 mg kg^{-1} (163.23 mg kg^{-1}) respectively during NEM. Pb exhibits the lowest concentration during NEM and ranges from BDL to 0.2 mg kg^{-1} with an average of 0.01 mg kg^{-1}. However, Zn content during NEM is comparable to SWM and ranges from 91.60 to 197 mg kg^{-1} (avg. 127.59 mg kg^{-1}). The concentration of Se varies from 494.3 to 931.6 mg kg^{-1} with an average of 744.01 mg kg^{-1}. The Cd concentration is also comparable between the seasons and it ranges from 0.96 to 1.53 mg kg^{-1}. Cr is recorded higher during NEM and its range is recorded as 99.3 to 113.3 mg kg^{-1} with an average value of 110.96 mg kg^{-1}. Except for Cr and Co concentrations, all other studied elements are enriched during SW monsoon compared to NE monsoon.

Table 5.1 Descriptive statistics of total trace metal (TTM) (n=36) concentration(in mg kg^{-1}) in sediments during SWM and NEM

Metals	SW Monsoon				NE Monsoon			
	Min	Max	Mean	St. Dev	Min	Max	Mean	St. Dev.
Co	796.5	2337.2	1318.11	355.27	1331.4	2902.9	1969.36	419.82
Cu	76.8	3901.3	1050.78	764.46	134	952.9	355.67	224.93
Mn	38.7	523.3	174.19	118.31	39	399.30	163.23	89.51
Pb	BDL	11.4	3.35	3.36	BDL	0.2	0.01	0.03
Zn	86.4	213.5	133.97	31.91	91.6	197	127.59	30.48
Se	527.7	1081.1	789.87	138.36	494.3	931.6	744.01	112.78
Fe	33205.7	90397.5	52496.3	15269.24	27673.6	65400.8	39527.7	10870.18
Al	16651.5	227258.1	110824.88	54123.51	1862.4	102302	27635.87	33237.45
Cd	0.99	1.74	1.25	0.19	0.96	1.53	1.18	0.14
Cr	29.7	113.8	92.63	22.99	99.3	113.3	110.96	2.15
Ba	774.1	7511.3	2301.48	1569.24	210.3	3186	1487.73	848.29

5.2.3 Partitioning mobility of elements

Sediments are a heterogenous mixture of dissimilar particles, which may be formed by an assemblage of both organic and inorganic compounds (Martin et al., 1987). In the case of an estuary, the sediments receive toxic elements continuously from various natural and anthropogenic sources. The point and non-point sources might include industrial discharge, agricultural input, river inputs and domestic discharges (Venkatramanan et al., 2015). Therefore, most of the studies concerning metal concentration focus on the total metal concentration in the sediments, which implies all forms of metal exhibiting equal impact on the environment in which overall, is not suitable while evaluating a short-term process (Tessier et al., 1979). According to Martin et al. (1987), the transportation medium of residual sediment is mainly associated with thermodynamically unstable sources such as carbonates, amorphous aluminosilicates, organic matter, etc., and normally coated with Fe and Mn oxides along with the organic matter. Therefore, the toxic impact of such element-carrying sediments can be exposed by determining the chemical forms exhibiting in them (Zhang et al., 2014). Along with that, it is a desirable criterion to discriminate between the different nature of elements in the sediments. These criteria can be easily achieved by speciation studies proposed by Tessier et al. (1979) while evaluating various processes in transportation and deposition of sediments in the downstream and release

of these elements from sediment to water table under varying environmental conditions.

In aquatic environments, sediments are identified to be the main source of metal assemblage. It also works as the major pathway for transportation and storage of potential noxious metals (Zhang et al., 2014). These metals get deposited on the sediment surfaces and become immobilized by incorporating themselves into the lattice structure of minerals such as Fe and Mn oxides and forming insoluble fraction such as metal sulfides (Lin et al., 2013). Thus, a very small quantity of metals stay soluble in water as compared to the 90% of the metals that get absorbed by the sediments and suspended solids under various environmental conditions (Zheng et al., 2008). Hence, the study of metal assemblage in sediments can provide a broad idea of anthropogenic influence in the aquatic system along with the potential risk associated with it. Hence, to avail the mobility and bioavailability of certain metals, extraction of partitioning particulate trace metals into chemical forms that are likely to be released under various chemical environments are done using protocols by Tessier et al. (1979). The extraction is done for metals like Co, Cu, Mn, Pb, Zn, Se, Fe, Al, Cd, Cr and Ba, where the mobile fraction is represented by the first 4 fractions (i.e., F1, F2, F3, F4) and the residual fraction is represented as F5 (Table 5.3 & 5.4). The distribution of all the analyzed metals in various fractions is presented in Figure 5.1 for SWM and NEM respectively.

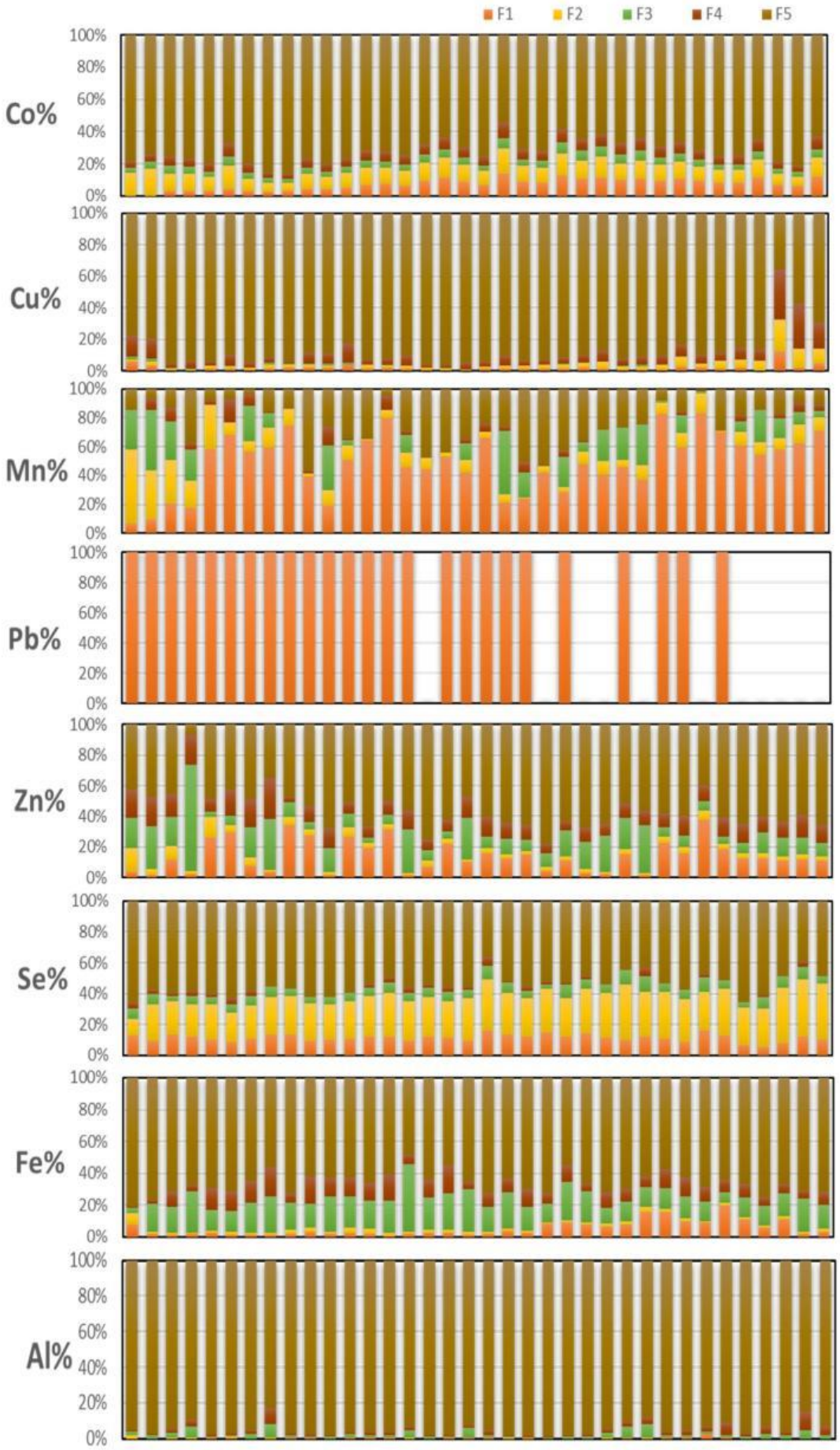
F1
F2
F3
F4
F5
Co%
Cu%
Mn%
Pb%
Zn%
Se%
Fe%
Al%
100%
80%
60%
40%
20%
0%

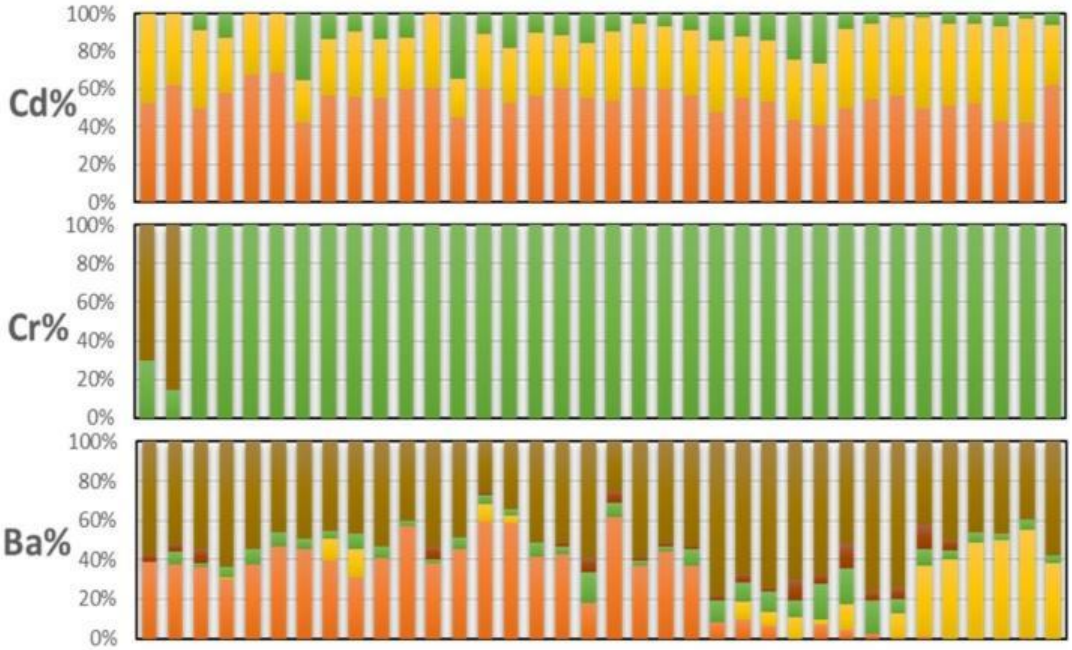

Fig. 5.1 The percentage distribution of trace metals in different fractions recorded during SWM

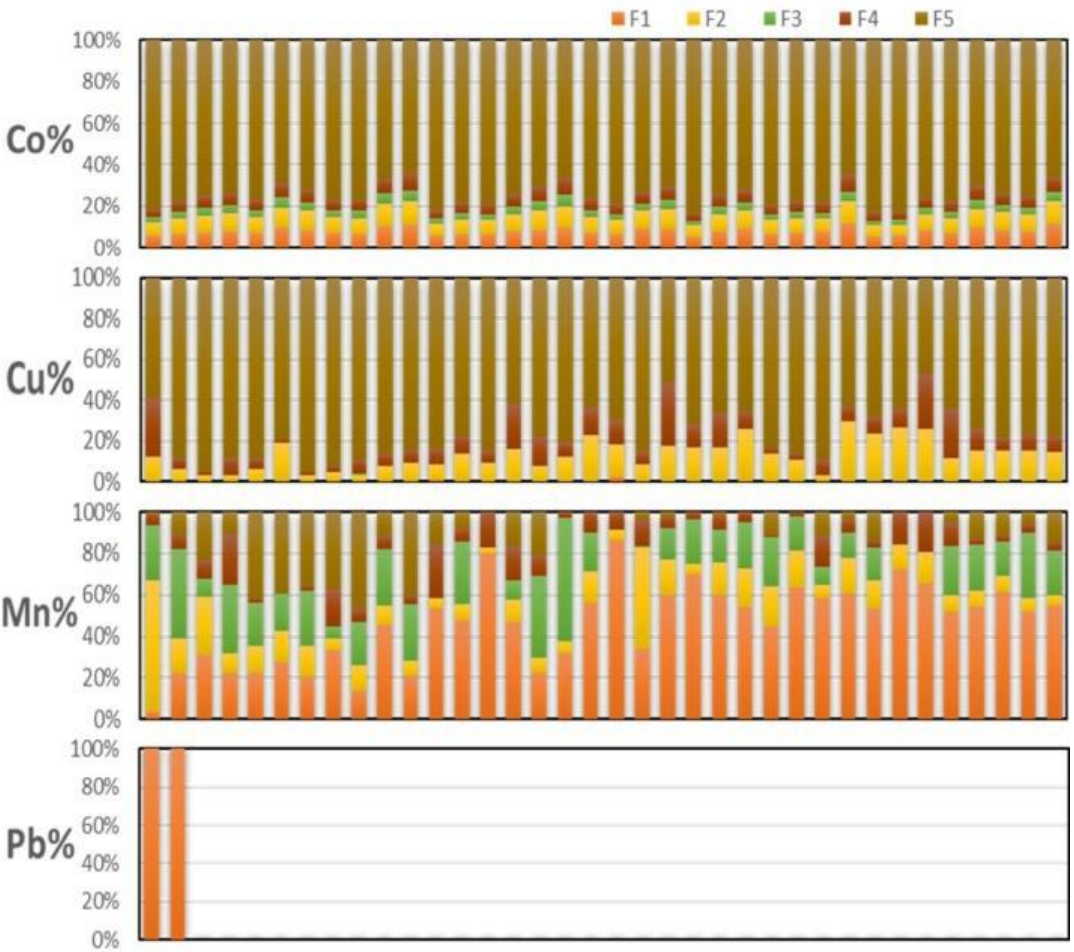

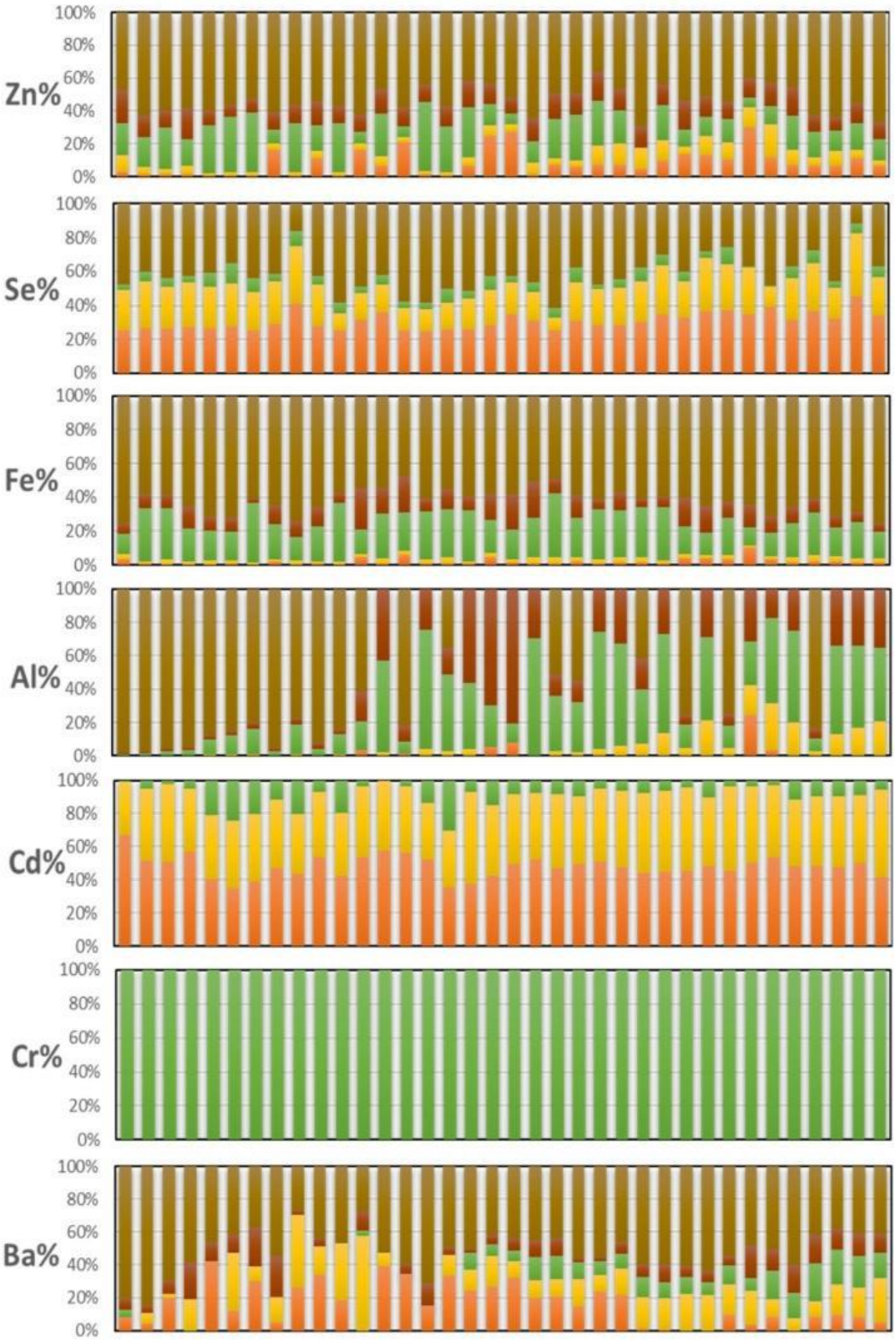

Fig. 5.2 The percentage distribution of trace metals in different fractions recorded during NEM

The partitioning of the metal concentrations between various fractions during SWM & NEM in descending order is as follows:

Table 5.2 Percentage of Metal contribution in various fractions shown in the descending order for SWM and NEM respectively

Elements	The concentration of elements in various fractions during SWM	The concentration of elements in various fractions during NEM
Co	F5>F2>F1>F4>F3	F5>F2>F1>F4>F3
Cu	F5>F4>F2>F1>F3	F5>F2>F4>F1>F3
Mn	F1>F5>F3>F2>F4	F1>F3>F2>F5>F4
Pb	F1>F2=F3=F4=F5	F1>F2=F3=F4=F5
Zn	F5>F3>F1>F4>F2	F5>F3>F4>F1>F2
Se	F5>F2>F1>F3>F4	F5>F1>F2>F3>F4
Fe	F5>F3>F4>F1>F2	F5>F3>F4>F2>F1
Al	F5>F3>F4>F1>F2	F5>F3>F4>F2>F1
Cd	F1>F2>F3>F4=F5	F1>F2>F3>F4=F5
Cr	F3>F5>F1=F2=F4	F3>F1=F2=F4=F5
Ba	F5>F1>F2>F3>F4	F5>F2>F1>F3>F4

*The similar trends observed between the season are underlined and highlighted.

5.2.3.1 Exchangeable Fraction (Fraction-1)

The exchangeable fraction mainly comprises of metals, which can be easily leached by a natural salt (Tack & Verloo, 1999) and readily absorbed and retained by weak electrostatic interactions (Rao et al., 2008). The associated metals with this fraction can be released by the ion-exchange process, which might influence the absorption and desorption reactions or can cause remobilization of metals with reducing pH conditions (áVan et al., 1995; Rao et al., 2008; Parker et al., 2001). This fraction is also marked as no specifically absorbed fraction and tend to be released by the action of K, Ca, Mg or NH4 with the displacement of metals with a tendency to form a weak electrostatic bond at organic and inorganic sites of the sediment's surface. These cations are highly reactive at relatively higher concentration situations (Rao et al., 2008; Beckett et al., 1989). The percentage of metals associated with this fraction during SWM in descending order can be arranged as Pb (100%)> Cd (53.67%)> Mn (46.99%)> Ba (22.99%)> Zn (13.32%)> Se (11.09%)> Co (7.04%)> Fe (4.92%)> Cu (1.47%%)> Al (0.2%)> Cr (0.00%) and during NEM as Pb (100%)> Cd (47.65%)> Mn (44.99%)> Se (30.12%)> Ba (12.63%)> Zn (7.60%)> Co (7.45%)> Fe (1.97%)> Al (0.27%)> Cu (0.09%)> Cr (0.00%).

It can be observed that Pb, Cd, Mn, Ba, and Zn are mainly associated with the exchangeable fraction in both seasons as compared to all other elements. However, the concentration of Pb is recorded very low during NEM and noted only at stations 1 and 2, whereas it recorded higher concentration at various stations during SWM. In contrast, Al, Cu and Cr are least associated with this fraction as compared to other fractions.

A relatively higher proportion of Mn is noted with the exchangeable fraction; however, it does not represent the anthropogenic influence in sediments as the element tends to present in less thermodynamically stable phases (Tessier et al., 1979; Prabakaran et al., 2019). On the other hand, a higher proportion of Cd and Pb can be attributed to the higher proportion of Mn and a higher concentration of Fe in exchangeable fraction as it can be absorbed by soil particles, Fe and Mn hydrated oxides, and humic acid (Yuan et al., 2004; Förstner et al., 2012). This kind of absorption of metals can attribute to a change in the water ionic strength (Yuan et al., 2004) and might represent an indicator of its anthropogenic nature of metals (Mohan et al., 2012) depending upon its source in the river basin.

5.2.3.2 The Carbonate Fraction (Fraction-2)

The metals bound to carbonate fraction are sensitive to pH changes and with the lowering of pH, sediments tend to release the metal cations into the water in absence of absorbents like Fe-Mn oxides and organic matter. The metals are loosely associated with the sediments and might represent their anthropogenic nature depending upon origin (Mohan et al., 2012; Prabakaran et al., 2019). The analyzed elements in this fraction during SWM in descending order can be presented as Cd (34.98%) > Se (25.80%) > Ba (16.69%) > Mn(12.13%) > Co (9.75%) > Zn (3.63%) > Cu (1.81%) > Fe (1.75%) > Al (0.14%) > Pb (0%) = Cr (0%) while during NEM, the descending order of metals associated with the carbonate fraction can be presented as Cd (42.27%) > Se (21.52%) > Ba (16%) > Mn (14.11%) > Cu (9.69%) > Co (7.87%) > Zn (5.80%) > Fe (2.30%) > Al (1.27%) > Pb (0%) = Cr (0%). It can be observed that Cd, Se, Ba and Mn have a significant presence (>10%) in fraction 2 for both seasons. The absorption of these metals by carbonate minerals shows similar character in both the seasons but lesser as compared to exchangeable fraction.

5.2.3.3 Reducible Fraction (Fraction-3)

Secondary oxides such as Fe and Mn coat themselves as fine discrete particles through the occurrence of various mechanisms, including absorption, ion exchange, coprecipitation, surface complex formation, etc. The scavenging nature of these oxides sorbs metals on the surface of the sediments initially in an exchangeable form, but over time, it becomes less mobile and converts into absorbed forms (Rao et al., 2008; Yuan et al., 2004). The metals added by these scavenging oxides can be released into water under reducing conditions (Mohan et al., 2012; Tack and Verloo, 1999). In the present study area, percentage of metals associated with fraction 3 during SWM can be presented as (descending order) Cr (87.77%) > Fe (17.55%) > Mn (15.87%) > Zn (15.36%) > Cd (11.35%) > Ba (6.08%) > Se (6.01%) > Co (4.18%) > Al (2.12%) > Cu (0.43%) > Pb (0%) while during NEM, the same can be presented as Cr (100%) > Fe (23.27%) > Mn (21.09%) > Zn (20.63%) > Al (12.98%) > Cd (10.08%) > Ba (10.02%) > Se (5.67%) > Co (3.36%) > Cu (0.04%) > Pb (0%). During the SWM, Cr, Fe, Mn, Zn and Cd show a significant association with a reducible fraction whereas Al and Ba show a significant association along with Cr, Fe, Mn, Zn and Cd during the NEM. The presence of Cr and toxic metals like Cd in both seasons shows a higher affinity towards Fe-Mn oxides and the formation and presence of stable phases in the sediments. The higher affinity of Zn towards Fe-Mn oxides as compared to carbonates in both seasons explains the higher stability constants that are formed in the sediments (Li et al., 2001). It also explains that the Fe-Mn oxides are the main carrier of Zn from the fluvial environment to the estuarine environment (Krupadam et al., 2006).

5.2.3.4 Oxidizable Fraction (Fraction-4)

This fraction also gives an idea about the elements that can be mobilized under changing environmental conditions and releases non-silicate bound forms that enter the soil environment (Rao et al., 2007). Such forms such as organic matter mainly consist of complex polymeric materials such as fluvic and humic acids, which have high metal absorption capacity and substances like carbohydrates, proteins, peptides, fat, amino acids, etc (Prabakaran et al., 2019). Such matters act as a sink for these metals and release them when the reacting conditions are oxidizing rather than reducing (Mohan et al., 2012). It efficiently releases metal sulfides in such conditions (Tack & Verloo, 1999). The elements associated with fraction 4 in the study area

during the SWM can be presented as Zn (11.33%) > Fe (9.19%) > Co (5.82%) > Cu (4.85%) > Mn (4.60%) > Ba (2.45%) > Se (1.80%) > Al (1.78%) > Pb (0%) = Cd (0%) = Cr (0%) while during the NEM, the association trend with this fraction can be presented as Zn (12.23%) > Fe (10.75%) > Ba (9.61%) > Cu (8.27%) > Mn (7.62%) > Al (6.8%) > Co (5.47%) > Pb (0%) = Cd (0%) = Cr (0%) = Se (0%). It is observed that Zn and Fe are the dominant metals in both seasons and the release is mainly associated with the degradation of organic matter in reducing conditions. This also can be interpreted as their ability to produce strong complexes with humic substances within natural waters (Marcovecchio et al., 2005). Metals like Cd and Pb have a lower tendency to form stable organic complexes in the aquatic system (Marcovecchio et al., 2005), which can be noticed during both seasons.

5.2.3.5 Residual Fraction (Fraction-5)

This fraction consists of primary and secondary minerals containing metals (Prabakaran et al., 2019; Gleyzes et al., 2002). These metals are strongly bound to the crystal structure of the minerals and not easily mobilized under varying natural environmental conditions because of their chemically stable and biologically inactive nature (Prabakaran et al., 2019). The metals associated with this fraction during the SWM can be presented as Al (95.76%) > Cu (91.54%) > Co (73.22%) > Fe (66.59%) > Zn (56.36%) > Se (55.30%) > Ba (51.79%) > Mn (20.42%) > Cr (12.23%) > Pb (0%) = Cd (0%) while during the NEM, the associated trend of the metals can be presented as Cu (81.91%) > Al (78.67%) > Co (75.84%) > Fe (61.67%) > Zn (53.74%) > Ba (51.74%) > Se (42.69%) > Mn (12.2%) > Cr (0%) = Pb (0%) = Cd (0%). All the metals except Pb, Cd and Cr have significant association with the residual fraction, which suggests that these metals are closely related to the crystalline structure of the minerals and are stable under natural conditions. Cu, Co, and Al in the study area seem to be closely bounded to the silicates as contribution of these metals in other fractions are very low.

Table 5.3 Trace metal concentrations (in mg kg^{-1}) in different fractions during SWM

Elements	F1			F2			F3			F4			F5		
	Min	Max	Mean	Min	Max	Mean	Min	Max	Mean	Min	Max	Mean	Min	Max	Mean
Co	0.70	149.00	92.49	95.30	167.30	128.12	34.30	73.70	54.96	42.60	101.10	76.47	456.30	1895.00	962.51
Cu	0.60	26.10	15.22	0.00	26.30	18.69	0.00	23.20	4.46	16.70	186.80	49.07	27.40	3645.00	946.51
Mn	3.00	309.90	80.16	0.30	178.40	20.69	0.00	216.60	27.07	0.00	58.00	7.84	0.00	114.00	34.83
Pb	BDL	11.40	3.56	BDL	BDL	BDL	BDL	BDL	BDL	BDL	BDL	BDL	BDL	BDL	BDL
Zn	1.30	49.50	17.52	2.00	14.80	4.78	3.50	84.00	20.21	3.80	45.70	14.90	7.90	135.50	74.14
Se	38.60	127.90	87.66	86.30	238.80	203.82	18.30	70.20	47.52	0.00	41.20	14.21	207.00	681.50	436.94
Fe	325.60	8102.00	2607.59	555.70	4616.00	925.76	2348.00	21230.00	9293.47	1046.00	15910.00	4865.00	21170.00	62160.00	35267.78
Al	BDL	1152.00	217.65	BDL	981.20	149.52	368.20	9026.00	2313.14	243.20	7802.00	1942.45	14125.00	224100.00	104369.86
Cd	0.43	0.84	0.68	0.32	0.75	0.44	BDL	0.60	0.14	BDL	BDL	BDL	BDL	BDL	BDL
Cr	BDL	BDL	BDL	BDL	BDL	BDL	16.80	152.20	91.59	BDL	BDL	BDL	BDL	362.50	12.76
Ba	BDL	2666.00	523.27	BDL	4119.00	379.68	BDL	423.20	138.43	BDL	260.40	55.84	325.00	3121.00	1178.56

Table 5.4 Trace metal concentrations (in mg kg^{-1}) in different fractions during NEM

Elements	F1			F2			F3			F4			F5		
	Min	Max	Mean	Min	Max	Mean	Min	Max	Mean	Min	Max	Mean	Min	Max	Mean
Co	127.40	173.00	147.39	145.70	164.30	155.66	55.50	76.70	66.49	97.60	118.30	108.29	856.20	2401.00	1500.26
Cu	BDL	4.30	0.32	19.90	59.50	34.03	BDL	4.60	0.13	2.30	63.50	29.05	85.20	854.60	287.71
Mn	2.10	238.70	72.08	1.50	83.80	22.61	BDL	164.10	33.79	0.00	52.10	12.20	0.00	69.00	19.54
Pb	BDL	2.70	0.08	BDL	BDL	BDL	BDL	BDL	BDL	BDL	BDL	BDL	BDL	BDL	BDL
Zn	1.10	31.90	9.52	2.40	22.50	7.26	BDL	70.30	25.84	8.50	23.90	15.31	20.00	111.50	67.29
Se	183.00	262.30	224.89	69.50	205.40	160.70	2.80	83.10	42.32	BDL	0.00	0.00	58.00	574.50	318.78
Fe	116.20	6586.00	768.30	637.30	1870.00	895.09	2060.00	20000.00	9059.31	1169.00	11380.00	4185.11	13160.00	42170.00	24021.67
Al	BDL	756.40	75.04	0.00	841.80	351.55	189.70	12635.00	3594.47	323.40	7656.00	1882.88	0.00	97450.00	21778.88
Cd	0.43	0.75	0.56	0.36	0.69	0.50	BDL	0.46	0.12	BDL	BDL	BDL	BDL	BDL	BDL
Cr	BDL	BDL	BDL	BDL	BDL	BDL	99.30	113.30	110.92	BDL	BDL	BDL	BDL	BDL	BDL
Ba	BDL	600.70	186.98	BDL	664.60	236.86	BDL	463.80	148.27	BDL	637.00	142.32	99.80	1568.00	766.03

5.3 Discussion

5.3.1 Seasonal and spatial distribution

5.3.1.1 Cobalt (Co)

The total concentration of Co shows a significant increase during the NEM compared to the SWM (Fig. 5.4) and the association of Co with residual fraction was noted highest during both seasons. This is mainly contributed by an increase in the concentration of Co in all the fractions during NEM as compared to SWM (Table 5.2). The percentage of Co associated with residual fraction stands highest at 73.22 and 75.84% during the SWM and NEM respectively, which indicates the association of Co with the crystal structure of the minerals and is mainly derived from geogenic source. The main medium of transportation for Co is through water run-off from the source area (Gleyzes et al., 2002; Yao et al., 2019). In the river basin, the highest average concentration of Co (102.64 mg kg^{-1}) has been observed in the shale and pyrite concretion found in Sibuti and Setap formation, followed by 23.4 mg kg^{-1} in Tukau formation (Nagarajan et al., 2017b). In the siliciclastic sediments of Sibuti and Lambir formations, 7.97 and 6.94 mg kg^{-1} of Co have been reported in rocks like arkose, lithrarenites, quartz arenites and wackes (Nagarajan et al., 2015; Nagarajan et al., 2017a). In the case of other fractions, the observed affinity of Co in descending order is: $Co_{carbonate}$ > $Co_{exchangeable}$ > $Co_{oxidizable}$ > $Co_{reducible}$ during both seasons (Table 5.3 and 5.4), from which oxidizable fraction and reducible fraction have an affinity with the metal which is not very significant but the increase in a concentration may be due to higher affinity of Co towards deposition under oxic condition than in sub-oxic conditions (Jones & Manning, 1994; Togunwa et al., 2017). A higher amount of diluent freshwater infusion into the estuary has been observed during the NEM, which leads to more precipitation (Yao et al., 2019) and deposition of Co containing minerals might lead to higher concentration in the residual fraction. Also, higher DO, higher pH and low salinity may influence Co concentration observed during the NEM compared to the SWM. The association of Co in the exchangeable fraction is higher during the NEM (7.45%), compared to the SWM (7.04%), whereas the percentage of Co association in carbonate and an oxidizable fraction (9.75 and 4.18%) are higher during the SWM, compared to the NEM (7.87 and 3.36%). This indicates the

conversion of mobile exchangeable Co to less mobile absorbed form (Rao et al., 2008; Yuan et al., 2004) during the cycle from NEM to SWM.

5.3.1.2 Copper (Cu)

Cu is one of the common metals present in the source rocks such as wacke, litharenite, arkose and ferruginous sandstone in the Sibuti Formation and Lambir formation (average concentration: 72.8 and 81.75 mg kg^{-1}), exposed in the river basin (Nagarajan et al., 2017a). Apart from that, the enrichment of Cu is also observed in terrigenous and lithic fragments particularly in clay minerals and phyllosilicates in SW part of Miri coastal region (217.5 mg kg^{-1}) and certainly much higher than continental crustal average values (UCC; McLennan, 2001; Nagarajan et al., 2019) and the source region of the Sibuti River basin. Previous study by Nagarajan et al. (2017b) revealed that the mean concentration of Cu in the Tukau Formation is around 41.32 mg kg^{-1}. Similarly, the concretion within shale beds in Sibuti and Setap formations have a mean concentration of the metal around 19.97 mg kg^{-1} (Azrul Nisyam et al., 2013). In addition, the coal layers within the source rocks exposed in the river basin are rich in chalcophile elements like Cu as well (Sia et al., 2012). In the estuary, Cu is in abundance during SWM as compared to the NEM (Fig. 5.4) where Cu concentrations during SWM and NEM are mainly associated with a residual fraction (91.54 and 81.91% respectively). Apart from that, SWM shares a higher proportion of Cu in exchangeable, reducible and oxidizable fractions, whereas carbonate fraction carries the majority of Cu during NEM. Lower sedimentation rate because of high flow rate during NEM might be the reason behind the decrease in concentration in the estuary (e.g. Samanta et al., 2017). However, higher pH observed during NEM might be giving rise to more Cu in the carbonate fraction. On the other hand, in the post-depositional period, intensifying coastal interference and acidification during SWM maybe removing Cu that consolidated with carbonates in the sediments (Drylie et al., 2019) as carbonates are not known to be the significant host of metals and act more as a diluent in acidifying conditions (Samanta et al., 2017; Cuong et al., 2006; Passos et al., 2010). The lack of higher association of Cu during NEM despite organic-rich freshwater infusion might be due to efficient bioturbation, mixing (Samanta et al., 2017; Banerjee et al., 2012) and high microbial activity, causing mineralization of organic matter thus giving rise to higher concentration of CO_2 in water (Canuel et al., 1993). In contrary, deposition of higher Cu containing sediments from the coastal end

with seawater seems to be a dominating process during the post-NEM period. The resuspension and stratification caused by this seawater intrusion might be causing a suboxic condition in the estuary and dissolution of Cu in carbonate fraction and reducible fraction during post-depositional suboxic diagenesis of sediments during the transition from NEM to SWM. This process is followed by re-precipitation in the zones where the mobilized Fe and Mn are fixed along with oxidizable fraction with decreasing microbial activity (Drylie et al., 2019) and exchangeable fractions (Samanta et al., 2017).

5.3.1.3 Manganese (Mn)

Manganese (Mn) is very commonly found in the form of oxides and hydroxides in the Earth's crust and an essential element for the biological system. The presence of the same forms of Mn has been noted in the sediments of the Sibuti river and majorly influenced by the Sibuti and Lambir formations and have an average concentration of 500 and 375 mg kg^{-1} (Nagarajan et al., 2015; Nagarajan et al., 2017a) respectively. Apart from that, Mn is reported in coastal sediments of SW part of the Miri coastal region (mean concentration: 26.6 mg kg^{-1}) (Nagarajan et al., 2019). Similarly, the Tukau Formation has recorded an average concentration of Mn around 94 mg kg^{-1} (Nagarajan et al., 2017b). Besides the above-mentioned sources, pyrite and other mineral concretions present within the shale beds of the Sibuti and Setap formations have the highest average concentration of Mn in the river basin (7700 mg kg^{-1}) (Azrul Nisyam et al., 2013), thus are expected to have maximum influence in riverine sediments. In the Sibuti estuarine sediments, Mn is recorded higher during SWM, compared to NEM (Fig. 5.4). Besides, the dominant fraction containing Mn is an exchangeable fraction contributing 46.99 and 44.99% of Mn during SWM and NEM respectively (Table 5.3 and 5.4), which indicates towards porewater induced ambient Mn concentration in the water table with saline water influenced stratification and suboxic condition in the estuary (Callaway et al., 1988; Turner et al., 2000) during both seasons and absorption of such on the surface of sediments with weak electrostatic bonds (Rao et al., 2008). More concentration in this fraction has been observed towards the upper part of the estuary (Fig. 5.1 and 5.2) and the reason behind this might be due to higher DO supporting the formation of a coating of Mn-hydroxides on sediments in the freshwater dominant region of the estuary (Duinker et al., 1979; Wollast et al., 1979; Reigner et al., 1993). In contrary, reducible fraction

shows a significant variation amongst all the fractions where Mn association with this fraction is increased from 15.87 to 21.09 % during the transition period from SWM to NEW, which might be due to the gradual transition of suboxic condition to the oxic condition observed during respective seasons while increasing the flocculation and precipitation of the metal in the sediments.

5.3.1.4 Lead (Pb)

Pb is usually found in the natural environment and is known for its toxicity in the aquatic environment. It is mostly immobile and tends to accumulate in sediments closest to point of its entry (Wuana et al., 2011; Dinsley et al., 2019) and is pH-dependent for sorption (Dinsley et al., 2019). The average concentrations of Pb in the Sibuti and Lambir formations and SW part of Miri coastal sediments are 47.6 mg kg^{-1} (Nagarajan et al., 2015), 18.23 mg kg^{-1} (Nagarajan et al., 2017a) and 7 mg kg^{-1} (Nagarajan et al., 2019) mg kg^{-1} respectively. In the concretion of shale and pyrite of Sibuti and Setap formation, the mean concentration is 12.38 mg/kg^{-1}, whereas Tukau formation in the source area has a higher average concentration of 60.7 mg/kg^{-1}. However, Pb concentrations in the study area are recorded to be relatively lower as compared to other metals and higher concentrations are observed in the majority of the stations during SWM (Fig. 5.4). In addition, Pb is only associated with an exchangeable fraction of the sediments during both seasons (Fig. 5.1 and 5.2). This association indicates towards the input of Pb from non-point sources of the study area, which includes the use of sulfate-based fertilizers in the agricultural fields around the river basin (Atafar et al., 2010; Ab Manan et al., 2018). The geogenic sources such as lignite beds in the river basin that are rich in Pb (Sia et al., 2012) and oxidation of shale and pyrite concretion (Anandkumar, 2016; Nagarajan et al., 2019) might be responsible for the presence of Pb in an exchangeable fraction of sediments.

5.3.1.5 Zinc (Zn)

Zn is the 23rd most abundant metal found in the Earth's crust and occurs naturally in sediments of the aquatic environment through weathering of Zn-bearing rocks. In the Sibuti river basin, the presence of Zn has been observed in clastic sediments of the Sibuti and Lambir formations with respective mean concentrations of 116.54 and 60.88 mg kg^{-1} respectively (Nagarajan et al., 2015; Nagarajan et al., 2017a). The recorded concentration is higher than PAAS (McLennan, 2001) in wackes, quartz

arenites, arkose and lanthanites of the Sibuti formation (Nagarajan et al., 2015). In SW part Miri coastal sediments, a higher presence of Zn was found in association with clay minerals and phyllosilicates and was enriched higher as compared to PAAS values (PAAS; McLennan, 2001; Nagarajan et al., 2019). In addition, the pyrite concretion within shale beds recorded a mean concentration of 66.35 mg kg^{-1} of Zn, whereas sediments of the Tukau Formation have an average concentration of 60.56 mg/kg^{-1} Zn (Nagarajan et al., 2017b). The variation of Zn is not significantly varying between SWM and NEM. However, a higher concentration of Zn is recorded during SWM (Fig. 5.4). Zn in the sediments of the Sibuti river estuary is mainly associated with the residual fraction followed by the reducible fraction in both seasons (Fig. 5.1 and 5.2). The percentage of Zn association in residual fraction during SWM and NEM is 56.36 and 53.74% respectively. In a reducible fraction, Zn seems to have a stable bond with Fe or Mn oxide coating and might be the carrier of Zn from the fluvial environment to the estuary (Li et al., 2000). This association with reducible fraction significantly decreases in the post-depositional period of NEM and shares a reduced percentage of 15.87% in SWM as compared to 20.63% during NEM. The Zn absorption onto Fe-Mn oxides is more stable than the carbonates (Fernandes et al., 1997; Ma et al., 1997; Li et al., 2000). Likewise, oxidizable fraction also represents a higher percentage of Zn, which is 12.23% during NEM and 11.33% during SWM (Fig. 5.1 and 5.2). On contrary, the exchangeable fraction has a significantly higher concentration of Zn during SWM (13.32%) than NEM (7.6%). This difference indicates the dissolution of Zn from both reducible and oxidizable fraction during post-depositional diagenesis due to the reduction of oxygenated condition with the saline water's influence in the transition towards SWM. The reduction in DO is inducing the breakdown of polymeric materials complexes of Zn and dissolution of Zn from Fe-Mn complexes due to stratification of water at the bottom (Mohan et al., 2012), which eventually is recycled in an exchangeable fraction of the sediments.

5.3.1.6 Selenium (Se)

Se is not considered to be one of the dominant metals in the earth's crust and is expected to be from anthropogenic sources in case of increased concentration. Irrigated river basins due to extensive agricultural activities containing marine shales are known to be the major source of selenate leached out of either from these agricultural fields or shale formations under alkaline or oxidizing conditions (May et

al., 2008) where these eventually settle in sediments in the form of insoluble selenide under salinity conditions in the aquatic system (Oremland et al., 1989; Peters et al., 1997). Such conditions prevail in the considered study area where major influencing formations like Sibuti and Lambir contain marine shales (Nagarajan et al., 2015; Nagarajan et al., 2017a). In addition, coal beds around the world and pyrites are one of the major sources of Se worldwide (Kieliszek et al., 2019; Bullock et al., 2018). The Se concentration has not been evaluated in any previous studies for the lithology exposed in the study area. Nonpoint sources like excessive fertilization in the agricultural area of the river can give rise to contamination Se in the river estuary (Kieliszek et al., 2019). Apart from this, the presence of lignite, and peat soil (Williams et al., 1934; Yudovich et al., 2006) is one of the major sources of Se in the Malaysian river, including Sarawak (Chang et al., 2020). The presence of these peat soil and lignite-bearing rocks are found in various formations such as Belait, Miri, Tukau, Lambir, Nyalau, Setap and Tangap (Fig. 1.6; Table 1.2). Se contents in coal-based oscillates were recorded at 6-8.4 g kg^{-1} in the Hubei province of China (Kieliszek et al., 2019) whereas 226 mg kg^{-1} of Se was noted in a Carboniferous coal bed in East Ayrshire, UK (Bullock et al., 2018). The Se concentration is higher in SWM as compared to NEM (Fig. 5.4). The majority of the Se during both seasons is associated with a residual fraction at 55.3% and 42.69% during SWM and NEM respectively (Fig. 5.1 and 5.2), indicating the source to be mainly geogenic. A significant concentration of Se in SWM and NEM is associated with an exchangeable fraction (11.09 and 30.12%), followed by carbonate fraction (25.8 and 21.58%) (Fig 5.1 and 5.2). Accumulation of Se in exchangeable fraction might be originating from the agricultural fields and mainly dependent on salinity and DO condition of estuarine water. Under salinity and anoxic conditions, these Se form selenide salts, which are insoluble and have higher tendency to get adsorbed in exchangeable fraction of sediments (Peters et al., 1997). In moderately reduced sediments and pH values between 4 and 7.5, adsorption mechanisms dominate Se behavior in the estuary (Peters et al., 1997), which might be the reason behind its significant association with carbonate fraction during both seasons and an increase in concentration during the post-monsoonal period in the same fraction.

5.3.1.7 Iron (Fe)

Fe is the most dominant metal found in sediments during NEM, whereas the concentration is 2nd dominant next to Al during SWM despite its higher concentration during SWM overall (Fig. 5.4). The presence of Fe in the estuary might have been derived from the geogenic sources through chemical and mechanical weathering. The majority of Fe concentration in estuarine sediments is in residual fraction (SWM; 66.59%; NEM; 61.67%), indicating its geogenic origin and immobile nature. This presence might be contributed by the presence of Fe in formations like Sibuti and Lambir in sandstones containing minerals like pyrite, ankerite and ferruginous sandstones rich in magnetite (Nagarajan et. 2017a; Nagarajan et al., 2015). Nagarajan et al. (2017a) also reported significant Fe leaching from the pore edges of the source rocks and coating of ferruginous sandstone grains with Fe-oxide. This might be the reason behind its significant presence in reducible fraction (SWM; 17.55%; NEM; 23.27%) and an oxidizable fraction (SWM; 9.19; NEM; 10.75%) (Fig. 5.1 and 5.2). The majority leached Fe due to chemical weathering might associate themselves with the dissolved organic matter in river water due to higher freshwater input during the NEM. This association is eventually decreasing in the transition towards SWM with increasing saline water domination in the estuary due to low flow of the river during the SWM, thus limiting the reach of organic matter in the estuary (Turner et al., 2008). An increase in Fe concentration in all the fractions during SWM indicates towards the seawater induced flocculation (Jilbert et al., 2016; Mayer et al., 1982). The precipitation of magnetite and goethite was noted before in saturation index in water samples (Fig. 4.27), which mainly happens because seawater cations neutralize the negatively charged iron-bearing colloids, and allowing flocculation (Boyle et al., 1977; Mayer et al., 1982; Hopwood et al., 2015).

5.3.1.8 Aluminum (Al)

Al is the most dominant metal during SWM and 2nd dominant element next to Fe during NEM (Table 5.1 and 5.2) (Fig. 5.4). The majority of Al is associated with residual fraction during both seasons, which is 95.76 and 78.67% during SWM and NEM respectively. Al-oxides have 2nd most dominant presence in Sibuti and Lambir formations and are found to be associated with clay minerals and phyllosilicates (Nagarajan et al., 2015; Nagarajan et al., 2017a). Other formations like the Tukau

formation (Nagarajan et al., 2017b) and concretion in Setap and Sibuti formations have reported the presence of Al oxides as well. The higher presence of Al in the residual fraction indicates its low solubility nature in the estuary and is mostly derived from the weathering in the source area (Hydes et al., 1977). In such a case, the lower sedimentation and higher erosion of Al bearing sediments are common phenomena during low tidal resistance and high flow of the river (Ferreira et al., 2018). This might be the condition in the estuary as the low tidal influence was observed during NEM as compared to SWM, leading to the removal of Al bearing clays from surface sediments. On the other hand, saline water influences during SWM due to high tide conditions causing more deposition and flocculation (Jilbert et al., 2016; Mayer et al., 1982) of such sediments lead to an increase in the concentration of Al. The 2nd most significant association of Al is noted with reducible fraction during the NEM, however, such association in the SWM is comparatively lesser. Al has amphoteric properties and depending on varying pH, it can produce varieties of species (Namieśnik et al., 2010). The pH of water varies from 4.6 to 7.6 and higher pH is observed in the upper part irrespective of the seasons (Fig. 4.2) with average pH being higher during NEM. In such acidic water condition, insoluble $Al(OH)_3$ is the dominant form (Driscoll et al., 1990; Habs et al., 1997) and becomes slightly soluble at pH 6.2 and produces series of intermediate forms such as $[Al(OH)_2(H_2O)_4]^+$ and $[Al(OH)(H_2O)_5]^{2+}$ (Namieśnik et al., 2010). Thus, higher oxygenated conditions in the upper part due to freshwater influence supporting the oxidization of Fe and Mn and leading to absorption of such forms of Al mentioned above are co-precipitating in the sediments (Walker et al., 2005; Namieśnik et al., 2010). In addition to that, higher turbidity, TSS (Fig. 4.4) and elevated concentration of Al in suspended solids (discussed in chapter-6) were also observed during NEM. So, the resuspension of clay minerals due to turbidity might be the reason behind the decrease in concentration of Al from station 12 to 36 (Fig. 5.3). In the lower part, the pH drop was observed during both seasons leading to domination of insoluble $Al(OH)_3$ while association of Al was not observed with any other fraction (Namieśnik et al., 2010) and its association with oxygenated conditions was observed (Fig. 5.1 and 5.2).

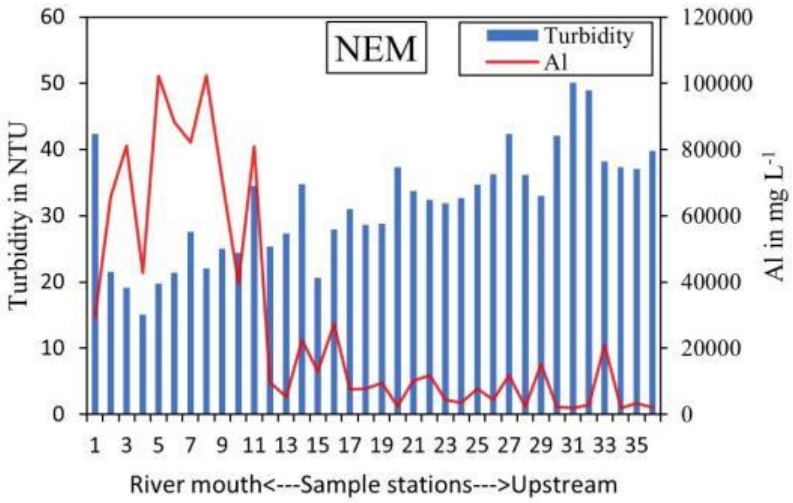

Fig. 5.3 Variation in concentration of Al with respect to Turbidity during NEM

5.3.1.9 Cadmium (Cd)

The presence of Cd rocks like phosphate rocks has not been noted in any previous studies, but the use of imported phosphate rocks for maximum yield through application of P-fertilizers is a common practice in Sarawak's peat soil for palm oil growth over the years where these fertilizers are identified as the major source of Cd in the SPM (Zaharah et al., 2014; De Boo et al., 1990). The nature of the Sibuti river basin is soil weathering prone and extensively agricultural in nature, which might be the reason behind the leaching of Cd into the river system through run-off and eventually reaching the estuary. Apart from that, leaching of Cd from shale and pyrite concretion in the SW part of Miri coastal water has been reported in a study by Anandkumar (2016). The leaching from these concretions present in Sibuti and Setap formations might be the source of Cd in estuarine sediments. The deviation of Cd concentration in the sediments is not significant during SWM and NEM. However, NEM shows a higher concentration of Cd in sediments and most of the Cd concentration is associated with exchangeable, carbonate and reducible fraction in the study area. The highest association (53.67 and 47.65% during SWM and NEM respectively) with an exchangeable fraction indicates the highly mobile nature of the metal and retention which is possible with weak electrostatic interactions (Rao et al., 2008). Association of Cd with carbonate fraction is significant and stands at 42.27% during the NEM indicating that carbonate minerals are the main carrier of Cd during the NEM, whereas higher dissolution of carbonate minerals is observed during the SWM, which reduces the Cd concentration in the fraction to 36.98%, and is further

confirmed based on the saturation index (Fig. 4.24). In the case of reducible fraction, 11.35% of Cd is associated with this fraction during SWM and 10.08% during NEM. This indicates the formation of a stable bond with Fe-Mn oxides in the post-depositional period in the estuary (Turner et al., 2008). Cd has a low affinity for organic ligands but a high affinity for the chloride ion (Tipping et al., 1998; Turner et al., 2008), which might be the reason behind its absence in oxidizable fraction.

5.3.1.10 Chromium (Cr)

The total concentration of Cr is higher in the sediments during NEM as compared to SWM (Table 5.1). The concentration of Cr is mainly associated with the reducible fraction of sediments in the estuary (SWM: 87.77%; NEM: 100%). The chromium in the Sibuti Formation exposed in the river basin and NW Borneo is mainly associated and controlled by the presence of chromite (Nagarajan et al., 2014; Nagarajan et al., 2017a). The average concentrations of Cr in the Sibuti and Lambir siliciclastic sediments were reported to be 53.33 and 51.5 mg kg^{-1} respectively (Nagarajan et al., 2017a). In addition, the pyrite concretion in the shales of the Sibuti and Setap formations recorded an average concentration of 110.76 mg kg^{-1} of Cr in them. The association of this metal with reducible fraction indicates that Fe oxides are the major carriers of Cr in the river from the source area and share a stable bond between themselves.

5.3.1.11 Barium (Ba)

The presence of Ba has been reported in the river basin, especially in arkoses, quartz arenites, wackes and lithrarenites in association with the clay minerals (Nagarajan et al., 2015; Nagarajan et al., 2017a). The respective mean concentrations in these formations are reported to be 774.1 and 140.25 mg kg^{-1} respectively. Additionally, the average concentration of Ba is reported in pyrite concretion in shale of Sibuti and Setap formations as 390.96 mg kg^{-1}. Ba shows an increase in concentration during the SWM than the NEM (Fig. 5.4). The majority of Ba is associated with a residual fraction (SWM: 51.79%; NEM: 51.74%) (Fig 5.1 and 5.2), which indicates the geogenic origin of the metal from the source region and is incorporated into the crystal structures of primary and secondary minerals (Zimmerman et al., 2010). Apart from that, the majority of Ba shows a significant affinity towards all other fractions during NEM, whereas Ba during SWM has a significant association with exchangeable and

carbonate fractions. A significant increase in percentage share in exchangeable fraction has been noticed during NEM (Fig. 5.1 and 5.2). The association of Ba in the exchangeable fraction is increased to 22.99% during NEM compared to SWM (12.63%). On contrary, the Ba concentration in the reducible and oxidizable fraction during NEM is higher than SWM, which might be the result of higher leaching from the pyrite concretion and shale, supported by high rainfall and absorption by Mn and Fe oxides (Namieśnik et al., 2010). Additionally, increasing salinity influence might be helping organic bound Ba to release and is resettling due to the ion exchange process under saline condition (Liguori et al., 2016; Coffey et. a. 1997; Yao et al., 2019) as an increase in exchangeable fraction has been noticed towards the lower part of the estuary (Fig. 5.1). The carbonate fraction bound Ba is significant during both seasons without much variation in their association, indicating that the carbonate minerals are the major carrier of Ba (Liguori et al., 2016). However, carbonate fraction-bound Ba is concentrated in the upper part during SWM (Fig. 5.1). The reducing condition (Fig. 4.2) and higher dissolution of carbonate minerals are observed (Fig. 4.24) in the estuary during SWM, where the associated Ba was released into the water in the lower part of the estuary. However, comparatively lower dissolution of such minerals was observed during NEM, which might be leading to precipitation of barium sulfate under higher salinity, turbidity (Gad et al., 2014) and organic respiration (Marchitto et al., 2013) in the lower part of the estuary. This might be the reason behind the well-spread association of Ba with carbonate fraction (Fig. 5.2) during NEM.

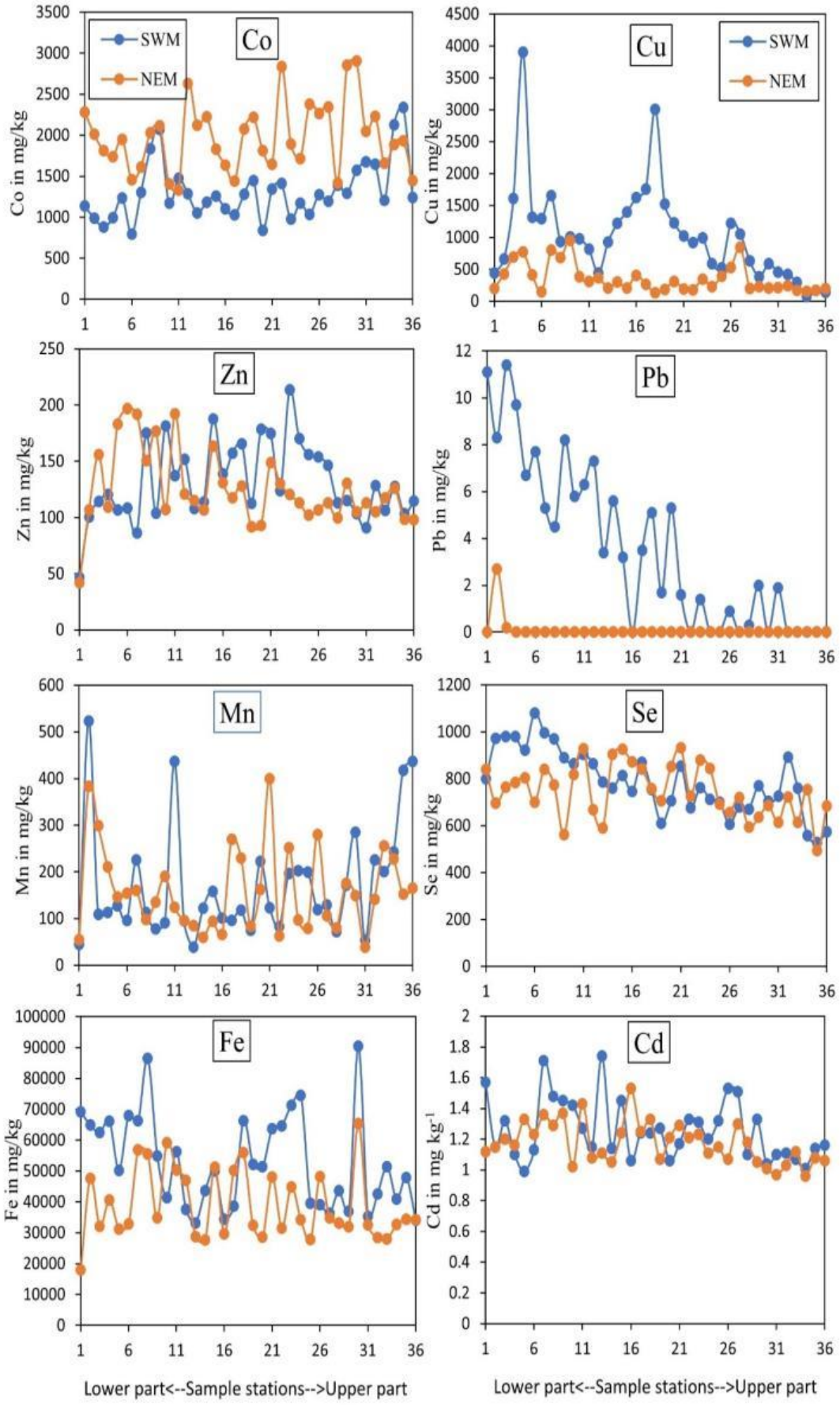
Co
SWM
NEM
Co in mg/kg
Cu
Cu in mg/kg
Zn
Zn in mg/kg
Pb
Pb in mg/kg
Mn
Mn in mg/kg
Se
Se in mg/kg
Fe
Fe in mg/kg
Cd
Cd in mg kg-1
Lower part<--Sample stations-->Upper part
Lower part<--Sample stations-->Upper part

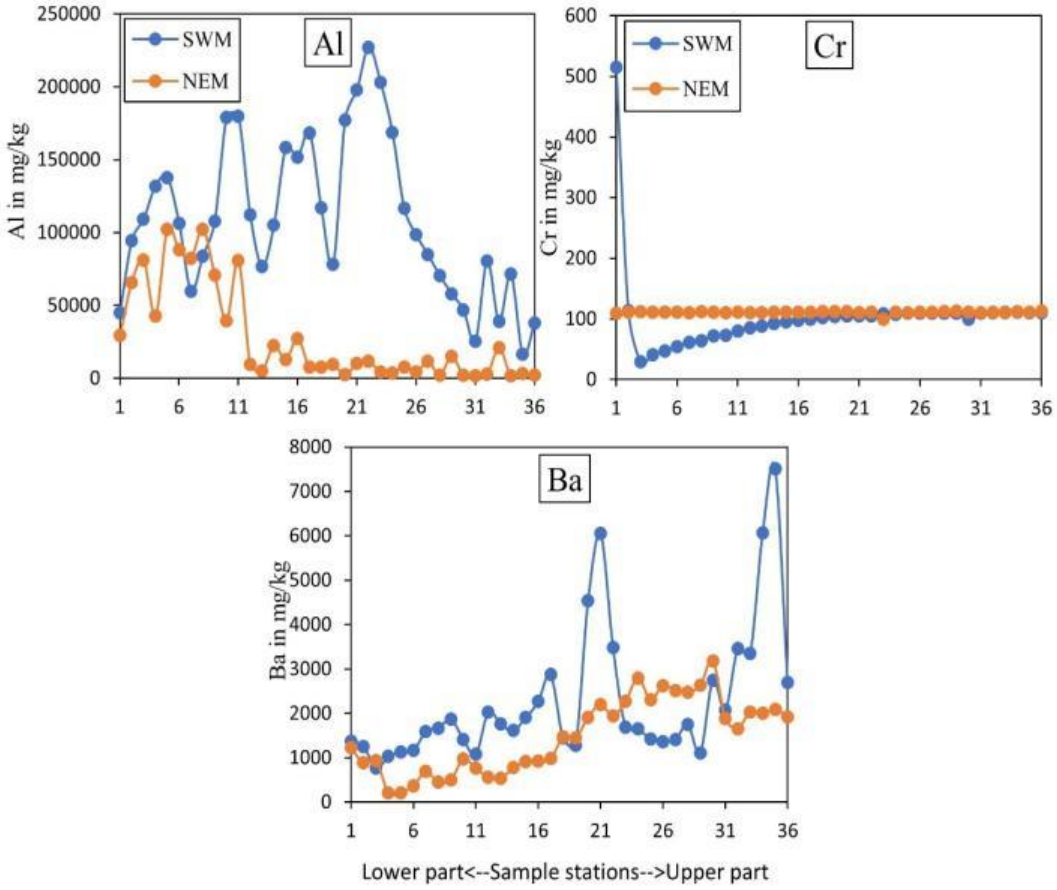

Fig. 5.4 Variation and distribution of trace metals in sediments during SWM and NEM

5.3.2 Statistical analysis

5.3.2.1 Inter-elemental relationships (Correlation Matrix)

Metals are vital in geochemical studies because of their genetic implications on the expected target mineralization and correlation of these metals helps to reveal the source and the process behind the transportation of such metals into an aquatic environment like estuaries (Li et al., 2012; Martin et al., 2012). In the current study, Pearson's correlation has been utilized to determine the inter-elemental relationship between various metals and their outcome for the SWM and NEM seasons is shown in Table 5.5 and 5.6 respectively.

5.3.2.1.1 South-West monsoon (SWM)

During SWM, Co and Ba share a significant correlation (r=0.525) between themselves, whereas Ba shows a weak negative correlation with Pb (r=-0.439) and Se (r=-0.445). Chalcophile element like Zn shares a significant correlation (r=0.676) with Al during SWM. In addition, Cu exhibits a weak correlation with Pb (r=0.413),

whereas the correlation between Se and Pb is strong (r=0.713). Metals like Pb and Se both show significant correlation with parameters like salinity (Pb: r=0.765 and Se: r=0.664), TSS (Pb: r= 0.681 and Se: 0.623) and turbidity (Pb: r= 0.620 and Se: 0.629) along with a weak negative correlation with pH (Pb: r=-0.416 and Se: -0.426) and DO (Pb: r=-0.566 and Se: -0.424). Apart from that, Cr shows a positive correlation with pH (r=0.531) and does not show any correlation with other metals or parameters.

The correlation of Ba and Co observed might be derived from the chlorites present in calcareous sandstones present in Sibuti Formation. The high correlation of chalcophile elements such as Se and Pb indicates the leaching of these metals from pyrites (Nagarajan et al., 2017a), lignite beds and peat soil as they are rich in chalcophile elements such as Pb, Cu and Se (Chang et al., 2020; Sia et al., 2012). The high positive correlation of salinity, turbidity and TSS with Pb and Se was also observed. These parameters (salinity, turbidity and TSS) are recorded high in lower part of the estuary due to seawater influence and gradually decreased in the upstream direction as discussed previously in water chapter (Fig. 4.3 and 4.4). So, this correlation mainly indicates towards the adsorption of Pb and Se on suspended solids in seawater induced turbidity zone of the estuary and eventually depositing as sediments.

The strong association of elements Zn with Al is mainly due to the clay minerals and phyllosilicates (Nagarajan et al., 2017a) and might be detrital in origin (Prabakaran et al., 2020) and derived from illite, kaolinite (Condie et al., 2001), pyrite of Sibuti formation (Nagarajan et al., 2017a). On the other hand, a moderate negative correlation of Co and Ba with Cu, Pb and Se might be due to the difference in origin and controlling factors. However, a moderate negative correlation of Co with Al indicates its association towards non-aluminous silicate minerals (Rahman et al., 2007; Nagarajan et al., 2015). The dissociation of Cr with any other element indicates towards its origin from chromite present in NW Borneo and Sibuti formation in the river basin (Nagarajan et al., 2014; Nagarajan et al., 2017a) while the strong association with pH indicates the deposition with Fe or Mn that precipitates under low acidic conditions (Bewers & Yeats, 1978; Campbell et al., 1984).

5.3.2.1.2 North-East monsoon (NEM)

During NEM, significant correlation of Al has been observed between Cu (r= 0.524), Zn (r= 0.683), and Cd (r= 0.501). In addition, Al shares high negative correlation with

pH (r=-0.628) and turbidity (r=-0.612). Apart from that, Cd shares a significant correlation with Zn (r= 0.592) and moderate correlation with Se (r= 0.402) and Cu (r= 0.403) and negative correlation with turbidity (r=-0.404). Meanwhile, Ba shares high negative correlation with Al ($r_=$ -0.687) and moderate negative correlation with Zn (r= -0.451). On the other hand, Pb shares significant positive correlation with salinity (r= 0.883) and DO (r= 0.501) and negative correlation with pH (r= -0.503).

The significant correlation of Al with chalcophile elements like Cu, Cd and Zn indicates that their distribution is associated with detrital clay minerals from the source area as the majority of Al oxides are mainly controlled by clay minerals. The significant correlation of Al, Cu and Zn with Cd during NEM might be due to the absorption of Cd by higher reactive carbonate clay minerals such as illite and kaolinite under higher salinity in the mixing zones of the estuary (Hao et al., 2020, Jian et al., 2014; Namiesnik et al., 2010). The high negative correlation of these elements with pH and turbidity indicates different controlling distribution factors such as the velocity of water and deposition in low turbid and low pH zones such as the lower part of the estuary. The moderate correlation of Se and Cd indicates a mixed source such as leaching from the shale and pyrite concretion (Anandkumar, 2016) and agricultural inputs because of higher run-off during NEM. The presence of chalcophile elements (Cu, Zn, Se) in lignite and peat soil in the study area (Chang et al., 2020; Sia et al., 2012) and the use of phosphate-based fertilizers (Zaharah et al., 2014; De Boo et al., 1990) in agricultural fields are acting as leaching source of these metals. The high negative correlation of Ba with Al might be due to its non-association with feldspar and clay mineral association in the source region (Nagarajan et al., 2015; Nagarajan et al., 2007a). On the other hand, a negative correlation of Ba with Cu, Zn, Cd and Co with Se and Cd are mainly due to the variation in the origin of the metals.

Table. 5.5 Correlation Matrix of Metals in Sediments during SWM

Parameters	pH	DO	Salinity	TSS	Turbidity	Co	Cu	Mn	Pb	Zn	Se	Fe	Al	Cd	Cr	Ba
pH	1.000															
DO	0.186	1.000														
Salinity	-0.343	-0.573	1.000													
TSS	-0.121	-0.472	0.627	1.000												
Turbidity	-0.165	-0.399	0.643	0.699	1.000											
Co	0.317	0.123	-0.261	-0.165	-0.034	1.000										
Cu	-0.384	-0.212	0.353	0.248	0.359	-0.374	1.000									
Mn	0.033	-0.062	-0.187	-0.030	-0.199	0.175	-0.331	1.000								
Pb	-0.416	-0.566	0.765	0.681	0.620	-0.312	0.413	-0.148	1.000							
Zn	-0.001	0.183	-0.078	-0.407	-0.362	-0.182	0.171	-0.050	-0.250	1.000						
Se	-0.426	-0.424	0.664	0.623	0.629	-0.347	0.380	-0.130	0.713	-0.048	1.000					
Fe	-0.079	-0.296	0.320	0.270	0.162	-0.010	0.221	0.100	0.281	0.025	0.371	1.000				
Al	-0.108	-0.068	0.217	0.006	-0.002	-0.381	0.340	-0.156	0.094	0.676	0.228	0.156	1.000			
Cd	0.064	-0.081	0.232	0.106	0.362	-0.077	0.065	-0.269	0.176	0.003	0.141	0.027	-0.020	1.000		
Cr	0.531	-0.099	0.088	0.149	-0.055	-0.021	-0.281	-0.089	0.122	-0.353	-0.212	0.078	-0.230	0.214	1.000	
Ba	0.298	0.168	-0.363	-0.349	-0.330	0.525	-0.347	0.282	-0.439	0.070	-0.445	-0.092	-0.053	-0.356	0.032	1.000

**Blue cells: Positive correlation; Grey cells: Negative correlation*

Table. 5.6 Correlation Matrix of Metals in Sediments during NEM

Parameters	pH	DO	Salinity	TSS	Turbidity	Co	Cu	Mn	Pb	Zn	Se	Fe	Al	Cd	Cr	Ba
pH	1.000															
DO	-0.213	1.000														
Salinity	-0.752	0.537	1.000													
TSS	0.037	0.296	0.278	1.000												
Turbidity	0.555	0.087	-0.158	0.242	1.000											
Co	0.110	0.050	0.017	-0.169	0.223	1.000										
Cu	-0.474	0.096	0.141	-0.155	-0.379	-0.006	1.000									
Mn	-0.077	0.047	-0.007	0.117	-0.219	-0.258	0.079	1.000								
Pb	-0.503	0.501	0.883	0.278	0.202	0.127	-0.114	-0.169	1.000							
Zn	-0.194	-0.279	-0.186	-0.107	-0.498	-0.282	0.313	0.117	-0.435	1.000						
Se	-0.250	-0.226	0.156	-0.177	-0.200	-0.324	0.012	0.106	0.137	0.208	1.000					
Fe	0.007	-0.220	-0.178	-0.298	-0.276	-0.096	0.173	0.355	-0.308	0.305	0.237	1.000				
Al	-0.628	0.061	0.398	0.028	-0.612	-0.272	0.524	0.095	0.023	0.683	0.177	0.165	1.000			
Cd	-0.281	-0.074	0.046	-0.159	-0.404	-0.334	0.403	0.026	-0.074	0.592	0.402	0.159	0.501	1.000		
Cr	0.056	-0.008	-0.041	-0.051	-0.016	0.022	0.015	-0.144	-0.096	0.056	-0.252	-0.113	0.120	-0.059	1.000	
Ba	0.544	-0.009	-0.375	0.056	0.684	0.304	-0.339	0.074	-0.061	-0.451	-0.224	-0.054	-0.687	-0.389	-0.098	1.000

**Blue cells: Positive correlation; Grey cells: Negative correlation*

5.3.2.2 Factor analysis of metals in sediments

Factor analysis was conducted with SPSS software using PCA (Principal component analysis) extraction and varimax rotation for both TTM (Total Trace Metals) and fraction-wise metals concentrations. The rotated component matrix of TTMs during SWM and NEM are presented in Table 5.7 and 5.8 respectively. The total variance of 72.66 and 72.87% for SWM and NEM respectively are explained. Furthermore, fraction-wise PCA is shown in Table 5.9 and 5.10, which represents the total variance of 83.76 and 82.32% during SWM and NEM respectively.

5.3.2.2.1 South-West monsoon (SWM)

Factor-1 represents 27.02% of the total variance and is explained by the significant positive loadings of Pb, Se, Fe, salinity, TSS and turbidity and a significant negative loading of DO. These elements are mainly associated with Fe-oxy-hydroxides and their concentrations are influenced by the salinity and DO. This indicates a common origin of these metals, which is leached from various geogenic sources like pyrites and lignite beds present in the Sibuti formation (Nagarajan et al., 2017a) and peat soil exposed within the river basin area as these elements are rich in Fe, Pb, Cu (Sia et al., 2012) and Se (Chang et al., 2020; Williams et al., 1934; Yudovich et al., 2006) (Fig. 5.5). Factor-2 has significant loading of Al and Zn with a variance of 12.411% during SWM. This association indicates that these elements are mainly associated with clay minerals like illite, chlorite and kaolinite in the estuarine sediments.

Factor-3 has a high loading of pH and Cr with the explained variance of 12.411% during this season. In a pH range of 5-7, Cr (III) prevails and easily associates with reducible organic matter (Pettine et al., 1990; Namieśnik et al., 2010). The dominant species of Cr (III) in the pH range of 4.5 to 7.5 are $Cr(OH)^{2+}$, $Cr(OH)_2^{+}$ which are susceptible to bioaccumulation through suspended solids and eventually depositing in sediments (Namieśnik et al., 2010). This association indicates leaching of Cr from mixed sources like pyrite and shale concretion in Sibuti formation and siliciclastic sediments of Sibuti and Lambir formation (Nagarajan et al., 2017a) rather than chromites present in NW Borneo and Sibuti formation in the river basin (Nagarajan et al., 2014). Chromites are predominantly acid-resistant in nature and do not leach Cr under the prevailing pH condition of the estuary (Weng et al., 1994; Weng et al., 2001).

Table 5.7 Rotated Component Matrix of Metals in Sediments during SWM

Parameters	Communalities	Component				
		1	2	3	4	5
pH	0.766	-0.234	0.040	0.754	0.357	0.120
DO	0.564	-0.732	0.000	-0.067	0.069	0.136
Salinity	0.760	0.822	0.086	-0.071	-0.171	0.205
TSS	0.729	0.809	-0.232	0.014	-0.109	0.098
Turbidity	0.846	0.725	-0.222	-0.217	0.115	0.460
Co	0.874	-0.119	-0.251	0.038	0.891	-0.032
Cu	0.554	0.335	0.316	-0.438	-0.261	0.287
Mn	0.614	0.035	-0.108	0.045	0.182	-0.752
Pb	0.809	0.816	-0.103	-0.116	-0.319	0.129
Zn	0.857	-0.267	0.876	-0.134	-0.016	0.026
Se	0.749	0.752	0.085	-0.334	-0.218	0.129
Fe	0.501	0.570	0.323	0.141	0.114	-0.195
Al	0.807	0.128	0.868	-0.101	-0.152	0.059
Cd	0.600	0.141	-0.016	0.199	-0.028	0.734
Cr	0.898	0.116	-0.215	0.900	-0.138	0.094
Ba	0.695	-0.265	0.099	0.140	0.673	-0.378
Percentage of Variance Explained		27.015	12.411	11.648	10.881	10.695
Total Variance Explained		72.651%				
Eigen Value		Greater than 1				

**Blue cells: Positive factor loading; Grey cells: Negative factor loading*

Factor-4 has significant loading of Co and Ba with a variance of 11.648%. Independent loading of Co and Ba and dissociation of these 2 elements from any other elements indicate its mixed origin like non-aluminous silicate minerals where both metals are not associated with Al oxides in the sediments of Sibuti formation (Nagarajan et al., 2019; Nagarajan et al., 2017a). In addition, carbonate (calcite, dolomite, and magnesite) or Fe oxide minerals such as goethite and pyrite might be a source as well (Dehaine et al., 2021). These minerals are abundant in shale and pyrite concretion of Sibuti and Setap formation.

Factor-5 has a higher loading of Cd with high negative loading of Mn with a variance of 10.695%. This might be due to the variation in the origin of both metals, where Cd is a major input from agricultural fields and Mn presence is mainly from geogenic sources in the study area (Fig. 5.5). Moderate loading of turbidity in this component indicates the desorption of Mn hydroxide bound Cd in high turbid conditions.

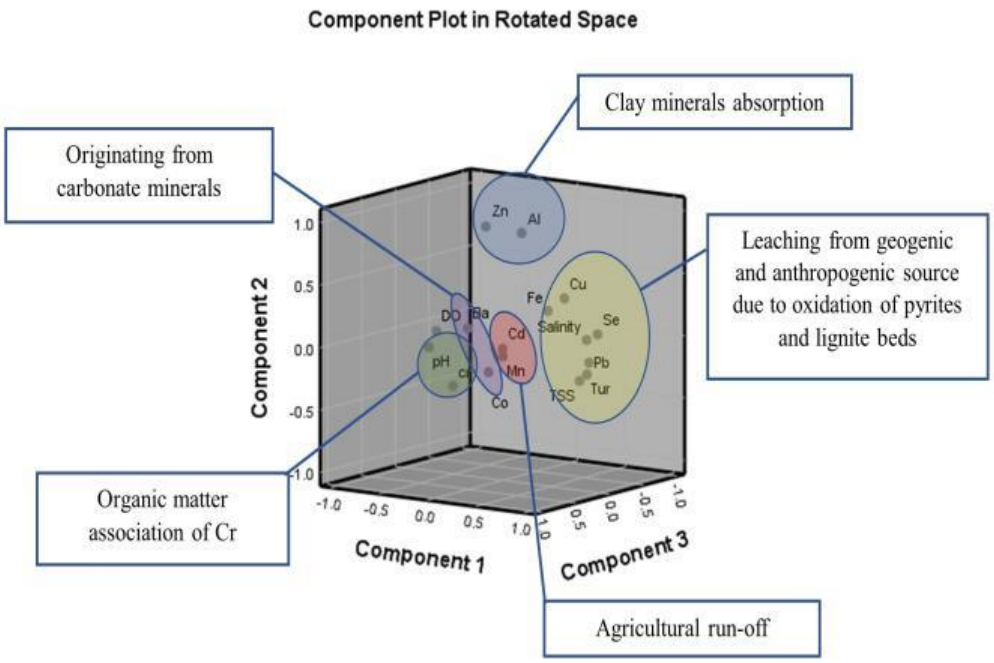

Fig. 5.5 Dominancy of principal components and associated sources in estuary during SWM

5.3.2.2.2 North-East monsoon (NEM)

Factor-1 has higher loading of Cu, Zn, Al, Cd and high negative loading of Ba, turbidity, and pH with 26.012% of the total variance. The chalcophile elements (Cu, Cd and Zn) are derived from pyrite and shale concretion and distribution is mainly controlled by clay minerals and phyllosilicates such as illite and kaolinite (Nagarajan et al., 2017a). The higher loading of Cd might be due to the absorption onto the clay minerals in the mixing zones of the estuary (Hao et al., 2020, Jian et al., 2014; Namiesnik et al., 2010) (Fig. 5.6). On the other hand, negative loading of Ba, turbidity and pH indicate absorption. The association of Ba with clay minerals is well observed in arkoses in Sibuti and Lambir formation (Nagarajan et al., 2015. Nagarajan et al., 2017a) which supports the association of Ba with clay mineral controlled factor (Factor-1). On the other hand, the presence of Ba in Sibuti and Tukau formation validates the leaching of this metal with chalcophile metals like Cu, Zn and Cd. These leached Ba in aquatic environment commonly precipitate as $BaSO_4$ or $BaCO_3$, where $BaSO_4$ precipitation is mainly associated with seawater introduction because of higher SO_4 content (Gad et al., 2014) and respiration of organic matter which is associated with acidic water (Marchitto et. al. 2013). But the formation of both precipitates is supported by absorption and by suspended solids and sedimentation (Gab et al., 2014).

$BaCO_3$ on the other hand, prevails under higher pH and relatively alkaline conditions (Gab et al., 2014).

Table 5.8 Rotated Component Matrix of Metals in Sediments during NEM

Parameters	Communalities	Components				
		1	2	3	4	5
pH	0.851	-0.631	-0.639	0.149	-0.047	0.142
DO	0.615	-0.058	0.687	0.318	0.118	0.156
Salinity	0.952	0.246	0.935	-0.099	-0.071	0.050
TSS	0.743	-0.166	0.329	0.225	0.028	0.746
Turbidity	0.684	-0.788	0.012	0.060	-0.214	0.121
Co	0.711	-0.324	0.152	0.314	-0.111	-0.687
Cu	0.581	0.619	0.115	0.203	0.231	-0.301
Mn	0.796	0.052	0.001	-0.017	0.852	0.258
Pb	0.927	-0.129	0.902	-0.203	-0.232	0.029
Zn	0.752	0.742	-0.413	-0.061	0.080	0.146
Se	0.804	0.224	0.015	-0.867	0.020	0.039
Fe	0.636	0.205	-0.278	-0.223	0.631	-0.263
Al	0.843	0.894	0.164	0.045	0.050	0.113
Cd	0.570	0.648	-0.128	-0.352	-0.042	0.093
Cr	0.481	0.192	-0.152	0.537	-0.362	0.040
Ba	0.713	-0.804	-0.155	0.081	0.170	-0.076
Percentage of Variance Explained		26.012	19.074	9.964	9.270	8.551
Total Variance Explained		72.87%				
Eigen Value		Greater than 1				

**Blue cells: Positive factor loading; Grey cells: Negative factor loading*

Comparing the conditions during NEM, low SO_4^{2-} concentration is observed in the upper part where the upper part has high SO_4^{2-} content in the estuary (Fig 4.8) and the turbidity of water has peaked in both ends while decreasing in the intermediate zone. In the case of pH, higher pH is observed in the upper part whereas relatively acidic conditions prevailed in the lower part (Fig. 4.2). To sum up the factor with the above discussion, $BaCO_3$ precipitation is evident in the upperpart and $BaSO_4$ precipitation in the lower part under high turbidity conditions mainly controlled by absorption and sedimentation of suspended solids in the estuary.

Factor -3 has high positive loading of Cr and high negative loading of Se with a variance of 9.964%. This kind of loading of these metals indicates the variation of origin for both metals where Cr is a ferromagnesian metal mainly derived from

chromite present in Sibuti formation (Fig. 5.6) (Nagarajan et al., 2014; Nagarajan et al., 2017a), while Se is a chalcophile metal mainly associated with lignite, peat soils, pyrites and/or other heavy minerals (Williams et al., 1934; Yudovich et al., 2006) in the source region.

Factor-4 has higher loading of Fe and Mn observed during NEM which might be due to the formation of Fe and Mn hydroxides and co-precipitation under well-oxygenated conditions observed during this season (Duinker et al., 1979; Wollast et al., 1979; Reigner et al., 1993). This factor has a variance of 9.270%. Apart from that, the Neogene sediments of Lambir, Miri and Tukau formations were deposited under oxic conditions (Togunwa et al., 2017), hence more Fe-Mn oxyhydroxides were retained in the estuary (Mortimer et al., 2000). The higher negative loading of Co and high positive loading of TSS in the factor-5 explain the variance of 6.551%. The major source of the metal in the source area is leaching of pyrites from the shale and concretions in Sibuti and Lambir formations under tropical condition (Nagarajan et al., 2014; Nagarajan et al., 2015). These oxidized metals are mainly transported in dissolved form or particulate form in river systems, where both phases pose a tendency to form metal humic-complexes (Tessier et al., 1984). In addition, Co is particle reactive and 90% of Co absorption by clay minerals is common in open river streams resembling the study area, whereas desorption up to 40-70% can happen with the introduction of seawater (Kharker et al., 1968; Anandkumar, 2016). Considering these observations, this association indicates towards the desorption of Co from suspended solids due to prevailing hydrological conditions like the flow velocity of currents, action by waves and tides, causing the breakdown of humic complexes with the introduction of seawater in the estuary.

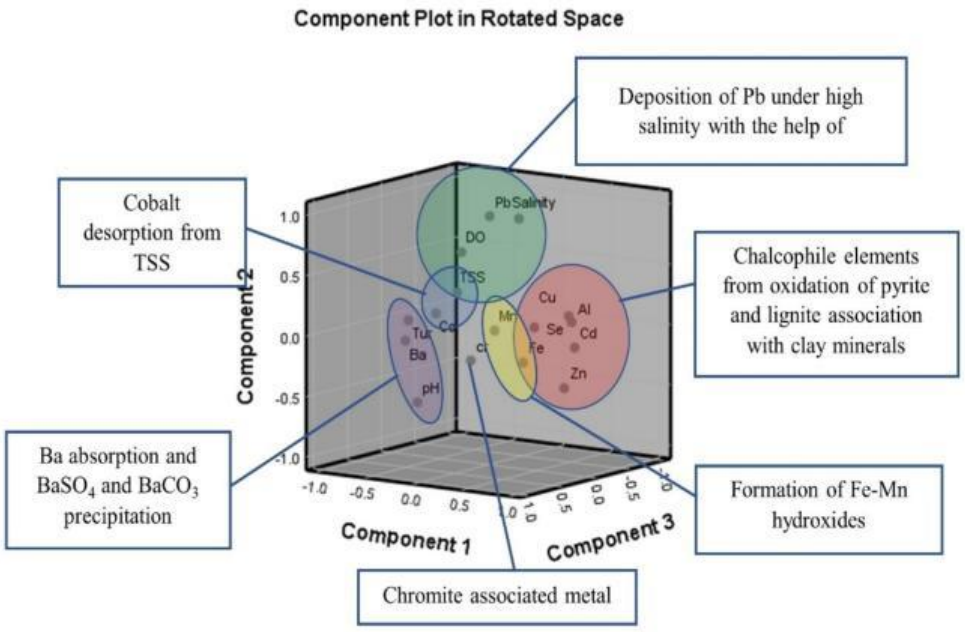

Fig. 5.6 Dominancy of principal components and associated sources in estuary during NEM

5.3.2.3 Factor analysis of metals in various fractions

In uncontaminated sediments, metals are usually associated with silicates and primary minerals (residual fraction) and therefore their mobility is limited (Kilink et al., 2019). But the metals associated with sediments through the process of ion exchange, carbonate absorption, oxide absorption and organic matter form relatively weaker bonds on the surface of sediments (Cui et al., 2015). The quantities of these metals within and adsorption on the surface of sediments are dependent on the local land use, geological substrate (bedrock), climate and even seasons (Namieśnik et al., 2015). These fractions are easily influenced by surrounding environmental conditions and are directly related to the mobility and toxicity of metals in aquatic systems (Sadhana et al., 2014; Cui et al., 2015). At present, sequential extraction (Tessier et al., 1979) has been a successful set of methods to quantify metal concentration in various speciation and bioavailability of trace metals and other elements in sediments. However, translation of this operational fractionation into chemical speciation is risky (Cui et al., 2015). Different species may be extracted in the same fraction and redistribution may take place depending upon the varying physico-chemical conditions (Nirel et al., 1990; Calmano et al., 2001; Cui et al., 2015). In such scenarios, geochemical models are well known to facilitate the discussion of cycling between the fractions, increase the level of understanding, increase the credibility of predictions of potential future

changes and relate the extracted fractions to specific chemical phases (Cui et al., 2015; Cao et al., 2015). To better interpret the chemical pools extracted from sequential extraction, a statistical factor model was used to keep the speciation of each metal as variables and are presented in Tables 5.9 and 5.10. As the form of occurrence of an element is strictly dependent on the changing physico-chemical conditions of water and affects the speciation of the compounds present in it (Namieśnik et al., 2015), major controlling parameters like pH, salinity and DO are taken into consideration to identify their influence of the speciations.

5.3.2.3.1 South-West monsoon (SWM)

Factor-1 has high positive loading of DO, CoF1, CoF3, CoF4, MnF1, CrF3, BaF2 and BaF3 along with moderate loading of FeF1. The high negative loading in this factor includes salinity, CuF1, CuF3, PbF1, ZnF2, SeF1, CdF1 and moderate negative loading of AlF2. This factor explains 23.52% of the total variance in the estuary. The positive loading is mainly observed in the upper part of the estuary whereas negative loading is dominant in the lower part (Table 5.10). The positive loadings indicate the formation of significant Mn oxides under well-oxygenated conditions than Fe oxides and scavenging metals like Co with weak electrostatic bonds. Furthermore, the association of F3 bound metals like Co and Cr with Mn and Fe hydroxides indicates stable formations between them (Li et al., 2001) whereas F2 and F4 bound Ba and Co indicate towards coating of Mn and Fe hydroxides on organic matter (e.g. Lion et al., 1982). On the other hand, observed negative loading of chalcophile metals such as Cu, Pb, Zn, Se and Cd along with weak loading Al indicates adsorption by the clay minerals and phyllosilicates (Al-hydroxides). The association of salinity with this group of metals and significant negative factor scores in the lower part of estuary (Table 5.9) indicate the saline water-induced resuspension, which is responsible for bringing these clay minerals and phyllosilicates into the water table. These chalcophile metals are the main products of leaching from geogenic sources like lignite beds, pyrites (Anandkumar, 2016) and anthropogenic sources like agricultural run-off in the river basin.

Factor-2 has higher positive loading of MnF1, FeF3, AlF3, AlF4, CuF4, CuF3, ZnF3, ZnF4 with total variance of 12.826%. The component is mainly associated with the middle part of the estuary (Table 5.13). The association of MnF1 with this fraction

indicates the ambient nature and flocculation of dissolved Mn. This process also forms the coating of Mn hydroxides on geogenic Fe, Al and carbonate minerals, which might be the result of periodic sub-oxic conditions initiated by tidal influence. The association of F1 bound Mn with F3 and F4 bound Cu and Zn indicates the cations competition with trace metals for negative sorption sites in these Mn bound sediments (Shafie et al., 2014) during the initial process and formation of a stable bond between Fe hydroxides, clay minerals and carbonates during the post-depositional diagenesis.

Factor-3 has high positive loading of pH, CoF2, FeF2, AlF2, CdF2 and CrF3 along with negative loading of SeF2 which represents 9.69% of the total variance. The association of Al and Fe with carbonate fraction signifies the formation of Fe carbonate cement on detrital clay minerals in the source area and absorption of metals like Co, Fe and Cd in the riverine system. This theory can be supported by the following observations: (1) Among all the carbonate cementations, Fe-calcite cementation is a major type and commonly observed to replace other detrital components in sandstone bodies (Lai et al., 2017) (2) Clay minerals associated with such cementation might be dioctahedral smectite and illite as these are formed through the transformation of detrital materials rich in Al and Fe (Dias et al., 2020) (3) In the case of the drainage basin, Nagarajan et al. (2015) and (2017a) reported the presence of smectite and illite ferruginous sandstones in Sibuti formation, which is found to be cemented with carbonates with Fe oxide coating on it. However, the negative loading of Se with this factor indicates ion exchange of Se with Co and Cd, and the release of Fe and Al hydroxide bound Se into water under low pH conditions. These Fe oxides are the main reason for the absorption of Co, Cd and Al in carbonate fraction (F3) and initial absorption of Cr in carbonate fraction (F3) while converting to form stable bonds with Fe and Al hydroxides during post-depositional diagenesis under high pH conditions.

Factor-4 has higher positive loading of MnF2, MnF3, MnF4, which explains 8.26% of the total variance. This association indicates that Mn (IV) or Mn oxide reduction is catalyzed by microorganisms. Organic matter in aquatic systems indirectly affects metal fate by forming a food source for microorganisms, which catalyze a series of redox reactions in the presence of electron acceptors (Du Laing et al., 2009). These reactions primarily affect the mobility and availability of metals in wetland soils. Furthermore, Du Laing et al. (2009) explained that water saturation during the

extended period of time changes the chemical properties of the sediments as well as the microbial population. Within this period, sediments undergo sequential redox reactions when redox status changes to anaerobic from aerobic, while Mn oxide reduction becomes a major mechanism under such conditions and are mainly catalyzed by microorganisms. The factor is dominant at station 2 having a factor score of 4.643 and nearer to the mouth of the river, thus it faces the highest resistance due to high tidal influence. This situation often leads to stratification of the water column where an anaerobic condition is inevitable at the bottom while injecting Mn from the sediments surfaces into the water column (Turner et al., 2000), which is mainly controlled by degrading microbial population (Patrick et al., 1992; Du Laing et al., 2009).

Factor-5 has a higher loading of ZnF2, AlF1 and moderate negative loading of CdF2 and addresses 5.75% of the total variance. This signifies the association of chalcophile minerals like pyrite from the source area and absorption by Al hydroxide coating on carbonate minerals in estuarine sediments mainly through ion exchange of Cd with Zn.

Factor-6 has higher loading of FeF4 and moderate loading of ZnF4, SeF1 along with moderate negative loading of CuF4 with a variance of 4.958%. This factor signifies the presence of Fe oxides on organic matter surface and ion exchange of chalcophile metals like Cu with Zn along with exchangeable Se on its surface. Factor-7 has higher loading of BaF1 with a variance of 4.889% indicating the absorption of Ba on clay minerals like mixed chlorite, illite and kaolinite (Eylem et al., 1990).

Factor-8 has high loading of FeF1 and BaF4 along with negative loading of MnF1 with a variance of 4.767%. This signifies coating of Fe oxides on the organic matter over Mn oxides in the lower part of the river as Mn reduction (Poggenburg et al., 2018) has been observed due to water stratification in factor-4 explained before. This is further validated by the high positive factor score at station 2 (Table 5.10). On the other hand, Mn oxide coating over organic matter is dominant in the upper part of the estuary with relatively aerobic conditions because of higher freshwater concentration (Duinker et al., 1979; Wollast et al., 1979; Reigner et al., 1993). The negative factor observed at various stations in the upper part validates this theory. The high positive

loading of Ba indicates absorption of the metal by organic matter mainly through Fe oxides rather than Mn.

Table 5.9 Rotated Component Matrix of Metals in various fractions of Sediments during SWM

Parameters	Communalities	Components									
		1	2	3	4	5	6	7	8	9	10
pH	0.848	0.398	-0.090	0.742	-0.010	0.161	-0.007	0.196	-0.136	0.110	-0.189
DO	0.676	0.612	0.099	0.025	-0.226	-0.045	-0.039	-0.315	0.225	0.206	0.209
Sal	0.744	-0.829	0.027	-0.014	0.007	-0.009	0.164	0.026	-0.115	0.000	0.121
CoF1	0.952	0.934	-0.132	0.005	-0.145	0.084	-0.071	0.059	0.061	-0.043	-0.140
CoF2	0.870	0.412	-0.179	0.546	0.461	-0.064	-0.177	-0.035	0.238	-0.225	-0.118
CoF3	0.824	0.874	0.099	0.009	-0.039	-0.052	-0.013	-0.123	0.081	0.151	-0.024
CoF4	0.959	0.941	-0.124	-0.004	-0.080	0.109	0.055	-0.032	-0.018	-0.053	-0.179
CuF1	0.869	-0.820	0.122	0.095	0.016	0.228	0.017	0.260	0.015	0.122	0.195
CuF2	0.561	0.401	0.325	-0.268	-0.084	-0.126	-0.171	0.351	0.096	0.187	0.053
CuF3	0.791	-0.506	0.587	-0.080	0.097	0.125	-0.037	-0.202	0.027	0.133	0.313
CuF4	0.898	-0.314	0.680	-0.002	0.120	0.123	-0.450	0.118	-0.032	-0.115	0.277
MnF1	0.791	0.537	0.532	0.024	0.255	0.155	0.151	-0.220	-0.513	-0.226	-0.100
MnF2	0.878	-0.177	0.019	-0.093	0.866	-0.114	-0.059	-0.171	-0.003	-0.194	0.061
MnF3	0.917	-0.102	0.086	-0.102	0.911	-0.199	-0.085	0.037	0.063	0.074	-0.004
MnF4	0.796	-0.123	-0.058	-0.162	0.802	-0.075	0.037	0.041	-0.305	-0.080	0.021
PbF1	0.917	-0.927	0.133	0.003	0.082	0.039	-0.067	-0.054	-0.005	-0.123	0.098
ZnF1	0.863	-0.099	-0.303	-0.142	-0.322	0.772	0.070	0.012	0.035	-0.139	-0.123
ZnF2	0.735	-0.535	-0.424	-0.107	-0.158	0.261	0.095	-0.300	0.071	-0.235	0.066
ZnF3	0.944	-0.032	0.923	-0.042	0.042	-0.225	-0.052	-0.043	0.034	0.141	0.102
ZnF4	0.885	-0.103	0.780	-0.124	0.129	-0.104	0.413	0.079	-0.096	-0.091	-0.168
SeF1	0.808	-0.579	0.108	-0.124	-0.141	-0.053	0.456	0.227	0.288	0.023	0.283
SeF2	0.831	0.085	0.209	-0.812	0.084	0.109	0.122	0.062	-0.042	0.118	-0.260
SeF3	0.808	-0.041	0.344	0.186	0.385	0.314	0.311	-0.214	0.062	0.273	0.430
SeF4	0.835	-0.248	0.128	0.120	0.039	0.019	-0.056	0.161	-0.110	0.093	0.831
FeF1	0.834	0.492	-0.124	0.370	-0.029	-0.009	0.127	-0.237	0.597	-0.074	0.070
FeF2	0.946	-0.449	-0.093	0.820	-0.115	-0.066	-0.075	-0.156	0.072	-0.044	0.087
FeF3	0.760	-0.105	0.679	-0.143	0.139	0.000	0.281	0.351	-0.155	-0.074	0.128
FeF4	0.930	-0.191	0.149	-0.234	-0.089	0.296	0.833	0.126	-0.072	0.078	-0.018
AlF1	0.894	-0.084	-0.214	-0.082	-0.173	0.866	0.122	-0.012	0.126	-0.063	0.139
AlF2	0.846	-0.377	0.294	0.661	-0.281	-0.202	-0.142	-0.062	0.071	0.099	0.147
AlF3	0.939	-0.086	0.893	-0.069	-0.167	-0.136	-0.120	-0.114	0.036	0.216	0.084
AlF4	0.921	0.009	0.743	-0.203	-0.210	-0.143	0.459	-0.117	-0.007	0.073	-0.182
CdF1	0.814	-0.643	0.104	0.190	-0.057	0.033	0.197	0.290	-0.074	0.421	-0.209

Parameters	Communalities	Components									
		1	2	3	4	5	6	7	8	9	10
CdF2	0.763	0.038	-0.179	0.514	-0.048	-0.415	0.082	-0.398	0.179	-0.306	-0.009
CdF3	0.763	0.050	0.139	-0.128	-0.160	-0.173	0.061	0.027	-0.142	0.792	0.136
CrF3	0.936	0.585	-0.201	0.651	-0.271	-0.074	-0.092	0.113	0.063	0.016	-0.160
BaF1	0.777	-0.273	-0.084	-0.041	-0.110	0.012	0.122	0.805	0.010	0.051	0.123
BaF2	0.874	0.510	-0.117	0.037	0.087	-0.192	-0.034	-0.294	-0.470	-0.496	-0.006
BaF3	0.714	0.753	-0.122	-0.031	-0.093	-0.148	-0.015	0.022	0.078	-0.232	0.201
BaF4	0.796	0.287	-0.107	0.041	-0.067	0.183	-0.061	-0.032	0.753	-0.237	-0.185
% of Variance Explained		23.52	12.83	9.69	8.26	5.75	4.96	4.89	4.77	4.68	4.43
Total Variance Explained		83.76%									
Eigen Value		Greater than 1									

**Blue cells: Positive factor loading; Grey cells: Negative factor loading*

Factor-9 has high loading of CdF3 and moderate loading of CdF1 and BaF2 with a variance of 4.677% in the estuarine sediments. The moderate association of Cd with an exchangeable fraction (F1) and high association with a reducible fraction (F3) indicate the transition between absorption of Cd through ion exchange on various oxides and formation of stable bonds during the post-depositional period. Factor-10 has high loading of SeF4 and weak loading of SeF3 with a variance of 4.425%. Se absorption in sediments is known to be strongly influenced by the presence of oxyhydroxides and organic matter under sub-oxic to anoxic conditions in both salt and freshwater interfaces (Oremland et al., 1989; Belzile et al., 2000; Hosseini et al., 2018). Oremland et al. (1989) specifically observed selenate reduction in water as the result of direct biological activity and elemental selenium as a respiratory end product of bacteria in estuarine sediments. Hoseini et al. (2018) concluded higher organic matter content of muddy sediment responsible for the higher accumulation of Se. Belzie et al. (2000) concluded that the main geochemical processes involving Se are adsorption of Se onto Fe and Mn oxyhydroxides and mineralization of organic matter in sediments. This process has a higher factor score both in the lower and upper part of the estuary (Table 5.10) and a sub-oxic condition (DO< 5 mg L^{-1}) of water was also observed during this season. These observations justify the higher association of Se with oxidizable and fraction and reducible fraction in the study area.

Table 5.10 Factor Score for Metals in various fraction of Sediments during SWM

Sample Stations	Components									
	1	**2**	**3**	**4**	**5**	**6**	**7**	**8**	**9**	**10**
1	-2.250	-0.744	4.888	-0.185	-1.126	-0.219	-0.506	0.430	-0.622	0.472
2	-1.289	0.153	-0.630	4.643	-0.380	-0.733	0.007	1.172	-0.283	0.182
3	-1.980	-0.566	-2.426	-0.799	-1.925	0.683	-1.684	0.748	-1.183	0.702
4	-0.981	3.211	-0.874	-0.473	-0.012	-1.984	-0.172	-0.133	-0.697	1.514
5	-1.327	-1.002	-1.020	-0.474	1.192	-0.090	-1.017	-0.265	-0.359	0.615
6	-1.064	0.064	0.025	-0.060	1.946	0.099	-0.114	-0.946	-0.379	1.179
7	-0.367	-0.696	-0.445	0.613	-0.527	1.194	0.424	-1.300	1.911	1.183
8	-0.560	2.769	0.031	-0.389	-0.742	4.204	-0.173	-0.236	-0.014	-1.600
9	-1.143	-0.834	-0.126	-0.867	-0.122	-0.200	0.089	-0.272	0.222	-0.594
10	-1.076	-0.087	-0.302	-1.009	1.175	-0.269	-0.327	-0.458	0.103	-1.195
11	-0.704	-0.230	-0.247	2.225	-0.395	0.407	0.338	-0.747	1.005	-0.905
12	-1.227	-0.270	0.176	-0.647	1.029	-0.119	-1.105	0.282	-0.567	-1.244
13	-0.497	-1.193	-0.522	-0.782	-0.416	-0.337	0.305	-0.687	2.383	0.096
14	-0.399	-0.261	-0.233	-0.174	1.690	-0.122	0.797	-0.857	0.183	0.402
15	-0.003	1.912	0.481	-0.431	-0.475	-0.937	1.267	-0.856	0.418	-0.017
16	-0.006	-0.957	-0.647	-0.662	-0.866	-0.215	0.757	-0.413	0.080	0.652
17	0.100	-0.420	0.100	-0.355	1.430	0.242	1.151	-0.030	0.349	0.439
18	0.148	1.785	0.317	-0.438	0.250	-1.368	0.965	-0.134	-0.737	-0.585
19	0.147	-0.294	-0.080	-0.314	-0.036	-0.070	0.941	0.096	0.041	0.653
20	0.221	0.216	-0.061	0.556	0.404	-0.470	2.069	0.930	-0.530	-0.384
21	0.222	-0.527	-0.225	-0.266	-0.164	0.802	2.682	0.447	-0.550	0.619
22	0.495	-0.854	-0.056	-0.935	-1.642	0.036	1.579	0.887	-0.167	0.101
23	0.624	0.314	0.488	0.421	0.378	1.118	-0.075	0.603	0.349	0.661
24	0.924	0.276	0.321	-0.043	-0.616	0.438	0.304	0.427	0.326	0.082
25	0.512	0.098	0.039	-0.103	-0.968	-0.604	-0.315	0.238	1.092	-1.000
26	0.557	0.770	-0.056	-0.143	0.970	-0.814	-1.342	0.753	1.476	-1.151
27	1.424	0.950	0.555	-0.246	-0.689	-0.243	-1.887	1.162	2.343	2.495
28	1.108	-0.538	-0.154	-0.418	0.561	-0.179	-0.314	1.787	-0.525	-0.147
29	0.638	-0.414	0.032	0.091	-0.113	-0.109	-0.224	0.332	0.321	-1.061
30	1.222	-0.325	0.570	0.593	2.662	1.747	-0.648	1.037	-0.825	1.130
31	0.640	-0.627	-0.480	-0.432	-0.534	-0.293	-0.218	2.285	-0.935	-0.939
32	0.831	-0.244	-0.197	0.061	-0.320	-0.525	-0.306	0.495	-0.910	-1.313
33	1.169	-0.436	0.123	0.218	-0.234	-0.503	-0.999	-0.973	0.175	-0.190
34	1.252	-0.283	0.300	0.089	-0.383	-0.382	-1.104	-1.290	-1.012	-0.333
35	1.703	-0.282	0.038	0.462	-1.157	0.323	-0.657	-2.430	-2.687	1.428
36	0.937	-0.440	0.297	0.672	0.157	-0.507	-0.486	-2.088	0.201	-1.944

**Blue cells: High positive loading; Grey cells: High negative loading*

5.3.2.3.2 North-East monsoon (NEM)

Factor-1 has high positive loading of pH, CoF1, SeF1, CoF2, BaF2, BaF3, CoF4, and BaF4 along with weak loading of AlF2, ZnF2 and MnF1. The high negative loading of salinity and CdF1 is also associated with this factor. 17.532% of the variance was explained by this factor during NEM. The high positive factor score in the upper part (Table 5.12) and positive loading of pH is indicative of absorption which is the main component of this factor in a freshwater dominated system. The moderate loading of Mn in F1 indicates freshly formed Mn hydroxides and absorption of leached Se and Co from the source area by Mn hydroxides that is taking place in well-oxygenated conditions (Shafie et al., 2014). Absorption of Co and Ba is mainly controlled by a mixed mechanism including clay minerals and carbonate minerals (Dehaine et al., 2021), where F2 absorption confirms carbonate mineral role and Al association with the same fraction signifies the association of clay minerals. Organic matter usually decreases in sediments towards the river mouth in such circumstances and is highly reactive in absorbing metals (Tomlinson et al., 1980). This factor mainly leads to the absorption of Co and Ba in the upper part. Higher positive and negative loading of Se, Mn and Cd in exchangeable fraction indicates towards ion exchange process of chalcophile metals under the influence of low pH and high saline water in the lower part.

Factor 2 is mainly associated with a reducible fraction (F3) and has higher loading of CoF3, ZnF3, SeF3, AlF2, AlF3, CdF3 with a total variance of 13.34%. This factor is mainly associated with the mixing zone in the estuary (Station 4 to 15) (Table 5.12). As clays, aluminosilicates and Fe and Al hydroxides are a major part of weathered sediments, an oxic condition in the aquatic system might give rise to coprecipitation of Al hydroxides and carbonates, adsorption, and cation exchange on clays (Horowitz et al., 1991; Iwegbue et al., 2015). The formation of Al hydroxides mainly depends upon decreasing stability of clays in suspension in intermediate zones with increasing salinity, causing coagulation and sedimentation in estuaries, and leading to fractionated sedimentation of different clay minerals (Edzwald et al., 1974; Eckert et al., 1976; Van et al., 1977). The association of reducible fraction indicates absorption and flocculation of these leached metals (Cd, Se, Cd and Co) which are mainly controlled by Al hydroxides formed in such condition due to the large surface area (Pokrovsky et al., 2008; Balistrieri et al., 2013; Liu et al., 2013).

Factor-3 has high loading of ZnF1, FeF1, AlF1 and FeF4 with a total explained variance of 9.642% in estuarine sediments. The high positive factor score suggests that this process is mainly taking place in the low salinity-influenced region that is far from the river mouth (Table 5.12). This suggests that Fe is forming complexes with organic matter in sediments with a high degree of humification (Barančíková et al., 2003) in a low salinity zone. On the other hand, this organic matter can play an important role in retaining the metals in exchangeable form (Zhang et al., 1997; Dar et al., 2016), which in this case, are Zn, Fe and Al (Barančíková et al., 2003) and are absorbed due to scavenging nature of Fe mainly in the mixing zone of the estuary. Similarly, Factor-4 has higher loading of CuF4, ZnF4, CdF1 and explains a total variance of 6.942%. Cu and Zn have strong affinity towards organic matter (Barančíková et al., 2003; Zhang et al., 1997). Association of both metals with fraction 5 suggests that Cu and Zn are predominantly bonded to organic matter with a high degree of humification and unavailable form. The predominant association of Cd with an aliphatic form of organic matter (Barančíková et al., 2003) might be the reason behind its association with this factor and its affinity towards exchangeable fractions.

Factor-5 has higher loading of MnF1, MnF2, FeF2 and moderate loading of FeF3. This factor explains 6.736% of the total variance. This factor is controlled by absorption of ambient Fe and Mn oxides in the exchangeable and carbonate fraction from the water table, as Fe is specifically converted into oxides, which is reflected as Fe in reducible fraction. In the case of Factor-6, high negative loading of Pb and salinity is observed with a variance of 6.279%. This signifies the deposition of freshwater-borne Pb due to high saline water-influenced suspended solids in the lower part of the estuary.

Factor-7 has high positive loading of CuF2 and ZnF2 along with negative loading of CrF3 with a variance of 5.683%. The controlling factor of Cu and Zn and Cr is mainly leaching shale and pyrites concretion in the study area (Anandkumar, 2016). The association of these 3 metals in this factor suggests that these metals originate from a single source (shale and pyrites concretion) but the distribution of Cu and Zn is mainly controlled through carbonate minerals. However, simultaneous negative loading of Cr in reducible fraction indicates its association with Fe and Mn oxides during release as these are the main contributing phases in weathering of Cr bearing minerals (Cheng et al., 2011; Ho et al., 2013).

Table 5.11 Rotated Component Matrix of Metals in various fractions of Sediments during NEM

Parameters	Communalities	Component										
		1	2	3	4	5	6	7	8	9	10	11
pH	0.852	0.766	-0.014	0.134	-0.055	-0.169	0.322	0.003	0.194	-0.139	0.154	-0.174
DO	0.823	-0.010	-0.172	-0.152	0.210	0.001	-0.425	-0.061	-0.069	0.715	0.107	-0.121
Sal	0.972	-0.571	-0.148	-0.121	0.073	0.042	-0.714	-0.062	-0.200	0.196	0.032	-0.091
CoF1	0.880	0.812	-0.281	-0.008	-0.056	-0.003	0.167	0.032	-0.160	-0.049	-0.264	0.115
CoF2	0.830	0.757	-0.048	0.107	0.191	-0.118	0.225	0.214	0.171	0.121	-0.219	0.067
CoF3	0.825	-0.224	0.712	0.036	0.168	0.128	0.382	0.074	-0.024	-0.024	0.263	-0.003
CoF4	0.833	0.854	-0.088	0.158	0.079	-0.029	0.072	0.111	-0.031	-0.190	0.064	0.065
CuF1	0.817	-0.015	-0.285	0.337	0.108	-0.322	-0.079	-0.308	0.231	-0.047	0.154	0.572
CuF2	0.867	0.390	-0.021	0.091	-0.080	-0.019	0.062	0.818	0.009	0.066	-0.132	0.074
CuF3	0.762	-0.012	0.333	-0.022	0.267	-0.121	0.105	-0.052	0.094	0.723	-0.136	0.035
CuF4	0.907	0.044	0.036	-0.082	0.907	-0.060	-0.193	0.048	0.035	0.170	-0.017	-0.024
MnF1	0.850	0.441	-0.114	0.120	0.014	0.666	0.057	0.072	0.190	-0.130	0.348	0.037
MnF2	0.770	-0.125	-0.145	-0.180	-0.002	0.819	-0.079	-0.020	0.073	0.106	0.068	0.056
MnF3	0.896	-0.142	-0.030	-0.229	-0.014	0.238	0.075	-0.070	-0.078	0.102	0.840	0.182
MnF4	0.887	-0.207	-0.348	0.320	0.481	0.427	0.281	-0.154	-0.201	0.170	0.170	-0.084
PbF1	0.928	-0.284	-0.207	-0.089	0.084	-0.012	-0.872	0.010	-0.037	0.094	-0.089	-0.102
ZnF1	0.871	0.258	-0.256	0.827	-0.080	-0.053	0.090	0.090	0.095	-0.123	-0.049	0.056
ZnF2	0.829	0.493	-0.319	-0.026	-0.021	-0.018	0.080	0.685	-0.007	-0.013	-0.041	-0.073
ZnF3	0.827	-0.306	0.787	-0.279	0.082	0.079	0.093	0.002	0.030	-0.067	0.088	-0.042
ZnF4	0.884	-0.119	0.355	-0.159	0.668	0.228	0.378	0.134	-0.045	-0.080	0.119	0.188
SeF1	0.778	0.539	-0.135	0.034	0.231	0.020	0.101	0.127	0.499	0.042	-0.369	-0.038
SeF2	0.690	-0.207	-0.021	-0.053	-0.335	0.126	-0.122	0.192	-0.247	0.611	0.171	-0.021
SeF3	0.781	-0.121	0.659	-0.304	-0.263	0.177	0.028	-0.293	0.029	-0.025	-0.055	0.219
FeF1	0.899	0.286	-0.112	0.811	-0.061	0.077	-0.063	0.187	-0.269	0.026	-0.110	-0.116
FeF2	0.883	0.266	0.378	0.028	0.324	0.576	0.018	-0.007	0.267	-0.389	-0.073	0.057
FeF3	0.732	-0.183	0.317	-0.046	0.103	0.467	0.182	0.196	0.065	-0.338	0.377	0.186
FeF4	0.905	-0.120	-0.252	0.803	0.140	0.040	0.323	-0.105	-0.034	-0.066	-0.165	0.108
AlF1	0.907	0.021	-0.102	0.848	-0.150	-0.191	-0.057	-0.121	0.316	-0.030	0.006	0.002
AlF2	0.923	0.425	0.708	-0.287	-0.088	-0.215	-0.037	0.125	-0.285	0.040	0.005	0.076
AlF3	0.955	-0.250	0.908	-0.159	0.087	-0.126	0.063	-0.037	0.039	0.064	-0.091	0.018
AlF4	0.915	-0.252	0.404	0.395	-0.070	-0.232	0.067	-0.237	0.553	-0.083	0.225	0.222
CdF1	0.849	-0.524	-0.206	-0.019	0.581	0.179	-0.254	-0.032	0.041	-0.017	-0.292	-0.098
CdF2	0.846	0.074	0.264	-0.057	-0.030	0.261	0.216	0.067	-0.052	-0.078	0.174	0.780
CdF3	0.827	-0.110	0.871	-0.050	-0.019	-0.109	0.044	-0.174	0.056	0.068	-0.041	0.018
CrF3	0.703	0.117	0.052	0.087	-0.352	-0.109	0.108	-0.625	-0.319	0.089	-0.163	0.068
BaF1	0.877	0.008	-0.005	0.029	-0.012	0.288	0.086	0.174	0.862	-0.088	-0.066	-0.011
BaF2	0.881	0.697	-0.116	0.176	-0.232	0.077	0.034	0.255	-0.186	0.138	-0.228	0.345
BaF3	0.945	0.881	-0.280	-0.197	-0.121	0.147	-0.094	0.049	0.060	-0.019	-0.006	-0.037
BaF4	0.869	0.749	-0.117	0.268	-0.147	0.192	-0.154	0.105	-0.217	0.026	0.007	-0.285
% of Variance Explained		17.53	13.34	9.64	6.94	6.74	6.28	5.68	5.62	5.10	4.60	3.85
Total Variance Explained		85.33%										
Eigen Value		Greater than 1										

**Blue cells: Positive factor loading; Grey cells: Negative factor loading*

Furthermore, the redox potential of Mn oxides is higher than any other naturally occurring oxidants, thus the ability of sediment to oxidize Cr might be more prominent

in the case of available reducible Mn than Fe (Bartlett and James, 1979; Ho et. al. 2013). Despite Fe oxides not being considered an oxidant for Cr because of the lower redox potential than Mn, the scavenging nature of Fe is unavoidable and might be playing a major role in absorbing a large proportion of Cr from the water table (Garnier et al., 2006).

Factor-8 has higher loading of AlF4 and BaF1 and indicates the humic coating on clay minerals and absorption of Ba on to the surface of such sediments. This factor shows 5.615% of the total variance. Factor-9 is associated with high loading of CuF3 and SeF2 indicating controlling source as pyrites where absorption of these metals on sediments is mainly associated with oxic conditions during NEM. Factor-10 has higher loading of Mn in reducible fraction (F3) and an increased formation of Mn hydroxides under an oxic condition in the estuary which has a major role in reducible fraction associated metals. This factor has a total variance of 4.602%. Factor-11 has high positive loading of chalcophile metals like Cu in F1 and Cd in F2. This signifies the absorption of these metals on the surface of carbonate minerals and are susceptible to minor variation of aquatic conditions.

Table 5.12 Factor Score for Metals in various fraction of Sediments during NEM

Sample Station	Component										
	1	2	3	4	5	6	7	8	9	10	11
1	-1.566	-1.113	-0.494	0.503	-0.125	-5.068	0.105	-0.149	0.504	-0.722	-0.648
2	-1.277	-1.313	-0.355	-0.177	0.714	-0.290	-0.623	-0.927	0.611	2.714	0.731
3	-1.592	-0.491	-0.501	-0.599	1.722	0.822	-0.299	-0.418	0.003	-0.363	0.004
4	-1.299	-1.216	-0.151	1.892	0.252	1.027	-0.609	-1.236	1.648	0.793	-0.772
5	-1.043	1.243	-0.525	-0.725	-0.379	-0.173	-0.285	-0.481	0.116	-0.082	-0.155
6	-0.915	1.822	-0.147	-1.804	-0.288	-0.245	-0.296	-0.591	0.062	0.175	-0.207
7	-0.711	1.935	-0.442	-0.860	0.072	-0.582	0.284	-0.130	-0.435	0.434	0.262
8	-1.173	-0.145	0.816	-0.003	-0.064	0.763	0.339	-1.028	-0.028	-0.628	-0.018
9	-0.068	1.942	-0.126	1.558	-0.708	0.613	-0.305	0.547	4.217	-0.792	0.202
10	-1.161	-0.869	0.015	-0.660	0.231	1.135	0.316	0.368	0.064	-0.046	-0.734
11	-0.386	1.374	-0.586	0.492	-0.355	0.019	-0.109	-0.192	-1.219	-0.656	0.806
12	-0.876	-0.855	1.861	0.559	-0.582	0.580	-0.402	-1.046	-0.962	-0.796	0.582
13	-1.069	-0.563	-0.478	0.302	-0.877	0.745	0.195	0.160	-1.568	-0.245	-0.487
14	-0.822	-0.776	0.967	-0.317	-0.805	0.565	-0.429	0.653	-0.885	-0.644	-1.163
15	-0.484	1.496	0.097	1.363	-0.091	0.183	-0.161	-0.078	-1.547	-0.209	-1.512
16	-0.025	2.277	-0.028	0.682	-0.833	-0.118	-0.402	0.594	-0.509	-0.232	-0.160
17	-0.339	0.085	-0.178	-0.191	-0.532	0.772	0.312	0.206	-0.290	3.120	1.537
18	0.100	0.606	2.380	-0.344	1.499	0.028	-0.620	0.921	-0.109	0.255	0.429
19	-0.065	-0.806	1.922	-0.559	-1.934	-0.582	-1.274	3.488	0.192	0.634	1.095
20	0.271	-1.245	-0.911	-0.239	1.720	0.849	-1.457	1.065	0.528	-2.210	-0.322
21	1.015	0.666	-0.028	1.999	3.191	-0.502	-0.700	0.793	-1.297	0.266	0.317
22	0.009	0.073	-0.583	-0.328	-0.183	0.278	-0.347	0.278	-0.403	-0.946	0.145
23	-0.274	-0.439	-0.563	1.557	0.697	0.086	3.473	2.037	0.179	0.758	0.120
24	0.018	-0.413	-0.578	-1.082	0.464	0.422	1.658	1.274	0.526	-1.005	0.320
25	0.538	-0.079	-0.818	-0.984	-0.531	-0.164	1.100	-0.697	-0.348	-0.500	1.139
26	1.030	0.340	-0.131	-0.754	1.127	-0.215	1.341	-0.653	-0.147	0.467	0.664
27	1.212	-0.715	0.066	1.743	-0.668	-0.380	-0.996	-1.315	-0.476	-0.974	3.469
28	0.349	-0.508	0.058	-0.807	-0.593	0.325	1.044	-1.347	0.280	-0.943	0.396
29	1.072	0.018	-0.391	-0.900	0.149	-0.098	0.774	0.063	0.656	-0.378	0.731
30	1.485	0.109	3.684	-0.431	0.649	-0.570	1.375	-1.524	0.792	-0.044	-1.249
31	1.338	-1.008	-0.618	1.311	-1.962	0.218	1.344	-0.073	-0.729	-0.272	-1.049
32	1.570	0.073	-0.535	1.097	-0.928	0.294	-0.743	-0.708	-0.025	1.220	-1.635
33	1.470	0.031	-0.531	-0.514	0.488	-0.709	-1.019	-0.018	-0.318	0.890	-0.919
34	1.418	-0.735	-0.777	-0.890	0.027	0.208	-0.773	0.532	-0.175	0.032	-1.182
35	1.066	-0.298	-0.528	-0.710	-0.392	-0.250	-0.643	0.011	0.433	1.009	-1.219
36	1.185	-0.504	-0.861	-1.183	-0.172	0.014	-1.168	-0.378	0.662	-0.080	0.485

**Blue cells: High positive loading; Grey cells: High negative loading*

5.3.3 Ecological risk assessment of sediments

Risk assessment of sediments in the Sibuti River estuary is done based on the various geochemical indices such as geo-accumulation index (I_{geo}) (Muller et al., 1981), Enrichment Factor (EF) (Bloundi et al., 2009), Contamination Factor (CF) (Hakansoon et al., 1980), Pollution Load Index (PLI) (Tomlinson et al., 1980), and Potential Ecological Risk Index (PERI) (Hakanson et al., 1980). These indices are widely used in evaluating sediment quality and toxicology of metals present in the various aquatic systems like estuaries (Elias et al., 2018; Zhu et al., 2012; Vu et al., 2018).

5.3.3.1 Geoaccumulation index (I_{geo})

During SWM, the decreasing order of metals according to their average I_{geo} values can be arranged as Se > Co > Cu > Cd > Ba > Zn > Fe > Cr > Pb > Mn. Considering the mean I_{geo} values (Fig. 5.7), the Sibuti estuarine sediments are extremely contaminated by Se and Co, strongly contaminated by Cd and Cu and moderately contaminated by Ba. The average I_{geo} values of elements such as Fe, Mn, Pb, Zn and Cr are in the uncontaminated category during SWM.

In the case of station-wise variation, 34 (94.44%) sites are reported to be uncontaminated with Fe and the rest fall under the uncontaminated to moderately contaminated category. Similarly, all the sites were uncontaminated with Mn and Pb and 19 (52.22%) and 35 (98.22%) of the stations are uncontaminated with Zn and Cr respectively, whereas the rest are in the uncontaminated to moderately contaminated category (Fig. 5.8). In the case of Ba, 22 (61.11%) sites reported uncontaminated to moderate contamination (Fig. 5.7). In addition, all the stations reported being moderately to strongly contaminated with Cd and Cu. In the case of Se, all the sites are extremely contaminated, whereas 26 (72.22%) of the sites are extremely contaminated with Cu and the rest show strong to extreme contamination (Fig. 5.8).

During NEM, the decreasing order of metals according to their mean I_{geo} values can be presented as Se > Co > Cd > Cu > Ba > Zn > Cr > Fe > Mn > Pb. The mean values indicate extreme contamination by Se and Co in Sibuti estuarine sediments, whereas moderate to strong contamination of sediments is by Cd and Cu. The metals like Zn

and Ba are in the moderate contamination category, whereas all other metals have I_{geo} values under the uncontaminated category (Fig. 5.7).

Station-wise variation indicates that 36 (100%) stations in the estuary are extremely contaminated with Se and Co and uncontaminated with Fe, Mn, Pb and Cr during this season. In the case of Cd, 23 (63.89%) of the stations show moderate to strong contamination where the rest are strongly contaminated. Similarly, 18 (50%) stations are moderately contaminated, and the rest 18 (50%) stations are under moderate to strong contamination (Fig. 5.8) category. In the case of Zn, 13 stations (36.11%) are uncontaminated to moderately contaminated, where the rest of the stations show no contamination of the metal in the sediments (Fig. 5.8).

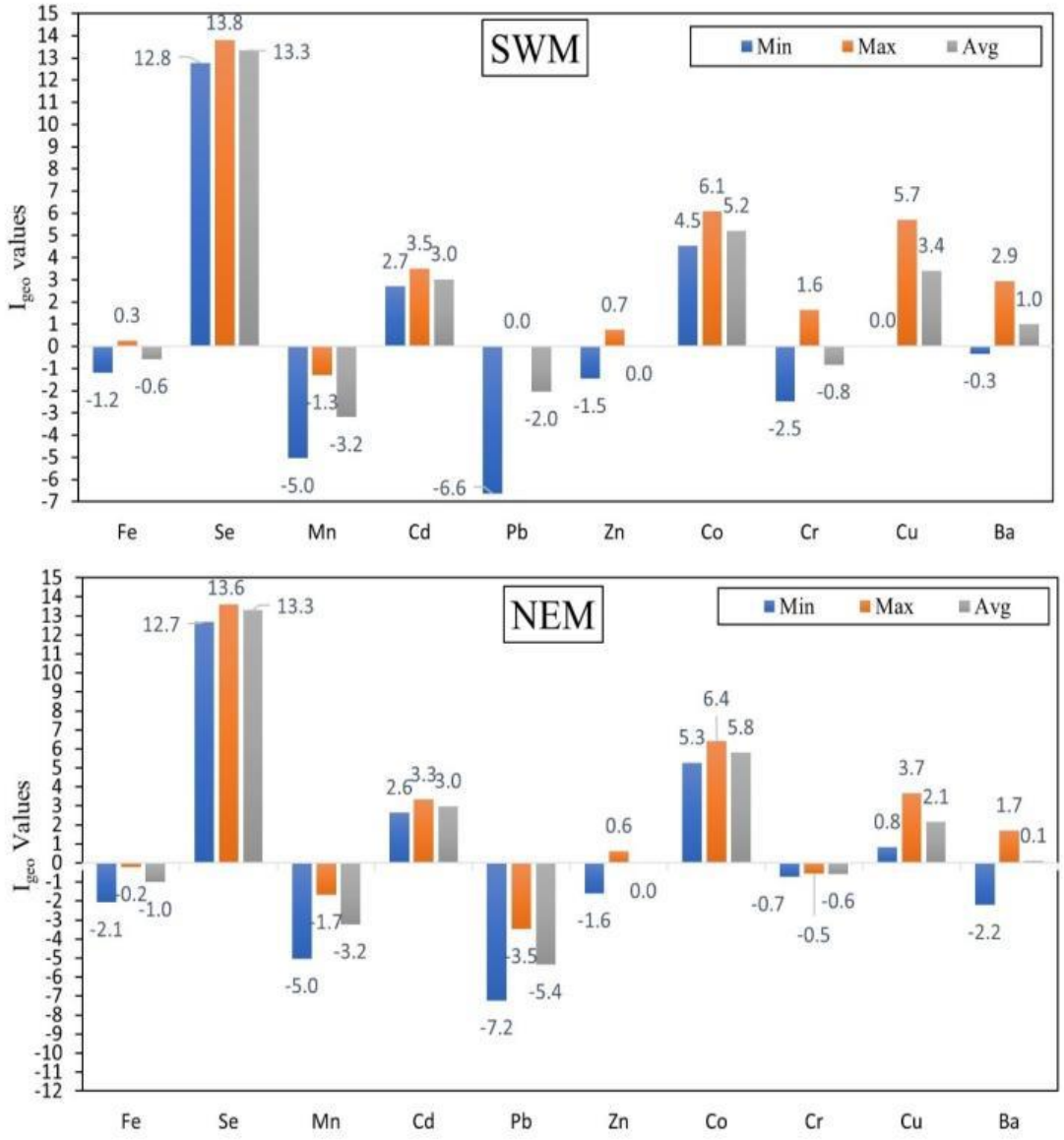

Fig. 5.7 Cluster plot showing Geo-accumulation index (I_{geo}) of metals during SWM and NEM

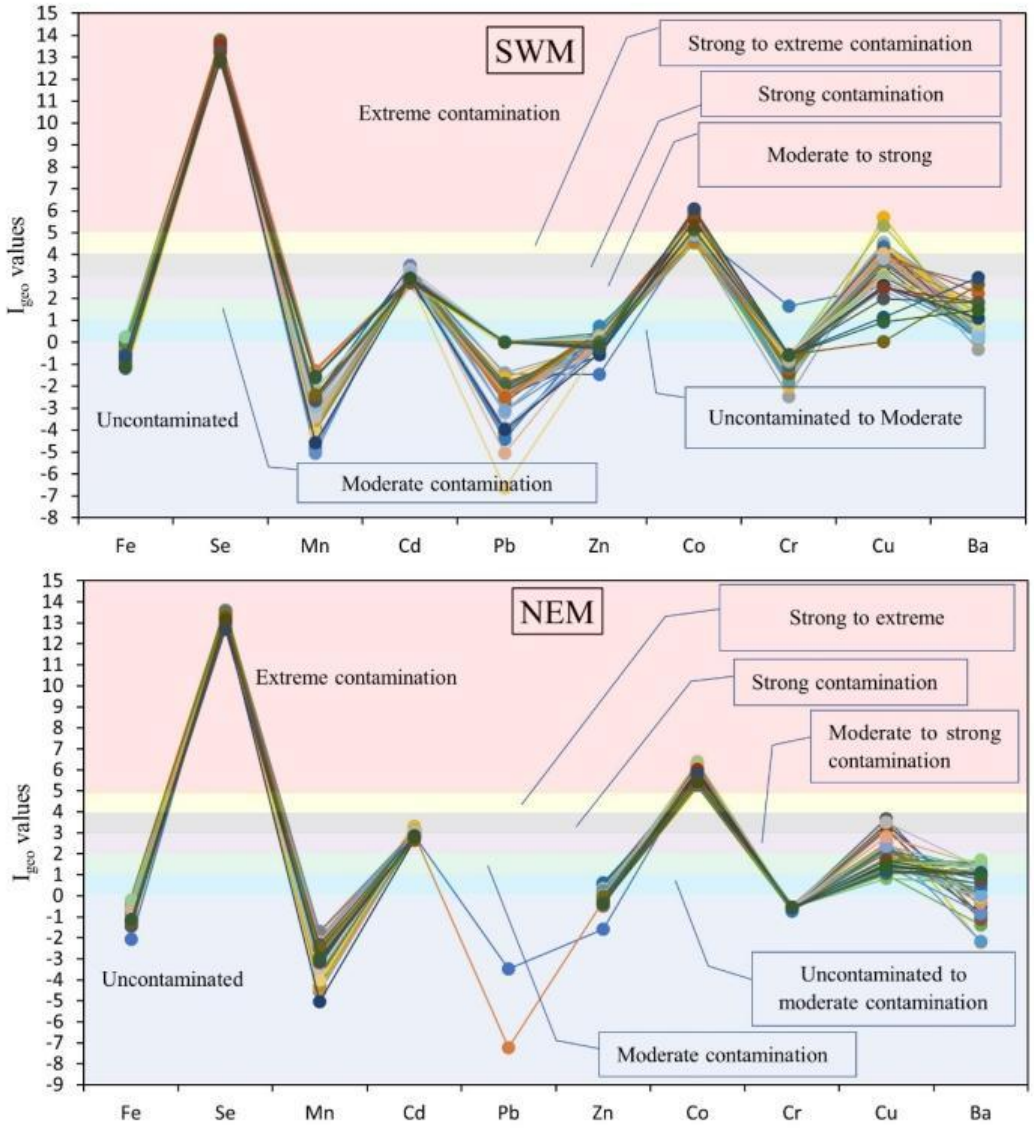

Fig. 5.8 Scatter plot showing I_{geo} value variation of metals in sediments during SWM and NEM

5.3.3.2 Enrichment factor (EF)

During SWM, the average EF values indicate extreme enrichment of Se and Co in Sibuti estuarine sediments (Fig. 5.9). In addition, significant enrichment of Cd and Cu is also observed in the sediments. Ba is moderately enriched in the sediments during this season and other metals like Fe, Mn, Al, Pb, Zn and Cr are observed to be in deficient to minimal enrichment condition (Fig. 5.9). The decreasing order of enrichment of metals can be shown as Se > Co > Cd > Cu > Ba > Zn > Fe > Cr > Mn > Pb.

In the case of station-wise enrichment, all the stations are heavily enriched with Se, whereas 21 (58.33%) stations are extremely enriched with Co, while the rest fall in the

very high enrichment category. Cd is enriched significantly in 27 (75%) stations in the estuary whereas the rest are in a very high enrichment category. In the case of Cu, 20 (55.55%) stations are significantly enriched with Cu and 12 (33.33%) stations show very high enrichment along with extreme enrichment in the rest of the stations. Ba is moderately enriched at 18 (50%) stations, 7 (19.44%) stations have significant to very high enrichment and the rest fall under the low enrichment category. Fe, Zn and Cr in 30 (83.33%), 30 (83.33%), 32 (88.89%) stations show minimal enrichment, and all the stations were recorded to be under minimal enrichment for Mn and Pb (Fig. 5.10).

During NEM, higher mean enrichment of metals has been observed for all the elements except Pb. The mean value of EF suggests that Se, Co, Cd and Ba are extremely enriched in the Sibuti estuarine sediments (Fig. 5.9). Fe, Zn and Cr are significantly enriched in the estuary whereas Mn and Pb are under minimal enrichment category during this season (5.8). The decreasing order of enrichment during this season can be observed as Se > Co > Cd > Cu > Ba > Zn > Cr > Fe > Mn > Pb.

Station-wise enrichment suggests extreme enrichment of Se and Co at all the stations. In the case of Cd, 26 (72.22%) of the stations are extremely enriched and are mostly situated away from the river mouth (Fig. 5.10). The stations near the mouth mostly fall under significant to very high enrichment of Cd. Ba is enriched extremely at 12 (33.33%) stations, significantly enriched at 8 (22.22%) stations and very highly enriched at 6 (16.66%) stations where highly enrichment stations are in the upper part of the estuary. The lower part shows minimal enrichment of Ba at the majority (9; 25%) of the stations (Fig. 5.10). Fe and Mn show significant enrichment mostly at stations situated in the upper part of the estuary. Considering all the stations, Fe is enriched in 13 (36.11%), 7 (19.44%), 1 (2.7%) station and fall in the significant, very high and extremely enrichment category respectively, whereas 8 (22.22%) stations are significantly enriched with Mn. Likewise, Zn and Cr show higher enrichment in the upper part as well during NEM where the lower part shows minimal enrichment. Among all the stations, 13 (36.11%) stations are enriched significantly with Cr and Zn. Extreme enrichment of Zn and Cr is observed at 6 (16.66%) stations and 4 (11.11%) stations respectively (Fig. 5.10).

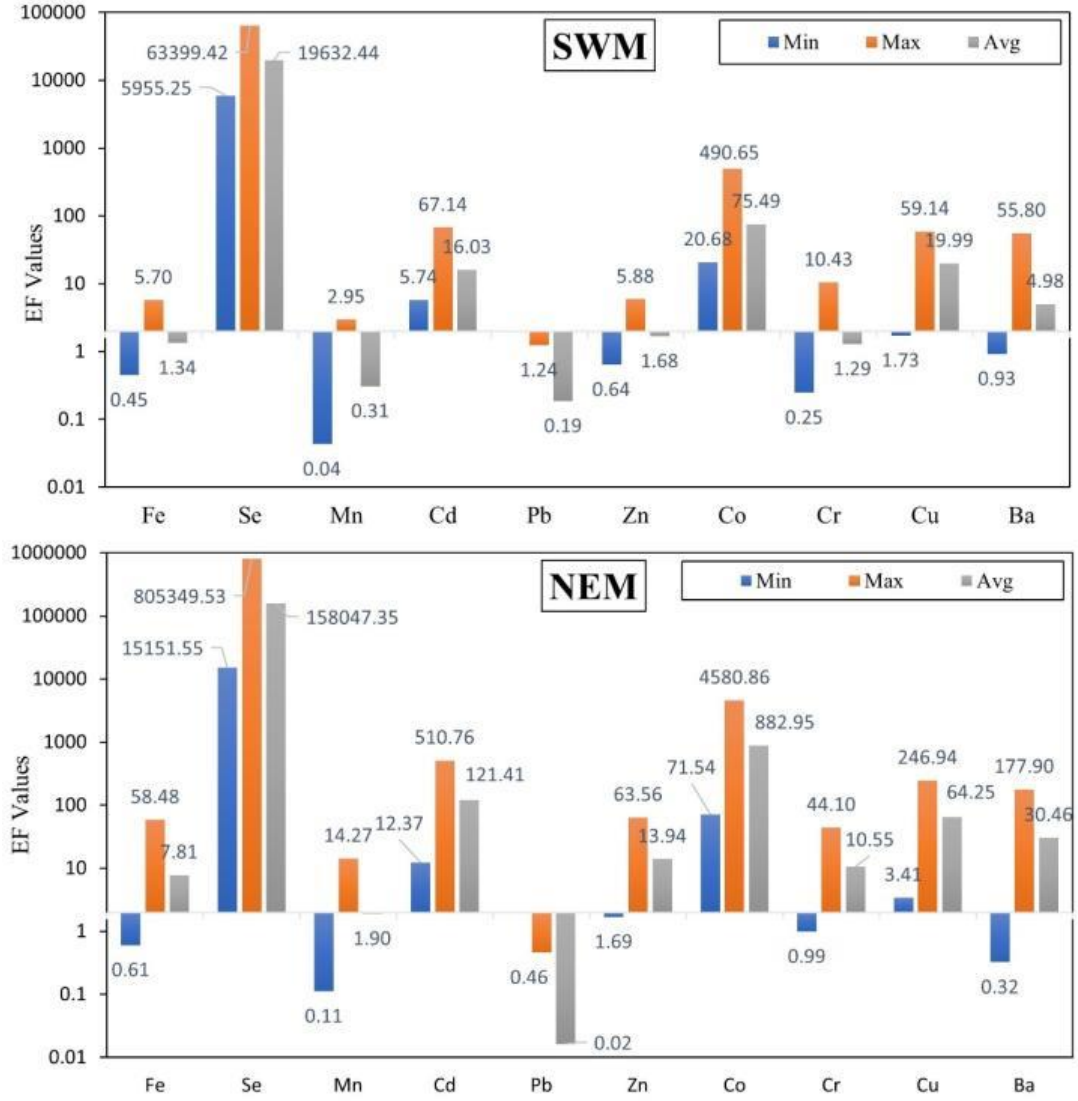

Fig. 5.9 Cluster column plot showing EF of metals during SWM and NEM

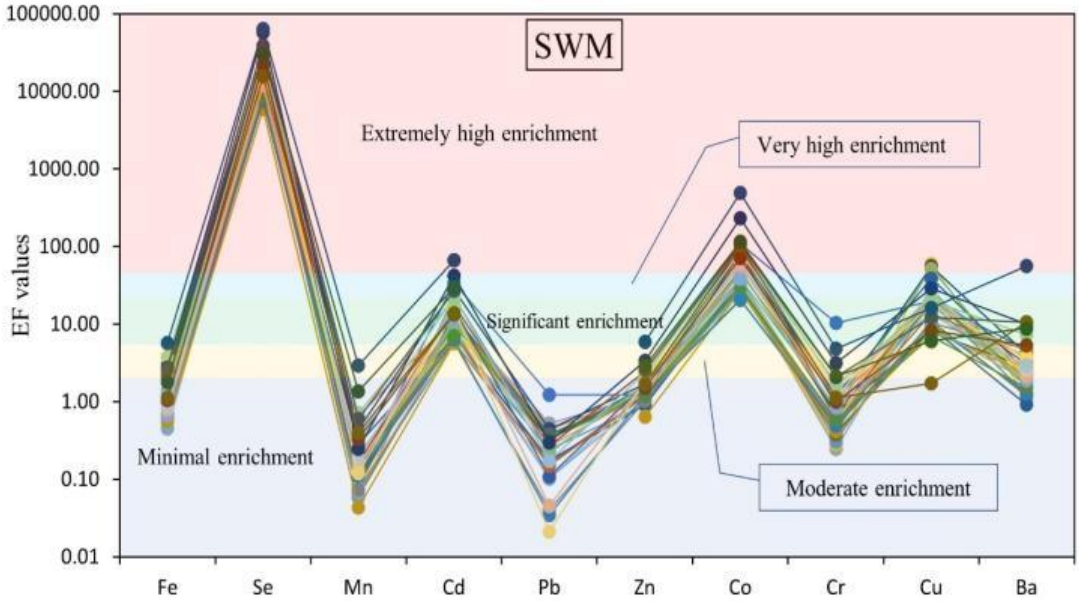

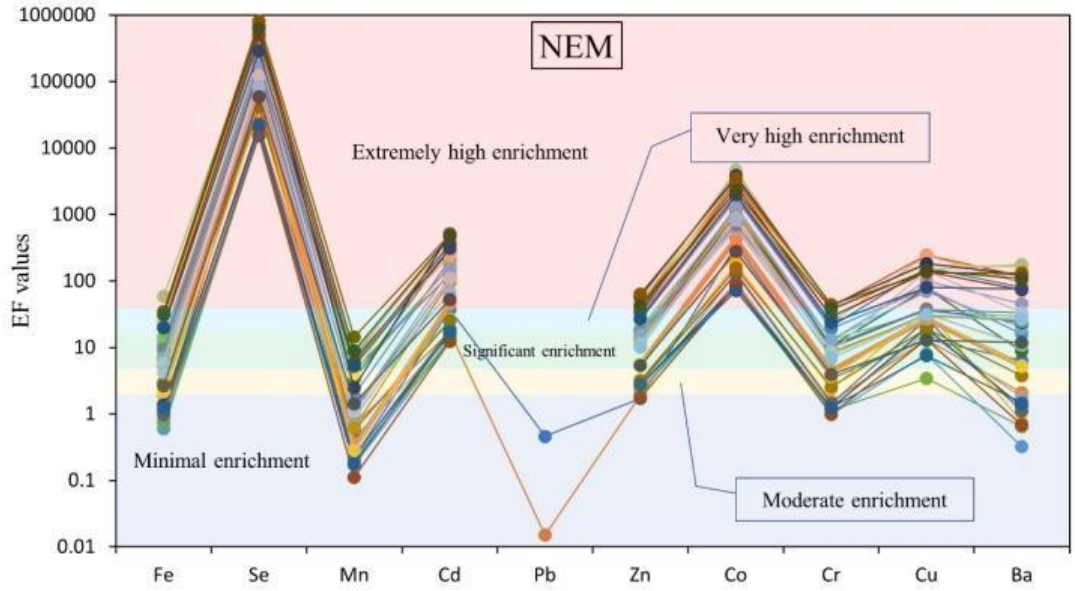

Fig. 5.10 Scatter plot showing EF variation of metals in sediments during SWM and NEM

5.3.3.3 Contamination factor (CF)

During SWM, the sequence of CF in decreasing order can be seen as Se > Co > Cu > Cd > Ba > Zn > Fe > Cr > Pb > Mn. The mean value of CF suggests that Se, Co, Cr and Cd are very highly contaminated in Sibuti estuarine sediments (Fig. 5.11). Meanwhile, the sediments are moderately contaminated by Ba, Fe and Zn. Elements like Pb, Zn and Cr mean values indicate low contamination of sediments with these elements (Fig. 5.11).

Stations-wise variation of CF suggests that all the stations are very highly contaminated by Se, Cd and Co, whereas 32 (88.89%) stations are very highly contaminated with Cu (Fig. 5.12) and the rest show moderate to considerable contamination. In the case of Ba, 4 (11.11%) and 9 (25%) stations show very high contamination and considerable contamination respectively, whereas the 23 (63.89%) stations are moderately contaminated. Moderate contamination of Zn was observed at 35 (97.22%) stations during this season. In the case of Fe, 17 (47.22%) stations are moderately contaminated, and the rest show low contamination. Likewise, contamination of Cr at 4 (11.11%) and 1 (2.78%) of the stations are moderate and considerable respectively whereas the rest 31 (86.11%) stations show low contamination. Metals like Mn and Pb show low contamination at all the stations during this season (Fig. 5.12).

During NEM, the decreasing sequence of metals can be observed as Se > Co > Cd > Cu > Ba > Zn > Cr > Fe > Mn > Pb. The mean CF values suggest that the majority of the sample stations are very highly contaminated with Se, Co, Cd and Cu. Metals like Ba, Cr and Zn are moderately contaminated whereas Fe, Mn and Pb are in a minimal contamination zone (Fig. 5.11) as compared to their PAAS values (Taylor & McLennan, 1985; McLennan, 2001).

Station-wise variation shows all the stations to be very highly contaminated with Se, Cd and Co during this season. In the case of Cu, 16 (44.44%) stations are very highly contaminated and the remaining 20 (66.66%) of the stations are in the considerable contamination category. In the case of Ba, 12 (33.33%) and 17 (47.22%) stations are considerable and moderately contaminated respectively. The contamination of Zn and Cr at 35 (97.22%) stations is moderate except the station nearest to the sea, whereas Fe, Mn and Pb show minimal contamination at all the stations (Fig. 5.12).

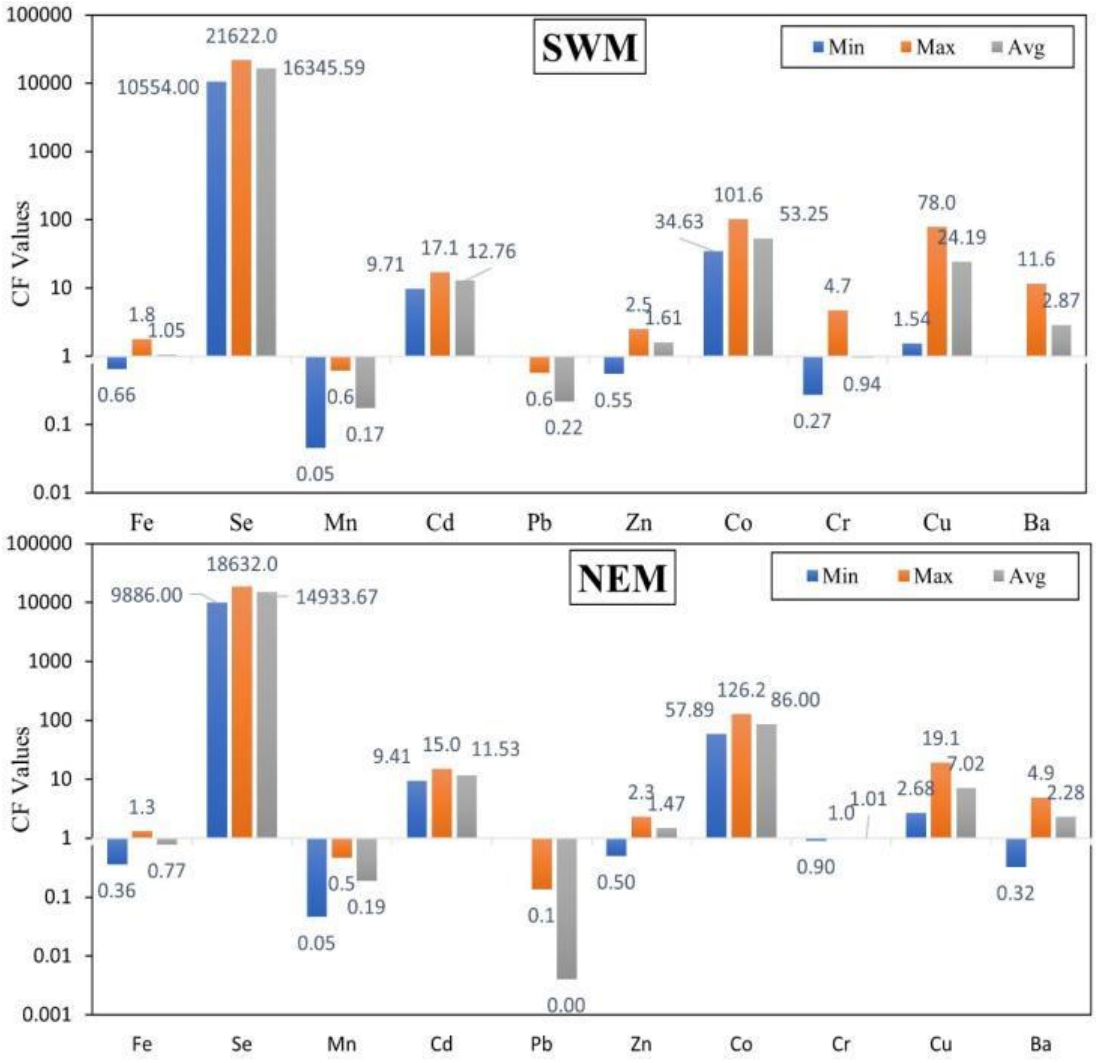

Fig. 5.11 Cluster column plot showing CF of metals during SWM and NEM

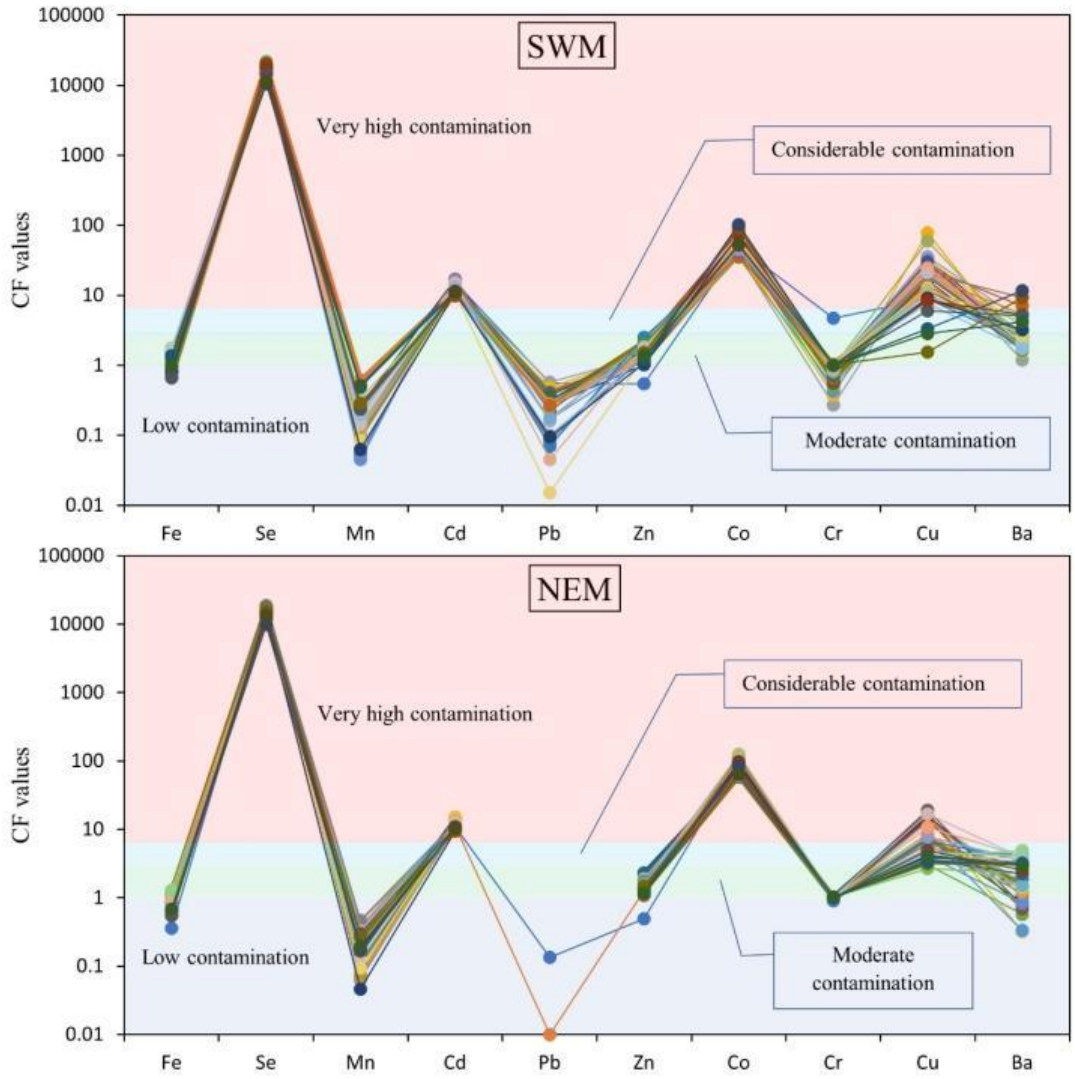

Fig. 5.12 Scatter plot showing CF variation of metals in sediments during SWM and NEM

5.3.3.4 Discussion

The very high enrichment and contamination of chalcophile elements like Se, Co along with Cu, Cd in the estuary were confirmed by all the above indices. Apart from that, moderate enrichment of Ba, Cr and Zn were also reported by these indices. High enrichment of these metals might be the result of heavy leaching from superficial sediments from the source region. The oxidation of metal sulfides (Hongxiao et al., 1994) from the source like pyrite concretions and shale beds with coal laminae (Nagarajan et al., 2017a; Williams et al., 1934), lignite beds (Sia et al., 2012; Yudovich et al., 2006) and weathering siliciclastic sediments of Sibuti and Lambir formations (Nagarajan et al., 2015; Nagarajan et al., 2017a) are combinedly contributing to such enrichment. This leaching process is enhanced by the tropical condition and high rain

in the region along with land-use changes like deforestation causing an increased soil erosion (Zhang et al., 2020) for the last 3 decades (Browne et al 2019; Bryan et al., 2013; Krawczyk et al., 2020). In addition, ideal conditions for absorption (pH: 5 to 7) have been observed in the estuary, leading to more deposition (Zhang et al., 2018) enhanced by tidal influence from the South China Sea. The river basin was reported to be rich in all these metals (Table 5.13). The clastic sediments of Sibuti Lambir formations have the highest concentration of Cu and Ba in it (Nagarajan et al., 2015; Nagarajan et al., 2017a) and are higher than the preindustrial PAAS values (Taylor & McLennan, 1985, 1995; McLennan, 2001), whereas a higher concentration of Co and Cr was reported in pyrite and shale concretions in Sibuti and Setap formations (Table 5.13). However, the availability of Cd and Se has not been considered in the source of Sibuti basin region in previous studies. However, the anthropogenic source like the agricultural activities in the river basin associated with peat soil in the NW of the Sarawak region are the main sources of Se (Chang et al., 2020) and Cd input, mainly from phosphate-based fertilizers (Zaharah et al., 2014; De Boo et al., 1990) where they are enhancing the contamination in riverine along with estuarine sediments. In the case of geogenic contributors, PCA analysis confirmed the association of Co and Se with other chalcophile elements such as Fe, Cu and Zn during both seasons (Fig. 5.5 and 5.6), indicating the origin from same sources.

Table 5.13 Comparison of selected metal average concentration (in mg kg^{-1}) in the sediments, various formations in the source area and PAAS values

Area of Study	Fe	Mn	Cu	Zn	Ba	Co	Se	Cr	References
Sibuti River Estuary	46012	168.71	703. 22	130.78	1894.6	757.24	-	101.795	**Present study**
Miri coast (SW part)	2948	26.6	217.5	95.6	-	1.3	-	49.48	Nagarajan et al., 2019
Lambir Formation	20340	375	81.75	60.88	140.25	6.94	-	51.5	Nagarajan et al., 2017a
Sibuti Formation	38900	500	72.8	116.54	774.1	7.97	-	53.33	Nagarajan et al., 2015; 2017a
Tukau Formation	21960	94	41.32	60.56	171.92	23.4	-	-	Nagarajan et al., 2017b
Shale and Pyrite concretion (Sibuti and Setap formation)	234600	7700	19.97	66.35	390.96	102.64	-	110.76	Azrul NIsyam et al., 2013
PAAS Values	50499	852	50	85	650	23	0.05	110	Taylor and McLennan, 1985;McLennan, 2001

5.3.3.5 Pollution load index (PLI)

The sediment quality is dependent on the contamination factor (CF) of the considered metals. Considering the calculated PLI in the current study area, all the stations have PLI values of more than 1 and are collectively polluted with considered metals (Fig. 5.13). The higher CF of metals like Se, Cd, Cu, Co, and Zn are mainly contributing towards the higher PLI values at all the stations. However, the majority of the metal contamination is through leaching of minerals from geogenic sources rather than anthropogenic influence. In addition, the present represents the fine fraction of the bulk sediments and thus normally accumulates more metal concentration than the bulk fraction which is the mixture of fine and coarse fractions of the sediments.

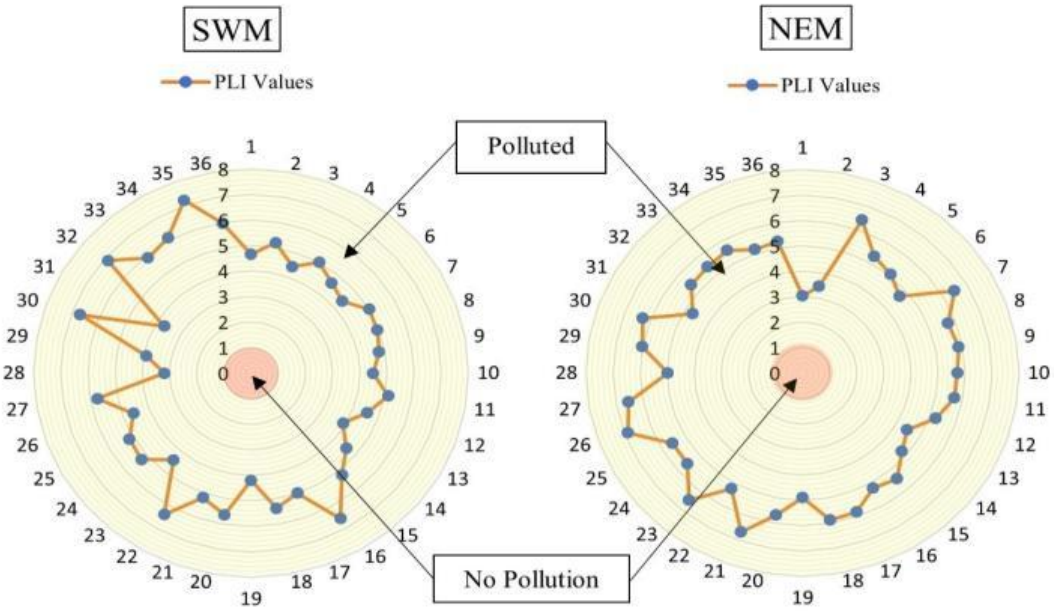

Fig. 5.13 Radial Plot showing PLI for SWM and NEM

5.3.3.6 Potential ecological risk index (PERI)

In the present study area, calculated PERI values range from 308.26 to 718.25 and 301.59 to 502.34 during SWM and NEM respectively. The average value of PERI during SWM (PERI: 478.4) and NEM (PERI: 384.63) falls under the considerable ecological risk category. Furthermore, 88.89 & 11.11% of the samples pose a considerable and very high ecological risk during SWM (Fig. 5.14) whereas all the stations are in the considerable risk category during NEM.

5.3.3.7 Sediment pollution index (SPI)

In the current study area, the SPI calculated during SWM & NEM ranges from 9.6 to 16.7 & 9.19 to 14.67 with respective mean values of 12.14 & 11.3. The plot (Fig. 5.15) reveals that 33 (91.66 %) stations during SWM and 31 (86.11%) stations during NEM fall under the highly polluted category, whereas the rest fall under the moderately polluted category. As SPI is dependent on trace metal concentration and consideration of the toxicity of the respective metal, higher enrichment of Cd (toxicity weight: 300; Singh et al., 2002) is mainly contributing towards higher SPI values at all the stations.

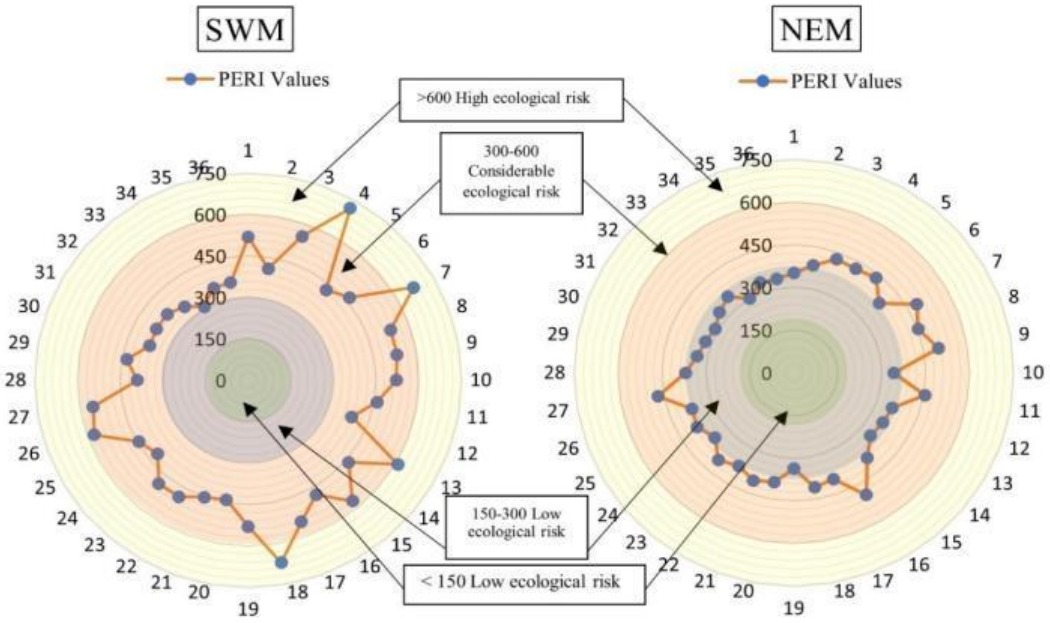

Fig. 5.14 Radial Plot showing PERI for SWM and NEM

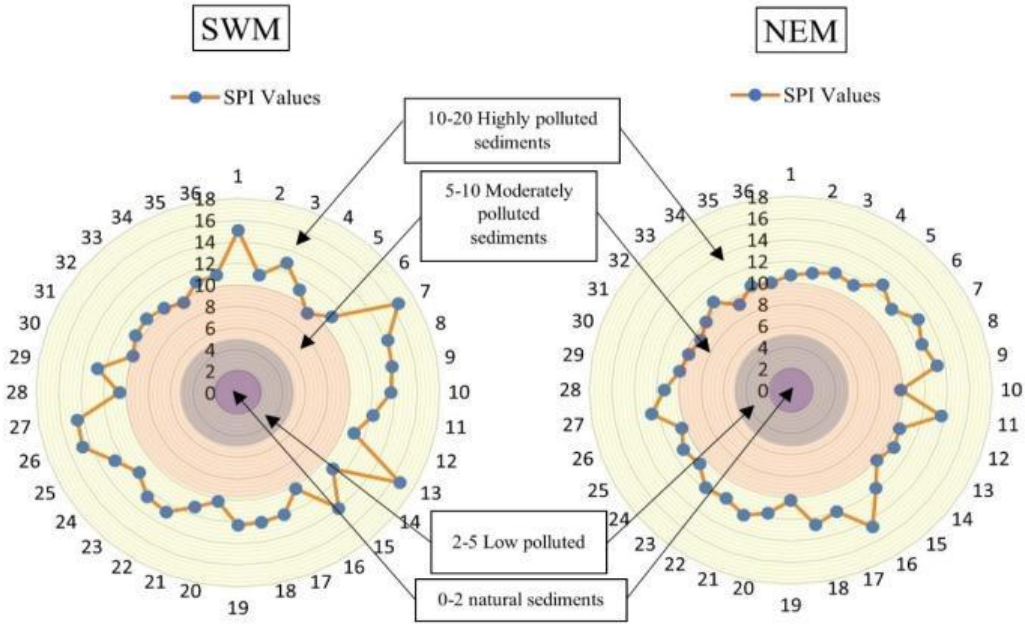

Fig. 5.15 Radial Plot showing SPI for SWM and NEM

5.3.3.8 Effect range low (ERL) and Effect range median (ERM)

During SWM, Cu concentration indicates the highest possible biological effects on living organisms as 91.66% of the sample stations have higher concentrations than ERM values. In addition, the Cr concentration nearest to the sea has a higher concentration than the ERM values. These 2 metals may pose frequent threats to the sediment-dwelling living organisms. Cr concentrations recorded in the range between ERL and ERM with 72.22% of the stations fall in this group and are most likely to have occasional adverse biological effects towards living organisms. Cr is followed by Zn (33.33% of sample stations in ERL-ERM) and Cu (8.33% of stations in ERL-ERM) and is likely to have such similar effects. Furthermore, Zn and Cr have concentrations in 66.66% and 25% of samples, lower than ERL values (Fig. 5.16). These elements do not pose any threats to the biological community in the estuary. The toxic metals Pb and Cd concentrations are recorded lower than the ERL values, indicating no threats are posed by these metals to the aquatic organisms. However, a significant portion of these metals is associated with an exchangeable fraction which may affect the aquatic system at certain conditions.

During NEM, Cu poses the highest adverse threat to the biological communities in the estuary as 47.22% of the stations recorded higher concentration than the ERM value. The occasional adverse effect can be expected from Cu, Zn and mainly from Cr as 100% of the stations recorded these elemental concentrations between ERL and ERM values, whereas 52.77% and 22.22% of stations recorded Cu and Zn concentrations between this range (Fig. 5.17). Elements like Pb and Cd recorded their concentrations lower than ERL at all the stations along with 77.77% of stations which recorded the Zn concentration to be lesser than the ERL values and pose little to no threat to the benthic organisms.

Table 5.14 Considered SQGs values and percentage of stations under biological effect of metals in surface sediments during SWM and NEM

Elements	Guidelines (Long et al., 1995) in mg kg^{-1}		Percentage of incidence effects		
	ERL	ERM	<ERL	ERL-ERM	>ERM
SWM					
Cu	34	270	0	8.33 (3/36)	91.66 (33/36)
Pb	46.7	218	100 (36/36)	0	0
Zn	150	410	66.66 (24/36)	33.33 (12/36)	0
Cd	1.2	9.6	100 (36/36)	0	0
Cr	81	370	25 (9/36)	72.22 (26/36)	2.77 (1/36)
NEM					
Cu	34	270	0	52.77 (19/36)	47.22 (17/36)
Pb	46.7	218	100 (36/36)	0	0
Zn	150	410	77.77 (28/36)	22.22 (8/36)	0
Cd	1.2	9.6	100 (36/36)	0	0
Cr	81	370	0	100 (36/36)	0

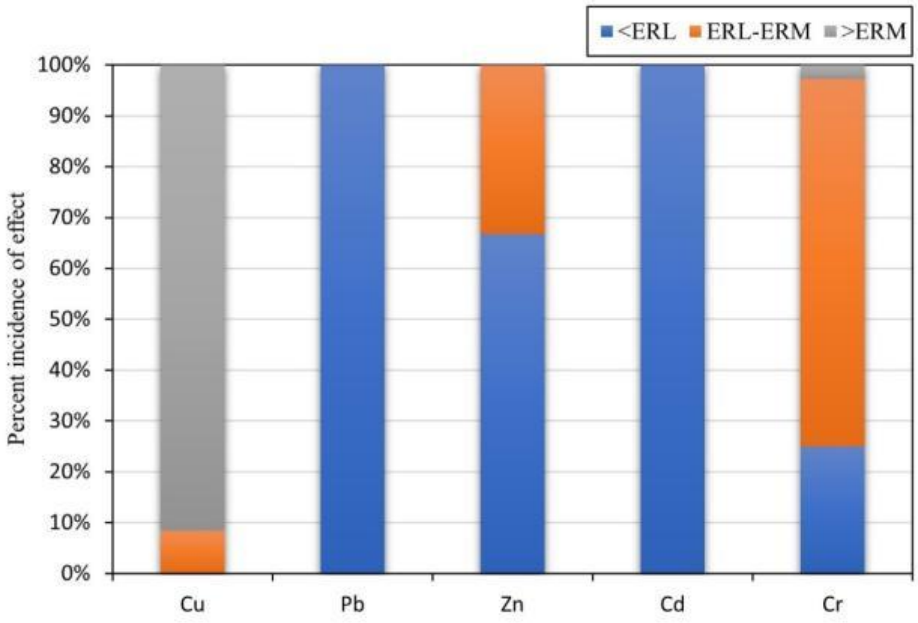

Fig. 5.16 Biological effect of metals in sediments during SWM

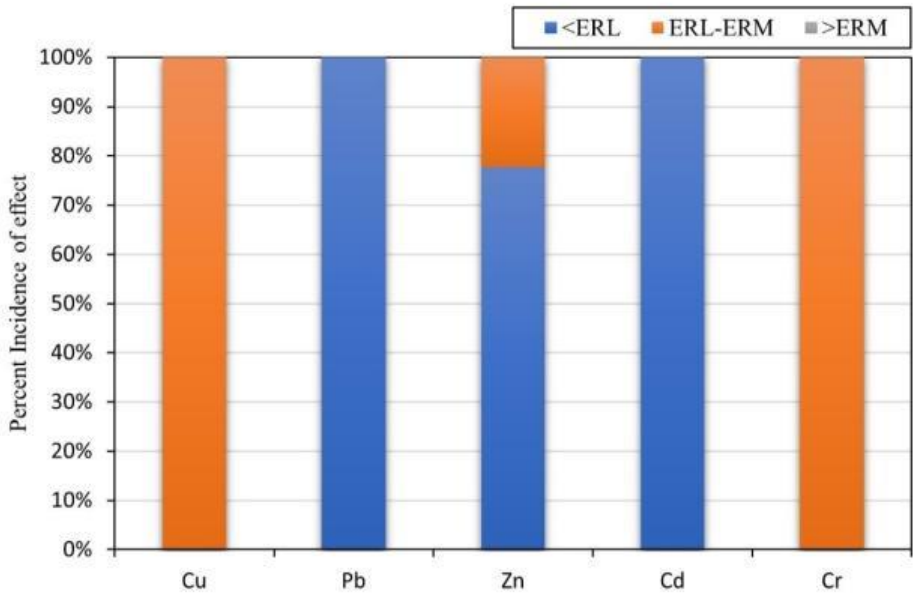

Fig. 5.17 Biological effect of metals in sediments during NEM

5.3.3.9 Risk assessment code (RAC)

In the current study, the association of metals like Co, Cu, Mn, Pb, Zn, Se, Fe, Al, Cd, Cr and Ba in exchangeable fraction and carbonate fraction are taken into consideration and the results are shown in Table 5.15 and 5.16. During SWM, Cd possesses the highest risk as all the stations are reported to be associated with the F1 and F2 fractions and thus it is very high in risk followed by 69.44% stations for Pb, 63.89% stations for Mn, and 13.89% of stations for Ba which show the high association of these fractions, thus they are very high-risk too. The high-risk category is dominated by Se (94.44% of stations), followed by Ba (61.11% of stations), Mn (27.78% of stations), Zn (19.44% of stations) and Cu (2.78% of stations). The medium-risk category is represented mainly by Co and Zn as 91.67% and 52.78% of the stations reported having 11-30% concentration in exchangeable and carbonate fraction. Cu and Fe at the majority of the stations fall under the low-risk category (1-10%) as 91.67% and 80.56% of stations show their association in exchangeable and carbonate fractions. In addition, Al and Cr in most of the stations are least associated with the carbonate and exchangeable fractions of the sediments and possess no risk to the benthic system in the estuary.

During NEM, Mn and Cd possess a major threat because of their mobility and their association with carbonate and exchangeable fractions. Cd in 100% of the stations reported to be very high-risk for Cd whereas 69.44% of the stations reported the same

for Mn during this season. Similarly, Ba and Mn at 30.56 and 22.22% of the stations are mainly associated with the F1 and F2 fractions and fall in a high-risk category, which are suspected to have an adverse effect on the benthic community during its mobility. In case of Co and Cu, 94.44% and 58.33% of the stations fall under medium risk category. Similarly, Zn, Fe and Al are in the low-risk category and pose little or no biological threat. Besides, 100, 94.44, and 30.56% of stations are reported to have Cr, Pb and Al concentration in F1 and F2 fractions at no risk category during this season.

Table 5.15 Station wise Risk assessment code (RAC) of sediments during SWM

Sample Stations	Co	Cu	Mn	Pb	Zn	Se	Fe	Al	Cd	Cr	Ba
1	M	L	V	V	M	M	M	L	V	N	H
2	M	L	H	V	L	H	L	N	V	N	H
3	M	L	H	V	M	H	L	N	V	N	H
4	M	L	H	V	L	H	L	N	V	N	H
5	M	L	V	V	H	H	L	N	V	N	H
6	M	L	V	V	H	M	L	N	V	N	H
7	L	L	V	V	M	H	L	N	V	N	H
8	L	L	V	V	L	H	L	N	V	N	H
9	L	L	V	V	H	H	L	N	V	N	H
10	M	L	H	V	H	H	L	N	V	N	H
11	M	L	M	V	L	H	L	N	V	N	V
12	M	L	V	V	H	H	L	N	V	N	H
13	M	L	V	V	M	H	L	N	V	N	H
14	M	L	V	V	H	H	L	N	V	N	V
15	M	L	V	V	L	H	L	N	V	N	V
16	M	L	V	N	L	H	L	N	V	N	H
17	M	L	V	V	M	H	L	N	V	N	H
18	M	L	H	V	M	H	L	N	V	N	M
19	M	L	V	V	M	H	L	N	V	N	V
20	M	L	M	V	M	H	L	N	V	N	H
21	M	L	M	V	M	H	L	N	V	N	H
22	M	L	H	N	L	H	L	N	V	N	H
23	M	L	H	V	M	H	L	N	V	N	L
24	M	L	V	N	L	H	L	N	V	N	M
25	M	L	H	N	L	H	L	N	V	N	M
26	M	L	H	V	M	H	L	N	V	N	M
27	M	L	H	N	L	H	M	N	V	N	L
28	M	L	V	V	M	H	M	N	V	N	M
29	M	L	V	V	M	H	M	N	V	N	L
30	M	L	V	N	H	H	L	L	V	N	M
31	M	L	V	V	M	H	M	N	V	N	H
32	M	L	V	N	M	H	M	N	V	N	H
33	M	L	V	N	M	H	L	N	V	N	H
34	M	H	V	N	M	H	M	N	V	N	H
35	M	M	V	N	M	H	L	N	V	N	V
36	M	M	V	N	M	H	L	N	V	N	H

****N**-No Risk; **L**-Low Risk; **M**- Medium Risk; **H**-High Risk; **V**-Very High Risk*

Table 5.16 Station wise Risk assessment code (RAC) of sediments during NEM

Sample Stations	Co	Cu	Mn	Pb	Zn	Se	Fe	Al	Cd	Cr	Ba
1	M	M	V	V	M	H	L	N	V	N	L
2	M	L	H	V	L	H	L	N	V	N	L
3	M	L	V	N	L	H	L	N	V	N	M
4	M	L	H	N	L	H	L	N	V	N	M
5	M	L	H	N	L	H	L	N	V	N	M
6	M	M	H	N	L	H	L	N	V	N	M
7	M	L	H	N	L	H	L	L	V	N	M
8	M	L	H	N	M	H	L	N	V	N	M
9	M	L	M	N	L	H	L	N	V	N	V
10	M	L	V	N	M	H	L	N	V	N	V
11	M	L	M	N	L	H	L	N	V	N	V
12	M	L	V	N	M	H	L	L	V	N	V
13	M	M	V	N	M	H	L	L	V	N	H
14	M	L	V	N	M	H	L	L	V	N	H
15	M	M	V	N	L	H	L	L	V	N	M
16	M	L	M	N	L	H	L	L	V	N	H
17	M	M	H	N	M	H	L	L	V	N	H
18	M	M	V	N	H	H	L	L	V	N	H
19	M	M	V	N	H	H	L	L	V	N	H
20	M	L	V	N	L	H	L	N	V	N	M
21	M	M	V	N	L	H	L	L	V	N	H
22	L	M	V	N	L	H	L	L	V	N	H
23	M	M	V	N	M	H	L	L	V	N	H
24	M	M	V	N	M	H	L	L	V	N	H
25	M	M	V	N	M	H	L	L	V	N	M
26	M	L	V	N	M	H	L	M	V	N	M
27	M	L	V	N	M	H	L	L	V	N	M
28	M	M	V	N	M	H	L	M	V	N	M
29	L	M	V	N	M	H	L	L	V	N	M
30	M	M	V	N	H	H	M	H	V	N	M
31	M	M	V	N	H	H	L	H	V	N	M
32	M	M	V	N	M	H	L	M	V	N	L
33	M	M	V	N	M	H	L	L	V	N	M
34	M	M	V	N	M	H	L	M	V	N	M
35	M	M	V	N	M	H	L	M	V	N	M
36	M	M	V	N	L	H	L	M	V	N	H

***N**-No Risk; **L**-Low Risk; **M**- Medium Risk; **H**-High Risk; **V**-Very High Risk*

5.4 Summary

- In sediments, trace metal concentrations such as Co, Cu, Pb, Al, Fe and Ba showed significant variation between the seasons, where Al and Fe concentrations being the highest during SWM and NEM respectively.
- Sequential extraction of sediments revealed that a higher proportion of Pb, Cd and Mn dominated the exchangeable fraction whereas Cd and Se were found in a higher proportion in carbonate fraction. The highest concentration of all the metals was found in the residual fraction except for Cd and Mn, which were found to be highest in the exchangeable fraction.
- Leaching of pyrite concretion and absorption of various metals such as Cu, Se and Zn were controlled by Fe oxyhydroxides and clay minerals during SWM, whereas chalcophile metals (Cu, Zn and Cd) were controlled by mainly clay minerals during NEM. Ba was controlled by reducible organic matter during SWM whereas precipitation of Ba in suspended solids was confirmed during NEM.
- Factor model of various fractions during SWM revealed the formation of Mn hydroxides and working as a major mechanism for absorption of Co, Cr, Cu, Zn and Ba in the lower part. Fe hydroxides and clay minerals mainly controlled metals such as Cu, Zn and Cd in the upper part of the estuary. Metals such as Se and Ba were mainly controlled by organic matter in the estuary.
- During Mn and Fe hydroxides formation under oxic conditions, absorption of Co and Ba along with Zn in upper part whereas clay and carbonate minerals in lower part were observed. Fe complexes with organic matter controlled Cu, Zn and Al absorption in exchangeable and reducible fractions.
- Estuarine sediments were found to be highly contaminated by Se, Co, Cu and Cd and possess high ecological risk on the aquatic biota.

Chapter-6

Geochemistry of Suspended solids

6.1 Introduction

The suspended solids (SS) refer to the concentration of organic and inorganic matter held in the water column of river water or streams due to the influence of turbulence and is a major influencer of turbidity (Bilotta et al., 2008). Rivers around the world carry 13.5×10^9 tons of suspended solids towards the sea (Eisma et al., 1988). All kinds of streams carry a certain amount of suspended solids in the water column under natural conditions (Ryan, 1991) and are mainly identified to be typically less than 63 μm in diameter (Waters, 1995; Bilotta et al., 2008). In an aquatic ecosystem like an estuary, hydrodynamic forces such as tides from the oceanic end and fluid transport from the riverine end are responsible for the majority of the suspended solids' concentration in water. Due to the influence and mixing of water from both ends, changes in the chemistry of suspended solids take place under varying hydrological conditions (Mehta et al., 1989; Regnier et al., 1993). At many river mouths, however, only very small amounts of bedload reach the sea, most of the supply being deposited in the lower reaches of the river, or the estuary (Eisma et al., 1988). In such an environment, cohesive aggregates play a major role in the sorption of various suspended and dissolved chemical constituents (Mehta et al., 1989; Kronvang et al., 2003). Likewise, the interaction of these suspended solids with estuarine sediments complicates the process more due to the heterogeneous physicochemical nature and content of detrital material of organic origin in bedload sediments. Thus, in a brackish water environment like an estuary, where a mixture of silt-and clay-sized sediments commonly occurs, the suspended solid concentration tends to be an agglomeration of aggregated and unaggregated sedimentary units with a wide range of sizes, shapes, strengths, densities and settling velocities (Mehta et al., 1989).

The enhancement of such particles is mainly contributed by anthropogenic/geogenic perturbations enhanced by the high flow rate of river, a higher rate of geogenic weathering in the river basin and flooding, decay of organic matter, which leads to physical and chemical changes in the waterbody (Bilotta et al., 2008; NRC, 1977). The particles of biogenic origin absorbed, or exchangeable substances do not

necessarily follow the resisting properties of bedload sediments. These particles can be mobilized frequently and follow much shorter cycles than the resistant sediment particles at the bottom (Eisma et al., 1988). Such chemical alterations with varying environmental conditions lead to the release of contaminants like various metals (Dawson et al., 1988; Kronvang et al., 2003; Bilotta et al., 2008). In addition, adsorbed substances like metals tend to associate with the fine size fractions which have a much larger specific surface, and due to the presence of clay minerals and organic matter, they are far more surface-active than comparatively larger sediments. The absorption of metals on suspended solids in the water column is also a prominent process in aquatic systems due to the availability in the water table besides working as a medium between metals that are dissolved and in particulate phase. This helps to describe the geochemical properties of such metals in such systems (Regnier et al., 1993). On the other hand, the accumulation of the trace elements on these particles induces harmful effects towards aquatic biota and initiates several complex chemical processes between water and sediment interface, while being a major source of transport of such to the sea (Song et al., 2010). Hence, the study of the composition of suspended solid matter is necessary along with the dissolved elements and settled sediments if the complete assessment of estuarine fluxes and pollution indicators are to be performed (Nasrabadi et al., 2018; Regnier et al., 1993; Wollast, 1982).

Considerable amounts of suspended solids can also come from coastal runoff, from erosion of older deposits along the shore or in the near-shore sea, from the atmosphere (mostly dust), waste dumping, and organisms. These contributions might be insignificant in the case of large river estuaries compared to river supply, however, small river estuaries like Sibuti can be highly influenced by such additions and help highlight the local source significance (Eisma et al., 1988). The Sibuti river estuary represents the continental input from the Sibuti river basin, which includes major geological formations like Sibuti and Lambir, that mainly consists of siliciclastic sedimentary rocks such as sandstones and shales with a thin layer of limestones (Nagarajan et al., 2017a). The formations like Sibuti and Setap have pyrite concretions within the shale beds, and the leaching of metals was reported in previous studies (Anandkumar, 2016; Nagarajan et al., 2019). These formations are prone to high chemical weathering under tropical weathering conditions and the erosion processes are enhanced due to the effect of the land use changes in the catchment area. The

deforestation happening over the years stands at 26% loss of forest cover since 1970 in Borneo and is contributing towards the physico-chemical weathering (Krawczyk et al., 2020). In such a case, the compositional study of particulate matter is necessary for the estuary to identify the contaminants interacting with it. In addition, a chemical tracer of such particles can be used to identify the effect on the coastal environment (Song et al., 2014; Daskalakis et al., 1995; Zhang et al., 1995) as it has been reported that these particulate matters were reported to be the major influencers of algae cover present on the Miri-Sibuti coral reefs (Browne et al., 2019). Taking the above mentioned scenarios into consideration including the geological conditions around the Sibuti river basin, the suspended sediment samples were collected from 5 stations during both seasons (SWM and NEM). The interval between each station was approximately 10 kms starting from the river mouth. In this chapter, variation and availability of identified metals such as Co, Cu, Mn, Fe, Al, Pb, Zn, Se, Cd, Cr and Ba associated with suspended solid matter during SWM and NEM are discussed. In addition to that, the source of the metals associated with the suspended solids, the degree of contamination and the depositional conditions in the estuary are also addressed.

6.2 Results

6.2.1 South-West Monsoon (SWM)

The descriptive statistics for the geochemistry of SS during the SW monsoon (SWM) are presented in Table 6.1. The concentration of Co during this season varies from 651 to 1650 mg kg1 with a mean value of 1145.4 mg kg^{-1}. The concentration of Cu varied from 752.3 to 1545 mg kg^{-1} with an average value of 1026.58 mg kg^{-1}, whereas Al concentration ranged from 17310 to 21045 mg kg^{-1} with a corresponding average of 19282 mg kg^{-1}. Likewise, metals like Mn ranged from 785.5 and 33430 mg kg-1 with a mean value of 1158.8 mg kg^{-1}, whereas Fe ranged from 1573 and 46890 mg kg^{-1} with average values of 38244 mg kg^{-1}. The concentration of Zn varied from 158.5 mg kg^{-1} to 279.5 mg kg^{-1} with an average of 232.6 mg kg^{-1}. The concentration of Cd ranged from 4.7 to 12.8 mg kg^{-1} with an average of 6.7 mg kg^{-1}. On the other hand, the concentration of Pb and Cr were observed below detection (BDL) levels in suspended solids during this season. The dominance of metals like Fe and Al has been noticed at all the stations (Fig. 6.1). The abundance of metals in descending order is as follows:

Fe > Al > Mn > Co > Cu > Ba > Zn > Se > Cd > Pb = Cr

6.2.2 North-East monsoon (NEM)

The descriptive statistics of metals observed during NEM are presented in Table 6.1. Co during NEM fluctuates from 1287 to 2389 mg kg^{-1} with a mean value of 1879.6 mg kg^{-1}. The fluctuation of Cu varied from 187.6 to 854.2 mg kg^{-1} with an average of 548.6 mg kg^{-1}, whereas Al ranged from 4335.5 to 10670 mg kg^{-1} with a mean value of 7645.1 mg kg^{-1}. The concentration of Mn varied from 1730 to 2902.5 with a mean value of 2321.8 mg kg^{-1}, whereas Fe ranged from 23340 and 37610 mg kg-1 with an average value of 29116 mg kg^{-1} Similarly, the concentration of Zn and Cd ranged from 111.5 and 3.55 mg kg-1 to 188.5 and 6.15 mg kg-1 with a respective average of 141.3 and 4.34 mg kg-1. The concentration of Pb and Cr were observed below detection (BDL) levels during NEM.

During NEM, trace metals like Fe and Al dominate in the suspended solids in the estuary (Fig. 6.1). However, the dominance of Mn has been noticed as compared to SWM (Fig. 6.1). The abundance of metals observed during NEM in descending order is as follows:

Fe > Al > Mn > Co > Ba > Cu > Se > Zn > Cd > Pb = Cr

Table. 6.1 Descriptive Statistics of Trace Metals in Suspended solids (n=5) during SWM and NEM (in mg kg^{-1})

Metals	SW Monsoon				NE Monsoon			
	Min	Max	Mean	St. Dev	Min	Max	Mean	St. Dev
Co	651	1650	1145.4	426.5	1287	2389	1879.6	416.5
Cu	752.3	1545	1026.6	322.3	187.6	854.2	548.6	315.
Mn	785.5	1573	1158.8	386.7	1730	2902.5	2321.8	503.5
Zn	158.5	279.5	232.6	60	111.5	188.5	141.3	30.7
Se	86	436	225.7	142.4	14	293	212.4	112.8
Fe	33430	46890	38244	5291.8	23340	37610	29116	6054.7
Al	17310	21045	19282	1609.6	4335.5	10670	7645.1	2533.2
Cd	4.7	12.75	6.68	3.45	3.55	6.15	4.34	1.1
Ba	507.5	279.5	826.4	502.6	563	1601.5	1059.8	452.1

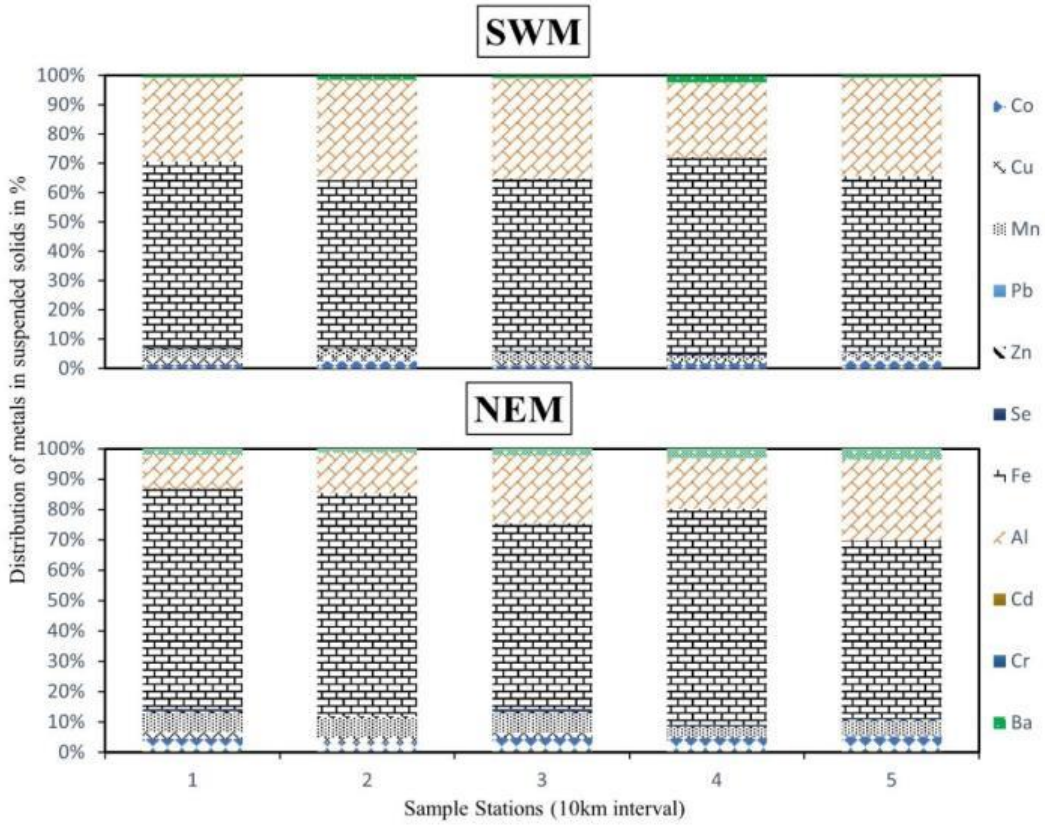

Fig. 6.1 Distribution of metals in SS samples during SWM and NEM

6.3 Discussions

6.3.1 Seasonal and spatial distribution of metals

6.3.1.1 Iron (Fe)

Fe is the dominating metal in suspended solid composition for both seasons, which might have been derived from the weathering of calcareous sandstones containing minerals like pyrite, ankerite and ferruginous sandstones rich in magnetite in Sibuti and Lambir formations (Nagarajan et. 2017; Nagarajan et al., 2015). Other than that, prominent sources of Fe in the river basin might include clastic sediments of Tukau formation (Nagarajan et al., 2017b), pyrite and shale concretion (Azrul NIsyam et al., 2013) and Miri coastal sediments (Nagarajan et al., 2019). The average concentration of Fe in these sources was briefed previously in Table 5.13. A higher concentration of Fe is noticed during SWM than NEM despite the increase in the share of Fe% at all the stations during NEM (Fig.6.1). Similar behavior of Fe was noticed for bedload sediments as well and is discussed in the previous chapter. The increase in concentration during SWM might be due to the seawater-induced turbidity and flocculation (Jilbert et al., 2016; Mayer et al., 1982), which forms Fe oxyhydroxides

and precipitation of goethite in saturation index during SWM confirms such process (Fig. 4.27). Such precipitation occurs on mixing because the seawater cations neutralize the negatively charged iron-bearing colloids, thus allowing flocculation (Boyle et al., 1977; Mayer et al., 1982; Hopwood et al., 2015). In addition, the aggregation of Fe and humic species at low salinities to form large colloids can remove almost 99% of dissolved Fe (Hopwood et al., 2015), which also has enhanced Fe concentration on suspended solids. However, during NEM, trace metals like Cu, Zn, and Fe shows a significant increase in the dissolved phase (Fig. 4.10) and decrease in solid phase (Table 6.1), while behaving non-conservatively towards mixing. This indicates the resuspension of Fe from the solid phase to the dissolved phase (Zhang et al., 1995) and working as a scavenger for these metals. On the other hand, the dominancy of freshwater during NEM is diminishing the influence of seawater-induced flocculation on suspended solids, indicating the dissolution of Fe from the suspended solids and increased in the liquid phase.

6.3.1.2 Manganese (Mn)

The behavior of Mn in SS shows an inverse nature and considerably high in concentration compared to bedload sediments. The higher average concentration observed in SS than sediments is indicative of its independence on riverine inputs during both seasons. The lower concentration of Mn during SWM (when low flow condition prevails) might be due to the higher residence time of Mn in pore waters and desorption from particles introduced due to resuspension within the estuary (Callaway et al., 1988). However, an increased concentration of Mn during NEM might be due to the oxidizing condition (Duinker et al., 1979; Wollast et al., 1979; Reigner et al., 1993), photodegradation and co-precipitation of Mn-hydroxides because of freshwater dilution (Mori et al., 2019; Oldham et al., 2017). Such Mn complexes are kinetically stabilized against Fe reduction even if the concentration of Fe is much higher in water (Oldham et al., 2017).

6.3.1.3 Aluminum (Al)

Al has been traditionally considered immobile during weathering process because of its low solubility in water. However, transport of the Al happens in the form of simple Al species in solution, polymeric materials and in small particles from the source rock in active weathering areas because of the mechanical and chemical attack on the parent

rocks (Hydes et al., 1977). Considering the fact that the geology of the Sibuti river basin is prone to mechanical and chemical weathering, this leads to the removal of mobile minerals such as clay minerals and enriches the residual elements (Nagarajan et al., 2015; Nagarajan et al., 2017a) of the river. The absence of dissolved Al in water during both the seasons (Table 4.4) and the high concentration Al in SS indicate that it is originating from catchment areas as detrital input. The alumino-oxides have dominance in clastic sediments of the river basin and are mainly found in aluminosilicates, which are common in Lambir and Sibuti formations (Nagarajan et al., 2017a). The addition of such materials in the river during the mechanical weathering process brings the existence of Al in SS. In addition, an increase in the concentration of Al has been noticed during SWM as compared to NEM. The concentration of Al is higher in the upper part of the estuary during both seasons (Fig. 6.2). However, the lower part of the estuary showed a significant spike in concentration during SWM whereas, a decline in concentration was noticed during NEM (between 30 to 0 km) (Fig. 6.1 and 6.2). The increase during SWM might be the effect of seawater-induced turbidity and resuspension of such Al-bearing particles from bed sediments into the water column in intertidal zones. On the other hand, during NEM, low tidal influence and settlement of riverine-induced particles near the river mouth lead to a decrease in the concentration of Al in SS towards the lower part of the estuary (Fig. 5.4 and Fig. 6.2).

6.3.1.4 Copper (Cu)

The sources of Cu in the river basin have been summarized in Table 5.13 in the sediment chapter and these sources are responsible for the concentration of Cu estuarine SS. In estuarine conditions, the concentration of Cu in SS during SWM was observed to be more than NEM and a gradual decline in concentration towards upstream of the estuary has been noticed during both seasons. This suggests the association of Cu with organic matter in riverine water (Regnier et al., 1993) input and eventually mineralizing on the surface of SS during the transport to sea with the effect of humic acid coating on the metalloids available on the SS (Regnier et al., 1993; Grassi et al., 2000; Mori et al., 2019; Oldham et al., 2017). The decrease in concentration during NEM can be attributed to destabilization in the influence of the seawater and progressive dilution along the mixing line cations, leading to the aggregation of colloidal materials and providing a mechanism for the removal of other

metals that tend to be adsorbed on colloid surfaces (Mosley et al., 2020; Regnier et al., 1993). In addition, desorption and solubility of Cu with organic matter in river water along with DO is a common observed factor (Regnier et al., 1993) and these oxidizing conditions favor higher particulate Mn metalloids (Duinker et al., 1979; Wollast et al., 1979). This might be the case in the flocculation of Cu in the estuary with Mn hydroxides (Fig. 6.1 and 6.2). To strengthen this further, saline water influence during high tide could reach more than 25 km in the estuary during high tide and low freshwater influx into the river, whereas during monsoons and high freshwater influx, the tidal influence is limited to 15 km as observed in previous described water chapter (Fig. 4.3). A gradual increase in the concentration of Cu and Mn has also been noticed after a 30 km distance towards the river mouth (Fig. 6.2) during NEM, which might be due to the absorption of Cu by Mn oxyhydroxides with an increase in saline water influence and diminishing humic substance strength on the metalloids. In addition, higher Cu association with reducible fraction among non-residual fraction is noticed in bedload sediments (Fig 5.1 and 5.2), which further strengthens the absorption of Cu by Mn oxyhydroxides in the lower part.

6.3.1.5 Zinc (Zn)

The presence of Zn in the Sibuti river basin and SW part of Miri coastal sediments has been reported by various previous studies (Nagarajan et al., 2015; Anandkumar et. al. 2016; Nagarajan et al., 2017a; Nagarajan et al., 2017b) and the average concentrations are summarized in Table 5.13. The concentration of Zn in the estuarine SS shows a similar pattern to that of Cu. Zn shows a higher concentration during SWM as compared to NEM. In addition, Zn has been noticed to be the highest among other metals in oxidizable fraction in bed sediment of the estuary (Fig 5.1 and 5.2). This might be the reason behind the decrease in concentration during NEM as it dissolve more under oxidizing conditions, diminishing the strength of humic acids under destabilization of saline water influence in an estuary (Mosley et al., 2020). However, the increase in concentration during SWM can be attributed to saline water-induced resuspension of Zn contained bedload sediments and absorption of Zn onto metalloids (Li et al., 2018).

6.3.1.6 Cobalt (Co)

Cobalt (Co) is uncommon as a free metal, but chemically combined forms of geogenic or anthropogenic origin are common and usually bound with other metals like Cu and Ni (Moreira et al., 2002). In the study area, Co was reported in clastic sediments of Sibuti and Lambir formation (Nagarajan et al., 2015; Nagarajan et al., 2017a) and Tukau formation (Nagarajan et al., 2017b). Other major sources include pyrite and shale concretion in Sibuti basial area and Miri coastal sediments (Anandkumar 2016; Nagarajan et al., 2019). The mean concentration of Co in the above-mentioned formations are summarized in Table 5.13, from which the shale and pyrite concretions were reported to have a maximum concentration of Co it (102.64 mg/kg^{-1}). In the estuarine SS, a higher concentration is observed at 40 km of the riverine end during both seasons and the overall increase in concentration during NEM indicates the association of Co in river-based SS as result of erosion from the river basin. But the concentration of Co in SS during both seasons is much higher than the average background values of any individual formation, thus indicating the combined influence of multiple geogenic sources available in the river basin (Table 5.13). The concentration of Co in SS favors a declining trend with salinity gradient in the estuary and behave accordingly between 10 and 30 km of the estuary (Fig. 6.2). The drop in concentration might be due to the flocculation of particles and settlement of sediments in the lower part of the estuary because of saltwater intrusion (Yang et al., 2017; Wang et al., 2003). Considering the trend of dissolved Co in water (Fig. 4.10) and concentration in SS (Fig. 6.2), they do not indicate the increase in the concentration of Co after 30 km distance, thus dissolution from the SS is not evident. Furthermore, the partitioning mobility index of bedload sediments discussed earlier shows that Co-contribution in sediments is more affiliated with the crystal structure of the minerals found in the study area (Fig. 5.1 and 5.2). So, the bedload sediments attributing more towards the absorption and desorption of Co concludes that SS is not a decisive factor for the change in concentration in the estuary (Yang et. a. 2017). These observations further strengthen the fact that gradual flocculation and settlement of SS are widespread in the estuary and the resuspension is bringing back Co-containing SS into the water table under varying conditions.

6.3.1.7 Cadmium (Cd)

Cadmium (Cd) is one of the least dominating metal in the estuarine SS (Table 6.1) but certainly has a higher concentration than bedload sediments (Table 5.1). The studies done previously on the formation situated in the Sibuti river basin have not reported or considered Cd. However, the leaching of Cd from shale and pyrite concretion was reported by Anandkumar (2016) in Miri coastal sediment studies. Apart from that, the possibility of leaching from agricultural fields from phosphate fertilizers is covered in the previous chapter under Cadmium briefing (5.3.1.9 Cd, Chapter 5). It was also noticed that Cd is mainly associated with mobile fractions like exchangeable, carbonate and reducible fractions. The property of Cd to exist as a positively charged divalent ion in the aquatic system allows it to adsorb onto solid surfaces with negative electrical charges (Benjamin et al., 1982), which includes clays, carbonate minerals and hydroxides of Fe and Mn. Cadmium is generally associated or adsorbed in SS as it is widely available in the water table and works as a major medium for absorption of leached Cd. Current observations indicate that the increase in concentration is mainly noticed in the middle region of the estuary specifically from 10 to 30 km distance from the sea and a declining trend is noticed towards the river mouth (Fig. 6.2). This enrichment of Cd in SS might be the result of leaching from agricultural fields situated around the estuary. The direct run-off from agricultural fields near Kampung Sinup and through tributaries such as Sungai Tiris near Bekenu and Sungai Kejapil (Fig. 1.4) might be the major contributors. Besides, the leaching from shale and pyrite concretion might be the contributor in the upstream region of the river. During SWM, the concentration is much higher in tributary-influenced areas and controlled by the absorption of Cd by clay minerals, and Fe and Mn hydroxides from the water table during high tide (Hao et al., 2020; Jiann et al., 2014). On the other hand, a spike in concentration is noticed during NEM in water table between 0 to 10 km distance indicating the desorption of Cd with decreasing pH and higher turbidity especially at station 1 and 2. This observation attributes to the fact that dilution of seawater influence during NEM is leading to relatively lower absorption of Cd onto the SS. Furthermore, while approaching the sea from the mixing zones, the concentration is decreasing during both seasons indicating desorption from clay minerals and favors the fact that clay minerals tend to desorb Cd from solid phase to liquid phase up to 20 to 30% with reducing pH (Hao et al., 2020). The absorbed Cd

onto Fe and Mn hydroxides can also enhance Cd desorption in the lower estuary and coastal regions where Cd chloro-complexes become dominant under seawater influence because of ion exchange (Jiann et al., 2014).

6.3.1.8 Barium (Ba)

Barium (Ba) was reported in all the major formations that have high potential to influence the river estuary and is summarized in Table 5.13. Among these sources, siliciclastic sediments of the Sibuti Formation (774.1 mg kg^{-1}) and shale and pyrite concretion (390.96 mg kg^{-1}) reported higher average concentrations. The concentration of Ba in SS is noted to be higher during NEM than SWM and the highest values were noticed at 30 km and further in the estuary (Fig. 6.2). The association and coprecipitation of Ba with Fe, Al or Mn oxides on SS in well-oxygenated conditions under the effect of freshwater infusion might be the reason behind such increased concentration (Mori et al., 2019). However, increasing saline water influence seems to be decreasing the concentration of SS containing Ba from the water table after 20km, as dissolution of Ba in estuarine water is very low and noted to be BDL at most of the stations away from the river mouth (Fig. 4.10). But higher salinity gradient near the river mouth has a strong influence on the desorption of the metal (Mori et al., 2019; Coffey et al., 1997) causing a further decrease in concentration. On the other hand, the addition of DO due to a higher amount of freshwater infusion and the addition of Ba-rich SS during NEM are the decisive factors for the notable higher concentrations.

6.3.1.9 Selenium (Se)

The presence of peat soil in various parts of Malaysia including Sarawak is identified to be the major source of Se in river streams (Chang et al., 2020). The erosion of such peat soil and lignite-bearing rocks in the various forms such as Belait, Miri, Tukau, Lambir, Nyalau, Setap and Tangap formations (Fig. 1.6; Table 1.2) can also contribute towards the Se bearing SS in estuarine water. A similar condition was reported in Hubei Province, China where Se content in coal oscillates is at 6-8.4 g/kg (Kieliszek et al., 2019). Apart from that, excessive fertilization in the agricultural area and anthropogenic activity happen through the combustion of coal, lignite, and crude oil (Kieliszek et al., 2019). According to Chang et al. (2020), Se found in Sarawak rivers is from organic inputs and shows higher affinity towards humification index and humic-like chromophoric dissolved organic matter in river streams. So, the

degradation of such organic matter under higher salinity conditions and Se affinity towards the formation of oxides (Hung et al., 1995; Kieliszek et al., 2019) along with its affinity to form metal compounds such FeSe (Dhillon et al., 2003) might be the main reason of increased concentration of Se in SS. In addition, the aerobic condition is dominant at 40 km as freshwater influence favors the presence of higher organic matter and form organic complexes with Se. This is the reason behind the higher concentration of Se reflected in a farther location from the sea. However, decreasing pH and increasing salinity towards the lower region is causing Se desorption from SS, which leads to a decrease in its concentration (Fig. 6.2).

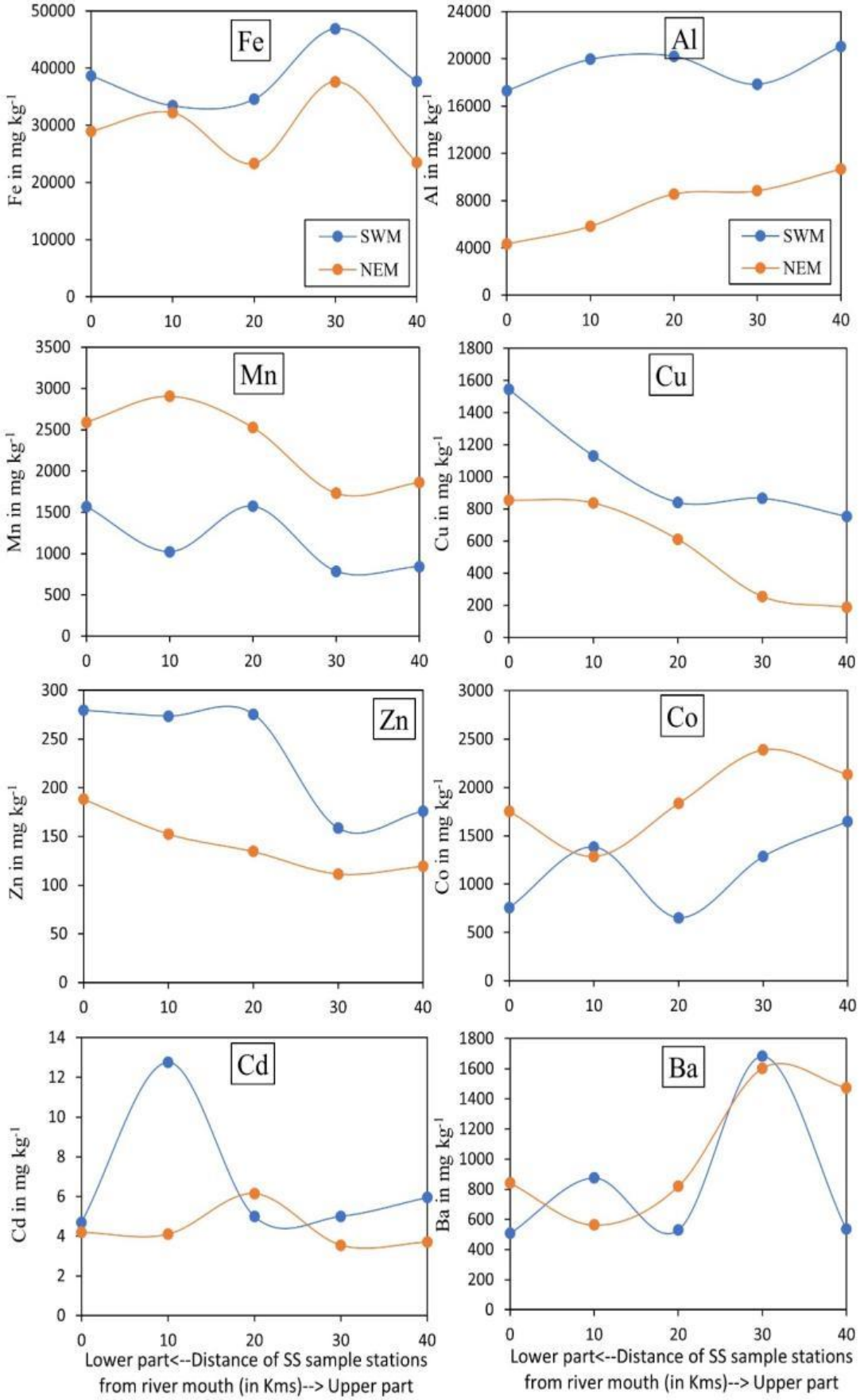
Fe
Fe in mg kg-1
SWM
NEM
Al
Al in mg kg-1
Mn
Mn in mg kg-1
Cu
Cu in mg kg-1
Zn
Zn in mg kg-1
Co
Co in mg kg-1
Cd
Cd in mg kg-1
Ba
Ba in mg kg-1
Lower part<--Distance of SS sample stations from river mouth (in Kms)--> Upper part

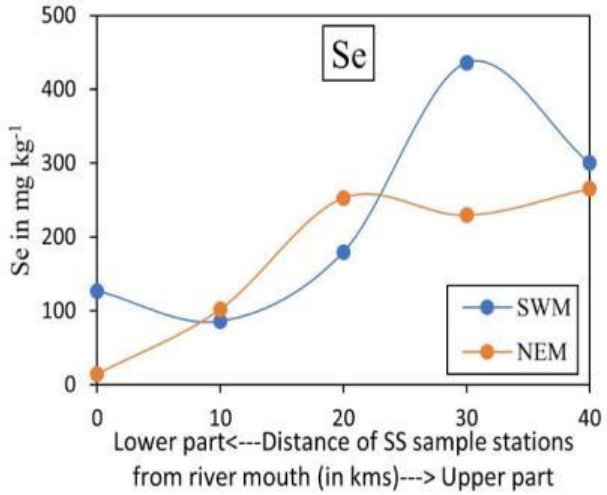

Fig. 6.2 Variation in concentration metals in SS with distance from the Sea during SWM and NEM

6.3.2 Statistical analysis

6.3.2.1 Inter-elemental relationships (Correlation matrix)

The Pearson's correlation has been utilized to determine the inter-elemental relationship between the trace metals. Physico-chemical parameters like pH, salinity, turbidity and TSS in estuarine water are reactive and have a higher tendency to control metal behavior (Thanh-Nho et al., 2018; Regnier et al., 1993; Turner et al., 2005; Morris et al., 1986; Mori et al., 2019; Coffey et al., 1997). Considering such tendency of these physico-chemical parameters, pH, salinity, turbidity and TSS (Total suspended solids) are also used in the correlation matrix to identify their influence over the metals. The correlation coefficient matrix is given in Table 6.2 and 6.3 for SWM and NEM respectively.

6.3.2.1.1 South-West monsoon (SWM)

Salinity in the estuary shows significant correlation with Cu, Mn, Zn, turbidity and TSS (r=0.961, 0.580, 0.773, 0.982 and 0.959) and significant negative correlation with Se and pH (r=-0.794, -0.944) (Table 6.2). On the hand, pH has positive correlation with Co, Se and Al (r= 0.655, 0.663 and 0.655) and negative correlation with Cu, Mn, Zn, Turbidity and TSS (r= -0.962, -0.707, -0.754, -0.958 and -0.963). Correlation of TSS and turbidity are similar to salinity in the estuary and share a positive correlation with Cu, Mn, Zn (TSS: r= 0.995, 0.527, 0.662 and Turbidity: r=0.991, 0.618, 0.661) and negative correlation with Se and Al (r= -0.666, -0.642 and -0.610, -0.615) (Table 6.3). Furthermore, metals like Co negatively correlated to Mn and Zn (r= -0.923 and -

0.670). Cu, Mn and Zn show a significant correlation with each other (Cu and Mn r= 0.539, Mn and Zn r= 0.829, Cu and Zn r= 0.621) while a negative correlation of Cu with Se and Al (r= -0.606 and -0.667), Mn with Se and Ba (r= -0.647 and -0.629) and Zn with Se, Fe and Ba (r= -0.939, -0.742 and -0.602) have been observed. In addition, Fe, Se and Ba are positively correlated to each other (Se and Fe r= 0.855, Se and Ba r= 0.687 and Fe and Ba r=0.779), whereas Se shares a negative correlation with Cd (r= -0.503) and Fe shows a negative correlation with Al and Cd (r=-0.612 and -0.524 respectively).

The reducing condition in the sediments favored by the low flow of the Sibuti river during the SWM is triggered by the degradation of organic matter. The reduced Fe and Mn, and presumably trace metals associated with hydroxide phases thereof, are injected into the overlying water column, where they precipitate and/or adsorb onto suspended particles and surficial sediments (Turner et al., 2000). The negative correlation of TSS, salinity and turbidity with pH can be justified as acidic condition that prevails in the lower part of the estuary leading to respiration of organic matter (e.g. Sun et al., 2020; Ishak et al., 2000). Such condition might be caused due to stratification of water with high tidal influence in this part of estuary while causing resuspension of SS, making the water more turbid. The positive interrelation of reduced Mn, Cu and Zn is associated with the coupling between redox processes occurring in the bed sediment and adsorption of metals (Mn, Cu, Zn) released from the pore waters onto ambient and diluent SS in the overlying water column (Turner et al., 2000; Callaway et al., 1988). Meanwhile, correlation with salinity indicates that the resuspension is mainly through saline water infusion during the low flow of the river. However, the abundance of Fe during SWM in SS suggests the ambient nature of Fe rather than resuspension and non-reactive. The changes in chemical composition are a dominant process happening due to Mn hydroxides in the study area. The positive correlation of Fe with Se and Ba indicates the absorption by Fe oxyhydroxides, whereas these 3 metals are found to be in negative correlation of Se with salinity, TSS and turbidity. The positive correlation of Fe, Se and Ba with pH suggests the absorption is mainly happening in the upper part of the estuary with low saltwater influence. Likewise, Al has a high negative correlation with salinity, TSS and turbidity, whereas it has a positive relation with pH along with Co and Cd in the estuary (Table 6.2). The absorption of Co and Cd on clay minerals like illite and

kaolinite in seawater are in dominating conditions during this season (Hao et al., 2020; Jiann et al., 2014; Namieśnik et al., 2010). The desorption of such metals from clay minerals can increase up to 20 to 30% under acidic conditions (Hao et al., 2020) in case of density stratification of water in the lower part, which justifies the correlation of Co and Al with pH. The negative association of Al and Co with saline water-induced salinity and turbidity indicates the origin of these metals are terrestrial as parameters such as turbidity are mainly induced by seawater during this season and limited to the lower part of the estuary. However, Cd do not share any positive or negative relationship with any physico-chemical parameters, indicating agricultural input (Zaharah et al., 2014; De Boo et al., 1990).

6.3.2.1.2 North-East monsoon (NEM)

During the NEM, salinity has a significant correlation with Cu and Zn (r=0.635 and 0.915) and a negative correlation with Al, turbidity and pH (-0.806, -0.807 and-0.900). In addition, a positive correlation of salinity with Mn and TSS (r=0.406 and 0.401) was also observed in the estuary. Trace metals like Mn, Cu and Zn have significant correlation among themselves (Cu and Mn r=0.950; Cu and Zn r=0.737; Mn and Zn r=0.876) and significant negative correlation with other metals such as Al, Ba and Se along with physico-chemical parameters like turbidity, SS and pH. Al during NEM shows significant positive correlation with Co, Ba, turbidity and pH (r=0.672, 0.721, 0.924 and 0.824), whereas Ba and Co share significant correlation with each other along with Se, SS, turbidity and pH (Co r=0.713, 0.949, 0.798, 0.628 and 0.602; Ba r=0.488, 0.834, 0.468, 0.695). On the other hand, Fe and Se are correlated to SS in the estuary with r=0.469 and 0.645.

An opposite trend of turbidity, TSS has been noticed to be higher during NEM as compared to SWM, where higher turbidity and TSS amount have been concentrated in the upper region of the estuary and a decline has been observed towards the lower region (Fig. 4.4). Hence, a negative correlation of turbidity is justified in the estuary. However, the seawater introduced TSS is dominating in the limited sea-influenced region, which is confirmed by the positive correlation between TSS and salinity. The inert relation of Mn, Cu, Zn and salinity is very similar to SWM, where resuspension occurs with the help of saline water intrusion. However, during this season, the region of influence of such process is lesser as compared to SWM and bioturbation, while

physical disturbance at the bottom responsible for inducing Mn, Cu and Zn rich pore water into diluents freshwater and settlement of these metals are happening on Mn oxides (Turner et al., 2000; Callaway et al., 1988; Mori et al., 2019; Oldham et al., 2017). Concurrently, metals like Mn from localized benthic sources in organic rich/mangrove dominated estuaries (e.g. Mori et al., 2019) are able to mix throughout the plume regions during high freshwater influx and precipitate more uniformly on the TSS and spiking the concentration upwards (Turner et al., 2000). Such Mn complexes are kinetically stabilized against Fe reduction even if the concentration of Fe is much higher in water (Oldham et al., 2017). The negative correlation of Mn, Cu and Zn with turbidity and pH indicates the limitation of the oxidation near the mouth region with high salinity influence. The interrelation of Al, Co and Ba indicates the terrestrial nature of these metals and shows a significant negative correlation with salinity while maintaining a positive correlation with turbidity and pH. Therefore, this association suggests the direct influence of weathering of these metal from the source area and are mainly controlled by absorption on clay minerals in the upper part of the estuary with the help of turbidity and high pH. The siliciclastic clay minerals such as illite and kaolinite have a higher content of Al and are known for their absorption of other metals such as Co and Ba on their reactive surfaces (Hao et al., 2020; Jiann et al., 2014; Namieśnik et al., 2010). The higher concentration of Fe in SS and no significant correlation with any metals ensure independence on the changes due to chemical reactivity in SS (Turner et. a. 2000). However, the total concentration of SS (TSS) has a higher correlation with particulate Co, Ba, Fe and Se and no other physico-chemical parameters are linked to this association indicating a common source. The pyrite and shale concretions in Sibuti and Tukau formation are rich in all these chalcophile metals (Azrul Nisyam et al., 2013; Anandkumar 2016; Nagarajan et al., 2019), hence it can be stipulated as a major source. Metal like Cd has a negative correlation with Fe and Ba and does not have any correlation with other parameters or metal, which might be due to the source variation of these metals. The leaching of Cd from agricultural fields might be playing a major role here whereas both Fe and Ba are found to be completely geogenic in origin.

Table. 6.2 Correlation Matrix of Trace Metals in SS during SWM

Parameters	pH	DO	Turbidity	Salinity	TSS	Co	Cu	Mn	Zn	Se	Fe	Al	Cd	Ba
pH	1.000													
DO	0.809	1.000												
Turbidity	-0.958	-0.943	1.000											
Salinity	-0.944	-0.928	0.982	1.000										
TSS	-0.963	-0.908	0.984	0.959	1.000									
Co	0.655	0.105	-0.417	-0.426	-0.500	1.000								
Cu	-0.962	-0.927	0.995	0.961	0.991	-0.447	1.000							
Mn	-0.707	-0.284	0.527	0.580	0.618	-0.923	0.539	1.000						
Zn	-0.754	-0.509	0.662	0.773	0.661	-0.670	0.621	0.829	1.000					
Se	0.663	0.624	-0.666	-0.794	-0.642	0.390	-0.606	-0.647	-0.939	1.000				
Fe	0.192	0.213	-0.194	-0.374	-0.184	0.157	-0.121	-0.457	-0.742	0.855	1.000			
Al	0.655	0.466	-0.610	-0.465	-0.615	0.420	-0.667	-0.216	-0.049	-0.121	-0.612	1.000		
Cd	-0.041	-0.326	0.181	0.291	0.024	0.420	0.087	-0.280	0.303	-0.503	-0.524	0.341	1.000	
Ba	0.273	0.281	-0.272	-0.383	-0.365	0.298	-0.252	-0.629	-0.602	0.687	0.779	-0.416	0.030	1.000

**Blue cells: Positive correlation; Grey cells: Negative correlation*

Table. 6.3 Correlation Matrix of Trace Metals in SS during NEM

Parameters	pH	DO	Turbidity	Salinity	TSS	Co	Cu	Mn	Zn	Se	Fe	Al	Cd	Ba
pH	1.000													
DO	-0.058	1.000												
Turbidity	0.942	0.221	1.000											
Salinity	-0.900	0.265	-0.807	1.000										
TSS	-0.033	0.340	0.121	0.401	1.000									
Co	0.602	0.600	0.798	-0.291	0.628	1.000								
Cu	-0.830	-0.507	-0.945	0.635	-0.172	-0.865	1.000							
Mn	-0.710	-0.604	-0.859	0.406	-0.457	-0.962	0.950	1.000						
Zn	-0.980	-0.045	-0.975	0.915	0.062	-0.647	0.876	0.737	1.000					
Se	0.838	0.145	0.914	-0.874	-0.149	0.605	-0.823	-0.650	-0.929	1.000				
Fe	0.272	-0.384	0.085	0.009	0.469	0.134	0.001	-0.153	-0.087	-0.260	1.000			
Al	0.824	0.347	0.924	-0.806	-0.141	0.672	-0.915	-0.757	-0.915	0.964	-0.281	1.000		
Cd	-0.244	-0.326	-0.171	-0.075	-0.206	-0.280	0.351	0.452	0.124	0.174	-0.563	-0.030	1.000	
Ba	0.695	0.609	0.834	-0.373	0.468	0.949	-0.937	-0.997	-0.710	0.601	0.198	0.721	-0.517	1.000

**Blue cells: Positive correlation; Grey cells: Negative correlation*

6.3.2.2 Factor analysis of metals in SS

A total of three principal components during each season has been extracted with an eigenvalue of > 1. The rotated component matrix of SWM and NEM is presented in Tables 6.4 and 6.5 with PC loading of each parameter and percentage variance, whereas the factor scores for respective seasons are shown in Fig. 6.3 and 6.5. A total variance of 95.17 and 93.62% has been explained during SWM and NEM by PCA analysis respectively.

6.3.2.2.1 South-West monsoon (SWM)

Factor-1 has strong positive loading (>0.5) of Cu, Mn, Zn along with saline water-induced parameters like salinity, turbidity and SS along with negative loading of pH, DO, Al and Se. This component represents 48.65% variance SWM while showing the highest positive factor score near the river mouth and lowest in the upper part (Fig. 6.3). The negative loading of Al and Se along with pH and DO indicate the absorption of Se by Al-oxyhydroxides under high pH and high DO conditions due to their reactive surfaces (Hsu et al., 1989; Nimiesnik et al., 2010; Jian et al., 2014; Hao et al., 2020). The low negative factor scores at station 20 and 40 km confirm such absorption in the upper part of estuary (Fig. 6.3). On the other end, the positive loading of Cu, Mn and Zn indicates towards the injection from the pore waters due to water density stratification, which causes organic respiration and maintains an acidic condition near the sediment-water interface (Turner et al., 2000). This can be confirmed by the negative loading of both pH and DO in this factor. These injected metals are getting absorbed with the help of Mn-oxyhydroxides formation on the ambient and diluent SS while replacing Fe and Al-hydroxides. In presence of organic acids generated from their respiration, Mn hydroxides have more reactive properties than Al hydroxides (Qin et al., 2018; Habibah et al., 2014). With this effect, Al and Fe are removed from the water column by the aggregation and precipitation of diaspore in distinct flocculation zones because of increasing ionic strength, as the water is subjected to steep pH and salinity gradients (Ferguson et al., 1999), whereas Se goes to dissolved phase with such effect and showing an increase in water during SWM (Fig. 4.10). This process has a dominating presence in the lower part of the estuary (Fig. 6.3 and 6.4).

Factor-2 has major loading of Se, Fe and Ba, meanwhile, there is a significant negative loading of Al, Mn, Zn representing 29.04% variance in the estuary during SWM. The

positive association of Fe, Se and Ba indicates the absorption of these metals by Fe-oxyhydroxides (Zhang et al., 2014) and a high positive factor score is observed at 30 km station (Fig. 6.3). As Fe is the dominating trace metal in the SS, the particulate Fe might indicate the presence of $Fe(OH)_3$ and $Fe(OH)_4^-$ (Ferguson et al., 1999). The tendency of Ba (Mori et al., 2019) and Se (Hung et al., 1995; Kieliszek et al., 2019) to form oxides with Fe in better-originated conditions far away from the sea is giving rise to the increase in the concentration of these metals in the estuary (Fig. 6.4), which eventually decreases towards river mouth (Fig 6.2). The negative loading of Al, Zn and Mn has been in the intermediate zone of the estuary, which is confirmed by the peak negative factor score from 20 to 30 km (Fig. 6.3). This part is the mixing zone with the partial influence of freshwater and saltwater and such association suggests the absorption of Zn by both ambient Mn-oxyhydroxides and diluent Al-oxyhydroxides. It works as a buffer zone for both oxyhydroxides as river mouth is dominated by Mn-oxyhydroxides due to organic respiration, acidic condition and heavily influenced by saltwater induced turbidity while the upper part is mainly dominated by Al-oxyhydroxides as discussed due to favoring DO and higher pH in Factor-1.

Factor-3 shows positive loading of Co and Cd along with negative loading of Mn while representing 17.5% of the total chemical process in the estuary. The high positive factor score is observed at a 10 km distance from the river mouth. This station is also associated with a major spike in the concentrations of Co and Cd during this season (Fig. 6.2). As discussed before, the decisive factor behind the control of Co into the water column is bedload sediments rather than suspended particulate matter in the estuary. The majority of Co occurs mainly in a non-reactive form and is buried with the accumulating sediments (Gendron et al., 1986). In the case of Cd, particulate Cd tends to settle at the sediment surface that is mostly bound to biogenic material present on it (Boyle et al., 1976; Gendron et al., 1986). But both these metals follow a redox-sensitive pattern of dissolution in the reducing zone of the sediments leading to vertical migration into the water column and enrichment by precipitation in the oxidized surface layer (Heggie et al., 1984). In addition, these metals have an affinity towards Mn-hydroxides during redistribution in particulate form (Gendron et al., 1986). The formation of particulate Mn hydroxides in reducing zones is evident from the factor 1 discussion. The association of Co and Cd from bed sediments and Mn hydroxide

presence as particulate matter might be responsible for the negative loading of Mn. The injected dissolved Co and Cd are being absorbed by the Mn hydroxides in the water table (Fig. 6.4), which explains this association and the spike in concentration observed at station 2 (10km).

Table 6.4 Rotated Component Matrix of Trace Metals in SS during SWM

Parameters	Communalities	Component		
		1	2	3
pH	0.991	-0.921	0.196	0.324
DO	0.946	-0.940	0.150	-0.198
Turbidity	0.997	0.981	-0.165	-0.084
Salinity	1.000	0.939	-0.342	-0.043
TSS	0.975	0.945	-0.179	-0.225
Co	0.917	-0.323	0.260	0.863
Cu	0.992	0.979	-0.102	-0.151
Mn	0.996	0.585	-0.549	-0.740
Zn	0.930	0.540	-0.756	-0.258
Se	0.992	-0.546	0.832	-0.034
Fe	0.999	-0.045	0.989	-0.141
Al	0.984	-0.699	-0.602	0.365
Cd	0.855	0.207	-0.395	0.810
Ba	0.748	-0.091	0.829	0.228
Percentage Variance Explained		48.65	29.04	17.5
Total Variance Explained		95.17%		
Eigen Value		Greater than 1		

**Blue cells: Positive fator loading; Grey cells: Negative factor loading*

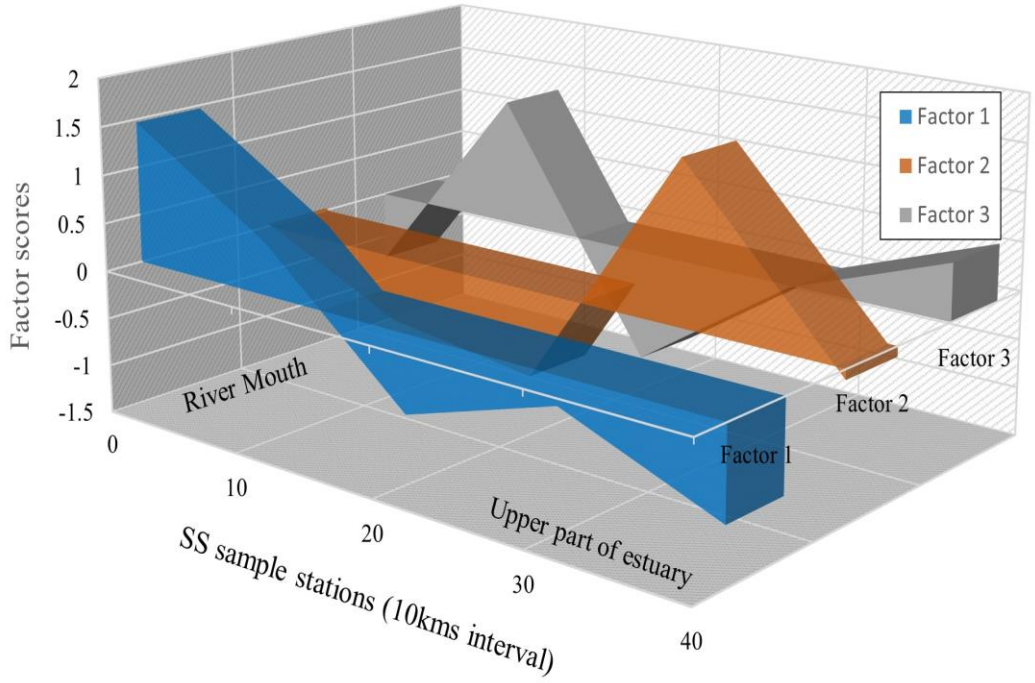

Fig. 6.3 Distribution of factor scores in the estuary during SWM

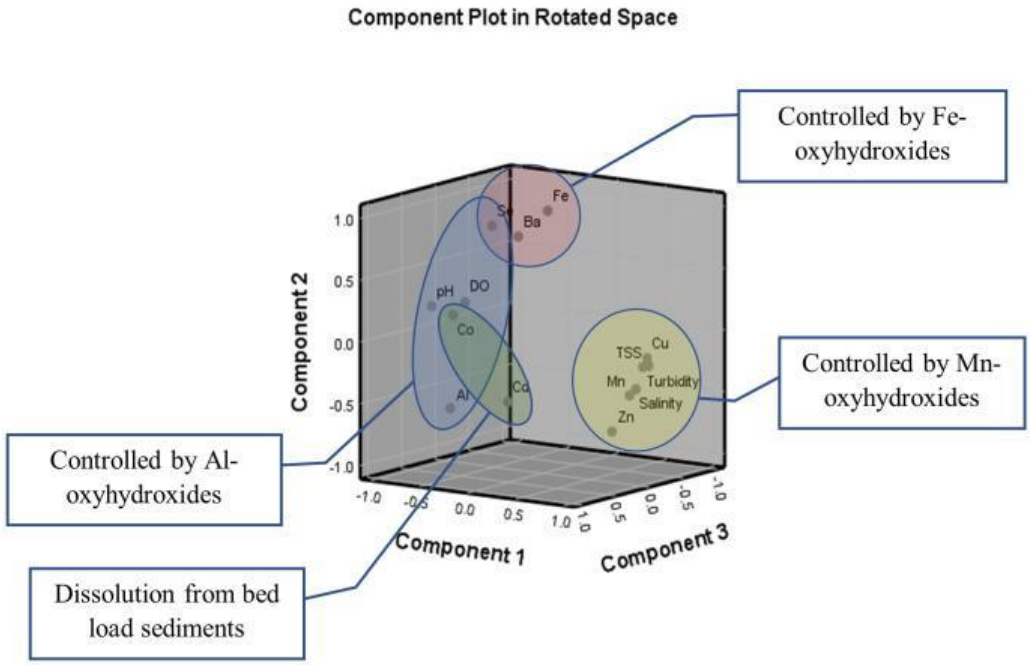

Fig. 6.4 Dominancy of principal components in estuary during SWM

6.3.2.2.2 North-East monsoon (NEM)

Factor-1 has a strong loading of Co, Se, Al, Ba, turbidity and pH along with negative loading of salinity, Cu, Mn and Zn which explains 51.49% of the total variance. This factor is very similar to the process observed in factor-1 during SWM. The association of Al, Se, Ba and Co indicates absorption by Al oxyhydroxides under ideal pH (4–7) levels in the upper region of the estuary. In this pH range, Al-oxyhydroxides stay in insoluble particulate form (Ferguson et al., 1999; Nimiesnik et al., 2010) and absorbing metals like Co, Se and Ba due to high surface reactivity (Hsu et al., 1989; Jian et al., 2014; Qin et al., 2018; Mori et al., 2019; Hao et al., 2020; Hao et al., 2020). But the influential region for this process in factor-1 (NEM) is higher as compared to SWM. The factor scores indicate the domination of positive factor in the upper part (20 to 40kms) due to freshwater domination and gradually decreasing towards the station at 10km with a gradual increase in salinity (Fig. 6.5). Starting from this point, negative factor score is observed to be dominating the lower part, with the higher loading of Mn, Zn and Cu (Fig. 6.5 and 6.6). This part of the estuary is controlled by reducing conditions due to stratification of salt and freshwater, and the pH drops due to respiration of organic matter, which are responsible for the injection of dissolved Mn, Cu and Zn from pore water into the water column (Turner et al., 2000). This leads to the formation of Mn-oxyhydroxides and the absorption of metals like Cu and Zn. The reactivity of Mn-hydroxides is supported by the presence of organic acids formed during the respiration of organic matter (Qin et al., 2018; Habibah et al., 2014) and are further enhanced in this reducing condition because of the aggregation and precipitation of Al-oxyhydroxides diaspore in distinct flocculation zones because of increasing ionic strength, as the water is subjected to steep pH and salinity gradients (Ferguson et al., 1999).

Factor-2 has significant loading of Co, Ba, DO and TSS along with negative loading of Cu and Mn, which explains 26.02% of the variance. This indicates towards the common origin of these metals and is mainly obtained from oxidation of shale and pyrite concretion in the upper stream. The presence of all the metals obtained in these factors is reported to be available in the concretion (Table 5.13). The DO in such process works as oxidant and the process is likely to take place in well-oxygenated condition (Moses et al., 1987). The association of TSS with these metals in absence of any controlling oxides or clay mineral indicates the absorption of Co and Ba by

particulate organic matter, which are highly reactive in prevailing condition (Tomlinson et al., 1980). The higher positive factor score in the upper part supports this theory as the upper part of the estuary is observed to be dominated by freshwater (Fig. 6.5). On the other hand, both Cu and Mn show a spike in trend in the lower part, and an especially significant negative factor score is obtained at station 2 (10km from the river mouth) (Fig. 6.5). This station falls under the high mixing zone in this season and higher seawater influence leading to respiration of the mentioned organic matter, thus leading to the dissolution of Co and Ba (Fig. 6.2), while making Mn oxyhydroxides more reactive with a generated organic acid in the process (Qin et al., 2018; Habibah et al., 2014) which leads to the absorption of Zn.

Table 6.5 Rotated Component Matrix of Trace Metals in SS during NEM

Parameters	Communalities	Component		
		1	2	3
pH	1.000	0.965	0.025	0.262
DO	0.943	-0.038	0.952	-0.190
Turbidity	0.993	0.938	0.314	0.118
Salinity	0.999	-0.961	0.263	0.080
TSS	0.700	-0.189	0.598	0.554
Co	0.939	0.541	0.764	0.251
Cu	0.988	-0.818	-0.557	-0.095
Mn	1.000	-0.642	-0.715	-0.278
Zn	0.999	-0.990	-0.110	-0.085
Se	0.982	0.939	0.170	-0.266
Fe	0.994	0.023	-0.187	0.979
Al	0.995	0.909	0.336	-0.238
Cd	0.576	-0.045	-0.318	-0.687
Ba	0.997	0.611	0.718	0.330
Percentage Variance Explained		51.49	26.02	16.11
Total Variance Explained		93.62%		
Eigen Value		Greater than 1		

**Blue cells: Positive factor loading; Grey cells: Negative factor loading*

Factor-3 has significantly higher loading of TSS and Fe and negative loading of Cd indicating towards the different origin of the metals, where most of the Fe concentration is geogenic and Cd concentration acquired from the SS is from

anthropogenic sources like agricultural inputs. The association of TSS and Fe indicates the present of particulate Fe in the water table and both the metals are associated with run-off water carrying SS from river basin and agricultural fields surrounding the river (Pobi et al., 2019). This factor explains 16.11% of the total variance.

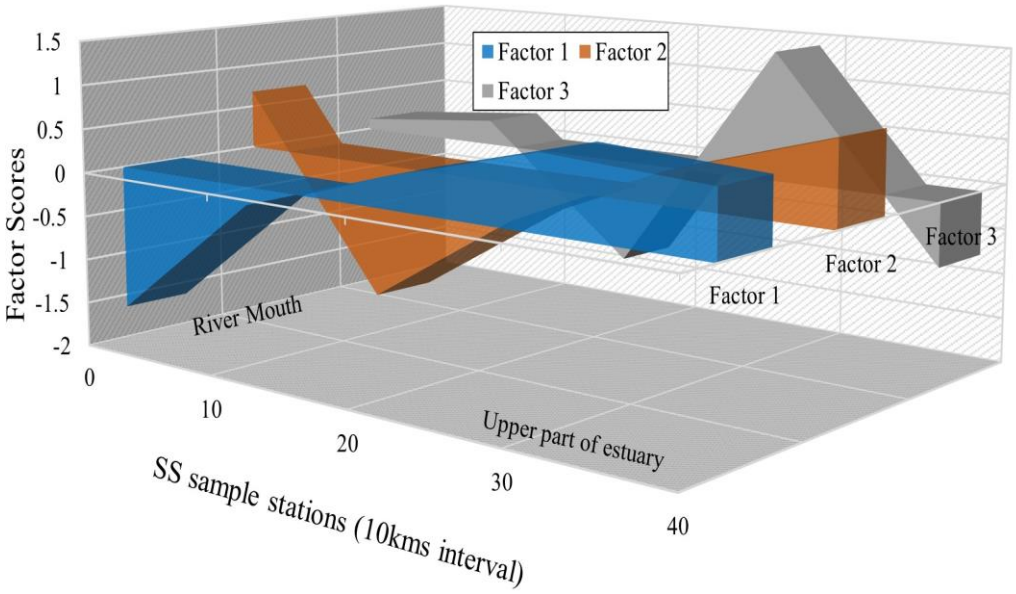

Fig. 6.5 Distribution of factor scores in the estuary during NEM

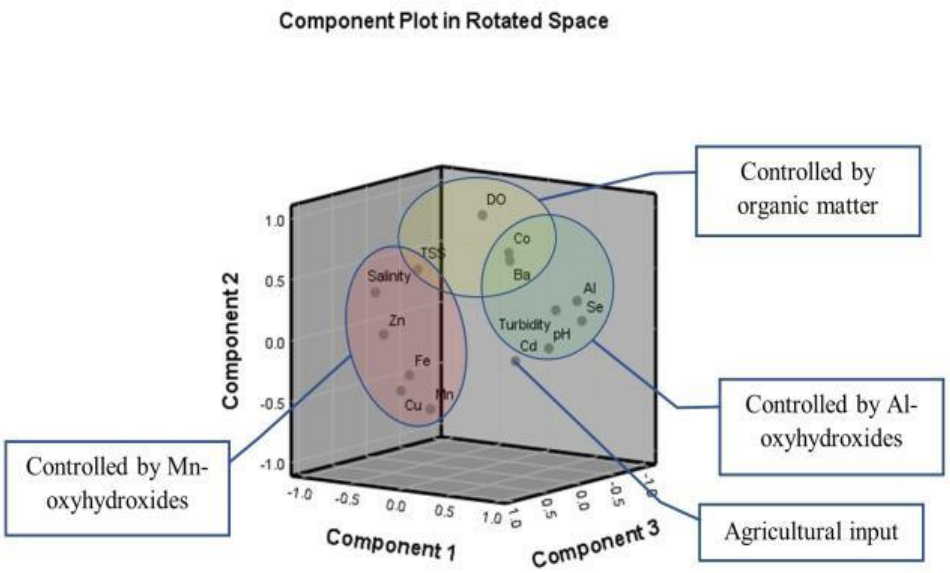

Fig. 6.6 Dominancy of principal components in estuary during NEM

6.3.3 Speciation of trace metals between particulate and dissolved phase

The speciation of trace metals in the aquatic system can be impacted by various controlling parameters such as pH, salinity, turbidity and amount of SS in the water column (Zhang et al., 2018; Yang et al., 2017; Kumar et al., 2010). In such a scenario, calculation of partition coefficient (K_d) helps to evaluate the partitioning balance of trace metals between particulate phase and liquid phase (Zhang et al., 2018; Zheng et al., 2013; Li et al., 2018). The calculation is done depending on the ratio of metals/metalloids in the particulate phase (Me_p) to metals/metalloids in the dissolved phase (Me_d), where Me_p is considered in mg kg^{-1} and Me_d is considered in mg L^{-1}.

$$K_d = {Me_p}/{Me_d} \text{.....(eq. 6.2)}$$

K_d is represented by the distribution co-efficient and expressed in mg metal per kg. The higher value of K_d (<3) shows the affinity of metals towards SS or absorption whereas, a lower value than 3 represents a higher affinity of metals towards liquid phase or dissolution under varying environmental conditions (Kumar et al., 2010; Zheng et al., 2013; Zhang et al., 2018; Li et al., 2018; Yang et al., 2017; Sedeño-Díaz et al., 2019).

6.3.3.1 South-West monsoon (SWM)

The average partition coefficient values during SWM for all the metals have recorded higher than 3 (Fig. 6.7), except for Cr which is present in the liquid phase but absent in suspended solids. This infers that the metal absorption from the liquid phase and particle reactivity of metals with SS is higher and it is a dominating process in the estuary (Li et al., 2018). The higher mobility of trace metals during SWM can be represented as Cr > Se > Cd > Ba > Zn > Mn > Cu > Co > Fe > Al. The presence of Al is only in the solid phase, which might be due to the higher pH (>4.5) observed during SWM as dissolved Al complexes is from a high acidic condition such as < 4.5 in water (Namieśnik et al., 2015). The absence of Cr indicates its complete independence of SS absorption, because of its readily soluble form of Cr(VI), which is stable even at lower oxidizing conditions (Namieśnik et al., 2015).

6.3.3.2 North-East monsoon (NEM)

Despite the increase in concentration in the liquid phase during NEM, the K_d for most of the metals except Cr was observed to be higher than 3 at all the stations. The higher mobility of trace metals with SS during NEM in descending order is observed as Cr > Se > Cd > Cu > Zn > Co > Ba > Fe > Mn > Al. The higher tendency of Mn to form hydroxides under oxidizing conditions because of freshwater dilution during NEM might be the reason for its increased reactivity towards SS (Duinker et al., 1979; Wollast et al., 1979; Reigner et al., 1993; Mori et al., 2019; Oldham et al., 2017). On the other hand, the behavior of Al and Cr remains the same as SWM as oxidizing conditions favor the formation of readily soluble Cr(VI) in water and the insoluble nature of Al under prevailing pH conditions which is resisting it from being mobile (Namieśnik et al., 2015). The highest amount of Se is desorbing from SS solids during this season as well. The K_d shown by Zn, Se, Fe and Cd is almost constant during both seasons (Fig. 6.7), whereas lower absorption of Co, Cu has been noticed during NEM and higher K_d values for Mn has been noticed during NEM, confirming the formation of the higher amount of Mn oxyhydroxides during NEM (Turner et al., 2000).

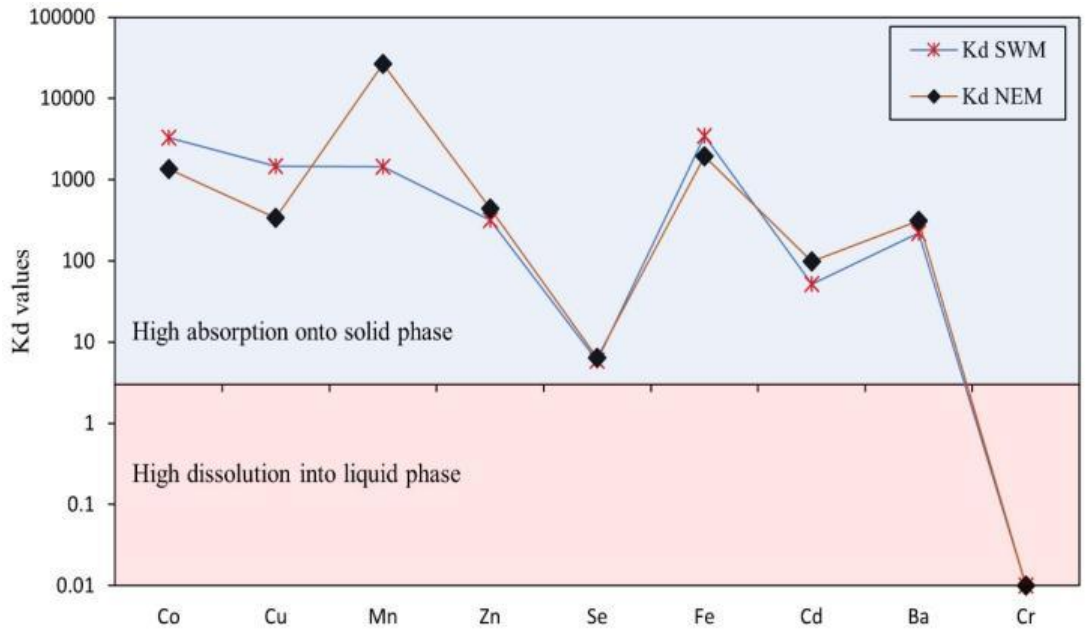

Fig. 6.7 Average values of K_d for considered metals during SWM and NEM

6.3.3.3 Correlation of K_d of metals and physico-chemical parameters during SWM

During SWM, factors like salinity, turbidity and TSS are behaving very similarly and are the major controlling factors in the lower part of the estuary. The positive correlation of metals like Co, Cu, Ba and Zn with these physico-chemical parameters (salinity, turbidity and TSS) (Table 6.6) indicates that the absorption of these metals are mainly controlled by the enhancement of reactively of suspended solids due to the saltwater influence in high turbidity zones (Kumar et al., 2010; Zheng et al., 2013; Sedeño-Díaz et al., 2020). On the other hand, higher pH, DO and temperature are the controlling factors in the upper part of the estuary (Fig. 6.3 and 6.4), and these parameters are positively correlated to metals such as Mn, Fe and Se, indicating absorption by Mn and Fe oxyhydroxides that are responsible for the higher K_d of Se in the estuary, whereas the drop in pH and DO in the lower part is leading to the dissolution of Se from these oxyhydroxides (Bjorn et al.,2015; Yang et al., 2017). The prominent property of Se to form an outer-sphere complex with oxyhydroxides such as goethite must be responsible for such absorption (Hayes et al., 1987). The conservative behavior of oxyhydroxides towards ambient pH is leading to such a scenario (Stumm et al., 2012).

6.3.3.4 Correlation of K_d of metals and physico-chemical parameters during NEM

During NEM, salinity, TSS and turbidity have a positive correlation with Co and Ba, which indicates towards an increase in absorption of these metals under high saline and turbid conditions (Allison et al., 2005; Sedeño-Díaz et al., 2020) in the estuary along the coastal zone (Table 6.7). However, pH has a negative correlation with the K_d of these two metals (Co and Ba) and hence acidic conditions might lead to dissolution (Yang et al., 2017). K_dFe and K_dCd are positively correlated to turbidity, which is higher in the upper part of the estuary during this season. Cd is known to form edge-sharing and corner-sharing inner-sphere complexes with Fe oxyhydroxides such as goethite (Spadini et al., 1994), yet while nearing to coastal environment, high Cl^- activity leads to the formation of mobile Cd-chloride complexes (Bjorn et al., 2015). This behavior is reflected by the negative correlation of Cd and Fe with DO and TSS, which are higher in the lower part of the estuary in this season despite the

fact that Fe oxyhydroxides are less mobile in the oxic environment (Bjorn et al., 2015). Similar behavior has also been noticed for Se and Fe, where conservative behavior of Fe oxyhydroxides towards ambient pH leads to desorption of Se from suspended solids (Stumm et al., 2012) and defines the negative correlation of Fe with Se. A negative correlation of K_dMn, K_dCu and K_dZn with DO indicates that the removal of Cu and Zn from liquid phase is caused due to reducing DO conditions at the bottom by Mn oxyhydroxides formed in the water column (Qin et al., 2018; Habibah et al., 2014).

Table 6.6 Correlation Matrix of K_d of metals and physico-chemical parameters during SWM

	K_d Co	K_d Cu	K_d Mn	K_d Zn	K_d Se	K_d Fe	K_d Cd	K_d Ba	Sal	pH	DO	Tur	Temp	TSS
K_d Co	1.000													
K_d Cu	1.000	1.000												
K_d Mn	-0.187	-0.187	1.000											
K_d Zn	0.047	0.047	-0.151	1.000										
K_d Se	-0.404	-0.404	0.600	-0.822	1.000									
K_d Fe	-0.578	-0.578	0.480	-0.725	0.949	1.000								
K_d Cd	-0.170	-0.170	-0.878	0.459	-0.672	-0.470	1.000							
K_d Ba	1.000	1.000	-0.187	0.047	-0.404	-0.578	-0.170	1.000						
Sal	0.641	0.641	-0.467	0.611	-0.889	-0.986	0.397	0.641	1.000					
pH	-0.851	-0.851	0.542	-0.240	0.695	0.835	-0.264	-0.851	-0.896	1.000				
DO	-0.777	-0.777	0.692	-0.238	0.670	0.655	-0.425	-0.777	-0.647	0.809	1.000			
Tur	0.858	0.858	-0.648	0.233	-0.708	-0.780	0.355	0.858	0.813	-0.958	-0.943	1.000		
Temp	-0.692	-0.692	0.688	-0.418	0.845	0.916	-0.511	-0.692	-0.944	0.958	0.805	-0.930	1.000	
TSS	0.928	0.928	-0.501	0.243	-0.673	-0.783	0.202	0.928	0.822	-0.963	-0.908	0.984	-0.899	1.00

**Blue cells: Positive correlation; Grey cells: Negative correlation*

Table 6.7 Correlation Matrix of K_d of metals and physico-chemical parameters during NEM

	K_d Co	K_d Cu	K_d Mn	K_d Zn	K_d Se	K_d Fe	K_d Cd	K_d Ba	Sal	pH	DO	Tur	Temp	TSS
K_d Co	1.000													
K_d Cu	-0.291	1.000												
K_d Mn	-0.443	0.69	1.000											
K_d Zn	-0.45	0.325	0.877	1.000										
K_d Se	0.723	-0.577	-0.18	0.097	1.000									
K_d Fe	-0.516	0.804	0.282	-0.03	-0.895	1.000								
K_d Cd	-0.504	0.758	0.214	-0.146	-0.94	0.976	1.000							
K_d Ba	0.797	0.14	-0.311	-0.401	0.355	0.023	-0.047	1.000						
Sal	0.724	0.251	-0.265	-0.401	0.233	0.154	0.085	0.991	1.000					
pH	-0.412	-0.533	-0.086	0.047	-0.048	-0.396	-0.264	-0.86	-0.9	1.000				
DO	0.509	-0.802	-0.709	-0.326	0.667	-0.628	-0.69	0.363	0.265	-0.058	1.000			
Tur	0.473	0.555	-0.099	-0.392	-0.144	0.501	0.461	0.858	0.917	-0.89	-0.098	1.000		
Temp	0.359	-0.534	-0.266	0.157	0.714	-0.55	-0.7	0.341	0.253	-0.246	0.861	-0.108	1.000	
TSS	0.903	-0.392	-0.38	-0.42	0.706	-0.662	-0.575	0.485	0.401	-0.033	0.34	0.188	0.119	1.000

**Blue cells: Positive correlation; Grey cells: Negative correlation*

6.3.4 Ecological risk assessment of suspended solids

6.3.4.1 Geoaccumulation index (I_{geo})

Depending on the I_{geo} values, the quality of the sediments can be classified into 7 categories and are tabulated in Table 3.7. The I_{geo} of the SS according to their abundancy as compared to their world average values (Viers et al., 2009) in descending order observed during SWM and NEM can be observed as SWM: Co > Cu > Cd > Ba > Zn > Mn > Fe and NEM: Co > Cu > Cd > Ba > Mn > Zn > Fe. Elements like Fe, Mn and Zn fall in the uncontaminated category during both seasons. The I_{geo} values of Ba indicate uncontaminated to moderate contamination during both seasons. Moreover, estuarine SS are moderately contaminated with Cd during both seasons, whereas Cu contamination is higher during SWM as compared to NEM and falls in the strong contamination category. The suspended solids are extremely contaminated with Co during both seasons (Fig. 6.8).

The site-wise variation revealed that all the sites are extremely contaminated by Co during NEM, whereas the sites in the upper part of the estuary (30 and 40kms) are extremely contaminated during SWM and the rest fall under the strong to extremely contaminated category. For Cu, sites in the upper part (20, 30 and 40km) are strongly contaminated whereas sites in the lower part show moderate to strong contamination during SWM (Fig. 6.8). During NEM, sites in the upper part (20, 30 and 40km) are moderate to strongly contaminated with Cu, whereas the lower part shows moderate contamination (Fig. 6.8). Likewise, all the sites during both seasons are moderately contaminated with Cd, except the site at 10 km, which shows moderate to strong contamination of Cd. In the case of Ba, sites at 10 and 40 km during SWM and site at 10km during NEM are uncontaminated, whereas the rest of the sites fall under the uncontaminated to moderate contamination category. All the sites for Fe, Zn, and Mn are uncontaminated during both seasons according to the acquired I_{geo} values, whereas contamination of Se could not be assessed due to the unavailability of average concentration in suspended solids of world rivers (Viers et al., 2009).

6.3.4.2 Enrichment factor (EF)

The sequential order of metals EF in descending order can be observed as Co > Cu > Cd > Ba > Zn > Mn > Fe and Co > Cu > Cd > Ba > Mn > Fe > Zn during SWM and

NEM respectively. Extreme enrichment of SS with Co and Cu are observed during both seasons except the site at 40km during NEM, which shows a significant enrichment of Cu. In the case of Cd, all sites are significantly enriched except the site at 10km during SWM, which shows very high enrichment (Fig 6.9). During NEM, all the sites in the upper part (20, 30 and 40km) are extremely enriched with Cd whereas sites in the lower part are significantly enriched (Fig. 6.9). In the case of Ba, all the sites during SWM are significantly enriched whereas very high enrichment has been noticed during NEM. Zn is enriched moderately in the upper part (30 and 40km) whereas the rest of the sites show significant enrichment during SWM. An increase in enrichment at upper part sites observed during NEM leads to significant enrichment of Zn at all the sites. In the case of Fe and Mn, NEM suspended solids are enriched more with these metals than SWM. Both the metals show moderate enrichment during SWM, whereas significant enrichment is observed during NEM (Fig. 6.9). Both the metals show high enrichment in the lower part of the estuary during NEM (sites: 10 and 20km), where Mn is very highly enriched.

6.3.4.3 Contamination factor (CF)

The sequential order of elements for CF during SWM and NEM can be represented as Co > Cu > Cd > Ba > Zn > Mn > Fe and Co > Cu > Cd > Ba > Mn > Zn >Fe. The suspended solids at all the sites are very highly contaminated with Co and Cu during both seasons except sites in the upper part during NEM (30 and 40km) (Fig. 6.10), which have moderate to considerable contamination. In the case of Cd, suspended solids at all the sites are considerably contaminated during SWM except the site at 10km whereas all sites are moderately contaminated during NEM except the site at 20km where contamination is at a considerable level (Fig. 6.10). In the case of Ba, all the sites show moderate contamination during both seasons. In the case of Zn, all sites show low contamination during both seasons except the sites at the lower part and mixing zone (10, 20 and 30km), which shows moderate contamination. During SWM, suspended solids show low contamination of Fe and Mn, whereas Mn shows moderate contamination during NEM at all the sites (Fig. 6.10).

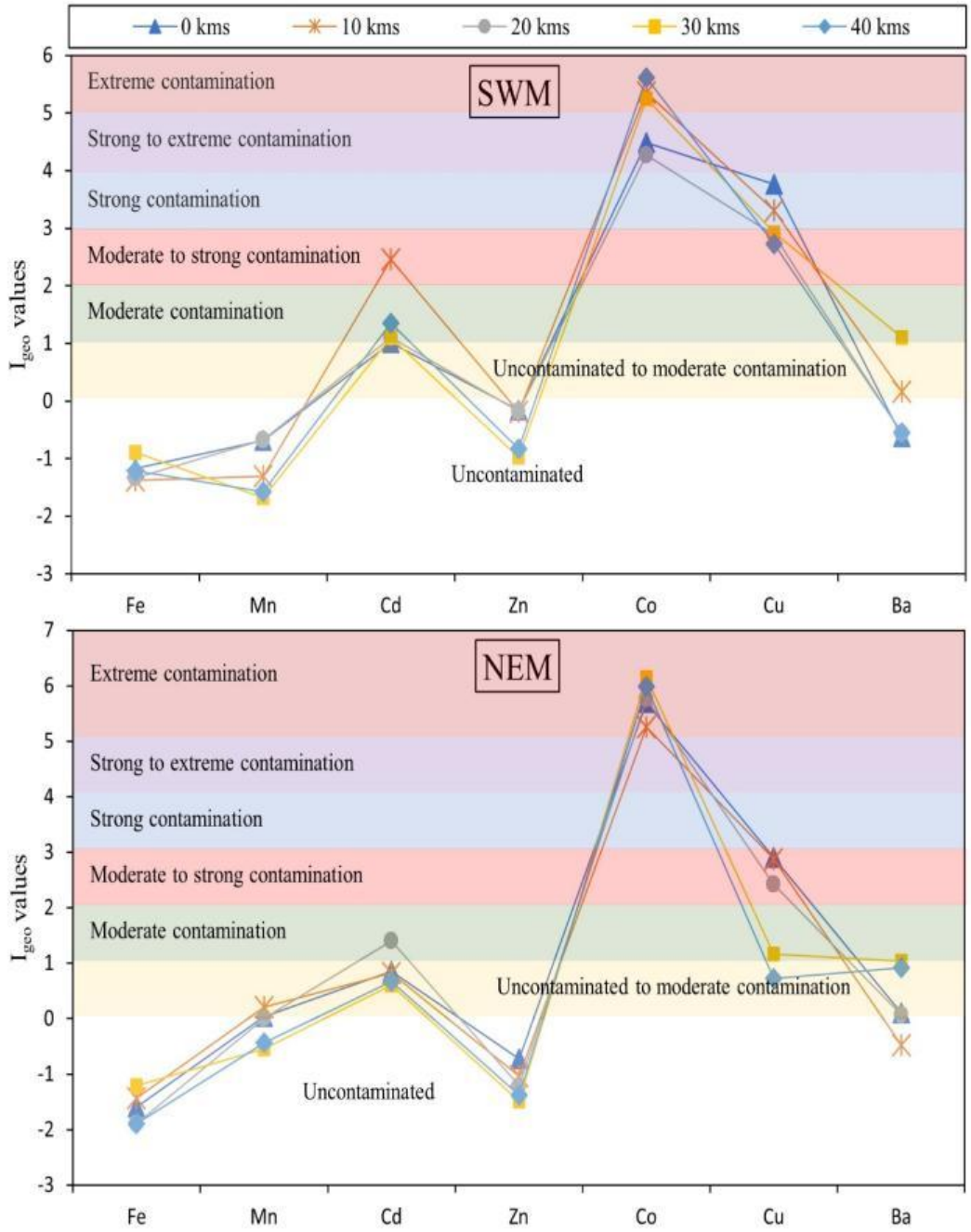

Fig. 6.8 Scatter plot showing I_{geo} index for SWM and NEM in suspended solids

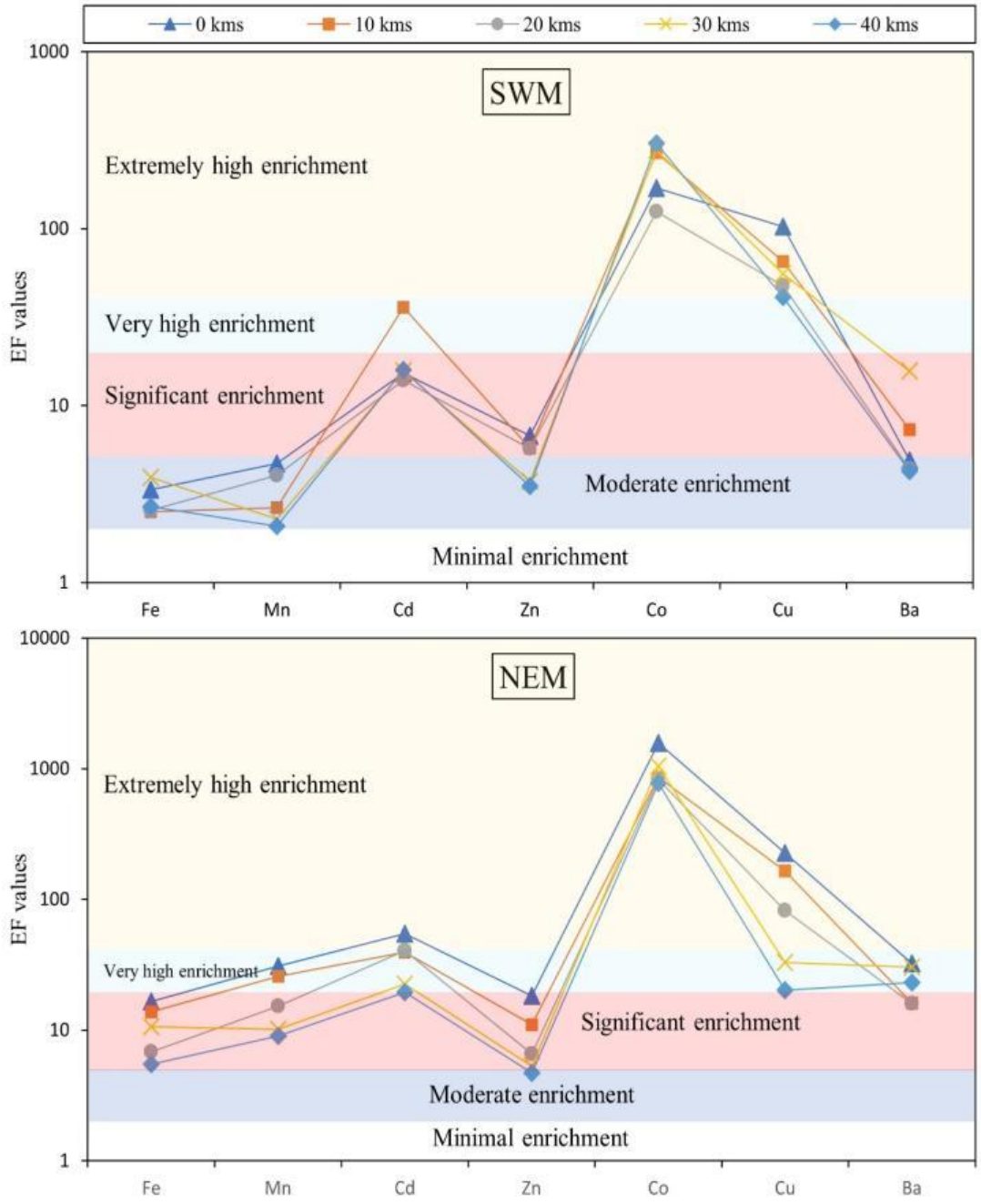

Fig. 6.9 Scatter plot showing EF variation during SWM and NEM in suspended solids

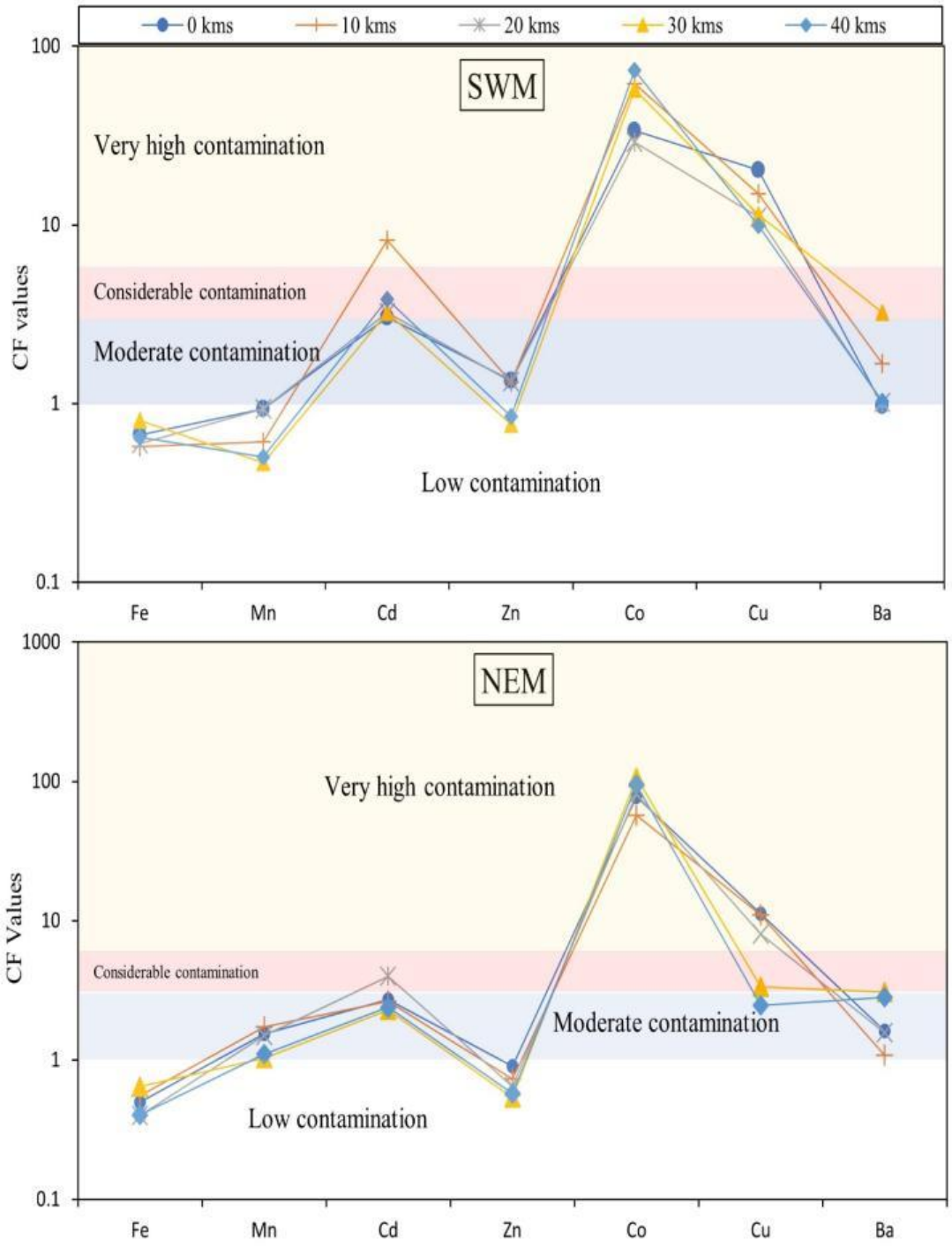

Fig. 6.10 Scatter plot showing CF variation during SWM and NEM in suspended solids

6.3.4.4 Discussion

The enrichment of Co in sediment of source area has been discussed before (Table 5.13) and are mainly controlled by clay minerals like chlorite. In addition, average concentration of Co in shale and pyrite concentration (Azrul Nisyam et al., 2013) is much higher than the average metal concentration of SS (Viers et al., 2009) and PAAS

(Taylor & McLennan, 1985, 1995; McLennan, 2001) (Table 6.9). The average Co concentration reported in estuarine SS is much higher than the concentration reported from the source region (Table 6.10) but is devoid of any anthropogenic influence. In such conditions, enhancement of Co in suspended solids by estuarine mechanisms along with the direct influence from the source region might be a feasible explanation. During SWM, Co is mainly controlled by the desorption of bedload sediment and absorption by Mn-oxyhydroxides and clay minerals (Fig. 6.4), whereas Co is controlled by clay mineral and organic matter during NEM. The spatially variable and oscillatory nature of estuarine tidal currents give rise to several sediment transport mechanisms, from which barotropic effect or tidal pumping and fluvial flow effect are a significant mechanism responsible for the up and down estuary transport of sediments during low flow and high flow, respectively. This leads to the formation of a zone of elevated SS and enhanced sediment trapping (Mathew et al., 2020). In such a transport limited regime, chemical weathering of bedload sediments will be faster than physical weathering (Stallard et al., 1983), leading to the removal of mobile elements such as Co (Viers et al., 2009). Tropical estuaries are dominant of weathering products i.e. clay minerals, oxyhydroxides and organic matter as suspended solids in general (Dupré et al., 1996) and the absorption by such matter can enhance the concentration of metals like Co in suspended solids. In the case of Cu, such effects are mainly controlled by Mn oxyhydroxides as indicated by PCA analysis during both seasons. But, this might be an advective suspended solids transport initiating entirely due to tidal waters (Mathew et al., 2020) as all the above indices indicated higher enrichment of Cu in SS in the lower part of the estuary. In addition, the precipitation of Mn oxyhydroxide as suspended solids is a dominating process in rivers with higher pH and temperature above 15°C with the presence of a large amount of biogenic particles (Pontér et al., 1992; Viers et al., 2009). To strengthen this further, enrichment of Cu is decreased during NEM, in which the estuary is dominated by freshwater and the average concentration of Cu is highest in Miri SW coastal sediments rather than major influencing formations like Lambir and Sibuti formation (Table 6.9). Metal like Cd behaved independently indicating an anthropogenic source such as agricultural input in PCA analysis (Fig. 6.4 and 6.6). Use of P-fertilizers in Sarawak is a common process for peat-based soil agriculture and enriches the suspended solids in the estuary with Cd as a result of leaching from these fields (Zaharah et al., 2014; De Boo et al., 1990). In case of Ba, all the formations in source area have considerable amount of

average Ba concentration it. However, siliciclastic sediment of the Sibuti formation is observed to have the highest concentration of Ba in it (Table 6.9) (Nagarajan et al., 2017a) and might be responsible for the high contamination of Ba in estuarine suspended solids.

Table 6.8 Comparison of selected metal average concentration (in mg kg^{-1}) in suspended solids of Sibuti estuary, world rivers and various formations in the source area

Area of Study	Fe	Mn	Cu	Zn	Ba	Co	Cd	Cr	References
Present study	37927	1740.3	787.6	186.95	943.1	1512.5	5.51	BDL	
Miri coast (SW part)	2948	26.6	217.5	95.6	-	1.3	-	49.48	Nagarajan et al., 2019
Lambir Formation	20340	375	81.75	60.88	140.25	6.94	-	51.5	Nagarajan et al., 2017a
Sibuti Formation	38900	500	72.8	116.54	774.1	7.97	-	53.33	Nagarajan et al., 2015, 2017a
Tukau Formation	21960	94	41.32	60.56	171.92	23.4	-	-	Nagarajan et al., 2017b
Shale and Pyrite concretion (Sibuti and Setap formation)	234600	7700	19.97	66.35	390.96	102.64	-	110.76	Azrul NIsyam et al., 2013
Average metal concentration of SS in world rivers	58100	1679	75.9	208	522	22.5	1.55	130	Viers et al., 2009

6.3.4.5 Pollution load index (PLI)

Considering the study area, all the PLI values at all the sites during SWM and NEM are observed to be heavily polluted, indicating collective enrichment of the considered elements. The PLI values range from 2.3 to 2.96 and 2.12 to 2.69 during SWM and NEM respectively. Sample site 2 (10 km from the sea) during SWM and site 1 (near the sea) are observed to be the most polluted sites in the estuary (Fig. 6.11). All the sites seemed to be affected by the enrichment of all the metals and mainly affected by heavy enrichment of Co, Cu and Cd during both seasons.

6.3.4.6 Potential ecological risk index (PERI)

The PERI values of the estuarine SS at all the sites fall under the high ecological risk category, which is mainly contributed by the elevated enrichment of Cd and its high toxicity levels (30) (Hakanson, 1980) during both seasons (Fig. 6.12). This indicates higher harmful effects of these metals on the biological community surviving in and

around the estuary (Kulbat et al., 2019; Gopal et al., 2018). SS site 2 and site 3 are major contributors of higher toxicity during SWM and NEM respectively.

6.3.4.7 Sediment pollution index (SPI)

The SPI value determined in the study area categorizes the estuarine SS in the dangerous category. Toxicity levels are very high at all the sites especially at site 2 during SWM and site 1 during NEM. Enrichment of Cu and Cd during both seasons is the main reason behind the elevated toxicity of SS in the estuary (Fig. 6.13).

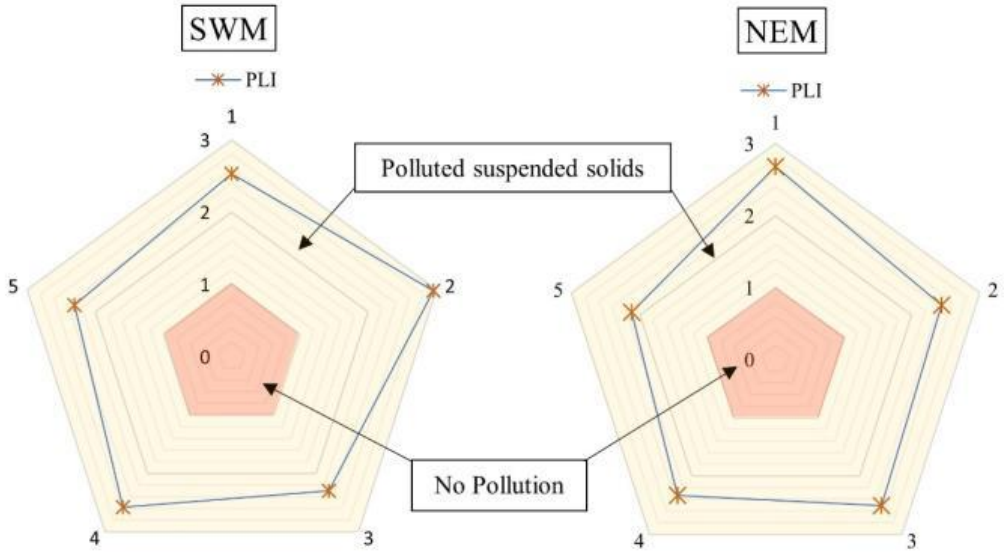

Fig. 6.11 Radial plot showing PLI variation during SWM and NEM

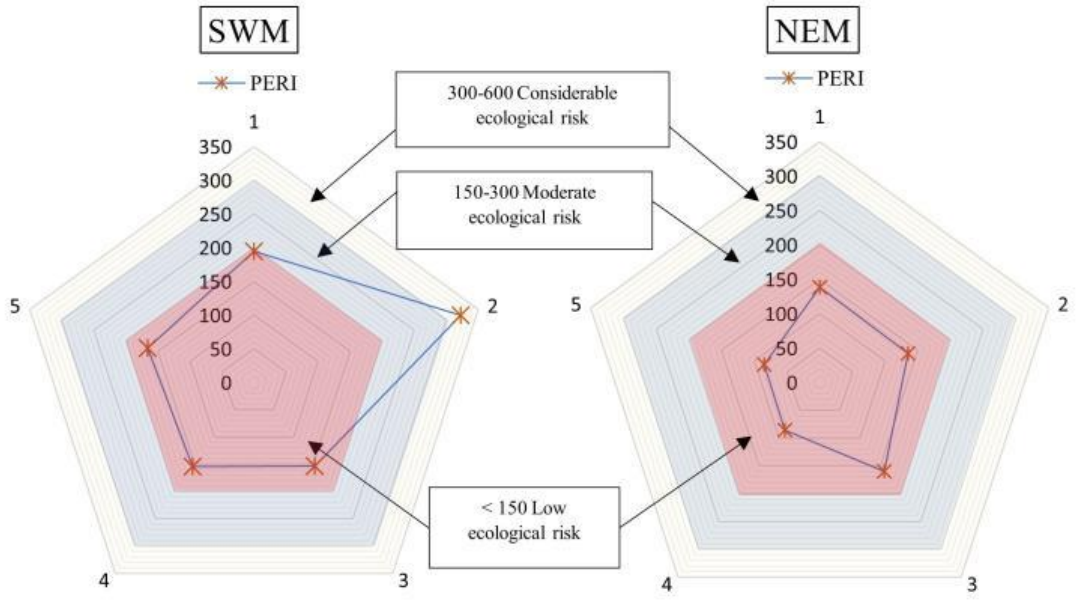

Fig. 6.12 Radial plot showing PERI variation during SWM and NEM

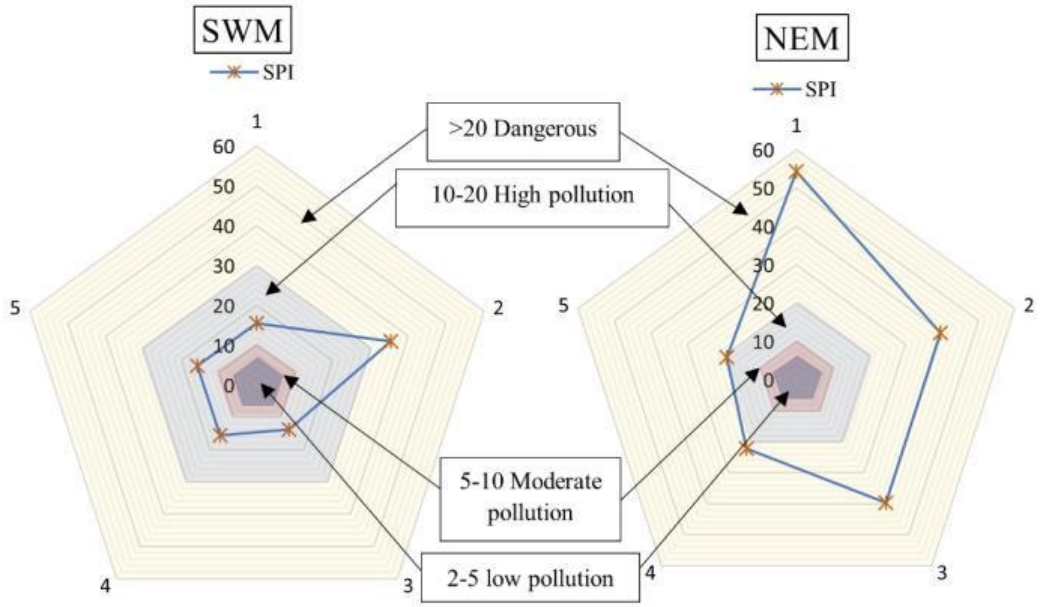

Fig. 6.13 Radial plot showing SPI variation during SWM and NEM

6.4 Summary

- A major fluctuation in concentration was observed in the case of Co, Cu, Mn, Zn, Fe, Al and Ba between the seasons, whereas Se and Cd show minor fluctuation during the same. Fe and Al are the dominating metals found in suspended solids during both seasons.
- In SWM, Mn hydroxides formation due to organic respiration mainly controlled the absorption of metals such as Cu and Zn in the lower and intermediate parts of the estuary. Such organic matter respiration is also found to be injecting metals such as Cd and Co into the water column as well. The Mn hydroxides in high turbid zones were found to be replacing the diluent Fe and Al hydroxides in the mixing zone, which are mainly responsible for the absorption of metals such as Se and Ba in the upper and intermediate parts of the estuary.
- During NEM, similar absorption behaviour of Al hydroxides and Mn hydroxides were also observed where clay minerals and particulate organic matter absorbed Se, Ba and Co under ideal pH conditions in the freshwater dominated upper part and Mn hydroxides absorbed Cu and Mn in the lower part of the estuary. The only exception in this season was the extension of the freshwater dominated zone which increased due to the monsoonal rainfall.

- Study of speciation of metals into solid and liquid phase revealed the absorption nature of the suspended solids in Sibuti river estuary where Cr showed highest tendency to be in dissolution phase than rest of the metals (Se, Cd, Cu, Zn, Co, Ba, Fe and Mn), which were found higher in solids phase.
- Suspended solids are heavily contaminated with Co, Cu and Cd during both seasons due to direct leaching from pyrite concretion and agricultural affluents. Ecologically suspended solids are heavily polluted and possess moderate to considerable ecological risk towards the aquatic biota.

Chapter-7

Influence of Sibuti River on Miri-Sibuti Coral Reefs (MSCR)

7.1 Introduction

Coral reefs are considered as the rainforest of the ocean and termed as labyrinths of living limestones associated with 25% of the marine life, covering 0.2% of the ocean floor worldwide and are present in coastlines of more than 100 countries and territories (Coral Guardian, 2020). Over the past 240 million years, corals have evolved into one of the most important and complex ecosystems on the planet and are benefiting 850 million people who live within 100 kilometers of reefs (UNEP, 2020; WWF, 2020). Meanwhile, these coral reefs provide about 10% of the fish caught worldwide where this figure rises to 20-25% in developing countries and 70-90% specifically in Southeast Asian countries (Wilkinson et al., 1995; Burke et al., 2002; Burke et al., 2011). Despite the benefits, climate change and local risks, mainly terrestrial inputs from rivers, have threatened coral reefs in various parts of the world and they are expected to disappear by 2050 if immediate actions are not taken for their conservation (Done et al., 2003; Freeman et al., 2013).

Considering the above factors, a key question prevails to many reefs worldwide in accordance with their relationship with the land and river-based pollutants in long term and their resilience towards it. To resolve such issues, many valuable studies have successfully pointed out various effects of such pollutants. The effects of these land and river-based pollutants might include changes in water quality, increased dissolved nutrients and fine sediments load with continuous changes in the respective coastal region and mainly responsible for the increase in algal density, changes in coral community composition, and diseases (Callender et al., 1984; Luke et al., 2003; Warne et al., 2005; Andrew et al., 2005; Mahdi et al., 2016; MacNeil et al., 2019).

The suspension of such fine particles' existence in river estuaries mainly leads these to the coastal environment and can affect the corals through microbial process triggered by the organic matter present in the sediments (Paul et al., 2014). Water quality issues impacting GBR (Great Barrier Reef) were found to be linked to the input of river plumes particularly during the wet season (La Niña influence) and washouts from river estuaries causing turbidity from fine sediment, high nutrients and high

phytoplankton biomass (De'ath et al., 2010; Fabricius et al., 2014; MacNeil et al., 2019). Similar sedimentation effects on coral reefs near Soufriere and Anse La Raye/Anse Galet river in Caribbean islands (Nugues et al., 2003) and Magdalena River influenced region in Columbia (Restrepo et al., 2016) were also associated with heavy rainfall (La Niña influence). These sediments have inhibitive effects on reef communities and the sedimentation processes, including various associations between substrate type, turbidity and light availability, affecting coral distributions on all scales from local depth restrictions to broad-scale biogeography (McLaughlin et al., 2003; Wolanski et al., 2003). In addition, riverine inputs of metals associated with water and sediments also work as a major stressor in the coral reef ecosystem (Ali et al., 2011). They can cause effects such as changes in the rate of photosynthesis which results in a decrease in coral calcification and growth rates during the juvenile polyp stage (Ferrier et al., 2001), increased coral bleaching (Sabdono et al., 2009), outright mortality in associated invertebrates and fishes (Peters et al., 1997) and physiological stress (Harland et al., 1989).

In the case of Miri-Sibuti coral reefs, it falls under endangered conditions globally, as 95% of the reef's decline is happening because of the local sources (Burke et. al. 2011). Major threats are identified to be local precipitation near the Miri coast and river discharge related to pacific decadal oscillation (PDO) (Krawczyk et al., 2020). The positive PDO mainly influences dry sinking air and reduced rainfall termed as South-west monsoon (SWM) and negative PDO brings more cold air and more rainfall termed as North-east monsoon (NEM). During the NEM, precipitation prevails in the southern region of the South China Sea (SCS) as an effect of high pressure over Asia and low pressure over Australia that pushes Intertropical Convergence Zone (ITCZ) towards the south resulting in the highest rainfall over Borneo and highest river run-off, whereas the vice versa effect is visible during the SWM (Steinke et al., 2010; Stephens et al., 2008) This monsoonal effect is mainly responsible for hydrological balance in the region and controlling the river run-offs (Krawczyk et al., 2020; Browne et al., 2019). The increased deforestation in Borneo since 1970 has resulted in the loss of 26% forest cover (Bryan et al., 2013) and has paved way for the increased in terrestrial sedimentation in the coastal environment through major rivers (Baram, Miri and Sibuti), aggravated by the above mentioned PDO (Krawczyk et al., 2020). Studies by Browne et al. (2019) in Miri-Sibuti coral reef region also indicated a 5-fold increase

in bioerosion and increase in bleaching of corals after the NEM during 2017 as compared to the SWM. High sedimentation rate and nutrients inputs were mainly responsible, where sediment accumulation rate, distance from local rivers and concentration of silt/clay fraction have played a major role. In addition, river mouths are identified to be key drivers of such sources. The presence of major rivers such as Baram, Miri (in NE part of Miri coast) and Sibuti (in SW part of Miri coast) are the major contributors of terrestrial pollutants in this coral reef region. The influence of the Sibuti river has been undermined despite being nearest to the coral reefs region and discharging directly into it in comparison to the Miri and Baram rivers due to a lack of compositional data related to water and sediment. As this study mainly focuses on the compositional character of water, sediments and suspended solids in the Sibuti river estuary, this chapter is mainly focusing on the comparison of acquired water data and its geochemistry with the seawater data acquired by Moollye (2017) from Eve garden, North Siwa and Annamone Garden situated in Miri-Sibuti coral reef region, geochemical seawater data from Miri coast acquired by Anandkumar (2016) (Fig. 7.1) and geochemical water data from the Lower Baram region acquired by Prabakaran (2017) to identify the influence of rivers into the coral reefs of this region. The area covered by these studies, and their sampling location with respect to Sibuti river estuary (Current study) is shown in Fig. 7.1. Moreover, no such comparison is made so far with the reef ecosystem. This study utilizes average concentrations of ions, nutrients and metals in the water and sediments from the present study and existing data sets generated by Anandkumar (2016), Prabakaran (2017) and Moollye (2017) and the geochemical interpretations are used as supporting literature to project the influence of Sibuti river estuary in the coastal region including Miri-Sibuti coral reefs.

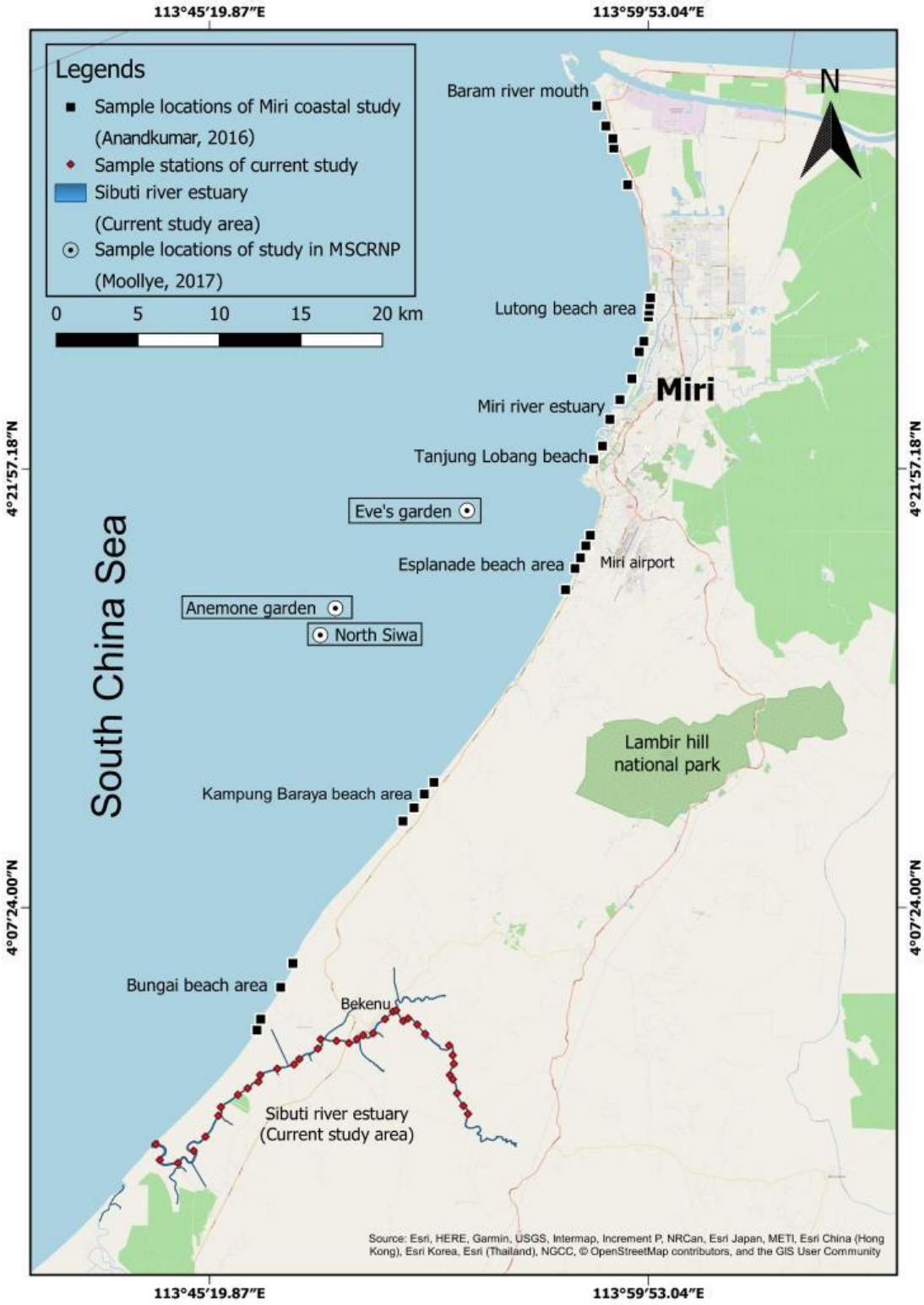

Fig. 7.1 Map showing study area considered by Anandkumar (2016) and Moollye (2017) for their and studies along with their sampling point locations with respect to the current study

7.2 Discussion

7.2.1 Seasonal seawater circulation in NW part of Borneo and sediment transport

River discharged sediment and water carried suspended solid transportation is strongly coupled with sea/ocean water circulation patterns all over the world. If the settling velocity is small enough for the sediment particles, it can spread over a large area sometimes in the entire basin (Poulain et al., 1996; Fohrmann et al., 2001). The exchange of such mass from ambient water mass from rivers and bottom currents are mainly responsible for the process (Fohrmann et al., 2001). In a tropical region like Borneo, where deforestation, temperature and rainfall change due to monsoon, it usually allows rivers to carry a large amount of sediments to the sea by suspension or saltation or even in solution (Whitmarsh et al., 1970). The total sediment loads from Borneo in the South China Sea (SCS) peaks at 910 million tons per year (Milliman et al., 1999; Liu et al., 2013) from major and minor rivers around the island. After entering the sea, the majority of sediment deposits on the continental shelf. However, a small percentage of such sediments were also observed in the abyssal basin of the South China Sea (Liu et al., 2011) from which the majority of the surface sediments including clay minerals are terrigenous in nature (Liu et al., 2013). Such transportation is highly dependent on oceanic circulation in the region (Whitmarsh et al., 1970). Considering the above observation, the Sibuti river carries sediments specifically, and is expected to get influenced by SCS water circulation pattern in SW part of Borneo coast where most of the deposits are expected to be scattered near the costal continental region. This study considers silt and clay fractions of the sediments and suspended solids in the Sibuti river estuary where they are usually the major components of such phenomenon (Liu et al., 2013). This can work as a strong tool to evaluate the transport of such mass on the Miri-Sibuti coral reef present in the region with the help of seawater circulation patterns. Studies done by Pa'Suya et al. (2014) in this region suggested that seawater circulation is in a northern direction throughout the year (Fig 7.3) except August when the direction varies and indicates the northeastern flow of oceanic currents (Fig. 7.2). This pattern indicates that the inputs from the Sibuti river is expected to get transported towards the northern and NE direction. In addition, considering study area by Moollye (2017) in Miri-Sibuti coral reef region and research area focused by Anandkumar (2016), the Miri coastal region

is also located in NE part of the Sibuti river estuary (Fig. 7.1) making it ideal to consider their findings to assess the influence of Sibuti river on Miri coastal region including the MSCRNP.

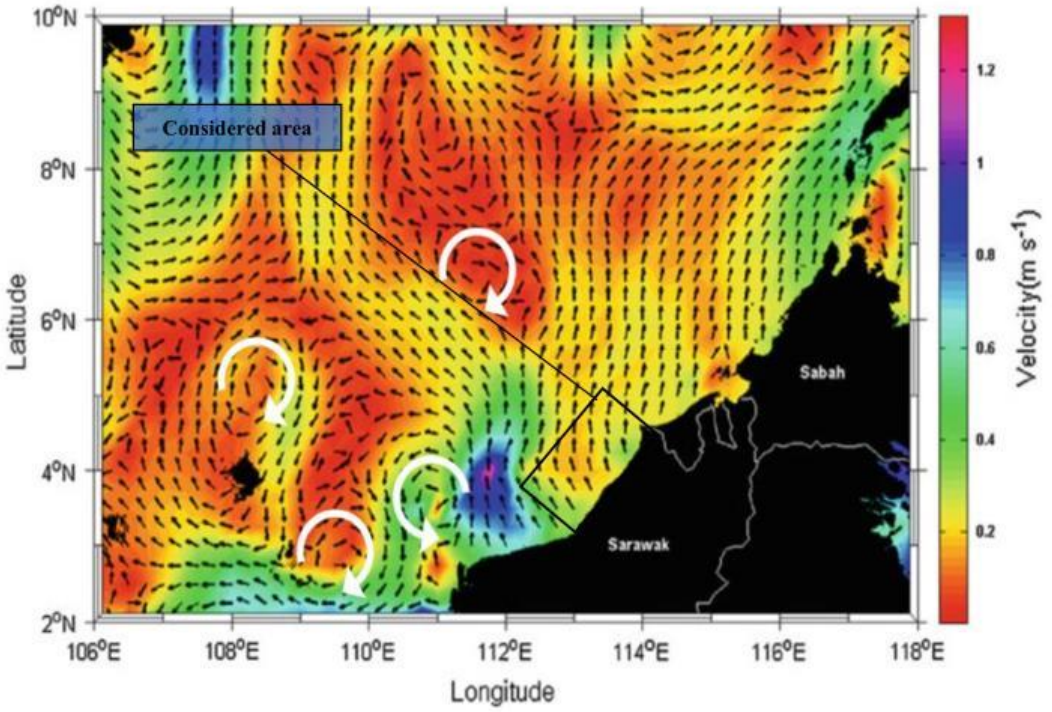

Fig. 7.2 South China sea water circulation during August (Pa'Suya et al., 2014)

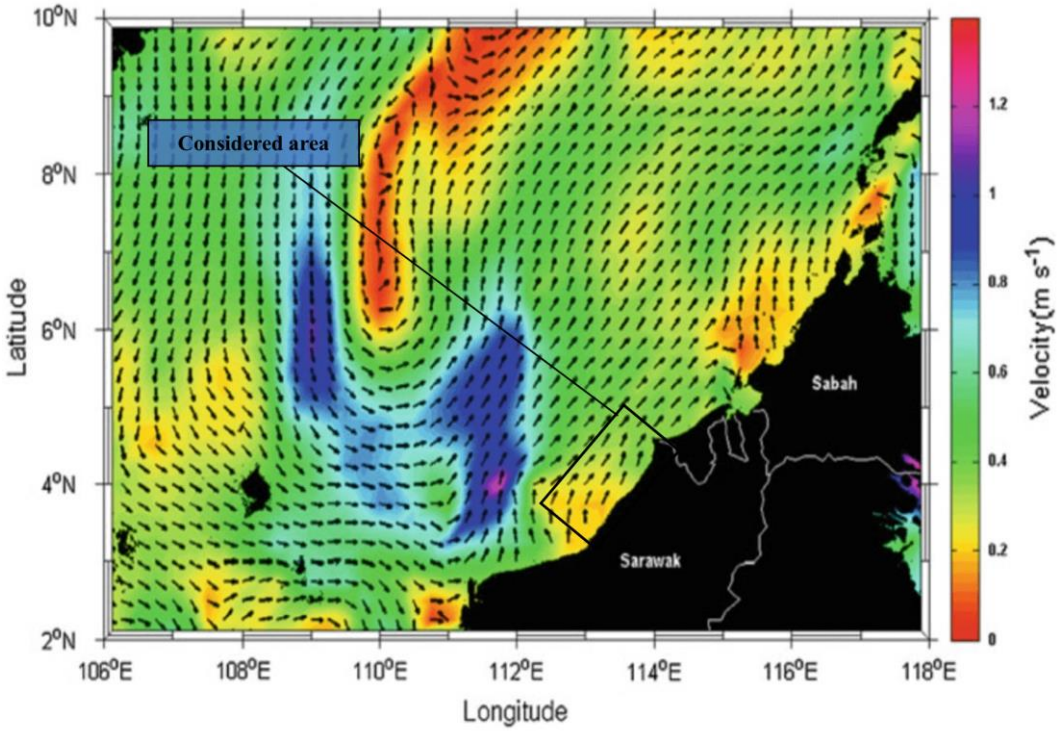

Fig. 7.3 South China sea water circulation during December and rest of the year (Pa'Suya et al., 2014)

7.2.2 Water quality data comparison of Sibuti river estuary and association with Miri coast and MSCRNP water

Water quality alteration in the coral reef ecosystem is complex stressors, which are mainly associated with terrestrial run-off from rivers. The nutrient and trace metal load in such systems are usually influenced by these terrestrial run-offs from rivers as it depends on the surrounding environment for such inputs (Cooper et al., 2009). These inputs are mainly responsible for causing reduced coral recruitment (Loya et al., 1976; Loya et al., 2004), modified trophic structures (Lapointe, 1997; Fabricius et al., 2005), altered biodiversity (Fallon et al., 1999) and coral mortality (Kline et al., 2006). Considering such observations, water quality data acquired from the Sibuti river estuary was compared to the water quality data acquired from Miri-Sibuti coral reef national park (MSCRNP) (Moollye, 2017) and with Miri coastal water quality data (Anandkumar, 2016). To identify major inputs from the rivers, the lower Baram water quality data (Prabakaran, 2017) was also taken into consideration and is shown in Table 7.1.

7.2.2.1 Influence of physico-chemical parameters

Among all the physico-chemical parameters, variation in turbidity between seasons is maximum at all the locations. Miri coastal water and MSCR region show a significant increase in turbidity during the NEM (Fig 7.3), indicating towards the riverine run-off due to the heavy rain and higher flow associated with this season. Turbidity is mainly caused by the transportation of particulate loads (silt, clay, plankton and organic-rich sediment flocs) by shore currents and can travel up to tens of kilometers away from the mouth (Fabricius et al., 2014). In comparison, the turbidity in MSCRNP is lower than both Sibuti and Miri coastal regions and the lower Baram river shows the highest turbidity among all the locations. But considering the sea currents in the South China Sea (Fig. 7.2), time of measurement in MSCRNP, which is during the pre-NEM period (which might increase during NEM), steady increase in all these 3 locations (Sibuti river, Miri coast and MSCRNP) validates that Sibuti river has induced turbidity to MSCRNP water.

In the case of salinity, average salinity at Miri coastal region and MSCRNP during both seasons remains significantly higher than the Sibuti estuary and the lower Baram region (Fig 7.4). The current study has indicated the dominance of saline water during

both seasons associated with high tidal circulation (Fig. 4.20 and 4.22) in the Sibuti river estuary. On contrary, studies carried out on sea surface salinity (SSS) variation and oxygen isotopes in MSCRNP by Krawczyk et al. (2020) revealed that it is influenced mainly during the winter season (NEM) and is associated with precipitation-evaporation balance along with freshwater discharges from the rivers around Miri region. The study also identified precipitation exceeding evaporation in the southern region and SSS (sea surface salinity) has a significant correlation with the Miri coast but not with the weather station situated at Marudi. In such a case, Sibuti is a major river on the southern coast of Miri and the sea currents aforementioned indicates the probable direct influence of the Sibuti river discharge in SCS regulation during winter season (NEM) along with other rivers like Miri river.

In the case of pH and DO, the average DO concentration in the Sibuti estuary is higher during NEM as compared to the coastal and lower Baram region, whereas pH in the Sibuti estuary is lower than the coastal area and MSCRNP region (Fig. 7.4). The DO concentration in MSCRNP seems to be constant during both seasons. Unlike freshwater system, seawater DO is regulated based on absorption from the atmosphere and photosynthetic production by marine plants (Song et al., 2019), whereas pH is regulated by mainly rainfall and absorption of atmospheric CO_2 (Caldeira et al., 1999). In general, riverine DO and pH inputs exhibit negligible influence on the coastal ecosystem. The same scenario applies to the current study area.

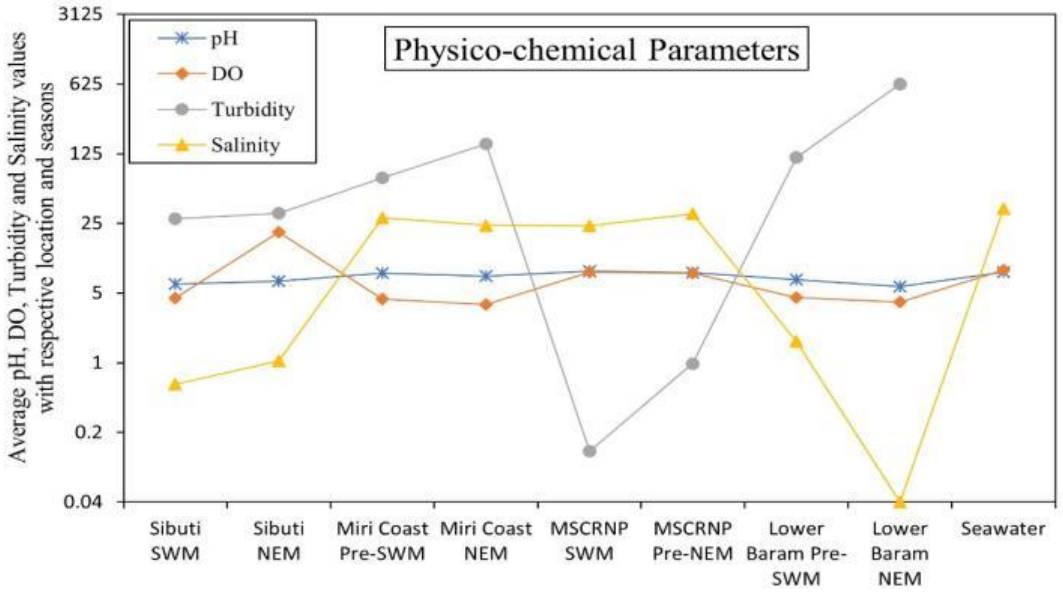

Fig. 7.4 Variation of physico-chemical parameters at Sibuti, Baram river estuary, Miri coastal water and MSCRNP

7.2.2.1.1 Statistical observations

Considering past studies done on the coastal environment including the coral reefs, (1) Anandkumar (2016) indicated that coastal turbidity is mainly influenced by the riverine inputs based on the statistical model. In this study, turbidity was highly correlated with riverine PO_4^{3-}, Ca^{2+}, Zn and Fe, whereas there is a negative correlation with salinity and Mg^{2+} during post-NEM period, where Fe association is assumed to be in colloid form and originating from the suspended particulate matter. He also predicted a reduction in photosynthetic activities related to the turbidity induced by riverine discharges. Comparison of this finding to the Sibuti estuarine chemistry shows a similar association of Fe and Zn with TSS during the NEM in water along with a positive correlation of PO_4^{3-} with velocity and velocity with TSS (Table 4.15) was observed. This indicates the potential washouts of suspended solids from the estuary where it plays a major role during post-NEM period in the coastal water while releasing Fe in colloidal form. Such similarity might be the effect of the proximity of the Sibuti estuary and sea currents in the region as explained before. Such association of turbidity with the mentioned parameters seems to be absent in the lower Baram waters (Prabakaran, 2017) but it also needs to be noted that TSS was not taken into consideration in the lower Baram study, which keeps influence of TSS from Baram unclear in this case. Considering the MSCRNP region, Moollye's (2017) statistical model showed a similar association of Fe and Zn in the region along with the association of turbidity with various nutrients such as NO_3^-, NH_3, SO_4^{2-} and cations like Ca^{2+} along with Cu (Table 7.2). He explained such association is mainly because of terrestrial riverine influence during post-NEM period. The concentration of NH_3 and NO_3^- were observed to be increasing during the NEM (Fig. 7.6) and the nitrification process has been observed in the presence of DO in the Sibuti river estuary, indicating the induced turbidity during post-NEM period in the MSCRNP region. However, the study ruled out SO_4^{2-} concentration in seawater which is already accompanying roughly 2700mg/L of SO_4^{2-} (Rakestraw, 1943; Anthoni, 2006). Browne et al. (2019) suggested that sediment traps, accumulation rate of sediments, concentration of silt/clay fractions and distance from river mouths controlled 62.5% of the benthic composition, among which river mouths in the region controlled 30% of it. The alteration of water quality in the coastal region is mainly influenced by the nutrients associated with sediment load and is the reason behind reduced diversity in

the region (Browne et al., 2019). However, studies done on MSCR region have taken major influence from Baram and Miri river into consideration to assess the riverine impact. On contrary, study done by Anandkumar (2016) showed significant influence of Sibuti river in the SW part of Miri's coastal waters. Furthermore, sea currents with varying seasons indicating a direct flow of Sibuti water carried suspended particles towards the MSCRMP region. A 5-fold increase in bioerosion and increase in bleaching of corals after NEM during 2017 associated with silt/clay fraction along with nutrients validates a scenario of Sibuti rivers' influence in major to minor category.

7.2.2.2 Influence of cations and anions

In the case of ions, measured concentrations at the Sibuti river estuary are comparatively low than the Miri coast (Anandkumar, 2016) and MSCRNP (Moollye, 2017) (Fig. 7.5). The cations and anions help incorporate into the carbonate lattice structure of the reefs in general and these coral reefs represent the major source of carbonate contributors to shallow marine sediments in general (Alharbi et al., 2017). The concentration of ions is much higher in typical seawater and tends to influence river estuaries in intertidal zones (Gasim et al., 2015). A similar case has been noticed where the concentration of ions measured is lower than typical seawater concentrations (Fig. 7.5). Furthermore, the statistical model used for the current study of water chemistry has shown the influence of seawater carried ion in the lower region of the estuary (Table 7.2) during both seasons. These observations indicate a very low to the negligible influence of riverine ions in the MSCRNP region.

The association of Ca^{2+}, Mg^{2+} and turbidity has been noticed during SWM at MSCRNP (Moollye, 2017) (Table 7.2). During the pre-NEM period, Ca^{2+} and Mg^{+2+} have increased in seawater with a decrease in pH in MSCRNP, which was attributed towards seasonal river run-off (Moollye, 2017). During NEM, the concentrations of Ca^{2+} and Mg^{2+} were observed to be much higher than that of during SWM in the Sibuti river estuary, indicating an increase of both ions in the coastal region along with post-NEM association with turbidity in the MSCRNP region. This influence is associated with higher run-off from the Sibuti river along with the northward sea current of SCS (Fig. 7.1 and 7.3).

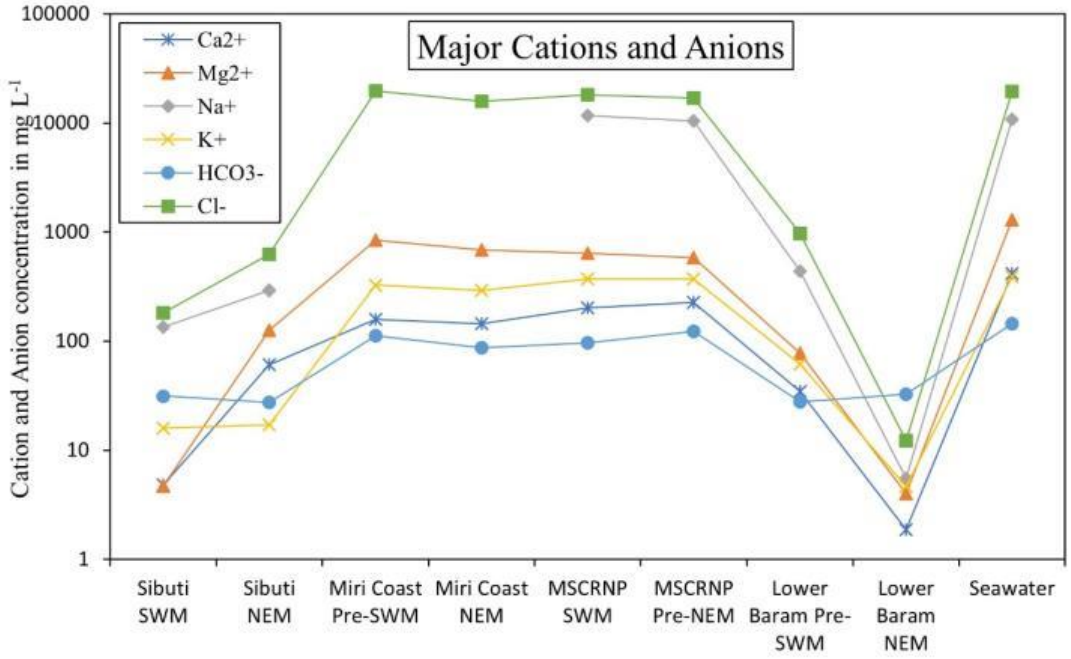

Fig. 7.5 Variation of cations and anions at Sibuti, Baram river estuary, Miri coastal water and MSCRNP

7.2.2.3 Influence of nutrients

The proximity of coast and river-off are the major source of nutrients in the coral ecosystem. It mainly depends on the surroundings of the inputs and river run-offs are the main identified source for dissolved inorganic nutrients in the coral environment (D'Angelo et al., 2014; Moollye, 2017). Similar closer proximity is associated with MSCRNP and these nutrients pose a higher threat as stressors and tend to cause eutrophication in association with turbidity in this region (Chislock et al., 2013; D'Angelo et al., 2014; Anandkumar, 2016; Moollye, 2017). In Miri coastal region, Anandkumar (2016) identified a major source of PO_4^{3-} as natural weathering of phosphorus-bearing minerals in the rocks and NO_3^- from anthropogenic sources such as fertilizer waste from agricultural fields. These nutrients are assumed to be direct input from river inputs in the region. In addition, he observed higher PO_4^- in the northern part of the Miri coast near the Baram river whereas higher NO_3^- and NH_3 concentrations are associated with the southern part (Bungai beach) of the Miri coast and are in close proximity to the Sibuti river mouth.

Considering the variation of nutrients, NO_3^- and NH_3 were observed to be increasing during NEM due to higher run-off (Fig. 7.6). However, the concentration of PO_4^{3-} is decreasing in the Sibuti river estuary during NEM because of the aerobic condition of the estuary and freshwater-dominated sediments favors PO_4^{3-} to bond with Fe (Roden

et. al. 1997; Gächter et. al. 2003; Hartzell et. al. 2012). During the post-NEM period, the average concentration of NO_3^- and NH_3 shows an increasing trend in Miri coastal waters and MSCRNP region (Fig. 7.6). In the case of PO_4^{3-}, a similar trend of the Sibuti river estuary has been observed in the Miri coast but opposite in the MSCRNP region where it increases during NEM. This might be the influence from the Baram river where fluctuation in PO_4^{3-} concentration is lesser (Fig. 7.6). SO_4^{2-} concentration of seawater is as high as 2700mg/L (Rakestraw, 1943; Anthoni, 2006), which can be observed to be much higher than both the averages for Sibuti and Baram river (Fig. 7.6) and devoid of riverine influence.

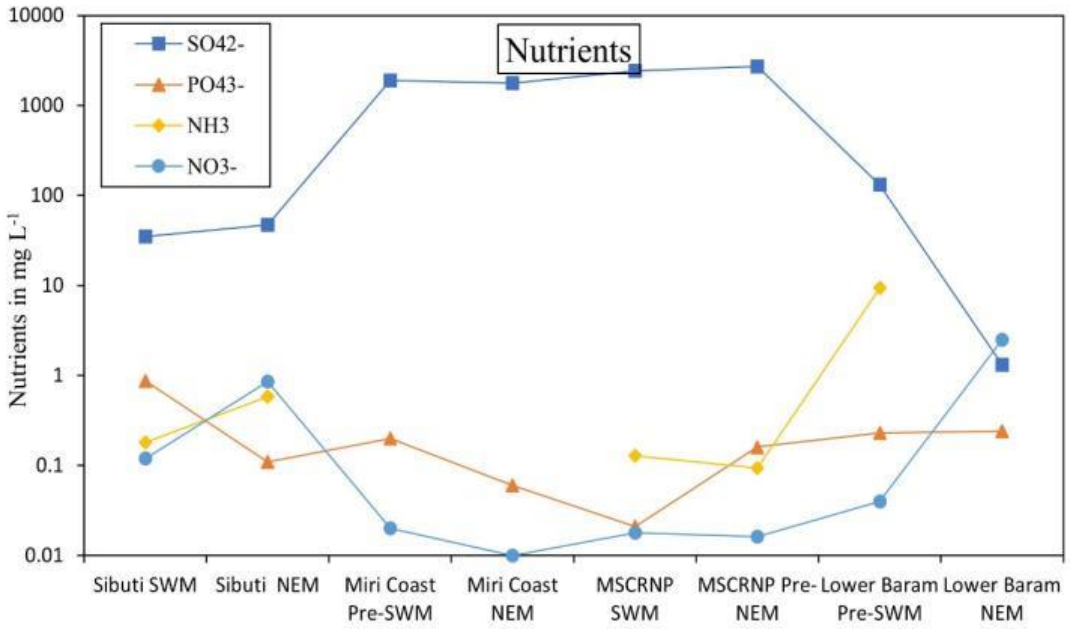

Fig. 7.6 Variation of Nutrients at Sibuti, Baram river estuary, Miri coastal water and MSCRNP

7.2.2.3.1 Statistical observations

The statistical analysis in the Sibuti river estuary is shown (Table 7.2), depicting an independent behavior of NO_3^- in the factor model and is a result of fertilizers from the agricultural fields, whereas NH_3 is associated with DO, indicating that nitrification process has occurred in the estuary during SWM. In the MSCRNP region, both were also found to be controlling major factors (Table 7.2). Similarly, a higher concentration of both were found in the river and nitrification process was observed to be dominant in the presence of DO in the estuary converting NO_3^- to NH_3 as discussed before where NO_3 was specifically found to be associated with turbidity in the estuary (Table 7.2). In the MSCRNP region, both NO_3^- and NH_3 were associated

with turbidity and river run-off during NEM (Moollye, 2017). In the case of PO_4^{3-}, association is mainly with TSS, specifically Fe particulate matter in the estuary and found to be associated with pH and other chalcophile metals in the MSCRNP region. This observation indicates a direct influence of the Sibuti river carrying nutrients on the MSCRNP water associated with the sea currents during both seasons.

7.2.2.4 Influence of metals

Metal concentration in seawater is less compared to freshwater streams (Md Yunus et al., 2015). Their solubility depends on the solvent characteristics and solubility constant for each metal, which determines its proportionality and abundance (Pizarro et al., 2001; Tang et al., 2010; Anandkumar, 2016). These can be observed in both intertidal waters and the surface water column (Tang et al., 2010; Md Yunus et al., 2015). In a coral ecosystem, dissolved metals can cause larval motility, larval settlement success and slower fertilization success (Kathryn et al., 2013; Reichelt et al., 2005). Studies revealed that trace metals such as Cu, Pb, Zn, Cd, and Ni can result in acute or chronic toxicity causing lethal effects or long-term impacts to key biological processes of corals, such as respiration, fertilization, and metamorphosis (Reichelt et al., 2005). As per ANZECC and ARMCANZ (2000) water quality guidelines, the trigger value for Cu in marine water to conserve 99% of species is 0.3µg/L, whereas the same percentage of species can be conserved with 2.2µg/L, 7.0µg/L, 7.0µg/L, 0.7µg/L of Pb, Zn, Ni, and Cd respectively.

In the current study area, the concentration of all the metals is higher than the typical seawater concentration and seems to be increasing during NEM, except for metals like Cd, Mn and Cr (Fig. 7.7) due to absorption by suspended solids and formation of Mn oxyhydroxides as previously discussed in section 4.4.3. In Miri coastal region, Zn, Cd and Mn during NEM and Cu, Pb, Co, Ni, Fe and Cr concentrations in the post-NEM period are higher for the samples collected near the riverine influence area (Anandkumar, 2016). In the SW region of Miri coastal water, higher enrichment of Co, Mn and Cu was shown compared to other metals during NEM and these metals were mainly originating from oxidation of shale and pyrite concretion situated from Tukau and Sibuti formations. Meanwhile, Fe concentration was found higher at Kampung Baraya beach situated in the northern region of the Sibuti river mouth (Anandkumar, 2016). In MSCRNP water, all the metal concentration is increasing

during NEM except Mn and Fe. The average concentrations are higher than the typical seawater concentration, indicating riverine influence in the region. The concentration of Co and Cu were found to be much higher during NEM and associated with turbidity in MSCRNP (Moollye, 2017). The average concentrations of these metals are higher in the Sibuti estuarine water than the lower Baram region (Fig. 7.7). The metal concentration variation in the Sibuti river, Miri SW coast and MSCRNP align very

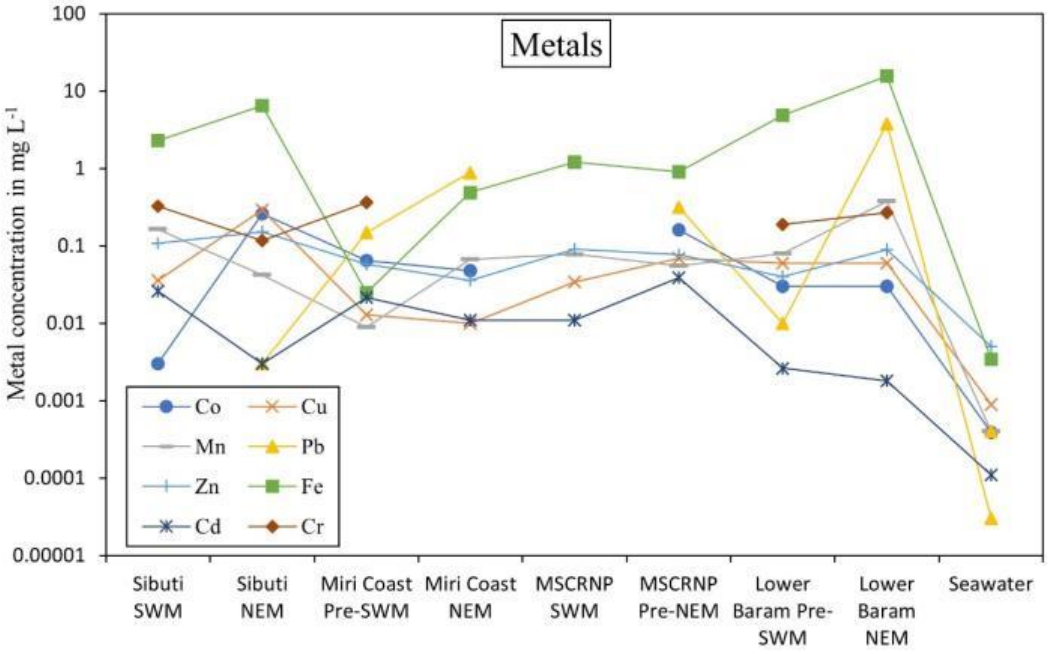

well with the sea current as discussed previously, which indicates a direct reach of these dissolved metals in MSCRNP water.

Fig. 7.7 Variation of Metals at Sibuti, Baram river estuary, Miri coastal water and MSCRNP

7.2.2.4.1 Statistical observations

Considering the statistical analysis done in the current study area, Miri coast and MSCRNP region, metals like Cu in MSCRNP water were associated with turbidity and played a major role in MSCRNP water chemistry compared to other metals (Moollye, 2017) (Table 7.2). Amongst the metals considered, Cu has a higher average value in Sibuti estuarine water than the Baram river inputs during both seasons (Fig. 7.7). The statistical model for the current study area also revealed its association with chalcophile metals like Zn during the SWM and Se during NEM and is a major input from oxidation of pyrite concretion from Tukau and Sibuti formation in the river basin (Nagarajan et al., 2017a; Anandkumar, 2016). Other metal associations like Fe and turbidity during SWM can be observed in both the Sibuti river estuary and Miri coast

(Anandkumar, 2016) (Table 7.2), Association with Fe, Zn and Mn can be observed during NEM in the Sibuti estuarine water and Miri coastal water whereas the same association was also found in MSCRNP region during the pre-SWM (post-NEM period) (Table 7.2). Such associations of Zn, Cd and Mn have been prominent in the Sibuti estuarine water, which were associated with TSS during NEM and the same association has been noticed in Miri coastal water. In the MSCRNP region, Cd and Zn were found together and considered as a result of riverine inputs, which contributes to a major part in the factor model of Moollye (2017). These associations of metals in river water, Miri coast and MSCRNP water indicate that the flow of the Sibuti river carried metals into the MSCRNP water through the northern and north-eastern sea currents during monsoon and post-monsoonal period.

Table 7.1 Comparison of Sibuti estuarine water quality parameters (Average) with Lower Baram, Miri coast and Miri-Sibuti coral reefs

Parameters	Unit	Sibuti river estuary (Current study)		Miri Coast (Anandkumar, 2016)		Lower Baram (Prabakaran, 2017)		Miri Sibuti Coral Reefs (Moollye, 2017)		Average typical Seawater quality parameters (Lenntech, 2005; Anthoni et al., 2006; Moollye, 2017)
		SWM	NEM	Pre-SWM	NEM	Pre-SWM	NEM	SWM	Pre-NEM	
Physico-chemical Parameters										
Temperature	℃	28.40	30.04	31.37	30.91	30.13	26.7	29.688	30	--
pH	--	6.16	6.61	7.94	7.40	6.82	5.81	8.352	8.068	8.1
DO	mg L^{-1}	4.44	20.49	4.37	3.86	4.53	4.05	8.109	7.918	8.5
Turbidity	NTU	27.90	31.69	71.70	156.59	114.77	627.76	0.13	0.981	--
Salinity	ppt	0.61	1.05	28.53	23.85	1.64	0	23.613	31.1	35
TSS	mg L^{-1}	55.62	156.81	--	--	--	--	--	--	--
Cations and Anions										
Ca^{2+}	mg L^{-1}	4.83	60.58	157.7	144.51	34.43	1.87	202.501	226.833	416
Mg^{2+}	mg L^{-1}	4.70	125.92	840.38	688.64	77.27	4	641.8	584.1	1295
Na^{+}	mg L^{-1}	134.70	292.97	--	--	437.62	5.54	11750	10400	10752
K^{+}	mg L^{-1}	15.89	17.10	325.89	292.91	61.48	4.67	373.85	374.05	390
HCO_3^{-}	mg L^{-1}	31.35	27.45	111.76	86.75	27.74	32.79	96.58	123.017	145
CO_3^{2-}	mg L^{-1}	BDL	BDL	8.70	7.49	BDL	BDL	--	--	--
Cl^{-}	mg L^{-1}	182.17	621.85	19764.5	15742.80	966.63	12.25	18103.87	16949.531	19345
Nutrients										
SO_4^{2-}	mg L^{-1}	34.97	46.86	1912.9	1760.71	131.13	1.31	2412.5	2712.5	--
PO_4^{3-}	mg L^{-1}	0.87	0.11	0.2	0.06	0.23	0.24	0.021	0.16	--
NO_3-N	mg L^{-1}	0.03	0.19	--	--	--	--	--	--	--
NH_3	mg L^{-1}	0.18	0.58	--	--	9.38	BDL	0.129	0.094	--
NH_4^{+}	mg L^{-1}	0.15	0.61	--	--	--	--	--	--	--
NO_3^{-}	mg L^{-1}	0.12	0.85	0.02	0.01	0.04	2.50	0.018	0.0163	--

Parameters	Unit	Sibuti river Estuary (Current study)		Miri coast (Anandkumar, 2016)		Lower Baram river (Prabakaran, 2017)		Miri-Sibuti coral reefs (Moollye, 2017)		Average typical Seawater quality parameters (Lenntech, 2005; Anthoni et al., 2006; Moollye, 2017)
		SWM	NEM	Pre-SWM	NEM	Pre-SWM	NEM	SWM	Pre-NEM	
Metals										
Co	mg L^{-1}	0.003	0.261	0.065	0.048	0.03	0.03	BDL	0.161	0.00039
Cu	mg L^{-1}	0.036	0.293	0.013	0.010	0.06	0.06	0.034	0.069	0.0009
Mn	mg L^{-1}	0.164	0.042	0.009	0.067	0.08	0.38	0.078	0.0554	0.0004
Pb	mg L^{-1}	BDL	0.003	0.149	0.887	0.01	3.75	BDL	0.316	0.00003
Zn	mg L^{-1}	0.109	0.151	0.058	0.036	0.04	0.09	0.091	0.077	0.005
Se	mg L^{-1}	6.236	5.522	--	--	--	--	--	--	--
Fe	mg L^{-1}	2.294	6.507	0.025	0.491	4.89	15.57	1.213	0.904	0.0034
Al	mg L^{-1}	BDL	BDL	--	--	2.28	17.07	--	--	--
Cd	mg L^{-1}	0.026	0.003	0.0214	0.011	0.00263	0.00181	0.011	0.039	0.00011
Cr	mg L^{-1}	0.324	0.118	0.365	BDL	0.19	0.27	--	--	--
Ba	mg L^{-1}	0.074	0.031	--	--	--	--	--	--	--

*-- Not measured

*BDL-Below detection limit

Table 7.2 Major statistical associations observed in Sibuti river estuary, Miri coast, MSCRNP and Lower Baram region

Sibuti River Estuary		**Miri Coast (Anandkumar, 2016)**		**Miri Sibuti Coral Reefs (Moollye, 2017)**		**Lower Baram (Prabakaran, 2017)**	
SWM	**NEM**	**Pre-SWM**	**NEM**	**SWM**	**Pre-NEM**	**Pre-SWM**	**NEM**
EC, TDS, Cl^-, Mg^{2+}, Cu, Na, K, SO_4^{2-}, NH_4^+, Ba, Cr (-ve) and Se (-ve)	EC, TDS, DO, salinity, HCO_3^-, Cl^-, Mg^{2+}, Ca^{2+}, K, SO_4^{2-}, Cd, Ba, Cr	Mn, Cd, Pb, Zn	Turbidity, Fe	Cl^-, Fe, Mn, Zn	pH, PO_4^{3-}, Cd, Co, Cu, Pb, Zn	Cl^-, SO_4^{2-}, Pb, Cd, Na^+, Cu, Mn (-ve), Cr (-ve), Al (-ve)	Pb, Zn, Mn, Cu, Co, Al
Fe, Mn, turbidity, salinity and DO (-ve)	EC, TDS, Mg^{2+}, Cl^-, Cu, SO_4^{2-}, NO_3^-, pH (-ve), Co (-ve), Cr (-ve), and turbidity(-ve)	Zn, turbidity	Cd, HCO_3^-	EC, TDS, salinity, Cd	EC, TDS, salinity, NO_3^-, Mg^{2+}, Cl^-, K^+	pH, DO	Fe, Al, K^+
pH, Ba, CO_2	TSS, Zn, Fe, Cd	Zn, SO_4^{2-} (-ve)	SO_4^{2-}, Fe	Turbidity, NO_3^-, NH_3^+, Cu	pH, NO_3^-, HCO_3^-	Cu	EC, Na, Cl^-
NO_3^-	DO, NH_3^+, NH_4	Mn, Fe	K^+, Co	Turbidity, Ca^{2+}, Mg^{2+}, Cu	Cd, Zn	NO_3^-	pH, DO
Cu, Zn	PO_4^{3-}, Velocity, TSS	Co, Fe (-ve), Mn (-ve)	K^+, Cd	Turbidity, SO_4^{2-}	NH_3	Zn, Al	Ca^{2+}, Mg^{2+}, Cl^-, HCO_3^-
SO_4^{2-}, PO_4^{3-}	HCO_3^-, Cu, Se	--	--	--	--	--	--
NH_3, DO	--	--	--	--	--	--	--
Cd, HCO_3^-	--	--	--	--	--	--	--

7.2.3 Sediment data comparison of Sibuti river estuary with Miri coastal sediments and MSCRNP water

Being an integral part of the biological community in the coastal ecosystem, it is important to consider the coastal behavior of the sediment compositions and its metal associations. As the coastal marine communities depend on the metal concentration in water for their survival, the concentration carried by sediment and suspended solids play a major role in transporting such metal from terrestrial source to marine waters. In such scenario, 30 to 98% of toxic materials like metals from geogenic/anthropogenic sources transported by rivers are associated with riverine sediments and suspended solids and behave differently under varying environmental conditions (Gibbs et al., 1973; Yang et al., 2017). Several studies have notified that the trace elements adsorption onto fine sediment particles and desorption happens in changing condition from river to sea with the help of remobilization and organic complexation during early diagenetic processes (Nyffeler et al., 1984; Horowitz, 1984; Impellitteri et al., 2006; Garnier et al., 2006). The size fraction of the sediment plays a major role in absorption of metals as with decreasing particle size, surface area of sediment and suspended solids increases, so as the absorption potential (Fernandes et al., 2015). Under estuarine and seawater conditions, Fe and Mn flocculates to form Fe or Mn hydroxides coating on the fine mineral particles of sediment and suspended solids along with riverine humic acid, making it an active site for metal absorption (Zhou et al., 1994; Fan et al., 2005; Dyer et al., 2005; Hassellov et al., 2008). Once adsorbed, these trace elements have the tendency to be released into the water column when these particles are exposed to reducing conditions. Especially in the case of organic-rich coastal waters in tropical regions like the Miri river, water is mainly associated with a lot of organic debris as it passes through deep forest that is prone to erosion due to deforestation occurring in the region (Anandkumar, 2016), in which, this favors the metals to be water borne in coastal waters. As the current study has considered and analyzed sediment particle <63µm and water borne suspended solids for metallic analysis, it will be helpful to indicate maximum influence in the coastal region because of their easy remobilization and higher tendency to enter the coastal waters through tidal, monsoonal variance along with sea currents observed in South China Sea over the years.

Considering these observations from previous studies, various metal concentrations of sediment and suspended solids from the Sibuti river estuary were taken into consideration along with the concentrations from the Miri coastal sediments and the lower Baram region. These average concentrations were compared with each other to estimate the influence of the Sibuti sediment carried metal influence in the coastal sediments in the absence of sediment data from the MSCRNP region. The observation indicates that the Sibuti riverine sediments and suspended solids are associated with higher concentration of metals than the lower Baram region except Mn and Pb (Fig. 7.8, Table 7.3). However, Mn concentration is significantly higher in Sibuti suspended solids. Average concentrations of metals like Fe, Cu and Co are mainly carried by both bed load and suspended sediments, whereas higher concentration of metals like Mn, Zn and Cd is associated with suspended solids in the Sibuti river estuary. On the other hand, Cr and Pb were only observed in bed load sediments during both seasons of the current study. In previous studies done by Anandkumar (2016), it showed higher concentration of metals like Cu, Co, Cr, Cd and Zn in the Miri coastal SW segment (i.e. Bungai beach and Kampung Baraya beach) which is in the closer proximity to the Sibuti river mouth. He termed these elevated concentrations as a result of leaching from the mineral concretions present in Sibuti basinal area mainly from pyrite concretions. Nagarajan et al. (2013) observed the concentration of acid-leachable metals like Co, Cr, Cu which have seen a 4-fold increase while metal like Zn has increased 2-fold as compared to beaches and bays around the world. These observations in the coastal area and higher concentration in the current study area (Fig. 7.8) indicates the direct influence of Sibuti river originated sediments dominating in the coastal region of Miri. In addition, considering the places in these studies are situated in northern region of the Sibuti river estuary, silt concentration is higher in SW section of the Miri coast and increasing towards the NE direction of the coast (Anandkumar, 2016). This validates the flow of these sediments and suspended solids from the Sibuti river estuary to the northern and NE coastal area with the help of sea currents during the SWM and NEM observed by Pa’Suya et al. (2014).

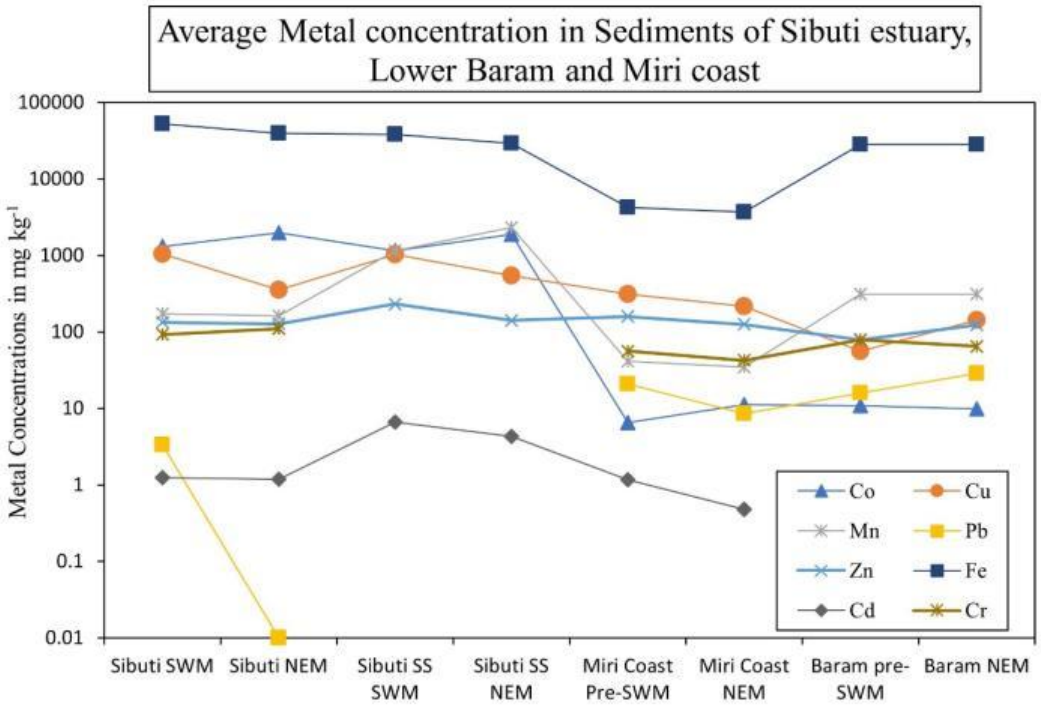

Fig. 7.8 Comparison of Metal concentration of Sibuti estuarine sediments and suspended solids with Lower Baram and Miri coastal sediments

7.2.3.1 Statistical observations

During the NEM, the major variance is controlled by Cu, Zn, Cd and Al in sediments, whereas association of Al, Co and turbidity dominated the variance suspended solids in Sibuti river estuary. These associations were mainly controlled by silt and clay minerals in the estuarine sediments. The high particle reactive nature of Co (Kharkar et al., 1968) and association with turbidity, TSS and Al might be due to the absorption of the metal by water borne suspended solids in the estuary. The same association of metals has also been found in the Miri coastal sediments and is mainly controlled by silt fraction in the sediments during the NEM. The variance of this association is highest in the PCA model done by Anandkumar (2016) (Table 7.4). However, negative association of Co has been noticed in the same component indicating desorption in seawater and forming cobalt-organic complexes in the seawater column (Anandkumar, 2016). Similarly, association of Fe and Mn was observed in both the Sibuti estuarine sediments and the Miri coastal sediments during the same season and assumed to be influenced by the Sibuti river (Anandkumar, 2016) and can be confirmed easily with current study area's findings. Similarly, during the SWM, association of Cu and Fe was found to be associated with silt fraction in both the Sibuti

river and the Miri coastal sediments, indicating direct influence of riverine silt and clay mineral carrying metal in both seasons.

These observations in the coastal environment have given an evidence on the direct influence of Sibuti river carried sediments and suspended solids in the Miri coastal environment and validated the movement of these sediments through sea current that were observed in the region. However, in absence of sediment data from MSCRNP region, a direct influence of sediments cannot be established. In such scenario, comparison with coastal sediment data with current study area can be fruitful is assessment of Sibuti river influence in this region. Findings such as (1) Presence of higher concentration of metals in sediments from current study area than the lower Baram region (Fig. 7.8), (2) Major similar association of metals in the coastal sediment statistical model with current study area (Table 7.4), (3) Oxygen isotopes in MSCRNP indicate direct influence from the Miri coastal precipitations (Krawczyk et al., 2020), (4) River mouths controlling concentration of silt and clay fractions are the key drivers in MSCRNP region (Browne et al., 2019), (5) There is a higher concentration of silt in the SW coast of Miri and its NE flow direction (Anandkumar, 2016), (6) Northern and NE Sea current direction (Pa'Suya et al., 2014) favours the flow of the Sibuti riverine particles towards the MSCRNP region, (7) Controlling factor associations like Cu with turbidity in MSCRNP water and (8) Identical and controlling statistical association in water discussed before (Table 7.2) were taken into consideration. Considering these all, it can be concluded that the Sibuti river has a significant influence on the MSCRNP region. However, the influence is primarily dependent on the seasonal rainfall in the region. In such scenario and above observations, heavy rainfall and higher terrestrial run-off are helpful to push the contaminants beyond estuarine boundaries into the sea during low tidal period. These contaminants eventually reach the MSCRNP region with the help of NE sea currents (Fig. 7.3 and Fig. 7.1) due to Coriolis effect. On the other hand, SWM, which is associated with low flow regime of river due to less rainfall has minor influence due to tidal water dominance in the estuary leading to more settlement in the estuary than washouts.

Table 7.3 Comparison of Average metal concentration in Sibuti estuarine sediments (Bed load and suspended) with Lower Baram and Miri coastal sediments

Metals	Unit	Sibuti river estuarine sediments (Current study)		Sibuti River Estuarine Suspended solids (Current study)		Miri Coast (Anandkumar, 2016)		Lower Baram (Prabakaran, 2017)	
		SWM	NEM	SWM	NEM	Pre-SWM	NEM	Pre-SWM	NEM
Co	mg kg^{-1}	1318.11	1969.36	1145.4	1879.6	6.56	11.21	10.8	9.8
Cu	mg kg^{-1}	1050.78	355.67	1026.58	548.56	313.84	217.21	56.3	142.8
Mn	mg kg^{-1}	174.19	163.23	1158.8	2321.8	41.33	34.9	310	310
Pb	mg kg^{-1}	3.35	0.01	BDL	BDL	20.88	8.59	15.8	28.5
Zn	mg kg^{-1}	133.97	127.59	232.6	141.3	159.32	125.48	78.4	123.1
Se	mg kg^{-1}	789.87	744.01	225.7	212.4	--	--	--	--
Fe	mg kg^{-1}	52496.30	39527.70	38244	29116	4260.07	3660.89	28466	28256
Al	mg kg^{-1}	110824.88	27635.87	19282	7645.1	--	--	63451	63398
Cd	mg kg^{-1}	1.25	1.18	6.68	4.34	1.16	0.48	--	--
Cr	mg kg^{-1}	92.63	110.96	BDL	BDL	56.37	42.6	79.1	64.7
Ba	mg kg^{-1}	2301.48	1487.73	826.4	1059.8	--	--	212.7	212.8

*-- Not measured

*BDL-Below detection limit

Table 7.4 Major statistical associations observed in Sibuti river estuarine and Miri coastal sediments

Sibuti estuarine sediments (Current study)		**Sibuti estuarine suspended solids (Current study)**		**Miri Coast (Anandkumar, 2016)**	
SWM	**NEM**	**SWM**	**NEM**	**Pre-SWM**	**NEM**
Cu, Pb, Se, Fe	Cu, Zn, Al, Cd, Ba (-ve), turbidity (-ve), pH (-ve)	Cu, Mn, Zn, salinity, turbidity, TSS, pH (-ve), Se (-ve), Al (-ve), Co (-ve)	Co, Al, Ba, turbidity, pH	Cu, Fe, silt	Cu, Zn, silt, Co (-ve)
Al	Pb, DO, salinity, pH (-ve)	Fe, Se, Ba, Al (-ve), Mn (-ve), Zn (-ve)	Co, Se, TSS, Ba, salinity	Pb, pH, SO_4	HCO_3, Cr, SO_4
pH, Cr	Cr, Se (-ve)	Co, Cd, Al	Fe, Cd (-ve)	Mn, Cr, Cu	Pb, Cd, silt
Co, Ba	Fe, Mn				Fe, Mn
Cd, Mn, turbidity	--	--	--	--	Cd, Cr (-ve), turbidity

Chapter 8

Conclusions and Recommendations

8.1 Conclusions

After identifying the extent of saltwater influence into the Sibuti river during high tide, surface water samples, bed load sediments and suspended solids were collected along approximately 35 km stretch of Sibuti in the upstream direction starting from the river mouth. The commonly observed monsoons spanning between SW monsoon (June-August) and NE monsoon (December- February) were considered for the sampling.

Objective-1: Geochemical processes

The study of hydrochemistry revealed that seawater intrusion in the estuary plays a major role in regulating the major ions (Cl^-, Mg^{2+}, Ca^{2+}, Na^+, K^+ , HCO_3^- and SO_4^{2-}) irrespective of the seasons. Low flow regime of the river (SWM) was found dominated with Na-Cl type of water major ions are mainly controlled by seawater. However, higher run-off and weathering in the upstream region of river, freshwater intrusion and intense mixing controlled the major ions giving rise to reverse ion exchange and Ca-Cl, Ca-Mg-Cl and Na-Cl type of water during NEM. Major controlling processes for nutrients such as NO_3^-, NH_3, NH_4^+ are found to be denitrification/nitrification and ammonification and are highly dependent on availability of DO in water table. Similarly, mobilization and precipitation of PO_4^{3-} from agricultural run-off is also controlled availability of DO with the help of denitrification coupled to sulfide oxidation and organic matter respiration/mineralization. Averaged Log pCO_2 values shown in the above atmospheric equilibrium (-3.5) indicated the role of respiration of organic matter and dissolution of various minerals in the acidic condition of the estuary. The residence time of river water was found higher during SWM compared to NEM giving rise to higher dissolution of carbonate minerals and precipitation of oxides and oxyhydroxides. During NEM, higher dissolution of sulfate and halide group of minerals are observed due to freshwater infusion and dilution of estuarine water.

In case of trace metals, chalcophile group of metals such as Fe, Mn, Cu, Zn and Se are controlled in water table by oxidation of pyrites and absorption/desorption from organic matter. Resuspension of bed load sediments and suspended solids in turbidity maximum zone is mainly responsible for increase in concentration of Fe and Mn in

water in the lower part of the estuary. This process is also evident in suspended solids where injection of metals especially Mn from bed load sediment into water column under anaerobic condition and through resuspension. It was catalysed by microorganisms, and enhanced by stratification of water and flocculation. The reactive nature of Mn in the presence of organic acid in overlaying oxygenated layer led to absorption of metals like Cu, Mn and Co in SS in the lower region and high turbid zone, which resulted in decrease in concentration of Mn in bed load sediments in the lower part of the estuary. On the other hand, absorption of metals by suspended clay minerals (Al-oxyhydroxides) and Fe oxyhydroxides under ideal pH (4-7), high organic matter concentration and DO condition controlled the distribution of metals such as Se, Co and Ba in the upper part of estuary.

In sediment factor model indicated that metal distribution and transport was mainly controlled by Fe and Mn hydroxides and clay minerals, whereas absorption/desorption was dependent on salinity variation, concentration of DO and pH in the estuary. It is regulated by resuspension and settlement as suspended solids under tidal influence. Furthermore, association of Mn with exchangeable and carbonate fraction as Mn-hydroxide controlled the majority of the processes in metals like Cu, Zn, Ba and Co. Fe and clay minerals with high degree of humification played a vital role in absorption of metals like Ba, Co, Cd, Zn, Cd and Cr in low salinity, high pH conditions along with the mixing zones. In addition, oxic environment during NEM gave rise to Al hydroxides with decreasing stability of clays in intermediate zones of the estuary and was responsible for flocculation of metals like Cd, Se, Cd and Co with increase in salinity.

Objective-2: Source of contaminants

The major ions (Cl^-, Mg^{2+}, Ca^{2+}, Na^+, K^+ , HCO_3^- and SO_4^{2-}) in the estuary are mainly derived from seawater during SWM whereas chemical weathering of rock in upstream region contributed higher concentration of ions like Mg^{2+}, Ca^{2+} and K^+ in the estuary. Nutrients NO_3^-, NH_3, NH_4^+, PO_4^{3-} are mainly originating from agricultural field irrespective of the seasons. Wastewater effluents from Bekenu played a major role in contribution of nutrients especially NH_3. Through the sequential extraction process in sediments, the exchangeable and carbonate fraction was dominated by metals such as Cd, Mn, Ba, Zn and Se whereas reducible fraction was dominated by Cr, Fe, Mn and

Zn. Consequently, Zn and Fe were the dominant metals in oxidizable fraction. The source of metals in the study area was found to be mainly from geogenic origin especially from shale and pyrite concretion of Sibuti formation and siliciclastic sediments of Sibuti and Lambir formation present in the study area. Higher deforestation coupled with high degree of chemical weathering due to higher rainfall contributing to such concentration. Metals such as Cd behaved independently in all the factor models and not associated with the residual fraction of sediments, which confirmed its origin from agricultural effluents, especially from phosphate-based fertilizers used for palm oil plantation in the river basin.

Objective-3: Risk Assessment

Water quality studies indicated the unsuitability of water for drinking purposes. The acidic condition of water and high turbidity at all the stations overwhelming the quantity of ions such as Na^{+}, Mg^{2+}, K^{+}, Cl^{+}, nutrients such as PO_4^{3-} and metals such as Fe, Mn, Cr, Se exceeded the WHO and Malaysian drinking water standards. In case of irrigation quality, estuarine water is found to be suitable by all the indices used. But Chances of sodium hazard are high as confirmed by SAR, Kelly's ratio and %Na index and less than 75% permeability during SWM due to seawater influence. In addition, water is found corrosive in nature, and it cannot be transported through metal pipes and transporting through PVC pipes will be a better option in such conditions.

Sediments were contaminated with Se, Co, Cu, Ba and Cd irrespective of the seasons whereas suspended solids are contaminated by Co, Cu, Cd and Ba at all stations. Contamination by Se and Co is very high compared to the other metals in sediments. Risk indexes like SPI, PLI and PERI categorized sediments as highly polluted with toxic metals and categorized suspended solids in the moderate to highly polluted category. Heavy leaching from the superficial sediment in the source region is responsible for such enrichment in the estuary. ERL and ERM values indicated Cu concentration at 91.66 and 47.22 % during SWM and NEM where it can have the highest possible biological effects to living organisms, whereas occasional adverse effects can be expected from Cu, Zn and Cr. Risk assessment code (RAC) placed Cd, Pb, Mn Se, Ba and Zn to be posing high risk during SWM, whereas Cd, Mn, Ba, Cu and Co during NEM posed medium to high risk towards benthic community of the estuary. The speciation of metals done between suspended solids and water (K_d) values

highlighted the absorption nature of suspended solids in the estuary under ideal pH (4-7) and salinity conditions in the estuary. The order of mobility of metals from solid phase during SWM and NEM can be seen as Cr > Se > Cd > Ba > Zn > Mn > Cu > Co > Fe > Al and as Cr > Se > Cd > Cu > Zn > Co > Ba > Fe > Mn > Al.

Objective-4: Effect of Sibuti river on Miri coastal and MSCR region

From the comparison of this study with previous studies such as Anandkumar (2016) and Moollye (2017), It can be deduced that Sibuti river discharges and its associated contaminants are reaching MSCR region with the help of Northern and NE Sea due to Coriolis effect. Such discharge includes higher concentration of terrestrial input from Sibuti river basin such as metals (Mn, Fe, Al, Se, Cu, Co, Cr, Cd and Zn) and nutrients (NO_3^-, NH_3, NH_4^+, PO_4^{3-}) found in sediments, suspended solids and water. Highest concentration PO_4^{3-} was observed in the current study area compared to Baram and continuous input of NO_3^-, NH_3, NH_4^+ were noticed during both seasons. Highest concentration of trace metals such as Co, Zn, and Cu are also observed in Sibuti river water compared to Baram river water whereas sediments and suspended solids carry highest amount of Cd, Mn, Fe, Co, Zn, Cu and Cr in current study area compared to Baram river inputs. The observed identical statistical associations observed in Sibuti river, coastal water/sediment and MSCR region especially with turbidity confirms such inputs are playing major role in coastal environment and MSCR region. So, it can be concluded that Sibuti river has minor to major influence in the Miri coast as well as MSCR region especially in case of nutrients and metal inputs depending upon monsoonal variation and sea currents observed in the region. This influence can be categorised as minor during SWM due to low flow regime of river and tidal dominance in the estuary especially during high tide. However, the high rainfall and high flow regime of river during NEM is effectively enhancing the contribution of river carried contaminants into South China sea, which eventually influencing the Miri coastal region and MSCR region with the help of sea currents.

8.2 Probable remedial measures for estuarine restoration

As riverine environment and its tributaries is major contributor to land-based contaminants, remedial measures should mainly focus on these contributions in order to preserve estuarine and coastal ecosystem (Md Anawar et al., 2020). In the current study area, various physical, chemical, biological, ecological and engineering based techniques can be utilized to improve the ecosystem.

For water quality improvement, mechanical aeration processes (Zhang et al., 2016; Bai et al., 2020), water transfer or diversion and dilution (Davies et al., 1992) and mechanical algae removal (Middlebrooks et al., 1974) can be utilized. Hydroponic floating beds can be utilized for P and N based nutrients using water spinach (Sun et al., 2017).

Chemical treatment such as flocculation, precipitation, oxidation and algaecides can remove suspended solids (SS) and algae from water (Peilin et al., 2019; Md Anawar et al., 2020). In the case of sediments, mechanical dredging of sediments could be an option as Sibuti river sediments were found to be heavily contaminated with toxic metals (Kondratyev et al., 2003; Md Anawar et al., 2020). In addition, mechanical algae removal, which would also be helpful for sediment as well as water quality improvement.

8.3 Recommendations and Future scope of work

1) This study has focused on geochemistry of bed load sediments and suspended sediments in the estuary. For detailed investigation on provenance and geochemistry of river sediments, undisturbed core samples can be studied in future to further enhance the evidence of their geochemical influence along with geological history of transport, paleo-climate and sediment maturity.

2) Isotopic studies can be considered for the sediment core and bed load sediments to further enhance the source tracing of contaminants like nutrients and metals in the river.

3) The river estuary has rich mangroves and Nipa palm (Mangrove palm) along with shore. The bioaccumulation of elements in these mangroves and in organic rich pore water can be studied. This will help to understand their influence on overlaying water chemistry and toxicity in mangrove system.

4) Numerical estuarine modelling can be done in order to predict the behaviour of pollutants and their impact on river system in response to changing climatic conditions and the influence of increasing anthropogenic activities. Various 2D or 3D numerical models can be adopted to show saltwater influence in estuary and density stratification with the help of data collected with varying depths at different stations. In addition, predictive numerical models of trace element transport to the ocean can also be done in the Sibuti river estuarine system.

5) Trace metals in the river estuary are mainly from oxidation of shale and pyrites from source area especially selenium, which is very high in concentration compared with other parts of the world. This metal has not been considered in any other studies, neither in the source area nor in the coastal region. Future studies can focus on the source of this metal in the river basin.

6) A geochemical fingerprinting or sediment provenance approach can be adopted to enhance the evidence of influence of Sibuti river sediments by identifying critical hot spots of erosion using the geochemical elements, TOC data as fingerprints and path of transport of sediments towards Miri-Sibuti coral reefs.

References

Ab Manan, W. N. A., Sulaiman, F. R., Alias, R., & Laiman, R. (2018). Determination of Selected Heavy Metal Concentrations in an Oil Palm Plantation Soil. Journal of Physical Science, 29, 63-70.

Abbaspour, N., Hurrell, R., & Kelishadi, R. (2014). Review on iron and its importance for human health. Journal of research in medical sciences: the official journal of Isfahan University of Medical Sciences, 19(2), 164.

Adams, J. B., Taljaard, S., Van Niekerk, L., & Lemley, D. A. (2020). Nutrient enrichment as a threat to the ecological resilience and health of South African microtidal estuaries. African Journal of Aquatic Science, 45(1-2), 23-40.

Adesina, R. B., & Ogunseiju, P. (2017). An assessment of bathymetry, hydrochemistry and trace metals in sediments of awoye Estuary in ilaje area, southwestern Nigeria. J. Geosci. Geomat, 5(2), 78-86.

Ahmad, F., Ushiyama, T., & Sayama, T. (2017). Determination of ZR Relationship and Inundation Analysis for Kuantan River Basin. Malaysia Meteorological Department: Petaling Jaya, Malaysia.

Ahmad, Z. Bin , Bee, . Ooi Jin , Leinbach, . Thomas R. and Lockard, . Craig A. (2020, April 13). Malaysia. Encyclopedia Britannica. https://www.britannica.com/place/Malaysia.

Ahmed, N., Siddiqui, N. A., Ramasamy, N., Ramkumar, M., Jamil, M., Usman, M., ... & Rahman, A. H. B. A. (2020). Geochemistry of Eocene Bawang Member turbidites of the Belaga Formation, Borneo: Implications for provenance, palaeoweathering, and tectonic setting. Geological Journal.

Ahnstrom, Z. A. S., & Parker, D. R. (2001). Cadmium reactivity in metal-contaminated soils using a coupled stable isotope dilution− sequential extraction procedure. Environmental science & technology, 35(1), 121-126.

Akram, S., & Rehman, F. (2018). Hardness in drinking-water, its sources, its effects on humans and its household treatment. J Chem Appl, 4(1), 1-4.

Al-Asadi, S. A., Al-Qurnawi, W. S., Al Hawash, A. B., Ghalib, H. B., & Alkhlifa, N. H. A. (2020). Water quality and impacting factors on heavy metals levels in Shatt Al-Arab River, Basra, Iraq. Applied Water Science, 10(5), 1-15.

Albarède, F. (2009). Geochemistry: an introduction. Cambridge University Press.

Alexander, R. B., Boyer, E. W., Smith, R. A., Schwarz, G. E., & Moore, R. B. (2007). The role of headwater streams in downstream water quality 1. JAWRA Journal of the American Water Resources Association, 43(1), 41-59.

Al-Ghanimy, M., Al-Mutawki, K. G., & Falah, H. H. (2019, September). Geochemical Modeling of Groundwater in AL Teeb Area (Northeast Missan Governorate). In Journal of Physics: Conference Series (Vol. 1294, No. 8, p. 082002). IOP Publishing.

Alharbi, W. R., Madkour, H. A., & El-Taher, A. (2017). Coral reefs as a tool for monitoring environmental and radiation hazards. Arabian Journal of Geosciences, 10(4), 89.

Ali, A. H. A., Hamed, M. A., & Abd El-Azim, H. (2011). Heavy metals distribution in the coral reef ecosystems of the Northern Red Sea. Helgoland marine research, 65(1), 67-80.

Ali, H., Khan, E., & Ilahi, I. (2019). Environmental chemistry and ecotoxicology of hazardous heavy metals: environmental persistence, toxicity, and bioaccumulation. Journal of chemistry, 2019.

Allersma, E., Hoekstra, A. J., & Bijker, E. W. (1967). Transport patterns in the Chao Phya estuary. In Coastal Engineering 1966 (pp. 632-650).

Allison, J. D., & Allison, T. L. (2005). Partition coefficients for metals in surface water, soil, and waste. Rep. EPA/600/R-05, 74.

Alsamadany, H., Al-Zahrani, H. S., Selim, E. M. M., & El-Sherbiny, M. M. (2020). Spatial distribution and potential ecological risk assessment of some trace elements in sediments and grey mangrove (Avicennia marina) along the Arabian Gulf coast, Saudi Arabia. Open Chemistry, 18(1), 77-96.

Alshameri, A., Wei, X., Wang, H., Fuguo, Y., Chen, X., He, H., ... & Xu, F. (2019). A Review of the Role of Natural Clay Minerals as Effective Adsorbents and an Alternative Source of Minerals. Minerals.

Annapoorna, H., & Janardhana, M. R. (2015). Assessment of groundwater quality for drinking purpose in rural areas surrounding a defunct copper mine. Aquatic Procedia, 4, 685-692.

Anschutz, A. J., & Penn, R. L. (2005). Reduction of crystalline iron (III) oxyhydroxides using hydroquinone: Influence of phase and particle size. Geochemical Transactions, 6(3), 1-7.

Anthoni, J. F. (2006). The chemical composition of seawater. Magnesium, 2701(7.68), 96-062.

Anthony, K. R., & Hoegh-Guldberg, O. (2003). Kinetics of photoacclimation in corals. Oecologia, 134(1), 23-31.

ANZECC, A. (2000). Australian and New Zealand guidelines for fresh and marine water quality. Australian and New Zealand Environment and Conservation Council and Agriculture and Resource Management Council of Australia and New Zealand, Canberra, 1-103.

APHA, (1998). Standard methods for the examination of water and wastewater (19th ed.). APHA, Washington, DC: USASS.

Aravindan, S., Manivel, M., & Chandrasekar, S. V. N. (2004). Groundwater quality in the hard rock area of the Gadilam River Basin, Tamil Nadu. JOURNAL-GEOLOGICAL SOCIETY OF INDIA, 63(6), 625-635.

Armitage, A. (2014). Coastal Wetland Ecology and Challenges for Environmental Management. Ecology and the Environment, 8, 425-456.

Anandkumar, A. (2016). Ecological risk assessment of the Miri coast, Sarawak, Borneo: A biogeochemical approach (Doctoral dissertation, Curtin University).

Asha, A. S., Saifullah, A. S. M., Uddin, M. G., Sheikh, M. S., Uddin, M. J., & Diganta, M. T. M. (2020). Assessment of trace metal in macroalgae and sediment of the Sundarban mangrove estuary. Applied Water Science, 10(1), 1-13.

Atafar, Z., Mesdaghinia, A., Nouri, J., Homaee, M., Yunesian, M., Ahmadimoghaddam, M., & Mahvi, A. H. (2010). Effect of fertilizer application on soil heavy metal concentration. Environmental monitoring and assessment, 160(1-4), 83.

áVan Rees, K. C. J. (1995). Speciation of particulate-bound cadmium of soils and its bioavailability. Analyst, 120(3), 659-665.

Ayers, R. S., & Westcot, D. W. (1985). Water quality for agriculture (Vol. 29). Rome: Food and Agriculture Organization of the United Nations.

Ayolabi, E. A., Folorunso, A. F., Odukoya, A. M., & Adeniran, A. E. (2013). Mapping saline water intrusion into the coastal aquifer with geophysical and geochemical techniques: The University of Lagos campus case (Nigeria). SpringerPlus, 2(1), 1-14.

Azrul NIsyam, B.K., Ching Siu, J., Joelle Lee, M.S., Lucian Ng, F.L., Mohammad Amir Syafiz, B.M.N., Muhammad Syafiz, B.R., Woon, Z. (2013) Geochemistry of Concretions in Sedimentary Rocks of Setap Shale, Northwest Borneo, Malaysia. BSC dissertation submitted to Curtin Unviersity, Malaysia (unpublished)

Bainbridge, Z. T., Wolanski, E., Álvarez-Romero, J. G., Lewis, S. E., & Brodie, J. E. (2012). Fine sediment and nutrient dynamics related to particle size and floc formation in a Burdekin River flood plume, Australia. Marine pollution bulletin, 65(4-9), 236-248.

Bai, X., Zhu, X., Jiang, H., Wang, Z., He, C., Sheng, L., & Zhuang, J. (2020). Purification effect of sequential constructed wetland for the polluted water in urban river. Water, 12(4), 1054.

Bakri, B., Sumakin, A., Widiasari, Y., & Ihsan, M. (2020). Distribution pattern of water salinity analysis in Jeneberang river estuary using ArcGIS. In IOP Conference Series: Earth and Environmental Science (Vol. 419, No. 1, p. 012116). IOP Publishing.

Balasubramanian, A. (1986). Hydrogeological investigations in the Tambraparani river basin, Tamil Nadu. Unpublished PhD Thesis, University of Mysore, Mysore.

Balistrieri, L. S., Borrok, D. M., Wanty, R. B., & Ridley, W. I. (2008). Fractionation of Cu and Zn isotopes during adsorption onto amorphous Fe (III) oxyhydroxide: experimental mixing of acid rock drainage and ambient river water. Geochimica et Cosmochimica Acta, 72(2), 311-328.

Banerjee, K., Senthilkumar, B., Purvaja, R., & Ramesh, R. (2012). Sedimentation and trace metal distribution in selected locations of Sundarbans mangroves and Hooghly estuary, Northeast coast of India. Environmental geochemistry and health, 34(1), 27-42.

Baran, A., & Tarnawski, M. (2015). Assessment of heavy metals mobility and toxicity in contaminated sediments by sequential extraction and a battery of bioassays. Ecotoxicology, 24(6), 1279-1293.

Barančíková, G., & Makovníková, J. (2003). The influence of humic acid quality on the sorption and mobility of heavy metals. Plant Soil Environ, 49(12), 565-571.

Barbieri, M. (2016). The importance of enrichment factor (EF) and geoaccumulation index (Igeo) to evaluate the soil contamination. J Geol Geophys, 5(1), 1-4.

Bardal, E., & Derby, B. (2004). Different forms of corrosion classified on the basis of appearance. Corrosion and protection, 89-191.

Baric, A., Kuspilic, G., & Matijevic, S. (2002). Nutrient (N, P, Si) fluxes between marine sediments and water column in coastal and open Adriatic. Hydrobiologia, 475(1), 151-159.

Barrio-Parra, F., Elío, J., De Miguel, E., García-González, J. E., Izquierdo, M., & Álvarez, R. (2018). Environmental risk assessment of cobalt and manganese from industrial sources in an estuarine system. Environmental geochemistry and health, 40(2), 737-748.

Bartlett, R., & James, B. (1979). Behavior of chromium in soils: III. Oxidation (Vol. 8, No. 1, pp. 31-35). American Society of Agronomy, Crop Science Society of America, and Soil Science Society of America.

Bartley, R., Bainbridge, Z. T., Lewis, S. E., Kroon, F. J., Wilkinson, S. N., Brodie, J. E., & Silburn, D. M. (2014). Relating sediment impacts on coral reefs to watershed sources, processes and management: A review. Science of the Total Environment, 468, 1138-1153.

Beck, M., Dellwig, O., Schnetger, B., & Brumsack, H. J. (2008). Cycling of trace metals (Mn, Fe, Mo, U, V, Cr) in deep pore waters of intertidal flat sediments. Geochimica et Cosmochimica Acta, 72(12), 2822-2840.

Beckett, P. H. (1989). The use of extractants in studies on trace metals in soils, sewage sludges, and sludge-treated soils. In Advances in soil science (pp. 143-176). Springer, New York, NY.

Beiras, R. (2018). Marine pollution: sources, fate and effects of pollutants in coastal ecosystems. Elsevier.

Belzile, N., Chen, Y. W., & Xu, R. (2000). Early diagenetic behaviour of selenium in freshwater sediments. Applied Geochemistry, 15(10), 1439-1454.

Ben Amor, R., Yahyaoui, A., Abidi, M., Chouba, L., & Gueddari, M. (2019). Bioavailability and assessment of metal contamination in surface sediments of rades-hamam lif coast, around meliane river (Gulf of Tunis, Tunisia, Mediterranean Sea). Journal of Chemistry, 2019.

Benjamin, M. M., & Leckie, J. O. (1982). Effects of complexation by chloride, sulfate, and thiosulfate on adsorption behavior of cadmium on oxide surfaces. Environmental Science & Technology, 16(3), 162-170.

Benson, N. G. (1981). The freshwater-inflow-to-estuaries issue. Fisheries, 6(5), 8-10.

Berry, K. L., Seemann, J., Dellwig, O., Struck, U., Wild, C., & Leinfelder, R. R. (2013). Sources and spatial distribution of heavy metals in scleractinian coral tissues and sediments from the Bocas del Toro Archipelago, Panama. Environmental monitoring and assessment, 185(11), 9089-9099.

Bewers, J. M., & Yeats, P. A. (1978). Trace metals in the waters of a partially mixed estuary. Estuarine and Coastal Marine Science, 7(2), 147-162.

Bianchi, T. S. (2007). Biogeochemistry of estuaries. Oxford University Press on Demand.

Biati, A., Karbassi, A. R., Hassani, A. H., Monavari, S. M., & Moattar, F. (2010). Role of metal species in flocculation rate during estuarine mixing. International Journal of Environmental Science & Technology, 7(2), 327-336.

Bilotta, G. S., & Brazier, R. E. (2008). Understanding the influence of suspended solids on water quality and aquatic biota. *Water research*, *42*(12), 2849-2861.

Bjorn, P., & Roychoudhury, A. N. (2015). Application, chemical interaction and fate of iron minerals in polluted sediment and soils. Current Pollution Reports, 1(4), 265-279.

Bloundi, M. K., Duplay, J., & Quaranta, G. (2009). Heavy metal contamination of coastal lagoon sediments by anthropogenic activities: the case of Nador (East Morocco). Environmental Geology, 56(5), 833-843.

Bolaños, R., Brown, J. M., Amoudry, L. O., & Souza, A. J. (2013). Tidal, riverine, and wind influences on the circulation of a macrotidal estuary. Journal of Physical Oceanography, 43(1), 29-50.

Boomer, K. M. B., & Bedford, B. L. (2008). Influence of nested groundwater systems on reduction–oxidation and alkalinity gradients with implications for plant nutrient availability in four New York fens. Journal of hydrology, 351(1-2), 107-125.

Boothroyd, J. C. (1978). Mesotidal inlets and estuaries. In Coastal sedimentary environments (pp. 287-360). Springer, New York, NY.

Borgese, L., Federici, S., Zacco, A., Gianoncelli, A., Rizzo, L., Smith, D. R., ... & Bontempi, E. (2013). Metal fractionation in soils and assessment of environmental contamination in Vallecamonica, Italy. Environmental Science and Pollution Research, 20(7), 5067-5075.

Boyd, C. E. (2014). Hydrogen sulfide, toxic but manageable. Global Aquaculture Advocate, 34-36.

Boyle, E. A., Edmond, J. M., & Sholkovitz, E. R. (1977). The mechanism of iron removal in estuaries. Geochimica et Cosmochimica Acta, 41(9), 1313-1324.

Boyle, E. A., Sclater, F., & Edmond, J. M. (1976). On the marine geochemistry of cadmium. Nature, 263(5572), 42-44.

Brandt J. Malcolm, K. Michael Johnson, Andrew J. Elphinston, Don D. Ratnayaka. (2017). Chapter 7 - Chemistry, Microbiology and Biology of Water, Twort's Water Supply (Seventh Edition), Butterworth-Heinemann, 235-321, ISBN 9780081000250, https://doi.org/10.1016/B978-0-08-100025-0.00007-7.

Brantley, S. L., Lebedeva, M. I., Balashov, V. N., Singha, K., Sullivan, P. L., & Stinchcomb, G. (2017). Toward a conceptual model relating chemical reaction fronts to water flow paths in hills. Geomorphology, 277, 100-117.

Brayner, F. M. M., da Silva, H. K. P., & de Freitas Barbosa, A. M. (2001). Speciation of heavy metals in estuarine sediments in the northeast of Brazil. Environmental Science and Pollution Research, 8(4), 269-274.

Breitfeld, H. T., Hall, R., Galin, T., & BouDagher-Fadel, M. K. (2018). Unravelling the stratigraphy and sedimentation history of the uppermost Cretaceous to Eocene sediments of the Kuching Zone in West Sarawak (Malaysia), Borneo. Journal of Asian Earth Sciences, 160, 200-223.

Briciu, A. E., Mihăilă, D., Graur, A., Oprea, D. I., Prisăcariu, A., & Bistricean, P. I. (2020). Changes in the Water Temperature of Rivers Impacted by the Urban Heat Island: Case Study of Suceava City. Water, 12(5), 1343.

Brodie, J., & Waterhouse, J. (2012). A critical review of environmental management of the 'not so Great'Barrier Reef. Estuarine, Coastal and Shelf Science, 104, 1-22.

Browne, N., Braoun, C., McIlwain, J., Nagarajan, R., & Zinke, J. (2019). Borneo coral reefs subject to high sediment loads show evidence of resilience to various environmental stressors. PeerJ, 7, e7382.

Bryan, J. E., Shearman, P. L., Asner, G. P., Knapp, D. E., Aoro, G., & Lokes, B. (2013). Extreme differences in forest degradation in Borneo: comparing practices in Sarawak, Sabah, and Brunei. PloS one, 8(7), e69679.

Bullock, L. A., Parnell, J., Perez, M., Boyce, A., Feldmann, J., & Armstrong, J. G. (2018). Multi-stage pyrite genesis and epigenetic selenium enrichment of Greenburn coals (East Ayrshire). Scottish Journal of Geology, 54(1), 37-49.

Burchard, H., Schuttelaars, H. M., & Ralston, D. K. (2018). Sediment trapping in estuaries. Annual review of marine science, 10, 371-395.

Burke, L., Reytar, K., Spalding, M., & Perry, A. (2011). Reefs at risk revisited. World Resources Institute.

Burke, L., WRI, L. S., & Spalding, M. (2002). Reefs at risk in Southeast Asia.

Burton, E. D., Phillips, I. R., & Hawker, D. W. (2006). Factors controlling the geochemical partitioning of trace metals in estuarine sediments. Soil and Sediment Contamination: An International Journal, 15(3), 253-276.

Byrd, J. T., Lee, K. W., Lee, D. S., Smith, R. G., & Windom, H. L. (1990). The behavior of trace metals in the Geum Estuary, Korea. Estuaries, 13(1), 8-13.

Caldeira, K., Berner, R., Sundquist, E. T., Pearson, P. N., & Palmer, M. R. (1999). Seawater pH and atmospheric carbon dioxide. Science, 286(5447), 2043-2043.

Callaway, R. J., Specht, D. T., & Ditsworth, G. R. (1988). Manganese and suspended matter in the Yaquina estuary, Oregon. Estuaries, 11(4), 217-225.

Calmano, W., Mangold, S., & Welter, E. (2001). An XAFS investigation of the artefacts caused by sequential extraction analyses of Pb-contaminated soils. Fresenius' Journal of Analytical Chemistry, 371(6), 823-830.

Campbell, J. A., & Yeats, P. A. (1984). Dissolved chromium in the St. Lawrence estuary. Estuarine, Coastal and Shelf Science, 19(5), 513-522.

Canfield, D. E., Jørgensen, B. B., Fossing, H., Glud, R., Gundersen, J., Ramsing, N. B., ... & Hall, P. O. (1993). Pathways of organic carbon oxidation in three continental margin sediments. Marine geology, 113(1-2), 27-40.

Canfield, D. E., Thamdrup, B., & Hansen, J. W. (1993). The anaerobic degradation of organic matter in Danish coastal sediments: iron reduction, manganese reduction, and sulfate reduction. Geochimica et Cosmochimica Acta, 57(16), 3867-3883.

Canuel, E. A., & Martens, C. S. (1993). Seasonal variations in the sources and alteration of organic matter associated with recently deposited sediments. Organic Geochemistry, 20(5), 563-577.

Cao, L., Tian, H., Yang, J., Shi, P., Lou, Q., Waxi, L., ... & Peng, X. (2015). Multivariate analyses and evaluation of heavy metals by chemometric BCR

sequential extraction method in surface sediments from Lingdingyang Bay, South China. Sustainability, 7(5), 4938-4951.

Caporale, A. G., & Violante, A. (2016). Chemical processes affecting the mobility of heavy metals and metalloids in soil environments. Current Pollution Reports, 2(1), 15-27.Okoro, H. K., Fatoki, O. S., Adekola, F. A., Ximba, B. J., & Snyman, R. G. (2012). A review of sequential extraction procedures for heavy metals speciation in soil and sediments.

Carugati, L., Gatto, B., Rastelli, E., Martire, M. L., Coral, C., Greco, S., & Danovaro, R. (2018). Impact of mangrove forests degradation on biodiversity and ecosystem functioning. Scientific reports, 8(1), 1-11.

Catianis, I., Secrieru, D., Pojar, I., Grosu, D., Scrieciu, A., Pavel, A. B., & Vasiliu, D. (2018). Water quality, sediment characteristics and benthic status of the razim-sinoie lagoon system, Romania. Open Geosciences, 10(1), 12-33.

Chabot, D., & Guénette, S. (2013). Physiology of water breathers: effects of temperature, dissolved oxygen, salinity and pH. Climate Change Impacts, Vulnerabilities and Opportunities. Analysis of the Marine Atlantic Basin, 16-44.

Chanda, S., Samanta, A., Paul, B. N., Ghosh, K., & Giri, S. S. (2017). Effect of dietary iron level on growth performance and enzyme activity in Rohu (Labeo rohita Hamilton) fingerlings. Indian Journal of Animal Nutrition, 34(2), 224-228.

Chandra, P., Sinha, S., Rai, U. N., Kruger, E., & Anderson, T. (1997, January). Bioremediation of chromium from water and soil by vascular aquatic plants. In ACS symposium series (Vol. 664, pp. 274-282). Washington, DC: American Chemical Society,[1974]-.

Chang, Y., Müller, M., Wu, Y., Jiang, S., Cao, W. W., Qu, J. G., ... & Mujahid, A. (2020). Distribution and behaviour of dissolved selenium in tropical peatland-draining rivers and estuaries of Malaysia. Biogeosciences, 17(4), 1133-1145.

Chapman, D. V. (Ed.). (1996). Water quality assessments: a guide to the use of biota, sediments and water in environmental monitoring. CRC Press.

Chapman, P. M., & Wang, F. (2001). Assessing sediment contamination in estuaries. Environmental Toxicology and Chemistry: An International Journal, 20(1), 3-22.

Chapman, P. M., Wang, F., Janssen, C., Persoone, G., & Allen, H. E. (1998). Ecotoxicology of metals in aquatic sediments: binding and release,

bioavailability, risk assessment, and remediation. Canadian Journal of Fisheries and Aquatic Sciences, 55(10), 2221-2243.

Chaudhuri, P., Chaudhuri, S., & Ghosh, R. (2019). The role of mangroves in coastal and estuarine sedimentary accretion in Southeast Asia. Sedimentary Processes-Examples from Asia, Turkey and Nigeria.

Chen, D., Hu, M., Guo, Y., & Dahlgren, R. A. (2015). Influence of legacy phosphorus, land use, and climate change on anthropogenic phosphorus inputs and riverine export dynamics. Biogeochemistry, 123(1), 99-116.

Chen, Y. M., Gao, J. B., Yuan, Y. Q., Ma, J., & Yu, S. (2016). Relationship between heavy metal contents and clay mineral properties in surface sediments: implications for metal pollution assessment. Continental Shelf Research, 124, 125-133.

Chenar, S. S., Karbassi, A., Zaker, N. H., & Ghazban, F. (2013). Electroflocculation of metals during estuarine mixing (Caspian Sea). Journal of Coastal Research, 29(4), 847-854.

Cheng, C. H., Jien, S. H., Iizuka, Y., Tsai, H., Chang, Y. H., & Hseu, Z. Y. (2011). Pedogenic chromium and nickel partitioning in serpentine soils along a toposequence. Soil Science Society of America Journal, 75(2), 659-668.

Chidambaram, S., Karmegam, U., Sasidhar, P., Prasanna, M. V., Manivannan, R., Arunachalam, S., ... & Anandhan, P. (2011). Significance of saturation index of certain clay minerals in shallow coastal groundwater, in and around Kalpakkam, Tamil Nadu, India. Journal of earth system science, 120(5), 897-909.

Chidambaram, S., Prasanna, M. V., Karmegam, U., Singaraja, C., Pethaperumal, S., Manivannan, R., ... & Tirumalesh, K. (2011). Significance of pCO_2 values in determining carbonate chemistry in groundwater of Pondicherry region, India. Frontiers of Earth Science, 5(2), 197.

Chidambaram, S., Prasanna, M. V., Singaraja, C., Thilagavathi, R., Pethaperumal, S., & Tirumalesh, K. (2012). Study on the saturation index of the carbonates in the groundwater using WATEQ4F, in layered coastal aquifers of Pondicherry. Journal of the Geological Society of India, 80(6), 813-824.

Chidambaram, S., Ramanathan, A. L., Prasanna, M. V., Lognatan, D., Srinivasamoorthy, K., & Anandhan, P. (2008). Study on the impact of tsunami on shallow groundwater from Portnova to Pumpuhar, using geoelectrical technique-southeast coast of India.

Chidambaram, S., Vijayakumar, V., Srinivasamoorthy, K., Anandhan, P., Prasanna, M. V., & Vasudevan, S. (2007). A study on variation in ionic composition of aqueous system in different lithounits around Perambalur region, Tamil Nadu. JOURNAL-GEOLOGICAL SOCIETY OF INDIA, 70(6), 1061.

Chislock, M. F., Doster, E., Zitomer, R. A., & Wilson, A. E. (2013). Eutrophication: causes, consequences, and controls in aquatic ecosystems. Nature Education Knowledge, 4(4), 10.

Choo-In, S. (2019). The Relationship Between the Total Dissolved Solids and The Conductivity Value of Drinking Water, Surface Water and Wastewater. In The 2019 International Academic Research Conference in Amsterdam (pp. 11-16).

Chopard, A., Plante, B., Benzaazoua, M., Bouzahzah, H., & Marion, P. (2017). Geochemical investigation of the galvanic effects during oxidation of pyrite and base-metals sulfides. Chemosphere, 166, 281-291.

Cochran , J. Kirk. (2014). Estuaries, Module in Earth Systems and Environmental Sciences, Elsevier, ISBN 9780124095489, DOI: https://doi.org/10.1016/B978-0-12-409548-9.09151-X.

Coffey, M., Dehairs, F., Collette, O., Luther, G., Church, T., & Jickells, T. (1997). The behaviour of dissolved barium in estuaries. Estuarine, Coastal and Shelf Science, 45(1), 113-121.

Cole, J. J., & Prairie, Y. T. (2014). Dissolved CO2 in freshwater systems.

Colin, Y., Goñi-Urriza, M., Gassie, C., Carlier, E., Monperrus, M., & Guyoneaud, R. (2017). Distribution of sulfate-reducing communities from estuarine to marine bay waters. Microbial ecology, 73(1), 39-49.

Condie, K. C., Lee, D., & Farmer, G. L. (2001). Tectonic setting and provenance of the Neoproterozoic Uinta Mountain and Big Cottonwood groups, northern Utah: constraints from geochemistry, Nd isotopes, and detrital modes. Sedimentary geology, 141, 443-464.

Conley, D. J., Paerl, H. W., Howarth, R. W., Boesch, D. F., Seitzinger, S. P., Karl E, K. E., ... & Gene E, G. E. (2009). Controlling eutrophication: nitrogen and phosphorus. Science, 123, 1014-1015.

Cooper, T. F., Gilmour, J. P., & Fabricius, K. E. (2009). Bioindicators of changes in water quality on coral reefs: review and recommendations for monitoring programmes. Coral reefs, 28(3), 589-606.

Coral Guardian, Importance of corals and their threats. (n.d.). Coral Guardian (December 5th, 2020). Retrieved, from https://www.coralguardian.org/en/coral-reefs/

Correns, C. W. (1969). Handbook of geochemistry.

Costanzo, S. D., O'Donohue, M. J., & Dennison, W. C. (2003). Assessing the seasonal influence of sewage and agricultural nutrient inputs in a subtropical river estuary. Estuaries, 26(4), 857-865.

Cui, Y., & Weng, L. (2015). Interpretation of heavy metal speciation in sequential extraction using geochemical modelling. Environmental Chemistry, 12(2), 163-173.

Cuong, D. T., & Obbard, J. P. (2006). Metal speciation in coastal marine sediments from Singapore using a modified BCR-sequential extraction procedure. Applied Geochemistry, 21(8), 1335-1346.

Cybulski, J. D., Husa, S. M., Duprey, N. N., Mamo, B. L., Tsang, T. P., Yasuhara, M., ... & Baker, D. M. (2020). Coral reef diversity losses in China's Greater Bay Area were driven by regional stressors. Science advances, 6(40), eabb1046.

D'Angelo, C., & Wiedenmann, J. (2014). Impacts of nutrient enrichment on coral reefs: new perspectives and implications for coastal management and reef survival. Current Opinion in Environmental Sustainability, 7, 82-93.

Dalrymple, R. W., Mackay, D. A., Ichaso, A. A., & Choi, K. S. (2012). Processes, morpho dynamics, and facies of tide-dominated estuaries. In Principles of tidal sedimentology (pp. 79-107). Springer, Dordrecht.

Dalrymple, R. W., Zaitlin, B. A., & Boyd, R. (1992). Estuarine facies models; conceptual basis and stratigraphic implications. Journal of Sedimentary Research, 62(6), 1130-1146.

Damashek, J., & Francis, C. A. (2018). Microbial nitrogen cycling in estuaries: from genes to ecosystem processes. Estuaries and Coasts, 41(3), 626-660.

Dan, S. F., Umoh, U. U., & Osabor, V. N. (2014). Seasonal variation of enrichment and contamination of heavy metals in the surface water of Qua Iboe River Estuary and adjoining creeks, South-South Nigeria. Journal of Oceanography and Marine Science, 5(6), 45-54.

Dang, D. H., Lenoble, V., Durrieu, G., Omanović, D., Mullot, J. U., Mounier, S., & Garnier, C. (2015). Seasonal variations of coastal sedimentary trace metals

cycling: Insight on the effect of manganese and iron (oxy) hydroxides, sulphide and organic matter. Marine pollution bulletin, 92(1-2), 113-124.

Dar, M. A., El-Metwally, M. E., & El-Moselhy, K. M. (2016). Distribution patterns of mobile heavy metals in the inshore sediments of the Red Sea. Arabian Journal of Geosciences, 9(3), 221.

Das, S., & Ting, Y. P. (2017). Evaluation of wet digestion methods for quantification of metal content in electronic scrap material. Resources, 6(4), 64.

Daskalakis, K. D., & O'Connor, T. P. (1995). Normalization and elemental sediment contamination in the coastal United States. Environmental science & technology, 29(2), 470-477.

Davidson, N. C. (2018). Estuary types. In C. M. Finlayson, M. Everard, K. Irvine, R. J. McInnes, B. A. Middleton, A. A. van Dam, & N. C. Davidson (Eds.), The Wetland Book I: Structure and function, management, and methods (pp. 1507-1513). Springer Netherlands. https://doi.org/10.1007/978-90-481-9659-3_338.

Davies, B. R., Thoms, M., & Meador, M. (1992). An assessment of the ecological impacts of inter-basin water transfers, and their threats to river basin integrity and conservation. Aquatic conservation: Marine and freshwater ecosystems, 2(4), 325-349.

Dawson, E. J., & Macklin, M. G. (1998). Speciation of heavy metals on suspended sediment under high flow conditions in the River Aire, West Yorkshire, UK. Hydrological Processes, 12(9), 1483-1494.

De Andrade Passos, E., Alves, J. C., dos Santos, I. S., Jose do Patrocínio, H. A., Garcia, C. A. B., & Costa, A. C. S. (2010). Assessment of trace metals contamination in estuarine sediments using a sequential extraction technique and principal component analysis. Microchemical Journal, 96(1), 50-57.

De Boo, W. (1990). Cadmium in agriculture. Toxicological & Environmental Chemistry, 27(1-3), 55-63.

De Souza Machado, A. A., Spencer, K., Kloas, W., Toffolon, M., & Zarfl, C. (2016). Metal fate and effects in estuaries: A review and conceptual model for better understanding of toxicity. Science of the Total Environment, 541, 268-281.

De'ath, G., & Fabricius, K. (2010). Water quality as a regional driver of coral biodiversity and macroalgae on the Great Barrier Reef. Ecological Applications, 20(3), 840-850.

Deborde, J., Anschutz, P., Chaillou, G., Etcheber, H., Commarieu, M. V., Lecroart, P., & Abril, G. (2007). The dynamics of phosphorus in turbid estuarine systems: Example of the Gironde estuary (France). Limnology and Oceanography, 52(2), 862-872.

Dehaine, Q., Tijsseling, L. T., Glass, H. J., Törmänen, T., & Butcher, A. R. (2021). Geometallurgy of cobalt ores: A review. Minerals Engineering, 160, 106656.

Devi, U., & Bhattacharyya, K. G. (2018). Mobility and bioavailability of Cd, Co, Cr, Cu, Mn and Zn in surface runoff sediments in the urban catchment area of Guwahati, India. Applied water science, 8(1), 1-14.

Devlin, M., Waterhouse, J., Taylor, J., & Brodie, J. (2001). Flood plumes in the Great Barrier Reef: spatial and temporal patterns in composition and distribution. GBRMPA research publication, 68.

Dhillon, K. S., & Dhillon, S. K. (2003). Distribution and management of seleniferous soils. Advances in agronomy, 79(1), 119-184.

Dias, I. A., Cury, L. F., Titon, B. G., Athayde, G. B., Fedalto, G., da Rocha Santos, L., ... & Manuela Bahniuk Rumbeslperger, A. (2020). The Occurrence of Authigenic Clay Minerals in Alkaline-Saline Lakes, Pantanal Wetland (Nhecolândia Region, Brazil). Minerals, 10(8), 718.

Dickson, A. G., Sabine, C. L., & Christian, J. R. (2007). Guide to best practices for ocean CO2 measurements. North Pacific Marine Science Organization.

Dinsley, J. M., Gowing, C. J. B., & Marriott, A. L. (2018). Natural and anthropogenic influences on atmospheric Pb-210 deposition and activity in sediments: a review.

Dollar, N. L., Souch, C. J., Filippelli, G. M., & Mastalerz, M. (2001). Chemical fractionation of metals in wetland sediments: Indiana Dunes National Lakeshore. Environmental science & technology, 35(18), 3608-3615.

Done, T., Whetton, P., Jones, R., Berkelmans, R., Lough, J., Skirving, W., & Wooldridge, S. (2003). Global climate change and coral bleaching on the Great Barrier Reef. Final Report to the State of Queensland Greenhouse Taskforce through the Department of Natural Resources and Mines, 49.

Doneen, L. D. (1964). Water quality for Agriculture, Department of Irrigation. University of California, Davis, 48.

Dooge, J. C. (Ed.). (2009). Fresh Surface Water. Eolss Publishers Company Limited.

Douglas, G. B., Ford, P. W., Palmer, M., Noble, R. M., & Packett, R. (2006). Fitzroy River, Queensland, Australia. II. Identification of sources of estuary bottom sediments. Environmental Chemistry, 3(5), 377-385.

Driscoll, C. T., & Schecher, W. D. (1990). The chemistry of aluminum in the environment. Environmental Geochemistry and Health, 12(1-2), 28-49.

Drogowska, M., Brossard, L., & Ménard, H. (1994). Comparative study of copper behaviour in bicarbonate and phosphate aqueous solutions and effect of chloride ions. Journal of applied electrochemistry, 24(4), 344-349.

Dronkers, J. (2005). Dynamics of coastal systems (Vol. 25). World Scientific.

Drylie, T. P., Needham, H. R., Lohrer, A. M., Hartland, A., & Pilditch, C. A. (2019). Calcium carbonate alters the functional response of coastal sediments to eutrophication-induced acidification. Scientific reports, 9(1), 1-13.

DSMOP, (Department of Statistics Malaysia Official Portal). (2020, June 25). Sarawak @ a Glance. www.dosm.gov.my. Retrieved from https://www.dosm.gov.my/v1/index.php?r=column/cone.

Du Laing, G., Rinklebe, J., Vandecasteele, B., Meers, E., & Tack, F. M. (2009). Trace metal behaviour in estuarine and riverine floodplain soils and sediments: a review. Science of the total environment, 407(13), 3972-3985.

Duinker, J. C., Wollast, R., & Billen, G. (1979). Behaviour of manganese in the Rhine and Scheldt estuaries: II. Geochemical cycling. Estuarine and Coastal Marine Science, 9(6), 727-738.

Dunn, J. G., Sammarco, P. W., & LaFleur Jr, G. (2012). Effects of phosphate on growth and skeletal density in the scleractinian coral Acropora muricata: A controlled experimental approach. Journal of Experimental Marine Biology and Ecology, 411, 34-44.

Duodu, G. O., Goonetilleke, A., & Ayoko, G. A. (2016). Comparison of pollution indices for the assessment of heavy metal in Brisbane River sediment. Environmental pollution, 219, 1077-1091.

Dupré, B., Gaillardet, J., Rousseau, D., & Allègre, C. J. (1996). Major and trace elements of river-borne material: The Congo Basin. Geochimica et Cosmochimica Acta, 60(8), 1301-1321.

Dyer, J. A., Trivedi, P., Scrivner, N. C., & Sparks, D. L. (2004). Surface complexation modeling of zinc sorption onto ferrihydrite. Journal of colloid and interface science, 270(1), 56-65.

Eaton, F. M. (1950). Significance of carbonate in irrigation water, soil sciences. 69.

Eckert, J. M., & Sholkovitz, E. R. (1976). The flocculation of iron, aluminium and humates from river water by electrolytes. Geochimica et Cosmochimica Acta, 40(7), 847-848.

Edokpayi, J. N., Odiyo, J. O., & Durowoju, O. S. (2017). Impact of wastewater on surface water quality in developing countries: a case study of South Africa. Water quality, 401-416.

Edzwald, J. K., Upchurch, J. B., & O'Melia, C. R. (1974). Coagulation in estuaries. Environmental Science & Technology, 8(1), 58-63.

Eisma, D. (1988). Transport and deposition of suspended matter in estuaries and the nearshore sea. In Physical and Chemical weathering in geochemical cycles (pp. 273-298). Springer, Dordrecht.

Elango, L., & Kannan, R. (2007). Rock–water interaction and its control on chemical composition of groundwater. Developments in environmental science, 5, 229-243.

Elderfield, H., & Hepworth, A. (1975). Diagenesis, metals and pollution in estuaries. Marine Pollution Bulletin, 6(6), 85-87.

Elias, M. S., Ibrahim, S., Samuding, K., Ab Rahman, S., & Hashim, A. (2018). The sources and ecological risk assessment of elemental pollution in sediment of Linggi estuary, Malaysia. Marine pollution bulletin, 137, 646-655.

Elias, M. S., Ibrahim, S., Samuding, K., Ab Rahman, S., & Hashim, A. (2018). The sources and ecological risk assessment of elemental pollution in sediment of Linggi estuary, Malaysia. Marine pollution bulletin, 137, 646-655.

Elliott, M., & McLusky, D. S. (2002). The need for definitions in understanding estuaries. Estuarine, coastal and shelf science, 55(6), 815-827.

EPA, (Environmental Protection Agency). (2016, December 19). Mangrove Swamps. Retrieved from https://www.epa.gov/wetlands/mangrove-swamps

Eylem, C., Erten, H. N., & Göktürk, H. (1990). Sorption-desorption behaviour of barium on clays. Journal of environmental radioactivity, 11(2), 183-200.

Fabricius, K. E. (2005). Effects of terrestrial runoff on the ecology of corals and coral reefs: review and synthesis. Marine pollution bulletin, 50(2), 125-146.

Fabricius, K. E., De'ath, G., Humphrey, C., Zagorskis, I., & Schaffelke, B. (2013). Intra-annual variation in turbidity in response to terrestrial runoff on near-shore coral reefs of the Great Barrier Reef. Estuarine, Coastal and Shelf Science, 116, 57-65.

Fabricius, K. E., Logan, M., Weeks, S., & Brodie, J. (2014). The effects of river run-off on water clarity across the central Great Barrier Reef. Marine pollution bulletin, 84(1-2), 191-200.

Facey, J. A., Apte, S. C., & Mitrovic, S. M. (2019). A review of the effect of trace metals on freshwater cyanobacterial growth and toxin production. Toxins, 11(11), 643.

Fallon, S. J., McCulloch, M. T., van Woesik, R., & Sinclair, D. J. (1999). Corals at their latitudinal limits: laser ablation trace element systematics in Porites from Shirigai Bay, Japan. Earth and Planetary Science Letters, 172(3-4), 221-238.

Fan, Z. (2005). Speciation analysis of antimony (III) and antimony (V) by flame atomic absorption spectrometry after separation/preconcentration with cloud point extraction. Microchimica Acta, 152(1-2), 29-33.

Farkas, A., Erratico, C., & Vigano, L. (2007). Assessment of the environmental significance of heavy metal pollution in surficial sediments of the River Po. Chemosphere, 68(4), 761-768.

Fatema, K., Maznah, W. W., & Isa, M. M. (2014). Spatial and temporal variation of physico-chemical parameters in the Merbok Estuary, Kedah, Malaysia. Tropical life sciences research, 25(2), 1.

Fenner, D. P. (2001). Malaysian hard corals. Department of Marine Park Malaysia, Putrajaya.

Fennessy, M. J., Dyer, K. R., & Huntley, D. A. (1994). INSSEV: An instrument to measure the size and settling velocity of flocs in situ. Marine geology, 117(1-4), 107-117.

Ferguson, A., & Eyre, B. (1999). Behaviour of aluminium and iron in acid runoff from acid sulfate soils in the lower Richmond River catchment. AGSO Journal of Australian Geology and Geophysics, 17(5/6), 193-202.

Fernandes, M. B., Sicre, M. A., Boireau, A., & Tronczynski, J. (1997). Polyaromatic hydrocarbon (PAH) distributions in the Seine River and its estuary. Marine Pollution Bulletin, 34(11), 857-867.

Fernandes, M. C., & Nayak, G. N. (2016). Role of sediment size in the distribution and abundance of metals in a tropical (Sharavati) estuary, west coast of India. Arabian Journal of Geosciences, 9(1), 33.

Fernandez, A., & Borrok, D. M. (2009). Fractionation of Cu, Fe, and Zn isotopes during the oxidative weathering of sulfide-rich rocks. Chemical Geology, 264(1-4), 1-12.

Ferreira, A. M. S., & Santos, C. S. (2018). Sedimentation and Erosion in Harbor Estuaries. Sedimentation Engineering, 31.

Ferrier-Pagès, C., Schoelzke, V., Jaubert, J., Muscatine, L., & Hoegh-Guldberg, O. (2001). Response of a scleractinian coral, Stylophora pistillata, to iron and nitrate enrichment. Journal of Experimental Marine Biology and Ecology, 259(2), 249-261.

Filgueiras, A. V., Lavilla, I., & Bendicho, C. (2002). Chemical sequential extraction for metal partitioning in environmental solid samples. Journal of Environmental Monitoring, 4(6), 823-857.

Fitzsimons, M. F., Lohan, M. C., Tappin, A. D., & Millward, G. E. (2012). The role of suspended particles in estuarine and coastal biogeochemistry.

Fohrmann, H., Backhaus, J. O., Blaume, F., Haupt, B. J., Kämpf, J., Michels, K., ... & Weber, M. (2001). Modern ocean current-controlled sediment transport in the Greenland-Iceland-Norwegian (GIN) Seas. In The Northern North Atlantic (pp. 135-154). Springer, Berlin, Heidelberg.

Foley, J. A., Defries, R., Asner, G. P., Barford, C., Bonan, G., Carpenter, S. R., ... & Snyder, P. K. (2005). Review global consequences of land use.

Fordyce, F. (2007). Selenium geochemistry and health. Ambio, 94-97.

Förstner, U., & Wittmann, G. T. (2012). Metal pollution in the aquatic environment. Springer Science & Business Media.

Frazar, S., Gold, A. J., Addy, K., Moatar, F., Birgand, F., Schroth, A. W., ... & Pradhanang, S. M. (2019). Contrasting behavior of nitrate and phosphate flux from high flow events on small agricultural and urban watersheds. Biogeochemistry, 145(1), 141-160.

Freeman, L. A., Kleypas, J. A., & Miller, A. J. (2013). Coral reef habitat response to climate change scenarios. PloS one, 8(12), e82404.

French, J. R., Burningham, H., & Benson, T. (2008). Tidal and meteorological forcing of suspended sediment flux in a muddy mesotidal estuary. Estuaries and Coasts, 31(5), 843-859.

Frota, F. F., Paiva, B. P., & Schettini, C. A. F. (2013). Intra-tidal variation of stratification in a semi-arid estuary under the impact of flow regulation. Brazilian journal of oceanography, 61(1), 23-33.

Gächter, R., & Müller, B. (2003). Why the phosphorus retention of lakes does not necessarily depend on the oxygen supply to their sediment surface. Limnology and Oceanography, 48(2), 929-933.

Gad S.C. (2014). Editor(s): Philip Wexler, Barium, Encyclopedia of Toxicology (Third Edition), Academic Press, 2014, Pages 368-370, ISBN 9780123864550. DOI: https://doi.org/10.1016/B978-0-12-386454-3.00819-8.

Galán, E., Gómez-Ariza, J. L., González, I., Fernández-Caliani, J. C., Morales, E., & Giráldez, I. (2003). Heavy metal partitioning in river sediments severely polluted by acid mine drainage in the Iberian Pyrite Belt. Applied Geochemistry, 18(3), 409-421.

Gandaseca, S., Rosli, N., Ngayop, J., & Arianto, C. I. (2011). Status of water quality based on the physico-chemical assessment on river water at Wildlife Sanctuary Sibuti Mangrove Forest, Miri Sarawak. American Journal of Environmental Sciences, 7(3), 269.

Gao, H., Bai, J., Xiao, R., Liu, P., Jiang, W., & Wang, J. (2013). Levels, sources and risk assessment of trace elements in wetland soils of a typical shallow freshwater lake, China. Stochastic Environmental Research and Risk Assessment, 27(1), 275-284.

Garel, E., Pinto, L., Santos, A., & Ferreira, Ó. (2009). Tidal and river discharge forcing upon water and sediment circulation at a rock-bound estuary (Guadiana estuary, Portugal). Estuarine, Coastal and Shelf Science, 84(2), 269-281.

Garnier, J., Billen, G., Vilain, G., Martinez, A., Silvestre, M., Mounier, E., & Toche, F. (2009). Nitrous oxide (N2O) in the Seine river and basin: observations and budgets. Agriculture, ecosystems & environment, 133(3-4), 223-233.

Garnier, J., Quantin, C., Martins, E. S., & Becquer, T. (2006). Solid speciation and availability of chromium in ultramafic soils from Niquelândia, Brazil. Journal of Geochemical Exploration, 88(1-3), 206-209.

Gasim, M. B., Khalid, N. A., & Muhamad, H. (2015). The influence of tidal activities on water quality of Paka River Terengganu, Malaysia. Malaysian journal of analytical sciences, 19(5), 979-990.

Gaulier, C., Zhou, C., Gao, Y., Guo, W., Reichstädter, M., Ma, T., ... & Billon, G. (2021). Investigation on trace metal speciation and distribution in the Scheldt estuary. Science of The Total Environment, 757, 143827.

Geisler, E., Bogler, A., Bar-Zeev, E., & Rahav, E. (2020). Heterotrophic Nitrogen Fixation at the Hyper-Eutrophic Qishon River and Estuary System. Frontiers in microbiology, 11, 1370.

Gendron, A., Silverberg, N., Sundby, B., & Lebel, J. (1986). Early diagenesis of cadmium and cobalt in sediments of the Laurentian Trough. Geochimica et Cosmochimica Acta, 50(5), 741-747.

Geography of Sarawak. (2015, April 23). www.spu.sarawak.gov.my. Retrieved from https://web.archive.org/web/20150423011032/http://www.spu.sarawak.gov.my/geography.html.

Geyer, W. R., & MacCready, P. (2014). The estuarine circulation. Annual review of fluid mechanics, 46, 175-197.

Ghazali, A. D. I. A. N. A., Shazili, N. A. M., Bidai, J. O. S. E. P. H., & Shaari, H. A. S. R. I. Z. A. L. (2016). The spatial distribution of Al, Fe, Cu, Cd and Pb in the surface sediment of Brunei Bay, Borneo during the southwest and northeast monsoons. Journal of Sustainability Science and Management, 11, 93-106.

Giacalone, A., Gianguzza, A., Orecchio, S., Piazzese, D., Dongarrà, G., Sciarrino, S., & Varrica, D. (2005). Metals distribution in the organic and inorganic fractions of soil: a case study on soils from Sicily. Chemical Speciation & Bioavailability, 17(3), 83-93.

Gibbs, R. J. (1970). Mechanisms controlling world water chemistry. Science, 170(3962), 1088-1090.

Gibbs, R. J. (1973). Mechanisms of trace metal transport in rivers. Science, 180(4081), 71-73.

Gibbs, R. J. (1986). Segregation of metals by coagulation in estuaries. Marine Chemistry, 18(2-4), 149-159.

Gleyzes, C., Tellier, S., & Astruc, M. (2002). Fractionation studies of trace elements in contaminated soils and sediments: a review of sequential extraction procedures. TrAC Trends in Analytical Chemistry, 21(6-7), 451-467.

Glynn, P. D., & Plummer, L. N. (2005). Geochemistry and the understanding of ground-water systems. Hydrogeology Journal, 13(1), 263-287.

Gómez-Álvarez, A., Valenzuela-García, J. L., Aguayo-Salinas, S., Meza-Figueroa, D., Ramírez-Hernándezc, J., & Ochoa-Ortega, G. (2007). Chemical partitioning of sediment contamination by heavy metals in the San Pedro River, Sonora, Mexico. Chemical Speciation & Bioavailability, 19(1), 25-35.

Gopal, V., Nithya, B., Magesh, N. S., & Jayaprakash, M. (2018). Seasonal variations and environmental risk assessment of trace elements in the sediments of Uppanar River estuary, southern India. Marine pollution bulletin, 129(1), 347-356.

Grassi, M. T., Shi, B., & Allen, H. E. (2000). Partition of copper between dissolved and particulate phases using aluminum oxide as an aquatic model phase: effects of pH, solids and organic matter. Journal of the Brazilian Chemical Society, 11(5), 516-524.

Greger, M., Kautsky, L., & Sandberg, T. (1995). A tentative model of Cd uptake in Potamogeton pectinatus in relation to salinity. Environmental and Experimental Botany, 35(2), 215-225.

Gu, X., & Evans, L. J. (2008). Surface complexation modelling of Cd (II), Cu (II), Ni (II), Pb (II) and Zn (II) adsorption onto kaolinite. Geochimica et Cosmochimica Acta, 72(2), 267-276.

Haaijer, S. C., Van der Welle, M. E., Schmid, M. C., Lamers, L. P., Jetten, M. S., & Op den Camp, H. J. (2006). Evidence for the involvement of betaproteobacterial Thiobacilli in the nitrate-dependent oxidation of iron sulfide minerals. FEMS microbiology ecology, 58(3), 439-448.

Habibah, J., Khairiah, J., Ismail, B. S., & Kadderi, M. D. (2014). Manganese speciation in selected agricultural soils of peninsular Malaysia. American Journal of Environmental Sciences, 10(2), 148.

Habs, H., BM (Bernie) Simon, Thimann, K. U., & Howe, P. (1997). Aluminium. Environmental Health Criteria 194.

Haile, N. S. (1974). Borneo. Geological Society, London, Special Publications, 4(1), 333-347.

Hakanson, L. (1980). An ecological risk index for aquatic pollution control. A sedimentological approach. Water research, 14(8), 975-1001.

Hall, R., & Breitfeld, H. T. (2017). Nature and demise of the proto-South China Sea.

Hamid, A., Bhat, S. U., & Jehangir, A. (2020). Local determinants influencing stream water quality. Applied Water Science, 10(1), 1-16.

Hamzaoui-Azaza, F., Tlili-Zrelli, B., Bouhlila, R., & Gueddari, M. (2013). An integrated statistical methods and modelling mineral–water interaction to identifying hydrogeochemical processes in groundwater in Southern Tunisia. Chemical Speciation & Bioavailability, 25(3), 165-178.

Handa, B. K. (1964). Modified Classification Procedure fro Rating Irrigation Waters. Soil Science, 98(4), 264-269.

Hao, W., Flynn, S. L., Alessi, D. S., & Konhauser, K. O. (2018). Change of the point of zero net proton charge (pHPZNPC) of clay minerals with ionic strength. Chemical Geology, 493, 458-467.

Hao, W., Flynn, S. L., Kashiwabara, T., Alam, M. S., Bandara, S., Swaren, L., ... & Konhauser, K. O. (2019). The impact of ionic strength on the proton reactivity of clay minerals. Chemical Geology, 529, 119294.

Hao, W., Kashiwabara, T., Jin, R., Takahashi, Y., Gingras, M., Alessi, D. S., & Konhauser, K. O. (2020). Clay minerals as a source of cadmium to estuaries. Scientific reports, 10(1), 1-11.

Harikumar, P. S., Nasir, U. P., & Rahman, M. M. (2009). Distribution of heavy metals in the core sediments of a tropical wetland system. International Journal of Environmental Science & Technology, 6(2), 225-232.

Harland, A. D., & Brown, B. E. (1989). Metal tolerance in the scleractinian coral Porites lutea. Marine Pollution Bulletin, 20(7), 353-357.

Hart, H. M. (2006). Effect of land use on total suspended solids and turbidity in the Little River Watershed, Blount County, Tennessee.

Hartzell, J. L., & Jordan, T. E. (2012). Shifts in the relative availability of phosphorus and nitrogen along estuarine salinity gradients. Biogeochemistry, 107(1-3), 489-500.

Hassani, S., Karbassi, A. R., & Ardestani, M. (2017). Role of estuarine natural flocculation process in removal of Cu, Mn, Ni, Pb and Zn.

Hassellov, M., & von der Kammer, F. (2008). Iron oxides as geochemical nanovectors for metal transport in soil-river systems. Elements, 4(6), 401-406.

Hayes, K. F., & Leckie, J. O. (1987). Modeling ionic strength effects on cation adsorption at hydrous oxide/solution interfaces. Journal of Colloid and Interface Science, 115(2), 564-572.

Haygarth, P. M., Bilotta, G. S., Bol, R., Brazier, R. E., Butler, P. J., Freer, J., ... & Naden, P. (2006). Processes affecting transfer of sediment and colloids, with associated phosphorus, from intensively farmed grasslands: an overview of key issues. Hydrological Processes, 20(20), 4407-4413.

He, Z., Li, F., Dominech, S., Wen, X., & Yang, S. (2019). Heavy metals of surface sediments in the Changjiang (Yangtze River) Estuary: distribution, speciation and environmental risks. Journal of Geochemical Exploration, 198, 18-28.

Heery, E. C., Hoeksema, B. W., Browne, N. K., Reimer, J. D., Ang, P. O., Huang, D., ... & Todd, P. A. (2018). Urban coral reefs: Degradation and resilience of hard coral assemblages in coastal cities of East and Southeast Asia. Marine pollution bulletin, 135, 654-681.

Heggie, D., & Lewis, T. (1984). Cobalt in pore waters of marine sediments. Nature, 311(5985), 453-455.

Hennessey, T. M. (1994). Governance and adaptive management for estuarine ecosystems: The case of Chesapeake Bay.

Herzog, S. D., Kvashnina, K., Persson, P., & Kritzberg, E. (2019). Organic iron complexes enhance iron transport capacity along estuarine salinity gradients. Biogeosciences Discussions, 1-20.

Hidayat, H., Vermeulen, B., Sassi, M. G., Torfs, P. J. J. F., & Hoitink, A. J. F. (2011). Discharge estimation in a backwater affected meandering river. Hydrology and earth system sciences, 15(8), 2717-2728.

Hing, L. S., Shah, M. N. M. A. H., Yusoff, N. M., & Ong, M. C. (2020). Fractionation of As, Co, Cu and Zn by Sequential Extraction in Surface Sediment of Kuala Terengganu River Estuary. Malaysian Journal of Applied Sciences, 5(2), 57-68.

Hirst, C., Andersson, P. S., Shaw, S., Burke, I. T., Kutscher, L., Murphy, M. J., ... & Porcelli, D. (2017). Characterisation of Fe-bearing particles and colloids in the Lena River basin, NE Russia. Geochimica et Cosmochimica Acta, 213, 553-573.

Ho, C. P., Hseu, Z. Y., Iizuka, Y., & Jien, S. H. (2013). Chromium speciation associated with iron and manganese oxides in serpentine mine tailings. Environmental Engineering Science, 30(5), 241-247.

Ho, H. H., Swennen, R., Cappuyns, V., Vassilieva, E., & Van Tran, T. (2012). Necessity of normalization to aluminum to assess the contamination by heavy metals and arsenic in sediments near Haiphong Harbor, Vietnam. Journal of Asian Earth Sciences, 56, 229-239.

Hongxiao, T., Zijian, W., Jingyi, L., & Müller, G. (1994). Ecological impacts of heavy metal pollution from Dexing Copper Mine to Poyang Lake-- recent research progress in CERP-continual phase. China Environmental Science, 5(2), 97-101.

Hopwood, M. J., Statham, P. J., Skrabal, S. A., & Willey, J. D. (2015). Dissolved iron (II) ligands in river and estuarine water. Marine Chemistry, 173, 173-182.

Horowitz, A. J. (1985). A primer on trace metal-sediment chemistry (p. 67). Washington, DC: US Government Printing Office.

Horowitz, A. J. (1991). A primer on sediment-trace element chemistry (Vol. 2). Chelsea: Lewis Publishers.

Hosseini, M., & Sajjadi, N. (2018). The comparison of selenium and lead accumulation between contaminated muddy and sandy sediments from four estuaries along the Persian Gulf: effect of grain size. Environmental geochemistry and health, 40(4), 1645-1656.

Howarth, R. W., Anderson, D. B., Cloern, J. E., Elfring, C., Hopkinson, C. S., Lapointe, B., ... & Walker, D. (2000). Nutrient pollution of coastal rivers, bays, and seas. Issues in ecology, (7), 1-16.

Hoz, L. R., Edwards, A. C., Romero, P. C., Jaime, C. M., & Santoyo, M. R. (2003). Physico-chemical seasonal variability of a tropical estuary: major and minor elements in water and air. Environmental Geology, 44(7), 790-798.

Hsu, P. H. (1989). Aluminum hydroxides and oxyhydroxides. Minerals in soil environments, 1, 331-378.

Hu, X., & Cai, W. J. (2013). Estuarine acidification and minimum buffer zone—a conceptual study. Geophysical Research Letters, 40(19), 5176-5181.

Hu, Y., Fitzgerald, N. M., Lv, G., Xing, X., Jiang, W. T., & Li, Z. (2015). Adsorption of atenolol on kaolinite. Advances in Materials Science and Engineering, 2015.

Huang, J., Huang, Y., & Zhang, Z. (2014). Coupled effects of natural and anthropogenic controls on seasonal and spatial variations of river water quality during baseflow in a coastal watershed of Southeast China. PloS one, 9(3), e91528.

Huang, Z., Liu, C., Zhao, X., Dong, J., & Zheng, B. (2020). Risk assessment of heavy metals in the surface sediment at the drinking water source of the Xiangjiang River in South China. Environmental Sciences Europe, 32(1), 1-9.

Hung, J. J., & Shy, C. P. (1995). Speciation of dissolved Selenium in the Kaoping and Erhjen Rivers and Estuaries, southwestern Taiwan. Estuaries, 18(1), 234-240.

Hunt, M., Herron, E., & Green, L. (2012). Chlorides in fresh water. The University of Rhode Island, collage of the environment and life sciences, University of Rhode Island, USA, URIWW, 4, 02881-0804.

Hunter, K. A., & Liss, P. S. (1982). Organic matter and the surface charge of suspended particles in estuarine waters 1. Limnology and Oceanography, 27(2), 322-335.

Hutchison, C. S. (1989). Geological evolution of South-east Asia (Vol. 13, p. 368). Oxford: Clarendon Press.

Hutchison, C. S. (1996). The 'Rajang accretionary prism'and 'Lupar Line'problem of Borneo. Geological Society, London, Special Publications, 106(1), 247-261.

Hutchison, C. S. (2005). Geology of North-West Borneo: Sarawak, Brunei and Sabah. Elsevier.

Hutchison, C. S. (2007). Geological Evolution of South-East Asia: Kuala Lumpur. Geological Society of Malaysia.

Hwang, J. S., Dahms, H. U., Huang, K. L., Huang, M. Y., Liu, X. J., Khim, J. S., & Wong, C. K. (2018). Bioaccumulation of trace metals in octocorals depends on age and tissue compartmentalization. PloS one, 13(4), e0196222.

Hydes, D. J., & Liss, P. S. (1977). The behaviour of dissolved aluminium in estuarine and coastal waters. Estuarine and Coastal Marine Science, 5(6), 755-769.

Ibrahim, T. N. B. T., Othman, F., & Mahmood, N. Z. (2020). Baseline study of heavy metal pollution in a tropical river in a developing country. Sains Malaysiana, 49(4), 729-742.

Idriss, A. A., & Ahmad, A. K. (2012). Concentration of selected heavy metals in water of the Juru River, Penang, Malaysia. African Journal of Biotechnology, 11(33), 8234-8240.

Iglesias, I., Avilez-Valente, P., Bio, A., & Bastos, L. (2019). Modelling the main hydrodynamic patterns in shallow water estuaries: the Minho Case Study. Water, 11(5), 1040.

Illuminati, S., Annibaldi, A., Truzzi, C., Tercier-Waeber, M. L., Nöel, S., Braungardt, C. B., ... & Scarponi, G. (2019). In-situ trace metal (Cd, Pb, Cu) speciation along the Po River plume (Northern Adriatic Sea) using submersible systems. Marine Chemistry, 212, 47-63.

Impellitteri, C. A., & Scheckel, K. G. (2006). The distribution, solid-phase speciation, and desorption/dissolution of as in waste iron-based drinking water treatment residuals. Chemosphere, 64(6), 875-880.

Ingri, J., Widerlund, A., Suteerasak, T., Bauer, S., & Elming, S. Å. (2014). Changes in trace metal sedimentation during freshening of a coastal basin. Marine Chemistry, 167, 2-12.

Ip, C. C., Li, X. D., Zhang, G., Wai, O. W., & Li, Y. S. (2007). Trace metal distribution in sediments of the Pearl River Estuary and the surrounding coastal area, South China. Environmental Pollution, 147(2), 311-323.

Ishak, A. K., Samuding, K., & Yusoff, N. H. (2000). Water and suspended sediment dynamics in the Sungai Selangor estuary; Dinamik air dan sedimen terampai di muara Sungai Selangor.

Islam, R., Faysal, S. M., Amin, R., Juliana, F. M., Islam, M. J., Alam, M. J., ... & Asaduzzaman, M. (2017). Assessment of pH and total dissolved substances (TDS) in the commercially available bottled drinking water. Iosr Journal of Nursing and Health Science Ver. IX, 6(5), 35-40.

Iwegbue, C. M., Eghwrudje, M. O., Nwajei, G. E., & Egboh, S. H. O. (2007). Chemical speciation of heavy metals in the Ase River sediment, Niger Delta, Nigeria. Chemical Speciation & Bioavailability, 19(3), 117-127.

Jarsjö, J., Chalov, S. R., Pietroń, J., Alekseenko, A. V., & Thorslund, J. (2017). Patterns of soil contamination, erosion and river loading of metals in a gold mining region of northern Mongolia. Regional Environmental Change, 17(7), 1991-2005.

Jarvie, H. P., Neal, C., Leach, D. V., Ryland, G. P., House, W. A., & Robson, A. J. (1997). Major ion concentrations and the inorganic carbon chemistry of the Humber rivers. Science of the Total Environment, 194, 285-302.

Jiang, S., Müller, M., Jin, J., Wu, Y., Zhu, K., Zhang, G., ... & Zhang, J. (2019). Dissolved inorganic nitrogen in a tropical estuary in Malaysia: transport and transformation. Biogeosciences, 16(14), 2821-2836.

Jiang, Y., Gui, H., Yu, H., Wang, M., Fang, H., Wang, C., ... & Huang, Y. (2020). Hydrochemical Characteristics and Water Quality Evaluation of Rivers in Different Regions of Cities: A Case Study of Suzhou City in Northern Anhui Province, China. Water, 12(4), 950.

Jiann, K. T., & Ho, P. (2014). Cadmium mixing behavior in estuaries: Redox controls on removal and mobilization. TAO: Terrestrial, Atmospheric and Oceanic Sciences, 25(5), 655.

Jilbert, T., Tiihonen, R., Myllykangas, J. P., Asmala, E., & Hietanen, S. (2016). Reactive iron and manganese in estuarine sediments of the Baltic Sea: Impacts of flocculation and redox shuttling. EGUGA, EPSC2016-14808.

Jokinen, S. A., Jilbert, T., Tiihonen-Filppula, R., & Koho, K. (2020). Terrestrial organic matter input drives sedimentary trace metal sequestration in a human-impacted boreal estuary. Science of the Total Environment, 717, 137047.

Jones, B., & Manning, D. A. (1994). Comparison of geochemical indices used for the interpretation of palaeoredox conditions in ancient mudstones. Chemical geology, 111(1-4), 111-129.

Jothivenkatachalam, K., Nithya, A., & Chandra Mohan, S. (2010). Correlation analysis of drinking water quality in and around Perur block of Coimbatore District, Tamil Nadu, India. Rasayan Journal of Chemistry, 3(4), 649-654.

Juen, L. L., Aris, A. Z., Shan, N. T., Yusoff, F. M., & Hashim, Z. (2015). Geochemical modeling of element species in selected tropical estuaries and coastal water of the Strait of Malacca. Procedia Environmental Sciences, 30, 109-114.

Kalin, R. M. (1996). Basic concepts and formulations for isotope geochemical modelling of groundwater systems (No. IAEA-TECDOC--910).

Karbassi, A. R., Bassam, S. S., & Ardestani, M. (2013). Flocculation of Cu, Mn, Ni, Pb, and Zn during Estuarine Mixing (Caspian Sea). International Journal of Environmental Research, 7(4), 917-924.

Karbassi, A. R., Heidari, M., Vaezi, A. R., Samani, A. V., Fakhraee, M., & Heidari, F. (2014). Effect of pH and salinity on flocculation process of heavy metals during mixing of Aras River water with Caspian Sea water. Environmental earth sciences, 72(2), 457-465.

Karbassi, A. R., Nouri, J., Mehrdadi, N., & Ayaz, G. O. (2008). Flocculation of heavy metals during mixing of freshwater with Caspian Sea water. Environmental geology, 53(8), 1811-1816.

Karbassi, A. R., Tajziehchi, S., & Adib, N. F. (2016). Role of estuarine natural processes in removal of trace metals under emergency situations. Global Journal of Environmental Science and Management, 2(1), 31.

Kärnä, T., & Baptista, A. M. (2016). Water age in the Columbia River estuary. Estuarine, Coastal and Shelf Science, 183, 249-259.

Kelly, W. P. (1940). Permissible composition and concentration of irrigated waters. Proceedings of the ASCF66, 607.

Kelly, W. P. (1963). Use of saline irrigation water. Soil science, 95(6), 385-391.

Kennish, M. J. (1994). Pollution in estuaries and coastal marine waters. Journal of Coastal Research, 27-49.

Kennish, M. J. (2002). Environmental threats and environmental future of estuaries. Environmental conservation, 78-107.

Kersten, M. (2002). Speciation of trace metals in sediments. Chemical speciation in the environment, 301-321.

Kersten, M., & Förstner, U. (1986). Chemical fractionation of heavy metals in anoxic estuarine and coastal sediments. Water Science and Technology, 18(4-5), 121-130.

Kessler, F. L. (2009). Observations on sediments and deformation characteristics, Sarawak Foreland, Borneo Island.

Kessler, F. L., & Jong, J. (2015). Northwest Sarawak: a complete geologic profile from the Lower Miocene to the Pliocene covering the Upper Setap Shale, Lambir and Tukau Formations.

Kharkar, D. P., Turekian, K. K., & Bertine, K. K. (1968). Stream supply of dissolved silver, molybdenum, antimony, selenium, chromium, cobalt, rubidium and cesium to the oceans. Geochimica et Cosmochimica Acta, 32(3), 285-298.

Khatoon, N., Khan, A. H., Rehman, M., & Pathak, V. (2013). Correlation study for the assessment of water quality and its parameters of Ganga River, Kanpur, Uttar Pradesh, India. IOSR Journal of Applied Chemistry, 5(3), 80-90.

Khatri, N., & Tyagi, S. (2015). Influences of natural and anthropogenic factors on surface and groundwater quality in rural and urban areas. Frontiers in Life Science, 8(1), 23-39.

Kieliszek, M. (2019). Selenium–fascinating microelement, properties and sources in food. Molecules, 24(7), 1298.

Klimchouk, A., Cucchi, F., Calaforra, J. M., Aksem, S., Finocchiaro, F., & Forti, P. (1996). Dissolution of gypsum from field observations. International Journal of Speleology, 25(3), 3.

Kline, D. I., Kuntz, N. M., Breitbart, M., Knowlton, N., & Rohwer, F. (2006). Role of elevated organic carbon levels and microbial activity in coral mortality. Marine Ecology Progress Series, 314, 119-125.

Klink, A., Dambiec, M., & Polechońska, L. (2019). Trace metal speciation in sediments and bioaccumulation in Phragmites australis as tools in environmental pollution monitoring. International Journal of Environmental Science and Technology, 16(12), 7611-7622.

Knox, A. S., Paller, M. H., Nelson, E. A., Specht, W. L., Halverson, N. V., & Gladden, J. B. (2006). Metal distribution and stability in constructed wetland sediment. Journal of Environmental Quality, 35(5), 1948-1959.

Koki, I. B. (2015). Efficiencies of acid digestion/leaching techniques in the determination of iron concentrations in soils from Challawa Industrial Estate Kano, Nigeria. Merit Res. J. Environ. Sci. Toxicol, 3(5), 65-71.

Kolahchi, Z., & Jalali, M. (2007). Effect of water quality on the leaching of potassium from sandy soil. Journal of arid environments, 68(4), 624-639.

Kondratyev, S. E. R. G. E. I. (2003). A system for ecological and economic assessment of the use, preservation and restoration of urban water bodies: St Petersburg as a case study. International Association of Hydrological Sciences, Publication, (281), 327-333.

Konig, A., Pearson, H. W., & Silva, S. A. (1987). Ammonia toxicity to algal growth in waste stabilization ponds. Water science and technology, 19(12), 115-122.

Koop, K., Booth, D., Broadbent, A., Brodie, J., Bucher, D., Capone, D., ... & Yellowlees, D. (2001). ENCORE: the effect of nutrient enrichment on coral

reefs. Synthesis of results and conclusions. Marine pollution bulletin, 42(2), 91-120.

Kopittke, P. M., Menzies, N. W., & Fulton, I. M. (2005). Gypsum solubility in seawater, and its application to bauxite residue amelioration. Soil Research, 42(8), 953-960.

Körner, S., Das, S. K., Veenstra, S., & Vermaat, J. E. (2001). The effect of pH variation at the ammonium/ammonia equilibrium in wastewater and its toxicity to Lemna gibba. Aquatic botany, 71(1), 71-78.

Krachler, R. F., Krachler, R., Stojanovic, A., Wielander, B., & Herzig, A. (2009). Effects of pH on aquatic biodegradation processes. Biogeosciences Discussions, 6(1), 491-514.

Krawczyk, H., Zinke, J., Browne, N., Struck, U., McIlwain, J., O'Leary, M., & Garbe-Schönberg, D. (2020). Corals reveal ENSO-driven synchrony of climate impacts on both terrestrial and marine ecosystems in northern Borneo. Scientific reports, 10(1), 1-14.

Kristensen, E., Kristiansen, K. D., & Jensen, M. H. (2003). Temporal behavior of manganese and iron in a sandy coastal sediment exposed to water column anoxia. Estuaries, 26(3), 690-699.

Kronvang, B., Laubel, A., Larsen, S. E., & Friberg, N. (2003). Pesticides and heavy metals in Danish streambed sediment. Hydrobiologia, 494(1-3), 93-101.

Kroon, F. J., Kuhnert, P. M., Henderson, B. L., Wilkinson, S. N., Kinsey-Henderson, A., Abbott, B., ... & Turner, R. D. (2012). River loads of suspended solids, nitrogen, phosphorus and herbicides delivered to the Great Barrier Reef lagoon. Marine pollution bulletin, 65(4-9), 167-181.

Krupadam, R. J., Smita, P., & Wate, S. R. (2006). Geochemical fractionation of heavy metals in sediments of the Tapi estuary. geochemical Journal, 40(5), 513-522.

Kulbat, E., & Sokołowska, A. (2019). Methods of assessment of metal contamination in bottom sediments (case study: Straszyn Lake, Poland). Archives of environmental contamination and toxicology, 77(4), 605-618.

Kumar, B., Senthil Kumar, K., Priya, M., Mukhopadhyay, D., & Shah, R. (2010). Distribution, partitioning, bioaccumulation of trace elements in water, sediment and fish from sewage fed fishponds in eastern Kolkata, India. Toxicological & Environ Chemistry, 92(2), 243-260.

Kumar, M., & Puri, A. (2012). A review of permissible limits of drinking water. Indian journal of occupational and environmental medicine, 16(1), 40.

Kumar, M., Kumari, K., Ramanathan, A. L., & Saxena, R. (2007). A comparative evaluation of groundwater suitability for irrigation and drinking purposes in two intensively cultivated districts of Punjab, India. Environmental Geology, 53(3), 553-574.

Kumar, N., Kumar, P., Basil, G., Kumar, R. N., Kharrazi, A., & Avtar, R. (2015). Characterization and evaluation of hydrological processes responsible for spatiotemporal variation of surface water quality at Narmada estuarine region in Gujarat, India. Applied Water Science, 5(3), 261-270.

Kumarasamy, P., Dahms, H. U., Jeon, H. J., Rajendran, A., & James, R. A. (2014). Irrigation water quality assessment—an example from the Tamiraparani river, Southern India. Arabian Journal of Geosciences, 7(12), 5209-5220.

Lackovic, K., Angove, M. J., Wells, J. D., & Johnson, B. B. (2003). Modeling the adsorption of Cd (II) onto Muloorina illite and related clay minerals. Journal of colloid and interface science, 257(1), 31-40.

Lafite, R. (2001). Impact de la dynamique tidale sur le transfert de sédiments fins. Université de Rouen: 80p.

Lai, J., Wang, G., Chen, J., Wang, S., Zhou, Z., & Fan, X. (2017). Origin and distribution of carbonate cement in tight sandstones: The Upper Triassic Yanchang Formation Chang 8 oil layer in west Ordos Basin, China. Geofluids, 2017.

Lambrechts, J., Humphrey, C., McKinna, L., Gourge, O., Fabricius, K. E., Mehta, A. J., ... & Wolanski, E. (2010). Importance of wave-induced bed liquefaction in the fine sediment budget of Cleveland Bay, Great Barrier Reef. Estuarine, Coastal and Shelf Science, 89(2), 154-162.

Lamers, L. P., Falla, S. J., Samborska, E. M., Dulken, I. A. V., Hengstum, G. V., & Roelofs, J. G. (2002). Factors controlling the extent of eutrophication and toxicity in sulfate-polluted freshwater wetlands. Limnology and oceanography, 47(2), 585-593.

Lapointe, B. E. (1997). Nutrient thresholds for bottom-up control of macroalgal blooms on coral reefs in Jamaica and southeast Florida. Limnology and Oceanography, 42(5part2), 1119-1131.

Lawrence, J. F. (1995). Digital Evaluation of Groundwater Resources in Ramanathapuram District, Tamil Nadu. Unpublished Thesis submitted to Manonmaniam Sundaranar University, Tirunelveli.

Lee, H. L., Tangang, F., Wahap, M. H., & YAng, S. (2016, July). Seasonal hypoxia occurrence at Terengganu estuary, Malaysia and its potential formation mechanisms. In IOP Conference Series: Materials Science and Engineering (Vol. 136, No. 1, p. 012068). IOP Publishing.

Lenntech. (2005). Composition of Seawater. Retrieved from http://www.lenntech.com/composition-seawater.html.

Lewis, S. E., Bainbridge, Z. T., Kuhnert, P. M., Sherman, B. S., Henderson, B., Dougall, C., ... & Brodie, J. E. (2013). Calculating sediment trapping efficiencies for reservoirs in tropical settings: a case study from the Burdekin Falls Dam, NE Australia. Water Resources Research, 49(2), 1017-1029.

Li, G., Liu, J., Diao, Z., Jiang, X., Li, J., Ke, Z., ... & Tan, Y. (2018). Subsurface low dissolved oxygen occurred at fresh-and saline-water intersection of the Pearl River estuary during the summer period. Marine pollution bulletin, 126, 585-591.

Li, H., Li, L., Su, F., Wang, T., & Gao, P. (2020). The Periodic Response of Tidal Flat Sediments to Runoff Variation of Upstream Main River: A Case Study in the Liaohe Estuary Wetland, China. Water, 12(1), 61.

Li, H., Shi, A., Li, M., & Zhang, X. (2013). Effect of pH, temperature, dissolved oxygen, and flow rate of overlying water on heavy metals release from storm sewer sediments. Journal of Chemistry, 2013.

Li, R., Tang, C., Cao, Y., Jiang, T., & Chen, J. (2018). The distribution and partitioning of trace metals (Pb, Cd, Cu, and Zn) and metalloid (As) in the Beijiang River. Environmental monitoring and assessment, 190(7), 399.

Li, X., Liu, L., Wang, Y., Luo, G., Chen, X., Yang, X., ... & He, X. (2012). Integrated assessment of heavy metal contamination in sediments from a coastal industrial basin, NE China. PloS one, 7(6), e39690.

Li, X., Shen, Z., Wai, O. W., & Li, Y. S. (2000). Chemical partitioning of heavy metal contaminants in sediments of the Pearl River Estuary. Chemical Speciation & Bioavailability, 12(1), 17-25.

Li, X., Shen, Z., Wai, O. W., & Li, Y. S. (2001). Chemical forms of Pb, Zn and Cu in the sediment profiles of the Pearl River Estuary. Marine Pollution Bulletin, 42(3), 215-223.

Li, Y., Wang, X. L., Huang, G. H., Zhang, B. Y., & Guo, S. H. (2009). Adsorption of Cu and Zn onto Mn/Fe oxides and organic materials in the extractable fractions of river surficial sediments. Soil & Sediment Contamination, 18(1), 87-101.

Liguori, B. T., ALMEIDA, M. G., & REZENDE, C. E. (2016). Barium and its Importance as an Indicator of (Paleo) Productivity. Anais da Academia Brasileira de Ciências, 88(4), 2093-2103.

Lim, W. Y., Aris, A. Z., & Zakaria, M. P. (2012). Spatial variability of metals in surface water and sediment in the Langat River and geochemical factors that influence their water-sediment interactions. The Scientific World Journal, 2012.

Lin, J., Zhu, G., Wei, J., Jiang, F., Wang, M. K., & Huang, Y. (2018). Mulching effects on erosion from steep slopes and sediment particle size distributions of gully colluvial deposits. Catena, 160, 57-67.

Lin, Y. C., Chang-Chien, G. P., Chiang, P. C., Chen, W. H., & Lin, Y. C. (2013). Multivariate analysis of heavy metal contaminations in seawater and sediments from a heavily industrialized harbor in Southern Taiwan. Marine pollution bulletin, 76(1-2), 266-275.

Lintern, A., Webb, J. A., Ryu, D., Liu, S., Bende-Michl, U., Waters, D., ... & Western, A. W. (2018). Key factors influencing differences in stream water quality across space. Wiley Interdisciplinary Reviews: Water, 5(1), e1260.

Lintern, D. G. (2003). Influences of flocculation on bed properties for fine-grained cohesive sediment (Doctoral dissertation, Oxford University, UK).

Lion, L. W., Altmann, R. S., & Leckie, J. O. (1982). Trace-metal adsorption characteristics of estuarine particulate matter: evaluation of contributions of iron/manganese oxide and organic surface coatings. Environmental Science & Technology, 16(10), 660-666.

Liu, H. C., You, C. F., Huang, B. J., & Huh, C. A. (2013). Distribution and accumulation of heavy metals in carbonate and reducible fractions of marine sediment from offshore mid-western Taiwan. Marine pollution bulletin, 73(1), 37-46.

Liu, J., Xiang, R., Chen, Z., Chen, M., Yan, W., Zhang, L., & Chen, H. (2013). Sources, transport and deposition of surface sediments from the South China Sea. Deep Sea Research Part I: Oceanographic Research Papers, 71, 92-102.

Liu, M., Chen, J., Sun, X., Hu, Z., & Fan, D. (2019). Accumulation and transformation of heavy metals in surface sediments from the Yangtze River estuary to the East China Sea shelf. Environmental pollution, 245, 111-121.

Lockard, C. A. , Leinbach, . Thomas R. , Bee, . Ooi Jin and Ahmad, . Zakaria Bin (2020, May 13). Malaysia. Encyclopedia Britannica. https://www.britannica.com/place/Malaysia.

Loitzenbauer, E., & Mendes, C. A. B. (2012). Salinity dynamics as a tool for water resources management in coastal zones: An application in the Tramandaí River basin, southern Brazil. Ocean & coastal management, 55, 52-62.

Loken, L. C., Small, G. E., Finlay, J. C., Sterner, R. W., & Stanley, E. H. (2016). Nitrogen cycling in a freshwater estuary. Biogeochemistry, 127(2-3), 199-216.

Long, E. R., MacDonald, D. D., Smith, S. L., & Calder, F. D. (1995). Incidence of adverse biological effects within ranges of chemical concentrations in marine and estuarine sediments. Environmental management, 19(1), 81-97.

Long, S. M. (2014). Sarawak coastal biodiversity: a current status.

Long, Y., Fang, Y., Shen, D., Feng, H., & Chen, T. (2016). Hydrogen sulfide (H_2S) emission control by aerobic sulfate reduction in landfill. Scientific reports, 6(1), 1-9.

Longphuirt, S. N., Mockler, E. M., O'Boyle, S., Wynne, C., & Stengel, D. B. (2016, January). Linking changes in nutrient source load to estuarine responses: an Irish perspective. In Biology and Environment: Proceedings of the Royal Irish Academy. Royal Irish Academy. Vol. 116, No. 3, pp. 295-311.

Looi, L. J., Aris, A. Z., Johari, W. L. W., Yusoff, F. M., & Hashim, Z. (2013). Baseline metals pollution profile of tropical estuaries and coastal waters of the Straits of Malacca. Marine pollution bulletin, 74(1), 471-476.

Lough, J. M. (2007). Tropical river flow and rainfall reconstructions from coral luminescence: Great Barrier Reef, Australia. Paleoceanography, 22(2).

Lough, J. M., Lewis, S. E., & Cantin, N. E. (2015). Freshwater impacts in the central Great Barrier Reef: 1648–2011. Coral Reefs, 34(3), 739-751.

Lower, S. K. (1999). Carbonate equilibria in natural waters. Simon Fraser University, 544.

Loya, Y. (1976). Effects of water turbidity and sedimentation on the community structure of Puerto Rican corals. Bulletin of Marine Science, 26(4), 450-466.

Loya, Y. (2004). The coral reefs of Eilat—past, present and future: three decades of coral community structure studies. In Coral health and disease (pp. 1-34). Springer, Berlin, Heidelberg.

Lu, L., Wang, R., Chen, F., Xue, J., Zhang, P., & Lu, J. (2005). Element mobility during pyrite weathering: implications for acid and heavy metal pollution at mining-impacted sites. Environmental geology, 49(1), 82-89.

Lučić, M., Jurina, I., Ščančar, J., Mikac, N., & Vdović, N. (2019). Sedimentological and geochemical characterization of river suspended particulate matter (SPM) sampled by time-integrated mass flux sampler (TIMS) in the Sava river (Croatia). Journal of soils and sediments, 19(2), 989-1004.

Ma, L. Q., & Rao, G. N. (1997). Chemical fractionation of cadmium, copper, nickel, and zinc in contaminated soils. Journal of Environmental Quality, 26(1), 259-264.

Mackay, D. W., & Fleming, G. (1969). Correlation of dissolved oxygen levels, freshwater flows and temperatures in a polluted estuary. Water Research, 3(2), 121-128.

Mackenzie, F. T., & Garrels, R. M. (1971). Evolution of sedimentary rocks. New York: Norton.

MacNeil, M. A., Mellin, C., Matthews, S., Wolff, N. H., McClanahan, T. R., Devlin, M., ... & Graham, N. A. (2019). Water quality mediates resilience on the Great Barrier Reef. Nature ecology & evolution, 3(4), 620-627.

Madon, M. (1999). Geological setting of Sarawak. The petroleum geology and resources of Malaysia, 1, 273-290.

MWQSI, (Malaysia Water Quality Standard and Index). (2021, April 5) Department of Environment. Retrieved from https://www.doe.gov.my/portalv1/en/standard-dan-indeks-kualiti-jabatan-alam-sekitar.

Malcolm, S. J., Battersby, N. S., Stanley, S. O., & Brown, C. M. (1986). Organic degradation, sulphate reduction and ammonia production in the sediments of Loch Eil, Scotland. Estuarine, Coastal and Shelf Science, 23(5), 689-704.

Manning, B. A., & Goldberg, S. (1997). Adsorption and stability of arsenic (III) at the clay mineral− water interface. Environmental science & technology, 31(7), 2005-2011.

MANRED, (Ministry of Modernisation of Agriculture, Native Land and Regional Development Sarawak). (2020, May 4). Retrieved from https://manred.sarawak.gov.my/modules/web/pages.php?mod=news&sub=news_view&nid=338.

Manullang, C. Y., Hutabarat, J., & Widowati, I. (2014). Bioaccumulation of cadmium (Cd) by white shrimp penaeus merguiensis at different salinity in kedungmalang estuary, jepara (central java). Marine Research in Indonesia, 39(1), 31-37.

Mapoma, H. W. T., Xie, X., Liu, Y., Zhu, Y., Kawaye, F. P., & Kayira, T. M. (2017). Hydrochemistry and quality of groundwater in alluvial aquifer of Karonga, Malawi. Environmental Earth Sciences, 76(9), 335.

Marchitto, T.M. (2013). Editor(s): Scott A. Elias, Cary J. Mock, Paleoceanography, physical and chemical proxies | Nutrient Proxies, Encyclopedia of Quaternary Science (Second Edition), Elsevier, Pages 899-906, ISBN 9780444536426, DOI: https://doi.org/10.1016/B978-0-444-53643-3.00291-0.

Marcovecchio, J., & Ferrer, L. (2005). Distribution and geochemical partitioning of heavy metals in sediments of the Bahía Blanca Estuary, Argentina. Journal of Coastal Research, 21(4 (214)), 826-834.

Martin, G. D., George, R., Shaiju, P., Muraleedharan, K. R., Nair, S. M., & Chandramohanakumar, N. (2012). Toxic metals enrichment in the surficial sediments of a eutrophic tropical estuary (Cochin Backwaters, Southwest Coast of India). The Scientific World Journal, 2012.

Martin, J. M., Nirel, P., & Thomas, A. J. (1987). Sequential extraction techniques promises and problems. Marine Chemistry, 22(2-4), 313-341.

Masindi, V., & Muedi, K. L. (2018). Environmental contamination by heavy metals. Heavy metals, 10, 115-132.

Mathew, R., & Winterwerp, J. C. (2020). Sediment dynamics and transport regimes in a narrow microtidal estuary. Ocean Dynamics, 70(4), 435-462.

Matson, E. A., & Brinson, M. M. (1985). Sulfate enrichments in estuarine waters of North Carolina. Estuaries, 8(3), 279-289.

Matthiessen, P., & Law, R. J. (2002). Contaminants and their effects on estuarine and coastal organisms in the United Kingdom in the late twentieth century. Environmental Pollution, 120(3), 739-757.

May, T. W., Fairchild, J. F., Petty, J. D., Walther, M. J., Lucero, J., Delvaux, M., ... & Armbruster, M. (2008). An evaluation of selenium concentrations in water, sediment, invertebrates, and fish from the Solomon River Basin. Environmental monitoring and assessment, 137(1), 213-232.

Mayer, L. M. (1982). Aggregation of colloidal iron during estuarine mixing: Kinetics, mechanism, and seasonality. Geochimica et Cosmochimica Acta, 46(12), 2527-2535.

McCabe, D. J. (2010). Rivers and streams: life in flowing water. Nature Education Knowledge, 1(4).

McCarthy, M. J., McNeal, K. S., Morse, J. W., & Gardner, W. S. (2008). Bottom-water hypoxia effects on sediment–water interface nitrogen transformations in a seasonally hypoxic, shallow bay (Corpus Christi Bay, TX, USA). Estuaries and Coasts, 31(3), 521-531.

McKinnon, A. D., & Thorrold, S. R. (1993). Zooplankton community structure and copepod egg production in coastal waters of the central Great Barrier Reef lagoon. Journal of Plankton Research, 15(12), 1387-1411.

McLaughlin, C. J., Smith, C. A., Buddemeier, R. W., Bartley, J. D., & Maxwell, B. A. (2003). Rivers, runoff, and reefs. Global and Planetary Change, 39(1-2), 191-199.

McLennan, S. M., Hemming, S. R., Taylor, S. R., & Eriksson, K. A. (1995). Early Proterozoic crustal evolution: Geochemical and NdPb isotopic evidence from metasedimentary rocks, southwestern North America. Geochimica et cosmochimica acta, 59(6), 1153-1177.

Md Anawar, H., & Chowdhury, R. (2020). Remediation of polluted river water by biological, chemical, ecological and engineering processes. Sustainability, 12(17), 7017.

Md Yunus, S., Hamzah, Z., Wood, A. K., & Ahmad. (2015, April). Assessment of heavy metals in seawater and fish tissues at Pulau Indah, Selangor, Malaysia. In AIP Conference Proceedings (Vol. 1659, No. 1, p. 050007). AIP Publishing LLC.

Mehta, A. J. (1989). On estuarine cohesive sediment suspension behavior. Journal of Geophysical Research: Oceans, 94(C10), 14303-14314.

Melville, F., & Pulkownik, A. (2006). Investigation of mangrove macroalgae as bioindicators of estuarine contamination. Marine Pollution Bulletin, 52(10), 1260-1269.

Mewes, A., Langer, G., de Nooijer, L. J., Bijma, J., & Reichart, G. J. (2014). Effect of different seawater Mg2+ concentrations on calcification in two benthic foraminifers. Marine micropaleontology, 113, 56-64.

Meybeck, M., & Moatar, F. (2012). Daily variability of river concentrations and fluxes: indicators based on the segmentation of the rating curve. Hydrological Processes, 26(8), 1188-1207.

Mhashhash, A., Bockelmann-Evans, B., & Pan, S. (2018). Effect of hydrodynamics factors on sediment flocculation processes in estuaries. Journal of Soils and Sediments, 18(10), 3094-3103.

Middlebrooks, E. J., Porcella, D. B., Gearheart, R. A., Marshall, G. R., Reynolds, J. H., & Grenney, W. J. (1974). Techniques for algae removal from wastewater stabilization ponds. Journal (Water Pollution Control Federation), 2676-2695.

Millward, G. E., & Liu, Y. P. (2003). Modelling metal desorption kinetics in estuaries. Science of the total Environment, 314, 613-623.

Mirlean, N., Bem, A. L. D., Quintana, G. C. D. R., Costa, L. P., & Ferraz, A. H. (2020). Sulfate reduction and alterability of sulfur species in sediments of an estuary with irregular hydrological regime. Ocean and Coastal Research, 68.

Mohamed, A. I. (2017). Irrigation water resources and suitability for crops in Egypt. Ground water, 11(15.30), 5-20.

Mohamed, C. A. R. P. S. & Yaacob, W. Z. W., (2019). Distribution of chromium and gallium in the Total suspended solid and surface sediments of Sungai Kelantan, Kelantan, Malaysia. Sains Malaysiana, 48(11), 2343-2353.

Mohan, M., Augustine, T., Jayasooryan, K. K., Chandran, M. S., & Ramasamy, E. V. (2012). Fractionation of selected metals in the sediments of Cochin estuary and Periyar River, southwest coast of India. The Environmentalist, 32(4), 383-393.

Mokhtar, N. F., Aris, A. Z., & Praveena, S. M. (2015). Preliminary study of heavy metal (Zn, Pb, Cr, Ni) contaminations in Langat river estuary, Selangor. Procedia Environmental Sciences, 30, 285-290.

Monbet, P. (2004). Seasonal cycle and mass balance of cadmium in an estuary with an agricultural catchment: The Morlaix River estuary (Brittany, France). Estuaries, 27(3), 448-459.

Moncmanová, A. (2007). Environmental factors that influence the deterioration of materials. Environmental Deterioration of Materials, 21, 1.

Monte, C. D. N., Rodrigues, A. P. D. C., de-Freitas, A. R., Freire, A. S., Santelli, R. E., Braz, B. F., & Machado, W. (2019). Dredging impact on trace metal behavior in a polluted estuary: a discussion about sampling design. Brazilian Journal of Oceanography, 67.

Mook, W. G., & Koene, B. K. S. (1975). Chemistry of dissolved inorganic carbon in estuarine and coastal brackish waters. Estuarine and Coastal Marine Science, 3(3), 325-336.

Moollye, S. V. (2017). A Comparative Study on the Seawater Quality of the Coral Environment between Miri (Sarawak) and Sipadan (Sabah) (Doctoral dissertation, Curtin University).

Moore, W. S., & Shaw, T. J. (2008). Fluxes and behavior of radium isotopes, barium, and uranium in seven Southeastern US rivers and estuaries. Marine Chemistry, 108(3-4), 236-254.

Moreira, F. R., Maia, C. B., & Ávila, A. K. (2002). Titanium as a chemical modifier for the determination of cobalt in marine sediments. Spectrochimica Acta Part B: Atomic Spectroscopy, 57(12), 2141-2149.

Mori, C., Santos, I. R., Brumsack, H. J., Schnetger, B., Dittmar, T., & Seidel, M. (2019). Non-conservative behavior of dissolved organic matter and trace metals (Mn, Fe, Ba) driven by porewater exchange in a subtropical mangrove-estuary. Frontiers in Marine Science, 6, 481.

Morillo, J., Usero, J., & Gracia, I. (2004). Heavy metal distribution in marine sediments from the southwest coast of Spain. Chemosphere, 55(3), 431-442.

Morris, A. W. (1986). Removal of trace metals in the very low salinity region of the Tamar Estuary, England. Science of the total Environment, 49, 297-304.

Morris, A. W., & Bale, A. J. (1979). Effect of rapid precipitation of dissolved Mn in river water on estuarine Mn distributions. Nature, 279(5711), 318-319.

Mortimer, R. J. G., & Rae, J. E. (2000). Metal speciation (Cu, Zn, Pb, Cd) and organic matter in oxic to suboxic salt marsh sediments, Severn Estuary, Southwest Britain. Marine Pollution Bulletin, 40(5), 377-386.

Moses, C. O., Nordstrom, D. K., Herman, J. S., & Mills, A. L. (1987). Aqueous pyrite oxidation by dissolved oxygen and by ferric iron. Geochimica et Cosmochimica Acta, 51(6), 1561-1571.

Mosley, L. M., & Liss, P. S. (2020). Particle aggregation, pH changes and metal behaviour during estuarine mixing: review and integration. Marine and Freshwater Research, 71(3), 300-310.

Mseddi, H., Ben Mammou, A., & Oueslati, W. (2010). Methodology for the extraction of carbonate-bound trace metals from carbonate-rich soils: application to Lakhouat soils, Tunis, Tunisia. Chemical Speciation & Bioavailability, 22(3), 165-170.

Mucci, A., Starr, M., Gilbert, D., & Sundby, B. (2011). Acidification of lower St. Lawrence Estuary bottom waters. Atmosphere-Ocean, 49(3), 206-218.

Muller, A. C., Muller, D. L., & Muller, A. (2016). Resolving spatiotemporal characteristics of the seasonal hypoxia cycle in shallow estuarine environments of the Severn River and South River, MD, Chesapeake Bay, USA. Heliyon, 2(9), e00157.

Müller, B., Meyer, J. S., & Gächter, R. (2018). Alkalinity and nitrate concentrations in calcareous watersheds: Are they linked, and is there an upper limit to alkalinity?. Biogeosciences Discussions, 1-19.

Muller, G. (1979). heavy metals in the sediments of the Rhine-verderungen since. Umshav, 79, 133-149.

Muller, G.(1969). Index of geoaccumulation in sediments of the Rhine River. Geojournal, 2, 108–118.

Murray, R. C. (1964). Origin and diagenesis of gypsum and anhydrite. Journal of Sedimentary Research, 34(3), 512-523.

Naderi, M., Raeisi, E., & Zarei, M. (2016). The impact of halite dissolution of salt diapirs on surface and ground water under climate change, South-Central Iran. Environmental Earth Sciences, 75(8), 708.

Nagarajan, R., Anandkumar, A., Hussain, S. M., Jonathan, M. P., Ramkumar, M., Eswaramoorthi, S., ... & Chua, H. B. (2019). Geochemical characterization of beach sediments of Miri, NW Borneo, SE Asia: Implications on provenance, weathering intensity, and assessment of coastal environmental status. In Coastal Zone Management (pp. 279-330). Elsevier.

Nagarajan, R., Armstrong-Altrin, J. S., Kessler, F. L., & Jong, J. (2017a). Petrological and geochemical constraints on provenance, paleoweathering, and tectonic setting of clastic sediments from the Neogene Lambir and Sibuti Formations, northwest Borneo. In Sediment provenance (pp. 123-153). Elsevier.

Nagarajan, R., Armstrong-Altrin, J. S., Kessler, F. L., Hidalgo-Moral, E. L., Dodge-Wan, D., & Taib, N. I. (2015). Provenance and tectonic setting of Miocene siliciclastic sediments, Sibuti Formation, northwestern Borneo. Arabian Journal of Geosciences, 8(10), 8549-8565.

Nagarajan, R., Armstrong-Altrin, J. S., Nagendra, R., Madhavaraju, J., & Moutte, J. (2007). Petrography and geochemistry of terrigenous sedimentary rocks in the Neoproterozoic Rabanpalli Formation, Bhima Basin, Southern India: implications for paleoweathering conditions, provenance and source rock composition. Journal-Geological Society of India, 70(2), 297.

Nagarajan, R., Jonathan, M. P., Roy, P. D., Wai-Hwa, L., Prasanna, M. V., Sarkar, S. K., & Navarrete-López, M. J. M. P. B. (2013). Metal concentrations in sediments from tourist beaches of Miri City, Sarawak, Malaysia (Borneo Island). Marine pollution bulletin, 73(1), 369-373.

Nagarajan, R., Roy, P. D., Kessler, F. L., Jong, J., Dayong, V., & Jonathan, M. P. (2017b). An integrated study of geochemistry and mineralogy of the Upper Tukau Formation, Borneo Island (East Malaysia): Sediment provenance, depositional setting and tectonic implications. Journal of Asian Earth Sciences, 143, 77-94.

Naidoo, S., & Olaniran, A. (2013). Treated wastewater effluent as a source of microbial pollution of surface water resources. International journal of environmental research and public health, 11(1), 249-270.

Najar, I. A., Ahmadi, R. B., Hamza, H., Sa'don, N. B. M., & Ahmad, A. (2020). First Order Seismic Microzonation of Miri district of Sarawak Malaysia using AHP-GIS Platform.

Namieśnik, J., & Rabajczyk, A. (2010). The speciation and physico-chemical forms of metals in surface waters and sediments. Chemical Speciation & Bioavailability, 22(1), 1-24.

Narayana, A. C. (2015). Shoreline Changes. Encyclopedia of Earth Sciences Series, 590–602. doi:10.1007/978-94-017-8801-4_118

Narwal, R. P., Singh, B. R., & Salbu, B. (1999). Association of cadmium, zinc, copper, and nickel with components in naturally heavy metal-rich soils studied by

parallel and sequential extractions. Communications in Soil Science and Plant Analysis, 30(7-8), 1209-1230.

Nasir, F. A. M., Suratman, S., & Le, D. Q. (2019). Distribution and Behavior Of Nutrients in Besut River Estuary, Terengganu, Malaysia. Malaysian Journal of Analytical Sciences, 23(6), 1077-1089.

Nasrabadi, T., Ruegner, H., Schwientek, M., Bennett, J., Fazel Valipour, S., & Grathwohl, P. (2018). Bulk metal concentrations versus total suspended solids in rivers: Time-invariant & catchment-specific relationships. PloS one, 13(1), e0191314.

NRC, (National Research Council & Safe Drinking Water Committee). (1977). Drinking Water and Health: Volume 1 (Vol. 1). National Academies Press.

NAWQA, (Corrosivity. National Water-Quality Assessment). (2021). Retrieved from https://www.usgs.gov/mission-areas/water-resources/science/corrosivity?qt-science_center_objects=0#qt-science_center_objects.

Nayak, G. N., Noronha-D'Mello, C. A., Pande, A., & Volvoikar, S. P. (2016). Understanding sedimentary depositional environments through geochemical signatures of a Tropical (Vaghotan) estuary, West Coast of India. Environmental Earth Sciences, 75(2), 111.

Nazeer, S., Hashmi, M. Z., & Malik, R. N. (2014). Heavy metals distribution, risk assessment and water quality characterization by water quality index of the River Soan, Pakistan. Ecological indicators, 43, 262-270.

Nemati, K., Bakar, N. K. A., Abas, M. R., & Sobhanzadeh, E. (2011). Speciation of heavy metals by modified BCR sequential extraction procedure in different depths of sediments from Sungai Buloh, Selangor, Malaysia. Journal of hazardous materials, 192(1), 402-410.

Ngatia, L., Grace III, J. M., Moriasi, D., & Taylor, R. (2019). Nitrogen and phosphorus eutrophication in marine ecosystems. Monitoring of Marine Pollution, 1-17.

NGS, (National Geographic Society). (2011, June 23). Cause and Effect: Tides. Retrieved from https://www.nationalgeographic.org/article/cause-effect-tides/.

Nieto, J. M., Sarmiento, A. M., Olías, M., Canovas, C. R., Riba, I., Kalman, J., & Delvalls, T. A. (2007). Acid mine drainage pollution in the Tinto and Odiel rivers (Iberian Pyrite Belt, SW Spain) and bioavailability of the transported metals to the Huelva Estuary. Environment International, 33(4), 445-455.

Nikanorov, A. M., & Brazhnikova, L. V. (2009). Water chemical composition of rivers, lakes and wetlands. Types and properties of water, 2, 42-80.

Nikanorov, A. M., & Khoruzhaya, T. A. (2012). Tendencies of long-term changes in water quality of water bodies in the South of Russia. Geography and Natural Resources, 33(2), 125-130.

Nirel, P. M. V., & Morel, F. M. (1990). Pitfalls of sequential extractions. Water research, 24(8), 1055-1056.

NIWA, (National Institute of Water and Atmospheric Research). (2020, October 5). Sediment, when soils erode, sediments are washed into waterways. Retrieved from https://niwa.co.nz/our-science/freshwater/tools/kaitiaki_tools/impacts/sediment#:~:text=When%20soils%20erode%2C%20sediments%20are%20washed%20into%20waterways.&text=Excess%20sediments%20can%20cause%20damage,to%20move%20around%20or%20feed.

Njitchoua, R., Dever, L., Fontes, J. C., & Naah, E. (1997). Geochemistry, origin and recharge mechanisms of groundwaters from the Garoua Sandstone aquifer, northen Cameroon. Journal of Hydrology, 190(1-2), 123-140.

NOAA, (National Oceanic and Atmospheric Administration). (2020, April 3). Professional Development – Estuaries. Retrieved from https://oceanservice.noaa.gov/education/pd/estuaries/welcome.html

Nugues, M. M., & Roberts, C. M. (2003). Coral mortality and interaction with algae in relation to sedimentation. Coral reefs, 22(4), 507-516.

Nyffeler, U. P., Li, Y. H., & Santschi, P. H. (1984). A kinetic approach to describe trace-element distribution between particles and solution in natural aquatic systems. Geochimica et Cosmochimica Acta, 48(7), 1513-1522.

Nystrand, M. I., Österholm, P., Nyberg, M. E., & Gustafsson, J. P. (2012). Metal speciation in rivers affected by enhanced soil erosion and acidity. Applied Geochemistry, 27(4), 906-916.

Nystrand, M. I., Österholm, P., Yu, C., & Åström, M. (2016). Distribution and speciation of metals, phosphorus, sulfate and organic material in brackish estuary water affected by acid sulfate soils. Applied Geochemistry, 66, 264-274.

Ohrel, R. L., & Register, K. M. (2006). Volunteer estuary monitoring: a methods manual. Ocean Conservancy.

Oldham, V. E., Miller, M. T., Jensen, L. T., & Luther III, G. W. (2017). Revisiting Mn and Fe removal in humic rich estuaries. Geochimica et Cosmochimica Acta, 209, 267-283.

Oliveira, H. (2012). Chromium as an environmental pollutant: insights on induced plant toxicity. Journal of Botany.

Omer, N. H. (2019). Water quality parameters. Water Quality-Science, Assessments and Policy, 18.

Ongley, E. D. (1996). Control of water pollution from agriculture (Vol. 55). Food & Agriculture Org.

Oremland, R. S., Hollibaugh, J. T., Maest, A. S., Presser, T. S., Miller, L. G., & Culbertson, C. W. (1989). Selenate reduction to elemental selenium by anaerobic bacteria in sediments and culture: biogeochemical significance of a novel, sulfate-independent respiration. Applied and Environmental Microbiology, 55(9), 2333-2343.

Orpin, A. R., & Ridd, P. V. (2012). Exposure of inshore corals to suspended sediments due to wave-resuspension and river plumes in the central Great Barrier Reef: a reappraisal. Continental Shelf Research, 47, 55-67.

Özkan, E. Y. (2012). A new assessment of heavy metal contaminations in an eutrophicated bay (Inner Izmir Bay, Turkey). Turkish Journal of Fisheries and Aquatic Sciences, 12(1), 135-147.

Pa'Suya, M. F., Omar, K. M., Peter, B. N., & Din, A. H. M. (2014). Seasonal Sea Surface Circulation in the Northwest Region Off the Borneo Island Based on Nineteen Years Satellite Altimetry Data. In Geoinformation for Informed Decisions (pp. 189-200). Springer, Cham.

Pađan, J., Marcinek, S., Cindrić, A. M., Layglon, N., Lenoble, V., Salaün, P., ... & Omanović, D. (2019). Improved voltammetric methodology for chromium redox speciation in estuarine waters. Analytica Chimica Acta, 1089, 40-47.

Paikaray, S. (2016). Origin, mobilization and distribution of selenium in a soil/water/air system: a global perspective with special reference to the Indian scenario. CLEAN–Soil, Air, Water, 44(5), 474-487.

Panda, B. R., Chidambaram, S., Ganesh, N., Adithya, V. S., Prasanna, M. V., Pradeep, K., & Vasudevan, U. (2018). A hydrochemical approach to estimate mountain front recharge in an aquifer system in Tamilnadu, India. Acta Geochimica, 37(3), 465-488.

Panigrahy, B. K., & Raymahashay, B. C. (2005). River water quality in weathered limestone: a case study in upper Mahanadi basin, India. Journal of earth system science, 114(5), 533-543.

Parker, D. R., Pedler, J. F., Ahnstrom, Z. A. S., & Resketo, M. (2001). Reevaluating the free-ion activity model of trace metal toxicity toward higher plants: Experimental evidence with copper and zinc. Environmental Toxicology and Chemistry: An International Journal, 20(4), 899-906.

Patra, S., Liu, C. Q., Wang, F. S., Li, S. L., & Wang, B. L. (2012). Behavior of major and minor elements in a temperate river estuary to the coastal sea. International Journal of Environmental Science and Technology, 9(4), 647-654.

Patrick Jr, W. H., & Jugsujinda, A. (1992). Sequential reduction and oxidation of inorganic nitrogen, manganese, and iron in flooded soil. Soil Science Society of America Journal, 56(4), 1071-1073.

Pavoni, E., Crosera, M., Petranich, E., Faganeli, J., Klun, K., Oliveri, P., ... & Adami, G. (2021). Distribution, Mobility and Fate of Trace Elements in an Estuarine System Under Anthropogenic Pressure: The Case of the Karstic Timavo River (Northern Adriatic Sea, Italy). Estuaries and Coasts, 1-17.

Pedersen, O., Colmer, T. D., & Sand-Jensen, K. (2013). Underwater photosynthesis of submerged plants–recent advances and methods. Frontiers in Plant Science, 4, 140.

Peilin, G., Meng, C., Lichao, Z., Yuejun, S., Minghao, M., & Lingyun, W. (2019, December). Study on water ecological restoration technology of river. In IOP Conference Series: Earth and Environmental Science (Vol. 371, No. 3, p. 032025). IOP Publishing.

Pejrup, M. (1986). Parameters affecting fine-grained suspended sediment concentrations in a shallow micro-tidal estuary, Ho Bugt, Denmark. Estuarine, Coastal and Shelf Science, 22(2), 241-254.

Peng, L. C., Hassan, K., Leman, M. S., Nasib, B. M., & Karim, R. A. (1997). Towards Producing a Stratigraphic Lexicon of Malaysia.

Perin, G., Craboledda, L., Lucchese, M., Cirillo, R., Dotta, L., & Zanette, M. A. Orio, A., 1985. Heavy metal speciation in the sediments of Northern Adriatic Sea. A new approach for environmental toxicity determination. In Proceedings of the International Conference “Heavy Metals in the Environment”. CEP Consultants, Athens, Greece (pp. 454-456).

Peters, E. C., Gassman, N. J., Firman, J. C., Richmond, R. H., & Power, E. A. (1997). Ecotoxicology of tropical marine ecosystems. Environmental Toxicology and Chemistry: An International Journal, 16(1), 12-40.

Peters, G. M., Maher, W. A., Barford, J. P., & Gomes, V. G. (1997). Selenium associations in estuarine sediments: redox effects. In the Interactions Between Sediments and Water (pp. 275-282). Springer, Dordrecht.

Pettine, M., & Millero, F. J. (1990). Chromium speciation in seawater: The probable role of hydrogen peroxide. Limnology and Oceanography, 35(3), 730-736.

Pfeiffer-Herbert, A. S., Kincaid, C. R., Bergondo, D. L., & Pockalny, R. A. (2015). Dynamics of wind-driven estuarine-shelf exchange in the Narragansett Bay estuary. Continental Shelf Research, 105, 42-59.

Pilcher, N., & Cabanban, A. (2000). The status of coral reefs in eastern Malaysia.

Piper, A. M. (1944). A graphic procedure in the geochemical interpretation of water-analyses. Eos, Transactions American Geophysical Union, 25(6), 914-928.

Pizarro, J., Rubio, M. A., & Lira, G. (2001). Optimization of a in situ sampling technique: Analysis of Cu and Fe in aquatic systems. Boletin De La Sociedad Chilena De Quimica, 46(3), 281-285.

Pobi, K. K., Satpati, S., Dutta, S., Nayek, S., Saha, R. N., & Gupta, S. (2019). Sources evaluation and ecological risk assessment of heavy metals accumulated within a natural stream of Durgapur industrial zone, India, by using multivariate analysis and pollution indices. Applied Water Science, 9(3), 58.

Poggenburg, C., Mikutta, R., Schippers, A., Dohrmann, R., & Guggenberger, G. (2018). Impact of natural organic matter coatings on the microbial reduction of iron oxides. Geochimica et Cosmochimica Acta, 224, 223-248.

Pokrovsky, O. S., Viers, J., Emnova, E. E., Kompantseva, E. I., & Freydier, R. (2008). Copper isotope fractionation during its interaction with soil and aquatic microorganisms and metal oxy (hydr) oxides: Possible structural control. Geochimica et Cosmochimica Acta, 72(7), 1742-1757.

Pontér, C., Ingri, J., & Boström, K. (1992). Geochemistry of manganese in the Kalix River, northern Sweden. Geochimica et Cosmochimica Acta, 56(4), 1485-1494.

Poulain, P. M., Warn-Varnas, A., & Niiler, P. P. (1996). Near-surface circulation of the Nordic seas as measured by Lagrangian drifters. Journal of Geophysical Research: Oceans, 101(C8), 18237-18258.

Prabakaran, K. (2017). Environmental Geochemistry of the Lower Baram River, Borneo (Doctoral dissertation, Curtin University).

Prabakaran, K., Eswaramoorthi, S., Nagarajan, R., Anandkumar, A., & Franco, F. M. (2020). Geochemical behaviour and risk assessment of trace elements in a tropical river, Northwest Borneo. Chemosphere, 252, 126430.

Prabakaran, K., Nagarajan, R., Eswaramoorthi, S., Anandkumar, A., & Franco, F. M. (2019). Environmental significance and geochemical speciation of trace elements in Lower Baram River sediments. Chemosphere, 219, 933-953.

Pradhanang, S. (2014). Distribution and fractionation of heavy metals in sediments of Karra River, Hetauda, Nepal. Journal of Institute of Science and Technology, 19(2), 123-128.

Prajith, A., Rao, V. P., & Chakraborty, P. (2016). Distribution, provenance and early diagenesis of major and trace metals in sediment cores from the Mandovi estuary, western India. Estuarine, Coastal and Shelf Science, 170, 173-185.

Prasad, B. S. R. V., Srinivasu, P. D. N., Varma, P. S., Raman, A. V., & Ray, S. (2014). Dynamics of dissolved oxygen in relation to saturation and health of an aquatic body: a case for Chilka Lagoon, India. Journal of Ecosystems, 2014.

Prasanna, M. V., Chidambaram, S., Hameed, A. S., & Srinivasamoorthy, K. (2010). Study of evaluation of groundwater in Gadilam basin using hydrogeochemical and isotope data. Environmental monitoring and assessment, 168(1-4), 63-90.

Prasanna, M. V., Ramdzani, I. A. B. A., Nagarajan, R., Chidambaram, S., & Venkatramanan, S. (2019, April). Geoelectrical Investigation Along Miri Coast, East Malaysia: Evaluate the Vulnerability of Coastal Aquifer. In IOP Conference Series: Materials Science and Engineering (Vol. 495, No. 1, p. 012042). IOP Publishing.

Priya, K. L., & Haddout, S. (2020, June). Trace metal partitioning in a shallow estuary, Muthupet, India. In IOP Conference Series: Earth and Environmental Science (Vol. 491, No. 1, p. 012016). IOP Publishing.

Priya, K. L., Jegathambal, P., & James, E. J. (2014). Trace metal distribution in a shallow estuary. Toxicological & Environmental Chemistry, 96(4), 579-593.

Prohić, E., & Kniewald, G. (1987). Heavy metal distribution in recent sediments of the Krka River estuary—an example of sequential extraction analysis. Marine chemistry, 22(2-4), 279-297.

Qian, W., Gan, J., Liu, J., He, B., Lu, Z., Guo, X., ... & Dai, M. (2018). Current status of emerging hypoxia in a eutrophic estuary: the lower reach of the Pearl River Estuary, China. Estuarine, Coastal and Shelf Science, 205, 58-67.

Qin, J., Enya, O., & Lin, C. (2018). Dynamics of Fe, Mn, and Al liberated from contaminated soil by low-molecular-weight organic acids and their effects on the release of soil-borne trace elements. Applied Sciences, 8(12), 2444.

Rabee, A. M., Al-Fatlawy, Y. F., & Nameer, M. (2011). Using Pollution Load Index (PLI) and geoaccumulation index (I-Geo) for the assessment of heavy metals pollution in Tigris river sediment in Baghdad Region. Al-Nahrain Journal of Science, 14(4), 108-114.

Rahman, M. J. J., & Suzuki, S. (2007). Geochemistry of sandstones from the Miocene Surma Group, Bengal Basin, Bangladesh: Implications for Provenance, tectonic setting and weathering. Geochemical Journal, 41(6), 415-428.

Rakestraw, N. W. (1943). The Oceans: Their Physics, Chemistry, and General Biology (Sverdrup, HU; Johnson, Martin W.; Fleming, Richard H.).

Ralston, D. K., Warner, J. C., Geyer, W. R., & Wall, G. R. (2013). Sediment transport due to extreme events: The Hudson River estuary after tropical storms Irene and Lee. Geophysical Research Letters, 40(20), 5451-5455.

Ramesh, K., & Jagadeeswari, B. P. (2012). Hydrochemical characteristics of groundwater for domestic and irrigation purposes in Periyakulam taluk of Theni district, Tamil Nadu. Int Res J Environ Sci, 1(1), 19-27.

Rao, C. R. M., Sahuquillo, A., & Sanchez, J. L. (2008). A review of the different methods applied in environmental geochemistry for single and sequential extraction of trace elements in soils and related materials. Water, Air, and Soil Pollution, 189(1-4), 291-333.

Rath, K. M., & Rousk, J. (2015). Salt effects on the soil microbial decomposer community and their role in organic carbon cycling: a review. Soil Biology and Biochemistry, 81, 108-123.

Ravikumar, P., & Somashekar, R. K. (2017). Principal component analysis and hydrochemical facies characterization to evaluate groundwater quality in Varahi river basin, Karnataka state, India. Applied Water Science, 7(2), 745-755.

Rawat, K. S., Singh, S. K., & Gautam, S. K. (2018). Assessment of groundwater quality for irrigation use: a peninsular case study. Applied Water Science, 8(8), 233.

RCM, (Reef Check Malaysia). (2018). Status of coral reefs in Malaysia, 2017. Reef check Malaysia survey report, Reef Check Malaysia.

Regarajan, R and Balasubramaniam, A. (1990) Corrosion and scale formation characteristics of Groundwater in and around Nagavalli, Salem District, Tamilnadu, J.Applied Hydrology,v.3,n2,pp 15-22

Regnier, P., & Wollast, R. (1993). Distribution of trace metals in suspended matter of the Scheldt estuary. Marine Chemistry, 43(1-4), 3-19.

Reichelt-Brushett, A. J., & Harrison, P. L. (2004). Development of a sublethal test to determine the effects of copper and lead on scleractinian coral larvae. Archives of environmental contamination and toxicology, 47(1), 40-55.

Reiss, A. G., Gavrieli, I., Rosenberg, Y. O., Reznik, I. J., Luttge, A., Emmanuel, S., & Ganor, J. (2021). Gypsum Precipitation under Saline Conditions: Thermodynamics, Kinetics, Morphology, and Size Distribution. Minerals, 11(2), 141.

Restrepo, J. D., Park, E., Aquino, S., & Latrubesse, E. M. (2016). Coral reefs chronically exposed to river sediment plumes in the southwestern Caribbean: Rosario Islands, Colombia. Science of the Total Environment, 553, 316-329.

Rich, C. I. (1968). Mineralogy of soil potassium. The role of potassium in agriculture, 79-108.

Richards, L. A. (1954). Diagnosis and Improvement of. Saline and Alkali Soils. USDA Handbook, 60.

Rieuwerts, J. S., Thornton, I., Farago, M. E., & Ashmore, M. R. (1998). Factors influencing metal bioavailability in soils: preliminary investigations for the development of a critical loads approach for metals. Chemical Speciation & Bioavailability, 10(2), 61-75.

Rigaud, S., Radakovitch, O., Couture, R. M., Deflandre, B., Cossa, D., Garnier, C., & Garnier, J. M. (2013). Mobility and fluxes of trace elements and nutrients at the sediment–water interface of a lagoon under contrasting water column oxygenation conditions. Applied Geochemistry, 31, 35-51.

Rinklebe, J., & Shaheen, S. M. (2014). Assessing the mobilization of cadmium, lead, and nickel using a seven-step sequential extraction technique in contaminated floodplain soil profiles along the central Elbe River, Germany. Water, Air, & Soil Pollution, 225(8), 1-20.

Robert, S., Blanc, G., Schäfer, J., Lavaux, G., & Abril, G. (2004). Metal mobilization in the Gironde Estuary (France): the role of the soft mud layer in the maximum turbidity zone. Marine Chemistry, 87(1-2), 1-13.

Roden, E. E., & Edmonds, J. W. (1997). Phosphate mobilization in iron-rich anaerobic sediments: microbial Fe (III) oxide reduction versus iron-sulfide formation. Archiv für Hydrobiologie, 347-378.

Rodgers, K. J., Hursthouse, A., & Cuthbert, S. (2015). The potential of sequential extraction in the characterisation and management of wastes from steel processing: a prospective review. International Journal of Environmental Research and Public Health, 12(9), 11724-11755.

Rosado, D., Usero, J., & Morillo, J. (2016). Ability of 3 extraction methods (BCR, Tessier and protease K) to estimate bioavailable metals in sediments from Huelva estuary (Southwestern Spain). Marine pollution bulletin, 102(1), 65-71.

Roy, K. J., & Smith, S. V. (1971). Sedimentation and coral reef development in turbid water: Fanning Lagoon.

Rusydi, A. F. (2018, February). Correlation between conductivity and total dissolved solid in various type of water: A review. In IOP conference series: earth and environmental science (Vol. 118, No. 1, p. 012019). IOP Publishing.

Ruttenberg, K. C. (1992). Development of a sequential extraction method for different forms of phosphorus in marine sediments. Limnology and oceanography, 37(7), 1460-1482.

Ryan, P. A. (1991). Environmental effects of sediment on New Zealand streams: a review. New Zealand journal of marine and freshwater research, 25(2), 207-221.

Rysgaard, S., Thastum, P., Dalsgaard, T., Christensen, P. B., & Sloth, N. P. (1999). Effects of salinity on NH 4+ adsorption capacity, nitrification, and denitrification in Danish estuarine sediments. Estuaries, 22(1), 21-30.

Ryznar, J. W. (1944). A new index for determining amount of calcium carbonate scale formed by a water. Journal-American Water Works Association, 36(4), 472-483.

Sabdono, A. (2009). Heavy metal levels and their potential toxic effect on coral Galaxea fascicularis from Java Sea, Indonesia. Research Journal of Environmental Sciences, 3(1), 96-102.

Saeedi, M., Karbassi, A. R., & Mehrdadi, N. (2003). Flocculation of dissolved Mn, Zn, Ni and Cu during the mixing of Tadjan River water with Caspian Sea water. International journal of environmental studies, 60(6), 575-580.

Saha, S., Reza, A. S., & Roy, M. K. (2019). Hydrochemical evaluation of groundwater quality of the Tista floodplain, Rangpur, Bangladesh. Applied Water Science, 9(8), 198.

Saifullah, A. S. M., Idris, M. H., Rajaee, A. H., & Johan, I. (2014). Seasonal variation of water characteristics in Kuala Sibuti river estuary in Miri, Sarawak, Malaysia. MJS, 33(1), 9-22.

Sakan, S., Frančišković-Bilinski, S., Đorđević, D., Popović, A., Škrivanj, S., & Bilinski, H. (2020). Geochemical Fractionation and Risk Assessment of Potentially Toxic Elements in Sediments from Kupa River, Croatia. Water, 12(7), 2024.

Salam, M. A., Paul, S. C., Rahman, F. N. B. A., Iqbal, M. A., Siddiqua, S. A., Rak, A., ... & A Kadir, W. R. (2021). Trace Metals Concentration and Associated Risk Assessment in Sediment of Kelantan Coastline Area Estuaries, Malaysia. Soil and Sediment Contamination: An International Journal, 1-20.

Salam, M. A., Paul, S. C., Zain, R. A. M. M., Bhowmik, S., Nath, M. R., Siddiqua, S. A., ... & Amin, M. F. M. (2020). Trace metals contamination potential and health risk assessment of commonly consumed fish of Perak River, Malaysia. Plos one, 15(10), e0241320.

Salas-Monreal, D., & Valle-Levinson, A. (2008). Sea-level slopes and volume fluxes produced by atmospheric forcing in estuaries: Chesapeake Bay case study. Journal of Coastal Research, (24), 208-217.

Saleem, M., Iqbal, J., & Shah, M. H. (2015). Geochemical speciation, anthropogenic contamination, risk assessment and source identification of selected metals in freshwater sediments—a case study from Mangla Lake, Pakistan. Environmental Nanotechnology, Monitoring & Management, 4, 27-36.

Saleh, A., Al-Ruwaih, F., & Shehata, M. (1999). Hydrogeochemical processes operating within the main aquifers of Kuwait. Journal of Arid Environments, 42(3), 195-209.

Samani, A. V., Karbassi, A. R., Fakhraee, M., Heidari, M., Vaezi, A. R., & Valikhani, Z. (2015). Effect of dissolved organic carbon and salinity on flocculation process of heavy metals during mixing of the Navrud River water with Caspian Seawater. Desalination and Water Treatment, 55(4), 926-934.

Samanta, S., & Dalai, T. K. (2016). Dissolved and particulate Barium in the Ganga (Hooghly) River estuary, India: Solute-particle interactions and the enhanced dissolved flux to the oceans. Geochimica et Cosmochimica Acta, 195, 1-28.

Samanta, S., Amrutha, K., Dalai, T. K., & Kumar, S. (2017). Heavy metals in the Ganga (Hooghly) River estuary sediment column: evaluation of association, geochemical cycling and anthropogenic enrichment. Environmental Earth Sciences, 76(4), 140.

Sanders, C. J., Barcellos, R. G., & Silva-Filho, E. V. (2012). Major element concentrations in mangrove pore water, Sepetiba Bay, Brazil. Brazilian Journal of Oceanography, 60(1), 33-39.

Santhi, C., Arnold, J. G., Williams, J. R., Dugas, W. A., Srinivasan, R., & Hauck, L. M. (2001). Validation of the swat model on a large rwer basin with point and nonpoint sources 1. JAWRA Journal of the American Water Resources Association, 37(5), 1169-1188.

Santos-Echeandia, J., Prego, R., Cobelo-García, A., & Millward, G. E. (2009). Porewater geochemistry in a Galician Ria (NW Iberian Peninsula): implications for benthic fluxes of dissolved trace elements (Co, Cu, Ni, Pb, V, Zn). Marine Chemistry, 117(1-4), 77-87.

Sarkar, S. K., Favas, P. J., Rakshit, D., & Satpathy, K. K. (2014). Geochemical speciation and risk assessment of heavy metals in soils and sediments. In Environmental risk assessment of soil contamination. IntechOpen.

Sassi, M. G., & Hoitink, A. J. F. (2013). River flow controls on tides and tide-mean water level profiles in a tidal freshwater river. Journal of Geophysical Research: Oceans, 118(9), 4139-4151.

Savci, S. (2012). An agricultural pollutant: chemical fertilizer. International Journal of Environmental Science and Development, 3(1), 73.

Sawyer, C. N., & McCarty, P. L. (1967). Chemistry for sanitary engineers.

Scanes, P., Ferguson, A., & Potts, J. (2017). Estuary form and function: implications for palaeoecological studies. In Applications of paleoenvironmental techniques in estuarine studies (pp. 9-44). Springer, Dordrecht.

Scavia, D., Bertani, I., Obenour, D. R., Turner, R. E., Forrest, D. R., & Katin, A. (2017). Ensemble modeling informs hypoxia management in the northern Gulf of Mexico. Proceedings of the National Academy of Sciences, 114(33), 8823-8828.

Schoeller, H, (1967). Qualitative evaluation of Ground Water Resources (in methods and techniques of Groundwater investigations and Development), water Resources Series,33, UNESCO, 44-52

Schoeller, H. (1965). Qualitative evaluation of groundwater resources. Methods and techniques of groundwater investigations and development. UNESCO, 5483.

Schoeller, H. (1977). Geochemistry of groundwater. In 'Groundwater Studies–an International Guide for Research and Practice'.(Eds RH Brown, AA Konoplyantsev, J. Ineson, and VS Kovalevsky.) pp. 1–18.

Schuler, L. J., Hoang, T. C., & Rand, G. M. (2008). Aquatic risk assessment of copper in freshwater and saltwater ecosystems of South Florida. Ecotoxicology, 17(7), 642-659.

Scott, C. R., Hemingway, K. L., Elliot, D. J. V. N., Pethick, J. S., Malcolm, S., & Wilkinson, M. (1999). Impacts of Nutrients in Estuaries: Phase 2, Summary Report. Environment Agency, Bristol.

Scully, M. E. (2016). Mixing of dissolved oxygen in Chesapeake Bay driven by the interaction between wind-driven circulation and estuarine bathymetry. Journal of Geophysical Research: Oceans, 121(8), 5639-5654.

Sedeño-Díaz, J. E., López-López, E., Mendoza-Martínez, E., Rodríguez-Romero, A. J., & Morales-García, S. S. (2020). Distribution coefficient and metal pollution index in water and sediments: Proposal of a new index for ecological risk assessment of metals. Water, 12(1), 29.

Seers, B. M., & Shears, N. T. (2015). Spatio-temporal patterns in coastal turbidity–long-term trends and drivers of variation across an estuarine-open coast gradient. Estuarine, Coastal and Shelf Science, 154, 137-151.

Sengupta, P. (2013). Potential health impacts of hard water. International journal of preventive medicine, 4(8), 866.

Senthilkumar, S., Balasubramanian, N., Gowtham, B., & Lawrence, J. F. (2017). Geochemical signatures of groundwater in the coastal aquifers of Thiruvallur district, south India. Applied Water Science, 7(1), 263-274.

Serder, M. F., Islam, M. S., Hasan, M. R., Yeasmin, M. S., & Mostafa, M. G. (2020). Assessment of coastal surface water quality for irrigation purpose. Water Practice & Technology, 15(4), 960-972.

Shafie, N. A., Aris, A. Z., & Haris, H. (2014). Geoaccumulation and distribution of heavy metals in the urban river sediment. International Journal of Sediment Research, 29(3), 368-377.

Shammi, M., Rahman, M. M., Islam, M. A., Bodrud-Doza, M., Zahid, A., Akter, Y., ... & Kurasaki, M. (2017). Spatio-temporal assessment and trend analysis of surface water salinity in the coastal region of Bangladesh. Environmental science and pollution research, 24(16), 14273-14290.

Shankar, K., Aravindan, S., & Rajendran, S. (2011). Hydrogeochemistry of the Paravanar River Sub-Basin, Cuddalore District, Tamilnadu, India. E-Journal of Chemistry, 8.

Shapiro, J. (1964). Effect of yellow organic acids on iron and other metals in water. Journal-American Water Works Association, 56(8), 1062-1082.

Sharma, A., Singh, A. K., & Kumar, K. (2012). Environmental geochemistry and quality assessment of surface and subsurface water of Mahi River basin, western India. Environmental Earth Sciences, 65(4), 1231-1250.

Shazili, N. A. M., Yunus, K., Ahmad, A. S., Abdullah, N., & Rashid, M. K. A. (2006). Heavy metal pollution status in the Malaysian aquatic environment. Aquatic Ecosystem Health & Management, 9(2), 137-145.

Sheeja, R. V., Sheela, A. M., Jaya, S., & Joseph, S. (2020). Assessment of water quality of a tropical river with special reference to ions. Current Journal of Applied Science and Technology, 97-116.

Sheikhy Narany, T., Ramli, M. F., Aris, A. Z., Sulaiman, W. N. A., Juahir, H., & Fakharian, K. (2014). Identification of the hydrogeochemical processes in groundwater using classic integrated geochemical methods and geostatistical techniques, in Amol-Babol Plain, Iran. The Scientific World Journal, 2014.

Shelton, J. L., Engle, M. A., Buccianti, A., & Blondes, M. S. (2018). The isometric log-ratio (ilr)-ion plot: A proposed alternative to the Piper diagram. Journal of Geochemical Exploration, 190, 130-141.

Sholkovitz, E. R. (1976). Flocculation of dissolved organic and inorganic matter during the mixing of river water and seawater. Geochimica et Cosmochimica Acta, 40(7), 831-845.

Sholkovitz, E. R. (1978). The flocculation of dissolved Fe, Mn, Al, Cu, NI, Co and Cd during estuarine mixing. Earth and Planetary Science Letters, 41(1), 77-86.

Shroff, P., Vashi, R. T., Champaneri, V. A., & Patel, K. K. (2015). Correlation study among water quality parameters of groundwater of Valsad district of south Gujarat (India). Journal of Fundamental and Applied Sciences, 7(3), 340-349.

Sia, E. S. A., Zhang, J., Jiang, S., Zhu, Z., Carrasco, G., Holt Jang, F., ... & Müller, M. (2019). Behaviour of Dissolved Phosphorus with the associated nutrients in relation to phytoplankton biomass of the Rajang River-South China Sea continuum. Biogeosciences Discussions, 1-35.

Sia, S. G., & Abdullah, W. H. (2012). Enrichment of arsenic, lead, and antimony in Balingian coal from Sarawak, Malaysia: Modes of occurrence, origin, and partitioning behaviour during coal combustion. International journal of coal geology, 101, 1-15.

Silburn, B., Kröger, S., Parker, E. R., Sivyer, D. B., Hicks, N., Powell, C. F., ... & Greenwood, N. (2017). Benthic pH gradients across a range of shelf sea sediment types linked to sediment characteristics and seasonal variability. Biogeochemistry, 135(1), 69-88.

Sim, S. F., Rajendran, M., Nyanti, L., Ling, T. Y., Grinang, J., & Liew, J. J. (2017). Assessment of trace metals in water and sediment in a tropical river potentially affected by land use activities in northern Sarawak, Malaysia. International Journal of Environmental Research, 11(2), 99-110.

Simon, K., Hassan, M. H. B. A., & Barbeito, M. P. J. (2014). Sedimentology and stratigraphy of the Miocene Kampung Opak limestone (Sibuti Formation), Bekenu, Sarawak.

Simonsen, M., Teien, H. C., Lind, O. C., Saetra, Ø., Albretsen, J., & Salbu, B. (2019). Modeling key processes affecting Al speciation and transport in estuaries. Science of the total environment, 687, 1147-1163.

Simpson, J. H., Brown, J., Matthews, J., & Allen, G. (1990). Tidal straining, density currents, and stirring in the control of estuarine stratification. Estuaries, 13(2), 125-132.

Simpson, S. L., Rosner, J., & Ellis, J. (2000). Competitive displacement reactions of cadmium, copper, and zinc added to a polluted, sulfidic estuarine sediment. Environmental Toxicology and Chemistry: An International Journal, 19(8), 1992-1999.

Singaraja, C. (2017). Relevance of water quality index for groundwater quality evaluation: Thoothukudi District, Tamil Nadu, India. Applied Water Science, 7(5), 2157-2173.

Singaraja, C., Chidambaram, S., Anandhan, P., Prasanna, M. V., Thivya, C., Thilagavathi, R., & Sarathidasan, J. (2014). Determination of the utility of groundwater with respect to the geochemical parameters: a case study from Tuticorin District of Tamil Nadu (India). Environment, development and sustainability, 16(3), 689-721.

Singh, M., Müller, G., & Singh, I. B. (2002). Heavy metals in freshly deposited stream sediments of rivers associated with urbanisation of the Ganga Plain, India. Water, Air, and Soil Pollution, 141(1-4), 35-54.

Singh, S. K., Subramanian, V., & Gibbs, R. J. (1984). Hydrous Fe and Mn oxides—scavengers of heavy metals in the aquatic environment. Critical Reviews in Environmental Control, 14(1), 33-90.

Sinkko, H., Lukkari, K., Sihvonen, L. M., Sivonen, K., Leivuori, M., Rantanen, M., ... & Lyra, C. (2013). Bacteria contribute to sediment nutrient release and reflect progressed eutrophication-driven hypoxia in an organic-rich continental sea. PloS one, 8(6), e67061.

Sivasubramanian, P., Balasubramanian, N., Soundranayagam, J. P., & Chandrasekar, N. (2013). Hydrochemical characteristics of coastal aquifers of Kadaladi, Ramanathapuram District, Tamilnadu, India. Applied Water Science, 3(3), 603-612.

Smith, V. H. (2003). Eutrophication of freshwater and coastal marine ecosystems a global problem. Environmental Science and Pollution Research, 10(2), 126-139.

Smith, V. H., & Schindler, D. W. (2009). Eutrophication science: where do we go from here? Trends in ecology & evolution, 24(4), 201-207.

Söderlund, M., Virkanen, J., Holgersson, S., & Lehto, J. (2016). Sorption and speciation of selenium in boreal forest soil. Journal of environmental radioactivity, 164, 220-231.

Somura, H., Takeda, I., Arnold, J. G., Mori, Y., Jeong, J., Kannan, N., & Hoffman, D. (2012). Impact of suspended sediment and nutrient loading from land uses against water quality in the Hii River basin, Japan. Journal of Hydrology, 450, 25-35.

Song, H., Wignall, P. B., Song, H., Dai, X., & Chu, D. (2019). Seawater temperature and dissolved oxygen over the past 500 million years. Journal of Earth Science, 30(2), 236-243.

Song, Y., Choi, M. S., Lee, J. Y., & Jang, D. J. (2014). Regional background concentrations of heavy metals (Cr, Co, Ni, Cu, Zn, Pb) in coastal sediments of the South Sea of Korea. Science of the Total Environment, 482, 80-91.

Song, Y., Ji, J., Mao, C., Yang, Z., Yuan, X., Ayoko, G. A., & Frost, R. L. (2010). Heavy metal contamination in suspended solids of Changjiang River—environmental implications. Geoderma, 159(3-4), 286-295.

Soo, C. L., Chen, C. A., & Mohd-Long, S. (2017). Assessment of near-bottom water quality of southwestern coast of Sarawak, Borneo, Malaysia: a multivariate statistical approach. Journal of Chemistry, 2017.

Spadini, L., Manceau, A., Schindler, P. W., & Charlet, L. (1994). Structure and stability of Cd2+ surface complexes on ferric oxides: 1. Results from EXAFS spectroscopy. Journal of Colloid and Interface Science, 168(1), 73-86.

Sposito, G., Skipper, N. T., Sutton, R., Park, S. H., Soper, A. K., & Greathouse, J. A. (1999). Surface geochemistry of the clay minerals. Proceedings of the National Academy of Sciences, 96(7), 3358-3364.

Sridhar, K. (2001). Artificial recharge potentials of upper Kadavanar basin, Dindigul Dsitrict, Tamil Nadu, using Remote Sensing and GIS. Unpublished Thesis, university of Madras, 265p.

Sridharan, M., & Nathan, D. S. (2017). Hydrochemical facies and ionic exchange in coastal aquifers of Puducherry region, India: Implications for seawater intrusion. Earth Systems and Environment, 1(1), 1-14.

Srinivasamoorthy, K., Gopinath, M., Chidambaram, S., Vasanthavigar, M., & Sarma, V. S. (2014). Hydrochemical characterization and quality appraisal of groundwater from Pungar sub basin, Tamilnadu, India. Journal of King Saud University-Science, 26(1), 37-52.

Środoń, J. (1999). Illite group clay minerals. Encyclopedia of Earth Science, 597-601.

Stallard, R. F., & Edmond, J. M. (1983). Geochemistry of the Amazon: 2. The influence of geology and weathering environment on the dissolved load. Journal of Geophysical Research: Oceans, 88(C14), 9671-9688.

Steinke, S., Mohtadi, M., Groeneveld, J., Lin, L. C., Löwemark, L., Chen, M. T., & Rendle-Bühring, R. (2010). Reconstructing the southern South China Sea upper water column structure since the Last Glacial Maximum: Implications for the East Asian winter monsoon development. Paleoceanography, 25(2).

Stephens, M., Mattey, D., Gilbertson, D. D., & Murray-Wallace, C. V. (2008). Shell-gathering from mangroves and the seasonality of the Southeast Asian Monsoon using high-resolution stable isotopic analysis of the tropical estuarine bivalve (Geloina erosa) from the Great Cave of Niah, Sarawak: methods and reconnaissance of molluscs of early Holocene and modern times. *Journal of Archaeological Science*, *35*(10), 2686-2697.

Storlazzi, C. D., Field, M. E., Bothner, M. H., Presto, M. K., & Draut, A. E. (2009). Sedimentation processes in a coral reef embayment: Hanalei Bay, Kauai. Marine Geology, 264(3-4), 140-151.

Stumm, W., & Morgan, J. J. (2012). Aquatic chemistry: chemical equilibria and rates in natural waters (Vol. 126). John Wiley & Sons.

Stumpf, R. P., Johnson, L. T., Wynne, T. T., & Baker, D. B. (2016). Forecasting annual cyanobacterial bloom biomass to inform management decisions in Lake Erie. Journal of Great Lakes Research, 42(6), 1174-1183.

Stuyfzand, P. J. (1989). A new hydrochemical classification of water types. Iahs Publ, 182, 89-98.

Subbarao, M., & Reddy, M. R. B. Groundwater Quality Assessment in Srikalahasthi Mandal, Chittoor District, Andhra Pradesh, South India (2018). IOSR Journal of Engineering (IOSRJEN). ISSN (e): 2250-3021, ISSN (p): 2278-8719 Vol. 08, Issue 8 (August. 2018), ||V (I) || 33-42

Sultan, K. (2012). Hydrochemistry and baseline values of major and trace elements in tropical surface waters of the Terengganu River (Malaysia). Water international, 37(1), 1-15.

Sun, J., Liu, L., Lin, J., Lin, B., & Zhao, H. (2020). Vertical water renewal in a large estuary and implications for water quality. Science of The Total Environment, 710, 135593.

Sun, S., Sheng, Y., Zhao, G., Li, Z., & Yang, J. (2017). Feasibility assessment: application of ecological floating beds for polluted tidal river remediation. Environmental monitoring and assessment, 189(12), 1-11.

Sun, X., Li, B. S., Liu, X. L., & Li, C. X. (2020). Spatial variations and potential risks of heavy metals in seawater, sediments, and living organisms in Jiuzhen bay, China. Journal of Chemistry, 2020.

Sunda, W. (2012). Feedback interactions between trace metal nutrients and phytoplankton in the ocean. Frontiers in microbiology, 3, 204.

Sundaray, S. K., Nayak, B. B., Lin, S., & Bhatta, D. (2011). Geochemical speciation and risk assessment of heavy metals in the river estuarine sediments—a case study: Mahanadi basin, India. Journal of hazardous materials, 186(2-3), 1837-1846.

Suratman, S., Aziz, A. A., Tahir, N. M., & Lee, L. H. (2018). Distribution and behaviour of nitrogen compounds in the surface water of Sungai Terengganu Estuary, Southern Waters of South China Sea, Malaysia. Sains Malaysiana, 47(4), 651-659.

Sutherland, R. A. (2000). Bed sediment-associated trace metals in an urban stream, Oahu, Hawaii. Environmental geology, 39(6), 611-627.

Szefer, P. (1998). Distribution and behaviour of selected heavy metals and other elements in various components of the southern Baltic ecosystem. Applied geochemistry, 13(3), 287-292.

Tack, F. M., & Verloo, M. G. (1999). Single extractions versus sequential extraction for the estimation of heavy metal fractions in reduced and oxidised dredged sediments. Chemical Speciation & Bioavailability, 11(2), 43-50.

Tahir, N. M., Suratman, S., Shazili, N. A. M., Ariffin, M. M., Amin, M. S. M., Ariff, N. F. M. N. I., & Sulaiman, W. N. H. W. (2008). Behaviour of Water Quality Parameters During Ebb Tide In Dungun River Estuary, Terengganu.

Takayanagi, K., & Gobeil, C. (2000). Dissolved aluminum in the upper St. Lawrence Estuary. Journal of oceanography, 56(5), 517-525.

Tang, A., Liu, R., Ling, M., Xu, L., & Wang, J. (2010). Distribution characteristics and controlling factors of soluble heavy metals in the Yellow River Estuary and adjacent sea. Procedia Environmental Sciences, 2, 1193-1198.

Tankere-Muller, S., Zhang, H., Davison, W., Finke, N., Larsen, O., Stahl, H., & Glud, R. N. (2007). Fine scale remobilisation of Fe, Mn, Co, Ni, Cu and Cd in contaminated marine sediment. Marine Chemistry, 106(1-2), 192-207.

Tarpley, D., Harris, C. K., Friedrichs, C. T., & Sherwood, C. R. (2019). Tidal variation in cohesive sediment distribution and sensitivity to flocculation and bed consolidation in an idealized, partially mixed estuary. Journal of Marine Science and Engineering, 7(10), 334.

Taylor, K. G., & Owens, P. N. (2009). Sediments in urban river basins: a review of sediment–contaminant dynamics in an environmental system conditioned by human activities. Journal of Soils and Sediments, 9(4), 281-303.

Taylor, M. P., Mackay, A. K., Hudson-Edwards, K. A., & Holz, E. (2010). Soil Cd, Cu, Pb and Zn contaminants around Mount Isa city, Queensland, Australia: Potential sources and risks to human health. Applied Geochemistry, 25(6), 841-855.

Taylor, S. R., & McLennan, S. M. (1985). The continental crust: its composition and evolution.

Taylor, S. R., & McLennan, S. M. (2001). Chemical composition and element distribution in the Earth's crust. Encyclopedia of Physical Science and Technology, 312.

Tchounwou, P. B., Yedjou, C. G., Patlolla, A. K., & Sutton, D. J. (2012). Heavy metal toxicity and the environment. Molecular, clinical and environmental toxicology, 133-164.

Tenaga, K. T. A. (2003). Updating of condition of flooding in Malaysia–main report. Drainage and Irrigation Department, Kuala Lumpur. Retrieved from https://www.water.gov.my/jps/resources/auto%20download%20images/5844e46d37d56.pdf.

Tessier, A. P. G. C., Campbell, P. G. C., Auclair, J. C., & Bisson, M. (1984). Relationships between the partitioning of trace metals in sediments and their accumulation in the tissues of the freshwater mollusc Elliptio complanata in a mining area. Canadian Journal of Fisheries and Aquatic Sciences, 41(10), 1463-1472.

Tessier, A., & Campbell, P. G. C. (1987). Partitioning of trace metals in sediments: relationships with bioavailability. In Ecological effects of in situ sediment contaminants (pp. 43-52). Springer, Dordrecht.

Tessier, A., Campbell, P. G., & Bisson, M. (1979). Sequential extraction procedure for the speciation of particulate trace metals. Analytical chemistry, 51(7), 844-851.

Thanh-Nho, N., Strady, E., Nhu-Trang, T. T., David, F., & Marchand, C. (2018). Trace metals partitioning between particulate and dissolved phases along a tropical mangrove estuary (Can Gio, Vietnam). Chemosphere, 196, 311-322.

Thayer, G. W., McTigue, T. A., Bellmer, R. J., Burrows, F. M., Merkey, D. H., Nickens, A. D., ... & Pinit, P. T. (2003). Science-based restoration monitoring of coastal habitats, volume one: A framework for monitoring plans under the Estuaries and Clean Waters Act of 2000 (Public Law 160-457).

Thilagavathi, R., Chidambaram, S., Prasanna, M. V., Thivya, C., & Singaraja, C. (2012). A study on groundwater geochemistry and water quality in layered aquifers system of Pondicherry region, southeast India. Applied water science, 2(4), 253-269.

Thivya, C., Chidambaram, S., Thilagavathi, R., Prasanna, M. V., Singaraja, C., Adithya, V. S., & Nepolian, M. (2015). A multivariate statistical approach to identify the spatio-temporal variation of geochemical process in a hard rock aquifer. Environmental monitoring and assessment, 187(9), 552.

Thompson, A., & Goyne, K. W. (2012). Introduction to the sorption of chemical constituents in soils. Nature Education Knowledge, 4(4), 7.

Thompson, T., Fawell, J., Kunikane, S., Jackson, D., Appleyard, S., Callan, P., ... & World Health Organization. (2007). Chemical safety of drinking water: assessing priorities for risk management. World Health Organization.

Tian, R. (2020). Factors Controlling Hypoxia Occurrence in Estuaries, Chester River, Chesapeake Bay. Water, 12(7), 1961.

Tiemann, T. T., Donough, C. R., Lim, Y. L., Härdter, R., Norton, R., Tao, H. H., ... & Oberthür, T. (2018). Feeding the palm: a review of oil palm nutrition. Advances in Agronomy, 152, 149-243.

Tipping, E., Lofts, S., & Lawlor, A. J. (1998). Modelling the chemical speciation of trace metals in the surface waters of the Humber system. Science of the Total Environment, 210, 63-77.

Todd DK. Groundwater hydrology. John Wiley and Sons Inc., New York, U.S.A.; 1980. p. 10-138.

Todd, D. K., & Mays, L. W. (2004). Groundwater hydrology. John Wiley & Sons.

Togunwa, O. S., & Abdullah, W. H. (2017). Geochemical characterization of Neogene sediments from onshore West Baram Delta Province, Sarawak: paleoenvironment, source input and thermal maturity. Open Geosciences, 9(1), 302-313.

Tomasko, D. A., Anastasiou, C., & Kovach, C. (2006). Dissolved oxygen dynamics in Charlotte Harbor and its contributing watershed, in response to Hurricanes Charley, Frances, and Jeanne—impacts and recovery. Estuaries and Coasts, 29(6), 932-938.

Tomaso, D. J., & Najjar, R. G. (2015). Long-term variations in the dissolved oxygen budget of an urbanized tidal river: The upper Delaware Estuary. Journal of Geophysical Research: Biogeosciences, 120(6), 1027-1045.

Tomlinson, D. L., Wilson, J. G., Harris, C. R., & Jeffrey, D. W. (1980). Problems in the assessment of heavy-metal levels in estuaries and the formation of a pollution index. Helgoländer meeresuntersuchungen, 33(1-4), 566-575.

Tosca, N. J., Jiang, C. Z., Rasmussen, B., & Muhling, J. (2019). Products of the iron cycle on the early Earth. Free Radical Biology and Medicine, 140, 138-153.

Tripathy, S. K., Panigrahy, R. C., Gouda, R., & Panda, D. (1990). Distribution of Calcium and Magnesium In The Rushikulya-Estuary (Orissa), East-Coast Of India.

Turner, A., & Mawji, E. (2005). Hydrophobicity and reactivity of trace metals in the low-salinity zone of a turbid estuary. *Limnology and oceanography*, *50*(3), 1011-1019.

Turner, A., & Millward, G. E. (2000). Particle dynamics and trace metal reactivity in estuarine plumes. Estuarine, Coastal and Shelf Science, 50(6), 761-774.

Turner, A., Le Roux, S. M., & Millward, G. E. (2008). Adsorption of cadmium to iron and manganese oxides during estuarine mixing. Marine Chemistry, 108(1-2), 77-84.

Turner, B. L., & Raboy, V. (2019). Phosphorus cycle. Access Science. Retrieved April 13, 2021, from https://doi.org/10.1036/1097-8542.508930

Ugwu, I. M., & Igbokwe, O. A. (2019). Sorption of heavy metals on clay minerals and oxides: a review. *Advanced sorption process applications*, 1-23.

Uncles, R. J., Elliott, R. C. A., & Weston, S. A. (1985). Observed fluxes of water, salt and suspended sediment in a partly mixed estuary. Estuarine, Coastal and Shelf Science, 20(2), 147-167.

UNEP, (United Nations Environment Programme). (2017). The Watershed: Water from the Mountains into the Sea, Lakes and Reservoirs vol. 2.

USEPA. (1992) (Digitally published: 2017, January 27). SW-846 Test Method 3005A: Acid Digestion of Waters for Total Recoverable or Dissolved Metals for Analysis by Flame Atomic Absorption (FLAA) or Inductively Coupled Plasma (ICP) Spectroscopy. Retrieved from https://www.epa.gov/hw-sw846/sw-846-test-method-3005a-acid-digestion-waters-total-recoverable-or-dissolved-metals.

Usero, J., Gamero, M., Morillo, J., & Gracia, I. (1998). Comparative study of three sequential extraction procedures for metals in marine sediments. Environment International, 24(4), 487-496.

USGS. (2021, January 3). Snowmelt Runoff and the Water Cycle. Retrieved from https://www.usgs.gov/special-topic/water-science-school/science/snowmelt-runoff-and-water-cycle?qt-science_center_objects=0#qt-science_center_objects.

USSL. (1954). Diagnosis and improvement of saline and alkali soils. USDA Handbook, 60: 147.

Van Dam, B. R., & Wang, H. (2019). Decadal-scale acidification trends in adjacent North Carolina estuaries: competing role of anthropogenic CO2 and riverine alkalinity loads. Frontiers in Marine Science, 6, 136.

Van Dam, J. W., Negri, A. P., Uthicke, S., & Mueller, J. F. (2011). Chemical pollution on coral reefs: exposure and ecological effects. In Ecological impacts of toxic chemicals (Vol. 9, pp. 187-211). Bentham Science Publishers Ltd.

Van der Weijden, C. H., Arnoldus, M. J. H. L., & Meurs, C. J. (1977). Desorption of metals from suspended material in the Rhine estuary. Netherlands Journal of Sea Research, 11(2), 130-145.

Van Maren, D. S., Liew, S. C., & Hasan, G. J. (2014). The role of terrestrial sediment on turbidity near Singapore's coral reefs. Continental Shelf Research, 76, 75-88.

Van Straaten, P. (2002). Rocks for crops: agromania’s of sub-Saharan Africa.

Vane, C. H., Turner, G. H., Chenery, S. R., Richardson, M., Cave, M. C., Terrington, R., ... & Moss-Hayes, V. (2020). Trends in heavy metals, polychlorinated biphenyls and toxicity from sediment cores of the inner River Thames estuary, London, UK. Environmental Science: Processes & Impacts, 22(2), 364-380.

Vaquer-Sunyer, R., & Duarte, C. M. (2008). Thresholds of hypoxia for marine biodiversity. Proceedings of the National Academy of Sciences, 105(40), 15452-15457.

Varade, A. M., Yenkie, R. O., Shende, R. R., Golekar, R. B., Wagh, V. M., & Khandare, H. W. (2018). Assessment of water quality for the groundwater resources of urbanized part of the Nagpur District, Maharashtra (India). American Journal of Water Resources, 6(3), 89-111.

Vasanthavigar, M., Srinivasamoorthy, K., Vijayaragavan, K., RAJIV, G. R., Chidambaram, S., Sarama, V. S., ... & Vasudevan, S. (2009). Hydro geochemistry of Thirumanimuttar basin: an indication of weathering and anthropogenic impact.

Vaughan, M. C., Bowden, W. B., Shanley, J. B., Vermilyea, A., Sleeper, R., Gold, A. J., ... & Schroth, A. W. (2017). High-frequency dissolved organic carbon and nitrate measurements reveal differences in storm hysteresis and loading in relation to land cover and seasonality. Water Resources Research, 53(7), 5345-5363.

Vengosh, A., Helvacı, C., & Karamanderesi, I. H. (2002). Geochemical constraints for the origin of thermal waters from western Turkey. Applied Geochemistry, 17(3), 163-183.

Venkatramanan, S., Chung, S. Y., Ramkumar, T., Gnanachandrasamy, G., & Kim, T. H. (2015). Evaluation of geochemical behavior and heavy metal distribution of sediments: the case study of the Tirumalairajan river estuary, southeast coast of India. International Journal of Sediment Research, 30(1), 28-38.

Venturelli, G., Boschetti, T., & Duchi, V. (2003). Na-carbonate waters of extreme composition: Possible origin and evolution. Geochemical Journal, 37(3), 351-366.

Verma, P., & Ratan, J. K. (2020). Assessment of the negative effects of various inorganic water pollutants on the biosphere—an overview. Inorganic Pollutants in Water, 73-96.

Viers, J., Dupré, B., & Gaillardet, J. (2009). Chemical composition of suspended sediments in World Rivers: New insights from a new database. Science of the total Environment, 407(2), 853-868.

Villars, M. T., & Delvigne, G. A. L. (2001). Estuarine processes. Literature Review.

Vu, C. T., Lin, C., Nguyen, K. A., Shern, C. C., & Kuo, Y. M. (2018). Ecological risk assessment of heavy metals sampled in sediments and water of the Houjing River, Taiwan. Environmental Earth Sciences, 77(10), 388.

Vu, C. T., Lin, C., Nguyen, K. A., Shern, C. C., & Kuo, Y. M. (2018). Ecological risk assessment of heavy metals sampled in sediments and water of the Houjing River, Taiwan. Environmental Earth Sciences, 77(10), 1-11.

Walker, C. H., Sibly, R. M., Hopkin, S. P., & Peakall, D. B. (2012). Principles of ecotoxicology. CRC press. Dan, S. F., Umoh, U. U., & Osabor, V. N. (2014). Seasonal variation of enrichment and contamination of heavy metals in the

surface water of Qua Iboe River Estuary and adjoining creeks, South-South Nigeria. Journal of Oceanography and Marine Science, 5(6), 45-54.

Walker, L. M., Montagna, P. A., Hu, X., & Wetz, M. S. (2020). Timescales and Magnitude of Water Quality Change in Three Texas Estuaries Induced by Passage of Hurricane Harvey. Estuaries and Coasts, 1-12.

Walker, T. A. (1981). Dependance of phytoplankton chlorophyll on bottom resuspension in Cleveland Bay, northern Queensland. Marine and Freshwater Research, 32(6), 981-986.

Wanda, E. M., Gulula, L. C., & Phiri, G. (2012). Determination of characteristics and drinking water quality index in Mzuzu City, Northern Malawi. Physics and Chemistry of the Earth, Parts A/B/C, 50, 92-97.

Wang, A. J., Bong, C. W., Xu, Y. H., Hassan, M. H. A., Ye, X., Bakar, A. F. A., ... & Loh, K. H. (2017). Assessment of heavy metal pollution in surficial sediments from a tropical river-estuary-shelf system: A case study of Kelantan River, Malaysia. Marine pollution bulletin, 125(1-2), 492-500.

Wang, A. Q., Huang, S. D., & Sun, T. H. (2001). Study on the coordinate periodic change and the relativity between pH and DO in shallow water with algae. Sichuan Environment, 20(2), 4-7.

Wang, D., Lin, W., Yang, X., Zhai, W., Dai, M., & Chen, C. T. A. (2012). Occurrences of dissolved trace metals (Cu, Cd, and Mn) in the Pearl River Estuary (China), a large river-groundwater-estuary system. Continental Shelf Research, 50, 54-63.

Wang, W., & Wang, W. X. (2017). Trace metal behavior in sediments of Jiulong River Estuary and implication for benthic exchange fluxes. Environmental Pollution, 225, 598-609.

Wang, X., Liu, B., & Zhang, W. (2020). Distribution and risk analysis of heavy metals in sediments from the Yangtze River Estuary, China. Environmental Science and Pollution Research, 27(10), 10802-10810.

Wang, Z. L., & Liu, C. Q. (2003). Distribution and partition behavior of heavy metals between dissolved and acid-soluble fractions along a salinity gradient in the Changjiang Estuary, eastern China. Chemical Geology, 202(3-4), 383-396.

Warren, L. A., & Haack, E. A. (2001). Biogeochemical controls on metal behaviour in freshwater environments. Earth-Science Reviews, 54(4), 261-320.

Waters, T. F. (1995). Sediment in streams: sources, biological effects, and control. American Fisheries Society.

Weber, M., De Beer, D., Lott, C., Polerecky, L., Kohls, K., Abed, R. M., ... & Fabricius, K. E. (2012). Mechanisms of damage to corals exposed to sedimentation. Proceedings of the National Academy of Sciences, 109(24), E1558-E1567.

Weiduo, H., Teruhiko, K., Jin, R., Takahashi, Y., Gingras, M., Alessi, D. S., & Konhauser, K. O. (2020). Clay minerals as a source of cadmium to estuaries. Scientific Reports (Nature Publisher Group), 10(1).

Wen, Y., Qiu, J., Cheng, S., Xu, C., & Gao, X. (2020). Hydrochemical Evolution Mechanisms of Shallow Groundwater and Its Quality Assessment in the Estuarine Coastal Zone: A Case Study of Qidong, China. International journal of environmental research and public health, 17(10), 3382.

Wen, Y., Xiao, J., Goodman, B. A., & He, X. (2019). Effects of Organic Amendments on the Transformation of Fe (Oxyhydr) Oxides and Soil Organic Carbon Storage. Frontiers in Earth Science, 7, 257.

Weng, C. H., Huang, C. P., & Sanders, P. F. (2001). Effect of pH on Cr (VI) leaching from soil enriched in chromite ore processing residue. Environmental Geochemistry and Health, 23(3), 207-211.

Weng, C. H., Huang, C. P., Allen, H. E., Cheng, A. D., & Sanders, P. F. (1994). Chromium leaching behavior in soil derived from chromite ore processing waste. Science of the total environment, 154(1), 71-86.

Wepener, V., & Vermeulen, L. A. (2005). A note on the concentrations and bioavailability of selected metals in sediments of Richards Bay Harbour, South Africa. Water SA, 31(4), 589-596.

Whitfield, A., & Elliot, M. (2011). Ecosystem and biotic classifications of estuaries and coasts. Treatise on Estuarine and Coastal Science.

Whitmarsh, R. B. (1970). Erosion and sediment transport beneath the sea. Science Progress (1933-), 1-25.

WHO, (World Health Organization). (1993). Guidelines for drinking-water quality. World Health Organization.

WHO, (World Health Organization). (2006). Concise International Chemical Assessment Document 69 Cobalt and inorganic cobalt compounds, Geneva, Switzerland (pp. 8–53).

WHO, (World Health Organization). (2009). Calcium and magnesium in drinking water: public health significance. World Health Organization.

WHO, (World Health Organization). (2011). Safe drinking-water from desalination (No. WHO/HSE/WSH/11.03). World Health Organization.

WHO, (World Health Organization). (2017). Water quality and health-review of turbidity: information for regulators and water suppliers.

Wiedenmann, J., D'Angelo, C., Smith, E. G., Hunt, A. N., Legiret, F. E., Postle, A. D., & Achterberg, E. P. (2013). Nutrient enrichment can increase the susceptibility of reef corals to bleaching. Nature Climate Change, 3(2), 160-164.

Wilcox, L. (1955). Classification and use of irrigation waters (No. 969). US Department of Agriculture.

Wilcox, L. V. (1948). The quality of water for irrigation use. US Department of Agricultural Technical Bulletin 1962. US Department of Agriculture, Washington, DC.

Wilkinson, C. R., Chou, L. M., Gomez, E., Ridzwan, A. R., Soekarno, S., & Sudara, S. (1995). Status of coral reefs in Southeast Asia: threats and responses. Oceanographic Literature Review, 8(42), 684.

Wilkinson, J. J., Chang, Z., Cooke, D. R., Baker, M. J., Wilkinson, C. C., Inglis, S., ... & Gemmell, J. B. (2015). The chlorite proximitor: A new tool for detecting porphyry ore deposits. Journal of Geochemical Exploration, 152, 10-26.

Williams, K. T., & Byers, H. G. (1934). Occurence of selenium in pyrites. Industrial & Engineering Chemistry Analytical Edition, 6(4), 296-297.

Williams, W. D. (1987). Salinization of rivers and streams. An important environmental hazard. Ambio, 16(4), 180-185.

Winter, T. C., Harvey, J. W., Franke, O. L., & Alley, W. M. (1998). Ground water and surface water: a single resource (Vol. 1139). US geological Survey.

Wolanski, E., Fabricius, K. E., Cooper, T. F., & Humphrey, C. (2008). Wet season fine sediment dynamics on the inner shelf of the Great Barrier Reef. Estuarine, Coastal and Shelf Science, 77(4), 755-762.

Wolanski, E., Richmond, R., McCook, L., & Sweatman, H. (2003). Mud, marine snow and coral reefs: the survival of coral reefs requires integrated watershed-

based management activities and marine conservation. American Scientist, 91(1), 44-51.

Wollast, R. (1982). Methodology of research in micropollutants–heavy metals. Water science and technology, 14(12), 107-125.

Wollast, R., Billen, G., & Duinker, J. C. (1979). Behaviour of manganese in the Rhine and Scheldt estuaries: I. Physico-chemical aspects. Estuarine and Coastal Marine Science, 9(2), 161-169.

Wong, M. K. (1980). A study of three extraction methods for hydrocarbons in marine sediment. Marine Chemistry, 9(3), 183-190.

Wooldridge, T. H., & Deyzel, S. H. P. (2012). Variability in estuarine water temperature gradients and influence on the distribution of zooplankton: a biogeographical perspective. African Journal of Marine Science, 34(4), 465-477.

Wu, Q., & Xia, X. (2014). Trends of water quantity and water quality of the Yellow River from 1956 to 2009: implications for the effect of climate change. Environmental Systems Research, 3(1), 1-6.

Wuana, R. A., & Okieimen, F. E. (2011). Heavy metals in contaminated soils: a review of sources, chemistry, risks and best available strategies for remediation. Isrn Ecology, 2011.

Xia, W., Zhao, X., Zhao, R., & Zhang, X. (2019). Flume Test Simulation and Study of Salt and Fresh Water Mixing Influenced by Tidal Reciprocating Flow. Water, 11(3), 584.

Xie, M., & Wang, W. X. (2020). Contrasting temporal dynamics of dissolved and colloidal trace metals in the Pearl River Estuary. Environmental Pollution, 265, 114955.

Yang, X., & Wang, Z. L. (2017). Distribution of dissolved, suspended, and sedimentary heavy metals along a salinized river continuum. Journal of Coastal Research, 33(5), 1189-1195.

Yao, K. M., Sangare, N., Trokourey, A., & Metongo, B. S. (2019). The mobility of the trace metals copper, zinc, lead, cobalt, and nickel in tropical estuarine sediments, Ebrie Lagoon, Côte d'Ivoire. Journal of soils and sediments, 19(2), 929-944.

Yuan, C. G., Shi, J. B., He, B., Liu, J. F., Liang, L. N., & Jiang, G. B. (2004). Speciation of heavy metals in marine sediments from the East China Sea by

ICP-MS with sequential extraction. Environment International, 30(6), 769-783.

Yuan, X., Zhang, L., Li, J., Wang, C., & Ji, J. (2014). Sediment properties and heavy metal pollution assessment in the river, estuary and lake environments of a fluvial plain, China. Catena, 119, 52-60.

Yudovich, Y. E., & Ketris, M. P. (2006). Selenium in coal: a review. International Journal of Coal Geology, 67(1-2), 112-126.

Zaharah, A. R., Gikonyo, E. W., Silek, B., Goh, K. J., & Amin, S. (2014). Evaluation of phosphate rock sources and rate of application on oil palm yield grown on peat soils of Sarawak, Malaysia. Journal of Agronomy, 13(1), 12-22.

Zahra, A., Hashmi, M. Z., Malik, R. N., & Ahmed, Z. (2014). Enrichment and geo-accumulation of heavy metals and risk assessment of sediments of the Kurang Nallah—feeding tributary of the Rawal Lake Reservoir, Pakistan. Science of the Total Environment, 470, 925-933.

Zaidi, F. K., Nazzal, Y., Jafri, M. K., Naeem, M., & Ahmed, I. (2015). Reverse ion exchange as a major process controlling the groundwater chemistry in an arid environment: a case study from northwestern Saudi Arabia. Environmental monitoring and assessment, 187(10), 1-18.

Zang, C., Huang, S., Wu, M., Du, S., Scholz, M., Gao, F., ... & Dong, Y. (2011). Comparison of relationships between pH, dissolved oxygen and chlorophyll a for aquaculture and non-aquaculture waters. Water, Air, & Soil Pollution, 219(1-4), 157-174.

Zeng, J., & Han, G. (2020). Tracing zinc sources with Zn isotope of fluvial suspended particulate matter in Zhujiang River, southwest China. Ecological Indicators, 118, 106723.

Zhang, C., Yu, Z. G., Zeng, G. M., Jiang, M., Yang, Z. Z., Cui, F., ... & Hu, L. (2014). Effects of sediment geochemical properties on heavy metal bioavailability. Environment international, 73, 270-281.

Zhang, C., Yu, Z. G., Zeng, G. M., Jiang, M., Yang, Z. Z., Cui, F., ... & Hu, L. (2014). Effects of sediment geochemical properties on heavy metal bioavailability. Environment international, 73, 270-281.

Zhang, H., Zhao, L., Sun, Y., Wang, J., & Wei, H. (2017). Contribution of sediment oxygen demand to hypoxia development off the Changjiang Estuary. Estuarine, Coastal and Shelf Science, 192, 149-157.

Zhang, J. (1995). Geochemistry of trace metals from Chinese river/estuary systems: an overview. Estuarine, Coastal and Shelf Science, 41(6), 631-658.

Zhang, J. Z., & Huang, X. L. (2011). Effect of temperature and salinity on phosphate sorption on marine sediments. Environmental science & technology, 45(16), 6831-6837.

Zhang, J., Zhou, F., Chen, C., Sun, X., Shi, Y., Zhao, H., & Chen, F. (2018). Spatial distribution and correlation characteristics of heavy metals in the seawater, suspended particulate matter and sediments in Zhanjiang Bay, China. PloS one, 13(8), e0201414.

Zhang, L. (2016). A Study of Polluted River Remediation by Aeration. In Proceedings of the 6th International Asia Conference on Industrial Engineering and Management Innovation (pp. 451-461). Atlantis Press, Paris.

Zhang, M., Alva, A. K., Li, Y. C., & Calvert, D. V. (1997). Chemical association of Cu, Zn, Mn, and Pb in selected sandy citrus soils. Soil Science, 162(3), 181-188.

Zhang, X., Müller, M., Jiang, S., Wu, Y., Zhu, X., Mujahid, A., ... & Zhang, J. (2020). Distribution and flux of dissolved iron in the peatland-draining rivers and estuaries of Sarawak, Malaysian Borneo. Biogeosciences, 17(7), 1805-1819.

Zhang, Y., Zhang, H., Zhang, Z., Liu, C., Sun, C., Zhang, W., & Marhaba, T. (2018). pH effect on heavy metal release from a polluted sediment. Journal of Chemistry, 2018.

Zhao, Y., Zou, X., Gao, J., Wang, C., Li, Y., Yao, Y., ... & Xu, M. (2018). Clay mineralogy and source-to-sink transport processes of Changjiang River sediments in the estuarine and inner shelf areas of the East China Sea. Journal of Asian Earth Sciences, 152, 91-102.

Zheng, N. A., Wang, Q., Liang, Z., & Zheng, D. (2008). Characterization of heavy metal concentrations in the sediments of three freshwater rivers in Huludao City, Northeast China. Environmental pollution, 154(1), 135-142.

Zheng, S., Wang, P., Wang, C., Hou, J., & Qian, J. (2013). Distribution of metals in water and suspended particulate matter during the resuspension processes in Taihu Lake sediment, China. Quaternary international, 286, 94-102.

Zhou, J. L., Liu, Y. P., & Abrahams, P. W. (2003). Trace metal behaviour in the Conwy estuary, North Wales. Chemosphere, 51(5), 429-440.

Zhou, J. L., Rowland, S., Fauzi, R., Mantoura, C., & Braven, J. (1994). The formation of humic coatings on mineral particles under simulated estuarine conditions—a mechanistic study. Water Research, 28(3), 571-579.

Zhou, Q., Liu, Y., Li, T., Zhao, H., Alessi, D. S., Liu, W., & Konhauser, K. O. (2020). Cadmium adsorption to clay-microbe aggregates: Implications for marine heavy metals cycling. Geochimica et Cosmochimica Acta, 290, 124-136.

Rigaud, S., Radakovitch, O., Couture, R. M., Deflandre, B., Cossa, D., Garnier, C., & Garnier, J. M. (2013). Mobility and fluxes of trace elements and nutrients at the sediment–water interface of a lagoon under contrasting water column oxygenation conditions. Applied Geochemistry, 31, 35-51.

Zhu, H. N., YUAN, X. Z., ZENG, G. M., JIANG, M., LIANG, J., ZHANG, C., ... & JIANG, H. W. (2012). Ecological risk assessment of heavy metals in sediments of Xiawan Port based on modified potential ecological risk index. Transactions of Nonferrous Metals Society of China, 22(6), 1470-1477.

Zhu, J., Weisberg, R. H., Zheng, L., & Qi, H. (2015). On the salt balance of Tampa Bay. Continental Shelf Research, 107, 115-131.

Zhu, W., Wang, C., Hill, J., He, Y., Tao, B., Mao, Z., & Wu, W. (2018). A missing link in the estuarine nitrogen cycle?: Coupled nitrification-denitrification mediated by suspended particulate matter. Scientific reports, 8(1), 1-10.

Zimmer, M. (2008). Detritus. Encyclopedia of Ecology, Academic Press, Pages 903-911, ISBN 9780080454054, https://doi.org/10.1016/B978-008045405-4.00475-4.

Zimmerman, A. J., & Weindorf, D. C. (2010). Heavy metal and trace metal analysis in soil by sequential extraction: a review of procedures. International journal of analytical chemistry, 2010.

Zogorski, J. S., Carter, J. M., Ivahnenko, T., Lapham, W. W., Moran, M. J., Rowe, B. L., ... & Toccalino, P. L. (2006). Volatile organic compounds in the nation's ground water and drinking-water supply wells. US Geological Survey Circular, 1292, 101.

"Every reasonable effort has been made to acknowledge the owners of copyright material. I would be pleased to hear from any copyright owner who has been omitted or incorrectly acknowledged."

Appendix

Appendix-1 The saturation index of mineral phases during SWM

Sample Stations	Carbonates				Sulfates		Halides	Oxides	
	Calcite	Magnesite	Aragonite	Dolomite	Gypsum	Anhydrite	Halide	Goethite	Magnetite
1	-2.06	-1.734	-2.207	-3.788	-2.708	-2.939	-4.354	-	11.036
2	-3.028	-3.388	-3.169	-6.367	-3.013	-3.221	-5.492	-	2.983
3	-4.19	-4.403	-4.331	-8.539	-7.56	-3.007	-5.032	-	-6.343
4	-3.004	-2.944	-3.146	-5.897	-2.707	-2.911	-4.431	-	3.032
5	-3.11	-3.528	-3.251	-6.581	-3.271	-3.472	-6.903	1.474	4.749
6	-3.061	-3.653	-3.201	-6.655	-3.146	-3.346	-6.265	1.542	4.93
7	-2.842	-3.279	-2.984	-6.075	-2.893	-3.103	-6.736	2.496	7.485
8	-3.219	-3.467	-3.36	-6.633	-3.241	-3.445	-6.439	2.129	6.527
9	-2.791	-3.041	-2.932	-5.781	-3.341	-3.547	-6.759	2.405	7.257
10	-2.864	-3.59	-3.006	-6.403	-3.381	-3.587	-6.718	1.957	6.042
11	-2.926	-3.183	-3.068	-6.062	-3.293	-3.502	-6.697	2.222	6.742
12	-2.882	-3.602	-3.023	-6.427	-3.359	-3.561	-7.177	2.499	7.493
13	-3.265	-4.171	-3.406	-7.386	-3.368	-3.575	-7.289	1.957	6.044
14	-3.104	-3.53	-3.246	-6.583	-3.592	-3.797	-7.24	2.144	6.514
15	-2.864	-3.774	-3.005	-6.59	-3.405	-3.614	-7.398	2.571	7.68
16	-2.931	-3.774	-3.072	-6.408	-2.903	-3.106	-7.398	1.699	5.355
17	-2.812	-3.532	-2.954	-6.312	-3.143	-3.352	-7.519	2.762	8.214
18	-3.244	-3.547	-3.385	-6.57	-3.336	-3.544	-7.44	1.968	6.057
19	-2.971	-3.375	-3.113	-6.635	-2.859	-3.068	-7.415	1.905	5.861
20	-3.176	-3.711	-3.318	-6.737	-3.29	-3.499	-7.453	2.221	6.717
21	-3.034	-3.61	-3.175	-6.44	-3.419	-3.624	-7.147	2.123	6.448
22	-2.865	-3.458	-3.007	-6.414	-3.039	-3.247	-6.979	2.517	7.516
23	-2.715	-3.599	-2.856	999	-3.025	-3.229	-7.157	2.768	8.203
24	-3.039	-	-3.181	-5.973	-3.626	-3.831	-7.01	2.751	8.113
25	-3.383	-2.987	-3.523	-7.128	-3.292	-3.492	-7.285	1.853	5.742
26	-3.264	-3.803	-3.405	-6.427	-3.241	-3.446	-7.403	2.09	6.362
27	-2.964	-3.215	-3.105	-6.607	-3.53	-3.737	-7.274	2.05	6.254
28	-2.789	-3.693	-2.93	-6.24	-3.53	-3.732	-7.519	2.418	7.238
29	-3.155	-3.508	-3.296	-6.184	-4.122	-4.32	-7.514	2.372	7.116
30	-2.742	-3.089	-2.883	-5.675	-3.715	-3.919	-7.554	2.356	7.057
31	-2.506	-2.987	-2.646	-5.974	-2.817	-3.017	-7.532	2.144	6.468
32	-2.776	-3.526	-2.917	-5.529	-3.107	-3.312	-7.424	2.447	7.291
33	-2.555	-2.805	-2.696	-5.95	-3.357	-3.559	-7.445	2.495	7.433
34	-2.453	-3.451	-2.594	-5.089	-3.101	-3.3	-7.137	3.157	9.225
35	-2.603	-2.695	-2.744	-5.743	-2.93	-3.131	-7.699	2.288	6.867
36	-2.7	-3.198	-2.841	-5.463	-2.903	-3.103	-7.411	2.793	8.213

Appendix-2 The saturation index of mineral phases during NEM

Sample Stations	Carbonates				Sulfates		Halides
	Calcite	Magnesite	Dolomite	Aragonite	Gypsum	Anhydrite	Halite
1	-2.26	-1.561	-3.755	-2.4	-2.15	-2.339	-3.786
2	-1.278	-1.051	-2.257	-1.416	-1.752	-1.936	-3.838
3	-1.48	-1.276	-2.689	-1.619	-1.752	-1.943	-4.798
4	-1.373	-1.443	-2.754	-1.513	-1.575	-1.77	-4.445
5	-1.555	-1.934	-3.429	-1.695	-1.739	-1.937	-4.698
6	-2.534	-1.069	-3.542	-2.674	-2.989	-3.184	-4.74
7	-2.121	-1.375	-3.436	-2.261	-2.459	-2.656	-4.88
8	-1.748	-1.894	-3.584	-1.889	-1.865	-2.064	-4.9
9	-1.585	-1.342	-2.868	-1.725	-1.954	-2.152	-5.009
10	-1.834	-2.63	-4.415	-1.976	-1.906	-2.113	-5.086
11	-1.335	-2.429	-3.712	-1.476	-1.675	-1.881	-5.342
12	-1.762	-1.302	-3.005	-1.902	-2.254	-2.454	-5.38
13	-1.787	-1.42	-3.153	-1.928	-2.321	-2.524	-5.935
14	-1.654	-2.809	-4.411	-1.795	-2.149	-2.354	-6.292
15	-1.348	-1.494	-2.786	-1.489	-2.143	-2.346	-6.38
16	-0.932	-2.42	-3.3	-1.073	-2.277	-2.483	-7.489
17	-0.909	-2.73	-3.584	-1.05	-2.288	-2.492	-7.84
18	-0.766	-1.471	-2.178	-0.906	-2.36	-2.56	-7.828
19	-0.806	-1.523	-2.27	-0.947	-2.51	-2.71	-7.961
20	-0.918	-1.225	-2.07	-1.057	-2.659	-2.845	-7.761
21	-1.081	-1.668	-2.681	-1.22	-2.211	-2.402	-7.178
22	-1.49	-1.183	-2.615	-1.631	-2.855	-3.054	-7.392
23	-1.059	-1.863	-2.858	-1.199	-2.523	-2.717	-7.798
24	-1.327	-1.988	-3.251	-1.467	-2.679	-2.873	-7.997
25	-1.922	-2.471	-4.338	-2.063	-3.245	-3.449	-8.301
26	-2.389	999	999	-2.53	-3.527	-3.726	-8.133
27	-1.919	-2.083	-3.951	-2.06	-3.196	-3.402	-8.341
28	-1.661	-1.059	-2.662	-1.802	-3.451	-3.651	-8.252
29	-1.297	-1.627	-2.859	-1.437	-3.092	-3.286	-8.447
30	-0.912	-1.7	-2.553	-1.052	-3.067	-3.267	-8.135
31	-0.819	-1.355	-2.119	-0.96	-3.024	-3.227	-8.344
32	-1.395	-1.813	-3.149	-1.535	-3.816	-4.016	-8.415
33	-2.239	-2.363	-4.55	-2.38	-4.206	-4.411	-8.488
34	-0.85	-1.538	-2.332	-0.991	-3.065	-3.266	-8.335
35	-1.842	-2.251	-4.031	-1.982	-4.578	-4.775	-8.408
36	-1.914	-2.02	-3.869	-2.053	-3.759	-3.953	-8.861

Appendix-3 Factor Score for Physico-chemical parameters, major ions, nutrients and trace metals during SWM

Sample Stations	F1	F2	F3	F4	F5	F6	F7	F8
1	4.383	0.390	3.003	0.587	0.277	-0.096	1.086	0.043
2	0.617	0.397	-0.765	-0.626	0.334	-1.239	1.301	-0.244
3	1.429	0.626	-3.952	0.161	-0.176	-0.540	0.984	0.643
4	2.974	0.319	-1.658	-1.340	0.286	0.129	-1.981	-0.100
5	-0.445	0.691	-0.217	-0.660	0.237	-1.536	0.063	-0.268
6	-0.266	1.445	-0.622	1.521	0.606	-0.604	-0.656	-0.652
7	-0.088	2.373	-0.347	0.314	-1.101	2.695	-0.802	-1.340
8	-0.313	1.342	0.245	-0.292	-1.328	-0.584	-0.110	0.088
9	-0.670	1.621	0.609	0.018	0.238	0.171	0.063	-0.355
10	-0.596	0.868	0.507	0.552	0.307	-1.270	0.245	-1.252
11	-0.598	1.678	0.810	0.812	1.893	0.340	-1.396	0.191
12	-0.429	0.040	0.064	-1.235	0.259	-1.568	0.001	1.125
13	-0.642	1.226	0.591	-0.511	-0.665	-0.206	-0.875	3.966
14	-0.555	0.454	0.522	-0.387	-0.453	-1.132	0.401	-0.304
15	-0.366	0.634	0.203	-0.454	-0.765	-0.133	-0.404	-1.002
16	-0.532	0.385	-0.645	-0.534	-0.178	0.055	1.804	0.020
17	-0.354	0.493	0.958	-0.904	-0.196	1.236	0.291	0.341
18	-0.687	0.444	0.093	-0.148	0.100	0.575	2.675	-0.462
19	0.076	-0.599	-0.293	-0.947	-0.147	0.182	0.132	0.141
20	-0.092	-0.345	-0.087	-0.497	0.112	1.636	-0.504	0.282
21	-0.569	-0.020	0.809	-0.911	2.027	-0.235	-0.163	0.808
22	-0.234	-0.718	0.519	0.211	-0.485	0.725	2.080	-0.407
23	0.049	-0.720	-0.139	1.794	-0.528	-0.428	1.450	0.572
24	-0.266	-0.678	0.086	1.780	-0.148	0.100	-0.731	-0.424
25	-0.132	-0.541	-0.676	1.916	-0.791	0.243	-0.410	0.025
26	-0.010	-0.859	-0.324	2.875	0.475	1.131	0.187	2.075
27	0.159	-1.281	0.784	0.230	-1.640	-0.875	-1.709	-0.195
28	-0.253	-1.356	0.490	-0.521	-0.633	-0.796	-0.184	0.352
29	-0.412	-0.913	-0.215	0.124	-0.795	-0.821	-0.810	0.078
30	-0.300	-0.869	0.388	-0.438	-0.765	-0.767	-0.544	-0.682
31	-0.289	-1.116	-0.403	0.488	3.844	-0.504	-0.530	-0.873
32	0.035	-0.910	0.337	0.264	-0.461	-0.086	-0.578	-1.431
33	-0.143	-0.979	-0.311	0.184	-0.909	-0.002	-0.681	-0.946
34	-0.300	-1.004	-0.298	-1.439	0.484	2.366	-0.056	-0.451
35	-0.196	-1.156	0.025	-1.091	0.520	0.488	0.305	-0.571
36	0.016	-1.362	-0.090	-0.895	0.163	1.350	0.056	1.210

Appendix-4 Factor Score for Physico-chemical parameters, major ions, nutrients and trace metals during NEM

Sample Stations	F1	F2	F3	F4	F5	F6
1	5.360	-0.877	-0.113	-0.282	-0.041	0.328
2	1.620	1.667	0.009	0.670	1.903	-0.746
3	0.259	1.315	1.022	-1.674	0.697	-0.027
4	0.360	1.859	0.107	-0.225	1.048	-0.803
5	0.118	1.394	-0.261	0.505	-0.213	-0.497
6	-0.048	1.680	1.011	0.171	-0.206	0.190
7	-0.288	1.321	-0.723	-0.530	0.020	3.958
8	-0.580	1.973	-0.401	1.276	-0.381	0.054
9	-0.299	1.855	0.111	2.001	0.609	0.062
10	-0.242	0.870	-0.589	0.607	-1.165	-0.430
11	0.220	0.482	0.346	-0.527	-3.014	0.822
12	-0.022	0.223	-0.659	-1.695	-0.330	0.332
13	-0.260	0.185	-0.624	-1.254	-1.006	0.239
14	0.117	-0.106	-0.765	-1.052	-1.640	-0.939
15	-0.362	0.206	1.044	-1.402	-0.342	-1.782
16	-0.416	-0.434	-0.471	-1.702	-0.126	-0.456
17	-0.545	-0.313	-0.532	-0.669	0.352	0.083
18	-0.713	-0.286	0.201	-0.679	1.629	-0.605
19	-0.619	-0.261	-0.619	-0.553	0.464	-1.051
20	-0.486	-0.714	-0.698	-0.213	1.817	-0.099
21	-0.277	-0.368	1.100	-0.480	0.426	-0.396
22	-0.355	-0.374	-0.191	-0.248	-0.503	-0.431
23	-0.394	-0.501	-0.412	-0.375	0.765	-0.089
24	-0.423	-0.492	-0.129	-0.460	0.719	-0.271
25	-0.097	-0.626	-0.610	-0.142	-0.968	0.526
26	-0.154	-0.783	0.341	-0.606	-0.032	0.011
27	-0.241	-0.625	-0.443	0.659	-0.884	0.620
28	-0.255	-0.805	-0.069	1.221	0.577	0.330
29	0.208	-0.451	-0.036	2.162	-1.820	-2.412
30	-0.265	-0.754	-0.076	1.166	-0.202	0.988
31	-0.287	-0.875	4.968	0.414	-0.294	0.866
32	-0.172	-1.168	-0.036	0.806	0.256	0.662
33	-0.112	-1.260	-0.315	0.461	0.367	-0.752
34	-0.005	-1.281	-0.221	0.198	1.091	0.869
35	-0.268	-0.811	-0.661	1.339	0.212	0.193
36	-0.078	-0.864	-0.605	1.114	0.214	0.653

Appendix-5 Factor Score for Trace Metals in SS during SWM

Sample Stations (Interval 10km)	Component		
	1	2	3
1	1.52034	0.18724	-0.55732
2	0.42122	-0.55946	1.49986
3	-0.42497	-0.98758	-1.16021
4	-0.45785	1.61587	-0.07832
5	-1.05874	-0.25608	0.29599

Appendix-6 Factor Score for Trace Metals in SS during NEM

Sample Stations (Interval 10km)	Component		
	1	2	3
1	-1.3366	1.10919	0.15519
2	-0.63585	-1.55418	0.6143
3	0.07311	-0.07598	-1.50282
4	0.95752	0.58665	1.09851
5	0.94181	-0.06568	-0.36518